

Metabolic significance of fumarate in *Plasmodium falciparum* and biochemical and structural characterization of class I fumarate hydratase from *Plasmodium falciparum* and *Methanocaldococcus jannaschii*

A Thesis Submitted for the Award of the Degree of

Doctor of Philosophy

By

Vijay. J



**Molecular Biology and Genetics Unit
Jawaharlal Nehru Centre for Advanced Scientific
Research (Deemed University)**

Bangalore-560064, India

January 2017

DECLARATION

I hereby declare that this thesis entitled “**Metabolic significance of fumarate in *Plasmodium falciparum* and biochemical and structural characterization of class I fumarate hydratase from *Plasmodium falciparum* and *Methanocaldococcus jannaschii***” is an authentic record of the research work carried out by me under the supervision of Prof. Hemalatha Balaram at the Molecular Biology and Genetics Unit, Jawaharlal Nehru Centre for Advanced Scientific Research, Bangalore, India and that this work has not been submitted elsewhere for the award of any other degree.

In keeping with the general practice of reporting scientific observations, due acknowledgements have been made wherever the work described has been based on the findings of other investigators. Any omission, which might have occurred by oversight or misjudgment, is regretted.

(Vijay. J)

Place:

Date:



Molecular Biology and Genetics Unit
JAWAHARLAL NEHRU CENTRE FOR ADVANCED SCIENTIFIC
RESEARCH
Jakkur, Bengaluru-560 064, India

Hemalatha Balaram, Ph.D.

Professor

CERTIFICATE

This is to certify that the work described in this thesis entitled “**Metabolic significance of fumarate in *Plasmodium falciparum* and biochemical and structural characterization of class I fumarate hydratase from *Plasmodium falciparum* and *Methanocaldococcus jannaschii***” is the result of investigations carried out by Mr. Vijay Jayaraman in the Molecular Biology and Genetics Unit, Jawaharlal Nehru Centre for Advanced Scientific Research, Bangalore, India under my supervision, and that the results presented in this thesis have not formed the basis for the award of any other diploma, degree or fellowship.

(Hemalatha Balaram)

JNCASR, Bangalore

December 2016.

◆Telephone:91-80-22082812 ◆Telefax: 91-80-22082766 ◆Email: hb@jncasr.ac.in

Acknowledgement

“Good company in a journey makes the way seem shorter” told by Izaak Walton aptly describes my Ph.D. career that lasted for over seven years. With a background in pharmaceutical sciences and very limited theory and experimental knowledge in molecular biology/biochemistry/structural biology to begin with, the work in this thesis wouldn't have been possible without the support of good, mentors, colleagues and friends. First and foremost, I would like to thank my principal investigator, Prof. Hemalatha Balaram who is an encouraging, enthusiastic, “protective” and a supportive mentor. I would always cherish the ‘tea-sessions’ I had with over both scientific and non-scientific topics. Importance of stating only facts in the data, avoiding over-interpretation and tall claims are some of the things that I learnt from her. I am also grateful to her for permitting me to attend Quantum mechanics course (as a part of my course-work) and providing an opportunity to teach metabolism as a part of the course, Basic Biological Chemistry. As a person, I always admire her for her patience, simplicity, and broad scientific knowledge.

I owe a deep sense of gratitude and respect to Dr. Joydeep Mitra, who was my mentor during my post-graduation. He had always advocated the importance of being generous and selfless in science. He helped me overcome the inertia I had in writing mails to authors, either for requesting reagents or protocols. Without this seemingly minor skill, majority of the work in the thesis wouldn't have been possible. I hope I will live up to the standards which he had inspired in us.

Working with Prof. Siddhartha P. Sharma, MBU, IISc was the best thing that happened to me during my Ph.D. I always admired his sportive spirit and infectious enthusiasm. Working with him helped me sustain my interests in NMR and also understand the topic in detail.

I thank Prof. P. Balaram for helping me in the interpretation of native ESI-MS data. I thank Prof. Gopal, MBU, IISc for providing access to MBU, X-ray diffraction facility, for the fruitful discussions and facilitating the use of ESRF synchrotron facility, France.

I thank Prof. S.V. Bhat for permitting me to use the EPR facility at Department of Physics, IISc and Bhagyashree for helping me with acquisition of EPR. I thank Ms. Sunitha for the helping me in acquiring of ESI-MS and native-ESI-MS.

I thank all the faculties of MBGU: Prof. M.R.S.Rao, Prof. Anuranjan Anand, Prof. Tapas Kumar Kundu, Prof. Uday Kumar Ranga, Prof. Kausav Sanyal, Prof. Maneesha Inamdar, Prof. Namitha Surolia, Dr. Ravi Manjithaya, Dr. Jamesh chellaiah for being always there for course work, suggestions and maintaining a streamlined infrastructure in MBGU.

Special thanks to Prof. Amitabh Joshi and the late Prof. V.K. Sharma for an informative course on Quantitative tools in biology.

*I thank the speakers of CCP4 workshop (2016) organized at RCB, Faridabad for helping me understand some basic concepts in X-ray crystallography. I thank Wellcome trust Sanger institute for selecting me as a part of their advanced course “Malaria experimental genetics, 2013”. The experience gained during the workshop has been instrumental in designing experiments on *P. berghei*.*

I thank Kumar, MBU, IISc for teaching me basics and practical aspects of X-ray crystallography. If not for him, I wouldn't have ventured into structural biology.

*I had inspiring, helpful and kind seniors like Bharath Srinivasan, Vinay Bulusu, Javaid, Vasudeva. S.P, Sanjeev Kumar and Sourav who are always a source of inspiration. My understanding on enzyme kinetics and metabolism wouldn't have been possible without the discussions I had with Vinay and Bharath. Special thanks to Vinay for training me in Plasmodium culture work and other regular molecular biology techniques including cloning, electrophoresis and microscopy. Thanks to Sanjeev, for being a compassionate and supportive senior. I would also thank Sanjeev for helping me in standardizing the protocol for *M. jannaschii* FH protein purification.*

One wouldn't ask for more in a lab if you get a wonderful and enthusiastic bunch of juniors like Arpit, Santosh, Lakshmeesha, Prasoon, Aparna, Arpitha, Asutosh and Neelakshi. Special thanks to Asutosh and Lakshmeesha who have always inspired me. I would like to thank Santosh for teaching me how to handle HPLC and stop-flow, Arpit and Lakshmeesha for regularly coming up with 'tricks' that makes an experiment work, Prasoon for the kindness she had always shown, Aparna and Arpitha for keeping the culture room up and running. I thank Arpitha, Jyothi, Umesh, Manu and Pavithra who have contributed significantly in this work. I thank Suresh. S.N, Meenakshi.P, Sarika with whom I had worked during their lab-rotation period.

I thank the 2 trios: first Avinash, Piyush, M.H.L.N Reddy for the wonderful time I had with them as a student representative, the second Arun, Anirudh and Neelakshi for being stress-busters especially during the fag end (and lonely period) of my Ph.D. I thank all my JNC friends; Rukshan and Priyank (for discussions on quantum mechanics), Anand (for solving my doubts in organic chemistry), Gopal, Vishwanath Reddy.

I thank my all my batchmates, Akhade, Rohan, Shilpee, Garima, Kirthana, and Parijat. I will always miss the company of my batchmates Hariraj Singh and Aditi who couldn't continue doing their Ph.D here in MBGU. I thank all my MBGU seniors, Mangai, Selvi, Kathigeyan, Manpreet, Praveen, Nikhil, Mishraji, Sreyoshi, Jitendra, Lakshmi Shankar Rai, Gautam Chatterjee, Mahesh Bacchu, Anjali verma, Venky, Kalpitha, Deeti shetty. I also thank other MBGU friends, Ramachandran Boopathi, Malini Menon, Sreedevi, Arnab, Surbhi, Shiny,

Simi, Rebu, Shambu, Prabhu, Gaurav, Veena, Piyush Mishra, Sundar, Adithya, Debosree, for reagents, space, and ideas.

I thank MBU friends Vidhi, Debarati, Moumita, Rustom, Swathi, Karuna, Abhinav, Anil, Disha, Santosh, for all the support they extended.

I thank all organizations and consortiums (MR4, CCP4, NCI, Addgene, PlasmoGEM) for providing us reagents, resources and training which was important for my work. I thank all central instrumentation facility at JNCASR: Suma for confocal microscope, Anitha for DNA sequencing, Dr. Prakash for Animal house facility, Mahesh for helping us with NMR facility.

I acknowledge CSIR for the fellowship. I thank Academic section (especially Sukanya ma'am), Admin. office, purchase section and security at JNCASR for making this place a conducive and efficient place to do research. Special thanks to Mr. A.N. Jayachandra, for being an able administrator of various aspects related to the institute. Thanks to Mr. Jayaramaiah for maintaining such a lush and green campus. I thank C.N.R. Rao foundation for providing me an opportunity to be a part of "Students Mentoring Programme".

None of this would have been possible without the unconditional love from my family members : Amma, Naina, Shijai, Bhuvana odhina, Pinni, Appiya, Vinu, Vithu, Bhava, Chelli mama, Vanaja attha, Prartana, Varnica and the most recent addition to the list "Bhushi" and thanks wouldn't suffice.

I am lucky to have friends like Karthik, Saravanan, Kumar, Antara and Shafqat Ali Khan. Karthik, whose mobile number was my emergency helpline number, has always inspired me and I have imbibed a lot of virtues from him. His thoughts on philosophy, conduct, and philanthropy have always influenced me. I thank Kumar and Antara for always being there in my life. Finally, it is hard to imagine the past 5 years of life without Amrutha. Her presence in my life has made it a more enriching experience.

Synopsis of the thesis entitled

**Metabolic significance of fumarate in *Plasmodium falciparum* and
biochemical and structural characterization of class I fumarate hydratase
from *Plasmodium falciparum* and *Methanocaldococcus jannaschii***

Submitted by

Vijay. J

*Molecular Biology and Genetics Unit, Jawaharlal Nehru Centre for Advanced
Scientific Research, Bangalore, India*

Energy metabolism in *Plasmodium falciparum* asexual stages is unique with respect to the set of pathways used to achieve the objective function of biomass production. ATP demand of the parasite is almost completely met by substrate level phosphorylation reactions of an unregulated glycolysis in the parasite with very low contribution from the tricarboxylic acid (TCA) cycle (Lang-Unnasch & Murphy, 1998; White et al., 1983). However, the TCA cycle in the intraerythrocytic stages of *Plasmodium* is completely operational with low flux and is largely anaplerotic in nature (Cobbold et al., 2013; MacRae et al., 2013). Anaplerotic contribution to the TCA cycle is mainly from three metabolites viz., phosphoenolpyruvate (PEP) derived from glycolysis, glutamine (derived from hemoglobin degradation and from host), and fumarate derived from purine nucleotide cycle (PNC). Purine nucleotide cycle is a set of reactions in the parasite cytosol, catalysed by three enzymes adenylosuccinate synthetase (ADSS), adenylosuccinate lyase (ASL) and adenosine monophosphate deaminase (AMPD), that involve the cyclic inter-conversion of IMP to AMP and the simultaneous conversion of one molecule of aspartate to one molecule of fumarate and ammonia. The fumarate generated enters the mitochondria and gets converted to malate and then to oxaloacetate through sequential action of the enzymes fumarate hydratase (FH) and malate-quinone oxidoreductase (MQO), the classical reactions of TCA cycle (Bulusu, Jayaraman, & Balaram, 2011). Oxaloacetate generated can have multiple fates in the cytosol.

Through a reverse genetic approach, the anaplerosis through PEP has been shown to be important for the asexual growth of the parasite (Storm et al., 2014). In a separate study it was shown that all the genes of the TCA cycle can be knocked out except for two, FH and MQO, implying two facts; (i) the essentiality of the enzymes FH and MQO and (ii) the dispensability of glutamine mediated anaplerosis (Ke et al., 2015). The metabolic significance of fumarate anaplerosis is still not clear.

In this work, we intended to study the metabolic significance of fumarate generated from PNC and biochemical characterisation of the first enzyme in fumarate metabolism, fumarate hydratase. The thesis is broadly divided into two sections: the first section of the thesis attempts to address the metabolic significance of fumarate generated from PNC. This section also deals with the development of a methodology to trace the fate of ammonia which subsequently can be used to trace the α -amino group of aspartate that feeds into the PNC. The second section deals with the biochemical and structural characterisation of fumarate hydratase from *P. falciparum* and *Methanocaldococcus jannaschii*.

Chapter 1 provides an introduction to energy metabolism in *P. falciparum* in particular covering glycolysis, TCA cycle and their cross talk with purine nucleotide cycle. Literature survey of studies done regarding these pathways/enzymes is presented and their implication in parasite metabolism is discussed. A comprehensive analysis of the distribution of purine salvage enzymes in Alveolates, comprising of Apicomplexans, Ciliates and Dinoflagellates is presented.

Chapter 2 addresses the importance of fumarate generated by PNC through an indirect approach. Depletion of fumarate generated from PNC by direct inhibition of either ADSS or ASL is not possible as it would interfere with the essential and the only step of AMP generation. To achieve selective depletion of fumarate, we have episomally expressed in *P. falciparum* an alternative AMP generating enzyme, *Saccharomyces cerevisiae* adenine phosphoribosyltransferase (ScAPRT) that makes AMP from adenine and phosphoribosylpyrophosphate. With two different sources of AMP, the endogenous AMP biosynthesis pathway in *P. falciparum* can be inhibited at the level of ADSS by the small molecule inhibitor, hadacidin. While the ScAPRT is functional, addition of hadacidin would selectively deplete fumarate but not the AMP pool from the parasite cytosol. The metabolic significance of fumarate can then be examined. This chapter deals with data regarding generation of transfectants expressing ScAPRT, validation of the transgenic parasites, functionality of the enzyme in the parasite compartment and hadacidin inhibition experiments to address the consequence of fumarate depletion.

Chapter 3 deals with a genetic strategy involving depletion of fumarate hydratase (FH) enzyme from the cell either by knocking out the gene in *P. berghei* or by conditionally knocking down the protein level in *P. falciparum*. Genetic manipulation in *P. berghei* was performed using a construct generated through recombineering strategy. A strategy involving tagging of *P. falciparum* FH with *E. coli* DHFR degradation domain was employed to knock down the level of the enzyme in the parasite. Validation of the genotypes of the transfectants will be discussed.

Chapter 4 describes the methodology developed to follow the fate of ^{15}N nitrogen. Following the fate of ammonia/amino group in any organism is conventionally done by mass spectrometry-based metabolomics. NMR analysis lags behind because of the low sensitivity of ^{15}N nitrogen but is advantageous in terms of spectral interpretation and metabolite identification. We have attempted to develop a methodology to follow the fate of ^{15}N ammonia using NMR-based techniques and standardized the same using *E. coli* as a metabolic system. The method was developed owing to availability of NMR machine time and non-availability of mass spectrometer locally for such analysis. The chapter will comprise the details about the metabolite derivatization methodology, NMR acquisition methods and the metabolites identified using the same in *E. coli*.

Fumarate hydratase (FH) enzymes are classified into class-I and class-II based on the presence or absence of iron-sulfur cluster in the protein (Woods, Schwartzbach, & Guest, 1988). Higher eukaryotes possess only the class II enzyme devoid of iron-sulfur clusters. Class I enzyme is present in many prokaryotes and lower unicellular eukaryotes. Class I enzymes contain iron-sulfur cluster and a thorough biochemical characterisation of the enzyme is absent. Class I enzyme comes in two variants- single subunit type and two subunit type. Section II deals with the biochemical and structural characterisation of class I fumarate hydratase of both single-subunit type exemplified by the *P. falciparum* enzyme and the two-subunit type exemplified by the *M. jannaschii* enzyme.

Chapter 5 provides an introduction to iron-sulfur cluster enzymes and principles of methods used to characterize them. The role of the iron-sulfur cluster in fumarate hydratase is suggested to be similar to that reported for aconitase- another iron-sulfur cluster containing enzyme for which a detailed biochemical characterization exists. A short description of the mechanism of action of aconitase is given as a primer for understanding the fumarate hydratase enzyme. A very brief introduction to solving the structure of a protein using X-ray is covered in this chapter.

Chapter 6 describes the efforts towards biochemical characterisation of fumarate hydratase from *P. falciparum*. We confirmed the annotation of the enzyme as fumarate hydratase by functional complementation in *E. coli* devoid of any fumarase activity. Details of the generation of such an *E. coli* strain are also presented. We generated various truncation constructs of the *Plasmodium* enzyme based on sequence alignment with other class-I enzymes. All the truncation constructs were tested for complementation in *E. coli*. All the constructs were also used for heterologous expression of the enzyme in *E. coli*. Although the protein was successfully expressed, it was found to be present largely as inclusion bodies. A small amount of protein was found in the soluble fraction and this was

found to be active. The protein was found to degrade with time and hence, activity was rapidly lost. Our efforts to improve the solubility, stability and activity of the enzyme will be discussed in this chapter.

Chapter 7 deals with two-subunit type class-I fumarate hydratase from *M. jannaschii* (Mj). Plasmid constructs for expression of the α and β subunits, together as well as individually, of the MjFH in *E. coli* were generated. Both subunits were over expressed and purified to homogeneity. Unlike the *Plasmodium* enzyme this enzyme was found to be stable. The subunits were biochemically characterized by mass spectrometry, fluorescence, circular dichroism, and analytical gel filtration. The α -subunit was found to be a constitutive dimer and the β -subunit a monomer; while the complex of α - and β -subunits was found to be a dimer of a heterodimer. Isothermal calorimetry based titration of the β - subunit with α -subunit indicated an endothermic heat change with a K_d value of 600 nM. For studying various aspects of the iron-sulfur cluster, the protein was reconstituted in an anaerobic chamber and subjected to different analyses. UV-visible spectrophotometry, visible CD, native protein mass spectrometry and electron paramagnetic resonance spectra of the reconstituted protein together suggested that the α -subunit alone harbours a 4Fe-4S cluster and that the β -subunit has no role in cluster formation. Fumarate to malate conversion by the reconstituted enzyme was monitored at 240 nm. Basic steady-state kinetic experiments suggested that both α -reconstituted and $\alpha\beta$ -complex-reconstituted with Fe-S cluster were active enzymes. However, the activity of the reconstituted alpha subunit was low and increased 56-fold upon addition of stoichiometric amounts of the β -subunit.

Structural analysis of the individual subunits of MjFH and the complex were attempted using x-ray crystallography. The crystallisation of both reconstituted and apoprotein preparations of the enzyme were set up under different conditions, with α -subunit alone, β -subunit alone and $\alpha\beta$ -complex. We successfully got crystals of β -subunit and of the apoform of $\alpha\beta$ -complex (apoprotein). The structure of β -subunit was solved using molecular replacement and is deposited in PDB. The structure solution of $\alpha\beta$ -complex was attempted using the structure of β -subunit for phasing.

Chapter 8 summarizes the entire work done as a part of the thesis and major conclusions are also presented. Future directions with respect different aspects of the work is also presented.

Taken together, the work attempts to probe the metabolic significance of the fumarate generated from purine nucleotide cycle in the intraerythrocytic stages of the parasite using two different strategies. Class-I fumarate hydratase has been biochemically

characterised from two organisms. Studies from the thermophilic two subunit enzyme showed that the α -subunit alone is sufficient for iron-sulfur cluster ligation and is active. The β -subunit interacts strongly with the α -subunit and enhances the activity of the α -subunit by 56-fold. The structure of β -subunit has been solved to a resolution of 2.34 Å.

References

- Bulusu, V., Jayaraman, V., & Balaram, H. (2011). Metabolic fate of fumarate, a side product of the purine salvage pathway in the intraerythrocytic stages of *Plasmodium falciparum*. *Journal of Biological Chemistry*, **286**(11), 9236–9245.
- Cobbold, S. A., Vaughan, A. M., Lewis, I. A., Painter, H. J., Camargo, N., Perlman, D. H., ... Llinás, M. (2013). Kinetic flux profiling elucidates two independent acetyl-CoA biosynthetic pathways in *Plasmodium falciparum*. *The Journal of Biological Chemistry*, **288**(51), 36338–50.
- Ke, H., Lewis, I. A., Morrisey, J. M., McLean, K. J., Ganesan, S. M., Painter, H. J., ... Vaidya, A. B. (2015). Genetic investigation of tricarboxylic acid metabolism during the *Plasmodium falciparum* life cycle. *Cell Reports*, **11**(1), 164–174.
- Lang-Unnasch, N., & Murphy, A. D. (1998). Metabolic changes of the malaria parasite during the transition from the human to the mosquito host. *Annual Review of Microbiology*, **52**, 561–90.
- MacRae, J. I., Dixon, M. W., Dearnley, M. K., Chua, H. H., Chambers, J. M., Kenny, S., ... McConville, M. J. (2013). Mitochondrial metabolism of sexual and asexual blood stages of the malaria parasite *Plasmodium falciparum*. *BMC Biology*, **11**, 67.
- Storm, J., Sethia, S., Blackburn, G. J., Chokkathukalam, A., Watson, D. G., Breitling, R., ... Müller, S. (2014). Phosphoenolpyruvate carboxylase identified as a key enzyme in erythrocytic *Plasmodium falciparum* carbon metabolism. *PLoS Pathogens*, **10**(1), e1003876.
- White, N. J., Warrell, D. A., Chanthavanich, P., Looareesuwan, S., Warrell, M. J., Krishna, S., ... Turner, R. C. (1983). Severe hypoglycemia and hyperinsulinemia in *falciparum* malaria. *The New England Journal of Medicine*, **309**(2), 61–6.
- Woods, S. A., Schwartzbach, S. D., & Guest, J. R. (1988). Two biochemically distinct classes of fumarase in *Escherichia coli*. *Biochimica et Biophysica Acta*, **954**(1), 14–26.
Retrieved from <http://www.ncbi.nlm.nih.gov/pubmed/3282546>

LIST OF PUBLICATIONS

- 1) **Bulusu V, Jayaraman V, Balaram H.** (2011) Metabolic fate of fumarate, a side product of the purine salvage pathway in the intraerythrocytic stages of *Plasmodium falciparum*. *Journal of Biological chemistry*, 286(11).
- 2) **Jayaraman V, Bulusu V, Balaram H.** (2012) Crosstalk between purine nucleotide metabolism and mitochondrial pathways in *Plasmodium falciparum*. *Current Science*, 102(5).
- 3) Structural and biochemical characterization of class-I fumarate hydratase from *Methanocaldococcus jannaschii* (manuscript under preparation).
- 4) Functional characterisation of class I fumarate hydratase from *Plasmodium falciparum* (manuscript to be submitted).
- 5) A novel methodology to follow the fate of nitrogen in general metabolic pathways using NMR (manuscript under preparation).
- 6) Metabolic significance of fumarate generated from purine salvage pathway in *Plasmodium falciparum* (manuscript under preparation).
- 7) Functional genomics of fumarate hydratase in *P. berghei* (manuscript under preparation).

List of Abbreviation

Å	Angstrom
aa	Amino acid
AAH	Adenine aminohydrolase
AAT	Aspartate amino transferase
ACO	Aconitase
AD	Aldolase
Ade	Adenine
ADA	Adenosine deaminase
ADP	Adenosine diphosphate
ADSS	Adenylosuccinate synthetase
ADA	Adenosine deaminase
AEC	Adenylate energy charge
AICAR	5-Aminoimidazole-4-carboxamide ribonucleotide
AK	Adenosine kinase
AMP	Adenosine 5 monophosphate
AMPD	AMP deaminase
APRT	Adenine phosphoribosyl transferase
ASL	Adenylosuccinate lyase
ATP	Adenosine triphosphate
α -KG	α -keto glutarate
α -KDH	α -keto glutarate dehydrogenase
BCAA	Branched chain amino acid
BCKDH	Branched chain keto acid dehydrogenase
BLAST	Basic Local Alignment Search Tool
bp	base pairs
BSA	Bovine serum albumin
β -ME	β -mercaptoethanol
CCP4	Collaborative Computational Project 4
CD	Circular Dichroism
CNT	Concentrative nucleoside transporter
CS	Citrate synthase

cDNA	Complementary deoxyribonucleic acid
DHAP	Dihydroxyacetone phosphate
DHFR	Dihydrofolate reductase
DHODH	Dihydroorotate dehydrogenase
DNA	Deoxyribonucleic acid
DTT	Dithiothreitol
ESI-MS	Electrospray Ionisation-Mass spectrometry
EDTA	Ethylenediaminetetraacetic acid
ENO	Enolase
ENT	Equilibrative nucleoside transporter
EPR	Electron paramagnetic resonance
EtBr	Ethidium bromide
ETC	Electron transport chain
E. coli	Escherichia coli
FAD	Flavin adenine dinucleotide
FAS	Fatty acid synthesis
FH	Fumarate hydratase
FNT	Facilitative nucleobase transporter
F 1,6-BP	Fructose 1,6- biphosphate
F 2,6,-BP	Fructose 2,6- biphosphate
GAPDH	Glyceraldehyde-3 phosphate dehydrogenase
GDH	Glutamate dehydrogenase
GMP	Guanosine 5' -monophosphate
GMPS	Guanosine 5'- monophosphate synthetase
GO-GAT	Glutamate-oxoglutarate: glutamine amido transferase
GTP	Guanosine triphosphate
G-3-P	Glyceraldehyde-3-phosphate
HEPES	4-(2-hydroxyethyl)-1-piperazineethanesulfonic acid
HGPRT	Hypoxanthine guanine phosphoribosyl transferase
HGXPRT	Hypoxanthine guanine xanthine phosphoribosyl transferase
hr	hour
Hyp	Hypoxanthine
IE	Intra erythrocytic

IDH	Isocitrate dehydrogenase
IMP	Inosine 5' monophosphate
IMPDH	Inosine 5' monophosphate dehydrogenases
IPP	Isopentenyl pyrophosphate
IPTG	Isopropyl thio - β -D-galactopyranoside
ITC	Isothermal calorimetry
kDa	kilo Dalton
LC	Liquid chromatography
LDH	Lactate dehydrogenase
LB	Luria broth
MDH	Malate dehydrogenase
MEGA	Molecular evolutionary genetics analysis
MES	2-(N-morpholino) ethanesulfonic acid
mg	milli gram
min	minute
Mj	<i>Methanocaldococcus jannaschii</i>
mM	milli Molar
MQO	Malate quinone oxidoreductase
MR	Molecular replacement
NaCl	Sodium chloride
NAD	Nicotinamide adenine dinucleotide
NADP	Nicotinamide adenine dinucleotide phosphate
NCBI	National Centre for Biological Information
NDH	NAD-dehydrogenase
Ni-NTA	Ni ²⁺ -nitrilotriacetic acid
nm	nano meter
NMR	Nuclear Magnetic Resonance
NPP	New permeability pathways
NTT	Nucleotide transporter
OD	Optical density
ORF	Open Reading Frame
OMPD	OMP decarboxylase
OPRT	Orotate phosphoribosyl transferase

PCR	Polymerase chain reaction
PDB	Protein data bank
PDH	Pyruvate dehydrogenase
PEG	Polyethylene glycol
PEI	Polyethylenimine
PEP	Phosphoenol pyruvate
PEPC	Phosphoenol pyruvate carboxylase
PEPCK	Phosphoenol pyruvate carboxykinase
Pf	<i>Plasmodium falciparum</i>
P _i	Inorganic phosphate
PFK	Phosphofructokinase
PGK	Phosphoglycerate kinase
PGM	Phosphoglycerate mutase
PK	Pyruvate kinase
PMSF	Phenylmethanesulfonyl fluoride
PP _i	Inorganic pyrophosphate
PRPP	5'- Phosphoribosyl-(α)1- pyrophosphate
PSP	Purine salvage pathway
PVDF	Polyvinylidene fluoride
PVM	Parasitophorous vacuolar membrane
PNP	Purine nucleoside phosphorylase
PNC	Purine nucleotide cycle
QFR	Quinol-Fumarate reductase
Q-sepharose	Quarternary ammonium sepharose
Q-TOF	Quadrupole time of flight
RMSD	Root mean square deviation
RNA	Ribonucleic acid
RP-HPLC	Reverse phase-High performance liquid chromatography
SAMP	Succinyl adenosine monophosphate
SCID	Severe combined immunodeficiency
SDS-PAGE	Sodium Dodecyl Sulphate-Polyacrylamide Gel Electrophoresis
SHAM	Salicylhydroxamic acid
Sc	<i>Saccharomyces cerevisiae</i>

SCOP	Structural classification of proteins
SDH	Succinate dehydrogenase
SDS	Sodium dodecyl sulphate
SA	Specific activity
SAICAR	Phosphoribosylaminoimidazolesuccinocarboxamide
TB	Terrific broth
TBAHS	Tetrabutyl ammonium hydrogen sulphide
TIM	Triose phosphate isomerase
TCA	Tricarboxylic acid cycle
UPRT	Uracil phosphoribosyl transferase
UV	Ultra violet
VC	Vector control
WT	Wild type
XMP	Xanthine 5 monophosphate

CONTENTS

Declaration	i
Certificate	iii
Acknowledgement	v
Synopsis	ix
List of publications	xv
List of abbreviations	xvii
Table of contents	xxiii

Chapter 1. An introduction to the crosstalk between purine and energy metabolism in the malaria parasite *Plasmodium falciparum*

1.1. General features of parasitism and apicomplexan lineage.....	1
1.2. Plasmodium: Hosts and life cycle.....	3
1.2.1. Asexual and sexual stage development.....	5
1.3. Energy metabolism.....	7
1.3.1. Glycolysis in <i>P. falciparum</i>	8
1.3.1.1. Variations and significance of glycolysis in apicomplexans.....	10
1.3.2. Pyruvate dehydrogenase (PDH) complex.....	11
1.3.3. Tricarboxylic acid cycle.....	12
1.3.3.1. Plasmodium TCA cycle.....	13
1.3.3.2. Source of acetyl-CoA	15
1.3.3.3. Anaplerosis in <i>Plasmodium</i> TCA cycle.....	16
1.3.3.4. Significance of TCA cycle enzymes	18
1.3.4. Mitochondria and electron transport chain	18
1.3.4.1. The role of mitochondrion in <i>P. falciparum</i>	19
1.3.4.2. Electron transport chain	20
1.3.4.3. <i>Plasmodium</i> electron transport chain.....	21
1.3.4.4. Mitochondrial dehydrogenases and their essentiality.....	25
1.3.5. Apicoplast and mitochondrial connection.....	25
1.3.6. Mitochondrial transporters.....	26
1.4. Purines and their biochemical roles.....	26
1.4.1. Purine synthesis <i>de novo</i> versus salvage.....	27
1.4.2. Modes of purine salvage	28
1.4.3. Purine salvage in <i>Plasmodium</i>	29
1.4.3.1. Transport of purines.....	29

1.4.3.2. Transport of purines across erythrocyte membrane.....	29
1.4.3.3. Transport of purines across parasite plasma membrane.....	30
1.4.4. Enzymes involved in purine salvage pathway	31
1.4.5. Adenylate energy charge	35
1.4.6. Purine nucleotide cycle	37
1.4.6.1. PNC in <i>Plasmodium</i>	38
1.4.6.2. Fate of fumarate generated from PNC in <i>Plasmodium falciparum</i>	38
1.4.6.4. Fate of ammonia generated from PNC.....	40
1.5. Objectives	41

Chapter 2. Probing the metabolic significance of fumarate generated from PNC by phenotyping transgenic *P. falciparum* expressing yeast adenine phosphoribosyl transferase (yAPRT)

2.1. Introduction.....	45
2.1.1. Metabolic and non-metabolic role of fumarate	45
2.1.2. Role of fumarate in <i>P. falciparum</i>	49
2.2. Objective and strategy.....	50
2.3. Materials and methods.....	50
2.3.1. Molecular biology reagents and chemicals.....	50
2.3.2. Bioinformatic analysis.....	51
2.3.3. Cloning, expression and purification of yeast adenine phosphoribosyl transferase (yAPRT).....	51
2.3.4. Antibody generation and purification.....	52
2.3.5. Western blot analysis of parasite proteins.....	53
2.3.6. <i>In vitro</i> culture of <i>Plasmodium falciparum</i>	54
2.3.6.1. Composition and preparation of complete culture media	54
2.3.6.2. Processing of human erythrocytes (O ⁺ and A ⁺) for <i>in vitro</i> culturing of <i>P. falciparum</i>	55
2.3.6.3. Regular maintenance of <i>Plasmodium</i> culture.....	56
2.3.6.4. Synchronisation of <i>P. falciparum</i> culture.....	56
2.3.6.5. Percoll enrichment of late stages of <i>P. falciparum</i>	57
2.3.6.6. Isolation of free parasites from infected erythrocytes using saponin treatment.....	57
2.3.6.7. Cryopreservation and revival of <i>P. falciparum</i> asexual stage cultures.....	58
2.3.6.8. Genomic DNA isolation.....	59

2.3.6.9. Enumeration of parasitemia using microscopy	60
2.3.6.10. Indirect immunofluorescence of asexual stages of <i>P. falciparum</i>	60
2.3.6.11. Live cell imaging of <i>P. falciparum</i> culture.....	61
2.3.7. Transfection of <i>P. falciparum</i>	61
2.3.7.1. Preloading of plasmid DNA into uninfected erythrocytes by electroporation.....	61
2.3.7.2. Direct electroporation of plasmid DNA into ring stage parasites.....	62
2.3.8. 2-Fluoroadenine inhibition of WT and <i>aprt</i> <i>E. coli</i> strains.....	63
2.3.9. <i>In vitro</i> activity of yAPRT	63
2.3.10. <i>In vivo</i> activity of yAPRT in <i>P. falciparum</i>	64
2.4. Results and discussion.....	64
2.4.1. Distribution of purine salvage pathway enzymes in alveolates.....	64
2.4.2. Comparison of thermodynamic/kinetic parameters of enzymes involved in purine salvage pathway.....	67
2.4.3. The choice of alternate AMP generating enzyme.....	68
2.4.4. Cloning, expression, purification and activity of recombinant yAPRT.....	69
2.4.5. Generation and purification of antibody.....	71
2.4.6. 2-FA toxicity as a reporter for <i>in vivo</i> activity of yAPRT	72
2.4.7. Generation and validation of <i>P. falciparum</i> strain expressing yAPRT/GFP.....	73
2.4.8. <i>In vivo</i> and <i>in vitro</i> activity of yAPRT in <i>P. falciparum</i>	76
2.4.9. Rescue of 2-FA mediated toxicity in 3D7-yAPRT parasites.....	77
2.4.10. Purine tolerance in 3D7-VC and 3D7-yAPRT	78
2.4.11. Rescue of hadacidin mediated inhibition as a probe for fumarate significance.....	81
2.5. Summary and future perspectives.....	82
Chapter 3. Functional genomics of fumarate hydratase in <i>Plasmodium falciparum</i> and <i>Plasmodium berghei</i>	
3.1. Introduction.....	83
3.2. Materials and methods.....	85
3.2.1. Chemicals, strains and molecular biology reagents	85
3.2.2. Expression and purification of <i>P. falciparum</i> FH C-terminal domain.....	85
3.2.3. Generation of gene targeting construct for the conditional knockdown of <i>P. falciparum</i> (Pf) fumarate hydratase (FH).....	86

3.2.4. Transfection and selection of parasites.....	87
3.2.5. Genotyping of the parasites.....	88
3.2.6. Strain of parasite and mice used for the study.....	88
3.2.7. Maintenance and assessment of parasites	88
3.2.8. Isolation of free parasites from infected mice erythrocytes.....	89
3.2.9. Cryopreservation and revival of <i>P. berghei</i>	89
3.2.10. <i>P. berghei</i> genomic DNA isolation	89
3.2.11. <i>P. falciparum</i> total RNA isolation.....	90
3.2.12. Maintenance of mice.....	90
3.2.13. Parasite administration and collection.....	91
3.2.14. <i>E. coli</i> strains, plasmids and <i>P. berghei</i> genomic clones used.....	91
3.2.15. Generation of <i>P. berghei</i> fumarate hydratase gene tagged and gene deletion constructs	91
3.2.16. Transfection of <i>P. berghei</i> using linear DNA.....	94
3.2.17. Nycodenz density gradient centrifugation.....	94
3.2.18. Southern blotting with <i>P. berghei</i> genomic DNA.....	95
3.2.19. Limiting dilution cloning.....	96
3.2.20. Sequence analysis.....	96
3.3. Results and discussion.....	97
3.3.1. Taxonomic distribution of class-I FH in eukaryotes.....	97
3.3.2. Expression analysis of fumarate hydratase in <i>P. falciparum</i>	99
3.3.3. Generation and validation of <i>FH-RFA</i> strain.....	101
3.3.4. Cellular localisation of FH.....	103
3.3.5. Generation of fumarate hydratase null (PbFHKO) and HA tagged (PbFHHA) strains of <i>P. berghei</i>	104
3.3.6. Generation of PbFH knockout construct.....	107
3.3.7. Genotyping of PbFHKO strain.....	108
3.4. Summary and future directions.....	110
Chapter 4. Tracing the cellular fate of ammonia: development of an NMR-based methodology	
4.1. Introduction.....	111
4.1.1. Nitrogen metabolism in organisms.....	111
4.1.2. Metabolic role of ammonia/ammonium.....	112
4.1.3. Generation and consumption of ammonia.....	112
4.1.5. Methodology to study ammonia metabolism.....	113
4.1.6. Rationale behind the methodology used.....	114

4.1.7. NMR techniques to establish metabolite identity.....	116
4.2. Materials and methods.....	117
4.2.1. Chemicals, Strains and Molecular biology Reagents Used.....	117
4.2.2. <i>E. coli</i> growth and metabolite extraction.....	117
4.2.3. Acetylation of metabolites.....	118
4.2.4. Estimation of level of acetylation.....	118
4.2.5. NMR acquisition and identification of metabolites.....	119
4.3. Results and discussion.....	119
4.3.1. Acetylation of standard metabolites.....	119
4.3.2. Quantification of extent of acetylation.....	122
4.3.4. Acetylation and NMR analysis of <i>E. coli</i> metabolites	124
4.3.4.1. 2D-HSQC analysis of acetylated metabolites.....	124
4.3.4.2. ¹⁵ N-edited TOCSY – HSQC analysis of acetylated metabolites.....	125
4.4. Summary and future directions	128
Chapter 5. An introduction to Fe-S cluster containing class I fumarate hydratase	
5.1. Fumarate hydratase.....	131
5.2. Physiological significance and localisation of FH (C I and C II).....	135
5.2.1. Class-II fumarate hydratase.....	135
5.2.2. Class-I fumarate hydratase.....	137
5.3. Mechanism and kinetic properties of CI and CII enzymes.....	138
5.4. Fe-S cluster.....	140
5.4.1. Types and chemical properties.....	141
5.4.2. Techniques to study Fe-S clusters.....	143
5.5. Physiological roles of iron-sulfur cluster containing proteins.....	145
5.5.1 Fe-S cluster as a Lewis acid.....	146
5.5.2. <i>Leishmania major</i> C I fumarate hydratase.....	149
5.6. Structural studies of proteins	153
5.6.1.1. Crystallisation of protein and data collection.....	153
5.6.1.2. Data processing.....	154
5.6.1.3. Model refinement and analysis.....	154
5.7. Objectives and strategy.....	155
Chapter 6. Preliminary biochemical characterization of <i>Plasmodium falciparum</i> fumarate hydratase	
6.1. Introduction.....	157
6.2. Materials and methods.....	158

6.2.1. Chemicals, strains and molecular biology reagents.....	158
6.2.2. Sequence analysis.....	158
6.2.3. Cloning, protein expression, and purification.....	159
6.2.4. Enzyme activity.....	159
6.2.5. Generation of fumarate hydratase null <i>E. coli</i> strain, <i>ΔfumACB</i>	160
6.2.6. Complementation assays in <i>E. coli</i>	161
6.2.7. Mercaptosuccinic acid mediated inhibition of FH.....	162
6.3. Results and discussion.....	162
6.3.1. Multiple sequence alignment.....	162
6.3.2. Prediction of mitochondrial targeting sequence.....	167
6.3.3. Cloning, expression and purification.....	169
6.3.4. Generation and testing of α -PffH Δ 40 antibody.....	171
6.3.5. Fumarate hydratase activity.....	172
6.3.6. Functional complementation of PffH in fumarate hydratase null <i>E. coli</i> strain	174
6.3.7. Functional complementation with PffH.....	175
6.3.8. Substrate promiscuity of PffH.....	176
6.3.8. Growth phenotype of cells expressing PffH on L-tartrate and itaconate...179	
6.3.9. Mercaptosuccinic acid mediated inhibition.....	181
6.3.10. Mercaptosuccinic acid mediated inhibition of <i>P. falciparum</i> <i>in vitro</i> cultures	183
6.4. Summary and future perspectives.....	183

Chapter 7. Biochemical and structural characterization of two subunit class I fumarate hydratase from thermophilic archaeon, *Methanocaldococcus jannaschii*.

7.1. Introduction.....	185
7.2. Materials and methods.....	187
7.2.1. Cloning, expression and purification of MjFH.....	187
7.2.2. Mass spectrometry	188
7.2.3. Interaction of MjFH α and MjFH β	188
7.2.3.1. Pull-down.....	188
7.2.3.2. Analytical gel filtration.....	189
7.2.3.3. Isothermal calorimetry.....	189
7.2.4. Characterization of iron-sulfur cluster.....	190
7.2.4.1. Reconstitution of the cluster	190
7.2.4.2. Spectroscopic methods.....	190

7.2.4.3. Colorimetric estimation of iron and acid-labile sulfide in the protein.....	190
7.2.4.4. Native mass spectrometry.....	191
7.2.4.5. Electron paramagnetic resonance.....	191
7.2.5. Thermostability of the individual subunits and the complex.....	192
7.2.6. Activity.....	192
7.2.6.1. Spectrophotometric assay.....	192
7.2.6.2. Complementation assay.....	192
7.2.7. Structure solution of MjFH beta subunit using X-ray crystallography.....	192
7.3. Results and discussion.....	193
7.3.1. Taxonomic distribution and phylogenetic analysis.....	193
7.3.2. Cloning, expression and purification.....	198
7.3.3. Oligomeric state and subunit interaction.....	201
7.3.4. Biophysical characterization and thermostability.....	204
7.3.5. Mass spectrometry of MjFH subunits.....	206
7.3.6. Type of the cluster and stoichiometry.....	208
7.3.6.1. Spectroscopic characterisation.....	208
7.3.6.2. Electron paramagnetic resonance (EPR).....	210
7.3.6.3. Stoichiometry of iron and sulfur.....	211
7.3.7. Functional complementation in <i>E. coli</i>	214
7.3.8. Activity.....	215
7.3.9. Structure of MjFH β subunit.....	216
7.3.9.1. Crystallisation, data collection and structure solution.....	216
7.3.9.2. Structural features of MjFH β	219
7.3.9.3. Comparison of MjFH β structure with other available class I FH structures	221
7.3.9.4. Malate binding sites in MjFH β subunit.....	224
7.4. Summary and future directions.....	225
Chapter 8. Conclusions and future directions	
8.1. Metabolic significance of fumarate generated from purine salvage pathway in <i>P.falciparum</i>	227
8.2. NMR-based strategy to study the cellular fate of ammonia.....	229
8.3. Biochemical and structural characterisation of class I fumarate hydratase.....	230
8.4. Taxonomic distribution of two classes of fumarate hydratase.....	231

Appendix I	235
Appendix II	249
References	257

Chapter 1

*An introduction to the crosstalk
between purine and energy
metabolism in the malaria parasite
Plasmodium falciparum*

Chapter 1

An introduction to the crosstalk between purine and energy metabolism in the malaria parasite *Plasmodium falciparum*

ABSTRACT

The two major objective of the thesis are to 1) investigate the metabolic significance of fumarate generated as a by-product of AMP generation in Plasmodium falciparum, and to 2) biochemically and structurally characterize iron-sulfur cluster containing class I fumarate hydratases from P. falciparum and Methanocaldococcus jannaschii. An introduction to both the objectives, experiments performed and the results are presented as two broad sections in the thesis. This chapter provides a general introduction and a summary of literature survey relevant to the topics discussed in section-I. A general introduction to parasitism and a description of the apicomplexan lineage is provided that includes the taxonomic positioning and the lifestyle of the organism of interest, P. falciparum. This is followed by a brief description of the various life-cycle stages of the parasite both in human and mosquito host. A brief introduction to energy metabolism is provided with a special focus on glycolysis, TCA cycle and electron transport chain of the parasite. Purine metabolism in the parasite is discussed with a special focus on purine salvage pathway, the enzymes and transporters involved. Finally, the objectives that were formulated, that formed the basis of the work in this section are presented.

1.1. General features of parasitism and apicomplexan lineage

Parasitism refers to an ecological relationship between heterologous organisms (either a prokaryote or a eukaryote), wherein the parasite survives and grows at the expense of the host. Parasitism can either cause morbidity, a diseased state, mortality i.e. death or even a behavioural change that lead to the above-mentioned states (Esch and Fernandez, 1993; Poulin and Morand, 2000). In cases where a parasite has many hosts, it may not share a parasitic relationship with all of them. Therefore, an organism can have a parasitic relationship with one host and a commensalistic/mutualistic relationship with another host. A parasite may need multiple hosts to complete its lifecycle; with sexual reproduction in the definitive host and asexual reproduction in the intermediate host. Around 40% of known species are parasitic in nature (Dobson et al., 2008). Adopting a parasitic lifestyle is known to be the major form of 'strategy' shifts that has occurred multiple times across many taxa. **Figure 1.1** schematically represents the relative abundance of the parasitic organisms in different taxa. As is evident from the figure some

taxa have organisms that are completely parasitic, others completely free living and few with an intermediate number of parasitic organisms (Rohde, 1993).

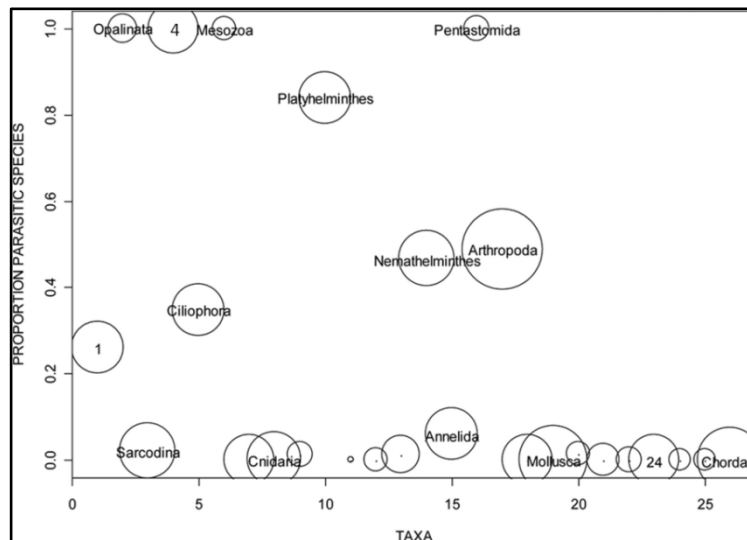


Figure 1.1. Relative abundance of different taxa, and the proportion of parasitic species in those taxa (figure reproduced from Rohde, 1982).

Taxa are numbered along the x axis as follows: 1, Mastigophora; 2, Opalinata; 3, Sarcodina; **4, Apicomplexa /Microspora**; 5, Ciliophora; 6, Mesozoa; 7, Porifera; 8, Cnidaria; 9, Ctenophora; 10, Platyhelminthes; 11, Priapulida; 12, Entoprocta; 13, Nemertina; 14, Nematelminthes; 15, Annelida; 16, Pentastomida; 17, Arthropoda; 18, Tentaculata; 19, Mollusca; 20, Echiurida; 21, Sipunculida; 22, Hemichordata; 23, Echinodermata; 24, Pogonophora; 25, Chaetognatha; 26, Chordata. The area of a circle corresponds to the natural log of the total number of species in a taxon, and the centre of the circle corresponds to the proportion of parasitic species in that taxon.

All apicomplexan organisms are eukaryotic, single-celled, obligate parasites that have evolved from a free-living flagellar photosynthetic ancestor (Arisue and Hashimoto, 2015). They are parasitic for a wide range of vertebrate and invertebrate organisms. Along with dinoflagellates and ciliates, the whole group is classified under the superphylum, alveolata. There are more than 300 genera in the apicomplexan phylum under which approximately 6000 species have been named. This accounts for only 0.1% of the estimated total number of organisms ($1.2-10 \times 10^6$) in this phylum (Morrison, 2009). The name apicomplexan is derived from the apical complex that these organisms possess, which is used for interaction with and invasion of the host cell surface. The apical complex consists of rhoptries and micronemes which are secretory organelles that contain the proteins necessary for motility and invasion processes. In apicomplexans, such as gregarines and coccidians, the apical complex additionally consists of a conical structure, the conoid which has unique protofilaments that help in mechanical aspects of

invasion into the host cell. Many apicomplexan organisms have been studied extensively from the perspective of biomedical and veterinary interests.

In all apicomplexan organisms, asexual cell division happens through closed mitosis (Francia and Striepen, 2014). The closed-type of mitosis can be divided into four representative types as exemplified by the kind of mitotic division seen in four major genera in the phyla; endodyogeny in *Toxoplasma* spp., schizogony in *Plasmodium* spp., host cell transformation in *Theileria* sp. and finally endopolygeny in *Sarcocystis* species. In schizogony, the nucleus divides multiple times in an asynchronous manner resulting in non-geometric expansion of daughter nuclei that assembles to form a structure called syncytium in the cytoplasm. The daughter cells are subsequently released by the rupture of the host cell. The complete cycle takes 48 h in *P. falciparum* but is different for different species of *Plasmodium*. A single apicomplexan species can use more than one mitotic strategy depending on the niche and the host cell type (Francia et al., 2012; Francia and Striepen, 2014). Features of sexual differentiation and meiosis in this phyla are reviewed in Smith et al. 2002. Metabolism is tightly interlinked with cell division (Lee and Finkel, 2013; Slavov et al., 2014). The metabolic features that support such complex cell division processes in apicomplexan parasites are still a fertile area of research.

1.2. Plasmodium: hosts and life cycle

Plasmodium, a genus under apicomplexa, consists of more than 200 diverse species that can cause infection in a wide range of vertebrate hosts (Yotoko and Elisei, 2006). Around 51 species are known to infect mammalian host, 89 species infect reptiles and 32 species infect avians. More species are being added to this genera with time. Except for the lizard malaria-causing parasite, *P. mexicanum* which uses sand flies as a definitive host, all other species use mosquito as their definitive host (Yotoko and Elisei, 2006). Another distinguishing feature that is shared by *Plasmodium* species infecting mammals is their habitation in anucleated erythrocyte, while in other species that parasitize lizard and birds, nucleated erythrocytes are infected. A major shift in the apicomplexan phylogeny is the event when *Plasmodium* evolved to use the mosquito as host. This adaptation to live in the insect enabled the parasite to explore a diverse vertebrates as hosts (Portman and Slapeta, 2014; Wellemis et al., 2009). Moreover, the severity of infection as seen in humans is not seen in other vertebrate hosts of the parasite. All the species are reported to have 14 chromosomes, a single mitochondrion in close association with a non-photosynthetic plastid-like organelle, the apicoplast, and the defining feature of apicomplexa, the apical body. *P. falciparum* is the deadliest of all human malaria parasites and is responsible for most of the mortality associated with the disease. Multiple drug resistant strains have

evolved in recent past and are a major concern in the endemic areas. *Plasmodium* species have 4 major stages in their life cycle shown schematically in **Figure 1.2**.

- a) Infective stage, when the parasite (sporozoites) enters through a mosquito bite into their vertebrate host
- b) Exoerythrocytic stage, when the sporozoites multiply through an asexual division called schizogony in the liver and get released into the blood as merozoites;
- c) Erythrocytic stage, when the released merozoites go through multiple rounds of schizogony in the erythrocytes of the host;
- d) Reproductive stage, in the mosquito where the parasite attains sexual maturity and multiplies through sexual reproduction.

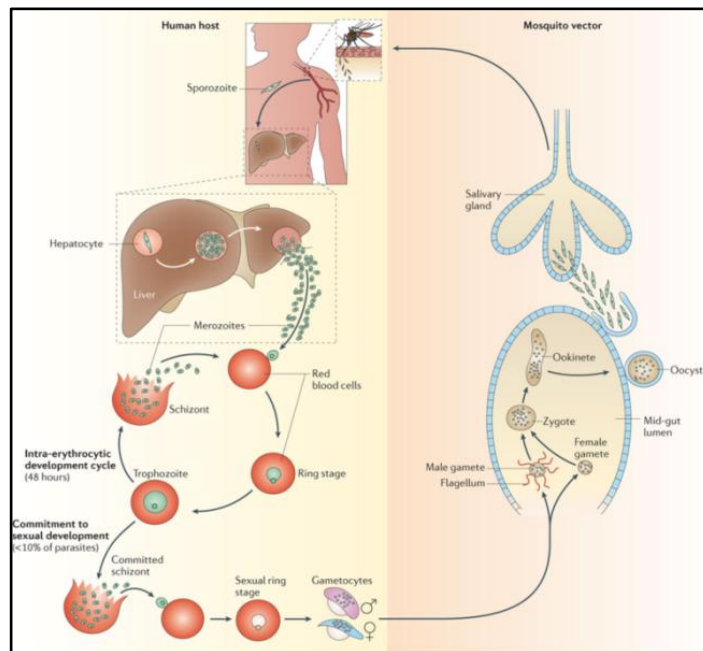


Figure 1.2. Complete life cycle of human malaria parasite *P. falciparum*

Sporozoites are transmitted to the human host via the bite of an infected *Anopheles* spp. mosquito and then travel to the liver. Following development in the liver, tens of thousands of merozoites are released into the blood and invade red blood cells. The parasites then undergo repeated rounds of asexual multiplication (the intra-erythrocytic developmental cycle), progressing through ring, trophozoite and schizont stages. In each cycle, a small proportion (<10%) of parasites begin to develop into the sexual form of the parasite, which is known as a gametocyte. This form is required for productive transmission to the mosquito host. Commitment to sexual development is thought to occur in schizont stage. After 10–12 days of development, mature male and female gametocytes are ready to undergo the sexual phase of the life cycle in the mosquito. Gametocytes differentiate into gametes and, after fertilization, the resulting zygote (which develops into a motile form known as the ookinete) develops into an oocyst. When the oocyst ruptures, haploid sporozoites are released, migrate to the salivary glands and can then be transmitted to humans. Figure reproduced from Ménard, 2005.

1.2.1. Asexual and sexual stage development

After the mosquito bite, the plasmodium sporozoites can either stay at the site of bite for a long time (Gueirard et al., 2010) or can invade through intracellular gaps and find their way to the liver. Once in the liver, the parasites under a process of merogony which is very similar to schizogony except for the fact that the daughter cells, though assembled, are not released from the cell immediately. The division continues until thousands of merozoites form and assemble in the mother cell. This marks the end of the exoerythrocytic stage (Arnot and Gull, 1998; Huff, 1947). The merozoites once released into the blood stream invade erythrocytes through their apical membrane complex and initiate the asexual intra-erythrocytic division (schizogony) which causes most of the symptoms associated with malaria. The intra-erythrocytic cycle of plasmodium species varies from 24 hours as in *Plasmodium knowlesi* to 72 hours as reported for *Plasmodium malariae*.

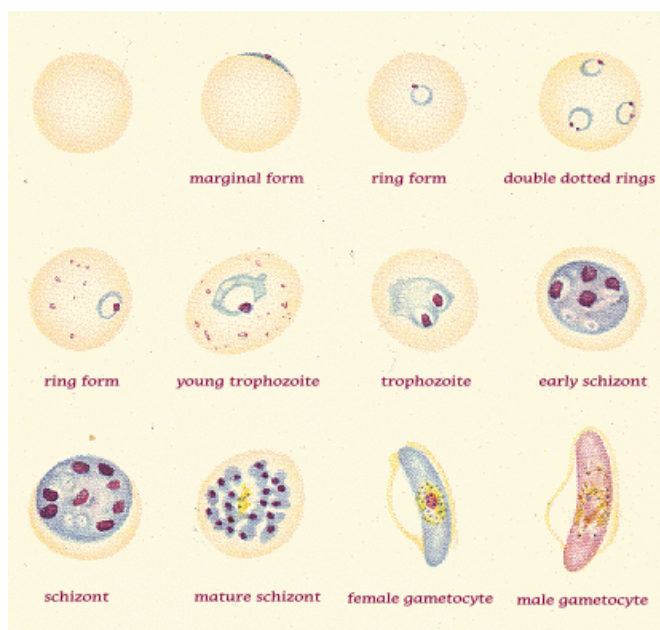


Figure 1.3. Life cycle stages of *P. falciparum*

An illustration showing different life cycle stages of *P. falciparum*. The morphology shown here closely resembles the one seen under the light microscope (100 X magnification) after staining the culture with Giemsa staining solution.

Various stages involved in schizogony are explained based on both the morphology of the parasite as it appears in the Giemsa-stained smear (**Figure 1.3**) of the infected blood as well as various molecular processes that happen within the cell (Hanssen et al., 2010; Bannister et al., 2000). Peculiar features associated with each of these stages are described below.

- a) Ring:** The name is derived from the fact that a merozoite after invasion into the erythrocyte assumes a ring-like structure. As the parasite invades, it surrounds itself with the erythrocyte membrane that subsequently buds off from the surface. The membrane remains around the parasite throughout schizogony and is called the parasitophorous vacuolar membrane (PVM). The mitochondrion stays in close association with the apicoplast and the association continues for the rest of the intraerythrocytic stages. Parasites have a sluggish metabolism in this stage and hence this form of the parasite is resistant to many drugs that target metabolic activity of the parasites. The stage typically lasts for 24 hours for *P. falciparum* and varies for different species of *Plasmodium*.
- b) Trophozoite:** The most metabolically active of all the erythrocytic stages where the raw materials needed for cell division is synthesized. Protein synthesis increases manifold as evident from an increase in the number of the free ribosomes and enlargement of the endoplasmic reticulum (ER). Mitochondria, apicoplast, and Golgi complex also increase in their sizes. Some of the striking morphological features that are apparent on imaging are the presence of membranous structure called Maurer's cleft extending from the parasite plasma membrane all the way up to the erythrocyte membrane and the brown coloured digestive vacuole. The role of Maurer's cleft is still not clear though there are speculations that it may be involved in the transport of molecules from the parasite to the erythrocytic surface. The brown colour of the digestive vacuole arises from the detoxified polymer of heme, hemozoin.
- c) Schizont:** The defining feature of the stage is the division of nucleus and assembly of the daughter cells. There is no tight control on the nuclear division process and a number of daughter cells ranging anywhere between 15-20. Protein synthesis and trafficking to the host cell surface continues during the stage. Mitochondria and apicoplast divide and enter into each merozoite which subsequently gets covered with a membrane through an unknown process. This leaves behind only the digestive vacuole in the cytosol of the schizont. At the end of schizogony, the merozoites rupture the host cell membrane and are released into the circulating blood ready for another round of erythrocyte lytic cycle. Unlike other Haemosporidia, plasmodium does not have a fixed number of lytic cycles before which sexual differentiation begins (Schuster, 2002). This forms the basis of the *in vitro* culture of the intraerythrocytic forms of the parasite which will proceed indefinitely provided suitable conditions are maintained.

Sexually dimorphic male and female gametocytes develop from merozoites of the asexual stages. The process is still intraerythrocytic and gametocytes in circulating

peripheral blood can be taken in by the mosquito where they undergo sexual reproduction. Therefore, gametocytes are called transmission stages. The process of gametocytogenesis takes around 8 days for *P. falciparum* and has five distinct stages. The commitment to gametocytogenesis takes place at the level of merozoites which can emerge directly from the liver stages or from one of the intraerythrocytic lytic stages. The committed merozoite differentiates and goes on to become either a male or a female gametocyte. Thus, malaria parasites are basically hermaphrodites (Talman et al., 2004).

Along with the bloodmeal, the male gametocyte, and the female gametocyte enter into the posterior midgut lumen of the mosquito. Here, the gametocytes differentiate and become increasingly dimorphic. The sequence of the events starting from the haploid gametocytes to haploid sporozoites that are ready to infect vertebrate tissue are described in Smith et al. 2002 and Talman et al. 2004, and will not be discussed as it is not relevant to this study.

1.3. Energy metabolism

All organisms need to spend energy to survive and propagate. Energy is generated and stored in the form of potential energy of a chemical bond in organic molecules. The enthalpy/energy needed to maintain this highly ordered state comes in two forms of disequilibria; the ATP/ADP chemical disequilibrium and the electrochemical disequilibrium between strong reductants in a cell (eg. NAD(P)H) and the usually more oxidizing environment (Schoepp-Cothenet et al., 2013). The ATP/ADP disequilibrium is a phenomenon in which, a cell maintains ATP, 5-10 times higher than the ADP concentration. There are only two ways in which ATP can be made in the cell from ADP; from substrate level phosphorylation and chemiosmotic coupling. Both these processes, though have different efficiency of ATP generation, rely on a common concept of harvesting energy from carbon-rich organic molecules, known as redox disproportionation (Weber, 1997). In substrate level phosphorylation, as it happens in glycolysis, there is a direct coupling of the energy derived, to synthesize ATP. Whereas, in chemiosmotic coupling, the ATP is made indirectly. In this process, the energy derived from redox disproportionation reactions (mainly reaction of the citric acid cycle) is stored as reducing equivalents, NADH, and FADH. Through a series of reactions constituting the electron transport chain the flow of electrons, facilitated by various electron carriers, is used to generate a proton gradient across a membrane (mitochondrial membrane/ plasma membrane). Finally, the energy is harvested in the form of ATP by coupling this proton gradient to the phosphorylation of ADP, in the enzyme complex called ATP synthase. The electrons are accepted by different terminal electron acceptors; oxygen

being the major electron acceptor in aerobic organisms. There are enormous variations seen in organisms, with respect to the enzymes, substrates, electron carriers, and terminal electron acceptors used to achieve the common goal of ATP synthesis (Voet and Voet, 2011). In the following section, the energy metabolism of *P. falciparum* is discussed with special emphasis on glycolysis, TCA cycle and electron transport chain.

1.3.1. Glycolysis in *P. falciparum*

Glycolysis comprises a set of biochemical reactions that converts carbohydrates (6 carbon) to pyruvate/lactate (3 carbons). The pathway constitutes the first component in the complete oxidation of carbohydrate to carbon dioxide and water, the other components being TCA cycle and electron transport chain. It was observed that *P. falciparum*-infected erythrocytes take up 100 times more glucose than the uninfected erythrocytes (Roth et al., 1988). Glucose once taken into the erythrocyte cytosol would be immediately converted to glucose 6-phosphate (G6-P) by the action of human hexokinase (HK). The subsequent action of a non-specific phosphatase on G6-P ensures that glucose is available to the parasite compartment. The increased consumption of glucose by the infected erythrocytes is attributed to both the transporters and the enzymes of the parasite compartment. The glucose uptake is through a high-affinity facilitative hexose transporter (PfHT) located in the parasite plasma membrane (Slavic et al., 2010; Woodrow et al., 2000). The transporter is expressed throughout the life cycle of the parasite and through the use of inhibitors, it has been shown to be essential for the intraerythrocytic parasite development. A thorough investigation into the mechanism of enhanced glycolytic flux is still missing, though we know a few contributing features of *Plasmodium* glycolysis.

- 1) Unlike the human glucose transporter, *glut1*, which is highly specific for glucose, PfHT can take in fructose as well. This differential substrate specificity has enabled the design of drugs which specifically target the parasite transporter (van Schalkwyk et al., 2008).
- 2) The key regulatory enzymes of glycolysis, hexokinase, and phosphofructokinase are reported to have low K_m values for their substrate (Mony et al., 2009; Chan and Sim, 2005; Kumar and Banyal, 1997). *P. falciparum* phosphofructokinase (PfPFK) has a higher specific activity compared to the mammalian enzyme. Additionally, allosteric regulation usually seen in PFK, mediated by fructose 2,6 biphosphate, phosphoenolpyruvate and citrate, are completely absent in the parasite enzyme (Mony et al., 2009).

- 3) The higher specific activity of pyruvate kinase and lack of inhibition by fructose 1,6 biphosphate (F1,6-BP) (Chan and Sim, 2005).
- 4) Unlike lactate dehydrogenase (LDH) from other organisms, the plasmodial enzyme is not inhibited by high concentrations of pyruvate, an adaptation reflective of the microaerophilic nature of the organism (Shoemark et al., 2007; Vander Jagt et al., 1981). The enzyme lactate dehydrogenase is essential for the parasite and is highly expressed (Vivas et al., 2005). The crystal structure of this enzyme is different from that of its host suggesting functional differences (Brown et al., 2004; Chaikuad et al., 2005).

For continuous operation of the conventional glycolytic pathway ATP, NAD⁺ and inorganic phosphate are needed. As ATP is available in excess in the cell, other factors would be key determinants in deciding the glycolytic flux. Metabolic labelling studies show that bulk of the glucose is metabolized to lactate ((Jensen et al., 1983)). The NAD⁺ generated by LDH reaction can fuel glycolysis. This would set in a self-sustaining glycolytic reaction without the need to rely on any mitochondrial reactions for NADH. Studies on intracellular inorganic phosphate levels are not performed in the parasite and hence it playing a regulatory role could not be commented upon. Interestingly, glycerol was found to be one of the metabolites formed from glucose in the intraerythrocytic parasite (Lian et al., 2009). This implies the possible presence of a functional glycerol-3-phosphate shuttle in *P. falciparum* and that the parasite has alternate mechanisms to reoxidise cytosolic NADH. However, the enzymes involved in the formation of glycerol are not known. Lian *et al.* have suggested the role of glycerol 3-phosphatase (unannotated) or glycerol kinase, operating in the reverse direction (thermodynamically unfavourable) as in trypanosomes, as probable enzymes involved in the formation of glycerol. Knockout of glycerol kinase in *P. falciparum* resulted in sub-optimal growth during asexual stages suggesting that it could have a significant role in the metabolism of the parasite (Naidoo and Coetzer, 2013). An alternative explanation suggests that a non-specific acid phosphatase can act upon glycerol 3-phosphate and form glycerol (Olszewski and Llinás, 2011). Further experiments would probably highlight the metabolic significance of glycerol production in the parasite. The high flux of glycolysis seen in *P. falciparum* is also seen in pathological states as in cancer (Roth et al., 1988). The cancer cells largely rely on aerobic glycolysis to meet their ATP and anabolic requirements (Warburg 1956).

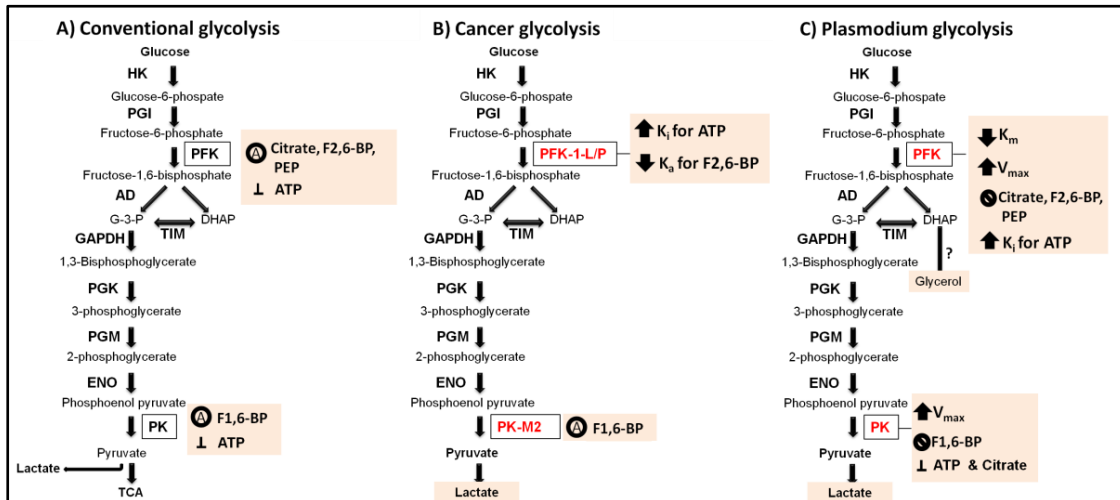


Figure 1.4. Unique features of glycolysis in cancer cells and in *Plasmodium*.

Panel A, B and C shows reactions of glycolysis. Key regulatory enzymes PFK and PK are enclosed in boxes. Shaded boxes in the inset show the regulatory properties of the enzymes. A black circle enclosing the alphabet A represents allosteric regulation by the metabolites that follow. An inverted T represents inhibitory potential by the metabolite that follows. An upward arrow indicates an increase in the value of the kinetic parameter that follows and the reverse holds true for the downward arrow. A circle with a cross indicates a lack of allosteric regulation by the metabolites that follow.

To achieve a higher flux of glycolysis most cancer cells express isoforms of key regulatory enzymes, PFK, and PK that have a lesser degree of allosteric regulation by the intermediates of the pathway (Schulze and Harris, 2012). In dysregulated glycolysis, the only limiting factor is the availability of substrates and co-factors, as many of the allosteric regulation of the enzyme is either lost or minimal as seen in cancer cells and *Plasmodium* parasites. Apart from glucose, another substrate that could decide the flux would be NAD^+ , inorganic phosphate, ADP, and ATP. The intracellular concentrations of these metabolites would place the upper limit on the flux of a dysregulated glycolysis. Rate-limiting enzymes/metabolites of plasmodium glycolysis are still not known. **Figure 1.4** shows unique features of *Plasmodium* glycolysis when compared to conventional glycolysis and to the one seen in cancer cells.

1.3.1.1. Variations and significance of glycolysis in apicomplexans

All the enzymes of the glycolytic machinery are present in apicomplexans and all organisms heavily depend on glycolysis for their ATP requirement. The excessive reliance on glycolysis in spite of retaining the entire Krebs's cycle machinery is thought to be an adaptation to avoid reactive oxygen species, though the exact reason is still not clear. A notable feature of the apicomplexan glycolysis is the presence of pyrophosphate-dependent PFK in *Eimeria*, *Cryptosporidium*, and *Toxoplasma* (Mony et al., 2009; Boitz et

al., 2013; Denton et al., 1994). Unlike the ATP-dependant PFK, the pyrophosphate-dependent PFK reaction is reversible under physiological conditions and hence, can be used for both glycolysis and gluconeogenesis (Mertens, 1991; Huang et al., 2008). The enzyme contributes to the energy economy of the cell by using the energy derived from pyrophosphate which otherwise would usually be hydrolyzed to inorganic pyrophosphate. The enzyme is thought to be evolved from ATP-dependent PFK and is seen in many anaerobic organisms. Moreover, the gluconeogenic enzyme fructose 1, 6 bisphosphatase is absent in *Cryptosporidium*, *Eimeria*, and *Plasmodia*. Further, gluconeogenic enzymes are reported to be essential for toxoplasma virulence and infectivity (Blume et al., 2015) especially owing to differential nutrient availability in the host system. Apart from their conventional role in glycolysis, certain glycolytic enzymes like enolase and pyruvate kinase are also known to be involved in cellular invasion machinery of the parasites (Pomel et al., 2008). In theileria and to a lesser extent in *Eimeria* and *Toxoplasma* infections, there is a parasite-induced increase in HIF-1 alpha levels that results in an increase of glycolytic flux in the host cell (Metheni et al., 2015; Menendez et al., 2015; Spear et al., 2006).

1.3.2. Pyruvate dehydrogenase (PDH) complex

Under aerobic circumstances, the pyruvate formed from glycolysis is converted to acetyl-coA by a multienzyme complex, pyruvate dehydrogenase. The enzyme PDH is closely related to alpha-keto glutarate dehydrogenase and is hypothesized to have evolved from a common ancestor, a branched chain keto acid dehydrogenase (Schreiner et al., 2005; Schnarrenberger and Martin, 2002) . The constituent parts of the complex perform the following function: E1 decarboxylates pyruvate and generates a covalent intermediate of thiamine pyrophosphate and the acetyl group of pyruvate; E2 transfers the acetyl group from thiamine pyrophosphate to lipoamide and subsequently on to a coenzyme A molecule covalently attached to one of its lysine; E3 is involved in the regeneration of lipoamide needed for E2 (Voet and Voet, 2011).

In all apicomplexans reported, pyruvate dehydrogenase (PDH) enzyme is either absent or is localized to the apicoplast of the organism, implying the uncoupling of glycolysis generated pyruvate and the OXPHOS pathway(van Dooren et al., 2006). However, the recent reports suggest that an alternative enzyme BCKDH, might take over the function of PDH and convert pyruvate to acetyl-CoA for use in TCA cycle (Oppenheim et al., 2014). The BCKDH gene is well conserved in apicomplexans and is localized to mitochondria in most of the apicomplexans studied. The enzyme is required for full virulence in both *Toxoplasma gondii* and *P. berghei* (Oppenheim et al., 2014). Glycolysis

seems to be a potential source of ATP, however, pyruvate derived acetyl-coA seems to be essential for these parasites.

1.3.3. Tricarboxylic acid cycle

Complete oxidation of any carbohydrate should result in the formation of carbon-di-oxide, equivalent to the number of carbon atom in the starting sugar. Glycolysis partially oxidizes glucose to pyruvate in which there are still reduced carbons available. PDH complex completes the oxidation of one carbon and couples it to the reduction of one NAD⁺ molecule. The process is put to completion by another set of enzymes that constitute the tricarboxylic acid cycle (TCA). The cyclical nature of the pathway was put forth by the classical paper of Hans Krebs (Krebs et al., 1938; Krebs, 1937) earning the cycle the name, Krebs cycle. The pathway results in the complete oxidation of all the carbons in acetyl-CoA. The net reaction of the cycle is the conversion of one molecule of acetyl-CoA to 2 molecules of CO₂. The process results in the formation of 3 molecules of NADH, one molecule of FADH and one molecule of GTP/ATP. A large number of moonlighting functions have been assigned to many enzymes of the pathway (Huberts and van der Klei, 2010)

Apart from the oxidative role of the cycle, the intermediates of the cycle are involved in many anabolic reactions and are siphoned off from the pathway, necessitating reactions that can replenish the intermediates that in turn can keep the primary function of the cycle, oxidation of carbons, still operative. Such reactions are called anaplerotic reactions (Gibala et al., 2000; Owen et al., 2002). The term anaplerosis was first used by Kornberg (Kornberg, 1966) to imply this phenomenon of C₄ and C₅ molecules feeding into the pathway. A fine balance of anaplerotic and cataplerotic reactions (lipogenesis and gluconeogenesis) is exploited by many human tissues to deal with varied metabolic challenges posed to them like; starvation, fasting, and exercise. The major anaplerotic enzyme in the eukaryotic system is pyruvate carboxylase that converts pyruvate to oxaloacetate. This happens when intermediates of TCA cycle leading to oxaloacetate formation are depleted or removed from the cycle for other functions. Other anaplerotic reactions of TCA cycle include, formation of α -ketoglutarate from deamination/deamidation of amino acids, the formation of oxaloacetate from phosphoenolpyruvate through the action of phosphoenolpyruvate carboxylase and generation of fumarate from purine nucleotide cycle that operates especially during exercise in skeletal muscles.

1.3.3.1. Plasmodium TCA cycle

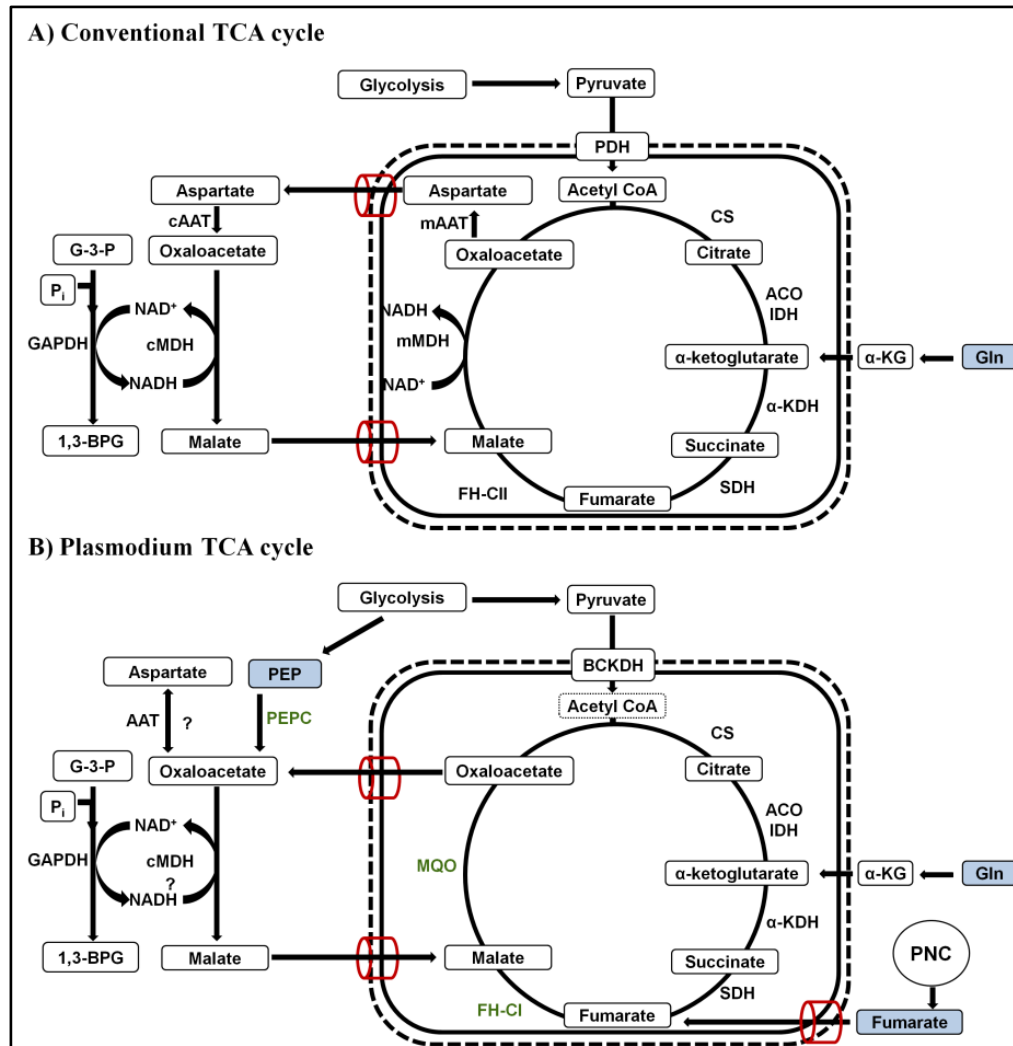


Figure 1.5. Unique features of Plasmodium TCA cycle.

The boxes with dashed and solid black line represent the outer and inner membrane of the mitochondrion. Red barrels represent transporters. Panel A shows typical citric acid cycle and its associated malate-aspartate shuttle (MAS). Oxidized NAD^+ that is generated in the cytosol as a result of MAS fuels the glyceraldehydes 3-phosphate dehydrogenase (GAPDH) reaction which could be rate limiting (see text). B) Plasmodium citric acid cycle driven mainly by anaplerosis from glutamine-derived α -ketoglutarate, PNC derived fumarate and glycolysis-derived PEP. The flux of glucose-derived pyruvate feeding the TCA cycle (through the reaction of BCKDH as acetyl-CoA) is minimal and is shown by a dashed box around acetyl-coA. Other notable differences are the exclusive cytosolic localization of aspartate aminotransferase (AAT), the type of fumarate hydratase enzyme used, and the fact that malate to oxaloacetate reaction is catalyzed by two different enzymes in cytosol (malate dehydrogenase) and mitochondria (malate-quinone oxidoreductase).

All the genes coding for a complete set of TCA cycle enzymes are present in the genome of *Plasmodium falciparum*. **Figure 1.5** compares and contrasts the features of *Plasmodium* TCA cycle with that of the conventional one. As discussed in section 1.2.1.3 most of the

ATP requirements of the asexual stages of the apicomplexan parasites are almost completely met by glycolysis in spite of retaining a complete set of genes for TCA cycle enzymes in the genome. The only exception to the above-mentioned metabolic feature is in cryptosporidium, where there is a complete absence of TCA cycle components. Unique features of apicomplexan TCA cycle are the presence of malate quinone oxidoreductase (MQO), an NADP⁺-dependent isocitrate dehydrogenase (IDH), and class-I iron-sulfur cluster dependent fumarate hydratase (FH). These genes are present in dinoflagellates, the free-living ancestor of apicomplexans and hence, these are not associated with parasitism (Jacot et al., 2016). A schematic representation of the gain and loss of certain metabolic pathway genes of mitochondria during apicomplexan evolution is given in **Figure 1.6**.

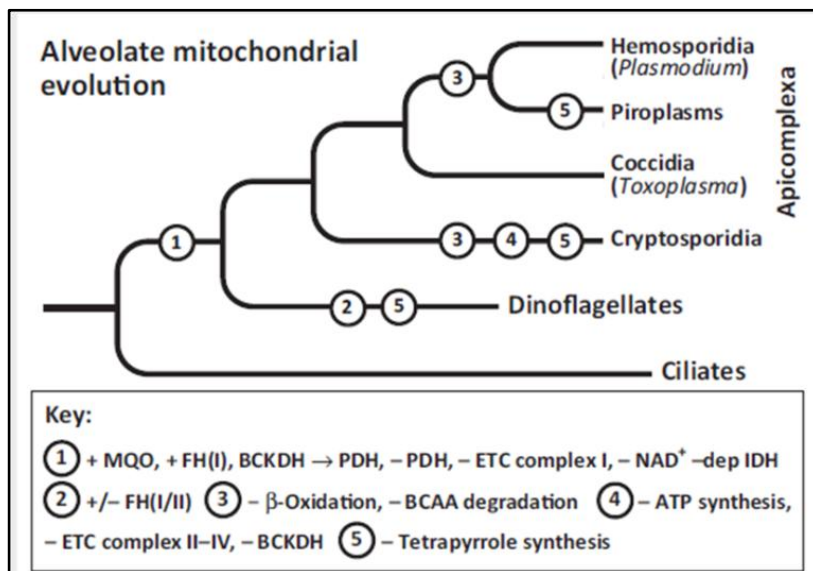


Figure 1.6. Gain and losses of genes in apicomplexan energy metabolism

Schematic representation of gains and losses of genes involved in mitochondrial metabolism of alveolates. Malate-quinone oxidoreductase (MQO), fumarate hydratase (FH), branched chain keto acid dehydrogenase (BCKDH), pyruvate dehydrogenase (PDH), electron transport chain (ETC) complex I, class I and class II fumarate hydratase (FH (I/II)), branched-chain amino acid degradation (BCAA), NAD⁺- dependent isocitrate dehydrogenase (IDH). The figure is reproduced from Jacot et al., 2016.

Various metabolic labelling experiments suggested that during intra-erythrocytic (IE) stages, the glucose derived acetyl-CoA formed by the action of BCKDH is insufficient to sustain the complete flux of TCA cycle but operates in a stage-independent manner. The anaplerotic flux through phosphoenolpyruvate carboxylase (PEPC) either through oxaloacetate or malate seems to be significant and operates in a stage-dependent manner, with peak contribution in the ring stages and then dropping off in trophozoites and

schizonts (Cobbold et al., 2013). Glutamine mediated anaplerosis is suggested to be the major flux driving the TCA cycle during the mature stages and minimal in the early stages. The contribution of fumarate anaplerosis and stage dependence is not yet characterized in the parasite asexual stages.

A study involving genetic knockout of each of the genes of the TCA cycle in *P. falciparum* revealed that except for two enzymes, FH and MQO, all other genes were amenable to genetic ablation in the intraerythrocytic stages of the parasite life cycle (Ke et al., 2015) and hence not essential. However, these parasites were not successful in establishing infection in mosquito implicating the essentiality of TCA cycle in sexual stages of the parasite. The role of FH and MQO in the parasite asexual stage growth is still not clear. The authors suggest the involvement of FH in aspartate generation and MQO in mitochondrial biogenesis. Conditional knockdown studies could throw light on the importance of these genes.

1.3.3.2. Source of acetyl-CoA

Feeble incorporation of label from glucose into TCA cycle intermediates implies that glycolysis is largely disconnected from the TCA cycle in the parasite. This is further supported by the finding that the pyruvate dehydrogenase (PDH) complex in *P. falciparum* localizes to the apicoplast and not to the mitochondrion. A study by Pei *et al.* showed that deletion of E1 α or E3 subunit genes of PDH complex in the rodent malaria parasite, *P. yoelli* caused no defect in blood, mosquito or early liver stage development. However, the knockout parasites could not initiate the blood stage infection as they were unable to develop into exoerythrocytic merozoites. This phenotype is similar to that observed for deletions of genes (e.g. FabI) involved in Type II fatty acid synthesis (FAS II) (Pei et al., 2010). Thus, these results indicate that the sole role of PDH is probably to provide acetyl-CoA for FAS II rather than the TCA cycle. A similar study conducted in *P. falciparum* indicated a dispensable role for the gene in the asexual stages of the parasite (Cobbold et al., 2013). The same study reported two independent sources of acetyl-CoA that is operating in these stages; 1) glucose-mediated acetyl-CoA production through an oxythiamine sensitive pathway, which the authors speculate to be BCKDH and 2) an acetate fixation pathway, wherein through the use of the enzyme acetyl-CoA synthetase (either AMP-forming/ ADP-forming) the parasite is able to convert exogenously supplied acetate to acetyl-CoA. They additionally also reported that percentage of label incorporation from glucose to acetate pool is less and hence alternate sources of acetate does exist in the parasite that accounts for the majority of acetyl-CoA pool of the parasite. Annotation for carnitine acetyltransferase is missing, however, carnitine has been shown

to provide growth support for erythrocyte free parasites in culture (Williams et al., 1998). Molecular mechanism behind the growth advantage is still not clear.

1.3.3.3. Anaplerosis in *Plasmodium* TCA cycle

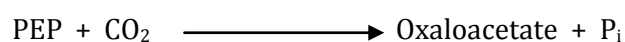
As evident from labeling studies on the *in vitro* culture of *P. falciparum*, TCA cycle is largely anaplerotic in nature. A summary of literature available on three major anaplerotic routes is presented here.

Glutamine mediated anaplerosis

¹³C-labeled glutamine incorporation into saponin released parasites, followed by mass spectrometry of metabolites extracted from the parasite suggested the operation of a complete oxidative TCA cycle (MacRae et al., 2013). The added glutamine must be converted to α -ketoglutarate through glutamate for being incorporated into the TCA cycle. The conversion of glutamine to glutamate can be brought about by various amidotransferases (eg. carbamoyl phosphate synthetase, GMP synthetase, glutamine:oxoglutarate aminotransferase etc.) that are present and expressed during the IE stages of the parasite. Glutamate dehydrogenase or aminotransferases were speculated to facilitate the subsequent conversion of glutamate to α -ketoglutarate. However, in a recent report by Storm *et al.*, using *GDHa* knockout strain of *P. berghei*, the non-involvement of this gene in the generation of α -ketoglutarate was shown (Storm et al., 2011). Also, through the use of the inhibitor L-cycloserine, it was shown that alanine and aspartate aminotransferases are also not involved in facilitating this conversion. In this context, an investigation into the role of GDHb and GDHc in generating α -ketoglutarate is warranted. The fact that none of these enzymes are mitochondrially localized raises serious doubts about the role of any GDH or aspartate aminotransferase in contributing to TCA cycle reactions. The transport of cytoplasmic pool of alpha-ketoglutarate generated by GDH (a/b/c) or by AAT, to the mitochondria still needs to be tested. The transporters that can facilitate the process could be either malate oxoglutarate transporter or the dicarboxylate-tricarboxylate transporter.

Phosphoenol pyruvate mediated anaplerosis

The enzyme PEPC, that converts phosphoenolpyruvate (PEP) to oxaloacetate, can divert the glycolysis generated PEP to fuel the TCA cycle. The reaction is schematically shown here.



Plasmodium also has the enzyme that can catalyze the reverse reaction, phosphoenol pyruvate carboxykinase (PEPCK). Transcriptional analysis revealed that the peak expression of these two enzymes varies during the intraerythrocytic cycle. PEPCK peaks during ring and trophozoite stages whereas, PEPCK peaks during schizont stage. The biochemical implication of this is still not clear. Metabolic labelling studies using ^{13}C labelled HCO_3^- showed that PEP indeed feeds anaplerotically into the TCA cycle. Recently, Storm *et al* reported the generation of PEPCK null *Plasmodium* strain (Storm et al., 2014). An interesting observation from their study is that the knockout strain was generated only upon supplementing the media with 5mM malate. The PEPCK null parasite has a stunted growth phenotype in normal RPMI containing growth medium and is rescued partially by supplementing the medium with either malate or fumarate but not by glycerol, citrate, aspartate, glycerol or succinate. This suggests the importance of cytosolic malate/oxaloacetate pools in spite of the fact that plasmodium secretes a lot of malate into the medium as a metabolic waste. The authors further showed the following metabolic remodeling in the PEPCK null parasites.

- 1) Glucose consumption by the PEPCK null parasite is reduced by half as compared to wild-type D10 parasite, and there is a decrease in the amount of lactate produced.
- 2) Increase in levels of pentose phosphate metabolites ribulose 5-phosphate and sedoheptulose 7-phosphate.
- 3) Increased levels of glyceraldehyde 3-phosphate/dihydroxyacetone phosphate suggestive of upregulated flux through glycerol-3 phosphate shuttle.
- 4) Reduced level of citrate production which in turn could reduce the NADPH production in the mitochondrion by isocitrate dehydrogenase.

Overall, the study suggests that cytosolic NAD^+ pools and cytosolic/mitochondrial NADPH pools are critical for the parasite and significant level of NAD and NADPH are generated by PEPCK mediated anaplerosis. However, the completely normal growth phenotype of IDH null parasite rules out any significant role of NADPH generated by the IDH reaction (Ke et al., 2015). Unlike in *P. falciparum*, the gene PEPCK could be knocked out without any phenotypic defect in *P. berghei* (Srivastava et al., 2015). This could be due to species-specific adaptation to different hosts.

The reaction of PEPCK also generates a molecule of inorganic phosphate in the cytosol. There are precedences where the concentration of cytosolic inorganic phosphate determines or is rate limiting for the glycolytic flux (Kubista and Foustka, 1962; Lee et al., 1967; Wu, 1965). The stunted growth phenotype exhibited by the PEPCK null parasites could be because of inorganic phosphate depletion. This speculation needs to be tested using appropriate experiments.

Fumarate anaplerosis

Fumarate is generated from the adenylosuccinate lyase (ASL) catalyzed reaction, that converts one molecule of succinyl-AMP to a molecule of fumarate and AMP. Upon incubation of the saponin released parasite with ¹³C-labeled fumarate, metabolites that were labeled include malate, aspartate, pyruvate, and lactate (Bulusu et al. 2011). It was further shown that conversion of fumarate to aspartate is mediated by the mitochondrial membrane potential-dependent enzyme, malate-quinone oxidoreductase and not malate dehydrogenase (a cytosolic enzyme). Fumarate anaplerosis can contribute to the following:

- 1) Cytosolic NAD⁺ levels that would be important for sustaining a higher flux of glycolysis.
- 2) The reaction of malate-quinone oxidoreductase could contribute to the mitochondrial membrane potential.
- 3) Aspartate generation which has multiple roles in the parasite viz. pyrimidine biosynthesis, purine salvage, and protein biosynthesis.

The inability to knock out the fumarate hydratase gene could be due to these contributions.

1.3.3.4. Significance of TCA cycle enzymes

Data from various studies, put together suggests that the parasite has a completely operative oxidative TCA cycle in the IE stages. The cycle is completely operational fuelled by glucose during the early stage and then by glutamine in the mature stages. However, most of the enzymes of the cycle except FH and MQO are dispensable for the parasite for its asexual growth, as evident from genetic knockout studies. Unlike in the asexual stages, both for gametocytogenesis and for sexual reproduction in the mosquito, all the genes of the TCA cycle seem to be essential. Moreover, metabolic labeling studies suggest that TCA flux in gametocyte is completely fuelled by glucose and there is no contribution from any anaplerotic reaction (MacRae et al., 2013). Moreover, the study also showed that inhibition of TCA cycle using sodium fluoroacetate prevented gametocyte formation.

1.3.4. Mitochondria and electron transport chain

Mitochondria are known to have been acquired by the eukaryotes by an endosymbiotic event. The organelle serves a multitude of function in eukaryotes (Voet and Voet, 2011). Of notable interests are

- 1) The source of ATP production as it harbors TCA cycle and the components of electron transport chain.

- 2) Serves as a calcium storehouse and hence involved in various signaling events
- 3) One of the iron-sulfur cluster assembly machinery is localized to the mitochondria and is essential for the function of many mitochondrial Fe-S enzymes.

Many of the genes from the mitochondrial genome have been transferred on to the nuclear genome of the host organism since the endosymbiosis event (Adams and Palmer, 2003; Kleine et al., 2009). Parasitic organisms have followed the generality of reductive evolution even in the case of the mitochondrion (Wolf and Koonin, 2013; Mendonça et al., 2011). Many anaerobic organisms including parasites have lost multiple functions associated with mitochondria and in extreme cases, the organelle itself (Karnkowska et al., 2016). Apicomplexan organisms have great diversity in the kind of mitochondria that its constituent organisms possess. An extreme example being *Cryptosporidium*, in which almost all the functions of the mitochondria are lost except for the Fe-S cluster biosynthesis machinery (Putignani et al., 2004; LaGier et al., 2003).

1.3.4.1. The role of mitochondrion in *P. falciparum*

Plasmodium species during the intraerythrocytic phase of their life cycle are known to possess a single mitochondrion. The mitochondrion among plasmodial spp. is heterogeneous with respect to size, shape, behaviour upon subcellular fractionation, the extent of internal structures etc. (Fry and Beesley, 1991). Obvious differences are the extent of oxidative phosphorylation and the alternative oxidase activity in different species. Rodent parasites, *P. yoelii* and *P. berghei* seem to have a higher rate of oxidative phosphorylation compared to *P. falciparum* (Fry and Beesley, 1991). *P. falciparum* unlike other species in the genus is reported to have an alternative oxidase activity (Murphy and Lang-Unnasch, 1999; Murphy et al., 1997). Although mitochondria underwent a reductive evolution in apicomplexan spp. its role seems to be essential for the survival of the parasites. The essentiality of this organelle may be due to many functions it performs viz. 1) it is the source of succinyl-CoA essential for heme biosynthesis, 2) source of orotate, an intermediate in *de novo* pyrimidine synthesis (Painter et al., 2007) and 3) iron-sulfur cluster biosynthesis (van Dooren et al., 2006) Although validated as a drug target for malaria, a clear understanding of the various functional aspects of the mitochondrion in *P. falciparum* is still lacking. Earlier studies have demonstrated that glycolysis and ETC are uncoupled and there is little if any, ATP contribution by oxidative phosphorylation (Ginsburg et al., 1986) Nevertheless, mitochondrial membrane potential has been proven to be an essential component for the survival of the parasite in the intraerythrocytic stages. The role of the membrane potential apart from being vital for respiration is also

implicated in the transport of small molecules and proteins across the inner mitochondrial membrane (van Dooren et al., 2006).

1.3.4.2. Electron transport chain

A conventional electron transport operates in the mitochondrial inner membranes and comprises of 1) 4 protein complexes (C-I to C-IV), that are oxidoreductases, 2) an ATP synthase complex which is a hydrolase, and 3) electron carriers ubiquinone (lipid-soluble) and cytochrome-c (water-soluble). Whereas complex-II is non-proton pumping, all other complexes (I, III and IV) are proton pumping, which means that the oxidation/reduction process is coupled to proton translocation from the matrix to the intermembrane space (Voet and Voet, 2011). Cytochrome-c is highly conserved in all kingdoms of life, unlike ubiquinone. Instead of ubiquinone, alternate electron carriers like menaquinone, and rhodoquinone are used in prokaryotes and lower eukaryotes respectively (Tielens and Van Hellemond, 1998). The nature of electron carrier decides the substrates used and the directionality of the reaction catalysed by complex-II.

Protein complexes I and II transfers electrons from the reducing equivalents NADH and FADH generated from TCA cycle reactions to ubiquinone thereby generating ubiquinol. Complex III transfers electrons from ubiquinol to cytochrome-c. Complex-IV, generally termed as cytochrome oxidase, transfers an electron from cytochrome to a final electron acceptor. In aerobic organisms, usually, oxygen is used as the final electron acceptor. Whereas in anaerobic eukaryotic organisms, fumarate is generally used as the terminal electron acceptor, anaerobic prokaryotes use a variety of electron acceptors like fumarate, sulphate, and nitrate. Complex V, an ATP synthase utilises the proton gradient generated to catalyse the phosphorylation of ADP thereby generating the much-needed molecule in the cell, ATP. The entire process of oxidation of substrates through TCA cycle and generation of ATP-fuelled by the proton gradient generated by the electron transport chain is called as oxidative phosphorylation. Apart from ATP synthesis, the mitochondrial membrane potential generated is needed for many vital processes as discussed in the section above (Voet and Voet, 2011).

Total mitochondrial membrane potential Δp is the sum of potential contributed by ΔpH (difference in concentration of H^+ ions) and $\Delta p\Psi$ (electron transfer potential). Complexes III and IV, that are proton pumping contribute to ΔpH whereas all the Complexes I to IV contribute to $\Delta p\Psi$. The contribution from alternative oxidase in *P. falciparum* is still not validated though 25% of the O_2 consumption is attributed to alternative oxidase activity (Murphy et al., 1997). Other components like the ATP/ADP

translocator is also hypothesised to contribute through ΔpH to the membrane potential (Vaidya and Mather, 2009).

1.3.4.3. Electron transport chain of *Plasmodium spp.*

P. falciparum has all the 5 respiratory complexes, though they are different from those of the mammalian mitochondria. The complexes are schematically shown in **Figure 1.7**.

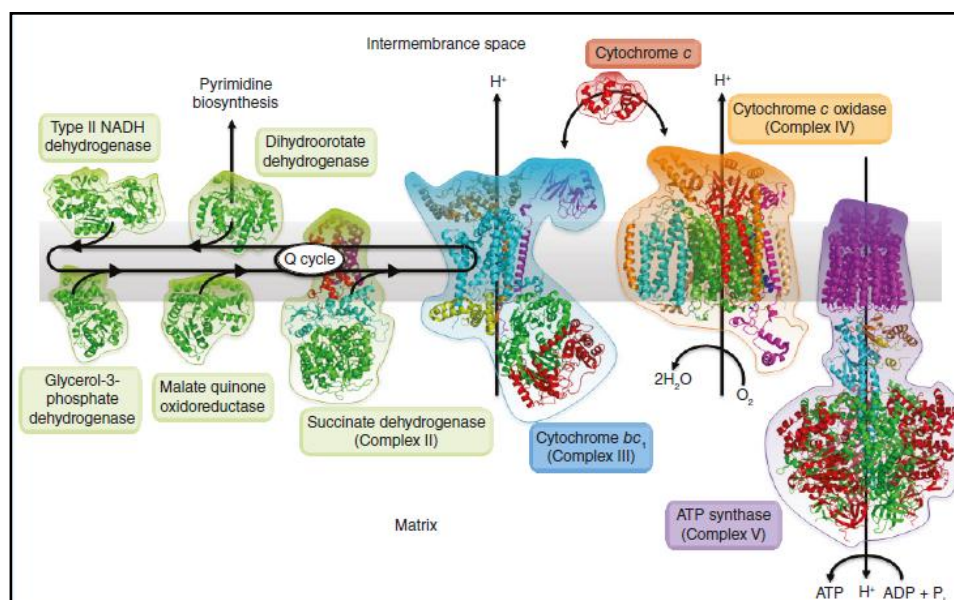


Figure 1.7. Mitochondrial complexes in the electron transport chain of *Plasmodium* species.

Complexes I-V and the dehydrogenases in *Plasmodium* are schematically represented. The proton pumping complex III and complex IV and the non-proton pumping complex V are also shown. The figure is reproduced from Nixon et al., 2013.

Complex I is rotenone-insensitive and non-proton pumping flavoenzyme and belongs to class II NADH dehydrogenase (NDH-2) (Biagini et al., 2006). The enzyme lacks a transmembrane domain and its orientation (internal/external) in the inner mitochondrial membrane is still not clear though biochemical studies in *P. yoelii* suggests an external type NDH-2 (Kawahara et al., 2009). *P. falciparum* enzyme has been shown to utilise menaquinone as electron acceptors apart from using ubiquinone, a classical electron acceptor (Tonhosolo et al., 2010). Tolerance to high levels of copper/hydrogen peroxide, oxidation of excess cytosolic NADH, and rapid quinone reduction/NADH oxidation are some of the physiological roles ascribed to NDH-2 in other organisms (Kerscher et al., 2008). This class of enzyme is sensitive to inhibition by flavin analogues as seen for yeast NDH-2. Extensive efforts had been put towards development of inhibitors directed towards PfNDH2 activity. However, a recent study excluded the essentiality of NDH2 in *P. berghei* (Boysen and Matuschewski, 2011). Knockout of *NDH2*

in *P. berghei* showed that the asexual stage parasites were viable with an intact mitochondrial membrane potential and normal virulence. However, these parasites were not able to undergo sporogony in the mosquito stages and showed arrest at the ookinete stage, though mitochondrial membrane potential in this stage was not lost. The authors suggest that processes involving high ATP requirement in the parasite during oocyst development, such as organelle disposal, could be severely affected. The essentiality and the physiological role of NDH-2 in *P. falciparum* still need to be examined by gene knockout studies.

Complex II or succinate dehydrogenase (SDH) converts succinate to fumarate. Experiments with isolated mitochondria have shown that the enzyme can act in a reversible manner when provided with appropriate electron acceptor (Fry and Beesley, 1991; Takeo et al., 2000; Saruta et al., 1996). The enzyme isolated from *P. yoelii* behaves similar to the human enzyme and gets inhibited by atpenin, a mammalian complex II inhibitor (Kawahara et al., 2009). Knockout studies in *P. berghei* showed that the enzyme is not essential for the asexual stages and is needed only for ookinete maturation in the mosquito stages (Hino et al., 2012). Conditional knockout of the SDHA subunit of the complex in *P. falciparum* has been shown to cause 50% inhibition in growth during asexual stages, that was rescued by addition of succinate but not fumarate (Tanaka et al., 2012). The study concluded that complex-II, although has the potential to act in a reversible manner, its quinol-fumarate reductase (QFR) activity (fumarate to succinate) is essential for optimal parasite growth and not the SDH activity. However, a subsequent study reported the successful knockout of the enzyme without causing any phenotypic effects to the growth of asexual stage parasite (Ke et al., 2015). In the same report, it has been shown that upon treatment of wild-type parasites with atovaquone, a complex III inhibitor, +3 isotopomer of succinate, derived from the anaplerotic influx from ¹³C-labeled glucose, accumulates. This was attributed to the reverse reaction of SDH. This, along with the fact that menaquinone, needed for the QFR activity, can be synthesised by the parasite supports that SDH can act in both the directions in the parasite. Finally, although it has been conclusively shown that SDH complex can potentially act in a reversible manner, activity in either direction seems not to be important for the intraerythrocytic growth of the *P. falciparum*.

Complex III, the cytochrome bc₁ complex (proton pumping), is the only complex which generates oxidised ubiquinone that is essential for the activity of many mitochondrial dehydrogenases, especially DHODH that generates dihydroorotate needed for pyrimidines biosynthesis. Various classes of inhibitors like naphthoquinones, pyridines, acridones, aridinediones and quinolones target the Q₀ site of complex III

resulting in the collapse of membrane potential (Fry and Pudney, 1992; Biagini et al., 2008; Rodrigues et al., 2010). Atovaquone is an inhibitor of the complex that binds the Qo site. Unfortunately, spontaneous mutations leading to rapid development of drug-resistant parasites is commonly seen for complex III inhibitors (Chiodini et al., 1995; Vaidya and Mather, 2000; Looareesuwan et al., 1996). However, proguanil along with atovaquone can kill the parasites effectively without leading to drug resistance (Canfield et al., 1995).

With respect to the rapid development of drug resistance against complex III inhibitors, it is relevant to discuss three novel resistance phenomenon exhibited by some laboratory generated drug resistant parasite to a complex III inhibitor and a DHODH inhibitor.

- 1) In a lead optimisation study of acridone derivative, 6-NH₂-Ac was found to be anti-malarial drug acting on cytochrome bc₁ complex (Winter et al., 2006). In a subsequent study, wild-type D6 parasites were grown in the presence of gradually increasing the concentration of the drug. Finally, a strain SB1-A6 was derived that was highly resistant to 6-NH₂-AC (Smilkstein et al., 2008). The resultant parasites were resistant to the drug as expected. Interestingly, the parasite line was resistant to other complex III inhibitors like atovaquone, antimycin, WR which acts at sites distal to the binding site of 6-NH₂Ac. Sequencing of the cytochrome bc₁ gene showed no mutations that could confer such a resistant phenotype. In order to evaluate the electron transport properties, cell-free preparations of cyt-bc₁ was prepared and tested for sensitivity to all the above-mentioned drugs. Remarkably, the activity of cyt-bc₁ was completely inhibited by these drugs at concentrations that were used for the wild-type cyt-bc₁. The authors offer multiple explanations for the phenotype with the most relevant being the fact that DHODH could use alternate electron acceptors. A subsequent report showing the capability of the parasite to biosynthesize menaquinone perfectly fits the explanation to support the phenotype of the SB1-A6 parasite. The fact that *H. pylori* enzyme can use menaquinone as an electron acceptor and recombinant Pf DHODH can use menadione, structurally similar to menaquinone, further supports the fact that PfDHODH could use menaquinone as an electron acceptor
- 2) In another study (Guler et al., 2015), *P. falciparum* strain Dd2 were made resistant to DSM1, a well characterised Pf DHODH inhibitor, by growing them with sub-lethal concentrations of the drug. Surprisingly, DSM1 resistant Dd2 parasite clones were tolerant to even 10 µM atovaquone, a potent cyt-bc₁ inhibitor. The authors found no sequence variation in cyt-bc₁ that can account for the tolerance behaviour. Two

possible explanations are discussed by the authors to explain the phenotype. One of them is the existence of a cyt-bc1 independent alternate mechanism for generation of oxidised ubiquinone, possibly by the reverse reaction of SDH, and the other being upregulation of copy number of a mitochondrial chaperone that enhances the protein import into the mitochondrion. It's known that fumarate reductase reaction doesn't have the redox potential to accept electrons from reduced ubiquinone and can only do so if reduced menaquinone is available.

- 3) The specific role of mitochondrial electron transport has been attributed entirely to generate ubiquinone necessary for the functioning of DHODH (Painter et al., 2007). The functioning of DHODH is essential for the de novo pyrimidine biosynthesis. Supplementing the parasite with yeast DHODH (yDHODH), a type 1 fumarate-dependent DHODH, makes the parasite resistant to atovaquone, a ubiquinone analogue that inhibits complex III by binding to cytochrome b subunit. However, different strains of transgenic *P. falciparum* expressing yDHODH from a single copy of the gene integrated into their genome show variation in susceptibility to atovaquone (Ke et al., 2011). This unexpected finding suggests that there is a strain-dependent variation in the essentiality of dehydrogenases other than DHODH. Upregulated menaquinone biosynthesis could be a potential mechanism that could explain the all the above resistance phenotype.

Complex IV which consists of cytochrome c oxidase (proton pumping) is sensitive to cyanide inhibition (Krungkrai et al., 1993; Scheibel and Pflaum, 1970; Krungkrai et al., 1997). Cyanide independent respiration in *P. falciparum* suggests the existence of alternate oxidase (Murphy et al., 1997). That atovaquone does not completely collapse the mitochondrial membrane potential indicated that a portion of the membrane potential is insensitive to atovaquone treatment (Painter et al., 2007). Proguanil, a dihydrofolate reductase (DHFR) inhibitor was, however, able to collapse this potential by an unknown mechanism (Canfield et al., 1995). It has been reported that alternate oxidase inhibitors, salicylhydroxamic acid (SHAM) and propyl gallate, potentiate the activity of atovaquone (Murphy and Lang-Unnasch, 1999). A recent study has examined the proteomic changes in *P. falciparum* caused by treatment with SHAM (Torrentino-Madamet et al., 2011). Upon the drug treatment, among other changes observed, a key change was the upregulation of the levels of some glycolytic enzymes. Alternate oxidase from plants is well characterised and the enzyme is active as a homodimer. It is known that organic acids (like pyruvate) allosterically activate alternative oxidase by promoting its dimerization (Millar et al., 1993). Increased pyruvate formation upon activation of glycolysis, is suggested to counteract inhibitory effect of SHAM in *P. falciparum*. It was also observed that under

hyperoxic conditions there was a dramatic drop in the inhibitory concentration (IC₅₀) of SHAM suggesting that the metabolic adaptation to oxygen rich environment is sensitive to SHAM. However, sequences with homology to alternative oxidases from other organisms have not been identified in *P. falciparum*.

Complex V, or ATP synthase complex in the parasite is still not well characterised, though recent bioinformatic analysis provides annotation for many additional subunits of the F₁ and F₀ complexes (Mogi and Kita, 2009). The essentiality of ATP synthase complex has been investigated in both *P. berghei* as well as in *P. falciparum* through genetic knockout studies. The beta subunit of the ATP synthase could be successfully knocked out in *P. berghei*, with only a marginal growth defect in the asexual stages but exhibited an arrested growth phenotype in the mosquito stages (Sturm et al., 2015). A similar attempt to knock out either the beta or the gamma subunit of ATP synthase in *P. falciparum* was unsuccessful. The authors suggest that the protein could be important for the local generation of ATP in the mitochondria (Balabaskaran Nina et al., 2011).

1.3.4.4. Mitochondrial dehydrogenases and their essentiality

There are at least 4 dehydrogenases viz., NADH dehydrogenase (complex I), succinate dehydrogenase (complex II), dihydroorotate dehydrogenase (DHODH), and glycerol 3-phosphate dehydrogenase whose activities contribute to the membrane potential of the *Plasmodium* mitochondrion (Uyemura, 2000; Biagini et al., 2006; Mogi and Kita, 2009; Saruta et al., 1996; Fry and Beesley, 1991; Kawahara et al., 2009). In addition, the activity of malate quinone oxidoreductase (MQO) also contributes to the membrane potential of the mitochondrion in the parasite (Storm et al., 2014; Bulusu et al., 2011a). DHODH which catalyses the conversion of dihydroorotate to orotate is an essential enzyme involved in pyrimidine biosynthesis. This belongs to type 2 class of DHODH and is dependent on the availability of oxidised ubiquinone for its function and hence, is dependent on complex III for its activity (Gutteridge et al., 1979). **Table A1 (Appendix I)** summarises all genetic knockout experiments performed to probe the essentiality of various genes involved in the energy metabolism in different *Plasmodium* species.

1.3.5. Apicoplast and mitochondrial connection

The apicoplast and the mitochondrion in *P. falciparum* are always seen to lie in close contact with each other. Hence, transport of metabolites across these organelles was hypothesised (Kobayashi et al.). The key pathways in apicoplast are type II fatty acid biosynthesis, iron-sulfur cluster biosynthesis, isoprenoid biosynthesis, and a portion of

heme biosynthesis. Using a chemical genetics approach Yeh *et al.* have shown that isoprenoid biosynthesis is probably the only key function of the apicoplast (Yeh and DeRisi, 2011). Inhibition with the anti-bacterial agent, fosmidomycin that targets isoprenoid biosynthesis was shown to be overcome by supplementing the parasite cells with isopentenyl pyrophosphate (IPP). The IPP rescued parasites seemed to be devoid of the apicoplast while, the mitochondrion was intact as evident by the measurement of mitochondrial/nuclear DNA ratio and mitotracker staining. In this context it will be interesting to examine the metabolic activities in the mitochondrion in the absence of apicoplast as the two organelles are closely associated in the parasite. The susceptibility of transgenic *P. falciparum* strain expressing yDHODH (fumarate-dependent and ubiquinone independent) to fosmidomycin suggests that IPP apart from serving as a precursor for menaquinone/ubiquinone biosynthesis might serve other essential roles. However, it is not possible to rule out the necessity of ubiquinone requirement for other dehydrogenases. This study also shows that apicoplast generated acetyl-coA is not essential for the parasite survival though it might be compensated for by the mitochondrial acetyl-CoA. This needs further investigation.

1.3.6. Mitochondrial transporters

The inner membrane of the mitochondrion is selectively permeable to metabolites and this necessitates the presence of transporters for the translocation of any polar metabolite across the organelle. Mitochondria of *Plasmodium* have many transporters to meet the metabolite traffic posed by its physiology. Transporters relevant to energy metabolism include pyruvate carrier protein, dicarboxylate transporter, malate-oxoglutarate transporter, ATP/ADP translocase etc.. To date, only the dicarboxylate transporter has been characterised in-vitro and is shown to transport α -ketoglutarate in exchange of both malate as well as oxaloacetate (Nozawa *et al.*, 2011). In *Arabidopsis*, the malate-oxoglutarate transporter is shown to have a dual role both in malate- α -KG exchange as well as in malate-oxaloacetate exchange (Kinoshita *et al.*, 2011). Whether such dual function is present for the plasmodium protein needs to be tested.

1.4. Purines and their biochemical roles

Purines are heterocyclic organic compounds ubiquitously found in all living organisms. This class of compounds has a pyrimidine ring fused to an imidazole ring. Purines can exist in a cell in many forms viz. nucleobase, nucleoside, and nucleotide (mono, di and triphosphates). Various purine derivatives are present in nature. Adenine and guanine are of special importance as their nucleotide form, AMP and GMP constitute the building

block of DNA/RNA. ATP and GTP are the major source of energy for diverse cellular processes. Apart from these roles, purines are required for the biosynthesis of essential biomolecules: co-factors like NADH, NADPH, Coenzyme A, SAM, and FAD; secondary messengers like cAMP, cGMP, ppGpp etc., that are involved in cellular signalling (Voet and Voet, 2011). Purines are also involved in purinergic signalling wherein molecules like adenosine and ATP can bind to specific receptors and cause varied responses. This kind of signalling is present in both plants and animals.

1.4.1. Purine synthesis *de novo* versus salvage

Purine demands of an organism can be met either through the *de novo* pathway, wherein the purine ring is synthesised inside the cell from simpler molecules or through salvage pathway, where the purine ring is directly taken into the cell from the surroundings using dedicated transporters. The *de novo* pathway is constituted by a set of 10 enzymatic transformations and is highly energy demanding. The enzymes of the pathway form a complex called as purinosomes in some organisms (Zhao et al., 2013, 2014). The *de novo* pathway is reported to have the higher regulatory capacity and directly correlated to growth rate when compared to that of salvage pathway. In organisms having both the pathways, the presence or absence of hypoxanthine seems to be the key deciding factor in the choice of the pathway (King et al., 1983; Yamaoka et al., 1997). Cells resort to salvage pathway either when they don't have the *de novo* enzymes or when there is a dearth of energy. Salvage pathway is additionally involved in the recycling of purines generated from catabolic reactions (Berg et al., 2002). In most organisms, IMP, the key intermediate of both the *de novo* and the salvage pathway is converted to AMP and GMP by a separate set of enzymes.

Studies over many decades have shown that presence of salvage pathway in humans is not superfluous as any mutations in the genes of the salvage pathway leads to various disorders, namely, 1) gout and Lesch-Nyhan syndrome caused by HPRT deficiency/mutation (Sculley et al., 1992; Torres and Puig, 2007), 2) severe combined immunodeficiency (SCID) caused by adenosine deaminase deficiency (Ozsahin et al., 1997), 3) exertional myalgia caused by AMP deaminase deficiency (Fishbein et al., 1978) and 4) autistic and epileptic features in adenylosuccinate lyase deficiency (Jinnah et al. 2013; Fu et al. 2015; Nyhan 2014; Nyhan 2005). Salvage enzymes regulate the steady state concentrations of IMP and GMP which in turn have a direct effect on the flux of *de novo* pathway (Lane and Fan, 2015). Purine salvage enzymes thus, are not just an alternative to *de novo* pathway but are necessary to maintain cellular homeostasis. In almost all the parasitic protozoa like *Plasmodium*, *Toxoplasma*, *Cryptosporidium*, *Eimeria*,

Theileria etc., the purine demands are completely met by the salvage pathway (Hassan and Coombs, 1988).

1.4.2. Modes of purine salvage

Unlike the *de novo* purine biosynthetic pathway that is well conserved, purine salvage pathway is highly variable. Variation can exist at three levels as shown in **Figure 1.8**:

- 1) The choice of purine: the choice of purine can be a nucleobase, nucleoside or a nucleotide. The choice of the purine depends largely on the kind of purine available in the local niche of the organism.

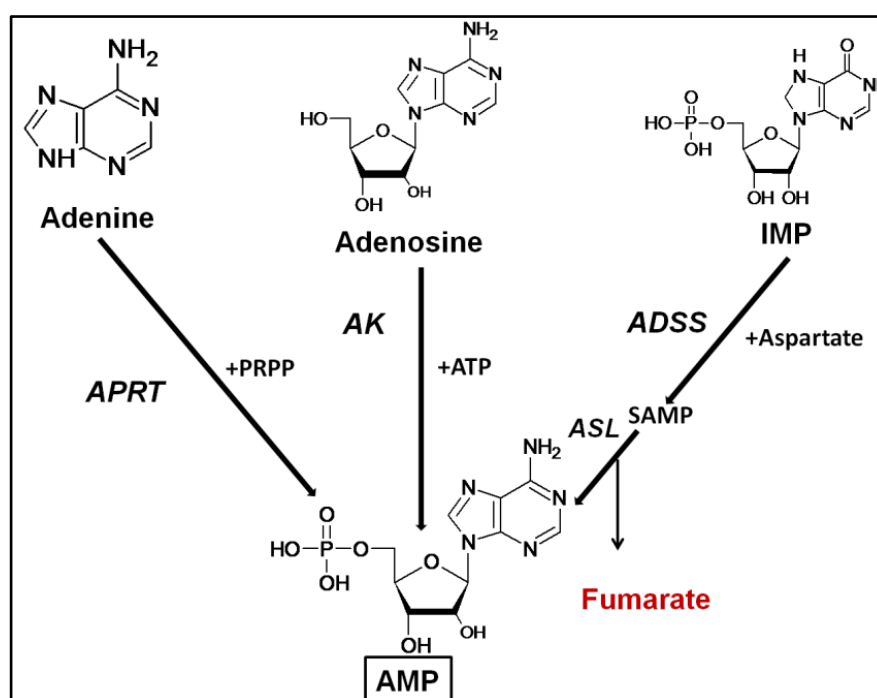


Figure 1.8. Different modes of salvage of AMP

The scheme represents different ways in which AMP can be made in a cell: adenine can be phosphoribosylated by APRT, adenosine can be phosphorylated by AK or IMP can be converted to AMP by the sequential action of ADSS and ASL. Fumarate is generated as a by-product when ADSS/ASL mode of AMP synthesis is used and is shown in red.

- 2) Nature of purine transporters: With the exception of adenine, all other forms of purines including the nucleobase, nucleoside, and nucleotide forms are cell impermeable. This necessitates the presence of transporters for these metabolites. Purine transporters come with various substrate specificities and affinities. Purine nucleoside transporters are broadly divided into concentrative nucleoside transporters (CNT) driven by the cation gradient across the membrane and equilibrative nucleoside transporter (ENT) that are driven by the concentration

gradient and hence bidirectional (Parkinson et al., 2011). The two families of transporters are completely unrelated with respect to structure/homology. Both these families can transport nucleobase and nucleosides. Nucleotide transporters (NTT's) are also reported to be present in many intracellular pathogenic fungi like microsporidia and intracellular pathogenic bacteria like Rickettsia and Chlamydia. They can transport both the dinucleotide and the mononucleotide form of purine (Landfear, 2011; Dean et al., 2014).

- 3) Enzymes used for purine salvage: If we consider a purine nucleotide (eg. AMP) as the ultimate requirement of the cell from purine salvage pathway enzymes, it can be met by three ways: a nucleobase can be phosphoribosylated by a phosphoribosyltransferase or a nucleoside can be phosphorylated by a nucleoside kinase or the nucleotide can be directly taken inside the cell. An organism can as well have a mixture of these strategies.

1.4.3. Purine salvage in *Plasmodium*

Purine salvage enzymes of plasmodium have drawn considerable attention as they are potential therapeutic targets (Downie et al., 2008). Literature is replete with information on various aspects the pathway. In summary, the available knowledge can be classified into 1) transporters of purines and 2) the enzymes of purine metabolism.

1.4.3.1. Transport of purines

During the intra-erythrocytic stage of the parasite, the metabolic needs are met by translocation of nutrients from the plasma into the parasite cytosolic compartment. There are three membranes any metabolite has to cross to reach the parasite cytosol: erythrocyte membrane, parasitophorous vacuolar membrane, and the parasite plasma membrane. It has been established that the PVM is a highly permeable membrane to most metabolites (Desai et al., 1993). This necessitates the presence of transporters at the level of erythrocyte and the parasite membrane for the translocation of any hydrophilic metabolite which is generally membrane impermeable. It has also been shown that the erythrocyte membrane becomes more permeable to metabolites post infection of the parasite through a set of transporters collectively called as new permeability pathways (NPP) (Ginsburg et al., 1983).

1.4.3.2. Transport of purines across erythrocyte membrane

Mature RBCs, unlike their precursor reticulocyte, have poorer metabolic activity (Pranker, 1955; Wiback and Palsson, 2002). With the loss of nucleus and the ability to

replicate, the nucleotide requirements of the mature RBCs are less. In spite of poor overall metabolic activity, the intraerythrocytic concentration of ATP is high, 2mM (Sarpel et al., 1982). The ATP is primarily synthesised by salvaging purines from plasma. Purine transport across the uninfected erythrocyte membrane is primarily driven through human facilitative nucleobase transporter (hFNT1) and human equilibrative nucleoside transporter (hENT1) (Kraupp et al., 1994; Domin et al., 1988). Infected erythrocyte membrane can additionally transport purines through NPP, though to a very limited extent. Whereas hFNT transports adenine and hypoxanthine, hENT can transport adenosine and uridine. The rate of purine import is doubled across the erythrocyte membrane post-infection implicating the higher metabolic demand of the parasite.

1.4.3.3. Transport of purines across parasite plasma membrane

Most of the protozoan parasites that are purine auxotrophs rely on ENT type of nucleoside transporter (de Koning et al., 2005). *Plasmodium* completely relies on nucleobase/ nucleoside salvage through the equilibrative type transporters (Quashie et al., 2010). Although there are reports that erythrocytic AMP pools can directly be transported to the parasite cytosol, the extent to which it contributes to the AMP requirement of the parasite is still not clear (Cassera et al., 2008). *P. falciparum* has four genes that code for the transporters, ENT1, ENT2, ENT3, and ENT4 (Gardner et al., 2002). The sequences of the proteins are highly divergent with only 2% sequence identity. ENT3 is present only in the *Plasmodium* species that infect humans and primates (Frame et al., 2015a; Riegelhaupt et al., 2010).

PfENT1 is the primary and essential transporter for purines in the parasite. Knockout of the gene in parasites grown in vitro at physiological hypoxanthine concentration (<10 μ M), turned out to be lethal (El Bissati et al., 2008). The Δ pfnt1 parasites could only be partially rescued by supplementing the growth media with supraphysiological concentrations of hypoxanthine (>50 μ M). The importance of the gene was further complemented by the knockout of the gene in *P. berghei* (Aly et al., 2010). The Δ pbent1 parasite was not able to kill mice. The maximum parasitemia load reached was 2%. The PfNT1 transporter has broad substrate specificity and can transport hypoxanthine, adenosine, guanine, guanosine and inosine. Through yeast based high throughput screens, inhibitors with nanomolar affinity have been reported for both Pf and PvENT1 (Frame et al., 2015b).

PfENT2 and 3, though not well characterised, initial reports suggest that they have minimal or no role in purine transport. PfNT2 has been shown to localise to the parasite endoplasmic reticulum (Frame et al., 2015a). PfENT4 is a purine transporter with low

affinity for adenine and 2'-deoxyadenosine (in millimolar range). The importance of these transporters for the parasite growth is still not clear.

1.4.4. Enzymes involved in purine salvage pathway

P. falciparum uses hypoxanthine, the most abundant purine in human plasma, as its primary purine source. The concentrations of other purines are catalogued in **Table 1.1**. Hypoxanthine is phosphoribosylated to IMP by hypoxanthine-guanine phosphoribosyltransferase (HGPRT). IMP is converted to AMP through the action of enzymes adenylosuccinate synthase (ADSS) and adenylosuccinate lyase (ASL). IMP is converted to GMP by the action of enzymes, inosine monophosphate dehydrogenase (IMPDH), and guanosine monophosphate synthetase (GMPS).

Table 1.1. Concentrations of different purines in human plasma

S.No	Purine	Concentration in human plasma (μM) (Chaleckis et al. 2016 and refs. therein)
1	Hypoxanthine	1-5
2	Adenine	0.3
3	Guanine	N.A
4	Adenosine	0.5
5	Guanosine	0.9
6	Inosine	1
9	AMP	6.2
10	ADP	48
11	ATP	433
12	GMP	0
13	GDP	15
14	GTP	25
15	Xanthine	1.27

Adenosine can also be used by the parasite. The first step in the utilisation of adenosine is its conversion to inosine by the action of the enzyme, adenosine deaminase (ADA). The inosine converted to hypoxanthine by the enzyme purine nucleoside phosphorylase (PNP). Thus, the hypoxanthine-IMP reaction catalysed by HGPRT forms a nodal reaction at which different purine sources converge. The reactions of the purine salvage pathway in the parasite are schematically presented in **Figure 1.9**. In addition to these reactions, AMP can be converted back to IMP by the enzyme Adenosine monophosphate deaminase (AMPD). The significance of this reaction to the parasite is still not clear. Other enzymes related to purine salvage like adenine phosphoribosyltransferase (APRT), adenosine kinase (AK), guanosine monophosphate reductase (GMPR), adenine aminohydrolase (AAH), and adenine deaminase (ADA) enzymes are absent in *Plasmodium* genome.

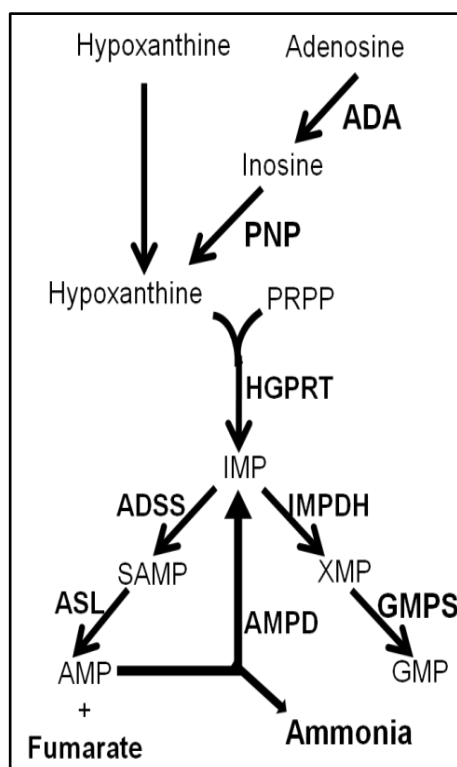


Figure 1.9. Purine salvage pathway of *P. falciparum*.

A schematic representation of the reactions of the purine salvage pathway. Adenosine is the major purine source available in the human plasma. A subset of reactions constituting the purine nucleotide cycle is also shown. Fumarate and ammonia are formed as by-products of the cycle.

A brief description of the enzymes involved in *Plasmodium* purine salvage pathway is given below:

Hypoxanthine-guanine phosphoribosyltransferase (HGPRT) (2.4.2.8)

This enzyme catalyses the phosphoribosylation of different substrates *viz.* hypoxanthine, guanine, and xanthine with variable efficiencies. Although the recombinantly expressed enzyme was found to be sluggish and exhibits a lag in the reaction progress curve, it was later found that the enzyme can be activated through its product IMP (Raman et al., 2005). PRPP one of its substrate can also activate the enzyme. Upon activation, the lag phase in the progress curve completely disappears. It was recently shown that the mechanism of activation involves both ligand-induced oligomerization and conformational changes. In particular, a change of trans to the cis conformation of Leu-Lys dipeptide is implicated in the activation mechanism (Roy et al., 2015). The feature of substrate/product activation is in contrast to the human counterpart. Unlike the human enzyme the parasite enzyme can also act on xanthine. Differences in the kinetic properties and substrate specificity between the human and the parasite enzyme have made PfHGPRT an attractive target for

malaria intervention. Many transition state inhibitors based on immucillin-H 5'P have been designed for this enzyme (Ducati et al., 2013). The need for the presence of phosphate groups for tight binding to the enzyme makes the transition state analogues impermeable to the membrane. Recently acyclic nucleoside phosphonate analogues that are cell permeable, hydrolysis-resistant, and highly selective to the parasite enzyme over the human enzyme have been described (Clinch et al., 2013; Hazleton et al., 2012). The IC₅₀ value of these drugs was reported to be around 1-50 μM and the drug inhibits hypoxanthine incorporation in *in vitro* culture of the parasite. Further modification of the scaffold to design inhibitors with nanomolar IC₅₀ could lead to a highly selective antimalarial drug.

Adenylosuccinate synthetase (ADSS) (6.3.4.4)

The enzyme is involved in catalysing the conversion of IMP to succinyl-AMP (SAMP). One molecule of aspartate is added on to a molecule of IMP resulting in the formation of SAMP. One molecule of GTP is also used up in the process. The plasmodium enzyme has been recombinantly expressed, kinetically characterised and the structure obtained (Jayalakshmi et al., 2002; Raman et al., 2004; Eaazhisai et al., 2004). Unlike ADSS reported from other organisms which follow a random mechanism of substrate binding, the plasmodium enzyme follows an ordered mechanism in which the substrates bind in the following order: IMP-GTP-aspartate. Another unique feature is the activation by fructose 1, 6-bisphosphate, an inhibitor of the mammalian enzyme. In-silico analysis to find most suitable drug targets in the parasite has revealed ADSS as the most druggable target (Ludin et al., 2012; Huthmacher et al., 2010). Hadacidin and hydantocidin are established inhibitors of the enzyme. IC₅₀ value for hadacidin is around 100 μM (Webster et al., 1984; Siehl et al., 1996) and the value for hydantocidin is not known. Although other inhibitors with better IC₅₀ values have been described they are not suitable scaffold for drug development.

Owing to the essentiality of the enzyme the knockout of the gene in *Plasmodium* is not possible. *Leishmania* has many redundant purine salvage pathways and hence generation of $\Delta adss$ parasites was feasible. The parasite load was significantly less in peripheral macrophages but not in other cell types (liver, spleen etc.) indicating cell type dependent usage of the salvage enzymes (Boitz et al., 2013).

Adenylosuccinate lyase (ASL) (4.3.2.2)

The enzyme belongs to the lyase family that also includes enzyme like class II fumarase, aspartase, and arginosuccinate lyase. The enzyme catalyses the reversible cleavage of

adenylosuccinate molecule into AMP and fumarate. In many cell types, it is involved in the maintenance of AMP and fumarate levels as it catalyses a constituent reaction of purine nucleotide cycle (van Waarde, 1988). The enzyme can also catalyse a chemically similar reaction of conversion of SAICAR to AICAR and fumarate. This reaction is part of de novo purine biosynthesis. Although the de novo pathway is absent from the parasite, the enzyme is reported to retain the activity. There is significant sequence divergence of the plasmodium enzyme when compared to that of the human enzyme making it a good drug target (Bulusu et al., 2011b). An ordered product release, AMP followed by fumarate, has been implicated for the lack of inhibition of the enzyme by dicarboxylic acids other than fumarate, for the *Saccharomyces* ASL. Such mechanism could still be in play for the plasmodium enzyme. The fact that the plasmodium enzyme still retained the catalytic activity on SAICAR was exploited to test the effect of the inhibitor, AICAR on the parasite and it was indeed proved that the compound could kill the parasite albeit with low efficacy (IC_{50} -160 μ M). The AICAR scaffold can be used to design more potent inhibitors of the plasmodium enzyme.

Despite redundant purine salvage pathways present in *Leishmania*, the knockout of the gene proved to be detrimental for the parasite growth in many host cell types (Boitz et al., 2013). The *asl* null parasites were rescued only upon the addition of a 6-oxypurine source and pharmacological inhibition of adenine aminohydrolyase by 2'-deoxycoformycin. The growth defect was ascribed to the accumulated succinyl-AMP (SAMP) pool acting as a dead sink thereby affecting the guanylate pool. Knockout of the gene in plasmodium would result in more severe phenotypes as there is complete dependence on this enzyme for AMP synthesis unlike in *Leishmania*.

Purine nucleoside phosphorylase (PNP)

The enzyme catalyses the conversion of inosine to hypoxanthine and ribose-1-phosphate. Just like the *P. falciparum* adenosine deaminase (PfADA), *P. falciparum* purine nucleoside phosphorylase (PfPNP) can act on methylthioinosine and convert it to hypoxanthine and methylthio ribose-1-phosphate (MTR1-P). The hypoxanthine generated is used for purine salvage by HGPRT and MTR1-P is used for methionine production. Inhibitors analogous to methylthioinosine like methylthio immucillin-H are effective against PfPNP and kill the parasite growth with an IC_{50} of 50 nM (Kicska et al., 2002; Taylor Ringia and Schramm, 2005). The structures of PfPNP with various inhibitors are available and corroborates to the promiscuous activity of PfPNP against the methylthio analogues of inosine (Donaldson et al., 2014). The importance of the ADA-PNP axis in the purine salvage pathway of the parasite is clear from the knockout studies done in *P. falciparum*. The Δpnp parasites were

generated with high hypoxanthine concentration in the *in vitro* culture compared to the plasma hypoxanthine concentration. At physiological concentrations of hypoxanthine, the Δpnp parasites failed to grow but were rescued upon supplementation with excess hypoxanthine, suggesting the importance of adenosine salvage / purine recycling in the parasite purine metabolism. Inhibitors of PNP were also able to clear the infection in *P. falciparum* infected Aotus monkey model adding validation to the importance of ADA-PNP axis (Madrid et al., 2008). Mice exposed to *P. yoelii* PNP knockout ($\Delta pypnp$) parasites were conferred with protective immunity and were able to survive a subsequent infection with wild-type parasites. Thus, Δpnp knockout parasites are considered an attenuated parasite based vaccine model (Ting et al., 2008).

Adenosine monophosphate deaminase (AMPD)

The enzyme catalyses the irreversible conversion of AMP to IMP and ammonia. The enzyme plays a key role in the maintenance of adenylate energy charge, particularly it has been shown in skeletal muscles that the activity of the enzyme meets the high energy demand during exercise (Hancock et al., 2006). The yeast enzyme is known to be regulated by various factors like binding to cytoskeletal elements, post-translational modifications and allosteric regulation by ATP, ADP, and inorganic phosphate. The enzyme is also activated by different alkali metal ions (Murakami, 1979). Human erythrocytes also possess this enzyme and is known to be activated by 2,3 bisphosphoglycerate (Sasaki et al., 1976). Because of the negative free energy of the reaction, at pH 7, the enzyme could be much more efficient in deamination of purines than that catalysed by GDH, which involves deamination of glutamate, to generate ammonia. Recent studies have reported small molecule inhibitors targeting the enzyme (Admyre et al., 2014; Plaideau et al., 2014). Anti-diabetic drug metformin is also known to inhibit the enzyme (Ouyang et al., 2011).

The enzyme is not well characterized in apicomplexans. With the presence of this enzyme along with ADSS and ASL, the purine nucleotide cycle can be operational in the parasite. The essentiality of the enzyme is still not clear. There are no reports on basic biochemical and structural characterization of the enzyme. Just like in other organisms the activity of the enzyme could help maintain AMP levels and hence indirectly regulate the adenylate kinase enzyme.

1.4.5. Adenylate energy charge

Adenylate energy charge (AEC) is the quantitative estimate that reflects the relative intracellular concentration of adenine nucleotides. The ratio served as a useful tool to

understand and deduce a pattern to explain the allosteric control of enzymes of different pathways, by different adenylate nucleotides (A Pradet and P Raymond, 1983). The relationship along with the graphical representation is shown in **Figure 1.10**.

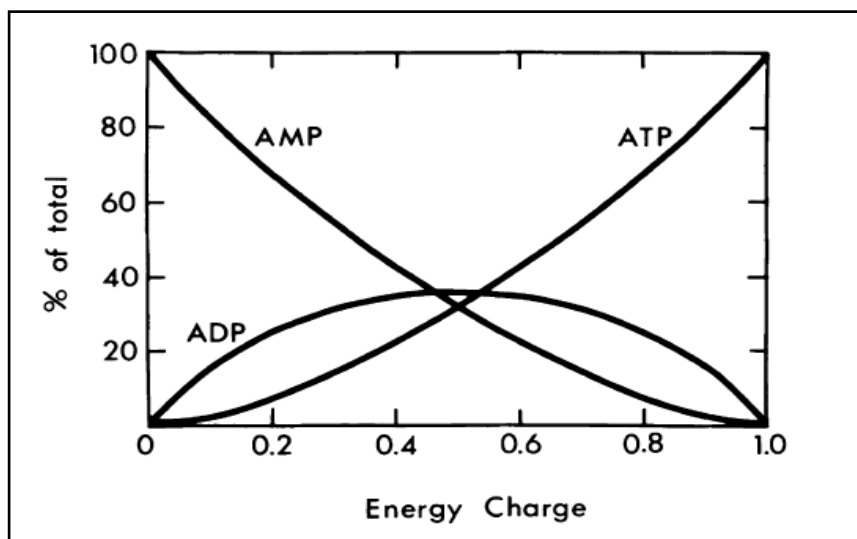


Figure 1.10. Adenylate energy charge

The schematic represents the relationship between different adenylate nucleotides.

A value of 1 indicates that all adenine nucleotides are present in the form of ATP, the value of 0 indicates that they are all present as AMP and when all nucleotides are present as ADP, the value is 0.5 (Atkinson and Walton, 1967). The ratio is a true representative of adenylate pool only if the enzyme adenylate kinase operates at near equilibrium. The alternate equation to establish a correlation between adenylate nucleotides which doesn't include this assumption is available (Bomsel and Pradet, 1968). However, the original equation developed by Atkinson is still widely used to quantitatively represent the adenylate pool in a cell. Rather than using the dynamic values of absolute concentration of these nucleotides, the ratio is more relevant for many cell types (De la Fuente et al., 2014).

A typical growing cell (prokaryotic/eukaryotic) has an adenylate energy charge value of 0.85. In many organisms the AEC value is maintained in the narrow range of 0.7-0.95. Some organisms tolerate big changes in AEC whereas some don't (Thomas and Dawson, 1977; Hill and London, 1978). Any change in the value will prompt changes such that the value is brought back to its initial value. Many enzymes are sensitive to this value and their enzymatic activity, in turn, maintains the cellular nucleotide balance. Whereas changes in adenylate energy charge are related directly to survival, guanylate energy charge is related to growth. Thus, if adenylate energy charge decreases (depletion of

ATP), the guanylate energy charge would decrease with immediate effect (GTP levels drops). The regulation is brought about by the enzyme nucleoside diphosphate kinase (Derr and Zieve, 1972; Karl, 1980).

Enzymes like adenylate kinase, adenylate/(AMP)deaminase and AMP-activated protein kinase (AMPK) are key in maintaining the AEC (A Pradet and P Raymond, 1983). Adenylate energy charge has been calculated for *P. lophurae* infected erythrocytes (Yamada and Sherman, 1980). In the first 20 hours of infection the value is maintained at 0.93, whereas during the last 14 hours, the value drops down with the lowest value being 0.6. The exact metabolic implication for the drop in AEC during the late stages of the parasite is still not known. All four enzymes involved in the maintenance of AEC viz., adenylate kinase, AMPK, nucleoside diphosphate kinase and adenylate/AMP deaminase are present in *Plasmodium*.

1.4.6. Purine nucleotide cycle

Purine nucleotide cycle is a set of three reactions catalysed by the enzymes, ADSS, ASL, and AMPD. The cycle was first discovered by Lowenstein (Tornheim and Lowenstein, 1972), in extracts of rat skeletal muscle. Working skeletal muscle is known to produce excess ammonia. High turnover of 6-aminogroup of AMP together with the absence of glutamate dehydrogenase hinted for an alternate pathway of ammonia production. It was finally reported that aspartate was the source of ammonia. The conversion required the presence of IMP or SAMP or AMP suggesting that these metabolites could be intermediates used in the conversion. It was also found that the conversion is GTP-dependent and GDP inhibits the process. Through classical biochemical techniques, it was found that enzymes ADSS, ASL, and AMPD were involved in the conversion and the whole pathway was collectively termed purine nucleotide cycle. The net reaction of the cycle is shown schematically in **Figure 1.11**. The stoichiometry of the cycle is such that for every molecule of aspartate and GTP consumed, the net products formed are 1) a molecule of fumarate 2) one molecule of GDP and inorganic phosphate and 3) a molecule of ammonia. In some organisms like rainbow trout (Mommensen and Hochachka, 1988), a temporally separated PNC has been reported wherein AMP producing reactions and ammonia producing reactions are temporally separated to achieve the objective function of meeting cellular energy needs (AMP) and maintaining pH balance (through protonation of ammonia).

Purine nucleotide cycle has AMP generating and consuming reactions and hence may be a key factor involved in regulation of adenylate energy charge. When ATP levels are high in the cell, then AMPD gets allosterically inhibited and steady state AMP levels go

up thereby, keeping the AEC under check. On the other hand, when ATP levels are low or in high demand, then adenylate kinase reaction would make more ATP. Under such circumstances, AMPD, by depleting AMP levels would fuel the adenylate kinase reaction thus, meeting cellular ATP demands.

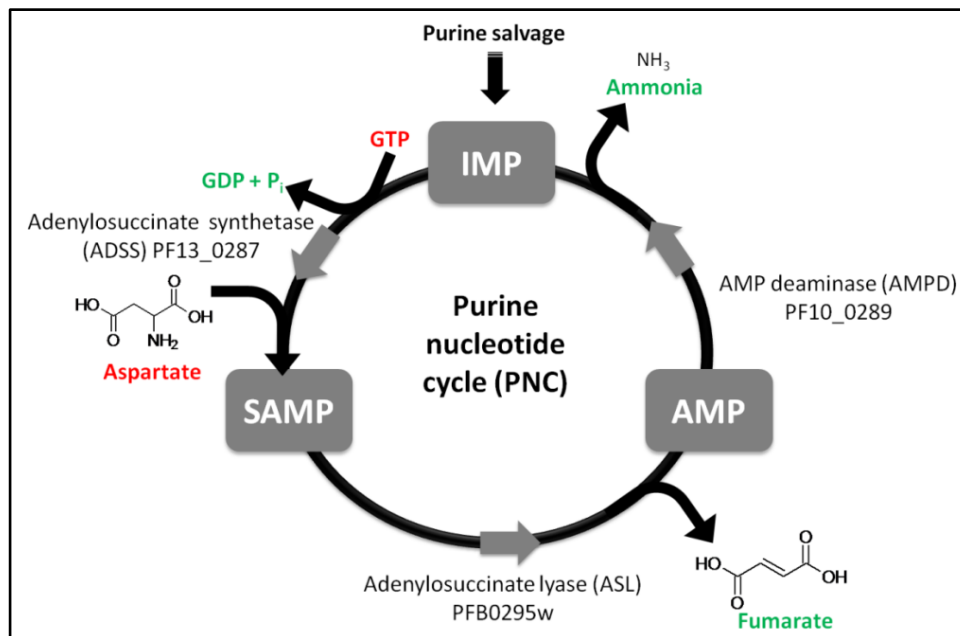


Figure 1.11. Purine nucleotide cycle (PNC).

The three reactions and the respective enzymes involved in purine nucleotide cycle are shown in the figure. The accession numbers correspond to the enzyme from *P. falciparum*. One molecule of fumarate, ammonia and inorganic phosphate are the net products formed from the complete operation of the cycle. The substrate consumed in the process is shown in red and net products formed are shown in green.

1.4.6.1. PNC in *Plasmodium*

The presence of all three enzymes in plasmodium suggests that the pathway might be operational in the parasite. Apart from the functionality of ADSS and ASL, AMPD was also shown to be functional by incorporation of ^{33}P into IMP when parasites are fed with [^{33}P]–AMP (Cassera et al., 2008). The operation of these reactions as a cycle or any temporal separation of the reactions as seen in rainbow trout is yet to be tested in various stages of the parasitic life cycle. The presence of PNC in *P. falciparum* suggests the need for regulation of AMP levels and a possible role for fumarate and ammonia in parasite metabolism.

1.4.6.2. Fate of fumarate generated from PNC in *Plasmodium falciparum*

Protozoan parasites are known to secrete organic acids such as lactate, malate, succinate, fumarate etc, (Marr et al., 1995). Through the use of ^{14}C labelled aspartate, recent studies

have shown that fumarate generated through PNC is not secreted as a metabolic waste in the intraerythrocytic (IE) stages of *P. falciparum* (Bulusu et al. 2011). Using intraerythrocytic *vitro* cultures of *P. falciparum*, ^{13}C -labelled fumarate (2, 3- $^{13}\text{C}_2$ fumarate) supplemented in the medium was shown to be metabolised to pyruvate and aspartic acid. The pathway for fumarate metabolism is shown in **Figure 1.12**.

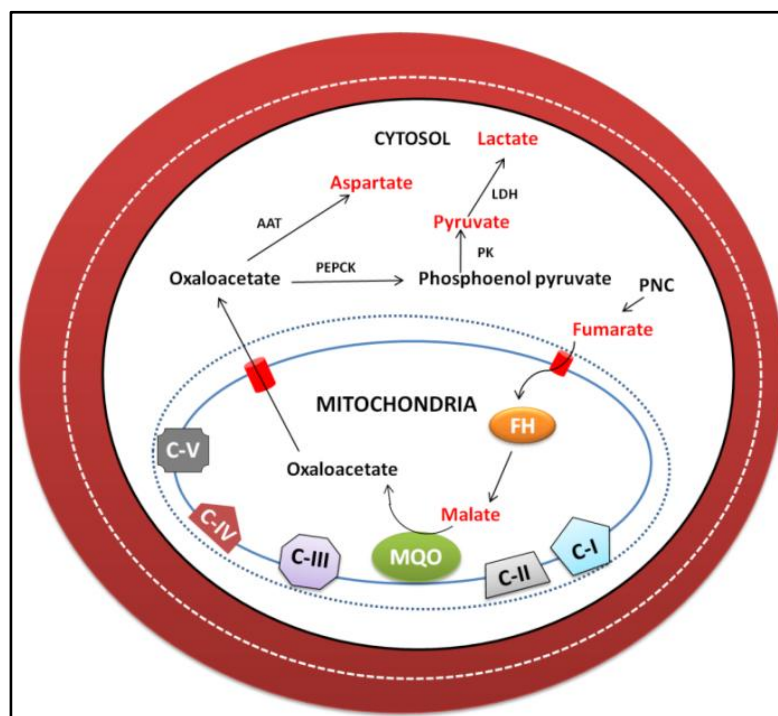


Figure 1.12. Fate of fumarate in *P. falciparum*.

Fumarate produced in the cytosol by PNC is shuttled into the mitochondrion where it is converted into oxaloacetate through the involvement of the enzymes fumarate hydratase (FH) and malate-quinone oxidoreductase (MQO). The oxaloacetate transported into the cytosol serves as the precursor for aspartate and pyruvate. Metabolites that incorporate ^{13}C label when saponin released parasites are fed with 2,3- ^{13}C -fumarate are coloured in red.

As shown in the figure, oxaloacetate generated from fumarate is the key intermediate that leads to the formation of aspartate and pyruvate. The fumarate hydratase activity which brings about the conversion of fumarate to malate has been shown to be localised to the mitochondrion in the parasite (Bulusu et al., 2011a). The subsequent conversion of malate to OAA by MQO was validated through the use of atovaquone. Atovaquone treated parasites failed to accumulate ^{13}C -labelled aspartate suggesting the role of mitochondrial MQO and not cytosolic MDH in the generation of OAA from malate. The conversion of OAA to aspartate is brought about by aspartate aminotransferase (AAT). Recombinant *P. falciparum* AAT has been shown to catalyse the reaction efficiently in both directions and localise to the cytosol (Wrenger et al., 2011). Specific inhibition of PfAAT by a peptide is also shown to inhibit parasite growth showing

the essentiality of the enzyme. The conversion of OAA to pyruvate must be through phosphoenolpyruvate carboxykinase (PEPCK) followed by pyruvate kinase. This conversion of fumarate to aspartic acid and pyruvate is compartmentalised between the mitochondrion and the cytosol. The whole process, therefore, requires the operation of shuttles that transport fumarate into the mitochondria and OAA out from this organelle. The possible metabolic significance of fumarate generated from PNC is reviewed and is schematically shown in **Figure 1.13**.

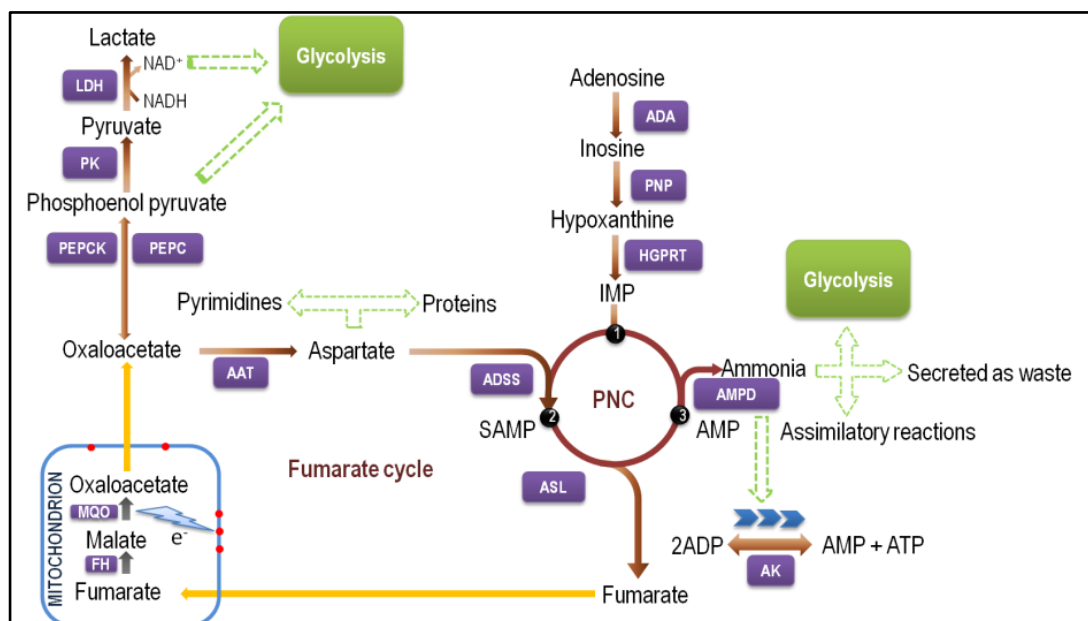


Figure 1.13. Cross talk of PNC with other metabolic pathways in *P. falciparum*.

The figure schematically shows the possible significance of fumarate generated from PNC in the intraerythrocytic stages of the parasite. Numbers 1, 2, and 3 in PNC refer to the metabolites IMP, SAMP and AMP, respectively. Brown arrows, enzymatic reactions in cytosol; grey arrows, enzymatic reactions in mitochondrion; orange arrows, transport processes; broken green arrows, possible role of metabolites (enzyme substrates or regulators); violet boxes, enzymes catalyzing the reaction; lightning bolt, electron donation to ubiquinone by MQO reaction; red filled circles, ubiquinone molecules; chevron arrows, preferred direction of the reversible reaction.

1.4.6.4. Fate of ammonia generated from PNC

Ammonia assimilation is suggested to be present in the parasite and hence, the ammonia generated through PNC can be used for such reactions. However, it should be noted that a considerable amount of ammonia is secreted as a metabolic waste by the parasite. In yeast, ammonia is reported to have a regulatory role in glycolysis by acting as an allosteric activator of PFK and the extent of its regulatory activities in *P. falciparum* is yet to be examined. The temporal separation of fumarate and ammonia generating reactions of PNC has been suggested to be involved in pH regulation in the skeletal muscles of rainbow

trout (Mommsen and Hochachka, 1988). The exact nature of PNC in terms of temporal separation of its reactions and its role in pH maintenance is yet to be validated in the parasite.

1.5. OBJECTIVES

Earlier work done in our laboratory addressing the fate of fumarate formed from ASL reaction, had provided first biochemical evidence for the operation of fumarate hydratase, and malate-quinone oxidoreductase in the IE stages of the parasite. These reactions are component parts of an oxidative citric acid cycle. Atovaquone based inhibition followed by metabolic tracing of labelled fumarate provided evidence for mitochondrial membrane potential-dependent activity of malate-quinone oxidoreductase. Subsequently, other studies (MacRae et al., 2013; Ke et al., 2015) showed convincing evidence for the operation of a complete oxidative citric acid cycle. From these studies, it is clear that glucose doesn't fuel citric acid cycle rather the flux of intermediates through the cycle is driven primarily in an anaplerotic fashion. Three enzymes could potentially be involved in the anaplerosis viz. FH, PEPC, and α -KDH. Reverse genetic approaches clearly showed the importance of FH and PEPC. The role of PEPC though seems to be essential, its molecular basis is still not clear. Malate/fumarate rescue of the PEPC null parasites suggests that the cytoplasmic oxaloacetate pool is important for the parasite. FH could potentially contribute to this pool although a quantitative analysis on the relative contribution is still not available. Essentiality of FH and MQO is puzzling, as other reactions of the citric acid cycle seem to be dispensable for the parasite. The thesis is an account of the experiments done to address the issues raised in the above discussion. The thesis is broadly divided into two sections. Section 1 deals with experiments done to address the biochemical importance the metabolites, fumarate and ammonia generated from purine nucleotide cycle and, the essentiality of the enzyme fumarate hydratase in *P. falciparum* and *P. berghei*. Section 2 deals with the experiments done towards biochemical and structural characterisation of class-I fumarate hydratases.

In order to find the significance of the fumarate metabolism, we followed two different strategies. In the first strategy discussed in chapter 2, we generated a transgenic parasite expressing yeast adenine phosphoribosyltransferase (yAPRT), which converts adenine to AMP. This is completely different from the endogenous AMP generating reaction, wherein one molecule of SAMP is converted to one molecule of fumarate and AMP by the enzyme adenylosuccinate lyase. Provided yAPRT generates enough AMP levels, the endogenous AMP generating pathway can be inhibited leading to depletion of fumarate generated from ASL reaction. In another strategy, discussed in chapter 3 we

attempted to know the functional significance of fumarate by either knockout of the enzyme fumarate hydratase in *P. berghei* or conditional knockout of the enzyme in *P. falciparum*.

Apart from fumarate, ammonia is another by-product that is generated upon complete operation of PNC. Although, there is considerable evidence of the fate of this ammonia in other systems (Arinze, 2005), its relevance in the parasite is still not clear. Evidence supporting the formation of ammonia from aspartate would also support the operation of PNC in the parasite. Ammonia is secreted into the spent media in the *in vitro* culture of *P. falciparum*. Whether ammonia generated from PNC forms a major fraction of this or is used in anabolic reactions, is still not clear. In order to find out the fate of ammonia in the parasite, we first standardised a metabolite derivatization methodology to follow the fate of ammonia in *E. coli* using NMR. The details and results are discussed in chapter 4.

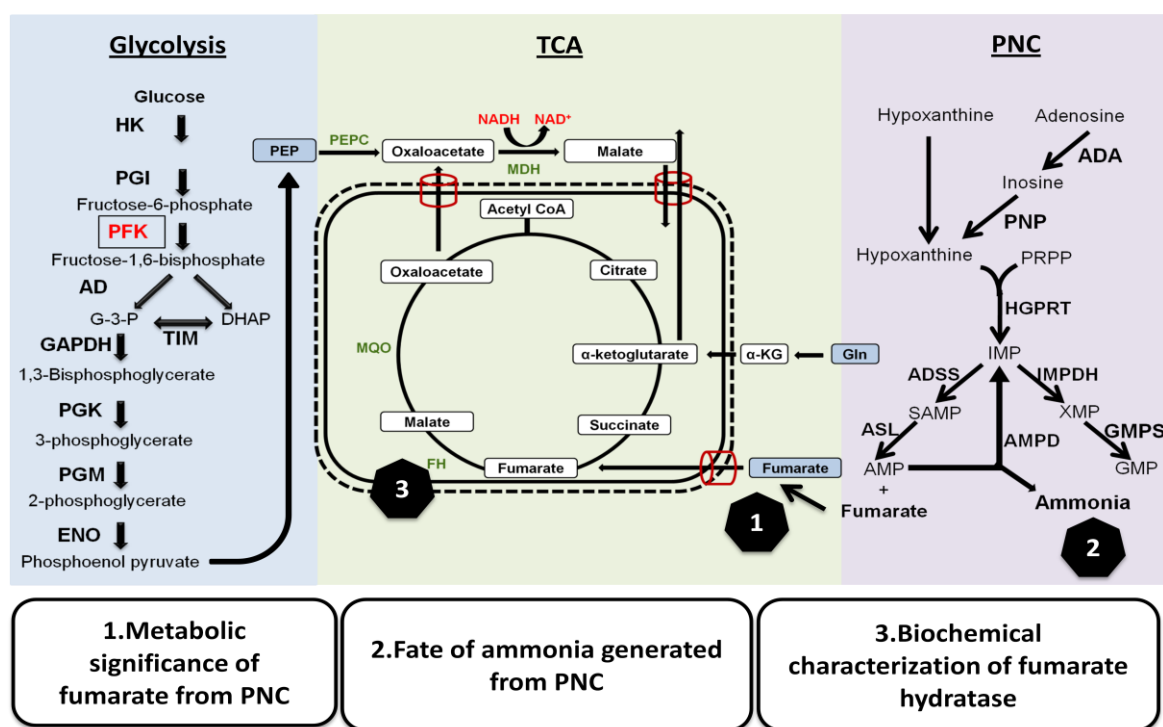


Figure 1.14. Schematic representation of the major objectives of the work addressed in the thesis.

Fumarate hydratase enzyme is present in two biochemically distinct forms. Class I fumarate hydratases are iron-sulfur cluster dependent, oxygen-sensitive enzyme, whereas class II enzyme is an iron-independent, and hence, insensitive to the presence of oxygen. Chapter 5 gives a general introduction to iron-sulfur cluster enzymes and principles of techniques used to study them. *Plasmodium* species has class I enzyme and

the human host has the class II enzyme. Class I enzymes are poorly characterised with regard to the biochemical and structural basis of catalysis. For this, enzyme from two different organisms was characterised; *M. jannaschii* fumarate hydratase discussed in chapter 7 and *P. falciparum* fumarate hydratase discussed in chapter 6. **Figure 1.14** schematically shows the main objectives of the thesis. Chapter 8 provides an overall conclusions derived from the experiments performed and future directions.

Chapter 2

***Probing the metabolic significance of
fumarate generated from PNC by
phenotyping transgenic P.
falciparum expressing yeast adenine
phosphoribosyl transferase (yAPRT)***

Chapter 2

Probing the metabolic significance of fumarate generated from PNC by phenotyping transgenic *P. falciparum* expressing yeast adenine phosphoribosyl transferase (yAPRT)

ABSTRACT

Fumarate is generated from both tricarboxylic acid cycle and from AMP synthesis during the intraerythrocytic growth of P. falciparum. With the presence of the gene encoding AMP deaminase (PF3D7_1329400), a functional purine nucleotide cycle (PNC) could amplify the levels of fumarate. This chapter deals with the study of the metabolic significance of fumarate generated specifically from PNC. Depletion of fumarate by using a small molecule inhibitor of either ADSS/ASL would be lethal to the parasite as this would also lead to depletion of AMP. Engineering an alternate pathway of AMP generation into the parasite followed by inhibition of ADSS/ASL pathway would enable one to selectively deplete fumarate. This would also inform on whether the parasite could survive with alternate modes of AMP generation that are present in other parasitic protozoa. Towards this end, we catalogued purine salvage pathway enzymes across apicomplexan parasites. Thermodynamic parameters of the reactions catalysed by these enzymes were compared and APRT was chosen as the alternate AMP generation pathway. For this, yeast adenine phosphoribosyltransferase (yAPRT) was expressed constitutively in the parasite. Expression of the protein and activity of the enzyme in the parasite was characterised by classic biochemical techniques. Results related to phenotyping of the yAPRT expressing parasite with regards to growth phenotype on different purine sources and upon depletion of fumarate by selective inhibition of ADSS will be presented.

2.1. INTRODUCTION

2.1.1. Metabolic and non-metabolic role of fumarate

Fumarate, an intermediate in TCA cycle, is a unique electrophilic metabolite in central carbon metabolism as it has a carbon-carbon double bond. PEP is the only other metabolite to share this chemical feature. Apart from being generated in TCA cycle, it is also generated in urea cycle and purine nucleotide cycle. There are only a handful of enzymes, catalogued in **Table 2.1**, present that is involved in fumarate metabolism.

Table 2.1. Enzymes that utilise fumarate as a substrate or generate it as a product.
 Enzyme list obtained from EC-Blast (Rahman et al., 2014), using keyword fumarate in the substructure search option. Only enzymes highlighted in green are present in *P. falciparum*.

Enzyme	E.C. No.	Reaction
Aspartate ammonia lyase	4.3.1.1	Aspartate + Water=Fumarate+Ammonia
Fumarate reductase (NADH)	1.3.1.6	Succinate + NAD ⁺ =Fumarate+NADH+H ⁺
Fumarate reductase (CoM/CoB)	1.3.4.1	Fumarate + CoM + CoB = Succinate + CoM-S-S-CoB
Dihydroorotate oxidase	1.3.98.1	(S)-dihydroorotate + Fumarate= Orotate + Succinate
2-hydroxy-6-oxonona-2,4-dienedioate hydrolase	3.7.1.14	(2Z,4E)-2-hydroxy-6-oxonona-2,4-diene-1,9-dioate + Water=(2Z)-2-hydroxypenta-2,4-dienoate + succinate
Succinate dehydrogenase	1.3.5.1	Succinate + Co-factor = Fumarate + reduced co-factor
Fumarate hydratase	4.2.1.2	Fumarate + Water = Malate
Carboxymethyloxy succinate lyase	4.2.99.12	Carboxymethyloxysuccinate + Water = fumarate + glycolate
3-fumarylpyruvate hydrolase	3.7.1.20	Fumarylpyruvate + Water = fumarate + pyruvate
Arginosuccinate lyase	4.3.2.1	Arginosuccinate + Water = Arginine + Fumarate
Adenylosuccinate lyase	4.3.2.2	Adenylosuccinate + Water = AMP + Fumarate
Benzylsuccinate synthase	4.1.99.11	Benzylsuccinate = Toluene + Fumarate
Fumaryl acetoacetase	3.7.1.2	Fumarylacetoacetate + Water= Fumarate + Acetoacetate

In the past decade, this metabolite has gained prominence as it is associated with multiple metabolic and non-metabolic roles in systems ranging from prokaryotes to eukaryotes (including animal and plant systems). Many of the roles of the metabolite are schematically represented in **Figure 2.1**. Due to rapid interconversion of fumarate and malate, by the enzyme fumarate hydratase, distinguishing the metabolic role of fumarate from malate is not trivial. A brief summary of the literature available on physiological role/significance of fumarate is provided below.

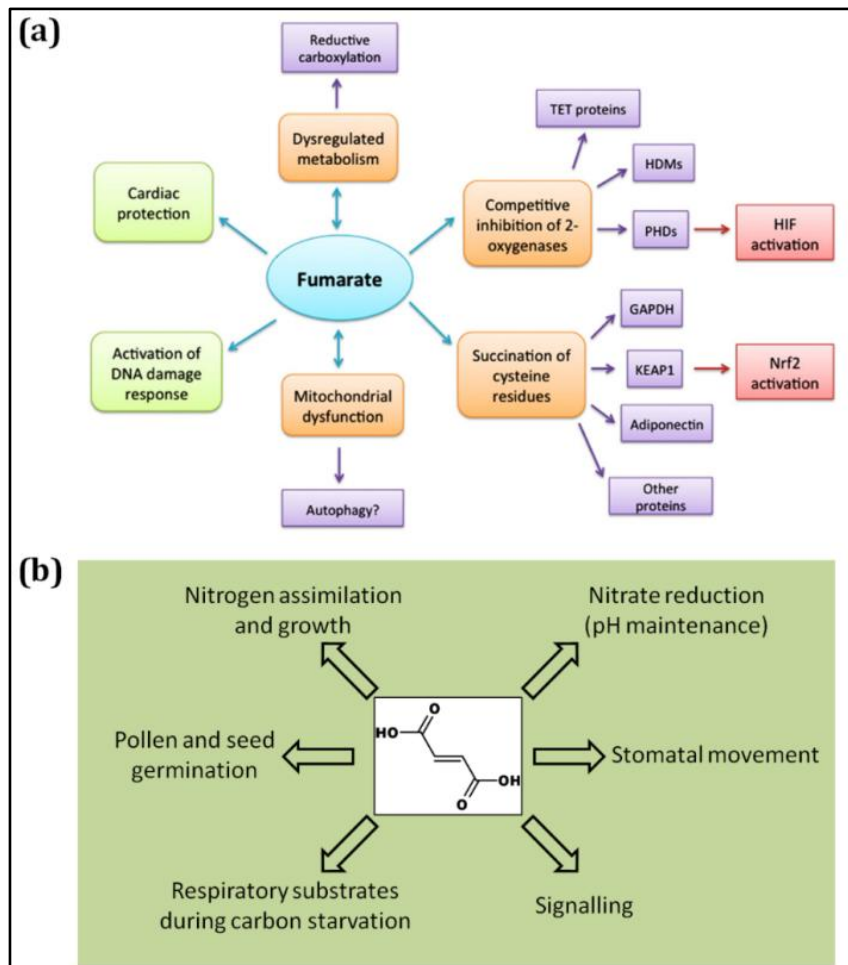


Figure 2.1. The role of fumarate in animal and plant cells.

(a) Schematic representation of molecular consequences of fumarate accumulation (*HIF* activation and *Nrf2* activation) in a cell shown in brown boxes; the functions in green boxes corresponds to the role of fumarate in certain cell types under normal physiological concentrations. **(b)** Collective representation of different physiological roles of fumarate in a plant cell. Panel a reproduced from Yang et al., 2012, Panel b modified and reproduced from Araújo et al., 2011.

In many prokaryotic systems, fumarate is used as a terminal electron acceptor in a process called as fumarate respiration (Kraeger et al., 1992). Fumarate is also known to regulate expression of many genes during the transition of *E. coli* from aerobic to anaerobic conditions (Zientz et al., 1998). Further, this metabolite is also known to be involved in regulation of flagellar motor switching in many bacteria (Barak et al., 1996; Prasad et al., 1998). In plant cells, the metabolite is used as a carbon sink and used during carbon starvation, functionally analogous to how starch is used. Fumarate is found in abundance in photosynthetic parts of plants (Araújo et al., 2011). Fumarate is also known to accumulate in plants grown on nitrate-rich conditions, where the metabolite is known to be involved in pH regulation, nitrogen and nitrate assimilation. Fumarate like malate plays a role in proper functioning of stomatal guard cells and thereby in the optimal

growth rate of plants (Nunes-Nesi et al., 2007). This is further supported by the fact that fast-growing plants accumulate more organic acids—one of the most significant differences seen—compared to slow growing plants (Poorter & Bergkotte 1992).

In animal cells, the physiological effects of fumarate can be divided based on its intracellular concentration. At normal physiological concentration, fumarate can act as an electron sink and support anaerobic respiration just as in prokaryotes (Krager et al., 1992). In exercising skeletal muscles, fumarate produced as a by-product of an upregulated purine nucleotide cycle, can act as an anaplerotic intermediate and sustain the flux of citric acid cycle thereby, catering to high ATP demands of the muscles (Lowenstein and Goodman, 1978). Recent studies have shown that fumarate can act as a cardio- and neuro- protectant by activating nuclear factor (erythroid-derived 2)-like 2 (Nrf2) antioxidant pathway (Linker et al., 2011; Ashrafian et al., 2012). This is achieved by fumarate covalently modifying critical cysteine residues in the protein Keap1 that is involved in ubiquitination and degradation of Nrf2 (Kinch et al., 2011). Further, local production of fumarate in the nucleus is known to promote DNA repair. This is achieved by direct inhibition of KDM2 histone demethylase by fumarate. The methylated histones are known to be a better template for recruitment of the factors involved in non-homologous end joining (NHEJ) - mediated double-stranded DNA break repair pathway (Jiang et al., 2015).

At high concentrations, fumarate can undergo Michael addition with reactive thiols in the cell. Michael addition is a non-enzymatic reaction that involves the addition of a nucleophile (thiol) onto α , β -unsaturated carbonyl compounds such as fumarate. Free reactive thiols can be present in metabolites like glutathione or in active site cysteines residues of certain enzymes; a schematic representation of the reaction involving both is shown in **Figure 2.2**. This covalent addition of fumarate onto a metabolite or a protein thiol is called succination. Succination can result in depletion of critical metabolites like GSH in a cell. Moreover, it can cause inhibition of many enzymes containing reactive cysteines in their active site thereby disturbing cellular homeostasis. Succination of many proteins has been observed in diabetes and obesity and is proposed to be a biomarker for nutrient excess and mitochondrial stress associated with these conditions (Thomas et al., 2012; Frizzell et al., 2009; Bardella et al., 2011).

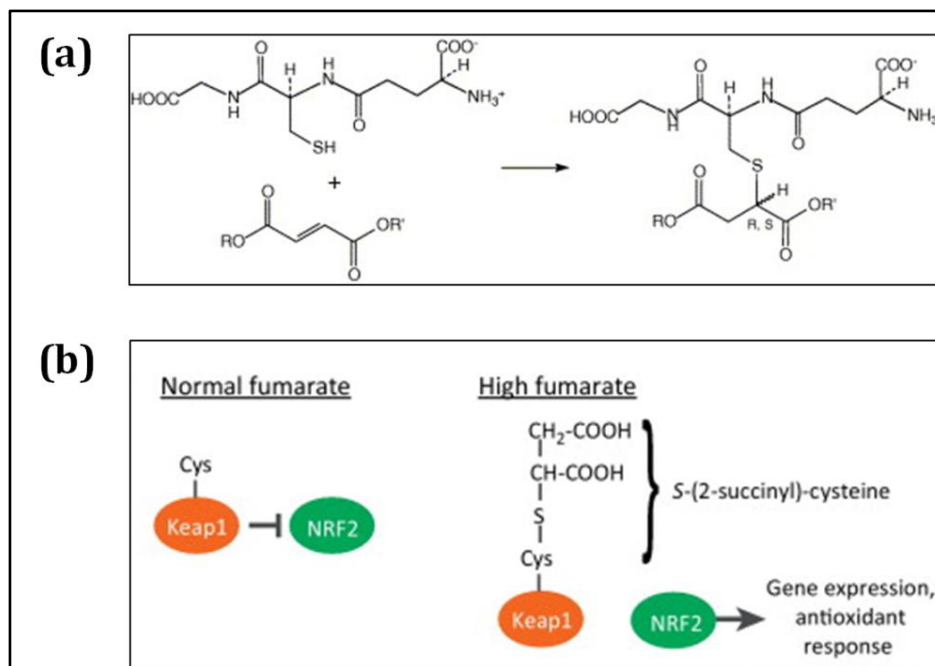


Figure 2.2. Michael addition involving fumarate in physiological conditions.

(a) Reaction showing the Michael addition between glutathione and dialkyl ester of fumarate. The reaction leads to depletion of intracellular concentration of glutathione in a cell. **(b)** Inactivation of Keap1 by succination reaction, thereby leading to activation of the NRF2 dependent antioxidant pathway. Panel (a) reproduced from Schmidt et al., 2007 and panel (b) reproduced from Mullen and DeBerardinis, 2016.

Apart from succination, at high concentrations, fumarate can act as a competitive inhibitor of 2-oxoglutarate dependent oxygenases like the prolyl hydroxylase domain (PHD) (King et al., 2006). PHDs catalyse oxygen-dependent hydroxylation of many critical transcription factors including hypoxia inducible factor-1 α (HIF). Hydroxylation acts as a signal for HIF degradation. Inhibition of PHD by fumarate leads to stabilisation of HIF-1 α that can activate multiple oncogenic pathways. Depletion of fumarate hydratase activity—through hereditary/acquired mutations—leading to accumulation of fumarate, is considered a prognosis for hereditary leiomyomatosis and renal cell cancer (HLRCC) (Tomlinson et al., 2002).

2.1.2. Role of fumarate in *P. falciparum*

Fumarate is generated by two independent pathways during the intraerythrocytic stage of *P. falciparum*; succinate dehydrogenase reaction of TCA cycle in the mitochondria and adenylosuccinate lyase reaction of the purine salvage pathway in the cytosol. Dependence of the parasite growth on TCA cycle is minimal and metabolic tracing experiments using ¹³C-labelled glucose shows very low flux of succinate to fumarate conversion (MacRae et al., 2013). The flux of fumarate generation through ASL reaction is expected to be high as

for every molecule of AMP— an essential molecule generated majorly through this reaction—one molecule of fumarate is also made. An indirect evidence suggesting significant steady-state cytosolic levels of fumarate comes from an experiment where a fumarate dependent-yeast dihydroorotate dehydrogenase was able to completely cater to the pyrimidine requirement of the parasite (Painter et al., 2007). As discussed in section 1.3.3.3 cytosolic malate/fumarate levels is suggested to be significant for maintaining the NAD⁺/NADH balance in the cytosol.

An earlier study performed in our laboratory has shown that fumarate generated in the parasite is not a metabolic waste but is converted through malate and oxaloacetate to aspartate which subsequently gets incorporated into proteins and in DNA as pyrimidines (Bulusu et al., 2011). NMR-based analyses also showed that the metabolite also gets converted to pyruvate through malate, oxaloacetate and phosphoenolpyruvate. Further, pyruvate formed is also converted by PflDH to lactate. A significant finding of the study was the dependence of fumarate metabolism on mitochondrial membrane potential at the step of MQO. This necessitates the transport of fumarate into and oxaloacetate out of the mitochondrial membrane for further metabolism. Malate-oxoglutarate/dicarboxylate transporter could be potential transporters involved in this processes.

2.2. OBJECTIVE AND STRATEGY

With a multitude of roles assigned to fumarate in different organisms, coupled with the finding that fumarate produced in *P. falciparum* is not a waste but is metabolised to different other intermediates raises the question on how important is fumarate metabolism to the parasite; specifically, the significance of fumarate generated by the adenylosuccinate reaction. Interfering with the function of the ASL enzyme to deplete the fumarate generated, would also deplete AMP levels thereby killing the parasite. By expressing an alternate AMP generating enzyme, we could potentially uncouple AMP and fumarate production following which fumarate could be selectively depleted by inhibition of either ADSS/ASL. This would also inform us on whether the parasite could survive with enzymes having alternate modes of AMP generation.

2.3. MATERIALS AND METHODS

2.3.1. Molecular biology reagents and chemicals

Regular cloning procedures related to plasmid DNA isolation, PCR product purification, and gel extraction were performed with kits procured from Qiagen, Germany. Plasmid DNA for *P. falciparum* transfection was prepared using Endofree-Plasmid Maxi kit from Qiagen, Germany. Oligonucleotides were custom synthesised from Sigma-Aldrich,

Bangalore. APRT null *E. coli* strain, JW0458-2 ($\Delta apt-754::kan$), was procured from Coli Genetic Stock Centre (CGSC), Yale, USA. 3D7 strain of *P. falciparum* was procured from Malaria Research and Reference Reagent Resource Center (MR4), USA. Centromere based plasmid pFCEN1 was a kind gift from Prof. Masao Yuda, Mie University, Japan. Plasmid pQE30 was procured from Qiagen, USA. Unless otherwise specified all chemicals used were of high quality and procured from Sigma-Aldrich, USA

Table 2.2. Sequences of primers used for cloning yAPRT in pET21b, pQE30 and pFCEN1.

S.NO	Primer name	Sequence (5' to 3')
1	Apt1FP_BamH1	CGCGGATCCTCTATAGCAAGTTATGCCCAAGAGTTG
2	Apt1RP_Sal1	ACGCGTCTGACTCATTTCATTTTCAACGCTTCCTTTTGAG
3	AptF_Bmt1	CTAGCTAGCTCTATAGCAAGTTATGCCCAAGAGTTG
4	AptR_BglII	AGCAGATCTTCATTTCATTTTCAACGCTTCCTTTTGAG

2.3.2. Bioinformatic analysis

To catalogue the purine salvage pathway enzyme in different parasites, BlastP tool (McGinnis and Madden, 2004) was used. Query sequences used for each enzyme are mentioned in the results section. The thermodynamic parameters for each of the reactions of the purine salvage pathway were obtained using eQuilibrator tool (Flamholz et al., 2012).

2.3.3. Cloning, expression and purification of yeast adenine phosphoribosyl transferase (yAPRT)

DNA corresponding to the coding sequence of yAPRT was amplified using *Saccharomyces cerevisiae* genomic DNA as template and primers 1 and 2 (Table 2.2). The gene was cloned in the vector pQE30 and pET21b using *BamHI* and *Sall* restriction sites. The protein will carry an N-terminal (HIS)₆-tag when expressed from pQE30 and pET21b. For recombinant protein expression, codon plus RIL strain was transformed with the pET21b-yAPRT plasmid. The cells were selected using ampicillin and chloramphenicol containing LB plate. Multiple colonies were used for inoculating into a 10 ml LB broth and grown overnight at 37 °C. 4 ml of the overnight culture was used as a pre-inoculum for scaling up the culture. For large scale culturing, 800 ml terrific broth in a 2L conical flask was used. Subsequent to inoculation, the flask was shaken at 180 rpm at 37 °C until the cells reached an OD₆₀₀ of 0.4-0.5. For pre-chilling, the cells were grown for 20 minutes at 18 °C. yAPRT expression was induced by addition of isopropyl thiogalactoside (IPTG) to a final concentration of 300 μM. The cells were grown for 18 hours after which they were

pelleted by centrifugation at 6000 x g. The cells were flash frozen and stored at -80 °C until further use.

For purification, the cell pellets were thawed at 4 °C in the lysis buffer containing 50 mM Tris-HCl, pH 7.4, 10% glycerol, 150 mM NaCl, 1 mM PMSF and 1 mM DTT. The cells were resuspended thoroughly to break all clumps and lysed by passing the slurry through 5 rounds of mechanical pressure in a French press. The lysate was clarified of the cell debris by centrifugation at 30000 x g. The supernatant was incubated with pre-equilibrated Ni-NTA sepharose beads for 2 h at 4 °C. The beads containing the bound protein were transferred to a glass column and washed with 50 column volumes each of lysis buffer and 5 mM imidazole containing lysis buffer to remove contaminating proteins that are non-specifically stuck to the beads. yAPRT was eluted with 1 ml each of increasing concentration of buffered imidazole (100 mM, 200 mM, 500 mM and 1 M). The eluted protein was analysed using SDS-PAGE. The protein was further purified by size-exclusion chromatography using Superdex 250. The column was equilibrated with a buffer containing 50 mM Tris-HCl, 1 mM DTT and 10% glycerol. 1.5 ml of protein solution eluted from Ni-NTA column was injected and allowed to separate at a flow rate of 1ml min⁻¹. The eluate from the column was monitored at a wavelength of 280 nm. The fractions corresponding to protein were collected peak wise and analysed using SDS-PAGE. The fractions corresponding to pure protein were pooled and used for further studies.

2.3.4. Antibody generation and purification

Pure protein obtained after size-exclusion chromatography was used for generation of antibody. New Zealand white rabbit was used for the generation of antibody. The immunisation regimen followed is given in **Table 2.3**.

Table 2.3. Immunisation regimen in rabbit using purified yAPRT as antigen

S.No	Day	Schedule	Amount of antigen (yAPRT)
1	0	Pre- immune sera collection	-
2	0	1° immunization-subcutaneous injection	500 µl protein (1 µg/µl)+ 500 µl Freund's complete adjuvant
3	14	Primary booster	500 µl protein (1 µg/µl)+ 500 µl Freund's incomplete adjuvant
4	28	Secondary booster	500 µl protein (1 µg/µl)+ 500 µl Freund's incomplete adjuvant
5	35	Test bleed	-
6	37	Major bleed	-

After the major bleed, the blood collected was allowed to clot overnight at 4 °C. The serum was carefully removed to avoid any carryover of cells. The serum was centrifuged

at high speed to remove any cellular components and debris. The supernatant was aliquoted into microcentrifuge tubes and stored frozen at -20 °C. For purification of antigen-specific antibody, the strip affinity protocol was followed. Briefly, the purified protein was subjected to SDS-PAGE and thereafter the protein on the gel was transferred onto a PVDF blot by electrophoresis. The blot was stained with Ponceau-S and the membrane containing the protein bands were selectively cut. The pieces of membrane were blocked overnight at 4 °C with 5 % skimmed milk solution made in PBS. The membrane pieces were incubated with the serum overnight at 4 °C and washed with 0.1% Tween20 solution in PBS. The bound antibody was eluted using 100 mM Tris-glycine buffer, pH 2.5 and immediately neutralised using 1 M Tris-HCl, pH 8. This elution was repeated three times and all the eluates were pooled and concentrated using centrifugal concentrators with a molecular weight cut-off of 10 kDa.

2.3.5. Western blot analysis of parasite proteins

Western blotting of proteins from parasite lysate can be difficult as the parasites contain a large amount of proteases that can degrade the protein of our interest if the samples are not handled and processed properly. In order to rule out the erythrocyte protein contamination, it is always recommended to extract proteins from erythrocyte lysate and use it as a control. Apart from this, other positive controls such as the relevant purified recombinant proteins were also used.

The parasite pellet stored in -80°C freezer or prepared freshly was used for Western blotting. 5 µl of protease cocktail inhibitor (Sigma-Aldrich, catalog# P8340) was added to 50-200 µl of parasite pellet immediately after removing it from the freezer or to a fresh pellet. An appropriate volume of SDS-loading dye solution was added and mixed well to solubilize the extracted proteins. The tube was placed in boiling water bath for 10 min. The lysate was centrifuged at 16000 x g for 15 min at room temperature. The supernatant was removed and transferred to a new tube and used for SDS-PAGE. For processing erythrocytes, 100 µl of 50% erythrocyte suspension was mixed with 300 µl of SDS-PAGE loading dye, the mixture was boiled for 10 min and then centrifuged at 16000 x g for 15 min at 25 °C.

The parasite and erythrocyte proteins were separated on a 10% SDS-PAGE gel. The PVDF membrane used for the transfer was activated by incubating the membrane in 100% methanol for 10 min. The gel was sandwiched along with the activated PVDF membrane between blotting pads that were wetted with the semi-dry transfer buffer that contains 24 mM Tris-HCl, 192 mM glycine, and 20% methanol. The transfer was done for 30 min at a constant current of 2 Amp and 25 Volts. After the transfer, the membrane was blocked with 5% (w/v) skim-milk solution made in PBS for 1 h at room temperature with

rocking. Appropriate dilution of primary antibody solution was added and incubated for 3h on a rocker. The blot was washed 3-4 times with PBS containing 0.1% Tween 20 (USB chemicals, 20605), with each wash for 10 min. Subsequently, the blot was incubated with a secondary antibody that is HRP conjugated and incubated for 3 h at room temperature on a rocker. The blot was thereafter washed with the wash buffer and developed using the developing buffer containing the colouring agent 3-amino-9-ethylcarbazole that forms a coloured product when acted upon by the enzyme horseradish peroxidase (HRP). The developing solution was made in 25 ml of PBS by adding 1ml of DMF containing 20 mg of the colouring agent, 833 μ l of 3 M sodium acetate, pH 5.2, and finally 50 μ l of hydrogen peroxide.

2.3.6. *In vitro* culture of *Plasmodium falciparum*

2.3.6.1. Composition and preparation of complete culture media

The complete medium for *in vitro* culturing of *P. falciparum* contains Roswell Park Memorial Institute medium-1640 (RPMI-1640) buffered with 4-(2-hydroxyethyl)-1-piperazineethanesulfonic acid (HEPES), sodium bicarbonate and Albumax I, a lipid-rich bovine serum albumin (a serum supplement). Additionally, the culture medium also contains glucose (carbon source), hypoxanthine (purine requirement), and Gentamycin (to avoid bacterial contamination). The exact composition of the complete medium is as given in **Table 2.4**.

A mixture containing RPMI-1640 and HEPES was prepared by dissolving appropriate amounts in autoclaved MilliQ water. The mixture was sterilised by filtration through NALGENE disposable Rapid flow filter (0.2 μ M) using a vacuum pump. Gentamicin was added to this mixture and the solution was stored at 4°C for a maximum period of 40 days. Albumax I, a lyophilized powder was added to autoclaved MilliQ water and incubated at 37 °C for at least 2 h to aid in complete solubilization. The viscous solution was filtered using a NALGENE Rapid flow filter, Thermo Scientific and aliquots of 50 ml made in sterile Falcon tubes were stored at 4 °C. 50 mM hypoxanthine stock solution was made by dissolving the powder in 125 mM NaOH and sterilised by filtration. Stock solutions of all other components were prepared in autoclaved MilliQ water, sterilised by filtration using 0.2 μ m syringe filter and stored at 4°C for a maximum period of 60 days.

Table 2.4. Composition of complete medium for *P. falciparum* in-vitro culture

S.No	Component name	Company/catalog no.	For 500 ml complete media
1	RPMI-1640	Sigma, R6504	5.2 g
2	HEPES, free acid	Sigma, H3375	2.97 g
3	Sodium bicarbonate	Sigma, S5761	20 ml (5% stock)
4	Albumax-I	Thermo Fisher scientific, 11020-021	25 ml(10% stock)
5	Hypoxanthine	Sigma, H9377	1ml (50 mM stock)
6	Glucose	Sigma, G5400	22.5 ml (10%stock)
7	Gentamycin	Abbott chemicals	500 µL or 40 mg/L

For the preparation of complete medium, all the individual components were transferred from 4 °C to 37 °C incubator and allowed to warm for at least 20 min. Once the components had warmed, the required amount of RPMI-HEPES mixture was transferred to a sterile glass reagent bottle followed by the addition of a mixture containing Albumax I, glucose, sodium bicarbonate, and hypoxanthine. The mixture was subjected to another round of filter sterilisation using 0.2 µm syringe filters. This complete medium was divided into small aliquots (50-200 ml) and stored at 4 °C for a maximum period of 7 days and pre-warmed at 37 °C before addition to *Plasmodium* culture. If this medium turned pink (due to CO₂ solubilization), it is not suitable for use in the culture and hence, discarded. To avoid/minimise this, the complete medium was stored in appropriate glass reagent bottles with a minimal headspace.

2.3.6.2. Processing of human erythrocytes (O⁺ and A⁺) for *in vitro* culturing of *P. falciparum*

Human erythrocytes from voluntary donors were collected following the institutional ethical norms. Both O⁺ and A⁺ erythrocytes were used for *in vitro* culturing of the parasite. 10/20 ml of the whole blood from healthy donors was collected in a 100 ml reagent bottle containing either 25/50 ml of acid-citrate-dextrose (ACD) buffer. 25 ml of ACD buffer contains 512.5 mg of glucose (Sigma-Aldrich, cat: G5400), 0.2 g of sodium citrate dihydrate (Sigma-Aldrich, cat: W302600), citric acid (Sigma-Aldrich chemicals, USA, cat: 251275), and sodium chloride (Sigma-Aldrich, cat: S9888). Immediately after collection of blood into the buffer, the bottle was swirled gently and stored at 8 °C for a maximum of 4-6 h. The blood was warmed to room temperature and the supernatant containing serum and the buffer was removed without disturbing the settled erythrocytes. The erythrocytes

were then suspended in PBS and aliquoted in multiple 15 ml conical Falcon tubes. The Falcons were then centrifuged at 800 x g using a REMI R8C centrifuge with a swing-out rotor for 5 min. After centrifugation, the leukocytes and other cell types that are lighter than erythrocytes form a thin, white layer (Buffy coat) on the top of the erythrocyte pellet. The supernatant was removed carefully along with the Buffy coat with minimal disturbance to the erythrocyte pellet. The erythrocyte pellet was washed with 2 volumes of PBS and supernatant removed. The resultant pellet was resuspended in equal volume of incomplete medium (complete medium without Albumax) and stored at 4 °C for a maximum period of 2 weeks.

2.3.6.3. Regular maintenance of *Plasmodium* culture

P. falciparum is a microaerophilic organism and is grown *in vitro* by the method established by Trager and Jensen (Trager and Jensen, 1976). Briefly, 5% hematocrit was maintained in the final culture and parasitemia was maintained between 0.5-4 %. Parasites were either thawed freshly from glycerol stock or were taken from the ongoing culture and expanded with fresh erythrocytes, such that the parasitemia does not exceed 4% and hematocrit 5%. On a regular basis, a 5 ml culture was maintained in a glass vial with a flat base and a loose lid and kept inside a candle jar with a candle kept lighted to remove oxygen, thus creating a microaerophilic condition. The lid of the jar was then slid over the body to close it tightly. Vacuum grease (Metroark 211 compound, Wacker chemicals) was applied to keep the jar airtight. Alternatively, the culture was also maintained in T75 flasks flushed with the gas mix (90% nitrogen, 5% carbon dioxide, and 5% oxygen). In both the methods, the spent medium was removed every day and replaced with fresh medium. Parasitemia was monitored by making a Giemsa-stained smear every alternate day.

Techniques for *P. falciparum* culture manipulation

2.3.6.4. Synchronisation of *P. falciparum* culture

P. falciparum asexual stages can be synchronised at either the ring stage (0-24 h post-invasion) using the sorbitol method or at the trophozoite/schizont stage (38-46 h post-invasion) using percoll gradient centrifugation. Mature asexual stages like trophozoites and schizonts have increased permeability to D-sorbitol because of up-regulation of new permeability pathways. This permeability results in lysis of the mature infected RBC's but not those with ring stage parasites.

In the sorbitol method, the parasite pellet, from 5/10 ml of 5% hematocrit culture predominantly with ring stage parasites, was mixed gently with 5 volumes of sterile 5%

sorbitol solution (0.5 g of D-sorbitol, catalogue No. S-1876, Sigma-Aldrich, dissolved in autoclaved MilliQ water and sterilized by filtration through a 0.2 µm syringe filter) and incubated for 5 min. The mature stages lyse during this time and the ring stages and uninfected erythrocytes were then recovered by centrifugation at 800 x g. The pellet was then washed with PBS and then again with the incomplete medium. The final pellet was resuspended in complete medium to attain 5% hematocrit. The procedure was repeated 48 h later in the next round of ring stage culture to attain a tighter synchronisation window.

2.3.6.5. Percoll enrichment of late stages of *P. falciparum*

Percoll (catalog# 17-0891-01) procured from Pharmacia Biotech AB, Uppsala, Sweden, is a density gradient media made of 23% w/w of colloidal silica coated with polyvinylpyrrolidone, in water. It can create a solution with a maximum density of 1.2 g/ml. The density gradient of percoll can be used to separate cells based on their mass. The density of the mature stages of the infected erythrocyte is greatly reduced, especially during the late trophozoite/schizont stage. This difference in density can be exploited to separate the mature stage from other asexual stages and uninfected erythrocytes (Rivadeneira et al., 1983). The percentage enrichment of schizont stages that can be achieved using percoll can be up to 80%.

A 90% percoll suspension was prepared by mixing 1ml of 10 X PBS and 9 ml of percoll. To this, 2.5 ml of PBS was added to get a 70% percoll suspension. The suspension was filtered using a 0.45 µm syringe filter. 40 ml culture containing predominantly late trophozoite/schizont stages is washed once with PBS and then a 10% suspension of cells was made using PBS. The cell suspension was carefully and slowly layered over the percoll in a 50 ml Falcon. The tube was then centrifuged at 800 x g for 30 min at room temperature after which, a distinct layer of hemozoin and another layer of late stage parasites are formed. The hemozoin band was removed and the parasite layer is collected in a fresh tube and washed with PBS. The cells were washed with incomplete medium and then used for further experiments.

2.3.6.6. Isolation of free parasites from infected erythrocytes using saponin treatment

For many applications related to only the parasite compartment, it is often necessary to isolate free parasites devoid of their host RBC components. Saponin lysis is the preferred method of choice. Saponins are amphipathic glycosides that interact with cholesterol in membranes and form pores thereby lysing most of the mammalian cell membranes.

Cholesterol poor plasmodium membranes are resistant to the saponin treatment and hence can be selectively enriched using this reagent (Christophers & Fulton 1939).

Parasite culture with predominantly trophozoite stages was subjected to saponin treatment. 0.15% of saponin solution was prepared by dissolving 15 mg of saponin (Sigma-Aldrich, Catalogue No. S-1252) in 10 ml of PBS. 2 volumes of this solution was added to 1 volume of culture pellet and incubated at room temperature for 4-5 min. The reaction was terminated by adding an excess of PBS. This results in almost complete lysis of the erythrocyte compartment. The solution was centrifuged at 1600 x g for 15 min in a REMI (RC8) centrifuge with a swing out rotor. After centrifugation, a black pellet of parasites along with some uninfected erythrocytes was obtained. The pellet was resuspended with 0.015% of saponin solution in PBS and centrifuged at 1600 x g for 15 min. We have observed that this additional wash step improves the parasite enrichment and ensures complete lysis of erythrocytes. The quality of the preparation can be checked using a Giemsa smear. The pellet was flash frozen in liquid nitrogen and stored at -80 °C or used directly.

2.3.6.7. Cryopreservation and revival of *P. falciparum* asexual stage cultures

For parasite cryopreservation, Stockholm sorbitol method (Lambros and Vanderberg, 1979) was used. 4-5 ml of parasite culture with 5% hematocrit, 3-10% parasitemia in predominantly ring stage is preferred. The culture was pelleted (pellet volume, approximately 0.2 ml) by centrifugation at 800 x g for 2-3 min at room temperature. The supernatant was removed and 0.3 ml of fetal bovine serum was added dropwise with gentle resuspension, by rocking the tube gently with hand, after every few drops. The cell suspension (now 40% hematocrit) was now mixed slowly, drop by drop, with 0.5 ml parasite freezing medium (28% glycerol, 3% sorbitol, and 0.65% NaCl). To make 250 ml of freezing medium, 180 ml of 4.2% sorbitol in 0.9% NaCl was mixed with 70 ml glycerol. The solution was filter sterilised and stored at 4 °C for up to 6 months. The addition of freezing medium should take around 1 min. The cell suspension was transferred to a sterile cryovial, the cap screwed tightly and the vial stored in liquid nitrogen until further use.

The frozen stock was revived by thawing with NaCl solution. For this, two different concentrations, 1.6% and 12% of sodium chloride solutions were used. The frozen vial was removed from the liquid nitrogen tank and thawed at 37 °C for 1 to 2 min. The cell suspension was transferred to sterile 50 ml centrifugal tubes. 0.1 volumes of 12% NaCl solution was added dropwise while swirling the tube. The tube was left to stand at room temperature for 5 min. 10 volumes of 1.6% sodium chloride solution was added slowly while swirling the tube simultaneously. The suspension was centrifuged at 500 x g

for 5 min at room temperature. The supernatant was removed and 10 volumes of complete medium were added dropwise while swirling the tube. The suspension was again centrifuged at 500 x g for 5 min. The supernatant containing lysed erythrocytes (both infected and uninfected) was removed and the cell pellet was resuspended in appropriate volume of complete medium for continuous *in vitro* culturing.

2.3.6.8. Genomic DNA isolation

Isolation of genomic DNA from parasites involves saponin lysis of infected erythrocytes to release free parasites and then a routine procedure based on phenol-chloroform extraction is followed. 40 ml culture (5% hematocrit) with 8-10% parasitemia is good for a high-yield of genomic DNA. Free parasite pellet was obtained from the culture using saponin lysis as described in section 2.4.3. The parasite pellet was either flash frozen in liquid nitrogen and stored at -80 °C for later use or directly used for genomic DNA isolation. In either case, the parasite pellet is resuspended in 1/100th the original culture volume in Tris-ethylenediaminetetraacetic acid (TE) buffer (10 mM Tris-HCl and 1 mM EDTA, pH 8.0). Proteinase K to a final concentration of 20 µg/ml and sodium dodecyl sulphate (SDS) to a final concentration of 0.5%, were added. The solution was mixed by gently inverting the tube, so as not to shear the genomic DNA. All the mixing steps were done gently and cut tips were used wherever possible. The mixture was incubated at 56-65 °C for 6-10 h. 1 volume of Tris-saturated phenol (should be yellow in colour) and 1 volume of chloroform were added to this solution. The tubes were inverted repeatedly for approximately 10 min until a clear separation of organic and aqueous phase is obtained. The tubes were centrifuged at 15000 x g for 5 min at room temperature.

The aqueous phase was transferred to a new tube without disturbing the interface and phenol-chloroform extraction was repeated. The final aqueous phase was mixed gently with 1 volume of chloroform for 5 min and centrifuged at 15000 x g for 5 min. The aqueous phase was transferred to a new tube and 1/10th volume of 3 M sodium acetate, pH 4.5 and 2.5 volumes of 100% ethanol were added and mixed well. The solution can be incubated at -20 °C freezer for at least 1 h to enhance the precipitation of DNA. The tubes were centrifuged at 15000 x g for 5 min. The supernatant was discarded and pellet washed with 500-1000 µl of 70% ice-cold ethanol, vortexed and centrifuged at 15000 x g for 5 min. The supernatant was discarded and the pellet air-dried by placing the tube in a dry bath set at 65 °C for 3-5 min. The dried DNA pellet was dissolved in 50-100 µl of TE, pH 8.0. The quality of the isolated genomic DNA was checked by electrophoresis on a 0.6% agarose gel.

Imaging techniques

2.3.6.9. Enumeration of parasitemia using microscopy

For routine parasite culture maintenance, the parasitemia was estimated every alternate day. This is done by Giemsa staining a thin smear of parasite culture and observing them under a light microscope. Giemsa staining solution (a mixture of methylene blue, eosin, and Azure B), stains the parasite differentially as it has a nucleus, unlike the host erythrocyte. For this, a 50 µl aliquot of the culture was centrifuged at 800 x g for 1 min. The pellet was resuspended in the small volume of spent media and a drop of this suspension was placed on a glass slide. A smear was made, air dried and fixed using methanol. The smear was layered with Giemsa staining solution and incubated for 5 min. The staining solution was prepared by mixing 300 µl of Giemsa staining solution with 900 µl Giemsa buffer. Giemsa buffer was prepared by dissolving 0.11 g of disodium hydrogen phosphate and 0.07 g of potassium dihydrogen phosphate in 100 ml water. The smear was washed to remove the staining solution and then observed under light microscope. For parasitemia estimation, infected erythrocytes in around 1000 erythrocytes were counted.

2.3.6.10. Indirect immunofluorescence of asexual stages of *P. falciparum*

0.5 ml of parasitized erythrocytes (5% hematocrit) was washed with PBS and the cells were fixed by resuspending in a solution containing 4% paraformaldehyde (cat) and 0.0075% glutaraldehyde (cat) for 30 minutes. The paraformaldehyde solution was made freshly before use. For this, 4 mg of paraformaldehyde powder was dissolved in 600 µl of PBS and then the tube was heated in hot water (60-70 °C) until the powder dissolved. The volume was made up to 1 ml with PBS. After incubation for 30 minutes, the cells were pelleted and washed with PBS. The cells were permeabilized by resuspension and incubation in a solution containing 0.1% TritonX-100 (USB chemicals, 22686) for 8-9 min. The cells were then washed with 500 µl of PBS twice and incubated with a 3% bovine serum albumin (BSA) solution prepared in PBS. The primary antibody of a required titre was added to the solution and incubated for 1 h at 25 °C. The cells were then washed with 500 µl of PBS three times, 10 min each. The secondary antibody of the required titre was added and cells were incubated in this solution for 1 hour in the dark. The cells were thereafter washed three times with PBS, with each wash lasting 10 minutes. Appropriate concentration of 4',6-diamidino-2-phenylindole (DAPI) (cat) or 2,5'-Bi-1H-benzimidazole, 2'-(4-ethoxyphenyl)-5-(4-methyl-1-piperazinyl) (Hoescht) (cat) was added and incubated for 10 minutes in the dark. The cells were washed again with PBS. A thick cell suspension

in PBS was made and 4 μ l of this suspension was used to prepare the slides as mentioned in the live cell microscopy section. The slides were imaged using a confocal microscope.

2.3.6.11. Live cell imaging of *P. falciparum* culture

Recombinant parasites in which a fluorescent tag is attached to the protein of interest, for analysis such as protein localisation, expression levels etc., are monitored using live cell microscopy. For this 100 μ l parasite culture (5% hematocrit) was centrifuged and the pellet resuspended in a small amount of the supernatant (typically 5-10 μ l). 4 μ l of the cell suspension is placed on a cover slip and the cover slip with cells was inverted over onto a glass slide slowly such that the suspension spreads to cover the entire area of the coverslip leaving no air bubbles. The cover slip was glued to the slide and immediately used for acquiring images.

2.3.7. Transfection of *P. falciparum*

Transfection of the parasites in asexual stages was done either by preloading the uninfected erythrocytes by electroporation with the plasmid of interest and then infecting them with the mature stage parasite culture or by direct electroporation of the plasmid of interest in the ring stage of the culture. In both cases, electroporation was done by using BioRad Gene Pulser Xcell (catalogue # 165-2660) using either the square wave or the exponential pulse protocol. The schematic representation of different methods is shown in **Figure 2.3**.

2.3.7.1. Preloading of plasmid DNA into uninfected erythrocytes by electroporation

0.5 ml of 50% erythrocyte suspension was used for each electroporation. The cells were washed with 5 ml of cytomix that is pre-warmed to room temperature, to remove the incomplete media completely. Cytomix is a solution containing a mixture of salts that is optimised for *P. falciparum* electroporation. Cytomix consists of 120 mM KCl, 0.15 mM CaCl₂, 2 mM EGTA, 5 mM MgCl₂, 10 mM K₂HPO₄/KH₂PO₄, pH 7.6, 25 mM HEPES, pH 7.6. For 100 ml of cytomix, 6 ml of 2 M KCl, 7.5 μ l of 2 M CaCl₂, 1 ml of 1 M K₂HPO₄/KH₂PO₄, pH 7.6 (for 10 ml of 1 M phosphate buffer, pH 7.6, mix 8.66 ml of 1 M K₂HPO₄ and 1.34 ml of 1 M KH₂PO₄), 10 ml of 250 mM HEPES/20 mM EGTA, pH 7.6 (pH to 7.6 using KOH), and 0.5 ml of 1 M MgCl₂ were mixed and made up to near 100 ml using MilliQ water. The pH was finally adjusted to 7.6 using 5/10 M KOH and volume made up to 100 ml. The solution was filter sterilised and stored at 4°C. This solution can be kept for 2-3 months. The washed erythrocytes were resuspended in cytomix, mixed with DNA and volume made up to 350-400 μ l with cytomix. A 2 mm electroporation cuvette was chilled for 30 min on ice

and the mixture containing the DNA and erythrocytes was transferred to the cuvette and kept on ice for at least 5 min. For electroporation using BioRad gene pulser, an exponential decay program set to 0.31 kV and 950 μ F was used. After electroporation, the time constant was noted and for a successful electroporation, it should be between 12-20 ms. The square wave pulse protocol when used was performed with 8 square-wave pulses of 365 V for 1 ms, separated by 100 ms. The contents of the cuvette were now transferred to a culture vial and excess complete medium of around 20 ml was added. After about 4 h the spent medium was removed along with lysed erythrocytes and replaced with fresh media. 1 ml healthy parasite culture, preferably in schizont stage (4-6% parasitemia) was added to this erythrocyte suspension and drug pressure applied after 48 h.

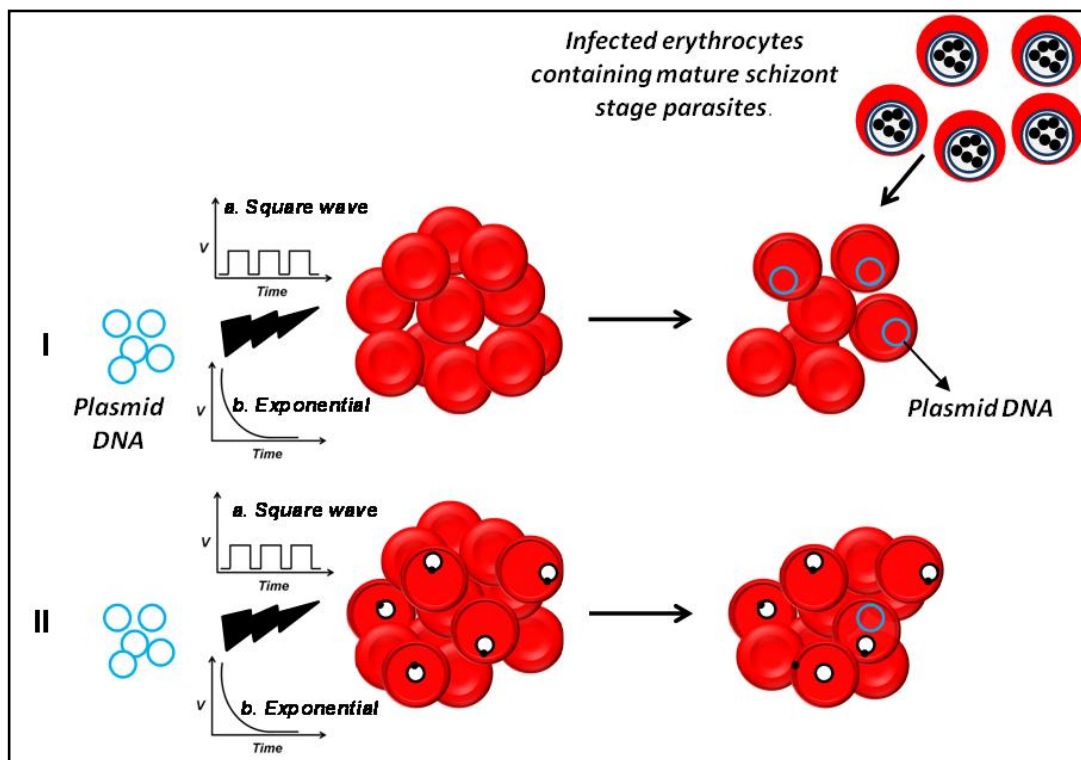


Figure 2.3. Transfection of *P. falciparum* asexual stages by electroporation.

I. The scheme describes the preloading method of transfection wherein, the uninfected red blood cells (uRBCs) are electroporated with plasmid DNA and mature stage parasite culture is added thereafter. **II.** The ring stages are directly used for transfection. In both the cases either square-wave or exponential decay pulse program can be used.

2.3.7.2. Direct electroporation of plasmid DNA into ring stage parasites

Direct electroporation of the asexual stages was done using a healthy ring stage culture (preferably mid-ring) with parasitemia around 8-10%. 5 ml culture was used for every electroporation. The cells were washed with 5 ml of cytomix and 75-100 μ g of DNA was

added to these cells and volume made up to 300-400 μl with cytomix. The sample was processed in a manner similar to that mentioned for the preloading method. Either square wave or exponential decay pulse was used. After electroporation, the cells were washed with pre-warmed complete medium and then transferred to the candle jar. The medium was changed twice within a span of 8 h to ensure removal of lysed cells. Fresh erythrocytes were added to the culture after 12 h to allow for reinvasion to happen. Drug selection was started after 48 h of electroporation.

2.3.8. 2-Fluoroadenine inhibition of WT and *Aprt* *E. coli* strains

JW0458-2 strain of *E. coli* with the copy of *Aprt* gene deleted (*Aprt*KO) was transformed with either pQE30 plasmid or the plasmid expressing yAPRT and the strains were denoted *Aprt*KO+pQE30 and *Aprt*KO + yAPRT respectively. The strains were selected on LB plate with both kanamycin and ampicillin. A single colony was picked and grown in 10 ml LB broth overnight. An equal number of cells, as ascertained by OD_{600} , were added to LB media containing different purine source with/without 2-fluoroadenine. The growth was monitored continuously and data from the time point representing the maximal change in growth phenotype is presented. For rescue experiments, involving relieving of inhibition by 2-fluoroadenine, adenine/hypoxanthine was added into the culture.

2.3.9. *In vitro* activity of yAPRT

In vitro activity of the recombinantly purified yAPRT was checked spectrophotometrically at 256nm ($\Delta\epsilon = 2.13 \text{ mM}^{-1}\text{cm}^{-1}$) in a 1 cm quartz cuvette. The reaction was performed in 100 mM Tris-HCl, pH 7.4 containing 100 μM of adenine, 500 μM of PRPP, and 10 mM of MgCl_2 in a final volume of 400 μl . The reaction was initiated by the addition of 0.6 ng of enzyme.

For checking the activity of the yAPRT in the parasite lysate, saponin pellets of both wild-type and yAPRT expressing *P. falciparum* strains were prepared and lysed by freeze-thawing. The lysate was dialysed extensively to remove small molecules. The protein content was normalised by using Bradford method (Bradford, 1976) and an equal amount of protein, from both the lysates, was used for the activity measurements. The assay was performed using the lysate, with adenine and PRPP as substrates and incubated for 2 h at 37°C. The protein was removed by TCA precipitation and the neutralised supernatant was injected into the C18 column. 4 mM tetrabutylammonium hydrogen sulphate was used as ion pairing agent. 50 mM sodium phosphate buffer, pH 6.2 was used as the equilibration buffer and the same buffer with 50% acetonitrile was used for gradient elution.

2.3.10. *In vivo* activity of yAPRT in *P. falciparum*

Susceptibility to 2-FA was used as a probe to qualitatively evaluate the *in vivo* activity of yAPRT in the parasite. To check the susceptibility of the parasites to 2-FA established protocols were used (Desjardins et al., 1979). Briefly, a synchronised culture of 3D7 and 3D7+yAPRT culture was used for the assay that was performed in a 96-well plate format. Parasite culture with an initial parasitemia of 1% and a hematocrit of 2% was used. The final culture volume was maintained at 200 μ l in each well. 2-FA was titrated using serial dilution method starting from 120 μ M to 230 nM (10 dilutions). After 98 h of incubation at 37 °C, smears were made, stained with Giemsa staining solution and parasitemia was estimated by counting at least 1000 RBCs in each condition under a microscope. As a control, parasitemia from a culture in which no 2-FA was added was estimated. The experiment was repeated twice with 2 technical replicates each time. The points were fit to an equation using log concentration of inhibitor versus response with a variable slope option, under non-linear regression analysis in GraphPad Prism 5.

2.4. RESULTS AND DISCUSSION

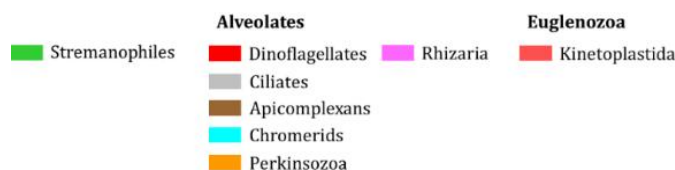
2.4.1. Distribution of purine salvage pathway enzymes in alveolates

Representative organisms belonging to alveolates, stremanophiles, rhizaria and kinetoplastids were surveyed for the presence/absence of enzymes involved in purine salvage and interconversion pathways. Similar analyses have been performed earlier but were limited only to a subsection of the organisms chosen here (Chaudhary et al., 2004). Moreover, whole-genome sequence information for many organisms is now available that would aid in a better comparative analysis. The analysis here includes both parasitic and non-parasitic organisms. For this analysis, Blast P tool was used and wherever possible protein sequences from *P. falciparum* was used as the query. For genes not present in *P. falciparum*, the corresponding protein sequence from a different parasitic organism belonging to any of the above-mentioned clades was used. For APRT, however, the sequence of *S. cerevisiae* was chosen as it gave a true representation of the distribution of the protein.

For multiple enzymes, more than one query was used for the following reasons; either the *Plasmodium* protein lacked homology to the protein present in some organisms as seen in the case of ADSS or a protein of a different superfamily performs the same catalytic function (exemplified by *Trypanosoma brucei* nucleoside hydrolase that converts inosine and guanosine to hypoxanthine and guanine, respectively, just like purine nucleoside phosphorylase of *Plasmodium*). The result of the analysis is catalogued in **Table 2.5.**

Table 2.5. Distribution of purine salvage/interconversion enzymes in representative organisms from alveolates, stremanophiles, kinetoplastids and rhizaria.

#	Organism	AAH Ld	ADA Pf	PNP Pf/ Ec/Ich /Tt-IUNH	HGPR T Pf/Gl	ADSS Pf/Tb	ASL Pf/Bh	AMPD Pf	IMPDH Pf/Ec	GMPS Pf	GMPR Ld/Hs	APRT Sc	AK Tg/Tv
1	<i>Paramecium tetraurelia</i>			1e-69 97,39	1e-13 47,35	5e-134 95,49	5e-133 95,45	1e-158 89,40	4e-96 96,37			2e-40 83,46	5e-29 94,29
2	<i>Tetrahymena thermophila</i>		1e-15 56,30	2e-150 98,72*	3e-16 70,31	3e-129 96,46	2e-141 95,48	8e-164 73,48	6e-106 95,37			7e-40 83,43	
3	<i>Oxytricha trifallax</i>	1e-06 33,32	4e-18 90,26	9e-31 86,31*	5e-32 97,30	1e-118 95,44	1e-144 97,46				9e-148 98,60	3e-38 90,41	4e-47 95,30
4	<i>Ichthyophthirius multifiliis</i>	3e-06 41,28	3e-14 49,28	0.0	5e-17 74,28	3e-130 95,46	2e-130 87,51	2e-161 74,48	4e-109 95,36				
5	<i>Plasmodium falciparum</i>		0.0	0.0	0.0	0.0	0.0	0.0	0.0	0.0			
6	<i>Toxoplasma gondii</i>	2e-27 93,34		2e-66 97,45	6e-77 95,51	2e-164 97,52	1e-144 98,43	0.0 89,56	0.0 99,50	0.0 99,47			0
7	<i>Cryptosporidium parvum</i>							0.0 82,48	2e-102 75,57	4e-62 98,29			3e-33 96,29
8	<i>Eimeria tenella</i>			8e-61 97,40	3e-72 90,48	5e-78 66,41	6e-36 55,36	0.0 69,59	0.0 98,53	3e-168 98,44			2e-07 19,41
9	<i>Neospora caninum</i>	2e-30 95,34		3e-57 97,42	1e-77 96,50	8e-162 97,50	2e-141 96,41	0.0 98,51	9e-174 99,59	0.0 99,46			1e-177 99,65
10	<i>Hammondia hammondi</i>	2e-27 95,34		4e-45 77,46	8e-77 95,51	1e-161 94,52	1e-144 98,43	0.0 89,56	0.0 99,52	0.0 99,47			0 100,81
11	<i>Theileria annulata</i>			8e-35 98,31		7e-118 92,45	2e-91 97,38	+	3e-176 99,50	3e-114 98,35	9e-40 95,32		
12	<i>Babesia bovis</i>		6e-72 94,34	7e-40 98,34		1e-126 96,45	8e-137 94,47		0.0 99,51	2e-112 98,35	1e-36 90,32		2e-20 93,26
13	<i>Gregarina niphandrois</i>			1e-76 95,53	3e-35 91,34	1e-107 95,38	4e-94 96,38	0.0 74,60	2e-103 73,53	2e-139 98,39	3e-44 92,36	6e-35 81,44	1e-25 92,28
14	<i>Trypanosoma brucei</i>			9e-18 91,29	7e-16 78,32	0.0	2e-115 95,39	3e-121 73,42	5e-134 99,41*	3e-60 98,30	0.0	2e-18 81,35	1e-47 95,34
15	<i>Leishmania donovani</i>	0.0		3e-60 95,35	2e-11 67,29	0.0	4e-115 95,40	3e-16 73,42	2e-137 99,42	5e-63 98,28	0.0	5e-18 88,33	2e-45 92,33
16	<i>Bodo saltans</i>	5e-137 95,48		1e-21 95,27	5e-07 64,28	0.0	9e-87 64,44	5e-120 73,42	1e-140 99,44*	4e-46 96,26		2e-24 86,35	4e-47 93,34
17	<i>Plasmodium brassicae</i>	2e-13 94,25	2e-20 88,24	6e-43 89,35*	2e-25 77,33	5e-144 95,49	0	3e-158 72,46	5e-173 97,50	1e-57 99,30	8e-179 99,68		1e-53 95,32
18	<i>Reticulomyxa filosa</i>	9e-13 90,24	5e-18 68,27	2e-15 74,26*	2e-18 74,31	4e-60 52,42	2e-63 31,59	1e-161 88,41	1e-141 99,40	3e-49 83,28	1e-170 99,68	8e-48 90,45	8e-51 96,32
19	<i>Blastocystis hominis</i>		8e-08 43,23	9e-43 57,43	1e-37 88,34	4e-131 95,46	0		7e-149 99,45	6e-163 99,43			
20	<i>Thalassiosira pseudonana</i>	+			+	+	0	+	+	+		+	+
21	<i>Chromera velia</i>	+			+	+		+	+	+		+	+
22	<i>V. brassicae formans</i>	+			+	+		+	+	+		+	+
23	<i>Symbiodinium minutum</i>	+			+	+		+	+	+			+
24	<i>Perkinsus marinus</i>	+			+	+		+	+	+		+	+
25	<i>Chlamydomonas reinhardtii</i>				+	+		+	+	+		+	+
26	<i>Giardia lamblia</i>			2e-40 93,32	0							2e-30 97,37	
27	<i>Trichomonas vaginalis</i>		6e-27 89,27	1e-97 97,59*	3e-16 77,28								0.0



Organisms from which the query sequences were used for BlastP search are indicated in the header row. When more than one sequence was used as the query, the query and the search results are given in the same colour. Every box contains numbers corresponding to e-value, sequence coverage and sequence identity in percentage, in that order, with respect to the query sequence. The first column of the table is coloured red for parasitic organisms and green for non-parasitic organisms. A plus sign in any box indicates the presence of the gene from earlier published data (Woo et al., 2015). A blue asterisk as superscript indicates the presence of two different genes encoding proteins with the same function but with distant homology. Pf, *P. falciparum*; Ld, *L. donovani*; Ec, *Escherichia coli*; Tb, *Trypanosoma brucei*; Tt-IUNH, *Tetrahymena thermophile inosine-uridine nucleoside hydrolase*; Gl, *Giardia lamblia*; Bh, *Blastocystis hominis*; Hs, *Homo sapiens*; Tv, *Trichomonas vaginalis*. AAH, adenine aminohydrolase/adenine deaminase; ADA, adenosine deaminase; PNP, purine nucleoside phosphorylase; HGPRT, hypoxanthine-guanine phosphoribosyltransferase; ADSS, adenylosuccinate synthetase; ASL, adenylosuccinate lyase; AMPD, adenosine monophosphate deaminase; IMPDH, inosine monophosphate dehydrogenase; GMPS, guanosine monophosphate synthetase; GMPR, guanosine monophosphate reductase, APRT, adenine phosphoribosyl transferase; AK, adenosine kinase; Ich, *Ichthyophthirius multifiliis*.

There are three categories into which organisms can be classified. Class1, those which depend on only phosphoribosylation based reactions to salvage purines as exemplified by *Giardia*; class2, those that use phosphorylation of nucleosides exclusively for salvage as seen in *Trichomonas*; and class3, that uses both ways as seen in ciliates and kinetoplastids. The following are the notable features brought out by this analysis:

1) With few exceptions, the general trend in purine acquisition amongst parasites as is evident from the table is that purine nucleosides and nucleobases are the preferred purine source. The nucleosides once transported into the cytosol are also converted to nucleobases by the action of enzymes, PNP or NH. The nucleobases are converted to their corresponding mononucleotide by the action of HGXPRT/APRT.

2) The enzymes HGPRT, PNP, ADSS, ASL, GMPS, IMPDH and AMPD are present in most of the organisms surveyed.

3) The enzymes ADA, AAH, APRT and GPRT are sparsely distributed. The most striking feature is almost complete absence of APRT in apicomplexan organisms, the exception being *Gregarina niphandrodes*.

4) In Apicomplexa, GMPR is restricted to organisms of the order Piroplasmida (*Theileria* and *Babesia*) and gregarines (*Gregarina niphandrodes*). It is perplexing that the enzyme AMPD that converts AMP back to IMP is more widely distributed than GMPR, that converts GMP to IMP.

5) The presence of the gene, inosine-uridine nucleoside hydrolase (IU-NH) can be considered as an indicator for the presence of pyrimidine salvage machinery in the corresponding organisms.

6) Strikingly, the gene corresponding to GMPS is absent in ciliates. With the absence of GMPS, the role of IMPDH, which is present in these organisms, is enigmatic. It is also possible that the annotation of IMPDH is wrong and the gene could actually be GMPR as these proteins exhibit high sequence conservation.

7) As established before, *Giardia lamblia* has the most simplistic purine salvage pathway with just NH, APRT and GPRT to meet the purine requirements. Interconversion of purines seems to be completely absent in this parasite.

8) Biochemical studies in *Trichomonas vaginalis* showed that adenosine is the primary source of all purine nucleotides in the parasite. Corroborating this, the corresponding enzymes are present in the organism. Although there is a protein homologous to HGPRT, biochemical studies show that phosphorylation of adenosine and guanosine by kinases is the major pathway of purine salvage. It has been suggested that contribution of adenosine to guanylate pool is facilitated by the enzymes, adenosine deaminase, purine nucleoside kinase, IMPDH and GMPS acting in tandem. Our bioinformatic analysis did not reveal the presence of IMPDH and GMPS in this organism. Although biochemical evidence exists for the presence of IMPDH and GMPS, further investigation is needed to confirm this at the sequence level. Another notable feature of this organism is the preferential action of PNP towards the formation of nucleosides, in a direction that is reverse to that seen in most other organisms (Munagala and Wang, 2003). Apart from the purine source available in the environment, which could be the primary determinant of the choice of salvage enzymes, other factors like, mode of pyrimidine metabolism (salvage vs *de novo*) and nature of energy metabolism (fermentative vs oxidative) could have also played a key role.

2.4.2. Comparison of thermodynamic/kinetic parameters of enzymes involved in purine salvage pathway

The introduction of a new enzyme to produce AMP in the parasite would mean sufficient substrate should be present in the parasite compartment and that the K_{eq} of the reaction is large enough to drive the reaction in the direction of AMP production and not the reverse. We obtained the K_{eq} values of all the enzymes of the purine salvage pathway using the tool eQuilibrator (Flamholz et al., 2012). From the values presented in **Table 2.6**, it can be seen that K_{eq} of APRT is 100 times greater than that of AK suggesting it to be a better candidate for AMP generation.

Table 2.6. Thermodynamic parameters of key enzymes in purine salvage metabolism. Highlighted in light green are the K_{eq} values that are positive. Highlighted in dark green are the most suitable enzymes for use as alternative modes of AMP generation in *P. falciparum*. Values were obtained from the tool eQuilibrator (Flamholz et al., 2012).

S.No	Enzyme	EC No.	$\Delta_r G'^m$ (kJ/mol)	$\Delta_r G'^o$ (kJ/mol)	K_{eq}
1	Adenosine deaminase (ADA)	3.5.4.4	40.1±1.4	22.9±1.4	1.1×10 ⁴
2	Purine nucleoside phosphorylase (PNP)	2.4.2.1	9.2±2.1	9.2±2.1	0.0248
3	Hypoxanthine phosphoribosyltransferase (HPRT)	2.4.2.8	26.7±3.1	26.7±3.1	4.8×10 ⁴
4	Adenylosuccinate synthetase (ADSS)	6.3.4.4	11.5±4.2	11.5±4.2	9.7×10 ⁻³
5	Adenylosuccinate lyase (ASL)	4.3.2.2	-7±2.7	10.1±2.7	0.0169
6	Adenosine monophosphate deaminase (AMPD)	3.5.4.6	48.7±3.8	31.6±3.8	3.4×10 ⁵
7	IMP dehydrogenase (IMPDH)	1.1.1.205	21.4±7.4	21.4±7.4	1.8×10 ⁻⁴
8	Guanosine monophosphate synthetase (GMPS)	6.3.5.2	N.D	N.D	N.D
9	Guanosine monophosphate reductase (GMPR)	1.6.6.8	N.D	N.D	N.D
10	Adenine aminohydrolase (AAH)	3.5.4.2	39.1±3.2	-22±3.2	7.2×10 ³
11	Adenine phosphoribosyltransferase (APRT)	2.4.2.8	17.1±2.6	17.1±2.6	1×10 ³
12	Guanine phosphoribosyltransferase (GPRT)	2.4.2.8	28.4±4.4	28.4±4.4	1×10 ⁵
13	Xanthine phosphoribosyltransferase (XPRT)	2.4.2.8	22.1±7.3	22.1±7.3	7.4×10 ³
14	Adenosine kinase (AK)	2.7.1.20	12.2±2.8	12.2±2.8	138
15	Guanosine kinase (GK)	2.7.1.73	20.5±6.7	20.5±6.7	4×10 ³
16	Adenylate kinase (ADK)	2.7.4.3	-2.6±0.3	-2.6±0.3	2.82

EC No., Enzyme commission number; $\Delta_r G'^m$, Gibbs free energy at a pH of 7.0 and ionic strength of 0.1 M, and 1 mM concentration of all reactants; $\Delta_r G'^o$, Gibbs free energy at a pH of 7.0 and ionic strength of 0.1 M, and 1 M concentration of all reactants; K_{eq} , rate enhancement of forward reaction over that of the reverse reaction. A value of 1 indicates an equal flux of forward and reverse reaction; a value of less than 1 indicates an increased flux of reverse reaction; and a value more than 1 indicates an increased flux of the forward reaction compared to that of the reverse reaction.

2.4.3. The choice of alternate AMP generating enzyme

Apart from the ADSS/ASSL pathway, two potential enzymes that could serve to produce AMP in *P. falciparum*, are APRT and AK. APRT uses a molecule of adenine and PRPP to produce AMP. AK uses one molecule of adenosine and ATP to generate AMP. For this work APRT was chosen as an alternate AMP generating enzyme for the following reasons;

- 1) The K_{eq} of APRT (10³) is much higher compared to that of AK (138) showing that APRT could be a better enzyme to drive the reaction away from equilibrium towards AMP generation.

- 2) Unlike adenosine which could be acted upon by adenosine deaminase in the parasite cytosol and hence diverting the flux into two different pathways (AK and ADA), there are no enzymes present in the parasite compartment that could act on adenine.
- 3) APRT is completely absent in all the organisms of Apicomplexa except for *Gregarina niphandrodes*. It would be interesting to examine the phenotype upon expression of APRT in *P. falciparum*.

One should note that these reasons do not warrant that AK cannot be used as an alternate AMP generating pathway, but just provide a rationale for choosing one over the other. For expressing APRT in *P. falciparum*, a centromere plasmid was chosen as it will be stably segregated across multiple generations. Moreover, since the copy number of the plasmid will be one, there would be minimal heterogeneity in phenotype across individuals in a population of parasites.

2.4.4. Cloning, expression, purification and activity of recombinant yAPRT

yAPRT was cloned in pET21b and expressed as an N-terminal (His)₆-tagged protein in *E. coli* (Figure 2.4). The cloned gene sequence was verified to be correct by DNA sequencing. The protein was purified to homogeneity by Ni-NTA followed by size-exclusion chromatography (Figure 2.5 b & c). The purified protein was found to be active as analysed by a spectrophotometric assay (Figure 2.5 f). The specific activity of the protein measured in Tris-HCl, pH 7.4 containing 100 μ M of adenine, 500 μ M of PRPP, and 10 mM of MgCl₂ was 13 μ mol min⁻¹mg⁻¹, which is comparable to the value reported in the literature (Alfonzo et al., 1997).

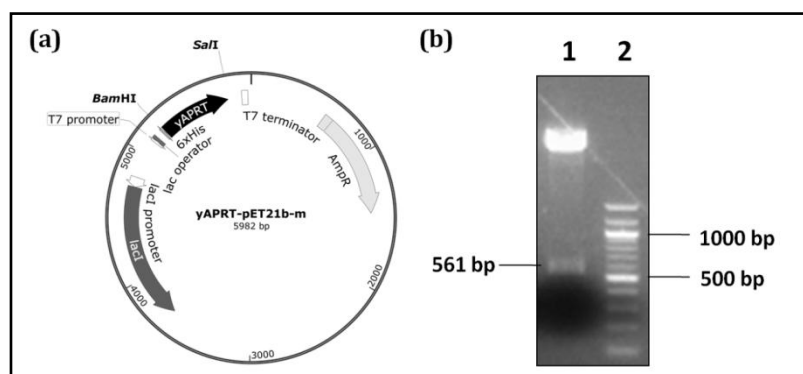


Figure 2.4. Cloning of *Saccharomyces cerevisiae* adenine phosphoribosyltransferase (yAPRT) into pET21b.

(a) Vector map showing key features of the plasmid used for recombinant expression of yAPRT. *LacI*- lac repressor protein, *AmpR*- β -lactamase enzyme, *Bam*HI and *Sal*I- enzymes used for cloning. **(b)** Validation of clone by restriction digestion and release of the DNA

fragment corresponding to *yAPRT* using *Bam*HI and *Sall*. Lane 1, restriction digestion mixture; and lane 2, 100bp DNA ladder. The clone was finally validated by DNA sequencing.

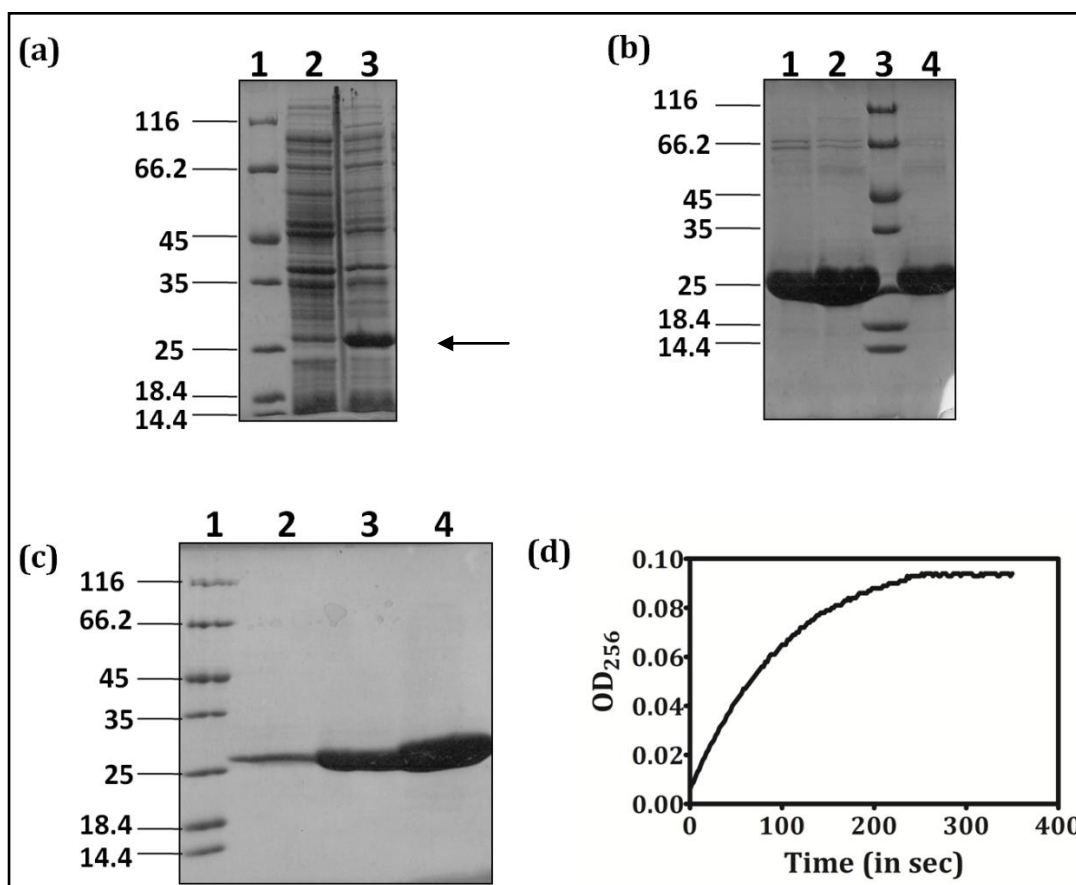


Figure 2.5. Expression, purification, and activity of recombinant *yAPRT*.

(a) SDS-PAGE analysis of whole cell lysate of BL21 (DE3) codon plus strain with pET21b-*yAPRT* plasmid, with and without IPTG induction. Lane 1, protein molecular weight marker; lane 2, uninduced cell lysate; and lane 3, induced cell lysate. Expressed *yAPRT* in lane 3 is indicated by an arrow. **(b)** SDS-PAGE analysis of eluates from Ni-NTA affinity chromatography. Lane 1, 100 mM imidazole eluate; lane 2, 200 mM imidazole eluate; lane 3, protein molecular weight marker; and lane 4, 500 mM imidazole eluate. **(c)** SDS-PAGE analysis of different fractions obtained after size-exclusion chromatography (SEC). Lane 1, protein molecular weight marker; lanes 2-4 correspond to different fractions of *yAPRT* after SEC. The molecular weight of marker proteins in panels a, b and c is shown in kDa. **(d)** Reaction progress curve showing the conversion of adenine to AMP.

For functional complementation in *E. coli* AptKO strain and for expression in *P. falciparum*, *yAPRT* was cloned into pQE30 and pFCENv1 vector. The clones were validated by sequencing and digestion using appropriate restriction enzymes (*Bam*HI and *Sall* for pQE30 vector and *Bgl*II and *Bmt*I in the case of pFCENv1 vector). For expression in *P. falciparum*, pFCENv1 vector was chosen as it will be stably segregated (due to the presence of centromere sequence) and only a single copy is maintained in each cell

avoiding any overexpression artefacts. yAPRT will be expressed from a *P. berghei* EF1 α promoter. The features of these plasmids are shown schematically in **Figure 2.6**.

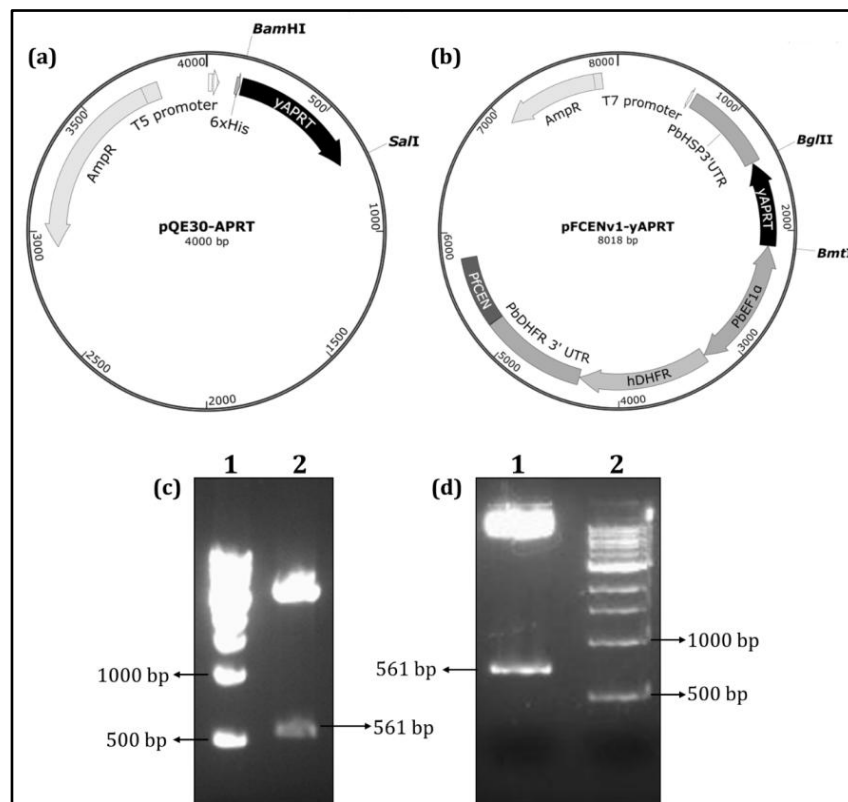


Figure 2.6. Cloning of yAPRT gene in pQE30 and pFCEN1.

(a) Schematic representation of the plasmid pQE30-yAPRT showing key features in the vector backbone. The position of constitutive T5 promoter and, BamHI and SalI sites used for cloning are also shown. **(b)** Schematic representation of key features of the plasmid pFCEN1-yAPRT. PbHSP3'UTR, 3'untranslated region of *P. berghei* heat shock protein; PbEF1 α , bidirectional promoter of *P. berghei* elongation factor 1 α ; hDHFR, human dihydrofolate reductase; PFCEN, *P. falciparum* centromere sequence 5.5 corresponding to chromosome 5, and positions of BglII and BmtI sites used for cloning yAPRT are shown. **(c)** Validation of cloning of yAPRT in pQE30 by using restriction enzymes BamHI and SalI. Lane1, 1 kb DNA ladder from New England Biolabs (NEB), USA; and lane2, digested plasmid DNA. **(d)** Validation of yAPRT cloning in pFCEN1 vector using enzymes BglII and BmtI. Lane1, digested plasmid DNA; and lane2, 1 kb DNA ladder from NEB. Enzymes mentioned in (a) and (b) were used for this restriction digestion. All the clones were confirmed by DNA sequencing.

2.4.5. Generation and purification of antibody

Antibody against recombinant yAPRT was generated in rabbit. The antibody was purified by using the strip-affinity method. The purified antibody was tested for its affinity to the recombinant protein by dot-blot. The antibody, even at a dilution of 1: 20,000 (**Figure 2.7**), reported back on the presence of the antigen. The antibody was used for both Western and indirect immunofluorescence to check the expression of yAPRT in 3D7-yAPRT parasites.

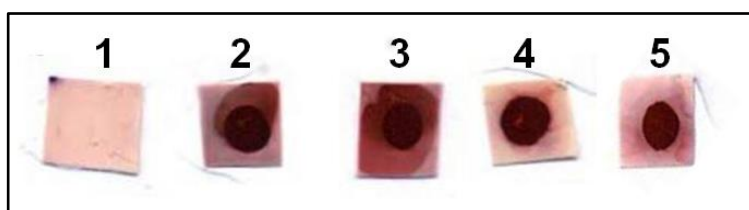


Figure 2.7. Purification of antibody using strip-affinity method and analysis using dot blot.

Antibodies were raised in rabbit. 1 ml of serum obtained from the rabbit was used for the purification process using the strip-affinity method. Different dilutions of the eluates obtained after purification were tested for their reactivity towards recombinant protein. 1, blot in which no protein was loaded; 2, blot containing 2 μg of yAPRT probed with unpurified serum containing anti-yAPRT antibodies; 3 to 5 correspond to the blot with 2 μg protein probed with different dilutions- 1:1000, 1:10000, and 1:20000, respectively of purified antibody.

2.4.6. 2-FA toxicity as a reporter for *in vivo* activity of yAPRT

Having established that yAPRT is active *in vitro*, the *in vivo* activity of yAPRT had to be established. 2-FA is a substrate analogue of adenine and gets catalysed to 2-fluoroadenosine monophosphate (2-FAMP) by APRT. 2-FAMP can inhibit many intracellular reactions where AMP/ADP/ATP is used and therefore, is toxic to the organism expressing APRT. The toxicity of 2-FA to an organism could serve as a surrogate for the *in vivo* activity of APRT. In order to check if yAPRT can catalyse the phosphoribosylation of 2-FA and produce toxic 2-FAMP, we performed 2-FA susceptibility studies in an *aprt* null *E. coli* strain, JW0458-2. As expected the strain grew well even at 0.5mM 2-FA. However, 2-FA turned out to be toxic for the strain expressing yAPRT as seen by the growth inhibition (**Figure 2.8b**), suggesting that 2-FA can act as a substrate for yAPRT (**Figure 2.8b**). The finding that the 2-FA mediated toxicity is specifically rescued by adenine but not hypoxanthine (**Figure 2.8b**) further substantiates the fact that 2-FA mediated toxicity can be used as a reporter for checking the *in vivo* activity of yAPRT.

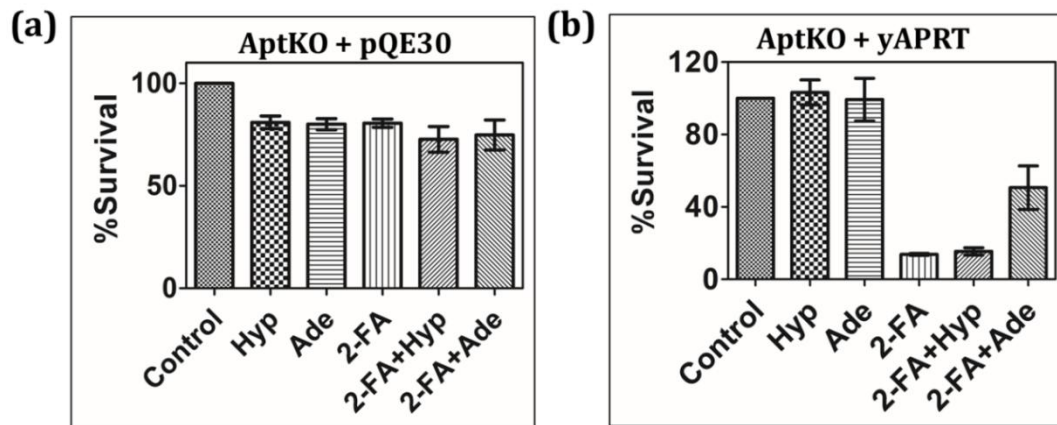


Figure 2.8. 2-FA adenine mediated toxicity and rescue in the *E. coli* strains AptKO+pQE30 and AptKO+ yAPRT.

(a) Bar graph showing normalised growth phenotype of *E. coli* strains AptKO+pQE30 in LB broth with different combinations of purine sources and 2-FA. Hyp, 1 mM of hypoxanthine; Ade, 1 mM of adenine, , 2-FA, 0.5 mM 2-fluoroadenine. The last two bars correspond to growth in condition where either 1mM hypoxanthine or 1mM adenine was added to compete with 2-FA to relieve the toxicity exhibited, if any. It can be seen there was no growth defect observed in any of the conditions tested. **(b)** Bar graph showing normalised growth phenotype of *E. coli* strains AptKO+pQE30 in LB broth with different combinations of purine sources and 2-FA. Unlike in (a), 2-FA is toxic to cells expressing yAPRT and the rescue is specifically relieved only by the addition of adenine (last bar) and not by hypoxanthine (last but one bar). AptKO is JM0458-2 strain in which the *aprt* gene is deleted. The experiment was done in duplicates and repeated twice. The error bars represent the standard error of the mean.

2.4.7. Generation and validation of *P. falciparum* strain expressing yAPRT/GFP

For all experiments related to yAPRT expression and phenotyping in the parasite, the pFCEN1 vector expressing GFP (pFCENv1-GFP) was used as a control and the strain would be referred to as 3D7-Vector control (VC). Transfection of *P. falciparum* with pFCEN1-APRT and pFCEN1-GFP was done by both preloading of erythrocytes and direct transfection of ring-stage *Plasmodium* culture. The time constant ranged from 14-18 ms in all these experiments. WR99210 was used as a selection marker and the drug resistant parasites were obtained anywhere between 15-40 days after transfection. PCR with gene specific primers and DNA from the transfected parasites as template showed the presence of the plasmid in this parasites (**Figure 2.10 a**).

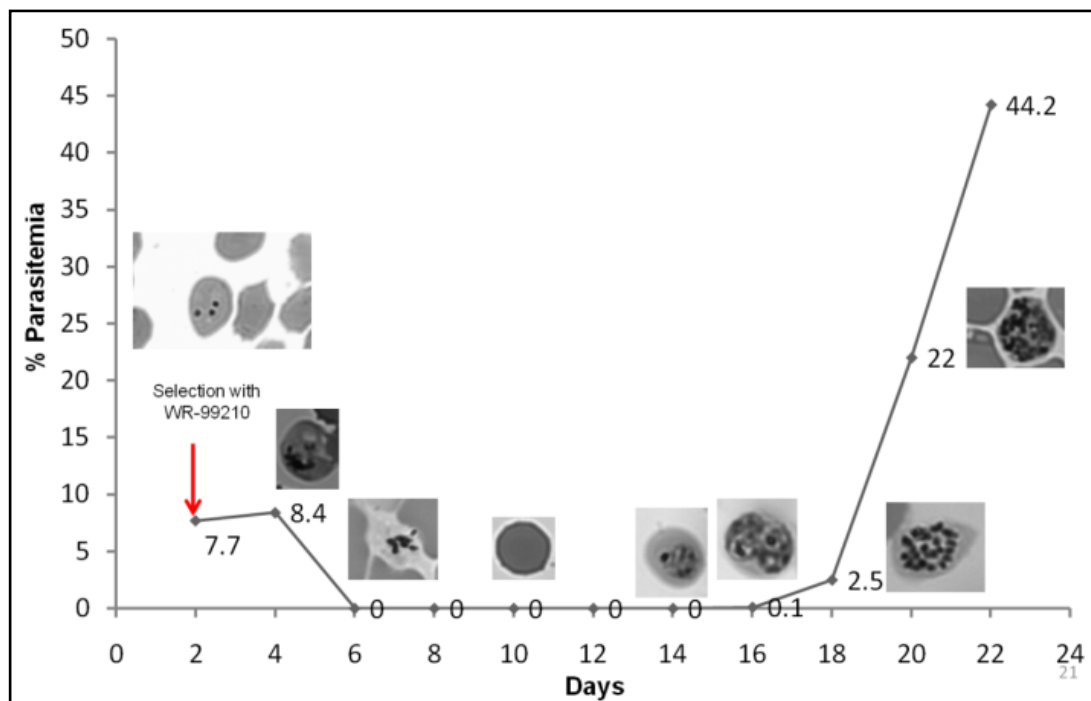


Figure 2.9. Schematic representation of growth pattern observed following DNA transfection and drug selection of asexual stage of *P. falciparum*.

Day 0 corresponds to transfection with ring stage culture using BioRad-XL electroporator. A snapshot of Giemsa-stained parasite/s is shown at different time points that best describes the health and stage of the culture. On day 2, after one generation time of the parasite following transfection, the transfected parasites were selected by applying an appropriate concentration of drug. On day 6, parasites could not be observed on the slide upon examining the usual number of fields. Depending on the transfection efficiency one can see the transfected parasites appearing on drug selection from anywhere between 10-40 days. In this particular transfection, we observed healthy parasites appearing from day 14 onwards. Parasitemia estimates on day 20 and 22 included the dilution factor that the cultures were subjected during continuous cultivation of the parasite.

Western blotting analysis performed on these parasite lysate using yAPRT specific antibody showed expression of yAPRT and GFP in the respective transfected parasites (**Figure 2.10 b**). Immunofluorescence microscopy of yAPRT parasites with antibody against yAPRT showed the presence of the protein in the parasite cytosol (**Figure 2.10 d**).

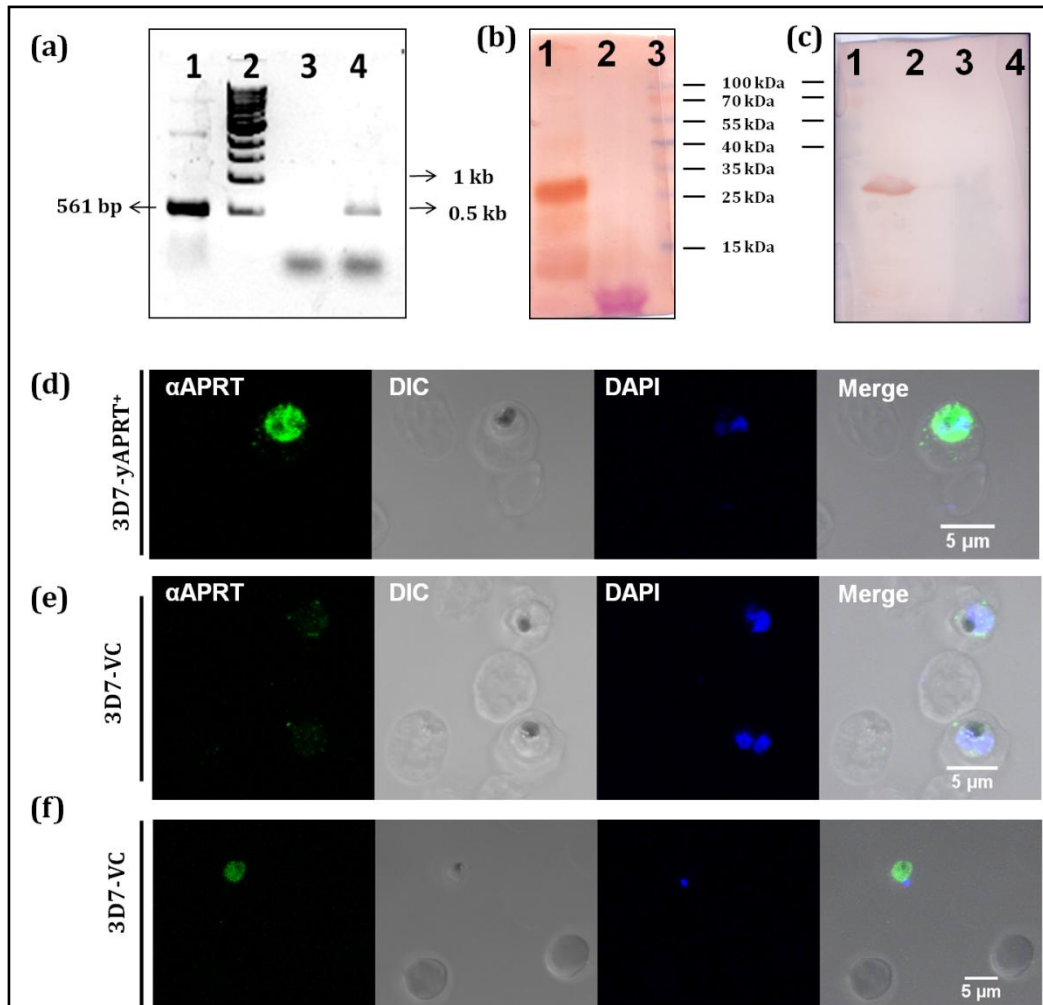


Figure 2.10. Validation of transfection and expression of yAPRT in *P. falciparum* 3D7 strain.

(a) PCR confirmation of the presence of plasmid pFCEN1-yAPRT in 3D7-yAPRT parasites. Lane1, PCR with plasmid pFCEN1-yAPRT as template; lane2, 1Kb DNA ladder; lane3, an aliquot of PCR product using genomic DNA isolated from 3D7-VC parasites as template; and lane4, an aliquot of PCR product using genomic DNA isolated from 3D7-yAPRT parasites. **(b)** Western blot analysis using α -APRT antibodies. Lane1, cell lysate of 3D7-yAPRT parasites after saponin treatment; lane2, cell lysate of 3D7-VC parasites after saponin treatment and lane3, prestained protein molecular weight marker (molecular weight shown in kDa). **(c)** Western blot analysis using α -GFP antibody. Protein equivalent to 10 ml culture of 5% hematocrit and 8% parasitemia was used for the analysis. Lane1 and 2, protein isolated from 3D7-VC parasites corresponding to 10 ml and 2 ml culture of 5% hematocrit and 8% parasitemia; lane3, protein isolated from 3D7-yAPRT parasite corresponding to 10 ml of culture of 5% hematocrit and 8% parasitemia; and lane4, prestained protein molecular weight marker (molecular weight shown in kDa). **(d)** Indirect immunofluorescence microscopy on 3D7-yAPRT parasites probed with α -APRT antibodies. **(e)** Indirect immunofluorescence microscopy on 3D7-VC parasites probed with α -APRT antibodies. **(f)** Live cell microscopy on 3D7-VC parasites showing the presence of GFP. In all immunofluorescence experiments, 10 images were collected in each experiment and representative images are shown.

2.4.8. *In vivo* and *in-vitro* activity of yAPRT in *P. falciparum*

To assess if yAPRT is functional in the parasite compartment, protein lysate from 3D7-yAPRT and 3D7-VC parasites were incubated with adenine. The incubation was followed by TCA precipitation of proteins, and analysis of reaction supernatant by ion-pair RP-HPLC to monitor the formation of AMP.

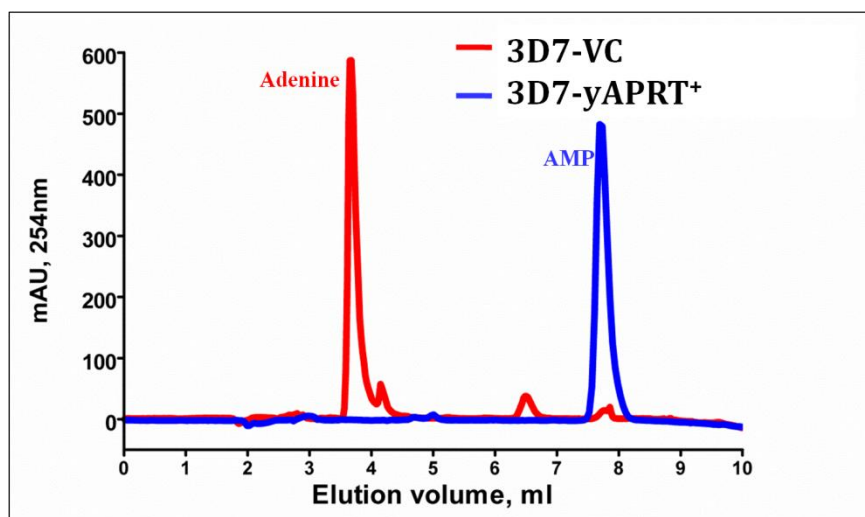


Figure 2.11. *In-vitro* activity of APRT in *P. falciparum* lysate.

Chromatogram from ion-pair RP-HPLC showing APRT activity in the cell lysate obtained from saponin-treated preparations of 3D7-VC (red line) and 3D7-yAPRT (blue line) parasites. There is a complete conversion of added adenine to AMP when protein lysate from 3D7-yAPRT parasite was used. The experiment was done twice.

As can be seen from the chromatogram, the lysate from 3D7-yAPRT brought about complete conversion of adenine to AMP compared to that from 3D7-VC strain (**Figure 2.11**). This shows the *in vitro* functionality of yAPRT expressed in *P. falciparum*. As described in the previous section, 2-FA toxicity can be used to check the *in vivo* functionality of yAPRT. As expected, the 3D7-yAPRT parasites were more sensitive to 2-FA as seen in the drop of IC_{50} from $8.66 \pm 0.02 \mu\text{M}$ for 3D7-VC parasites to $1.30 \pm 0.02 \mu\text{M}$ for 3D7-yAPRT parasites (**Figure 2.12** left panel). This corroborates with the results seen in *E. coli* experiments (section 2.11.6) and supports the *in vivo* functionality of yAPRT in the parasite 3D7-yAPRT. It should be noted that 2-FA is toxic to the 3D7-VC parasite because of the presence of human APRT in the erythrocyte compartment. The drop in IC_{50} of 2-FA for 3D7-yAPRT parasite is due to the presence of yAPRT in the parasite compartment in addition to hAPRT in the erythrocyte compartment, thereby producing excess 2-FAMP when compared to that of 3D7-VC parasites (**Figure 2.12** right panel). From this result, it can be concluded that yAPRT is functional in the parasite compartment thereby causing increased sensitivity of 3D7-yAPRT parasites towards 2-FA.

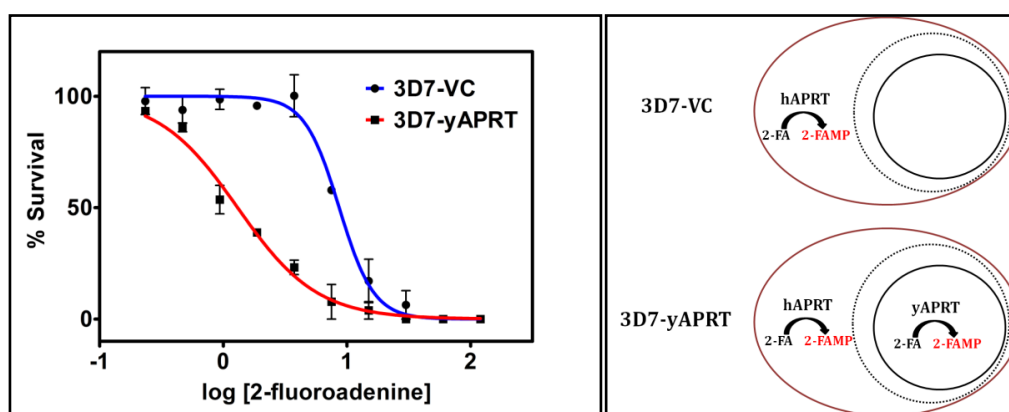


Figure 2.12. The in vivo activity of yAPRT in 3D7-APRT parasite cytosol.

The left panel shows the susceptibility of 3D7-VC (blue line) and 3D7-yAPRT (red line) parasites to 2-fluoroadenine. An IC_{50} value of $1.30 \pm 0.02 \mu\text{M}$ was obtained for 3D7-APRT parasites and $8.66 \pm 0.02 \mu\text{M}$ for 3D7-VC parasites. The drop in IC_{50} value in 3D7-APRT parasite can be attributed to the activity of yAPRT in parasite compartment in addition to the activity of human APRT (hAPRT) in erythrocytes cytoplasm. The experiment was done in duplicates and repeated twice. The error bars represent the standard error of the mean. The right panel shows the metabolic scenario causing higher sensitivity of 3D7-yAPRT parasites to 2-FA. The brown line corresponds to erythrocyte membrane, the dotted black line corresponds to parasitophorous vacuolar membrane and the black line corresponds to the parasite plasma membrane. hAPRT, human adenine phosphoribosyltransferase; 2-FA, 2-fluoroadenine; 2-FAMP, 2-fluoroadenosine mono phosphate; yAPRT, yeast adenine phosphoribosyltransferase.

2.4.9. Rescue of 2-FA mediated toxicity in 3D7-yAPRT parasites

The addition of adenine should compete for 2-FA as a substrate for yAPRT/hAPRT and hence should relieve toxicity of 2-FA. We attempted to rescue both the parasites from 2-FA by the addition of 100 μM adenine. All regular *in vitro* *P. falciparum* growth culture media contained 100 μM hypoxanthine. We had also observed that addition of up to 1mM adenine along with 100 μM hypoxanthine to a culture of 3D7 parasites enhances growth (data not shown). Based on this observation, 100 μM hypoxanthine and 100 μM adenine were added to the medium for the rescue experiment.

We observed that, while adenine supplementation was able to rescue the 3D7-VC parasites from 2-FA mediated growth inhibition, no rescue was seen with 3D7-yAPRT parasites (**Figure 2.13**). Around 60% drop in parasitemia was observed at a 2-FA concentration of 2 μM for 3D7-yAPRT parasites grown in 100 μM hypoxanthine only containing medium (**Figure 2.13 b**). This is in agreement with the IC_{50} value for 2-FA (1.2 μM) for 3D7-yAPRT parasites (**Figure 2.12**). Surprisingly, the presence of 100 μM adenine rather than rescuing the parasite caused complete death of 3D7-yARPT parasites

(Figure 2.13 b). This prompted us to compare the growth of 3D7-yAPRT and 3D7-VC parasites in medium containing either adenine or hypoxanthine or a combination of both.

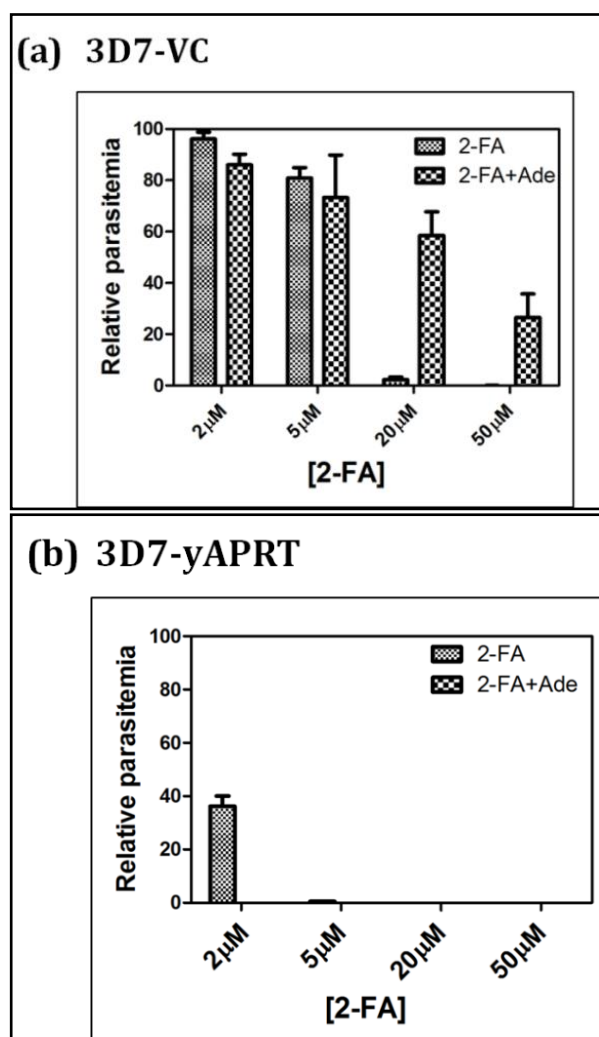


Figure 2.13. Rescue of 2-FA inhibition by adenine supplementation.

(a) Rescue of 2-FA inhibition by addition of 100 μM adenine in 3D7-VC parasites and **(b)** Rescue of 2-FA inhibition by addition of 100 μM adenine in 3D7-yAPRT. Four different concentrations of 2-FA- 2,5,20, and 50 μM-were used for the assay. The culture medium already contained 100 μM hypoxanthine. In addition to the hypoxanthine present, 100 μM adenine was used for the rescue experiment. The parasitemia of both 3D7-VC and 3D7-yAPRT shown in the figure is normalised with respect to the parasitemia in culture grown in regular culture medium containing 100 μM hypoxanthine alone. The experiment was done in duplicates and repeated twice. The error bars represent the standard error of the mean.

2.4.10. Purine tolerance in 3D7-VC and 3D7-yAPRT

The growth of both the parasites was examined in the presence of either 100 μM adenine/hypoxanthine alone or both purine bases together. Notably, the growth of 3D7-yAPRT parasites was severely inhibited in the presence of both the purine sources while

when the purines were singly provided, the parasites grew normally (**Figure 2.14**). 3D7-VC parasites showed no difference in growth under all three conditions of purine source.

Adenine mediated toxicity has been reported for some wild-type and mutant *E. coli* strains (Levine and Taylor, 1982; Xi et al., 2000). The mechanism of adenine toxicity in these cases is attributed either to inhibition of pyrimidine biosynthesis (caused by excess ATP and low PRPP levels) or to drop in guanylate pool due to depletion of PRPP. Trypanosomal parasites are sensitive to high concentrations of adenine and the mechanism is independent of the presence of APRT (Lüscher et al., 2014). This is unlike the phenotype seen in 3D7-yAPRT strain where the combined presence of hypoxanthine and adenine along with a functional APRT is needed to exhibit toxicity. In the context of *Plasmodium* purine and pyrimidine metabolism, the toxicity seen in 3D7-yAPRT parasites could be due to either excess AMP formation or depletion of PRPP or both. These changes might cause toxicity through the following ways that is discussed below and also schematically shown in **Figure 2.15**.

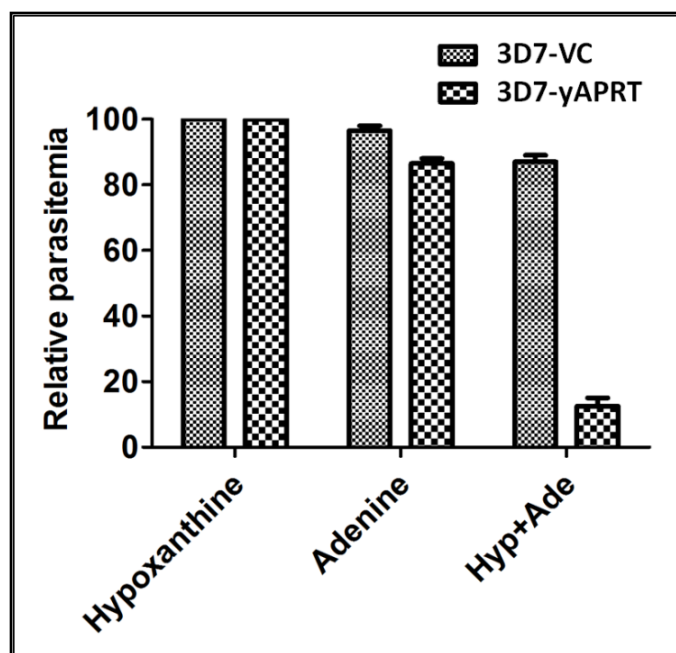


Figure 2.14. Growth phenotype of 3D7-VC and 3D7-yAPRT parasites in media containing different purine sources.

There is a selective inhibition of growth seen with 3D7-yAPRT parasite in media containing both hypoxanthine and adenine. The growth of 3D7-VC parasites was normal in all the conditions tested. Both adenine and hypoxanthine were used at a concentration of 100 μ M. The experiment was done in duplicates and repeated twice. The error bars represent the standard error of the mean.

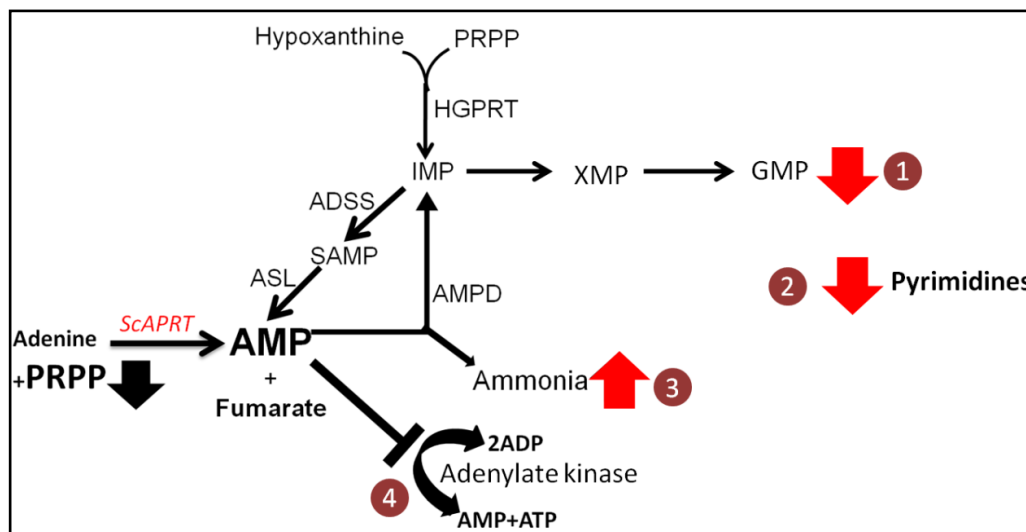


Figure 2.15. Metabolic consequences of PRPP depletion and AMP accumulation.

1, Drop in PRPP can result in insufficient IMP production that might result in lower GMP levels; 2, PRPP depletion can also cause a drop in pyrimidine levels; 3, excess AMP might be converted to IMP by AMP deaminase. This results in the formation of a molecule of ammonia which is toxic to the parasite; 4, Excess AMP might inhibit adenylate kinase thereby perturbing adenylate energy charge of the parasite.

1) The presence of yAPRT might divert a large pool of PRPP into AMP production. This may result in insufficient PRPP that would be needed for the production of guanylate pool (through the sequential action of HGPRT, IMPDH, and GMPS). If this is the case addition of guanosine could rescue the adenine toxicity observed in 3D7-yAPRT parasites. Guanosine can get converted to guanine by the action of the enzyme PfPNP (Kicska et al., 2002). The guanine thus formed can be phosphoribosylated to GMP by PfHGPRT thereby restoring GMP levels.

2) The drop in PRPP could also affect de novo pyrimidine biosynthesis at the level of orotate phosphoribosyltransferase.

3) *P. falciparum* has a functional AMP deaminase (Cassera et al., 2008). Excess AMP generated by the simultaneous functioning of yAPRT and PfASL might be converted to IMP by the action of AMP deaminase. This would also result in the production of one molecule of ammonia for every molecule of AMP converted to IMP, in the parasite compartment. It has been shown earlier that ammonia is toxic to the parasite (Zeuthen et al., 2006). This hypothesis could be tested by quantifying ammonia in the spent media.

4) Excess AMP production might also inhibit adenylate kinase thereby, perturbing the adenylate energy charge in the parasite.

Redundant pathways for purine salvage do exist in organisms and such a phenotype wherein the toxicity is exhibited only in the combination of purine sources has not been reported previously. The observation on the phenotype of 3D7-yAPRT in the presence of hypoxanthine and adenine prompts us to speculate on a possible reason for

the absence of APRT in apicomplexans. This result also suggests medium composition to be used for hadacidin rescue experiments for 3D7-yAPRT parasites.

2.4.11. Rescue of hadacidin mediated inhibition as a probe for fumarate significance.

With the results in this chapter suggesting that adenine is taken up into the parasite compartment and yAPRT can function to produce AMP, it should be possible to inhibit the essential enzyme ADSS, without compromising the AMP needs of the parasite. This would enable selective depletion of fumarate upon hadacidin addition. Complete rescue of hadacidin inhibition would mean that yAPRT generates sufficient AMP to support parasite growth and that fumarate generated by ASL is not essential for the parasite.

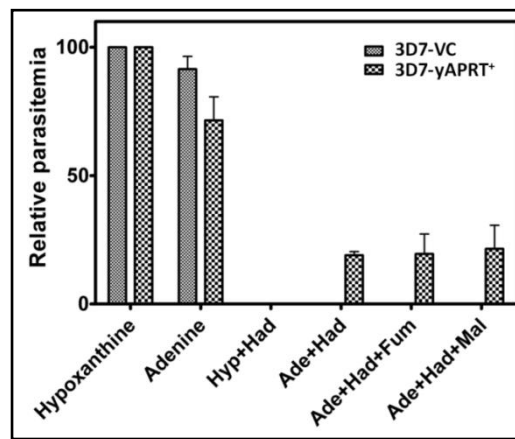


Figure 2.16. yAPRT as an alternative purine source.

Parasite grown on different purine sources was used as a control. The growth inhibition exhibited by hadacidin (1 mM) could only be partially rescued by addition of adenine. The addition of excess fumarate or malate (5 mM each) did not help the parasite to grow better. The experiment was done in duplicates and repeated twice. The error bars represent the standard error of the mean.

It was observed that with adenine as the sole purine source, hadacidin inhibition on 3D7-yAPRT was only partly rescued. However, the rescue is significant when compared to that of 3D7-VC in which there were no parasites seen. The lack of complete rescue could have multiple explanations; 1) AMP generated by yAPRT was not enough to support parasite growth, 2) fumarate generated by the pathway is essential for the parasite or 3) hadacidin at the concentration used might have non-specific effects.

To differentiate between these possible explanations, excess (5 mM) fumarate/malate was added to the medium along with adenine and hadacidin (**Figure 2.16**). However, we did not observe any additional growth advantage in excess of that seen with adenine alone containing medium. Studies on *pepc* null parasites showed that

excess malate/fumarate could rescue the growth defect. This study also showed that externally supplemented fumarate/malate was taken up by the infected erythrocyte and met cellular demands. However, it is still not clear whether the mitochondrial levels of these metabolites were restored by external supplementation in the medium. Other seeming possibilities for failure to rescue hadacidin toxicity include loss of cross-regulation between adenylate and guanylate arms of the purine salvage pathway, fumarate in the medium could have different fate compared to the locally generated one, and involvement of SAMP in essential roles other than AMP generation. Further, experiments are needed to test these hypotheses.

2.5. SUMMARY AND FUTURE PERSPECTIVES

In order to probe into the essentiality of fumarate generated as a by-product of ADSS/ASL pathway, we attempted to bypass the endogenous AMP synthesis route, by incorporating an alternate AMP generating enzyme in the parasite. Comparative analysis of enzymes involved in purine salvage pathway from different organisms and comparison of thermodynamic parameters of multiple reactions of purine salvage pathway enzymes hinted at APRT as the best candidate for the bypass. yAPRT was chosen for this and the protein was recombinantly expressed in *E. coli*, purified and antibodies generated in rabbit. The purified recombinant protein was found to be active *in vitro* using a spectrophotometric assay. Toxicity towards 2-FA was used as a phenotype to infer upon the *in vivo* activity of yAPRT in *E. coli*. Following this preliminary study, yAPRT was expressed episomally under a constitutive promoter in *P. falciparum*. The localisation of the protein was found to be cytosolic by using immunofluorescence. The activity of the protein in the parasite lysate was validated by RP-HPLC. A drop in IC₅₀ value of 2-FA suggested that the protein is functional *in vivo* and that adenine is utilised in the parasite compartment. Unlike in *E. coli*, the addition of adenine failed to rescue the 2-FA induced toxicity in the presence of yAPRT. Instead, the addition of adenine in the presence of hypoxanthine was found to be toxic for the 3D7-APRT parasite but not for the 3D7-VC parasite. The exact molecular mechanism of the toxicity in the combined presence of adenine and hypoxanthine is not clear. While 3D7-VC could not be rescued of hadacidin toxicity using adenine, there was partial rescue seen with 3D7-yAPRT parasites. The extraneous addition of either fumarate or malate did not confer any additional growth advantage. Identification of proper additives in the culture medium to meet the metabolic requirements of the parasite in the presence of hadacidin (like supplementation of guanosine or orotate) might aid the growth rescue. Further experiments could be focused in this direction. This would throw light on the importance of fumarate generated from PNC in the parasite.

Chapter 3
Functional genomics of fumarate
hydratase in Plasmodium
falciparum and Plasmodium
berghei

Chapter 3

Functional genomics of fumarate hydratase in *Plasmodium falciparum* and *Plasmodium berghei*

ABSTRACT

A direct approach to know the metabolic significance of the metabolite fumarate would be to knockout/knockdown the enzyme, fumarate hydratase that metabolizes it to malate. While the knockout of the gene has not been attempted in P. berghei, the same has been attempted in P. falciparum (Ke et al., 2015). The study shows that though the gene locus is susceptible to recombination, knockout of the gene was not possible; a direct evidence showing the essentiality of the protein. This chapter briefly summarizes the study of fumarate hydratase in different organisms in the perspective to its localization and essentiality. Following this, the objectives are presented. A detailed description of the study on conditional knockdown of fumarate hydratase protein using a degron-based strategy in P. falciparum, and knockout of the fumarate hydratase gene in P. berghei are provided.

3.1. INTRODUCTION

Fumarate hydratase (FH) (E.C. no. 4.2.1.2) catalyses the interconversion of fumarate to malate. There are two biochemically distinct FH present in organisms. Class I fumarate hydratases are iron-sulfur cluster containing enzymes, whereas, class II enzymes are iron independent. Only a few eukaryotic organisms are known to have Class I type FH. All apicomplexa have the C-I type enzyme and they lack C-II type FH (Danne et al., 2013). However, the list of eukaryotes having C-I FH is still not catalogued. It would also be an interesting exercise to check if all other eukaryotes having C-I FH also have C-II FH. Moreover, it would be informative to catalogue eukaryotes having C-I FH on the basis of their organisation (unicellular/multicellular), lifestyle (parasitic/free-living) and redundancy in fumarase activity (whether or not they have both types of FH). This cataloguing might be useful to draw any possible correlation between these parameters and the type of FH an organism possess.

As discussed in the previous chapter, fumarate is known to perform a multitude of functions and the role of the enzyme fumarate hydratase (FH) is critical in dictating the intracellular level of the metabolite. Substantiating this fact is the accumulating evidence wherein mutation/s leading to FH inactivation has been implicated in renal cancer, epithelial to mesenchymal transition, diabetes and obesity (Adam et al., 2013; Boettcher

et al., 2014; Sciacovelli et al., 2016; Frizzell et al., 2012; Thomas et al., 2012). As all TCA cycle reactions occur mainly in the mitochondria, the enzyme is expected to be mitochondrially localized in eukaryotes. However, dual localisation of fumarate hydratase (class II type) to both mitochondria and cytosolic compartments and the molecular mechanism of localization has been studied in the yeast, *Saccharomyces cerevisiae* (Knox et al., 1998). Upon DNA damage the cytosolic enzyme also relocalizes to the nucleus and has been shown to be important in initial recruitment of DNA repair machinery to the site of damage (Yogev et al., 2010). In yeast, though fumarate is generated mostly in mitochondria the role of the cytosolic enzyme is still not clear. The enzyme has been localized and biochemically characterised in *Trypanosoma cruzi* (Coustou et al., 2006). The organism has two isoforms of the enzyme, with both belonging to the iron-sulfur cluster containing class-I type FH. Through RNAi mediated knockdown of the transcripts, it was shown that the enzyme is essential for the viability of the parasite. Notably, the defective growth phenotype of the FH knockdown parasite was rescued by addition of fumarate. The authors postulate that the essentiality of the fumarate is because of the dependence of the cytosolic enzyme dihydroorotate dehydrogenase (DHODH) on fumarate for the conversion of dihydroorotate to orotate, an essential metabolite in the *de novo* pyrimidine biosynthesis. This implies that malate to fumarate conversion is important for parasite growth which is also substantiated by the fact that addition of fumarate rescued the defective growth phenotype.

Leishmania donovani, the parasite that causes leishmaniasis has two genes LmjF24.0320 and LmjF29.1960 that encode for fumarate hydratase LmFH-1 and LmFH-2 enzymes, respectively. Both the enzymes belong to class I type, Fe-S cluster containing fumarase. LmFH-1 localizes to the mitochondria and LmFH-2 localizes predominantly to the cytosol with some localisation seen in glycosomes as well. Both enzymes were thermolabile and exhibit difference in secondary structural features as examined by circular dichroism (Feliciano et al., 2012). The exact molecular reason behind using a thermolabile, iron-sulfur cluster containing enzyme for catalysis instead of a thermostable iron-independent enzyme is still not clear. Aconitase, an iron-sulfur cluster containing enzyme is present in all organisms that has an intact TCA cycle. Apart from being an enzyme the protein is also involved in gene regulation. In times of iron deficiency, the protein undergoes a drastic change in structure and transforms to a RNA binding protein. Specifically, it binds to the mRNA of proteins involved in iron metabolism to re-establish intracellular iron levels in the cell (Beinert et al., 1996). Whether such moonlighting function exists for fumarate hydratase is not known.

3.2. Materials and methods

3.2.1. Chemicals, strains and molecular biology reagents

Plasmid pGDB and the Plasmepsin-I knockout (PM1KO) *Plasmodium* strain, obtained from Prof. Daniel E. Goldberg's lab (Washington university, USA) were used for the conditional knockdown study of fumarate hydratase. *Plasmodium berghei* ANKA strain was procured from MR4. For regular cloning procedures, plasmid DNA isolation kit, PCR product purification kit, and gel extraction kit were procured from Qiagen, Germany. Oligonucleotides were custom synthesized from Sigma-Aldrich, Bangalore. Unless otherwise specified all chemicals used were of high quality and procured from Sigma-Aldrich, USA.

3.2.2. Expression and purification of *P. falciparum* FH C-terminal domain

DNA fragment corresponding to the C-terminal domain of PffFH was PCR amplified using primers mentioned in **Table 3.1** and genomic DNA of *P. falciparum* as template. Using regular cloning procedures, the PfCTD was cloned in pET21b vector using NdeI and XhoI restriction sites.

Table 3.1. Primers used for cloning PfCTD in pET21b vector

FHCTDF_NdeI	CCGAATTCATATGGCTGTAAAATTGATTTAAATCAAATATGGAAC
FHCTDR_XhoI	CCGCTCGAGTGATGGTAACCATTTATTATAAAAATCATTGCC

For purification, BL21(DE3)-RIL strain was transformed with pET21b plasmid with PffHCTD and selected on LB plate containing ampicillin and chloramphenicol. Multiple colonies were picked and inoculated into a 10 ml LB broth. The culture was grown for 6 h at 37 °C. Thereafter, the cells were pelleted, washed with antibiotic free LB broth and then used for inoculating a 800 ml culture. The cells were grown at 30 °C until the OD₆₀₀ reached 0.5, thereafter induced with 100 µM IPTG and grown further for 16 h at 16 °C. The cells were harvested by centrifugation and resuspended in lysis buffer containing 50 mM Tris-HCl, pH 7.4, 150 mM NaCl, 1 mM PMSF, and 10% glycerol. The cells were lysed using 4 cycles of French press at 1000 psi and the lysate cleared by centrifuging at 30,000 x g for 30 minutes. The supernatant was carefully removed without disturbing the pellet and 1 ml slurry of Ni-NTA beads (Novagen) that was pre-equilibrated with lysis buffer was added for binding of the His-tagged protein. The binding was done at 4°C for 3 h and thereafter, the beads were washed with 50 ml lysis buffer and the protein was eluted with different concentrations of imidazole. The eluates were further purified by size-exclusion chromatography using Superdex-200 PG (16/600) from GE healthcare Life Sciences. The column was equilibrated with buffer containing 50 mM Tris-HCl, pH 7.4, 150 mM NaCl,

and 1 mM PMSF and the protein was eluted with the same buffer at a flow rate of 1 ml/min.

3.2.3. Generation of gene targeting construct for the conditional knockdown of *P. falciparum* (Pf) fumarate hydratase (FH)

Standard protocols were followed for cloning (Sambrook and Russell, 2001). *P. falciparum* 3D7 genomic DNA was used as template and the oligonucleotides mentioned in **Table 3.2** were used for the amplification of the coding sequence of PffH. The PCR product was digested with *XhoI* and *AvrII* and subsequently cloned in between these sites into the plasmid pGDB to generate the construct pGDB-FH.

Table 3.2. The primers used for amplifying the coding sequence of the gene for fumarate hydratase for cloning into pGDB using *XhoI* and *AvrII* restriction sites (underlined).

Primer name	Primer sequence (5' to 3')
FHpGDB-Xho1_FWD	GACTTACTCGAGATGATAAAGTTTAAAGAAGCTTCCATTTTGTAC
FHpGDB-AvrII_REV	GACTTACCTAGGTGATGGTAACCATTATTATAAAAATCATTGCC

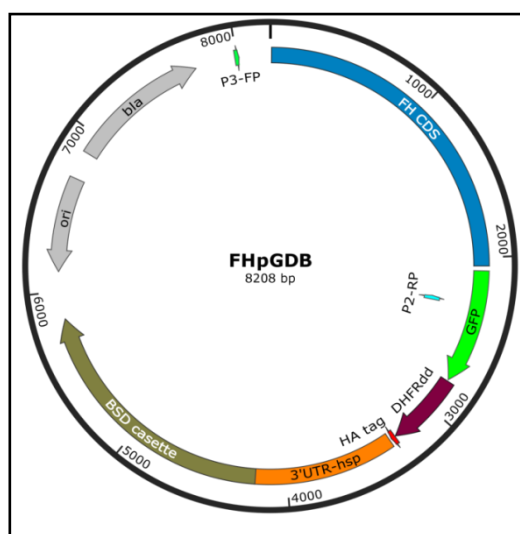


Figure 3.1. A schematic representation of key features in the plasmid pGDB-FH.

FH CDS- fumarate hydratase coding sequence, *GFP*-green fluorescent protein, *DHFRdd*-dihydrofolate reductase degradation domain, *HA tag*- haemagglutinin tag, *BSD cassette*-encodes the gene blasticidin deaminase, *bla*- encodes beta lactamase, *P3-FP* and *P2-RP* are primer positions for diagnostic PCR to differentiate between episomal copy and integration event.

This plasmid contains the complete ORF of PffH followed by green fluorescent protein (GFP), *E. coli* DHFR degradation domain (DD) and 3XHA tag, that together constitute a regulatable fluorescent affinity tag (RFA) as shown in **Figure 3.1**. The strategy has been successfully used to conditionally knockdown multiple essential genes (Muralidharan et

al., 2011; Florentin et al., 2016) at the level of protein. A protein tagged with the degradation domain will be stable only upon binding of the small molecule trimethoprim. Upon withdrawal of the drug from the medium, the protein along with the degradation domain will be targeted to proteasomal degradation.

3.2.4. Transfection and selection of parasites

PM1KO strain was used for this experiment. For the generation of parasites in which the fumarate hydratase can be conditionally knocked down, the plasmid pGDB-FH was used. **Figure 3.2** a schematically shows the effect of presence/absence of TMP on the protein level within the cell.

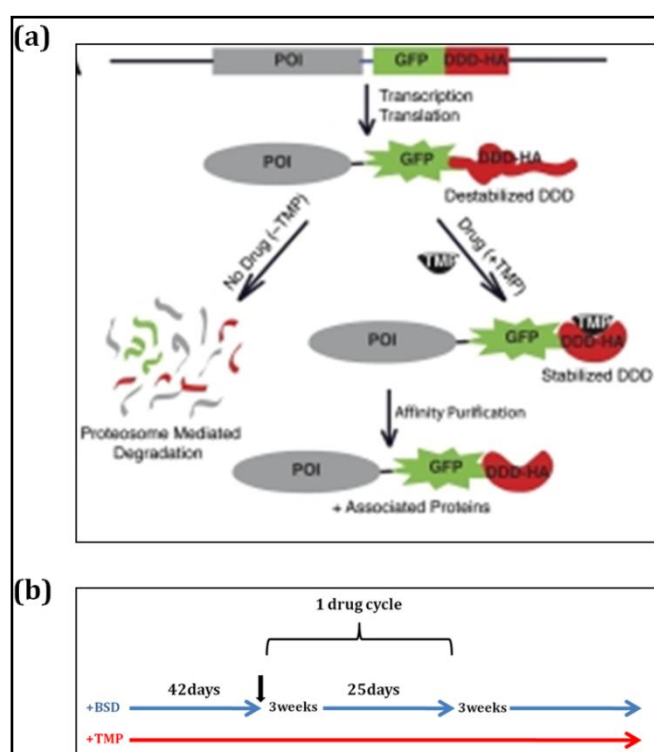


Figure 3.2. Schematic showing the conditional knockdown strategy of the protein of interest using the RFA tag.

(a) The effect of TMP on the stability of the protein of interest and the use of fusion protein to pull down interacting partners is shown. DDD, DHFR degradation domain; TMP, trimethoprim; POI, protein of interest; HA, hemagglutinin tag. The figure is reproduced from Muralidharan et al. 2011. **(b)** The drug cycling regimen. The blue arrows indicate the presence of 2.5 $\mu\text{g}/\text{ml}$ of blasticidin and the red arrow indicates the presence of 10 μM trimethoprim. The duration corresponding to the removal of blasticidin for 3 weeks and reintroducing for 25 days constitute one drug cycle. Multiple drug cycles ensure the removal of the episomal copy of the plasmid pGDB-FH.

The plasmid DNA was isolated using EndoFree plasmid maxi prep. kit from Qiagen, USA. An aliquot of the eluted plasmid was run on the gel to check for purity and relative

amounts of supercoiled population. 100 µg of plasmid was mixed with 50 µl of cytomix and incubated overnight at 4°C. Electroporation using the plasmid was performed using both methods mentioned in section 2.6. When the parasitemia reached 4-6%, 2.5 µg/mL blasticidin and 10 µM trimethoprim (TMP) were added to the medium. From this point onwards trimethoprim was always retained in the culture medium. **Figure 3.2 b** schematically shows the drug cycling strategy used. When the parasitemia reached around 5%, blasticidin was removed from the medium while trimethoprim was retained. The parasites were grown for 3 weeks without blasticidin after which it was again reintroduced. These steps constitute one drug cycle. 3 drug cyclings were done so as to enrich the culture with stable integrant population of parasites. This cycling should be repeated until the parasites carrying the episomal copy are not detected by PCR. The strain of the parasites generated will henceforth be referred to as PffH-RFA.

3.2.5. Genotyping of the parasites

Confirmation of integration of the RFA tag into the right locus in the chromosome of the parasite, PffH-RFA, was done by PCR with the appropriate set of primers. The presence of an episomal copy of plasmid was also tested by PCR with primers of right combination. The primers used are given in **Table 3.3**.

Table 3.3. List of oligonucleotides used for validation of integration of RFA tag into the right FH gene locus.

S.No	Primer	Primer sequence (5' to 3')	Purpose
1	P1 and P2	P1:GCCATTAAAAAATAGGATAACATATATAAAAATGCACAAT CC P2:CATATGATCTGGGTATCTCGCAAAGCATTG	5' integration
2	P2 and P3	P2:CATATGATCTGGGTATCTCGCAAAGCATTG P3: GGAGACGGTCACAGCTTGTCTGTAAG	Episomal copy check
3	P3 and P4	P3: GGAGACGGTCACAGCTTGTCTGTAAG P4:GTTGTGATATTGCACATGAATGGATCCAATC	3' integration

Plasmodium berghei culturing and manipulation

3.2.6. Strain of parasite and mice used for the study

Plasmodium berghei strain ANKA (MRA-671,MR4, ATCC Manassas Virginia) was used for the study. The strain was procured from Malaria Research and Reference Reagent Resource Center, USA (MR4). For routine maintenance of wild-type and mutant *P. berghei* strains, BALB/c mice (either male or female) were used.

3.2.7. Maintenance and assessment of parasites

For routine maintenance, 50-100 µl of parasite cell suspension from frozen glycerol stock

was injected intraperitoneally into a BALB/c mouse. For parasitemia estimation, the mice were bled through the tail vein, a thin smear of the blood was made on a glass slide and stained with Giemsa solution similar to that followed for *P. falciparum* culture. The parasitemia estimation is best when done in the second half of the day (14.00-16.00 h) as the parasites are mostly in mature stages and hence, easier for visual examination.

3.2.8. Isolation of free parasites from infected mice erythrocytes

Isolation of free parasites is achieved by lysing the erythrocytes selectively leaving the parasites intact. This is done using erythrocyte lysis buffer (ELB) that contains 150 mM ammonium chloride, 10 mM potassium bicarbonate, and 1 mM EDTA. For preparing 1 litre of 10X stock of ELB, 80.20 g of ammonium chloride, 10.0 g of potassium bicarbonate and 3.70 g of EDTA were mixed and the volume was made up to 1 liter using autoclaved MilliQ water. The solution was filter sterilized and stored at 4°C for up to 6 months. The infected mouse was bled through the retro-orbital vein for collecting parasites. Approximately, 700 - 1000 µl of whole blood was obtained from each mouse. The blood sample was centrifuged and the cells resuspended in ELB. For up to 1 ml of blood, 10 ml of ice-cold ELB was used. The suspension was left on ice for 3-5 min when erythrocyte lysis occurs and free parasites are released. The solution turned red due to hemolysis and was centrifuged at 800 x g for 8 min at room temperature, to pellet the parasites. The parasite pellet was directly processed for other applications or was flash frozen in liquid nitrogen and stored at -80°C until further use.

3.2.9. Cryopreservation and revival of *P. berghei*

Blood containing infected erythrocytes (0.7-1.0 ml) at parasitemia between 1 and 10%, was collected from mice in an equal volume of incomplete medium containing 200 U/ml heparin (Cat. no. Sigma-H3149). The blood was mixed with 1 ml of glycerol-PBS solution (30% glycerol: v/v), containing 0.05 ml of heparin stock solution (200 U/ml was made by dissolving the heparin powder at a concentration of 1mg/ml) . The solution was transferred to a sterile cryovial, flash-frozen and stored in liquid nitrogen. The parasites were revived by simply thawing the frozen stocks at 37°C for 1-2 min and 50-100 µl of the cell suspension was injected into mice intraperitoneally.

3.2.10. *P. berghei* genomic DNA isolation

The parasite pellet was resuspended in 700 µl Tris-sodium chloride-EDTA (TNE) buffer containing 10 mM Tris-HCl, pH 8, 100 mM sodium chloride, 5 mM EDTA, pH 8. The volume was made up to 1 ml and incubated for 10 min at 37°C. Thereafter, 200 µg of proteinase K

(20 µl of 10 mg/ml solution) was added and the incubation was continued for 1 h at 37°C. Buffered phenol was added up to 1.5 ml, tubes were inverted several times and the solution was centrifuged at 16000 x g for 5 min. The aqueous phase was transferred to a new tube and chloroform: isoamyl alcohol mixture (24:1) was added up to 1.5 ml. The tubes were inverted several times and centrifuged at 16000 x g for 5 min. The aqueous phase was transferred to a new tube and 0.1 volume of 3 M sodium acetate, pH 5.2 and 2 volumes of absolute ethanol were added. The tubes were inverted several times and the solution was incubated in -20 °C freezer overnight to enhance the precipitation of DNA. The solution was centrifuged for 10 min at 16000 x g for 15 min at 4 °C. The DNA pellet was washed with 70% ethanol and dried in a dry bath at 60 °C. The DNA was resuspended in 50-300 µl of autoclaved MilliQ water.

3.2.11. *P. falciparum* total RNA isolation

Saponin released parasites from 40 ml of culture with 5% hematocrit and 6-8 % parasitemia was used for RNA isolation using standard protocol (Ménard, 2013). Briefly, the saponin released parasites were washed with PBS twice and 1 ml of TRIzol® reagent was added to the washed saponin pellet. The pellet was resuspended thoroughly with pipette such that there are no clumps and the solution was incubated at RT for 15-20 min. The solution was centrifuged at 16000 x g for 10 minutes and the supernatant obtained was mixed well with 200 µl of chloroform by inverting the tube. The sample was centrifuged at 16000 x g for 30 minutes at 4°C to separate the organic and the aqueous phase. The supernatant containing the RNA fraction was carefully removed and transferred to another microcentrifuge tube without disturbing the interface layer. The supernatant was mixed with 400 µl of isopropanol by gently inverting the tubes 2-3 times and left at RT for 10 minutes. The sample was centrifuged at 16000 x g at 4°C for 5 minutes. The pellet containing RNA was washed with 1 ml of 75% ethanol and the washed pellet was air dried. The pellet was dissolved in 20- 50 µl of DEPC treated distilled water and used for subsequent experiments.

3.2.12. Maintenance of mice

BALB/c mice were used for regular maintenance of parasite. The infected mice were kept in a filter-top cage so that the infection does not spread to other mice through a mosquito bite. The mice were fed with regular mice feed and autoclaved water for drinking. Institutional animal ethics committee clearance for all animal-related experiments and procedures was obtained.

3.2.13. Parasite administration and collection

The parasites were administered to mice through different routes based on the application. For establishing a fresh infection from glycerol stock, the intraperitoneal route was used. For limiting dilution cloning, the intravenous route, either through tail vein or retro orbital plexus was used. For parasite collection, the mice were bled by the puncture of retro-orbital plexus. The use of retro-orbital plexus for parasite administration is adopted based on Yardeni et al., 2011.

Generation of plasmid constructs for targeted gene replacement using recombineering.

3.2.14. *E. coli* strains, plasmids and *P. berghei* genomic clones used.

Generation of gene modification (tagging or deletion) constructs using recombineering strategy involves use of a set of reagents comprising of both plasmid DNA and *E. coli* strains modified to handle the AT-rich *Plasmodium* genes as well as aid in manipulating such sequences. TSA *E. coli* cells, Lucigen, Wisconsin, USA, was used for the study. Other plasmids used in the generation of knockout constructs are listed in **Table 3.4** and were obtained from GeneBridges, Heidelberg, Germany. *E. coli* strains E5555 and E5454 were used for the maintenance of the plasmid with a pR6K origin of replication. The strains were a kind gift from Prof. Herbert Schweizer, Colorado State University, Colorado.

Table 3.4. List of plasmids used in the generation of *P. berghei* fumarate hydratase knockout construct.

S.No.	Name of the construct	Purpose
1	PbG01-2466a09	<i>P. berghei</i> genomic clone used for generation of tagging or knockout constructs of fumarate hydratase.
2	pSC101gbdA-tet	Encodes the lambda phage red operon that is used in phage recombination and proofreading machinery and <i>E.coli recA</i> .
2	R6K_R1R2_Zeo PheS	Used as a template for generating the Zeo-PheS cassette
3	R6K GW 3XHA ko (2X PbDHFR 3'UTR)	Used in <i>in vitro</i> LR-Clonase reaction to introduce DHFR marker into pJAZZ vector for 3XHA tagging or knockout construct generation.
4	GW R6K mCherry	Alternative to plasmid mentioned in 3. The tag here is mCherry instead of 3X HA.

3.2.15. Generation of *P. berghei* fumarate hydratase gene tagged and gene deletion constructs

The recombination efficiency of exogenous constructs in *Plasmodium berghei* is very low, necessitating the usage of long homology arms of a minimum length of 1kb. Cloning AT-

rich genes and intergenic segments of the *P. berghei* genome using conventional restriction-ligation based cloning is a daunting task. Recombineering is an alternative for regular cloning procedures that does not involve PCR, restriction digestion, and ligation. The method is based on published protocols (Pfander et al., 2011). **Figure 3.3** describes the steps involved in the recombineering. The two major-steps involved in generation of gene targeting constructs involve, first the conversion of the genomic clone, containing the gene of interest (GOI) along with its flanking regions, to an intermediate vector using Red recombinase producing *E. coli* cells. The second step involves the conversion of the intermediate vector to the final gene targeting vector by use of *in-vitro* LR-Clonase based reaction. PlasmogEM is a repository containing a library of *P. berghei* genomic DNA clones and their targeting constructs. A brief protocol describing the steps involved in generation of FH targeting constructs (both tagging and knockout) from the fumarate hydratase genomic clone, PbG01-2466a09 is given below,

- 1) The genomic clone PbG01-2466a09 procured from PlasmogEM was validated by PCR using the quality control primers, QC1 and QC2 as well as by restriction mapping.
 - 2) A PCR was performed with primers RECupR2 and RECdownR1 using R6K- R1R2-Zeo-PheS plasmid as the template. The PCR product was subjected to DpnI digestion and then purified by gel extraction.
 - 3) The TSA cells containing the genomic clone PbG01-2466a09 (TSA_FH) were made recombination proficient by transforming it with temperature sensitive plasmid pSC101-gbdA-tet that expresses Red recombinase enzymes upon arabinose induction.
 - 4) The PCR product generated in step 2 was introduced into the recombination proficient TSA_FH cells by electroporation. The cells were selected on Zeocin plate at 37 °C. This ensures selection of transformants as well as curing of temperature sensitive pSC101 plasmid. The *E. coli* strain at this stage, called TSA_FHIV, has the FH ORF replaced with Zeo/Phe cassette, a positive/negative selection marker of *E. coli*. The vector at this stage is the intermediate vector (FHIV) and is validated using the PCR with primers QC1 and PheSR2, the details of which are given in **Table 3.5**.
 - 5) To ensure complete elimination of the parent construct, PbG01-2466a09, the FHIV plasmid was isolated from TSA_FHIV and used for transformation of fresh TSA cells and subjected to selection on zeocin plate. The process was repeated until there was no PCR product obtained using QC1 and QC2 using the plasmid isolated from zeocin selected TSA cells as a template.
 - 6) The FHIV plasmid was mixed with pR6K-L1L2-hdhfr-yfcu and subjected to *in vitro* LR-clonase reaction. The Clonase enzyme mix promotes the recombination between *attL* and *attR* sites. The reaction was performed at 16°C for 16 h. After the reaction, the
-

contents were desalted by disc dialysis or five times water diluted reaction mixture was used directly for electroporation in fresh TSA cells. The cells were plated on a YEG-Cl plate which is toxic for cells containing undesired products of LR-Clonase reaction and the plasmid FHIV. This process will generate strains carrying the plasmid in which the FH gene is either tagged (FHHA) or is knocked out (FHKO). The plasmids were isolated from the colonies and validated using QC1 and *hdhfr* reverse primer. Positive bands indicate the presence of the gene targeting construct for use in *P. berghei* transfection, after *NotI* digestion and gel purification. FH tagging construct was generated following a similar procedure as a part of the Wellcome trust advanced course on malaria genetics, 2013, Sanger Institute, UK.

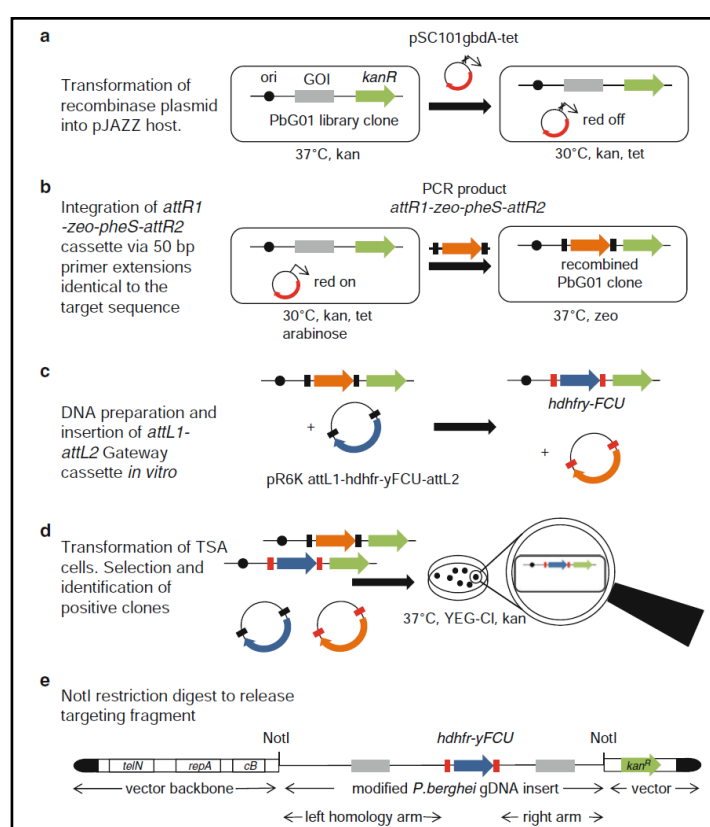


Figure 3.3. Overview of steps involved in the generation of gene targeting constructs for *P. berghei*.

(a) Making TSA cells containing the genomic clone of interest, recombination proficient by transforming it with *pSC101-gbdA-tet*. **(b)** Arabinose induction of red operon followed by electroporation with the PCR construct that contains 50bp homology arms targets and replaces the gene of interest in the pJAZZ vector with Zeo-PheS cassette. **(c)** The intermediate vector is used in the *in vitro* Clonase reaction with *attL1/L2* containing plasmids to replace the bacterial selection cassette with the *Plasmodium* selection cassette. **(d)** Transformation of TSA cells with LR-clonase reaction mix and growing it on negative selection plate. **(e)** Confirmation of the final construct by PCR and the *NotI* released fragment can be used for transfection into *P. berghei*. The figure is reproduced from Ménard 2013.

Table 3.5. Oligonucleotides used for the generation of fumarate hydratase knockout construct

S.No	Primers	Sequence (5' to 3')
1	QC1	CATTATCTTTTTCTTTTTTGCACATATTTAAAACG
2	QC2	CCTTTTTCTTCAAACCTCAAAAATATCTAAGAAATTG
3	PheSR2	TCATTCTTCGAAAACGATCTGCG
4	Hdhfr-yfcu	ACTTCTTAAACCTAATCTGTAGTAAGGAAGGGATTG
5	RECupR2	GATTTTGTGTGAAATTTATTTAATAAATTTGTAAATTTTGAACCTCA ACACCGCTACTGCGACTATAGA
6	RECdownR1	TTAAAACCTTATGAGTTTTTTTTTCCAACAATGTACATATTTTTGGAA AAAAAGGCGCATAACGATACCAC
7	5'intcheckPbFHHA_F P	CGAACTATGGGCATGGTAATAATAATGGAAATAGCG
8	3'intcheckPbFHHA_R P	CCTCAGTATATGAACAAATGAATGACCATATTAAGTG
9	FPbFHHA	GGGAAGTATTGGAGGCCAGGTGCAATATTAGC
10	RPbFHHA	GTGGATGAAAATATTACTGGTGCTTTGAGGGGTGAGC

3.2.16. Transfection of *P. berghei* using linear DNA.

50-100 µl of glycerol stock of infected blood containing *P. berghei* ANKA strain was injected intra-peritoneally into two mice. The parasitemia was monitored by making Giemsa smears from tail blood. At 1-3 % parasitemia, the mice were bled by retro-orbital plexus puncture. Around 0.8-1.0 ml of blood was obtained from each mouse. The blood was collected in incomplete medium with heparin to a final concentration of 200 U/ml. The parasites were now mixed with the medium containing RPMI-1640 with glutamine, 25 mM HEPES, 10 mM NaHCO₃ and 20% fetal bovine serum. Around 50 ml of the cell suspension was taken in 250 ml reagent bottle, gassed for 2 min with malaria gas (5% oxygen, 5% carbon dioxide and 90% nitrogen) and then tightly sealed. The bottle was shaken at an optimal speed (120-150 rpm) so that the cells don't settle. The culture was grown overnight at 36.5 °C, during which early stages like rings and trophozoites mature to form mature schizonts and this was monitored by making a Giemsa smear. All the parasites that mature to schizont stage are arrested at this stage. If the parasite maturation had not occurred the growth was continued under the same condition for few more hours and then examined again using Giemsa smear.

3.2.17. Nycodenz density gradient centrifugation

Once the parasite cells had achieved good synchrony, they were subjected to Nycodenz based gradient centrifugation. The process enriches the mature stage parasites. Nycodenz

enrichment of schizont stage parasites was achieved by using 55% / 60% Nycodenz gradient. The 50 ml culture suspension was divided equally among two 50 ml conical tubes and 10 mL of Nycodenz is layered below carefully. The centrifugation was done at 800 x g for 30 min during which the separation of the mature stages happens and forms a darkly coloured ring-like layer is formed in the gradient. The band was carefully collected and washed with PBS. The cells were pelleted and an aliquot was used to make smear to check the level of enrichment. The collected schizonts should be sufficient enough for 10 different transfections. Around 5-10 µg of DNA was used for every transfection. The DNA was mixed with 100 µl of nucleofector solution (Lonza) from the parasite nucleofector kit P1. The schizonts were mixed with this solution and transferred to the nucleofector cuvette using a sterile Pasteur pipette supplied with the nucleofector kit. Transfection was done using Amaxa 2D-nucleofector using the program U-33. Immediately after the transfection the contents of the cuvette were injected through intravenous administration. We preferred the retro-orbital plexus route as the tail vein injections resulted in necrosis and complete removal of the tail, making subsequent parasitemia estimation difficult. The mice were maintained normally and the drug pressure was started 24 h after the transfection by feeding the mice with pyrimethamine-containing water for around 10 days or up to the appearance of the transfectants. For genotyping the transfected parasites, primers #7-10 given in Table 3.4 were used.

3.2.18. Southern blotting with *P. berghei* genomic DNA

Standard protocols were followed for Southern blotting (Ménard, 2013). Briefly, the *P. berghei* genomic DNA was isolated by phenol-chloroform method and equal amount of this DNA from PbWT and drug-selected recombinant parasites were subjected to restriction digestion overnight using specific restriction enzymes. For *Bst*BI digestion, the incubation temperature was 65°C. The digested DNA was subjected to agarose gel electrophoresis to separate the DNA fragments based on molecular weight. The separated DNA was depurinated by incubating the gel in 0.25 M HCl for 5 minutes. The gel was neutralized by incubating in solution containing 1 M NaOH, 1.5 M NaCl (alkaline transfer buffer). The DNA on the gel was transferred onto a Zeta probe hybridisation membrane by capillary transfer for 18 h. The DNA was crosslinked to the membrane by exposure to UV following which it was incubated with pre-hybridisation buffer (for 200 ml; SDS-10 g, NaCl- 5.8 g, 0.5 M EDTA- 2.4 ml, 1 M Sodium phosphate, pH7 -20 ml and 30 µl of salmon sperm DNA of concentration 0.75 mg/ml: dissolve in 150 ml and bring up to 200 ml) containing carrier DNA for 1 hour at 65°C. The radiolabeled probe (synthesized using random primer kit) was added to 20 ml of pre-hybridization solution (sans carrier DNA)

and boiled for 15 minutes in water-bath. The hot solution was directly added to the membrane and incubated at 65°C for 18 h. After incubation the membrane was washed using sodium citrate buffer (dissolve 175.3 g of NaCl, 88.2 g of sodium citrate in 800 ml of water. Adjust the pH to 7 with a few drops of concentrated HCl. The volume was adjusted to 1 L with water, dispensed into aliquots and sterilized by autoclaving. The final concentrations of the ingredients are 3M NaCl and 0.3 M sodium citrate). The membrane was exposed to a phosphoscreen overnight in lightproof cassette and developed using a phosphor imager.

3.2.19. Limiting dilution cloning

For limiting dilution cloning, standard procedures were followed (Janse et al., 2006). Briefly, blood from the mouse infected with *P. berghei* recombinant parasites were collected in RPMI medium containing heparin. Appropriate dilution of the whole blood was made and the total number of erythrocytes in a known volume of blood was estimated using hemocytometer-based counting. The parasitemia was estimated by counting at least 1000 RBCs in a Giemsa stained smear prepared from the same blood. Based on the total cell count and the parasitemia estimated, the blood was serially diluted using incomplete RPMI medium such that 10 parasites are present in 1 ml of solution. 100 µl of this solution was injected intravenously into 10 different mice. Similar calculation was used for injecting more number of mice. The presence of parasites was monitored by making Giemsa stained smears of the blood collected from these mice at regular intervals.

3.2.20. Sequence analysis

E. coli Fum A sequence was used as a query in BLASTP to fetch a list of eukaryotic organisms having class I FH. The search was restricted to eukaryotes and the maximum target hits was changed from a default value of 200 to 20,000. Each of these eukaryotic organisms was individually searched for the presence of class II FH using *E. coli* FumC as the query sequence for BLASTP. Hits with an e-value of 10^{-10} was considered significant and used for the analysis.

3.3. RESULTS AND DISCUSSION

3.3.1. Taxonomic distribution of class-I FH in eukaryotes

Table 3.6. List of eukaryotic organisms that have class-I type fumarate hydratase.

	Organism	Annotation/Accession no.	Life style	C-II FH
Alveolata	<i>Perkinsus marinus</i>	FH: XP_002769256	[P][U]	A
	<i>Babesia bovis</i>	FH: XP_001608904	[P] [U]	A
	<i>Theileria annulata</i>	FH: XP_954791	[P] [U]	A
	<i>Plasmodium falciparum</i>	FH: XP_001352143	[P] [U]	A
	<i>Toxoplasma gondii</i>	FH: XP_002368801	[P] [U]	A
	<i>Cryptosporidium muris</i>	FH: XP_002140038	[P] [U]	A
	<i>Neospora caninum</i>	FH: XP_003880843	[P] [U]	A
	<i>Hammondia hammondi</i>	FH: XP_008887656	[P] [U]	A
	<i>Eimeria tenella</i>	FH: XP_013233133	[P] [U]	A
Kinetoplastids	<i>Leishmania donovani</i>	FH: XP_003862626	[P] [U]	A
	<i>Trypanosoma cruzi</i>	FH: XP_814517	[P] [U]	A
	<i>Leptomonas pyrrocoris</i>	FH: XP_015659024	[P] [U]	A
	<i>Phytomonas sp. isolate Hart1</i>	UP: CCW67322	[P] [U]	A
	<i>Strigomonas culicis</i>	FH: EPY34169	[P] [U]	A
	<i>Bodo saltans</i>	FH: CUE71425	[P] [U]	A
	<i>Angomonas deanei</i>	FH: EPY26539	[P] [U]	A
Flat worms	<i>Hymenolepis microstoma</i>	FH:CDS31600	[P][M]	A
	<i>Echinococcus granulosus</i>	FH: CDS20347	[P] [M]	A
	<i>Schistosoma mansoni</i>	PR: CCD75592	[P] [M]	P
	<i>Clonorchis sinensis</i>	FH: GAA32985	[P] [M]	P
	<i>Opisthorchis viverrini</i>	HP: XP_009168721	[P] [M]	P
Green algae	<i>Volvox carteri f. nagariensis</i>	FH: XP_002956431	[FL] [M]	P
	<i>Chlamydomonas reinhardtii</i>	FH: XP_001696634	[FL] [U]	P
	<i>Bathycoccus prasinos</i>	FH: XP_007514405	[FL] [U]	P
	<i>Gonium pectorale</i>	HP: KXZ553026	[FL] [U]	A
	<i>Ostreococcus lucii marinus CCE9901</i>	FH: XP_003078640	[FL] [U]	P
	<i>Micromonas commoda</i>	FH: XP_002501905	[FL] [U]	P
Dia.	<i>Phaeodactylum tricornutum CCAP 1055/1</i>	PF:XP_002179239	[FL] [U]	P
	<i>Thalassiosira pseudonana CCMP1335</i>	FH: XP_002289528	[FL] [U]	P
Gast.	<i>Aplysia californica</i>	UP: XP_12940821	[FL] [M]	P
	<i>Lottia gigantea</i>	HP: XP_009058873	[FL] [M]	P
	<i>Biomphalaria glabrata</i>	FH: XP_013081380	[FL] [M]	P
	<i>Trichuris trichiura [nematods]</i>	FH: CDW56990	[FL/P][M]	P
	<i>Caenorhabditis remanei [nematods]</i>	HP: XP_003087664	[FL] [M]	P
	<i>Ricinus communis [eudicots]</i>	FH: EEF26711	[FL] [M]	P
	<i>Lingula anatina [brachiopods]</i>	FH: XP_013411739	[FL] [M]	P
	<i>Helobdella robusta [segmented worms]</i>	HP: XP_009028259	[FL] [M]	P
	<i>Capitella teleta [segmented worms]</i>	HP: ELT88058	[FL] [M]	P
	<i>Plutella xylostella [moths]</i>	UP: XP_011567445	[FL] [M]	P
	<i>Trichoplax adhaerens [placozoa]</i>	HP: XP_002113462	[FL] [M]	P
	<i>Crassostrea gigas (Pacific oyster) [bivalves]</i>	FH: EKC28844	[FL] [M]	P
	<i>Octopus bimaculoides [cephalopods]</i>	HP: KOF97915	[FL] [M]	P
	<i>Emiliana huxleyi CCMP1516 [haptophytes]</i>	FH: XP_005760439	[FL] [U]	A
	<i>Chrysochromulina sp. [haptophytes]</i>	FH: KO053837	[FL] [U]	A
	<i>Monosiga brevicollis [choanoflagellates]</i>	HP: XP_001745789	[FL] [M]	P
	<i>Salpingoeca rosetta [choanoflagellates]</i>	FH: XP_004991224	[FL] [M]	P
	<i>Strongylocentrotus purpuratus [sea urchins]</i>	UP: XP_782370	[FL] [M]	P

	<i>Guillardia theta</i> CCMP2712[<i>cryptomonad</i>]	HP: XP_005839918	[FL] [U]	Am
	<i>Ectocarpus siliculosus</i> [<i>brown algae</i>]	FH: CBJ30095	[FL] [M]	P
	<i>Priapulius caudatus</i> [<i>priapulids</i>]	FH: XP_014672575	[FL] [M]	P
	<i>Naegleria gruberi</i> [<i>percolozoa</i>]	FH: XP_002683156	[FL] [U]	P
	<i>Acanthamoeba castellanii</i> str. Neff	FH: XP_004336044	[FL/P] [M]	P
	<i>Blastocystis hominis</i> [<i>stremanophiles</i>]	UP: XP_012899223	[P] [U]	Am
	<i>Capsaspora owczarzewski</i> [<i>opisthokont</i>]	FH: XP_004345167	[Sy][U]	P
	<i>Thecamonas trahens</i> ATCC 50062	FH: XP_009058873	[FL] [U]	P
	<i>Beauveria bassiana</i> D1-5 [<i>ascomycetes</i>]	FH: KGQ11123	[P] [U]	P
	<i>Branchiostoma floridae</i> [<i>lancelets</i>]	HP: XP_002613780	[FL] [M]	P
	<i>Saccoglossus kowalevskii</i> [<i>hemichordata</i>]	UP: XP_006819722	[FL] [M]	P
	<i>Pantholops hodgsonii</i> [<i>even toed ungulates</i>]	UP: XP_005976865	[FL] [M]	P
	<i>Entamoeba histolytica</i> [<i>Amoebazoa</i>]	FH: XP_001913833	[P][U]	A
	<i>Aureococcus anophagefferens</i> [<i>pelogophytes</i>]	HP: XP_009035148	[FL] [U]	P
	<i>Batrachochytrium dendrobatidis</i> [<i>chytrids</i>]	HP: XP_006683538	[P][U]	P
	<i>Nannochloropsis gaditana</i> [<i>algae</i>]	FH: EWM30255	[FL] [U]	P
	<i>Vitrella brassicaformis</i> [<i>chromerida</i>]	UP: CEM21256	[FL] [U]	P
	<i>Sphaeroforma arctica</i> [<i>opisthokont</i>]	FH: XP_014156242	[FL] [U]	P

FH, fumarate hydratase; [H], hypothetical protein; [UP], unknown protein; [PR], pol related; [P], parasitic; [FL], free living; [Sy], symbiont; [U], unicellular; [M], multicellular. The common names of the organism are given in square brackets following the Latin names. The list of organisms were obtained from the output of BLAST P using *E. coli* class-I fumarate hydratase protein sequence as the query. An e-value cut-off of 10^{-10} was used for selecting the protein sequences from organisms. The name of the taxon to which the organisms belong is indicated in some cases in the second column. *E. coli* FumC protein sequence was used as a query to know the presence or absence of class-II fumarate hydratase in these organisms. P, present; A, absent; Am, ambiguous; Dia., diatoms; Gast., gastropods.

Class-I-FHs are present in only few eukaryotic organisms. **Table 3.6** lists the representative organisms from different genera, the annotation status of FH protein in them, lifestyle of the organism (parasitic or free living) and whether the organism is unicellular or multicellular. *E. coli* FH protein sequence was used as the query and its homologous sequences in the non-redundant protein database were obtained using the BLAST P tool (McGinnis and Madden, 2004). The Blast P search was confined to eukaryotic sequences. The number of expected target sequence was changed from a default value of 100 to 20,000. Sequence hits with only significant e-value were used for the analysis (least e-value being 10^{-38}). The results are presented in Table 3.5. Examination of the table leads to the following key observations;

1) Organisms belonging to Alveolata, Kinetoplastida and other organisms such as *Entamoeba histolytica*, *Emiliania huxleyi*, *Hymenolepis microstoma*, *Echinococcus granulosus*, *Gonium pectorale*, *Chrysochromulina* sp., have only class-I type fumarate hydratase. Most of the other eukaryotes having class-I FH also have the gene corresponding to class-II FH.

2) *Hymenolepis microstoma* and *Echinococcus granulosus* (flatworms) are the only multicellular organisms relying entirely on class-I fumarate hydratase.

3) *Emiliania huxleyi*, *Chrysochromulina sp.*, and *Gonium pectorale* are the only free-living organisms relying exclusively on C-I FH. This negates any correlation between the type of FH and the life-style (parasitic vs free-living) of the organism.

4) *Vitrella brassiciformis*, a photosynthetic ancestor to apicomplexans has both Class I and Class II genes, suggesting a gene loss event with respect to C-II FH during the evolution of apicomplexan lineage.

Overall, the bioinformatic analysis suggests that there could have been a gene loss event (corresponding to C-II FH) associated with the evolution of apicomplexan lineage. There is no correlation between parasitic life-style and the type of FH and hence the reason behind the presence of class I FH instead of a class II enzyme in apicomplexa is not clear.

3.3.2. Expression analysis of fumarate hydratase in *P. falciparum*.

To check if fumarate hydratase is expressed during intra-erythrocytic stages, expression analysis was performed both at RNA and protein level. **Figure 3.4** shows the presence of transcripts corresponding to the full-length fumarate hydratase gene. Along with PfFH, it was found that MQO (Pf malate-quinone oxidoreductase), AAT (aspartate aminotransferase), MOG (malate-oxoglutarate transporter) that are involved in fumarate metabolism are also expressed in the intra-erythrocytic stage of the parasite.

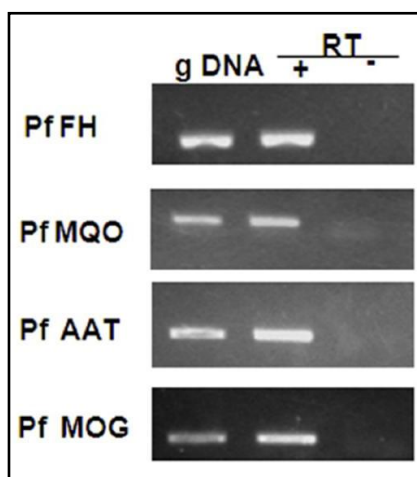


Figure 3.4. Validation of the presence of transcripts of genes involved in fumarate metabolism

Expression of Pf fumarate hydratase along with other genes that are involved in fumarate metabolism was checked by performing PCR. Gene specific primers were used with cDNA prepared from asexual stage culture of *P. falciparum* as template. FH, fumarate hydratase; MQO, malate-quinone oxidoreductase; AAT, aspartate aminotransferase; MOG, malate-oxoglutarate transporter; gDNA, genomic DNA; RT (+/-), presence and absence of reverse transcriptase enzyme.

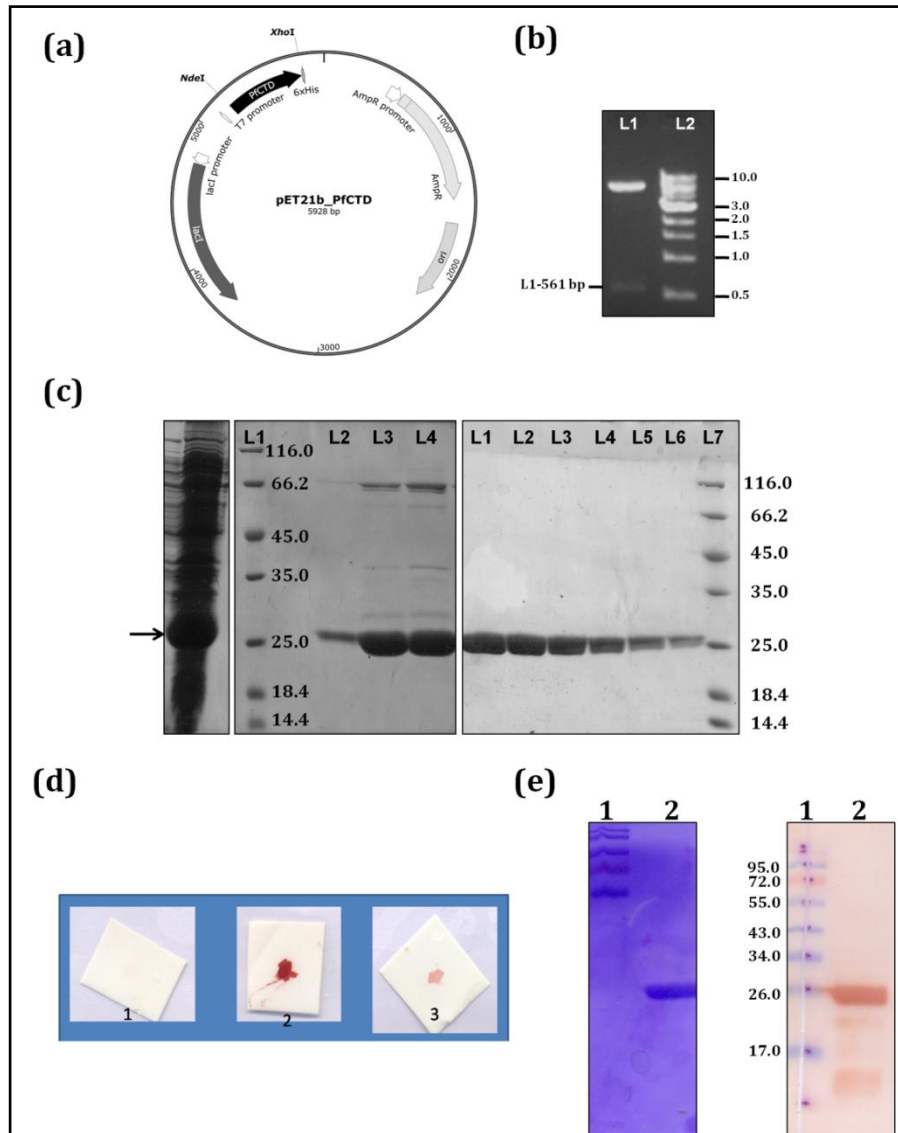


Figure 3.5. Purification of recombinant PfCTD followed by generation and characterization of PfCTD- specific antibody

(a) pET21b based expression construct for purification of recombinant PfCTD. AmpR, β -lactamase gene; 6XHIS, 6X histidine tag; T7, T7 phage promoter; CTD, C-terminal domain. **(b)** Cloning of PfCTD in pET21b vector validated using the enzyme NdeI and XhoI. L1, insert released corresponding to PfCTD (561 bp); L2, 1kb DNA ladder. Clone was confirmed by sequencing. **(c)** The left panel shows overexpression of PfCTD in the whole cell lysate of BL21 (DE3) strain. The middle panel shows the purification profile of PfCTD after Ni-NTA affinity chromatography. L1, protein molecular weight marker; L2, 10 mM wash fraction; L3 and L4, 250 mM imidazole eluates. Right panel, L1-L6 shows different fractions of protein collected after size-exclusion chromatography; L7, protein molecular weight marker. The size of the molecular weight proteins is in kDa. **(d)** Dot blot to validate the antibody after purification using antigen-affinity protocol. 1, pre-immune serum; 2, immune serum (unpurified); 3, purified antibody (eluate 1). **(e)** Validation of purified α -PfCTD antibody. The left panel shows the CBB stained SDS-PAGE gel containing purified PfCTD. L1, protein molecular weight marker; L2, purified PfCTD. The right panel shows the blot containing PfCTD probed with α -PfCTD antibody. L1, prestained protein molecular weight marker (molecular weight of protein in kDa) and L2, purified PfCTD.

In order to check the expression of PfFH, protein-specific antibody was raised against the C-terminal domain of the protein. For this, C-terminal domain of PfFH was expressed and purified. The DNA fragment corresponding to the protein was cloned in pET21b and expressed in *E. coli* as a C-terminal (His)₆-tagged protein (**Figure 3.5 a and b**) and purified to homogeneity using Ni-NTA affinity chromatography followed by size-exclusion chromatography (**Figure 3.5 c**). The purified protein was used to raise antibodies in rabbit. The protein specific antibody was purified from the immune serum using antigen-affinity based purification (**Figure 3.5 d**). Western blotting using the purified antibody showed that it can specifically detect recombinant PfCTD (**Figure 3.5 e**). Following this, the antibody was used to check the expression of PfFH in the whole cell lysate of *P. falciparum*. The result shows that the protein is expressed during the intraerythrocytic stages (**Figure 3.6**).

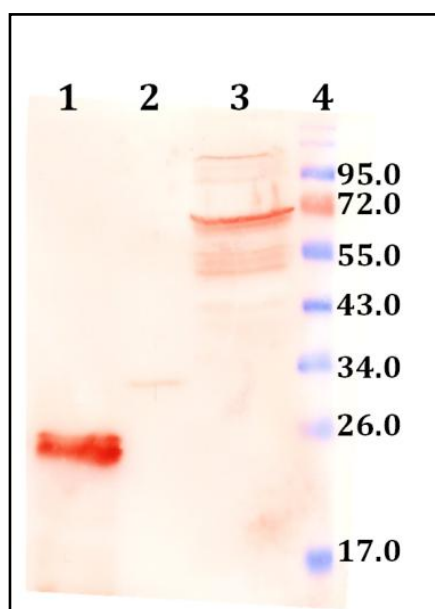


Figure 3.6. Examination of the expression of PfFH using PfCTD-specific antibody

Expression of fumarate hydratase in the asexual intra-erythrocytic stage of P. falciparum. L1, purified PfCTD protein; L2, lysate of human erythrocytes; L3, lysate of P. falciparum asexual stage culture; L4, prestained protein molecular weight marker (size of proteins is indicated in kDa).

3.3.3. Generation and validation of FH-RFA strain

Full length coding sequence of the fumarate hydratase gene was cloned into the plasmid, pGDB and PM1KO parasites (Muralidharan et al., 2011) at ring stage was transfected using both the square wave (Goldfless et al., 2014) and exponential decay protocol using BioRad-XL electroporator. When the parasitemia reached 4-6%, trimethoprim and blasticidin were added to the culture for stabilization of protein and selection of the

parasites, respectively.

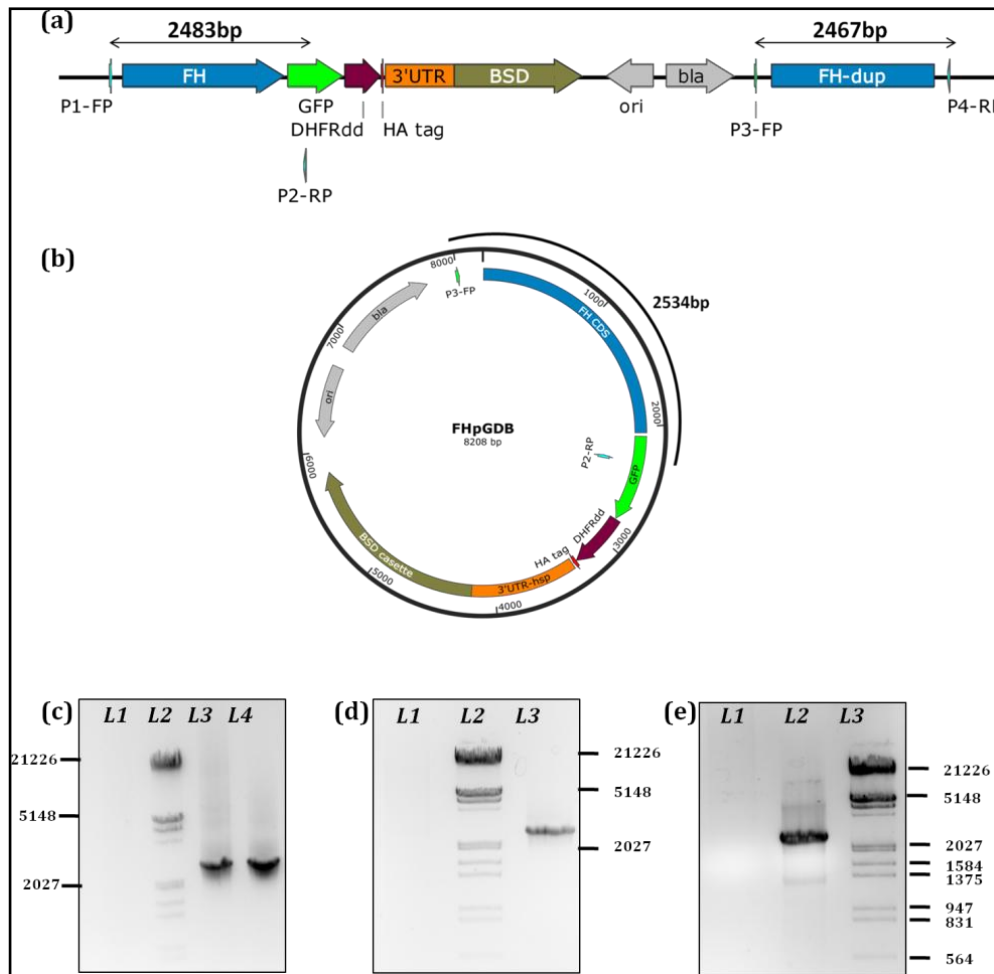


Figure 3.7. Genotyping of P_fFH-RFA parasites.

(a) Scheme showing the integration locus with the RFA tag in tandem with FH gene locus in the strain P_fFH-RFA. Primers P1-FP and P2-RP were used for checking the 5' integration. Primers P3-FP and P4-RP were used to check the 3' integration. **(b)** Position of the primers P3-FP and P2-RP used for checking the presence of episomal copy of the plasmid. **(c)** Genotyping by PCR for validating the removal of episomal copy using primers P3-FP and P2-RP. The templates used in different lanes are as follows; L1- *P. falciparum* PM1KO genomic DNA, L2- marker, L3- pGDB-FH plasmid, L4- PM1KO-FHpGDB after 3 rounds of drug cycling. Band of size 2534 bp seen in L3 and L4 shows that the episomal copy is still retained. **(d)** Genotyping by PCR for validating 5' integration using primers P1-FP and P2-RP. The templates used for the different PCRs were; L1-PM1KO genomic DNA, L2-marker, L3-PM1KO-FHpGDB after 3 rounds of drug cycling. A band of size 2483 bp validates 5' integration. **(e)** Genotyping by PCR for validating 3' integration using primers P3-FP and P4-RP. The templates used for the different PCRs were; L1-PM1KO genomic DNA, L2-PM1KO-FHpGDB genomic DNA after 3 rounds of drug cycling, L3-marker. A band of size 2467 bp validates 3' integration. BSD, blasticidin deaminase; ori, the origin of replication; FH, fumarate hydratase; FH-dup, duplicated copy of the FH gene. FP, forward primer; RP, reverse primer. 3'UTR, 3' untranslated region; bla, beta-lactamase gene, P1-4, primers listed in Table 3.2.

Parasites appeared 40 days after drug selection in culture where square wave based transfection protocol was used but not when exponential decay pulse was used. The drug cycling schedule followed to remove the episomal copy of the plasmid is given in Figure 3.2 b. To validate the integration at 5' and 3' regions of the FH gene locus, genomic DNA from the *P. falciparum* strain containing RFA tagged FH locus (PfFH-RFA) parasites was isolated and used as template in PCR reaction along with different primer combinations. These results confirmed single crossover event at FH gene locus (**Figure 3.7 d and e**). PCR with appropriate primers showed the presence of the episomal copy of the plasmid even after three rounds of drug cycling (**Figure 3.7 c**). Cloning of these parasites was attempted using limiting dilution cloning but were not successful. However, as the gene in the plasmid lack the promoter needed for expression the presence of episomal copy of the plasmid would not be a hindrance in the TMP based protein knockdown or in localisation studies.

There was no growth defect observed upon removal of TMP from the culture medium. This is possible if the protein is compartmentalized and therefore is inaccessible to the proteasomal machinery that is predominantly present in the cytosol. To test the localisation of the protein live-cell imaging was performed on FH-RFA strain.

3.3.4. Cellular localisation of FH

Live cell microscopy of the DAPI stained parasites showed punctate appearance of GFP signal in the parasite compartment (**Figure 3.8**). The ratio of GFP⁺ to GFP⁻ parasites would serve to report on the enrichment of PM1KO-FH-RFA parasites over parasites having only the episomal copy of the plasmid (and hence no fluorescence) achieved by drug cycling. Towards this, a culture containing mature parasites was subjected to percoll treatment and the parasites were used for imaging using confocal microscopy after staining with DAPI. Analysis of various fields showed that though most of the parasites were GFP⁺, there were few parasites from which no GFP signal could be observed (Figure 3.8). Mitochondrion was stained with MitoTracker and the parasites were imaged to see the localisation of the protein. **Figure 3.9** clearly shows that the colocalization of GFP signal with the MitoTracker staining. This proves mitochondrial localisation of fumarate hydratase in *P. falciparum*. Hence, it is possible that the even upon TMP removal, the protein is not accessible to the proteasomal machinery for degradation. This can be attributed to the lack of any observable phenotype in the viability of the FH-RFA parasites.

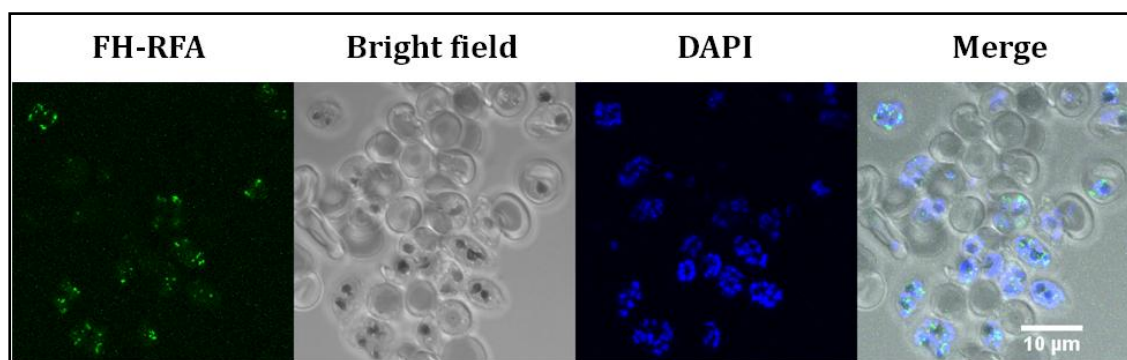


Figure 3.8. Localisation of fumarate hydratase in P. berghei.

A punctate localization of GFP signal was seen (FH-RFA panel) with varying intensities.

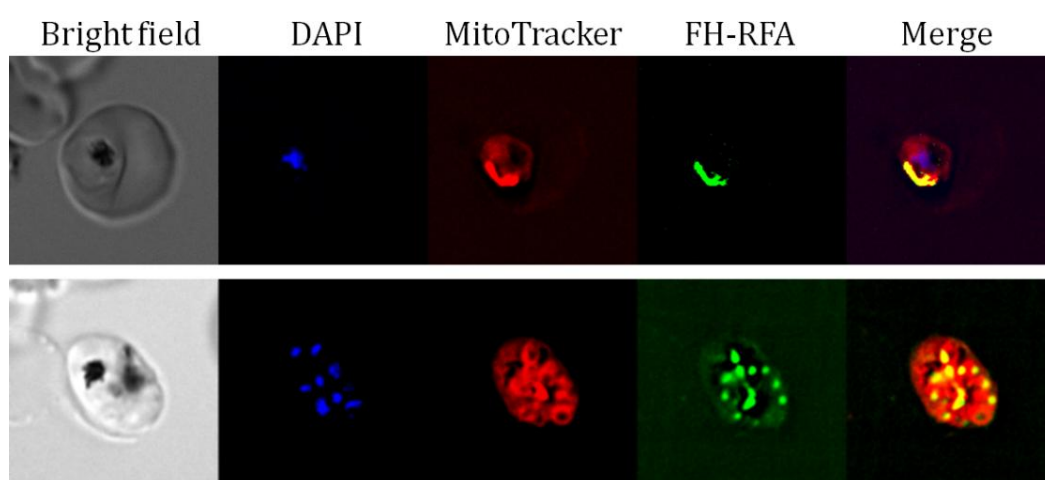


Figure: 3.9. Co-localisation of fumarate hydratase with MitoTracker.

Upper panel shows a mature trophozoite and the lower panel, a schizont. As it is evident from the merge (right most subpanel), the protein has mitochondrial localisation.

3.3.5. Generation of fumarate hydratase null (PbFHKO) and HA tagged (PbFHHA) strains of *P. berghei*.

Increased efficiency of transfection makes *P. berghei* an attractive system to test the essentiality of genes of *Plasmodium* spp. in general. However, there have been instances wherein genes shown to be essential to *P. falciparum* could be knocked out in *P. berghei* with only minor or no phenotypic differences in asexual stage growth (Srivastava et al., 2015; Sturm et al., 2015). Parasite or host specific factors could be responsible for this difference. As the *P. falciparum* gene could not be knocked out, before proceeding to knockout the *PbFH* (*P. berghei* fumarate hydratase), we tested if the gene locus is susceptible to recombination. For this, we attempted to insert a HA tag at the 3' end of the gene, in frame with P. berghei ORF using double crossover homologous recombination.

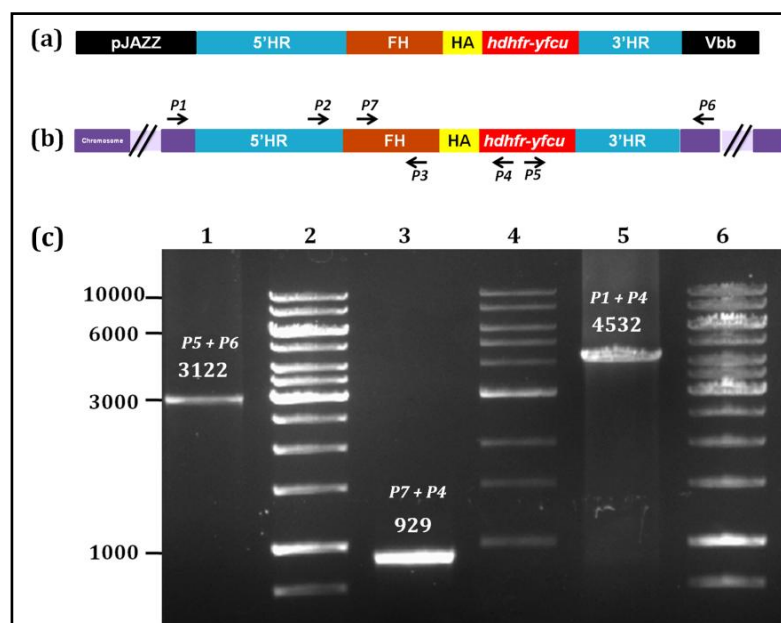


Figure 3.10. Genotyping of the PbFHHA parasites by PCR

(a) Schematic representation of the fumarate hydratase, HA tagging construct generated using recombineering strategy. 5'HR- 5' homologous region, FH-full length coding sequence of fumarate hydratase, HA- haemagglutinin tag, 3'HR- 3' homologous region, pJAZZ Vbb-vector backbone of the pJAZZ linear plasmid, *hdhfr-yfcu* (human dihydrofolate reductase and a bifunctional protein containing yeast cytosine deaminase and uridyl phosphoribosyltransferase)- positive/negative selection cassette for use in *P. berghei*. **(b)** Fumarate hydratase genomic locus after integration of the tagging construct by double crossover homologous recombination. The position of the primers used for genotyping the drug selected parasites are indicated. **(c)** Genotyping of the transfectants. With the genomic DNA isolated from transfected and drug selected parasites different PCRs were done to verify the integration of the *hDHFR* cassette. L1- primers P5 and P6 were used to check 3' integration (expected band size: 3122 bp), L2- marker, L3- primer P7 and P4 were used to check the presence of the *hDHFR* cassette in the right orientation with respect to the FH gene (expected band size: 929 bp), L4- marker, L5- primers P1 and P4 were used to check the 5' integration (expected band size: 4532 bp), L6-marker.

The cloning of AT-rich intergenic fragments of *Plasmodium* genome for generating gene manipulation constructs is often fraught with difficulties. Use of PCR-free recombineering based strategy offers better and faster way to generate constructs for knockout or tagging. PbFH HA tagging construct was generated as a part of a training program at Wellcome Trust Sanger Institute. The construct (**Figure 3.10 a**) was used directly for transfection. Pyrimethamine selection was started 24 hours after transfection. Drug resistant parasites were obtained 10 days after the selection. The parasites grew normally and were able to successfully establish lethal infection in mice. The integration of the selection cassette (both at 5' and 3' ends) was checked by PCR using appropriate primers with genomic DNA isolated from uncloned population of the parasites as template

(Figure 3.10 b). The results suggest that the selection cassette is integrated at the right genomic locus (Figure 3.10 c).

In order to further validate the right integration of the drug selection cassette and to rule out any gene duplication events, Southern blotting was performed using a radioactively labelled gene probe. The result (Figure 3.11) suggests that the integration has happened at the right locus and there is no gene duplication event. This suggests that the PbFH gene locus is susceptible to homologous recombination and hence a direct gene knockout experiment can be attempted.

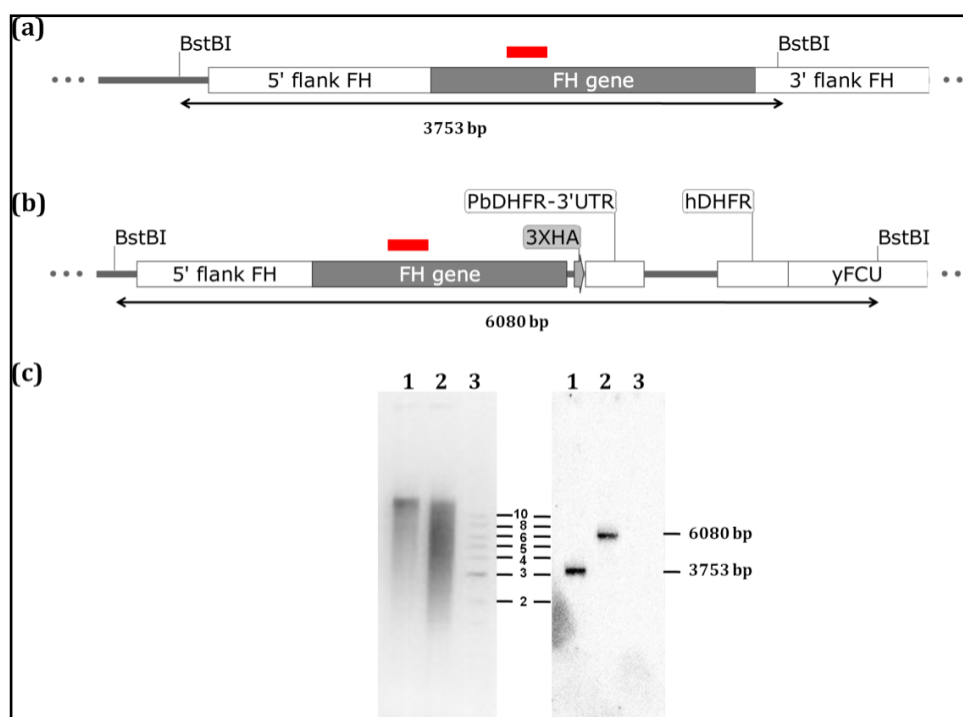


Figure 3.11. Southern blotting using *FH* gene probe to validate the 3' integration of HA-tag

(a) Schematic representation of *FH* gene locus in the wild-type *P. berghei* along with the 5' and 3' flanking regions. The position of the radiolabeled probe used for southern blotting and the *Bst*BI restriction sites are indicated. (b) Schematic representation of the expected *FH* gene locus after double crossover recombination of the 3' HA tagging construct. The location of 3X HA tag, yFCU/DHFR, radiolabeled probe - used for southern blotting and the *Bst*BI restriction sites are indicated. (c) The left panel shows EtBr stained agarose gel loaded with *Bst*BI digested genomic DNA of both the wild-type (lane 1) and the transfected parasites (lane 2). Lane 3 has 1 kb DNA ladder from NEB; the molecular weight corresponding to different bands are shown in kilobase pairs. The right panel shows the Southern blot of genomic DNA from the PbWT and the PbFHHA uncloned population digested with *Bst*BI and probed with the *FH* gene probe showing a single 6 kb band for PbFHHA (lane 2) and the expected 3.7 kb band for PbWT parasites (lane 1).

3.3.6. Generation of PbFH knockout construct

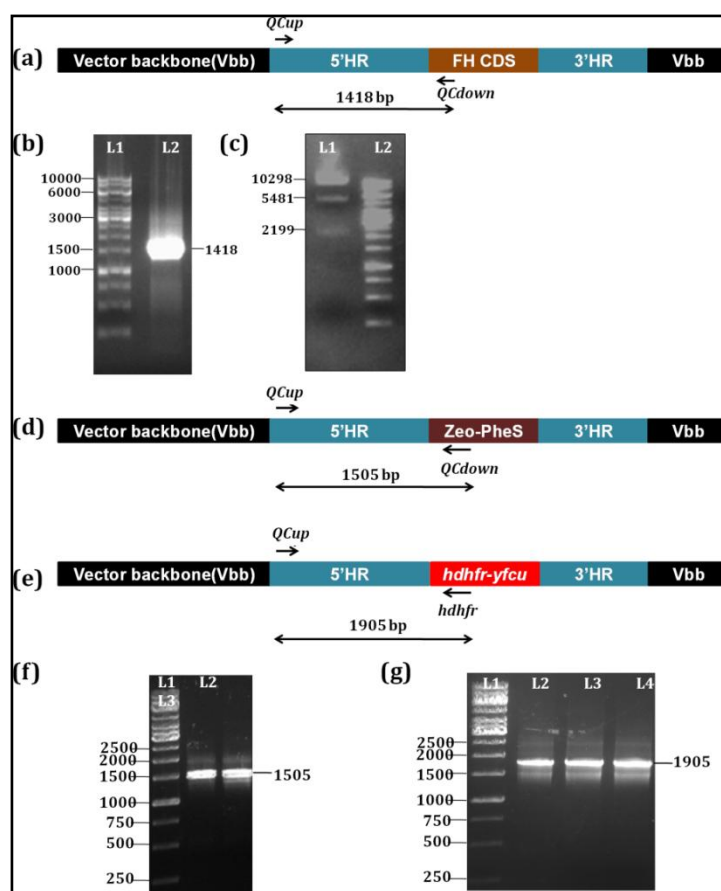


Figure 3.11. Generation of FH-knockout construct using recombineering.

(a) Schematic representation of the FH genomic clone obtained from PlasmoGEM. The position of primers used for validation, QCup and QCdown are also indicated. **(b)** Validation of the genomic clone by PCR using primers QCup and QCdown. L1, DNA ladder and L2, PCR product obtained upon using primers QCup and QCdown with FH genomic clone as template. **(c)** Validation of the genomic clone by *NotI* digestion. An expected pattern of bands were seen. **(d)** Schematic representation of the intermediate vector, FHIV (see text). Position of validation primers QCup and PheSR2 are indicated. **(e)** Schematic representation of the final gene targeting construct and the position of validation primer QCup and *hdhfr* primers are indicated. **(f)** Validation of FHIV. L1, DNA ladder (sizes indicated in base pairs); L2 and L3, PCR product obtained (1505 bp) using primers QCup and PheSR2 using FHIV isolated from two different colonies as template. **(g)** Validation of the FH gene targeting construct. L1, DNA ladder L2-L4, PCR product using primers QCup and *hdhfr* primers and FH gene targeting construct isolated from three different colonies as template.

The genomic clone of fumarate hydratase (**Figure 3.11 a**) was obtained from PlasmoGEM and was validated using PCR and *NotI* restriction digestion (**Figure 3.11 b and c**). Using published protocol (Pfander et al., 2011) the genomic clone was used as a template for the generation of the knockout construct (schematically shown in **Figure 3.11 e**). The generated construct was validated using PCR (**Figure 3.11 f and g**). Transfection of wild-type *P. berghei* ANKA strain with these constructs resulted in parasites appearing in mice

at around 10 days after drug selection. The *P. berghei* FH knockout strain (PbFHKO) was viable; could be propagated from one mouse to the other and could cause lethality to mice.

3.3.7. Genotyping of PbFHKO strain.

The genotype of PbFHKO was validated by PCR using appropriate primers. The position of the primers is schematically shown in **Figure 3.12 a and b**. PCR results suggest successful integration of the selection cassette both at the 3' and 5' end. The genotype was further validated using Southern blotting.

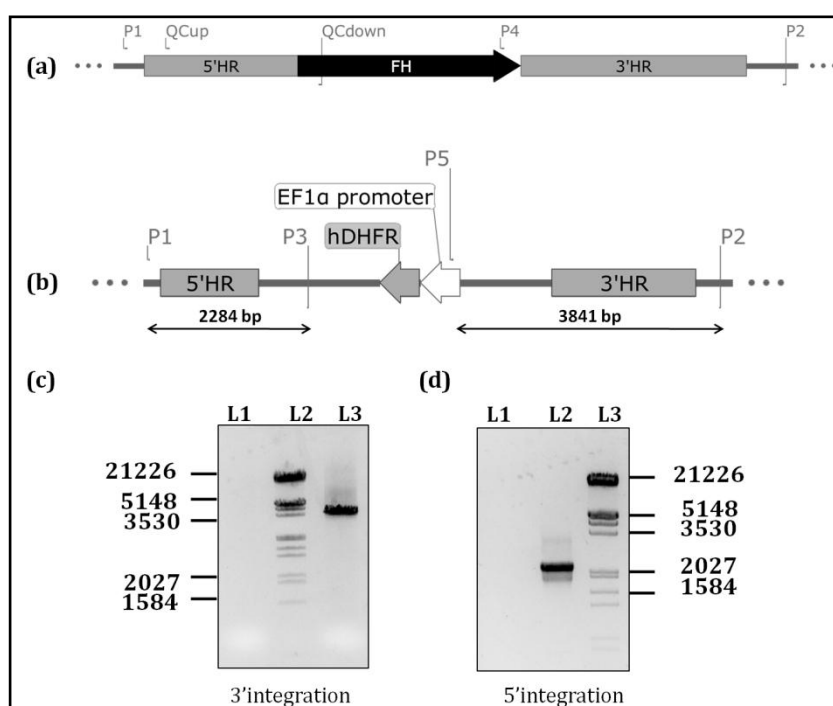


Figure 3.12. Genotyping of the fumarate hydratase knockout parasites.

(a) Schematic representation of fumarate hydratase gene and the homologous regions used for double crossover recombination. **(b)** Genomic locus after double crossover recombination of the wild-type fumarate hydratase gene with hDHFR cassette. The position of the primers used for verifying the integration is also shown. Primers P1 and P3 were used to verify the 5' integration. Primers P5 and P2 were used for verification of 3' integration. The expected band size of amplicon in each of these cases is shown with double headed arrows. **(c)** PCR for the validation of 3' integration (P5 and P2). The templates used corresponding to different lanes are, L1, wild-type *P. berghei* ANKA genomic DNA; L2, marker; L3, *P. berghei* fumarate hydratase knockout genomic DNA. **(d)** PCR to verify the presence of 5' integration (P1 and P3). The templates used corresponding to different lanes are, L1- wild-type *P. berghei* ANKA genomic DNA, L2- *P. berghei* fumarate hydratase knockout genomic DNA, L3-marker.

The Southern blotting of the *Bst*BI digested genomic DNA from the PbWT and PbFHKO parasites using PbDHFR 3'UTR probe shows that the drug selection cassette has

integrated at the right loci. The fact that even upon multiple passaging between mice, the uncloned FHKO parasite was viable, shows that the gene is not essential for the intraerythrocytic growth of the parasite. Limiting dilution cloning was attempted by intravenous injection of 1 parasite per mouse and 15 mice was used in each attempt. Unfortunately, no parasites appeared even 15 days after initial parasite administration. However, in mouse injected with 100 parasites, the parasitemia reached around 5%, 10 days after the administration. Phenotyping of a clonal population of PbFHKO parasite on both asexual and sexual stages would add further evidence to the importance of the gene. The fact that the gene could not be knocked out in *P. falciparum* but could be knocked out in *P. berghei* could be attributed to host and/or parasite specific differences.

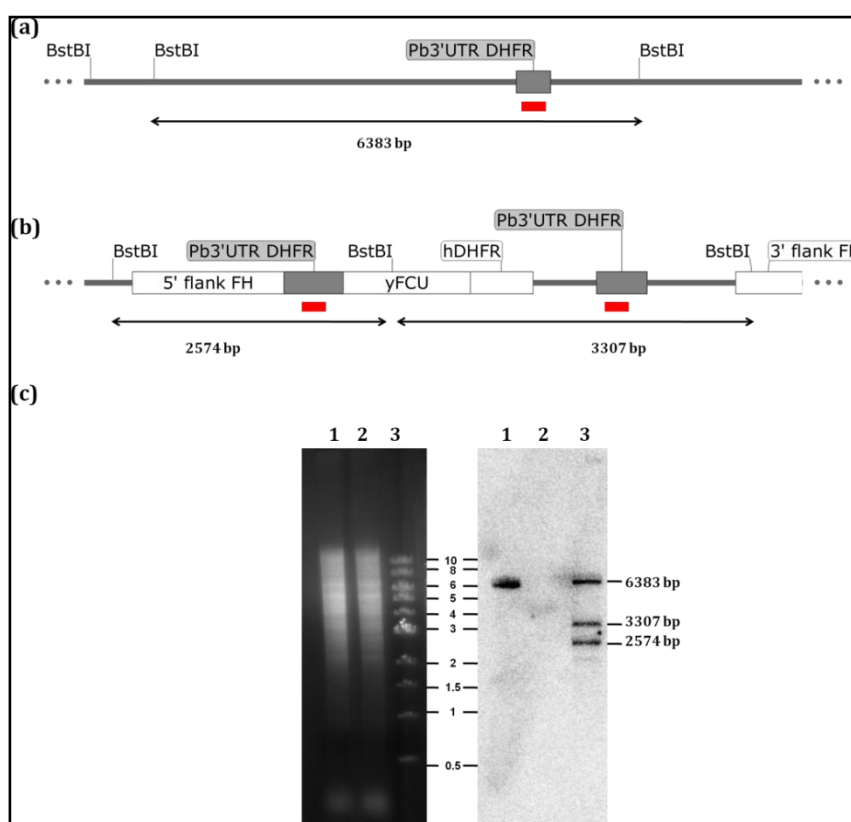


Figure 3.13. Southern blotting using *FH* gene probe to validate the 3' integration with HA-tag

(a) Schematic representation of *PbDHFR* 3'UTR gene locus in the wild-type *P. berghei*. The position of the radiolabeled probe used for Southern blotting and the *BstBI* restriction sites are indicated. **(b)** Schematic representation of the expected *FH* gene locus after double crossover recombination with the knockout construct. The location of *Pb* 3'UTR region, *yFCU*/*DHFR* ORF's, radiolabeled probe used for Southern blotting and the *BstBI* restriction sites are indicated. **(c)** The left panel shows *EtBr* stained agarose gel loaded with *BstBI* digested genomic DNA of both the wild-type (lane 1) and the transfected parasites (lane 2). Lane 3 has 1 kb DNA ladder from *NEB*; the molecular weight corresponding to different bands are shown in kilo

base pairs. The right panel shows the Southern blot of genomic DNA from the PbWT and the PbFHKO uncloned population digested with *Bst*BI and probed with the PbDHFR 3'UTR probe showing an expected single band around 6 kb band for PbWT (lane 1) and the three bands of different molecular weights (6383, 3307, and 2574 bp) for PbKO parasites (lane 1). A faint band was also seen below the 2574 bp band. The reason for the occurrence of this band is not clear.

3.4. SUMMARY AND FUTURE DIRECTIONS

Class I fumarate hydratases are present in mostly unicellular eukaryotes; notably in organisms belonging to apicomplexa and kinetoplastida. Most of the unicellular eukaryotes harbouring the gene have parasitic life-style though there is no causal relationship between the presence of the gene and the life-style. Only single subunit class I fumarate hydratases are present in eukaryotes. The advantage of having class- I FH over class II in some organisms is still not clear. RT-PCR experiment using gene specific primers showed that FH, MQO and AAT all involved in fumarate metabolism are expressed during the intraerythrocytic stages of the parasite. Western blot analysis on the parasite lysate using PffH-CTD specific antibody showed that the protein which is close to the expected molecular weight is expressed during intra-erythrocytic stages. By tagging the 3' end of the endogenous FH gene locus with GFP, the protein was found to be localised to the parasite mitochondria.

Gene tagging studies on *P. berghei* showed that the *PbFH* gene locus is susceptible to homologous recombination. Knockout of the gene was successful as shown by PCR and Southern blotting. The gene is not essential for *P. berghei* asexual stage growth. Cloning of parasites by limiting dilution was not successful for both FHKO and FHHA parasites. Upon obtaining a clonal population of parasites phenotyping of PbFHKO parasites on both sexual and asexual growth can be performed. With many genes of TCA cycle shown to be essential for sexual growth of the parasites in mosquitoes, one would expect the PbFHKO parasites to exhibit similar phenotype.

Chapter 4

Tracing the cellular fate of ammonia: development of an NMR-based methodology

Chapter 4

Tracing the cellular fate of ammonia: development of an NMR-based methodology

ABSTRACT

*Mass spectrometry-based metabolomics approaches remains one of the widely used technique to study nitrogen metabolism. NMR-based approaches involving the use of ¹⁵N-labelled metabolites as tracers are few and suffer from the low sensitivity of the ¹⁵N-nucleus. We proposed to develop an NMR based strategy to trace the fate of nitrogen in cellular system. The strategy was first tested in *E. coli*, as the cells can be easily grown. Once standardized in *E. coli*, depending on the sensitivity, this strategy could be extended to other cell types including *P. falciparum*.*

4.1. INTRODUCTION

Nitrogen is a widely present element in key biomolecules that includes amino acids, nucleotides, and cofactors. It is incorporated into these molecules by three major means; incorporating precursors that already have nitrogen (eg. the nitrogen at the second position of the pyrimidine ring of adenine is obtained by incorporation of aspartate backbone), fixation of atmospheric nitrogen, and incorporation of ammonia/ammonium. Amongst these, very few organisms like plants have the capacity to fix atmospheric nitrogen, and majority of the nitrogen atom is incorporated into biomolecules by either transfer of primary amino group from one molecule to another catalyzed by transaminases or through incorporation of ammonia catalyzed by amino/amidotransferase class of enzymes (Buchanan, 1973; Lin & Stewart, 1998; Wang, Shen, Xu, & Guo, 2014; Webster, 1955; Zalkin, 1985). This chapter deals with developing a novel methodology to identify and hence trace the fate of ammonia in metabolic reactions of the cell. This section provides brief information on multiple roles of ammonia in cellular metabolism, schemes of ammonia metabolism in different organisms, and discusses various methodologies available to trace the amino groups in metabolic reactions.

4.1.1. Nitrogen metabolism in organisms

Nitrogen assimilation is a process of converting inorganic nitrogenous compounds like nitrate, atmospheric nitrogen etc. to organic molecules like amino acids. Plants generally

use either nitrate or ammonium to meet their nitrogen requirements (Wang et al., 2014). The nitrate acquired is also converted by the action of nitrite and nitrate-reductase to ammonia. Glutamine synthetase-glutamate synthase (GS-GOGAT) reaction constitutes the major pathway for the incorporation of ammonia thus generated, into amino acids. Thus, ammonia/ammonium is generally the final form of inorganic compound that ultimately gets converted to organic compounds. Unlike plants, some free-living and symbiotic microorganisms can fix atmospheric nitrogen in the form of NH_4^+ (Cheng, 2008; Lee, Ribbe, & Hu, 2014). Animals are completely dependent on exogenous sources (plant, microorganism) for their nitrogen requirements. Organisms can also be classified into ammonotelic and non-ammonotelic depending on whether they excrete ammonia/ammonium to their environment. On similar lines, organisms can be classified to ureotelic and non-ureotelic pertaining to their excretion of urea. Protozoan parasites are generally ammonotelic as one or more of the urea cycle enzymes are absent. Among the protozoa, kinetoplastids like *Leishmania* and *Trypanosoma* are well studied for their ammonotelic properties (Yoshida & Camargo, 1978). *P. falciparum* is also an ammonotelic organism.

4.1.2. Metabolic role of ammonia/ammonium

In general, in prokaryotes, plants and in animals, ammonia/ammonium gets incorporated into amino acids through the action of either glutamate dehydrogenase GDH or GS-GOGAT pathway (van Heeswijk, Westerhoff, & Boogerd, 2013). The pathway comprising the GDH and GS/GOGAT reactions are shown in **Figure 4.1**. Besides this anabolic role, ammonia has multiple other functions reported;

- 1) Ammonia is known to regulate nitrogen metabolism in yeast by controlling the expression of genes involved in the process (Schure et al., 1998).
- 2) Ammonia can allosterically regulate phosphofructokinase thereby, controlling glycolytic flux (Yoshino & Murakami, 1982)
- 3) In excess amount ammonia is known to cause neurological pathology (Wilkinson, Smeeton, & Watt, 2010)

4.1.3. Generation and consumption of ammonia

Figure 4.1 shows a generalised scheme of ammonia metabolism that is prevalent in many organisms across all three domains of life (including plants, prokaryotes and animals). As one can see from the figure, ammonium can be directly translocated from the extracellular niche or can be generated from inorganic precursors like nitrite or nitrogen.

However, in general the capacity to generate ammonia from nitrogen is present only in some bacteria and from nitrite only in plants. Once generated, ammonia is used in many assimilatory and anabolic reactions primarily through glutamate. This is catalysed by the enzyme glutamate dehydrogenase (GDH). Ammonia can be incorporated into glutamine by the action of the enzyme glutamine synthetase. Unlike GDH reaction, this requires ATP hydrolysis and hence is an energy-consuming reaction. The glutamine generated can also be converted back to glutamate by the action of glutamine: oxoglutarate amidotransferase (GOGAT). The GOGAT reaction generates two molecules of glutamate from a molecule of α -ketoglutarate and glutamine.

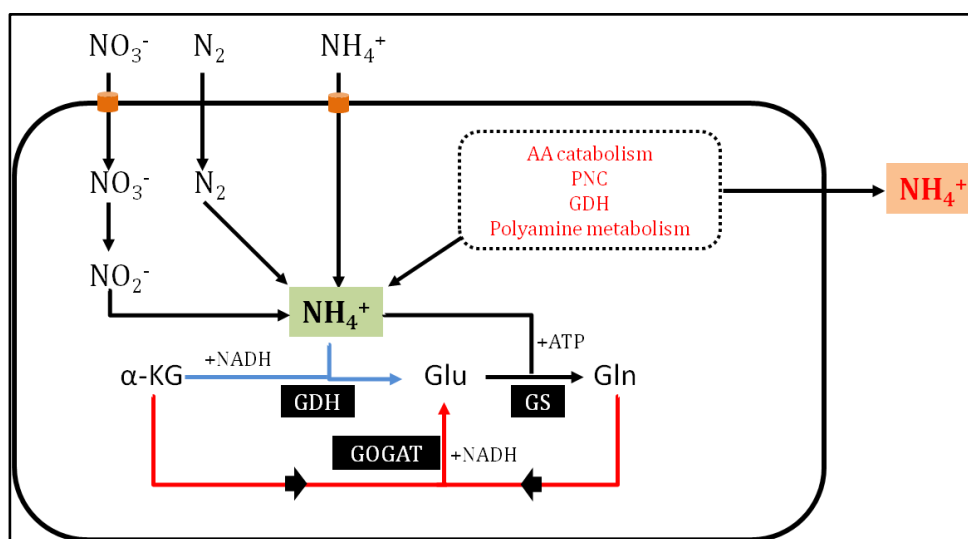


Figure 4.1. An overview of ammonia metabolism

The GOGAT and GDH based ammonia assimilation is shown schematically in the figure. Sources of ammonia can be inorganic, starting from nitrate or nitrogen or organic when obtained from amino acid catabolism, purine nucleotide cycle, GDH reaction and polyamine metabolism. GOGAT, glutamine: oxoglutarate glutamine amidotransferase; GDH, glutamate dehydrogenase; NADH, nicotinamide adenine dinucleotide; α -KG, α -keto glutarate; Gln, glutamine; Glu, glutamate; GS, glutamine synthetase; PNC, purine nucleotide cycle; AA catabolism, amino acid catabolism.

The glutamate and glutamine thus generated are used in a multitude of reactions inside the cell. The majority of these reactions involve transamination reactions and reactions that involve the transfer of amido group from glutamine, in the form of ammonia that gets incorporated into biomolecules (like purines, pyrimidines etc.).

4.1.5. Methodology to study ammonia metabolism

Mass spectrometry and to a lesser extent NMR has been used to study nitrogen metabolism in many organisms. Isotope labelling of metabolites using ^{15}N -labelled precursor followed by mass spectrometric analysis of extracted metabolites is a very

sensitive technique to map nitrogen metabolism. This strategy has been used successfully in many cell types and organisms (Gaudin et al., 2014; Liu et al., 2015). Mass spectrometry requires a low amount of the metabolite for analysis, unlike NMR. Both the techniques have their own advantages and limitations and are reviewed in Emwas, 2015 and Dieterle et al., 2011. One should note that these techniques provide complementary information and wherever possible, both must be employed.

^{14}N is a quadrupolar nucleus with spin greater than $\frac{1}{2}$. Though NMR sensitive, we cannot observe signal from ^{14}N for most metabolites owing to quadrupolar relaxation, a phenomenon affected by the symmetry and size of the metabolite (Günther, 2013). Hence, metabolite precursors containing ^{15}N nucleus which have a spin $\frac{1}{2}$ are used to trace nitrogen metabolism. However, the fact that ^{15}N nuclei have a negative gyromagnetic ratio, studying its metabolism using ^{15}N -NMR i.e., in direct dimension, suffers from sensitivity issues. Reports, where nitrogen metabolism has been traced through the indirect dimension of protons attached to a ^{15}N , has been performed and this doesn't have the problem of sensitivity as much as in ^{15}N -NMR (Paul Juretschke, 1984). We proposed to develop a methodology to study nitrogen metabolism using *E. coli* as a model system using multidimensional NMR experiments.

4.1.6. Rationale behind the methodology used

The line shape of the signal from an NMR sensitive nucleus is dictated by two modes of relaxation. Spin-lattice relaxation, which affects peak intensity, is indicated by the parameter T1 and spin-spin relaxation, that affects peak width, is indicated by T2. T2 is highly dependent on a phenomenon called chemical exchange (Cavanagh, Fairbrother, Palmer III, Rance, & Skelton, 2007). **Figure 4.2** schematically shows the effect of the rate of this exchange on the line shape in NMR. Fast exchanging protons give broad lines as compared to slow exchanging protons. As we intended to study nitrogen metabolism using protons attached to ^{15}N nuclei, chemical exchange of these protons with solvent would dictate the quality of the spectra. The exchange rate of protons attached to nitrogen nuclei is dependent on the chemical environment in the molecule. Protons attached to aliphatic primary amines exchange rapidly with water and hence are not observed due to line broadening. The exchange is slower for protons in aliphatic secondary amines, aromatic amines (both primary and secondary), and amide nitrogen and hence can be studied by NMR. Nevertheless, aliphatic primary amines constitute a major functional group in majority of the metabolites (like amino acids, polyamines etc.) involved in nitrogen metabolism. In order to obtain a signal from the proton attached to aliphatic primary amines, we intended to derivatize these metabolites such that the exchange rate

of the protons can be reduced. Acetylation of aliphatic primary amine groups using acetic anhydride is an established derivatization method in organic chemistry for various applications (Naik, 2004; Phukan, Ganguly, & Devi, 2009).

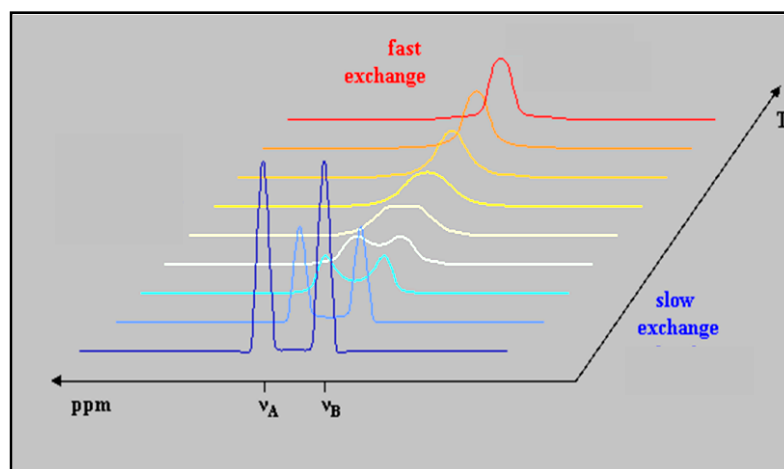


Figure 4.2. Effect of chemical exchange on the line shape in NMR

The schematic shows a series of hypothetical ^1H -NMR spectra. The spectra are coloured from violet, corresponding to slow exchange to red corresponding to fast exchange, as a function of temperature. ν_A and ν_B correspond to the chemical shift values of two different protons A and B. Even at constant temperature the proton exchange rates would determine the spectral pattern obtained. Figure reproduced from <http://www2.fci.unibo.it/~mazzand/dnmr.html> after modifications.

As shown in **Figure 4.3** the derivatization procedure results in the conversion of a primary amine group (containing fast exchanging protons) to an amide group (with slow exchanging protons) thereby enabling detection of these protons using NMR. It should be noted that the procedure followed would not result in acetylation of aromatic primary amines.

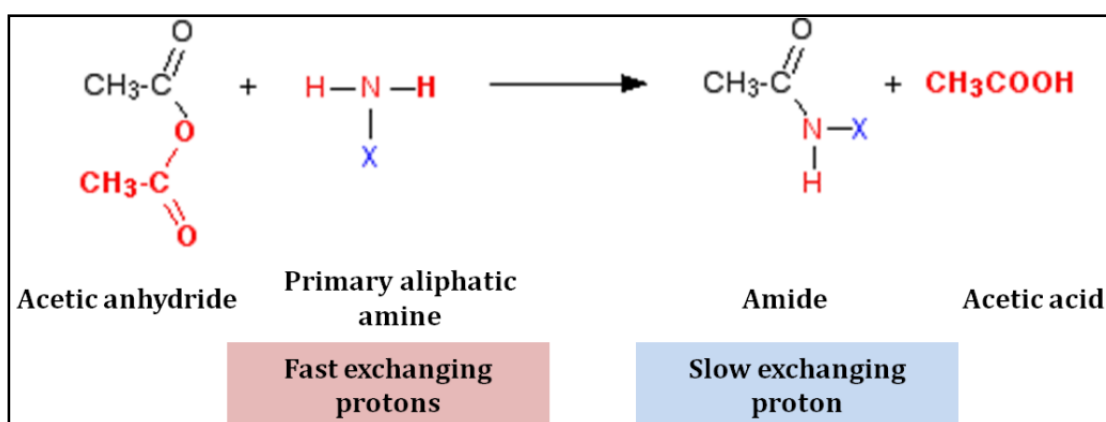


Figure 4.3. Acetylation of primary amines to reduce exchange rates.

4.1.7. NMR techniques to establish metabolite identity

NMR techniques involving 1D, 2D and 3D has been successfully used in both qualitative and quantitative metabolomics. The details of these techniques are comprehensively presented in many reviews (Cerdan & Seelig, 1990; Kruk et al., 2016; Markley et al., 2017). Metabolites involved in primary metabolism are composed of carbon, oxygen, nitrogen, sulfur and hydrogen nuclei. Amongst all, proton is a highly NMR sensitive nucleus as it has a higher gyromagnetic ratio. Owing to higher sensitivity and short acquisition time, 1D proton NMR is routinely used to check signal to noise ratio (S/N), and resolution that can be obtained with the sample of interest. However, 1D-H-NMR suffers from poor chemical shift dispersion (1- 10 ppm), and often results in resonance overlap especially when studying metabolites belonging to one chemical class which differ from each other by only few atoms (like amino acids, polyamines, nucleotides etc.). This necessitates the use multidimensional experiments (2D, 3D) to establish the identity of metabolites. Though multidimensional NMR experiments have lower sensitivity, resolution of signals is enhanced, which is most often desired in NMR based experiments.

Studying ammonia metabolism employing ^{15}N -labelled precursors and by $1\text{D}^{15}\text{N}$ -NMR has been reported previously in many model systems (Haran, Kahana, & Lapidot, 1983; Kanamori, Weiss, & Roberts, 1989; Legerton, Kanamori, Weiss, & Roberts, 1981; Yamada & Sherman, 1980). ^{15}N nuclei has a very broad chemical shift dispersion ranging from 0-900 ppm. However, ^{15}N has a low and negative value of gyromagnetic ratio and the sensitivity of a 1D N-NMR is much lower when compared to that of the proton. A two-dimensional heteronuclear NMR experiment that involves monitoring proton in direct dimension (F1) and nitrogen in indirect dimension (F2) offers a combination of higher sensitivity associated with protons and wide chemical shift dispersion associated with nitrogen. A 2D ^1H - ^{15}N -HSQC (heteronuclear single quantum coherence) is one such experiment that is used in this work to trace the metabolites in *E. coli* that have incorporated ^{15}N from ^{15}N -labelled ammonium chloride. There are no reference databases that we could use to establish the identity of the metabolite using the data just from ^1H - ^{15}N -HSQC, as the existing NMR based metabolome databases do not have information of the proton and the nitrogen chemical shift values for different acetylated metabolites. To establish the identity of metabolites, a three-dimensional NMR experiment, 3D TOCSY-HSQC (total correlation spectroscopy – heteronuclear single quantum coherence) was performed. This involves a homonuclear 2D-TOCSY pulse sequence followed by a heteronuclear 2D- ^1H - ^{15}N HSQC. The amide proton is monitored in F1 dimension, other correlated protons in F2 dimension and the amide nitrogen in F3 dimension (Marion et

al., 1989). This is generally used to identify amino acids in proteins. On similar lines, the experiment described in this chapter was used to find the chemical shift of the protons correlated to the amide proton in the acetylated metabolite which in turn can be used to identify different metabolites.

4.2. MATERIALS AND METHODS

4.2.1. Chemicals, Strains and Molecular biology Reagents Used

Media components were procured from HiMedia, India. Metabolites were extracted from the *E. coli* strain BL21 (DE3) and used for NMR experiments. *P. falciparum* strain 3D7 was used for all metabolite extraction experiments. ¹⁵N- labelled ammonium chloride was procured from Sigma-Aldrich, USA. Acetic anhydride, triethylamine, methanol, o-phthalaldehyde used in various steps of metabolite extraction, derivatization and analysis were procured from Sigma-Aldrich, USA.

4.2.2. *E. coli* growth and metabolite extraction

A single colony of BL21 (DE3) was used inoculate a 10 ml LB-medium and allowed to overnight. The cells were pelleted and washed thoroughly three times with M9 minimal medium such that any trace of LB medium is removed completely. Cells corresponding to 200 µl of this saturated culture were used for secondary inoculation into 10 ml M9-minimal medium containing ¹⁵N-labelled ammonium chloride at a concentration of 2 g/l. The culture was grown for 10 h at 37 °C with shaking at 180 rpm. The cells were separated by centrifugation and the cell pellet was stored at -80 °C until further use.

For metabolite extraction, published protocols were followed (Prasad Maharjan & Ferenci, 2003; Shryock, Rubio, & Berne, 1986). Briefly, the pellet corresponding to 5 ml of overnight culture was resuspended in 5 ml of water. To this, 120 ml of methanol: water mixture (2:1 v/v) was added and cells resuspended immediately. The suspension was incubated in a 70 °C water bath for 30 min. The suspension was centrifuged at 4000 x g for 30 min at 4 °C to remove the cellular debris and precipitated proteins. The supernatant was subjected to evaporation in a rotovac to remove methanol completely. The solution was then lyophilized to obtain a solid mass containing the metabolites. The lyophilized material was dissolved in 20 mM potassium phosphate, pH 7.4. The solubilized material was subjected to acetylation reaction. Triethylamine was first added to make the pH of the solution alkaline and acetylation of metabolites was performed as mentioned below.

4.2.3. Acetylation of metabolites

For standardisation of the acetylation protocol, ^{15}N -labelled ammonium chloride was used. Apart from this, the methodology was also performed on γ -amino butyric acid (GABA), glutamic acid and asparagine. A 1 mM solution of each of these compounds was made by dissolving them in distilled water. For acetylation of metabolites, the concentration of the reactive primary amine was first estimated using OPA assay (described in section 4.2.4). Acetic anhydride was used in 4-fold molar excess to ensure complete acetylation of all metabolites. Triethylamine was used as a base in the reaction. To begin acetylation a small aliquot (0.5-1 μl) of triethylamine was added to a well-stirred metabolite solution such that a basic pH is established. Thereafter, an equal volume of acetic anhydride was added to this solution under constant stirring for a minute. The pH of the solution was constantly monitored to ensure that a basic pH is always maintained. This procedure involving alternate addition of acetic anhydride and triethylamine was continued until four equivalents of acetic anhydride were added to the metabolite solution. An aliquot of the solution was used for o-phthalaldehyde (OPA) assay to check the level of acetylation. For NMR experiments, the solution was lyophilized to remove water and triethylammonium acetate following which the powder was dissolved in 600 μl of 20 mM potassium phosphate, pH 6.4 containing 10 % D_2O .

4.2.4. Estimation of level of acetylation

The degree of acetylation of metabolites/standard compounds was indirectly estimated using o-phthalaldehyde (Roth, 1971). The reagent provides a quantitative estimate of aliphatic amino groups present in a solution. This can be used to estimate the concentration of primary amino group of unacetylated metabolites and hence would provide an estimate of the degree of acetylation. For the assay, a buffered reagent containing 1.5 ml of o-phthalaldehyde solution (10 mg/ml in ethanol), 90 ml of borate buffer of pH 9.5 (for amino acids) and 7.4 (for ammonia) and 1.5 ml of a solution of 2-mercaptoethanol (5 μl /ml in ethanol) was prepared. To a 100 μl of the test solution containing aliphatic compounds with amino group in the concentration ranging from 0.1-1 mM, 3 ml of the buffered reagent was added and incubated for 25 min. The fluorescence of this solution was measured at 455 nm with an excitation wavelength of 340 nm. A known concentration of aspartate was used to plot a standard curve and this was used to calculate the concentration of primary aliphatic amino groups in the metabolite extract by interpolation.

4.2.5. NMR acquisition and identification of metabolites

All NMR data were acquired on Varian (Agilent) 600 MHz NMR Spectrometer equipped with a cryogenically cooled triple resonance probe that was fitted with a Z-axis PFG gradient accessory. Spectra were acquired at 25 °C. Solvent suppression was achieved using either solvent presaturation or by pulsed field gradients using the Excitation-Sculpting pulse program (Hwang & Shaka, 1995). Spectra were sampled over a bandwidth of 10000 Hz. A total of 16384 data points were acquired. The time-domain data were zero-filled once prior to Fourier transformation. Two - dimensional ^1H - ^{15}N HSQC spectra were acquired in gradient selected and sensitivity enhanced mode (Kay, Keifer, & Saarinen, 1992). A proton spectral width of 8000 Hz was sampled in all 2D heteronuclear NMR experiments. Nitrogen spectral widths of 6000 Hz and 1992 Hz were recorded on samples of cell lysates and standard amino acid, respectively. Three-dimensional ^{15}N -edited TOCSY - HSQC spectra (Cavanagh et al., 2007) were recorded on the lysate of an *E. coli* culture that was grown on $^{15}\text{NH}_4\text{Cl}$ as the sole source of nitrogen. Proton spectral widths of 8000 Hz and 3873 Hz were recorded during the acquisition period (t_3) and during the indirectly detected t_1 time dimension, respectively. A nitrogen spectral width of 1945 Hz was recorded in the indirectly detected t_2 time dimension. Data were zero-filled once in each dimension prior to Fourier transformation. CCPN analysis tool (Vranken et al., 2005) was used for visualization of slices and generating figures. All data were processed using VNMRJ, ACD Spectrum viewer or NMRPipe / NMRDraw software (Delaglio et al., 1995).

4.3. Results and discussion

4.3.1. Acetylation of standard metabolites

Amino acids aspartate, asparagine, glutamate and metabolites like GABA and ammonia were individually acetylated with acetic anhydride in the presence of triethylamine in potassium phosphate buffer, pH 6.4. The reaction mixture was lyophilized to remove the volatile salt triethylammonium acetate and the powder was resuspended in water containing 10% D_2O and used for acquiring NMR spectra. The effect of acetylation on enhancing the signal from the proton attached to the nitrogen is shown in **Figure 4.4**. Upon acetylation with acetic anhydride a sharp peak at 7.8 ppm corresponding to the amide proton is clearly seen in the spectra.

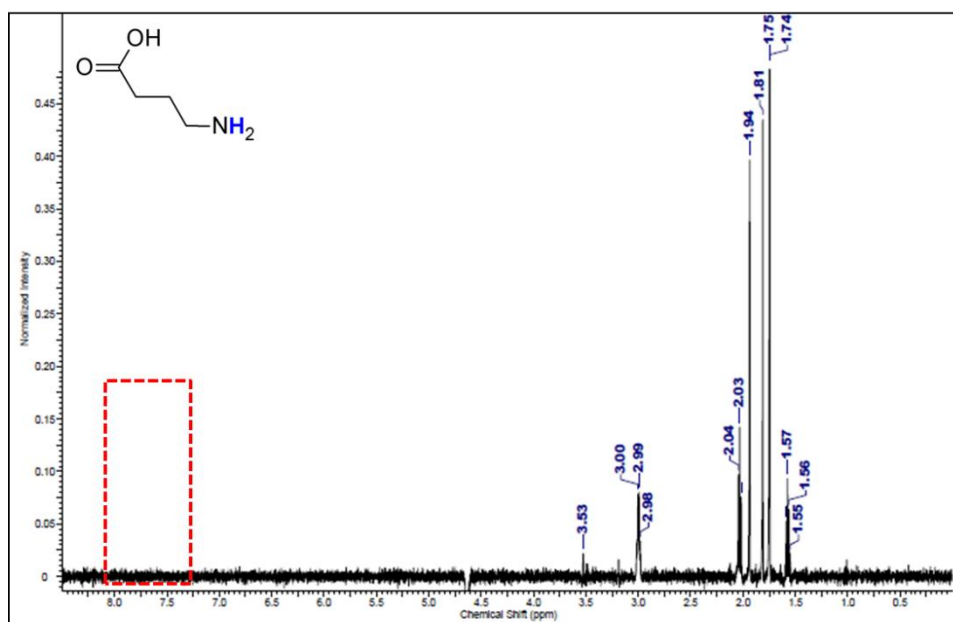
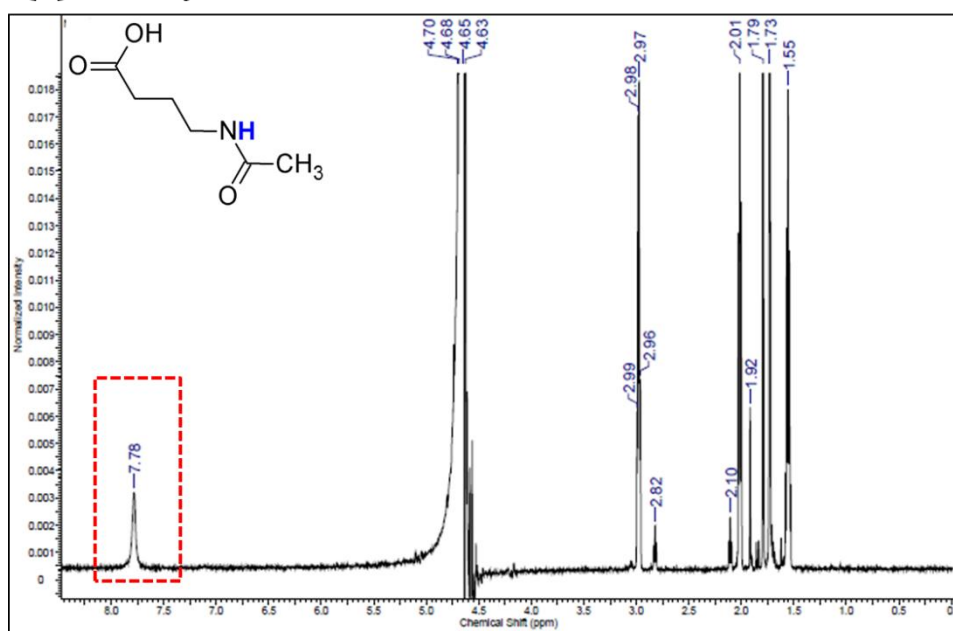
(a) GABA**(b) N-acetyl GABA**

Figure 4.4. Effect of acetylation on the signal intensity of proton attached to nitrogen in GABA

(a) GABA was mixed with acetic acid and triethylamine and the 1D proton spectrum was acquired. A broad peak corresponding to protons in primary amine group is highlighted with a dashed blue outline. The structure of GABA with the protons of interest shown in blue is given in the inset. **(b)** GABA was acetylated using acetic anhydride in the presence of triethylamine. The reaction mixture was directly used for acquiring 1D proton spectra. A sharp peak corresponding to the amide proton is highlighted. The chemical structure of N-acetyl GABA is shown in the inset. Note that GABA used is not enriched in ^{15}N .

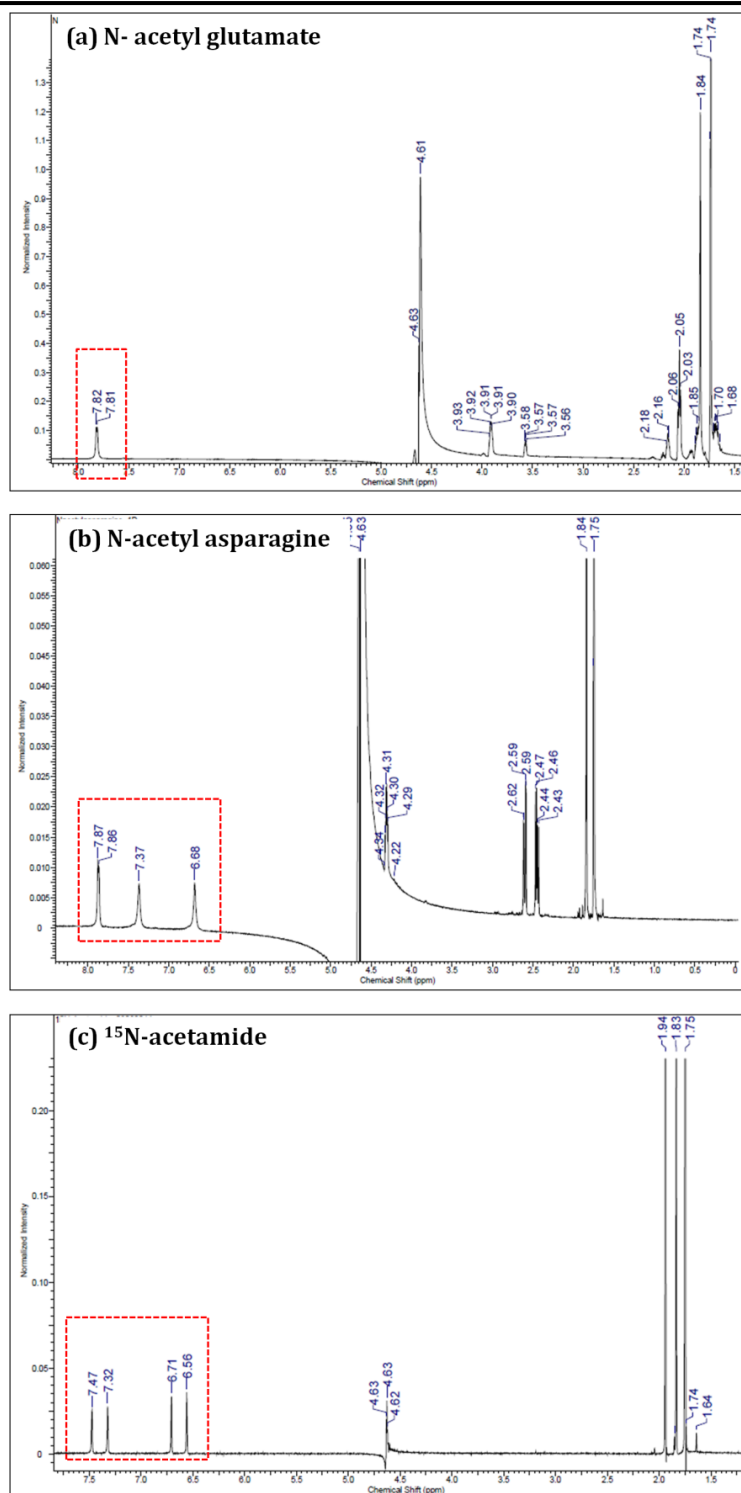


Figure 4.5. 1D proton NMR spectra of the reaction mixture after acetylation of the indicated metabolites

(a) The amide proton of N-acetyl-glutamate at 7.81 ppm is highlighted using a dashed red outline. **(b)** The side chain amide protons in N-acetyl asparagines are seen at 7.37 and 6.68 ppm. The main chain amide proton is seen at 7.87 ppm. **(d)** ^{15}N labelled ammonium chloride was acetylated and the two amide protons have non-equivalent spins and hence seen as a doublet of a doublet one centred at 7.4 and the other at 6.6 ppm. Note that the above compounds are not ^{15}N enriched.

The 1D proton spectra of other acetylated standards are shown in **Figure 4.5**. In these spectra, the amide proton is visible in the 6.0-8.0 ppm range. These samples were also analysed by heteronuclear single quantum coherence (HSQC) in proton and nitrogen dimensions. The resultant spectra are shown in **Figure 4.6**. As these are ^1H - ^{15}N -HSQC spectrum, only proton attached to ^{15}N -nitrogen will be observed. This shows that under the reaction conditions used these metabolites are acetylated. Low normalized intensity value of the peaks corresponding to amide protons in all the spectra shown in Figure 4.4 and 4.5 might either be due to low levels of acetylation or due to low natural abundance of ^{15}N (0.01%). In order to discriminate between the two, a fluorimetric assay was used to quantify the extent of acetylation in each of the reactions.

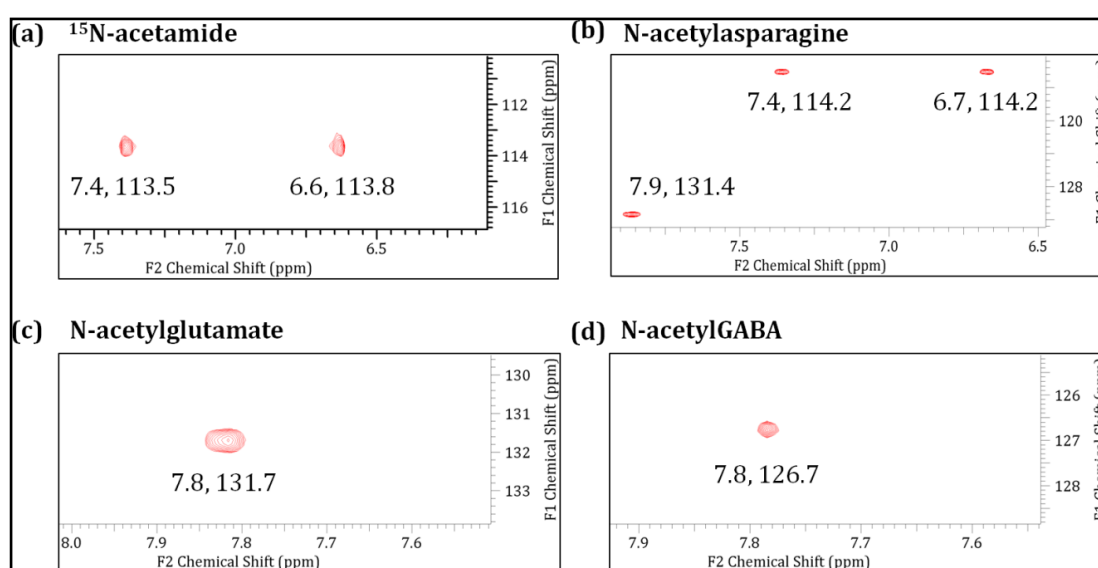


Figure 4.6. ^1H - ^{15}N -HSQC of standard acetylated metabolites

Chemical shift value of proton and nitrogen of the amide are indicated for each cross-peaks. The vertical and horizontal axis shows the chemical shift value of nitrogen and proton, respectively (shown as F1 and F2). **(a)** Two cross peaks corresponding to non-equivalent protons in ^{15}N labelled-acetamide. **(b)** Two cross peaks at the nitrogen chemical shift value of 114.2 correspond to the side chain amide of asparagine. The amide proton obtained after acetylation has a nitrogen chemical shift value of 131.4 ppm. **(c)** and **(d)** shows the cross peak corresponding to N-acetylglutamate and N-acetylGABA.

4.3.2. Quantification of extent of acetylation

Quantification of unacetylated metabolites would require an assay that can quantitate the unreacted amines in the reaction mixture. For this we resorted to a fluorimetric assay involving o-phthalaldehyde (OPA). OPA has a reactive aldehyde group that reacts with aliphatic primary amines in the presence of a reducing agent and at pH 7.4 to give a fluorescent adduct. The reaction is shown in **Figure 4.7**.

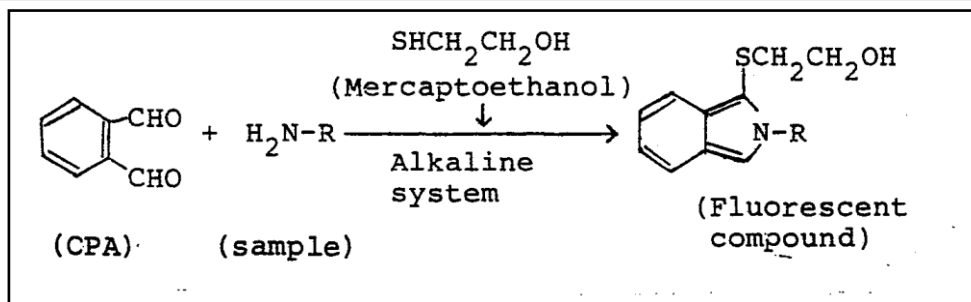


Figure 4.7. OPA assay for quantitation of unreacted amines after the acetylation reaction

The assay involves the formation of a fluorescent adduct between the amino acid, OPA and β -mercaptoethanol. The intensity of the fluorescence can be used as a direct estimate of the concentration of the primary amine.

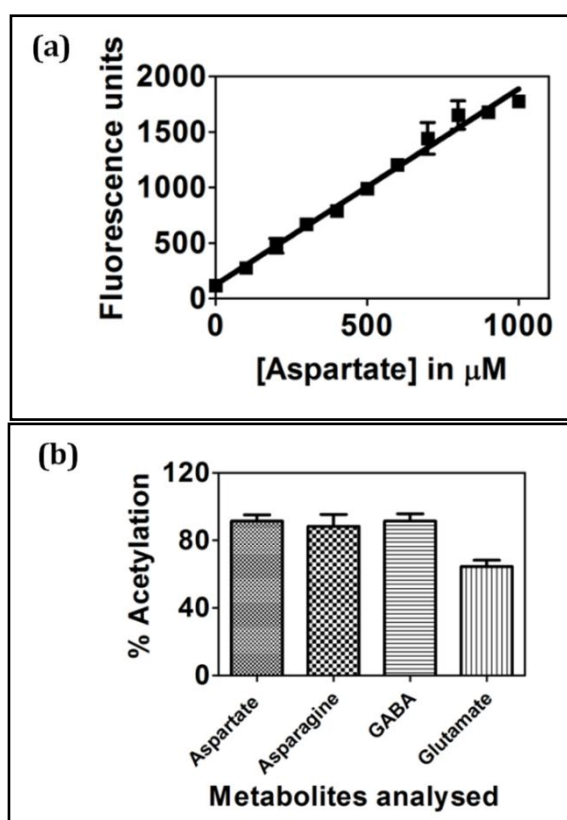


Figure 4.8. Quantitation of the extent of acetylation using OPA assay.

(a) Standard plot showing a linear correlation between the concentration of aspartate and the fluorescence intensity of the OPA-aspartate adduct. **(b)** From the OPA assay, the amount of unacetylated metabolite was quantified and used to estimate the extent of acetylation. Acetylation was close to 90% for both aspartate and GABA. The least level of acetylation was seen for glutamate (65 %).

A standard plot corresponding to known concentrations of any amino acid can be used to estimate the absolute concentration of the primary amines in the reaction mixture. One such standard plot using aspartate is shown in **Figure 4.8 a**. By using the

fluorescence intensity values of the reaction mixture before and after acetylation, the percent unreacted amines and hence, the unacetylated amines were quantitatively estimated. From this, the percentage of metabolites that are N-acetylated was inferred. As shown in **Figure 4.8 b** the acetylation procedure yielded good amounts of N-acetylated metabolites with the least being 65 % for glutamate and the maximum being 90% for aspartate.

4.3.4. Acetylation and NMR analysis of *E. coli* metabolites

4.3.4.1. 2D-HSQC analysis of acetylated metabolites

Hot-methanol extraction was used for the extraction of metabolites from *E. coli* cultures grown on minimal media containing ^{15}N labelled-ammonium chloride as the sole nitrogen source. The metabolites were resuspended in 20 mM sodium phosphate buffer, pH 6.4 containing 10 % D_2O and used for recording NMR spectrum. The 1D proton spectrum of the metabolites with the amide region expanded is shown in **Figure 4.10**.

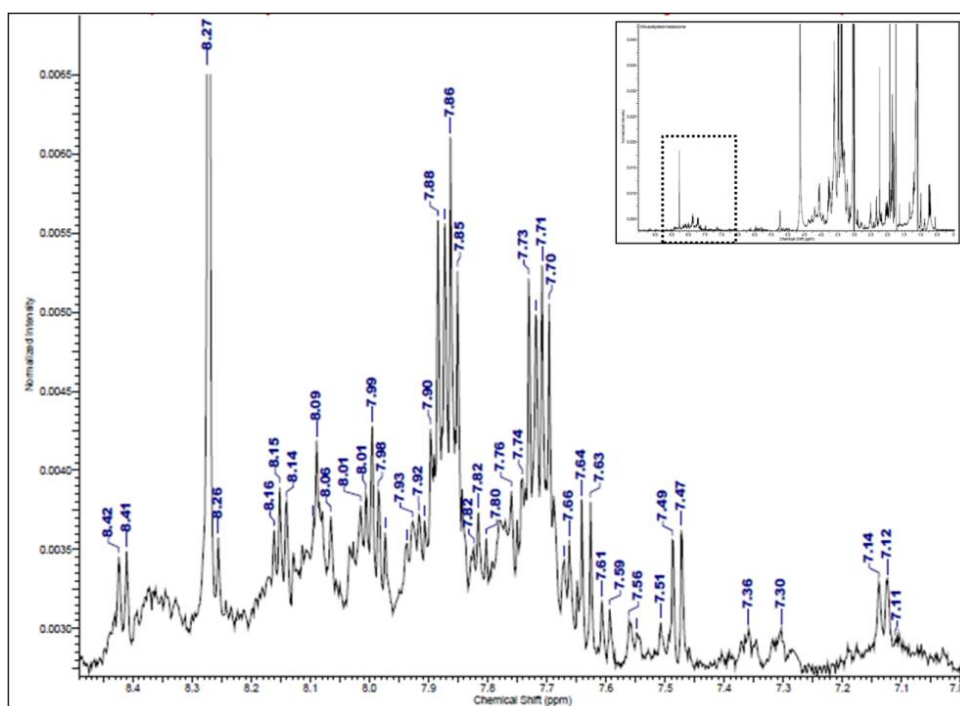


Figure 4.9. 1D proton NMR spectra of acetylated *E. coli* metabolites

The panel shows the peaks in the amide region (7.0-8.5 ppm). The full spectrum is shown in the inset.

The acetylated metabolite mixture was then analysed using 2D-HSQC in the proton (F1) and nitrogen (F2) dimension. The plane showing $^{1}\text{H}^{\text{N}}/\text{N}$ cross peaks is shown in **Figure 4.10**. Multiple cross peaks corresponding to different metabolites were observed and they were well separated in nitrogen dimension if not in the proton. A total number of 47 cross

peaks were seen. The nitrogen and the proton chemical shift values for each cross-peak is presented in **Table A 4.1 (Appendix-I)**, and each of these peaks could correspond to 47 different metabolites. All of the correlation cross-peaks were found in between 7.5 and 8.5 ppm (amide region). To our knowledge, there is no information available from any of the standard NMR metabolome databases about the chemical shift values of N-acetylated metabolites which could be used as a reference for metabolite identification. Hence, to identify the metabolites from this data, a ^{15}N -HSQC-TOCSY experiment on the acetylated metabolite extract was performed.

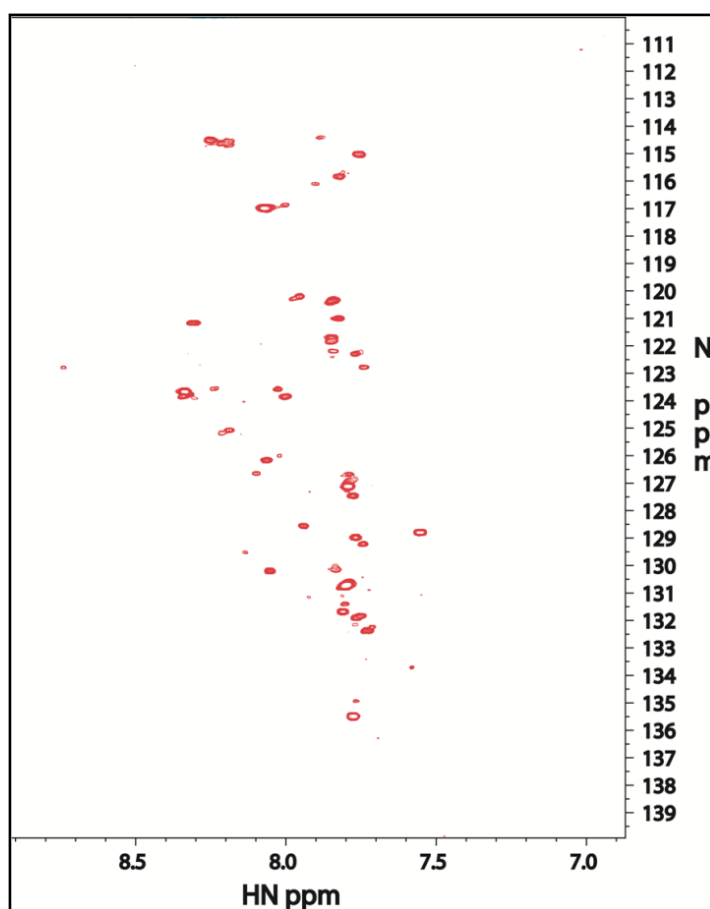


Figure 4.10. 2D-HSQC of acetylated *E. coli* metabolites

The plane shows the cross-peaks corresponding to different metabolites. Amide proton chemical shift is shown in the horizontal axis and the nitrogen chemical shift is shown in the vertical axis.

4.3.4.2. ^{15}N -edited TOCSY – HSQC analysis of acetylated metabolites

Figure 4.11 shows the two-dimensional HN-H projection of the 3D- ^{15}N -edited TOCSY – HSQC. The experiment involves the transfer of magnetisation from the amide proton to amide nitrogen (HSQC) and then on to protons attached to all the carbons in the molecule

in a manner similar to a regular TOCSY experiment. This would give cross-peaks corresponding to the amide proton and the correlation cross peaks corresponding to the protons attached to all the carbon atoms in the molecule.

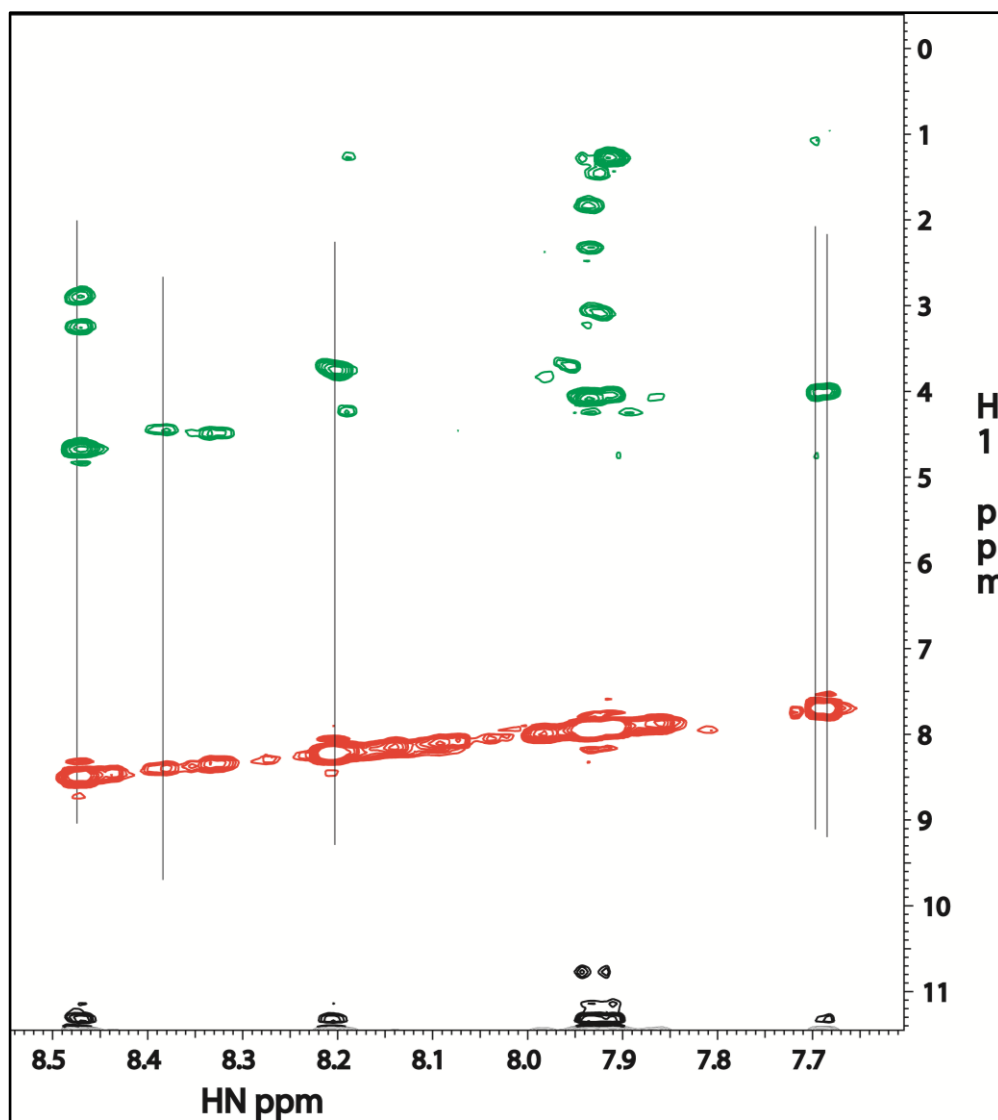
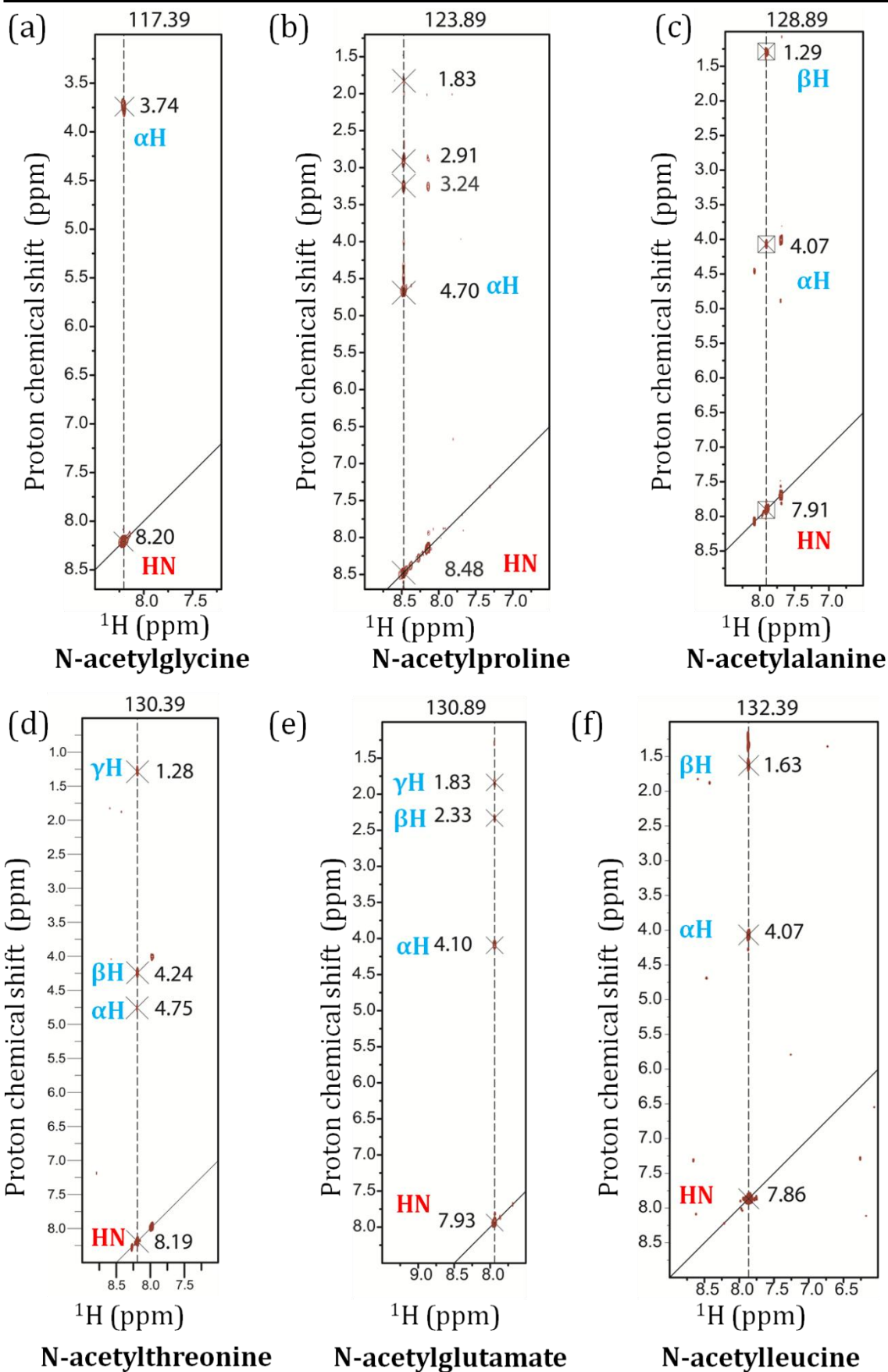


Figure 4.11. Two-dimensional HN (F1)-H (F3) projection of ^{15}N edited 3D-TOCSY- HSQC spectra of the acetylated ^{15}N -labelled *E. coli* metabolites.

Coloured in red are the NH cross-peaks. Coloured in green are the correlated cross-peaks. Connected by dashed lines are a set of cross-peaks corresponding to 4 different metabolites.



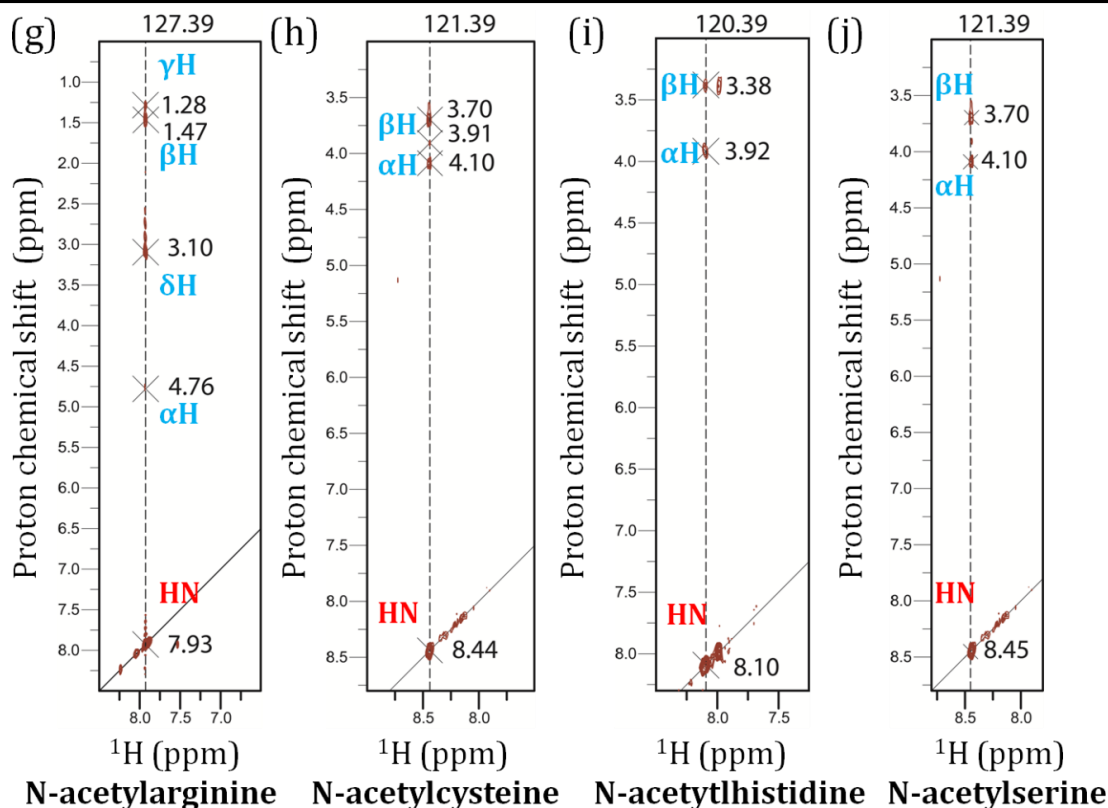


Figure 4.12. Strip plot showing the amide and correlated cross peaks for different metabolites identified.

The line running 45° to the horizontal axis corresponds to the ^1H - ^{15}N HSQC and hence the cross-peak on the line corresponds to the amide proton. The amide proton (F1 dimension) chemical shift value (ppm) is shown in the horizontal axis and the chemical shift value (ppm) for protons in F2 dimension is shown in the vertical axis. ^{15}N (F3 dimension) chemical shift (ppm) is noted at the top of each strip. Assignment of the metabolite was based on comparison of the chemical shift values (ppm) to standard values available in literature.

There are a total of 30 cross peak seen for the amide proton at different nitrogen chemical shifts values (**Appendix I-Table A4.2**). There are 27 correlation cross peaks seen that correspond the proton/s attached to the carbon atom that is directly bonded to the nitrogen (**Appendix I-Figure A4.1**). Using this data, N-acetylated species of 10 different metabolites were identified; glycine, proline, alanine, glutamate, threonine, leucine, arginine, cysteine, histidine and serine could be tentatively identified (**Figure 4.12**).

4.4. CONCLUSION AND FUTURE PERSPECTIVE

Acetylation of the extracted metabolite using the procedure was complete as we could hardly detect any unreacted primary amines in the OPA assay after the acetylation procedure. Metabolites were extracted from only 5 ml of *E. coli* culture which might not have yielded high concentration of individual metabolites. This might have led to certain

metabolites present at concentrations insufficient for a 3D-NMR experiment in spite of the total scanning time of 3 days. Moreover, the efficiency of magnetisation transfer diminishes as the number of bonds involved increases. High-intensity signal will require much larger metabolite concentration. For detecting metabolites having secondary amine groups (eg. polyamines), which cannot be acetylated by the protocol used, dissolving the extracted metabolites in aprotic solvent like DMSO (where proton exchange will be absent), will aid in their detection using similar NMR experiments adopted for primary amines.

Chapter 5

An introduction to Fe-S cluster containing class I fumarate hydratase

Chapter 5

An introduction to Fe-S cluster containing class I fumarate hydratase

ABSTRACT

*The structure of a macromolecule dictates its function. But there can be more than one structure that could perform the same function. Fumarate hydratase (FH) presents one such example wherein two different classes of the enzyme with bare minimal sequence similarity perform the same function. Two biochemically distinct forms of fumarate hydratase have been characterised from different organisms, one with the iron-sulfur cluster (class I) and the other without (class II). Iron-sulfur cluster is known to act as a Lewis acid and is an essential part of the catalytic cycle of this class of enzyme. This section presents our efforts to study a single subunit class-I FH from a mesophile, *P. falciparum* and two-subunit class-I FH from a thermophile, *Methanocaldococcus jannaschii* (Mj). This chapter provides an introduction to the reactions catalysed by the enzyme, compare and contrast the enzymatic mechanism of two classes of FH, and an introduction to the types of the iron-sulfur cluster, their properties and methods used to study them. Finally, a section is dedicated describing the basics of X-ray crystallography which has been exploited to understand the function of MjFH.*

5.1. Fumarate hydratase

Fumarate hydratase (FH) (4.2.1.4) belongs to the carbon-oxygen hydrolyase category of enzymes that catalyses the reversible conversion of fumarate to malate. Fumarate to malate conversion involves the *anti* addition of water molecule across the carbon-carbon double bond of fumarate and the reverse reaction involves cleavage of carbon-oxygen bond and removal of a proton from 2nd and 3rd carbon of malate, respectively. The reaction is a part of the TCA cycle, which is present ubiquitously across all kingdoms of life. This reaction can be catalysed by two distinct classes of fumarate hydratases as discovered first in *E. coli*. Class I fumarate hydratases (C I-FH) are iron-sulfur cluster containing thermolabile enzymes. Class II type fumarate hydratase (C II-FH) are iron-independent and relatively more thermostable enzymes. Other than the fumarate recognition motif, there is no sequence conservation between two classes of enzymes (Woods et al., 1988). The iron-sulfur cluster in C I-FH is susceptible to oxidative damage

even in the presence of trace amounts of oxygen. This posits the use of anaerobic environment/strategies in various steps involved in the biochemical and structural characterization of the enzyme.

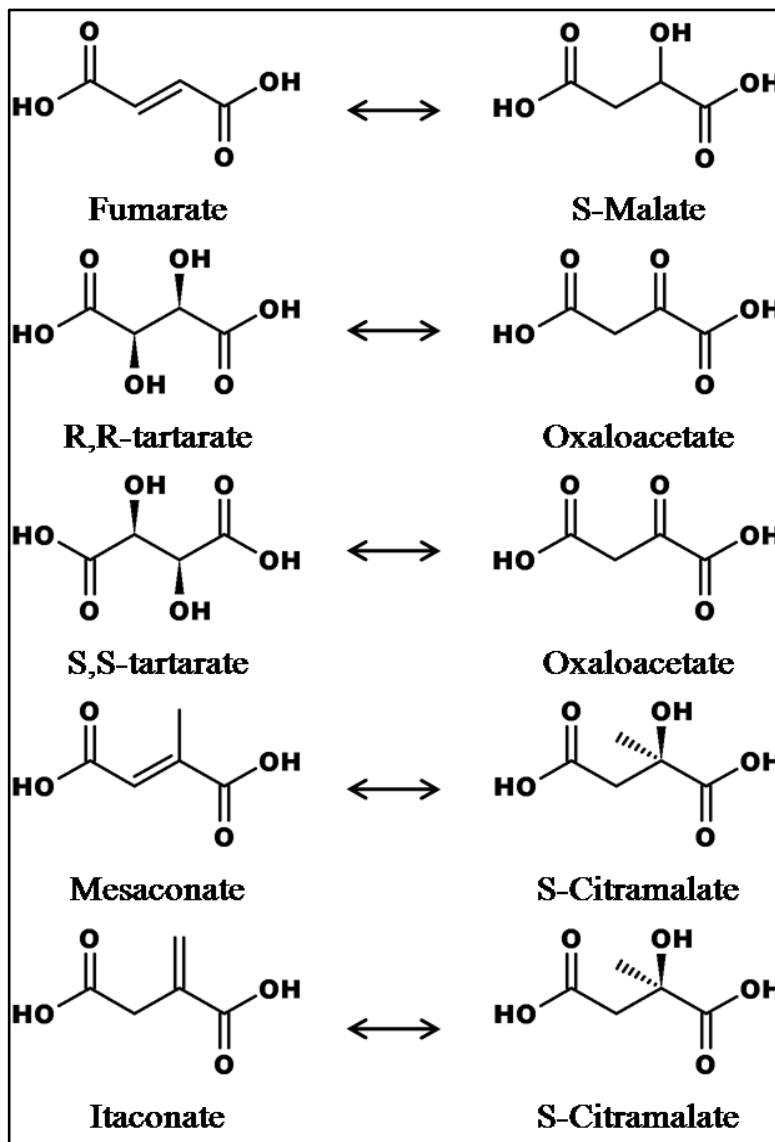


Figure 5.1. Reactions catalysed by fumarate hydratase (fumarate to malate, mesaconate to citramalate, and D-tartrate to oxaloacetate), itaconate dehydratase (itaconate to citramalate), mesaconase (mesaconate to citramalate and fumarate to malate) and L-tartrate dehydratase (L-tartrate to oxaloacetate).

Apart from malate dehydration, the enzyme displays promiscuous activity on substrates like D-tartrate and mesaconate (van Vugt-Lussenburg et al., 2013; Kronen et al., 2015) converting them to oxaloacetate and citramalate, respectively. Fumarase A (FumA), one of the C I-FH from *E. coli* has been reported to act on fluoro fumarate, acetylene dicarboxylate and enol-oxaloacetate as well (Flint, 1994). **Figure 5.1** is a compilation of reactions catalysed by fumarases and the related enzymes, mesaconase

and L-tartrate dehydratase. On comparison of the K_{eq} values of the reactions catalysed by fumarase (Table 5.1), it is interesting to note that unlike the reaction involving fumarate and mesaconate, that proceeds close to equilibrium (and hence reversible reactions), the tartrate to oxaloacetate reaction is far from equilibrium (and hence almost an irreversible reaction).

Table 5.1. Thermodynamic parameters of different reactions catalysed by fumarate hydratase. Values obtained from eQlibrator tool (Flamholz et al., 2012).

S.No	Reaction	$\Delta_r G'^m / \Delta_r G^\circ$ (KJ/mol)	K_{eq}
1	Malate to fumarate	3.5 ± 0.6	0.248
2	Tartrate to oxaloacetate	-35.3 ± 3.9	1.6×10^6
3	Mesaconate to citramalate	2.9 ± 4.7	0.316

$\Delta_r G'^m$, Gibbs free energy at a pH of 7.0 and ionic strength of 0.1 M, and 1 mM concentration of all reactants; $\Delta_r G^\circ$, Gibbs free energy at a pH of 7.0 and ionic strength of 0.1 M, and 1 M concentration of all reactants; K_{eq} , rate enhancement of forward reaction over that of the reverse reaction. A value of 1 indicates an equal flux of forward and reverse reaction; a value of less than 1 indicates an increased flux of reverse reaction, and a value more than 1 indicates an increased flux of the forwards reaction compared to that of the reverse reaction.

A search of the Pfam database using the keyword 'fumarate hydratase' was carried out to examine the distribution of the two distinct classes of fumarases. PF10415 is the Pfam ID for class II fumarases and PF05683 and PF05681 for class I enzymes. Figure 5.2 shows the distribution of both classes of enzymes. Both classes of enzymes are present in all three kingdoms of life, with some organisms especially bacteria encoding both types of fumarate hydratases as exemplified by *Escherichia coli*. Based on subunit organisation, class-I fumarate hydratases can be further subdivided into single subunit- and two subunit- type enzymes. Distribution of C I- and C II-FH is given in Figure 5.2. Similar to *E. coli*, many organisms do possess both classes of enzymes. Exact reason as to the need of an oxygen sensitive C I-FH when a more robust C II gene is present is still not known. Similarly, the distribution of two-subunit and single subunit C I FH is still not completely catalogued. The nature of the ancestral protein with respect to domain architecture (single/ two subunit) is still not known. A thorough phylogenetic analysis and taxonomic distribution would throw light on many such unanswered questions. It has been hypothesised that the kind of fumarate hydratase present (C I vs C II) might determine the prokaryotic lifestyle- with respect to sensitivity to oxygen of an organism (Shimoyama et al., 2007a).

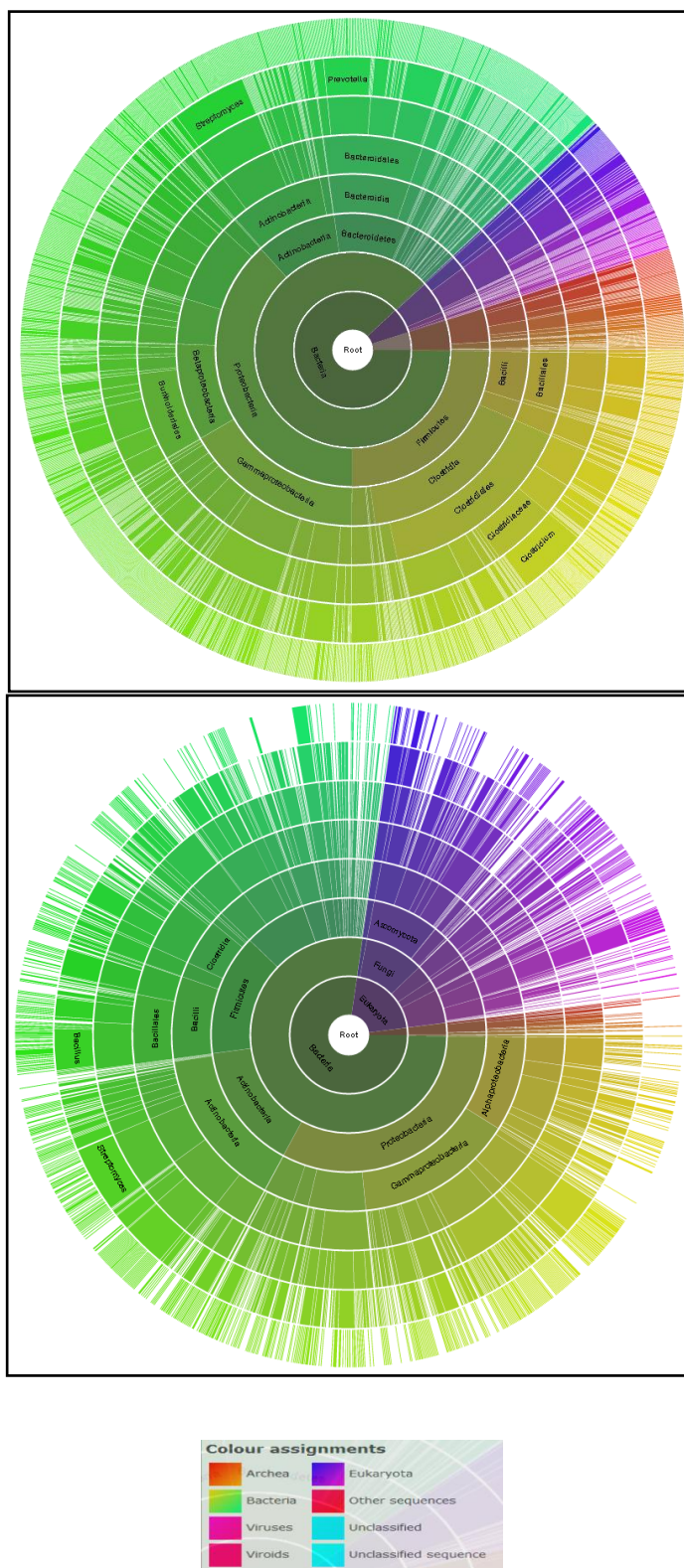


Figure 5.2. Distribution of C I-FH (left panel) and C II-FH (right panel).

It can be seen that C II-FH is present in very few archaea and present in more eukaryotic organisms than C I-FH. The figures have been adapted from Pfam database (Punta et al., 2012). The legend for the colour coding is provided.

The class I enzyme has been studied from a few organisms and the findings are summarised in table 5.2.

Table 5.2. Summary of literature available on C I- FH from various organisms.

<i>Organism</i>	<i>Type</i>	<i>Findings</i>	<i>Reference</i>
<i>Escherichia coli</i>	SS	Cluster type, kinetic characterisation, substrates catalysed	(Woods et al., 1988; Flint, 1993; van Vugt-Lussenburg et al., 2013)
<i>Leishmania major</i>	SS	Cluster type, kinetic characterisation and localisation	(Feliciano et al. 2012)
<i>Burkholderia xerovorans</i>	SS	Substrate promiscuity and kinetic characterisation	(Kronen et al., 2015)
<i>Pelotomaculum thermopropionicum</i>	TS	Cluster type and kinetic characterisation	(Shimoyama et al., 2007a)
<i>Pyrococcus furiosus</i>	TS	Cluster type and kinetic characterisation	(van Vugt-Lussenburg et al., 2009a)
<i>Archaeoglobus fulgidus</i>	TS	Structure of β -subunit	PDB id: 2ISB

SS-single subunit, TS-two subunit.

5.2. Physiological significance and localisation of FH (C I and C II)

Enzymatic function of both classes of fumarate hydratase remains the same; conversion of fumarate to malate. Hence, it is important to understand the physiological significance of both classes of enzymes in different systems.

5.2.1. Class II fumarate hydratase

Class II fumarate hydratases are extensively studied from both structural and functional perspective. In many eukaryotes, the enzyme is localised to both mitochondria and cytosol. Multiple strategies are found in different organisms by which the enzyme is dual localised to both the compartments. Summary of the strategies used from some of the well-studied systems are given below:

- 1) Yeast has a single gene, *Fum1*, that encodes a mitochondrial FH which after the removal of the signal peptide in the mitochondria undergoes retrograde transport to cytosol (Knox et al., 1998),
- 2) Many plant species like Arabidopsis and tomato have two genes encoding two different proteins with and without the mitochondrial targeting sequence (MTS) (Pracharoenwattana et al., 2010),
- 3) In rat liver cells the FH gene is transcribed to a single mRNA with two translational initiation sites such that two different proteins are made from the same mRNA one with the MTS and that other without the MTS (Tuboi et al., 1986),

4) In humans, alternative transcription initiation from a single gene result in two different mRNA one coding for the cytosolic isoforms and the other for the mitochondrial enzyme (Dik et al., 2016).

In mitochondria, the primary role of the enzyme is to act in congruence with other citric acid cycle enzymes. Diverse roles are associated with cytosolic fumarate hydratase; involvement in urea cycle in mammalian cells (Adam et al., 2013), nitrogen assimilation of plants (Pracharoenwattana et al., 2010; Nunes-Nesi et al., 2010), seed germination (maize) (Eprintsev et al., 2014), carbon storage in plants (Zell et al., 2010) and DNA repair pathway of yeast and mammalian cells (Jiang et al., 2015). In mammalian cells, the major role of cytosolic FH seems to be to keep the fumarate levels under control. Elevation of fumarate levels due to mutation and inactivation of FH leads to pathologic consequences. Biallelic inactivation of fumarate hydratase has been associated with a genetic disorder called Hereditary leiomyomatosis and renal cell carcinoma (HLRCC) and encephalopathies (Tomlinson et al., 2002).

Molecular basis associated with pathogenicity of fumarate accumulation are perturbation of urea cycle metabolism (Adam et al., 2013), succination of thiols in proteins/metabolites (Blatnik et al., 2008; Thomas et al., 2012) , and HIF1- α stabilization and a glycolytic shift in cellular metabolism (Pollard et al., 2005; Tong et al., 2011a; b). However, it has been reported that the consequence of FH inactivation is cell type-specific and cannot be generalised (Raimundo et al., 2008). Succination and HIF1- α stabilisation are some of the recently discovered molecular consequences of fumarate accumulation. Fumarate accumulation in cells causes reversal of arginosuccinate lyase reaction: arginosuccinate to arginine and fumarate, thereby causing depletion of arginine. FH-deficient cells become auxotrophic for arginine. The role of the enzyme in DNA repair is an exciting finding (Jiang et al., 2015). It has been shown in both yeast and in mammalian cell lines, that upon DNA damage the cytosolic enzyme relocates to the nucleus where it is involved in the recruitment of key enzymes involved in DNA repair. Exposure of cell to ionising radiation causes an increased association of fumarate hydratase to histones in particular histone variant H2A.Z. Subsequently, DNA-dependent protein kinase acts on fumarate hydratase and phosphorylates threonine 236. The phosphorylated FH recruits more of DNA-PK at the double stranded break (DSB) region. Finally, fumarate generated locally at the site causes inhibition of H3 demethylases thereby, enhancing dimethylation of histone H3. Dimethylated histone H3 is known to bind Ku70, a protein involved in non-homologous end joining based repair pathway. Overall, the study suggests the importance of both the physical presence of the phosphorylated enzyme and the enzymatic activity of FH for DNA repair of cells exposed to ionising radiations.

Arabidopsis has two genes that encode mitochondrial and cytosolic form of FH. The mitochondrial enzyme is essential whereas the cytosolic enzyme is not. However, the cytosolic enzyme is needed for nitrogen assimilation and growth in the presence of high nitrogen content (Pracharoenwattana et al., 2010). Fumarate is proposed to act as a counter ion for nitrate during nitrogen assimilation. In a study done in maize seeds, the cytosolic isoform of the enzyme has been shown to be involved in the metabolism of succinate generated in glyoxylate pathway (Eprintsev et al., 2014). The cytosolic isoforms have been shown to have an optimal pH of activity 1 unit lesser than that of the mitochondrial isoforms. The physiological implication of this is proposed to be the involvement of the enzyme in low-pH-induced germination of maize seeds. The cytosolic isoform is also shown to be more efficient in catalysis when compared to the mitochondrial isoforms.

5.2.2. Class I fumarate hydratase

As discussed in section 6.1 this class of enzymes are predominantly present in bacteria and archaea. Only a few eukaryotes have been reported to have this class of enzyme. The two subunit type enzyme has been characterised only from two organisms: *Pelotomaculum thermopropionicum* (Shimoyama et al., 2007b)- an anaerobic, thermophilic bacterium belonging to clostridial firmicute, and *Pyrococcus furiosus*, a hyperthermophilic euryarchaeota. Though known for its role in TCA cycle, the role of FH in these organisms might not be directly related the cycle itself. In *P. thermopropionicum*, a propionate oxidising bacteria, fumarate hydratase is involved in methylmalonyl-coenzyme A pathway (Kosaka et al., 2006) where removal of formed fumarate is essential to avoid energetically unfavourable succinate oxidation (Van Kuijk et al., 1998). The metabolic role of the enzyme in *P. furiosus* is still not clear as many of the TCA cycle enzymes are missing in the annotated genome (van Vugt-Lussenburg et al., 2009a).

However, transcriptome analysis has shown that there is a two-fold increase in the fumarase levels in cells grown on sulphur suggesting a possible bioenergetic role of the enzyme in this organism (Schut et al., 2001). It has been suggested that fumarate generated by the enzyme may also play a role in flagellar switching as seen in many bacterial species but in a fumarate reductase independent fashion (Marwan et al., 1990; Cohen-Ben-Lulu et al., 2008).

Discovered first in *E. coli* (Woods et al., 1988) , single subunit CI-FH has been studied in organisms like *Leishmania* (Feliciano et al. 2012), *Syntrophobacter fumaroxidans* (Kuijk et al., 1996), *P. falciparum* (Ke et al., 2015), and *Burkholderia xenovorans* (Kronen et al., 2015). The physiological significance of the enzyme in these

organisms seems to be associated with its role in TCA cycle. However, the promiscuous activity of the fumarases on mesaconate support certain organisms like *B. xerovorans* to grown on substrates like itaconate and mesaconate. The *E. coli* enzyme is also known to act on the substrate D-tartrate (Kim et al., 2007). In *E. coli* there are two genes *fumA* and *fumB*, both belonging to C I-FH that catalyses the reversible conversion of fumarate to malate. However, *fumA* is the major protein expressed during aerobic condition with about 80% of the fumarase activity attributed to it. *FumB* is expressed only during anaerobic conditions. However, both *FumA* and *FumB* are shown to be upregulated in *E. coli* when grown on glycerol as the sole carbon source (Martínez-Gómez et al., 2012). The notion that *FumA* is more efficient in fumarate to malate conversion and *fumB* for the reverse reaction has been recently disproved (van Vugt-Lussenburg et al., 2013). The authors show that both the enzymes display comparable efficiency in catalysing the reaction in either direction. The only significant difference found between these enzymes was in the dehydration of D-tartrate. *FumB* acts on D-tartrate 4 times more efficiently than *FumA*. Owing to the stereospecificity of the reaction, none of class I enzymes characterised so far is shown to act on L- or meso tartrate.

5.3. Mechanism and kinetic properties of C I and C II enzymes

C II-FH belongs to aspartase/fumarase superfamily of enzymes that share a common tertiary and quaternary fold. Aspartase (4.3.1.1), fumarase (4.2.1.2), adenylosuccinate lyase (4.3.2.2), and arginosuccinate lyase (4.3.2.1) are among the well-studied enzymes in this family. These enzymes are usually tetramers with four different active sites. They catalyse anti addition/elimination of water molecule. A scheme representing the different substrates used by this family of enzymes is given in Figure 5.1. As can be seen in the figure, the enzymes recognise a succinyl group in the substrates which is converted to fumarate after catalysis. The proposed mechanism of catalysis is given in **Figure 5.3** (Puthan Veetil et al., 2012). Briefly, the first step involves abstraction of a proton from the C3-carbon of the substrate resulting in the formation of a carbanion. Multiple pieces of evidence suggest a conserved serine present in the signature sequence GSSXXPKXNPXXXE acts as a catalytic base that is involved in this proton abstraction. Stabilisation of the charge on the carbon leads to the formation of an enediolate intermediate. Kinetic isotope experiments, crystal structure of the enzyme with substrates bound and inhibition of the enzyme activity by the nitro analogues of the substrate supports the existence of an enediolate intermediate in the reaction landscape (Blanchard and Cleland, 1980; Fibriansah et al., 2011).

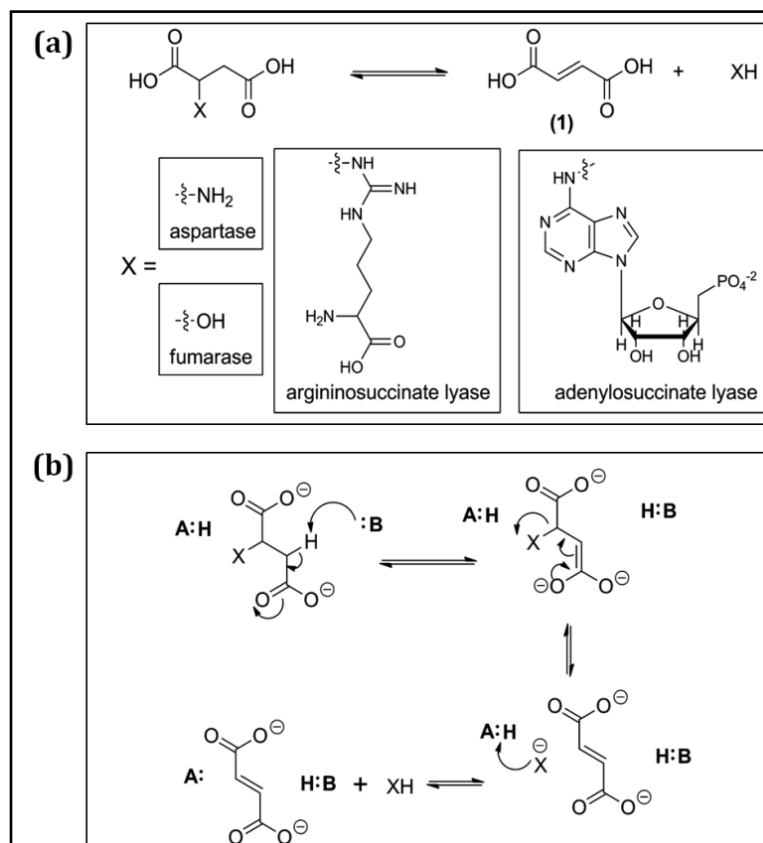


Figure 5.3. Common catalytic strategy of aspartase/fumarase superfamily enzymes

(a) Common chemical features in reactions catalysed by aspartase/fumarase superfamily of enzymes. (b) Proposed reaction mechanism of fumarase superfamily enzymes. Formation of enediolate intermediate is shown in the figure (Puthan Veetil et al., 2012)

The leaving group in fumarase reaction is actually the hydroxyl group which is protonated to water by a catalytic acid in the protein. Though there are reports suggesting that a conserved histidine might act as the catalytic acid, further studies need to be performed to unambiguously assign the residue (Puthan Veetil et al., 2012). Finally, fumarate and a second product (water in case of fumarase reaction and ammonia in case of aspartase reaction) are released from the enzyme. C II fumarases are one of nature's perfected enzymes achieving rate enhancement of over 10^{15} fold over the uncatalyzed reaction. One remarkable feature of C II enzyme is the extent to which the transition state stabilisation is achieved, 30 kcal/mol. This value is not achieved by enzymes like triosephosphate isomerase or other isomerases that catalyse C-H bond cleavage (Bearne and Wolfenden, 1995). The structure of this class of enzyme has been solved from multiple organisms (Weaver and Banaszak, 1996; Weaver et al., 1998; Mechaly et al., 2012; Weaver, 2005).

C I-FH uses an iron-sulfur cluster as a cofactor for substrate binding and catalysis. The mechanism involved is similar to aconitase which is another iron-sulfur cluster protein that catalyses the conversion of citrate to isocitrate (Flint and Allen, 1996a). In iron-sulfur cluster dependent hydrolyases the cluster is known to perform two functions, one, to bind the substrate and the other, to activate the leaving group which in the case of the fumarase reaction is a hydroxyl moiety acting as a Lewis acid. The proposed reaction mechanism is shown in **Figure 5.4**. It has been proposed that all other steps involved in the catalysis are similar to that observed in class-II fumarases (Flint and Allen, 1996a). Fumarase A from *E. coli* has been studied extensively for the elucidation of the reaction mechanism of class I-FH (Flint et al., 1992; Flint, 1993, 1994). The mechanism is discussed in detail in section 5.6.1. A brief introduction to Fe-S cluster with respect to its types and the techniques used to study them is given in next section.

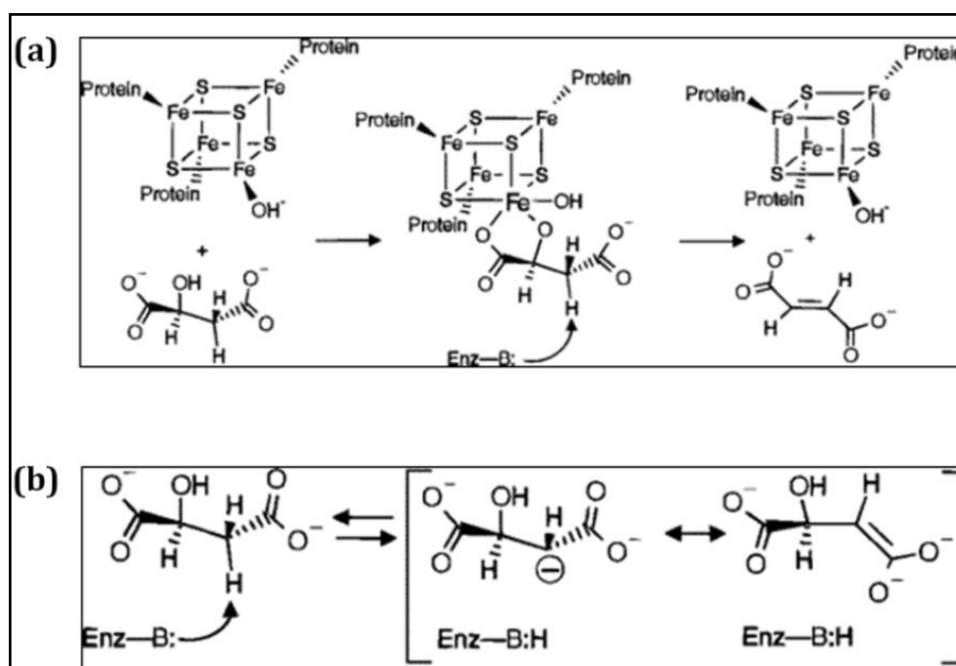


Figure 5.4. Proposed reaction mechanism for C I-FH.

(a) Involvement of the cluster in substrate binding and catalysis. **(b)** Formation of enediolate intermediate in a fashion similar to that seen for C-II FH. Figure reproduced from Flint & Allen 1996.

5.4. Fe-S cluster

Iron-sulfur clusters constitute inorganic cofactors containing different stoichiometry of iron and sulphur and are found in multiple proteins belonging to different superfamilies. These constitute one of the ancient cofactors that either in the form of minerals (pyrite) or along with proteins as clusters are proposed to have catalyzed multiple primordial

enzymatic transformation and hence thought to have played a key role in the origin of life—the proposition surmising the iron-sulfur world hypothesis (Wächtershäuser, 1990, 1992; Wachtershauser, 2008). The two components of the cluster, iron and sulphur, offer unique chemical properties and are exploited in biological systems. Sulphur can take variable oxidation states and hence offers versatility in the number of bonds that it can form and break. Iron, on the other hand, seems to be the best metal of choice to work with sulfur as this metal has the least inner sphere reorganization energy, the energy required for a species to stabilize itself upon loss/gain of electrons, thereby making iron-sulfur pair based clusters an optimal co-factor used in multiple electron transfers and Lewis acid-based reactions in biology (Beinert, 2000; Jensen, 2006).

5.4.1. Types and chemical properties

Iron-sulfur clusters come in different shapes and sizes differing majorly in the number of iron and sulphur and in the presence of additional metal ions as a part of the cluster (**Figure 5.5**). Iron binds usually to the γ S of the cysteine residues in proteins, but other residues like histidine can also bind iron (eg. Rieske cluster with two histidines involved in [2Fe-2S] cluster). In clusters with more than one iron, inorganic sulphur atoms form linkages to hold the iron known as μ S linkages (Collins et al., 2011). 90% of the iron-sulfur cluster proteins in *E. coli* belong to [4Fe-4S] type and the remaining 10% to [2Fe-2S] and [3Fe-4S] types (Fontecave, 2006).

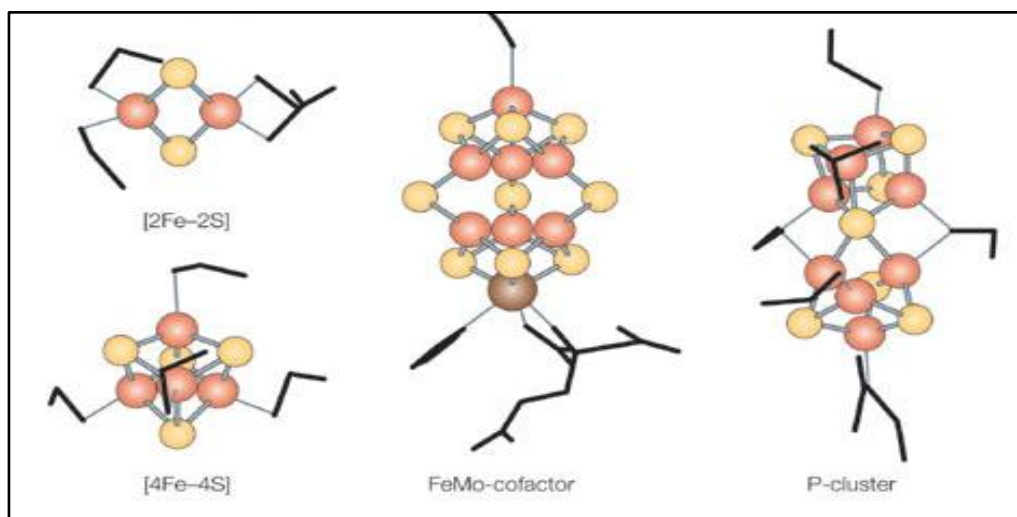


Figure 5.5. Types of iron-sulfur cluster.

Solid black lines indicate sidechain residues from protein backbone (usually cysteines); orange spheres indicate iron atom and yellow spheres, inorganic sulphur atoms. Figure reproduced from (Rouault and Tong, 2005)

Metal-thiolate bonds are known to have a covalent bond character with iron-thiolate bonds exhibiting more of σ -character (Solomon et al., 2006). Iron-sulfur (inorganic) bonds are 2 to 3 times more covalent than the iron-thiolate bond. The bond covalency and redox potential of the cluster can be significantly affected by hydrogen bonding with protein backbone amide or residue side chains (Kolling et al., 2007; Birrell et al., 2016; Collins et al., 2011). Bond length of Fe-S $_{\gamma}$ is usually between 2.2-2.4 Å and bond angles of μ S/S $_{\gamma}$ -Fe- μ S/S $_{\gamma}$ range from 75-115°. The geometrical parameters of a typical [3Fe-4S]⁺ in ferredoxin II from *Dosidicus gigas* is shown in **Figure 5.6 a** (Cammack, 1999). Despite high covalency, the Fe-S bonds are shown to have surprisingly low mechanical stability (Zheng and Li, 2011). A recently published high resolution (0.48 Å) structure of HIPIP containing 4Fe-4S cluster subjected to charge-density analysis has provided a detailed snapshot of the electron distribution around different constituent atoms of the cluster (Hirano et al., 2016) as shown in **Figure 5.6 b**. The authors have attributed the asymmetry of the iron-sulfur cluster and the protein environment as the structural basis of the charge storage property of the cluster. Similar data if available for a 3Fe-4S cluster in an enzyme, it would provide insight into the mechanism by which these cofactors are used as electron storage devices as seen in HIPIP proteins and as a Lewis acid as present in fumarase.

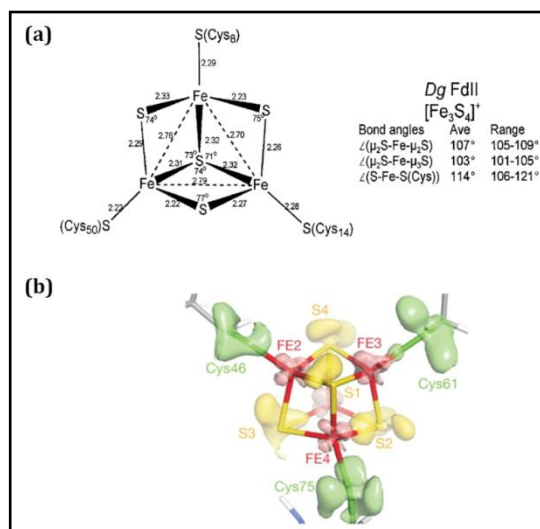


Figure 5.6. Geometry of Fe-S cluster

(a) Geometrical properties of a [3Fe-4S]⁺ cluster of Ferredoxin II from *Dosidicus gigas*. μ S corresponds to inorganic sulphur in the cluster. **(b)** Electron density around different atoms of the 4Fe-4S cluster in HIPIP protein from *Thermochromatium tepidum*. Green, yellow and red represents the distribution of charge around cysteinyl sulphur, inorganic sulphur and iron respectively, as calculated from charge density analysis. Panel (a) is reproduced from Cammack, 1999 and panel (b) reproduced from Hirano et al., 2016.

The iron in the cluster has been shown to have a distorted tetrahedral geometry (Collins et al., 2011). The clusters have both electronic and magnetic properties, with electronic properties localised more on sulphur and the magnetic/spin properties on the iron. The cluster can exist in different oxidation states; shown as a superscript in the usual representation of the cluster; $[2\text{Fe-2S}]^{2+}$ shows the 2+ oxidation state of the cluster), with each oxidation state having different properties. The oxidation state of the cluster is known to have an inverse relationship with the Fe-S bond distance and hence on the cluster geometry (Collins et al., 2011; Mousesca and Lamotte, 1998). Only certain oxidation states of the cluster can have physiologically relevant functions.

5.4.2. Techniques to study Fe-S clusters

The techniques used to study the cluster are based on its electronic and magnetic properties. Important characteristics of the cluster that need to be studied are the stoichiometry of iron and sulphur, oxidation state, and the redox potential. These features can be studied by well-established techniques used widely in bioinorganic chemistry. **Table 5.3** lists different techniques used to study Fe-S clusters and the information we gain from each of them.

Table 5.3. Techniques to study Fe-S cluster proteins. Various techniques used to study Fe-S clusters and the information obtained from them. A suitable reference that most widely covers the basic aspects of the technique as used for Fe-S cluster is provided

S.No	Technique	Property studied	Information about cluster	Reference
1	EPR	Paramagnetic property of iron	Type and spin state (indirect inference of oxidation state)	(Androes & Calvin 1962; Noodleman et al. 1995)
2	Ultraviolet-Visible Spectrophotometer	Thiolate-Metal charge transfer	Type and purity	(Dailey et al., 1994)
3	Atomic emission spectroscopy	Quantitative estimate of Fe and S	Stoichiometry	(Pierik et al. 1992)
4	Native mass spectrometry	Quantitative estimate of the mass of the protein with cluster	Stoichiometry	(Gao et al., 2007; Hernández et al., 2001)
5	Colorimetry	Reactivity of iron and sulphide	Stoichiometry	(Suhara et al., 1975; Beinert et al., 1983)

6	Magnetic circular dichroism	Magnetic property of iron in the cluster	Spin state and hence the type	(Stephens et al., 1978)
7	Visible circular dichroism	Charge transfer band of Fe-S	Presence and monitoring formation during in-vitro reconstitution	(Bonomi et al., 2008)
8	Electron nuclear double resonance(ENDOR) and (advanced EPR)	Paramagnetic property of iron	Enzyme mechanism, structure of cluster, ligand identification and protein dynamics	(Cutsail et al., 2015)
9	Electron spin echo envelope modulation (ESEEM)	Paramagnetic property of iron	Enzyme mechanism, structure of cluster, proton environment and protein dynamics	(Cutsail et al., 2015; Kolling et al., 2009)
10	Double electron-electron resonance (DEER)	Paramagnetic property of iron	Enzyme mechanism, structure of cluster, proton environment and protein dynamics	(Noodleman et al., 1995; Bertrand et al., 1994; Roessler et al., 2010)
11	Crystallography	Anomalous scattering of iron and sulphur	Type, geometry, molecular environment and stoichiometry	(Lauble et al., 1992; Lloyd et al., 1999)
12	Mossbauer spectroscopy	Magnetic property of iron	Electronic property of individual Fe atom, Fe-Fe coupling and oxidation state	(Pandelia et al., 2015)
13	Resonance Raman	Fe-S stretching vibrations	Type (especially useful when more than one cluster type is present)	(Sanders-Loehr, 1988)
14	X-ray absorption spectroscopy	Absorption of iron	Local electronic environment and geometry	(Penner-Hahn, 1988)

Two of the techniques that pertain to this thesis will be discussed in detail; EPR and UV-visible spectroscopy. The ligand to metal charge transfer results in a weak electronic transition causing brownish colouration of the iron-sulfur cluster containing proteins with absorption in the visible region. Depending on the type of the cluster the absorption peaks differ. For [2Fe-2S] clusters display an absorption band at 330 nm with broad shoulders at 460 nm and 550 nm. The [4Fe-4S] cluster exhibits a single absorption band ranging anywhere between 390-420 nm (Dailey et al., 1994; Agar et al., 2000). The

ratio of $A_{420}:A_{280}$ ranging between 0.30-0.32 is taken as a measure for complete reconstitution of apoprotein.

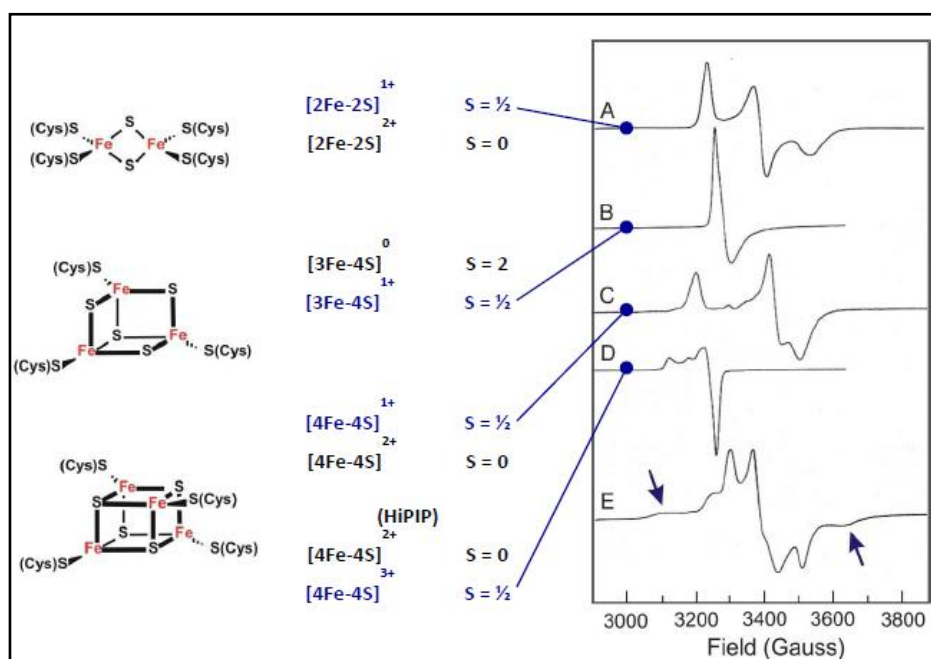


Figure 5.7. EPR spectra of different types of iron-sulfur clusters.

On the left, the basic structure of the cluster types is shown. In the middle column, redox states and their respective spin states are indicated. The panels on the right show the EPR spectra of the iron-sulfur clusters in ferredoxins from *Mastigocladus laminosus* (A), *Desulfovibrio gigas* (B), *Bacillus stearothermophilus* (C), *Chromatium vinosum* high-potential iron-sulfur protein (HiPIP) (D), and *Clostridium pasteurianum* 8Fe ferredoxin (E). Figure and legend reproduced from https://www.auburn.edu/~duinedu/epr/1_theory.pdf.

The principle of EPR is based on the interaction of a free electron with the electromagnetic radiation (microwave radiation) in the presence of externally applied magnetic field. Therefore the basic minimum criteria for a molecule to be EPR active is that it should have an unpaired electron. Only a few oxidation states of Fe-S cluster have an unpaired electron and hence are EPR active. Moreover, from the line shape of the spectra, one can infer the type of the cluster as well. **Figure 5.7** shows characteristic EPR spectra of different Fe-S clusters. Temperature dependent relaxation rates of the electron are slow for [2Fe-2S] and rapid for [4Fe-4S] clusters. So at 60K, a [2Fe-2S] cluster would still give an EPR spectra unlike a [4Fe-4S] cluster (Hanson & Berliner 2010).

5.5. Physiological roles of iron-sulfur cluster containing proteins

Peculiar electronic properties conferred by Fe-S cluster have been exploited by proteins for multiple functions in the cell. The physiological role of Fe-S clusters can be divided under following broad categories; 1) structural stability to proteins; 2) electron transport

and storage eg., electron transport chain complexes like ferredoxin, and rubredoxin; 3) free radical mediated catalysis/ source of sulfur eg., adenosyl SAM enzymes; 4) as a Lewis acid, involved in substrate binding and catalytic transformation of electron rich compounds like aconitic acid, fumarate, mesaconate etc.; 5) sensing and gene regulation eg., IRP1, SoxR, and FNR; 6) DNA replication and repair eg., DNA polymerase, primase, Xeroderma pigmentosum protein and glycosylases; 7) tRNA maturation and hence in translational fidelity. For the purview of the thesis, only the role of the iron-sulfur cluster as a Lewis acid will be discussed in detail. Other functions of the cluster are reviewed elsewhere (Fontecave, 2006 and references therein).

5.5.1 Fe-S cluster as a Lewis acid

Table 5.4 lists the enzymes (hydro-lyases) reported to have an iron-sulfur cluster. To date, Aconitase is the only enzyme of this class that has been completely characterised both structurally and biochemically. Very recently, malate bound structure of C I-FH from *Leishmania* has been reported (Feliciano et al., 2016). Another enzyme for which structural and preliminary biochemical data is available is serine dehydratase and quinolinate synthase. These enzymes adopt a common catalytic strategy and the cluster is primarily involved in the activation of hydroxyl group thereby, making it a better leaving group.

Table 5.4. Enzymes belonging to the hydrolyase family dependent on iron-sulfur cluster for substrate binding and catalysis.

#	Enzyme	E.C. No	Substrate and product	Pathway involved	References
1	Fumarate hydratase	4.2.1.2	Fumarate to S-malate	TCA cycle	(Woods et al., 1988)
2	Homoaconitase	4.2.1.36	Homocitrate to homo isocitrate	Lysine and Coenzyme B biosynthesis	(Drevland et al., 2008)
3	Aconitase	4.2.1.3	Citrate to isocitrate	TCA cycle	(Beinert et al., 1996)
4	Isopropylmalate dehydratase	4.2.1.33	2-isopropylmalate to 3-isopropylmalate	Leucine biosynthesis	(Skala et al., 1991)
5	Maleate hydratase	1.2.1.31	Maleate to R-Malate	Gentisic acid degradation	(Ueda et al., 1993)
6	Dimethyl maleate hydratase	4.2.1.85	Dimethyl maleate to dimethyl maleate	Nicotinic acid degradation	(Kollmann-koch & Eggerer 1984)

7	Mesaconate	1.2.1.34	Methylfumarate to S-methylmalate	Glutamate fermentation	(Kronen et al., 2015)
8	Citraconate	1.2.1.35	Methylfumarate to R-methylmalate	Glutamate fermentation	(Subramanian and Rao, 1968)
9	L-Tartrate dehydratase	4.2.1.32	Oxaloacetate to L-tartrate	Glyoxylate and dicarboxylate metabolism	(Kelly and Scopes, 1986)
10	Dihydroxyacid dehydratase	4.2.1.9	Dihydroxymethylbutanoate to α -ketoisovaleric acid	Branched chain amino acid metabolism	(Flint et al., 1993)
11	Phosphogluconate dehydratase	4.2.1.12	6-phospho-D-gluconate to 2-dehydro-3-deoxy-6-phospho-D-gluconate	Pentose phosphate pathway	(Kovachevich and Wood, 1955)
12	Serine dehydratase	4.2.1.16	Serine to pyruvate	Gluconeogenesis	(Grabowski et al., 1993)
13	Quinolinate synthase	2.5.1.72	Glyceronephosphate+ imino succinate to pyridine 2,3 dicarboxylate	NAD biosynthesis	(Ollagnier-de Choudens et al., 2005)

Various steps involved in catalysis where Fe-S cluster acts as Lewis acid is detailed below;

1. Substrate binding: All these enzymes have a $[4\text{Fe-4S}]^{2+}$ cluster coordinated by 3 conserved cysteines with the fourth iron held loosely by a hydroxyl ion called the Fe_a site (**Figure 5.8**). Binding of the substrate to the labile Fe_a with the help of both hydroxyl and carboxyl groups, thereby forming a hexadentate coordination with the metal is shown in **Figure 5.9**. In enzymes like quinolinate synthase or radical SAM enzymes only pentadentate coordination is observed where only one group of the substrate (mostly hydroxyl) interacts with Fe_a .

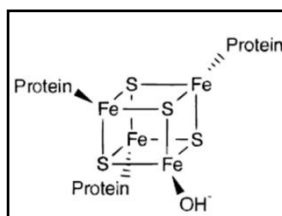


Figure 5.8. A 3Fe-4S cluster

Schematic representation of a $[4\text{Fe-4S}]$ cluster with three irons ligated by cysteine residues from the protein backbone and one iron held loosely by a hydroxyl ion. Figure reproduced from Flint & Allen 1996a.

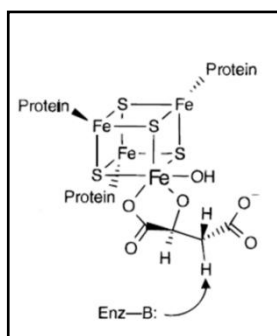


Figure 5.9. Substrate-bound 3Fe-4S cluster

Substrate binds to the Fe_a site thereby, forming a hexadentate ligand-metal complex. Figure reproduced from Flint & Allen 1996a.

2. Base catalysed proton removal: This involves abstraction of a proton from the carbon adjacent to the hydroxyl carrying carbon by a catalytic base which is validated as serine in aconitase. Though the serine residue in other iron-sulphur cluster dependent hydrolyases (Table 5.4) has not been unambiguously identified, a mechanism similar to that seen in Aconitase has been suggested. This results in the formation of enediolate intermediate as shown in **Figure 5.10**. Inhibition of fumA by the nitronate analogue of fumarate just like in mammalian fumarase supports the formation of this intermediate. Further, the absence of any kinetic isotope effect on the use of deuterated malate suggests that the formation of carbanion is not the rate limiting step (Flint, 1994).

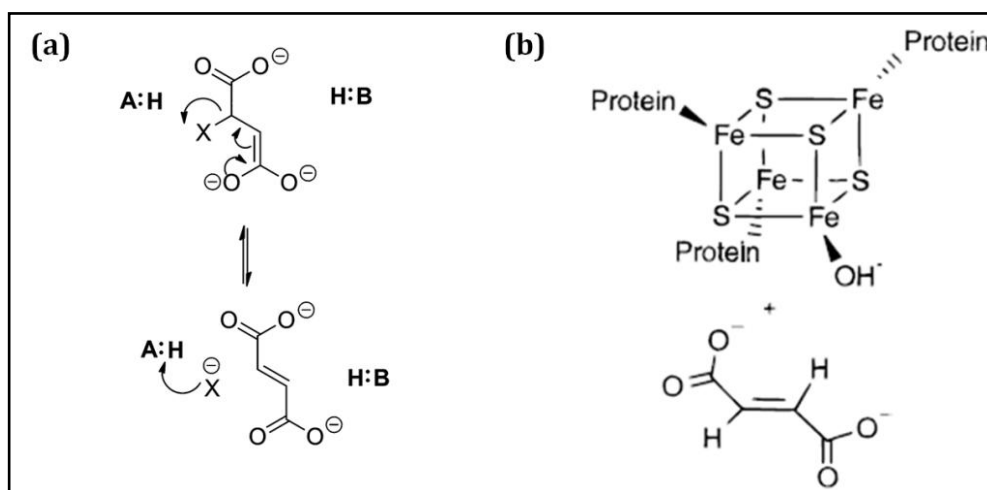


Figure 5.10. Mechanism of malate dehydration

(a) Formation of enediolate intermediate. (b) The release of fumarate and reformation of the cluster with tetradentate Fe_a site ready for next round of catalysis. Figure reproduced from Flint & Allen 1996a.

3. Lewis acid (the cluster) mediated activation of hydroxyl removal: Activation of the hydroxyl group by Fe_a makes it a better leaving group by accepting electrons of the C-O bond. Removal of the proton from the C3- carbon and the Fe_a mediated removal of the hydroxyl group from C2-carbon results in the formation of the olefinic bond between C2- and C3-carbon. The presence of a [4Fe-4S] cluster has been validated in these enzymes by EPR, Mossbauer, UV-spectrophotometer and in few cases by crystal structures as well. Most of these enzymes have been expressed in *E.coli* as recombinant proteins and were found to be inactive immediately after purification. Activation of the cluster was performed by the addition of iron and sulphide in the presence of thiol under anaerobic conditions. The reconstituted enzyme is sensitive to oxygen but can be reactivated by addition of iron and thiol. However, the enzyme dihydroxy acid dehydratase once degraded oxidatively could not be reconstituted again suggesting differences in the local environment of the cluster.

5.5.2. *Leishmania major* C I fumarate hydratase

While our study on Class I FH from *M. jannaschii* and *P. falciparum* was in progress, a report on the structure of *Leishmania major* fumarate hydratase-2 (LmFH-2) was published (Feliciano et al., 2016). The study reported the first structure of single subunit class I fumarate hydratase with L-malate bound to a 4Fe-4S cluster. *Leishmania* is a eukaryotic unicellular parasite belonging to group *Trypanosomatidae* and is the causative agent for leishmaniasis. Currently, there is no direct evidence that unambiguously shows the essentiality of the enzyme in *Leishmania* parasites. The organism has two Class I fumarate hydratase, one localised to mitochondria denoted LmFH-1 and the other to the cytosol, denoted as LmFH-2. Both the proteins were recombinantly expressed and kinetically characterised (Feliciano et al., 2012). The pH optimum of the activity for both the substrates is 8.5 for LmFH-1 and 9.0 for LmFH-2. It corroborates well with the pH optima of C I-FH from other organisms like *Euglena gracilis* and MPOB bacteria (Shibata et al., 1985; Kuijk et al., 1996). The K_m values for the *Leishmania* enzyme were found to be relatively high compared to other class-I FHs reported. **Table 5.5** shows the kinetic parameters of FH characterised till date. High K_m value for both the substrates is correlated with high intracellular concentrations of these metabolites in the organism

Table 5.5. Kinetic parameters of FH from different organisms

Organisms	Fumarate			Malate			Reference
	K_m (mM)	V_{max} ($\mu\text{mol min}^{-1}$ mg^{-1})	k_{cat} (s^{-1})	K_m (mM)	V_{max} ($\mu\text{mol min}^{-1}$ mg^{-1})	k_{cat} (s^{-1})	
<i>E. coli</i> Fum A Fum B	0.46 0.32	1900 1430	1932 1440	0.7 0.3	720 490	700 480	(van Vugt-Lussenburg et al., 2013)
<i>L. major</i> LMFH-1 LMFH-2	2.5 5.7	26.4 182.6	28.3 204.2	2.3 12.6	11.8 138.1	12.9 151.4	(Feliciano et al., 2012)
<i>P. furiosus</i> FH	0.34	1376	1088	0.41	1892	25.37	(van Vugt-Lussenburg et al., 2009b)
<i>P. thermop.</i> MmcBC	0.43	201	219	0.59	23.7	25.2	(Shimoyama et al., 2007b)
<i>E. gracilis</i>	0.031	N.A	N.A	0.14	N.A	N.A	(Shibata et al., 1985)
MPOB	0.25	N.A	690	2.38	N.A	540	(Van Kuijk et al., 1996)
<i>B. xerov.</i>	0.1	296	280	0.28	118	111	(Kronen et al., 2015)

The structure of LmfH-2 is the only model currently available in PDB for full length C I-FH. The protein has two domains, an N-terminal domain (NTD) and a C-terminal domain (CTD) connected by a linker region. Because of the lack of electron density corresponding to the residues in the linker region, it is not mapped on to the final structure. The N-terminal domain and C-terminal domain of single subunit C I-FH are homologous to α and β -subunits of two-subunit type C I-FH present in many archaea and some bacteria. Crystal structure corresponding to the β -subunit of two subunit type C I-

FH is already available in PDB (2ISB and 5DNI). The condition under LmFH-2 was crystallized had Tacsimate, which is a mixture containing multiple dicarboxylic acids that includes 1.8305 M malonic acid, 0.25 M ammonium citrate tribasic, 0.12 M succinic acid, 0.3 M DL-malic acid, 0.4 M sodium acetate trihydrate, 0.5 M sodium formate, and 0.16 M ammonium tartrate dibasic. Apart from the electron density of the protein, there were additional densities corresponding to ligands. Two molecules of L-malate, two molecules of malonate and one [4Fe-4S] cluster were fit to these observed additional densities (per monomer). The dimeric structure (PDB ID: 5L2R) of LmFH-2 is presented in **Figure 5.11**, and the Fe-S cluster highlighted in each monomer. The structure has a unique arrangement of α -helices and strands that is not found in any other structure in PDB and hence possess a unique protein fold. The residues involved in Fe-S cluster binding are solely from the N-terminal domain (NTD) with no contribution from the C-terminal domain (CTD).

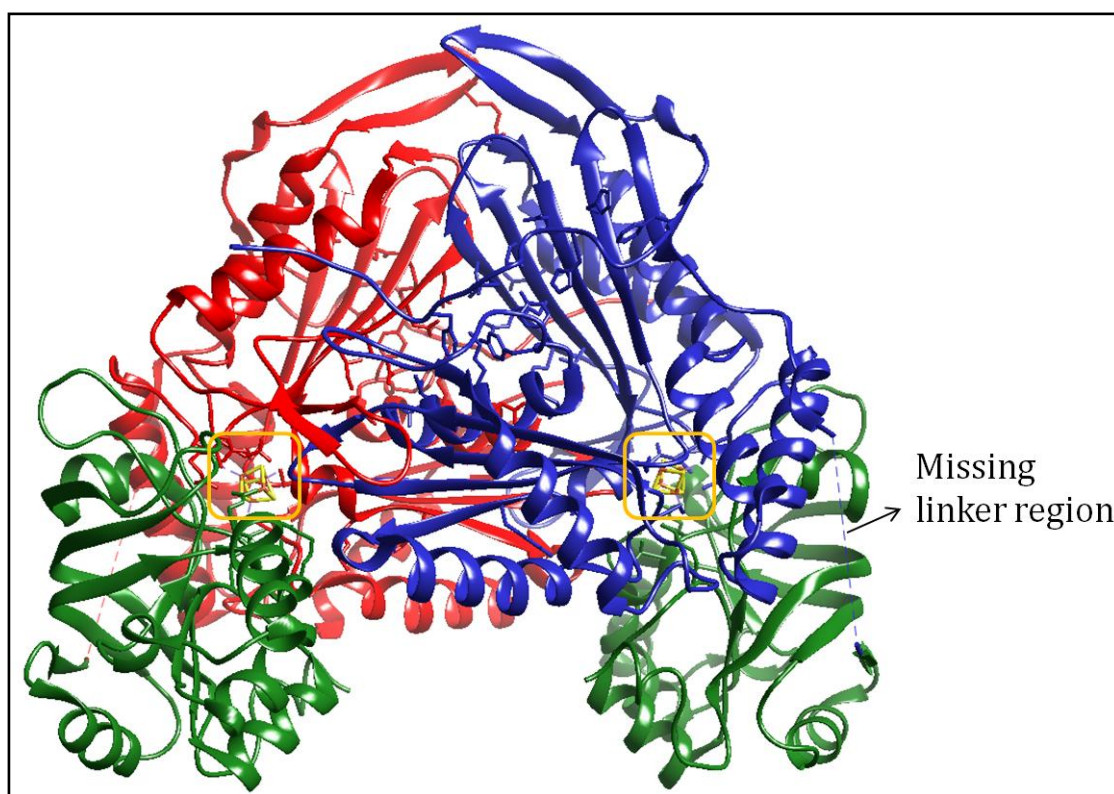


Figure 5.11. Structure of LmFH-2 (PDB ID: 5L2R)

The dimeric structure of LmFH-2 is shown with the NTD from the two different chains coloured red and blue. The CTD in both chains is coloured green. The Fe-S cluster is present in the interface of NTD and CTD and is outlined by a yellow box. Electron density corresponding to residues connecting NTD and CTD was absent and hence this polypeptide segment is missing in the final structure. The missing linker region is shown as dashed line in both chains.

One L-malate molecule was bound to one of the Fe atoms in the cluster. Apart from the cluster, the residues involved in malate binding are shown in **Figure 5.12**. All the residues directly binding the ligand in a subunit belong to the same chain suggesting that the monomer has all the components required for substrate binding.

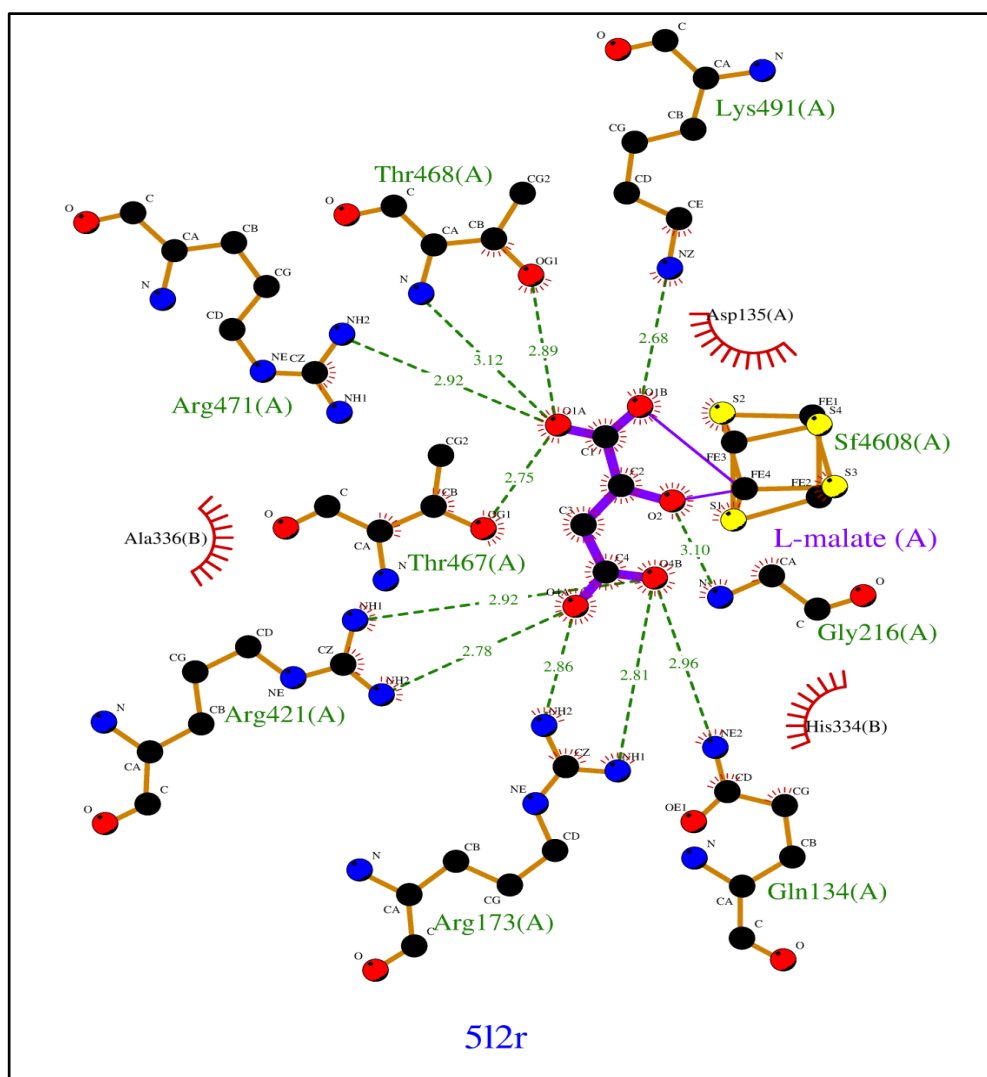


Figure 5.12. The active site of LmFH-2 with bound L-malate (PDB ID: 5L2R).

The active site of the protein includes the iron-sulfur cluster and the substrate binding residues. The residues involved in malate binding and their corresponding distance from the different atoms of malate are shown. Residues involved in non-bonded interactions are shown as red spikes.

As discussed earlier, catalysis in class I FH is thought to proceed through a carbanion intermediate. In the first step that involves the formation of the intermediate, the role of a catalytic base that deprotonates the C3 carbon of malate is implicated. The authors propose that the residues Arg-421, Arg-471, or a water molecule in the vicinity

might play this role. The subsequent step in catalysis involves protonation of the hydroxyl group of malate resulting in its elimination as a water molecule. Asp-135 and, His-334 from the neighbouring chain is thought to be involved in this step. The proposed catalytic mechanism as presented in the report is reproduced in **Figure 5.13**.

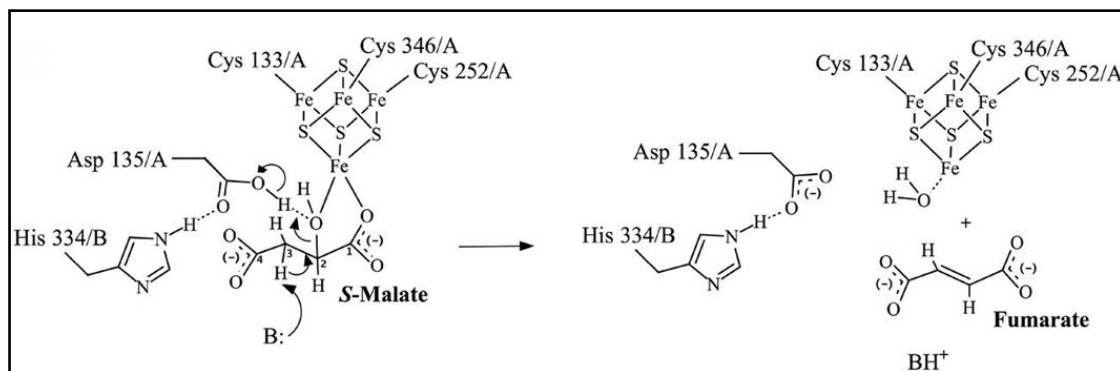


Figure 5.13. Proposed catalytic mechanism of LmFH-2

The catalytic base involved in the generation of carbanion intermediate and the catalytic acid that is involved in the protonation of the hydroxyl group of malate are shown. Figure reproduced from (Feliciano et al., 2016).

5.6. Structural studies of proteins

Knowing the structure of macromolecules to atomic detail provides valuable information for understanding multiple aspects related to its function. The structure of the MjFH β subunit was solved as a part of this work and this section provides a brief introduction to various steps involved in solving a protein structure using X-ray crystallography. The technique depends on the scattering of X-rays by atoms, more specifically by the electron cloud of atoms in the crystal, thereby generating a characteristic diffraction pattern, exclusive to the crystal, which can be recorded as spots on a detector. The position of the spots and the intensity has complete information of all atoms in the protein. Because of the limitations in data collection technology, the information about temporal separation of waves scattered by the atoms or more appropriately the phase of the scattered waves is lost. Using mathematical tools, multiple ingenious ways have been developed to overcome the phase problem. Molecular replacement and anomalous diffraction are widely used methodologies to solve the phase problem in protein crystallography. Three major steps involved in protein crystallography are discussed below (Rupp, 2010; Rhodes, 2006).

5.6.1.1. Crystallisation of protein and data collection

Crystallisation is a precipitation phenomenon that is ordered thereby resulting in the formation of a crystal. Unfortunately, the factors governing this seemingly simple process

are still not completely understood, making the process trial and error in nature and more so in protein crystallization. Vapour diffusion, hanging drop and sitting drop techniques are the three widely used strategies to obtain protein crystals. The commonality in all these methods is that the protein solution is mixed with a solution containing small molecules and polymers of different nature and let to undergo a slow but controlled evaporation thereby pushing the protein towards precipitation. Kits containing different solutions of defined compositions are available from different manufacturers that are screened against the protein of interest to obtain a crystal. Key factors that govern crystallisation are protein concentration, purity, pH, temperature and the precipitant used. Once a crystal has been obtained its diffraction quality can be further improved by using soaking the crystal in cryoprotectants like glycerol and PEG of different concentrations. The crystal is placed in a goniometer and diffracted with an X-ray source usually Cu-K α . The diffracted rays are recorded on a detector which can either be CCD or image plate based. Few images are acquired and used for indexing, a process that informs one about the most probable space group of the crystal, and also examined for the data collection strategy to be used. The strategy mainly pertains to the number of angles the data should be collected to get complete information of the atoms in the crystal (Rupp, 2010; Rhodes, 2006).

5.6.1.2. Data processing

Major steps in data processing are the integration of multiple 2D frames containing diffraction spots based on the space group of the crystal, scaling of spot intensities, and phasing to derive electron density from intensity values and information from one of the phasing methods like MR, SAD/MAD, IMR etc. Molecular replacement is the best option when a structure model of another protein with sequence similarity of greater than 40% is available. If the protein has a good number of cysteines then anomalous data collected at an appropriate wavelength for sulfur-SAD can be used to obtain phases. If no known structures exist or if molecular replacement fails the method of choice is either Se-SAD (single wavelength anomalous dispersion)/MAD (multi-wavelength anomalous dispersion) where selenomethionine incorporated recombinant protein is used for crystallisation. Anomalous scattering from selenium can be a very useful in obtaining phase information (Rupp, 2010; Rhodes, 2006).

5.6.1.3. Model refinement and analysis

The model generated after phasing would have errors with respect to geometric parameters (bond angles, bond length etc.) as the experimental data has fewer

parameters than is actually needed to describe these to high levels of accuracy. This demands statistical averaging of geometric parameters driven by optimal fit to the observed electron density. The geometric constraints library derived from accurate small molecule structures are used in the refinement. Thus macromolecular model refinement can be conceived of as an optimisation problem entailing mathematical parameters to instruct the tools when it has found an optimal solution (Tronrud et al., 2004). Most modern refinement tools use maximum likelihood based methods with parameters like R_{work} and R_{free} as indicators that reflect the optimal fit of the model to the experimental data (Murshudov et al., 2011). However, it has to be borne in mind that averaging of parameters causes a lot of information loss in terms of microscopic heterogeneity that a model could offer (Kuzmanic et al., 2014) .

5.7. OBJECTIVES AND STRATEGY

The primary objective was to understand class I FH from structural and biochemical perspective. *P. falciparum* FH, a single subunit class I FH and *M. jannaschii* FH, a two subunit class I FH were recombinantly expressed in *E. coli* for the same.

Chapter 6

Preliminary biochemical characterization of Plasmodium falciparum fumarate hydratase

Chapter 6

Preliminary biochemical characterization of *Plasmodium falciparum* fumarate hydratase

ABSTRACT

Plasmodium falciparum (Pf) genome has one gene that codes for the single subunit, class I type iron-sulfur cluster containing, fumarate hydratase (FH). The protein catalyzes the reversible conversion of fumarate to malate. Recent genetic studies have shown that the gene is essential for the parasite and cannot be knocked out (Ke et al., 2015). This chapter summarizes the results pertaining to biochemical characterization of the recombinant *Plasmodium* enzyme. Bioinformatic analyses, based on protein primary sequence were performed in order to predict the mitochondrial targeting sequence at the N-terminus, conserved cysteines, and the domain boundary. Based on these analyses, expression constructs containing DNA sequence coding for different N-terminal truncations viz, PffH Δ 40, PffH Δ 120, and the full-length coding sequence of PffH were generated and used for recombinant protein expression in *E. coli*. The recombinant proteins PffH Δ 40 was used for raising antibodies in mice. Our efforts to improve the solubility of the protein, PffH Δ 40 that include optimization of growth conditions, use of different expression strains, co-expression of chaperones, and purification conditions are summarized. Ni-NTA agarose beads were used to purify the PffH Δ 40. PffH Δ 40 was partially purified and was found to be highly unstable and degrade with time. However, the freshly purified protein was found to be active by both UV-spectrophotometric and NMR-based assays. A fumarate hydratase null *E. coli* strain, Δ fumACB, was generated using Lambda Red recombinase-based strategy. The genotyping of the strain by PCR and phenotyping by growth on fumarate-containing minimal medium were performed. Growth phenotype for the strain expressing different PffH constructs was also scored on substrates on which Class I FH shows promiscuous activity. The observation regarding growth phenotype on these substrates are presented and the results discussed. The strain was also used to test the inhibitory potential of malate analogue mercaptosuccinic acid on both PffH expressing *E. coli* strain of Δ fumACB and on the asexual stages of *P. falciparum* in *in vitro* culture.

6.1. INTRODUCTION

Class I FHs are divided into single and two subunit type enzymes and catalyze reversible conversion of fumarate to malate. Class-I type FH is present in around 60 eukaryotic organisms (both free-living and parasitic). All these organisms have single subunit type

FH. The *P. falciparum* enzyme is also a single subunit type, class I fumarate hydratase. The genome has one copy of the gene on chromosome 9, which is intron less, and encodes for a protein of 681 amino acids in length. The protein is putatively annotated as fumarate hydratase (PlasmodDB id: PF3D7_0927300). High-throughput transcriptome analysis shows that the protein is expressed throughout the asexual and sexual stages of the parasite (Young et al., 2005; Llinas et al., 2006; Ngwa et al., 2013). Biochemical evidence suggests that the protein is mitochondrially localized (Bulusu et al., 2011), though a canonical targeting sequence is missing in the primary sequence of the protein. *Leishmania donovani* fumarate hydratase is the only C-I single subunit type eukaryotic FH for which information on structural, biochemical and kinetic characterization is available (Feliciano et al., 2012, 2016).

In this study, we have done a preliminary biochemical characterization of the *Plasmodium* enzyme. We have recombinantly expressed the N-terminal truncated version of the PffH and shown that it is active. A fumarate null *E.coli* strain was generated, that can be used for the functional complementation of fumarate hydratase (class I/II) from any organism as well as for screening inhibitors against the enzyme. The PffH enzyme was shown to functionally complement the fumarate hydratase deficiency in this strain. Further, the strain expressing the PffH enzyme was used for screening few substrate analogues that could be potential inhibitors.

6.2. Materials and methods

6.2.1. Chemicals, strains and molecular biology reagents

All chemical reagents used were obtained from Sigma Chemicals Co., USA. Ni-NTA conjugated agarose beads and Phusion high-fidelity DNA polymerase was procured from Thermo Fisher Scientific Inc. Restriction enzymes, T4 DNA ligase and Lemo21 (DE3) were from New England Biolabs, MA, USA. Primers were custom synthesized from Sigma-Aldrich, Bangalore. Media components were from Himedia laboratories, Mumbai, India. Plasmid pDB1818 was a kind gift from Prof. Dennis R. Dean, Virginia Tech, USA. *E. coli* strain Δ iscR was a kind gift from Prof. James R. Swartz, Stanford University, USA.

6.2.2. Sequence analysis

Sequences of fumarate hydratase were obtained from NCBI BLAST-P tool using *P. falciparum* fumarate hydratase as the query sequence. ClustalW (Thompson et al., 1994) was used for multiple sequence alignment and the output was processed using ESPRIPT (Robert and Gouet, 2014) for visualization.

6.2.3. Cloning, protein expression, and purification

DNA fragments corresponding to the entire open reading frame (ORF) and the N-terminal deletion constructs were amplified by PCR using the parasite genomic DNA as template and cloned into a modified pET21b vector using the enzymes *Bam*HI and *Sal*I, such that the (His)₆-tag is at the N-terminus. The sequences of oligonucleotides used are given in **Table 6.1**. *E. coli* strain BL21(DE3)-RIL was used for expressing PffH Δ 40 and PffH Δ 120. For purification, the pET21b plasmid with PffH Δ 40 was transformed into BL21(DE3)-RIL strain and selected on LB plate containing ampicillin and chloramphenicol. Multiple colonies were picked and inoculated into a 10 ml LB broth. The culture was grown for 6 h at 37 °C. Thereafter, the cells were pelleted, washed with antibiotic free LB broth and then used for inoculating an 800 ml culture. The cells were grown at 30 °C until the OD₆₀₀ reached 0.5, thereafter induced with 0.05 mM IPTG and grown further for 16 h at 16 °C. The cells were harvested by centrifugation and resuspended in lysis buffer containing 50 mM Tris-HCl, pH 7.4, 150 mM NaCl, 1 mM PMSF, and 10% glycerol. The cells were lysed using 4 cycles of French press at 1000 psi and the lysate cleared by centrifuging at 30,000 x g for 30 minutes. The supernatant was carefully removed without disturbing the pellet and 1ml slurry of Ni-NTA beads (Novagen) pre-equilibrated with lysis buffer was added for binding of the His-tagged protein. The binding was done at 4°C for 3h and thereafter, the beads were washed with 50ml lysis buffer and protein eluted with different concentrations of imidazole.

Table 6.1. Oligonucleotides used for this study

S.No	Primer Name	Primer sequence (5' to 3')
1	FHF_BamH1_FL	CGCGGATCCATAAAGTTTAAAGAAGCTTCCATTTTG
2	FHR_Sal1_FL	ACGCGTCGACTTATGATGGTAACCATTTATTATAAAAATC
3	FHF_BamH1_Δ40	CGCGGATCCAGTTTAAATAGTTTTATAGACATTTTAAAGCTTTAG
4	FHF_BamH1_Δ120	CGCGGATCCAATTATGAAAAAGAATATATACATATCCCACC
5	P1	CGGAACACCCGCCAGAGCATAACCAAACCAGGCAGTAAGTGA GAGAACAGTGTAGGCTGGAGCTGCTTC
6	P2	GCGCAGCCGCTTCGTTTGATCATTCCACGGCTGCACCTGTATGTTGC AGACTGTCAAACATGAGAATTAATTCCG
7	P3	CTGAGTTAATGAGTTTTTGCATGATCAATCCCTG
8	P4	CACAGCGGGTGCATTGTGTGAGTTG
9	P5	GGCAGATAAGCTGTGGGGCGCAC
10	P6	GCGTCTGGTACAAAGGAGATCAAAAACAAGTCC

6.2.4. Enzyme activity

The conversion of fumarate to malate was monitored spectrophotometrically by a drop in absorbance at 240nm caused by fumarate depletion ($\epsilon_{240}=22,400 \text{ M}^{-1}\text{cm}^{-1}$). For NMR, the purified recombinant PffH Δ 40 was incubated with 2, 3-[¹³C]-fumarate for 30 min. The

protein was precipitated with TCA and the supernatant, neutralized with 5 N KOH was used for recording ^{13}C -NMR spectrum. D_2O was added to a final concentration of 10 % to the sample for signal lock.

6.2.5. Generation of fumarate hydratase null *E. coli* strain, ΔfumACB

In order to generate a fumarate hydratase null strain, JW4083-1 (*fumB748 (del)::kan*), an *E. coli* strain in which *fumB* is replaced with a kanamycin selection cassette flanked by flippase recognition target (FRT) sites (part of Keio collection), was obtained from Coli Genetic Stock Centre (CGSC) (Baba et al., 2006). To remove the kanamycin cassette flanked by FRT sites and to subsequently knockout the genes *fumA* and *fumC*, standard protocols were followed (Datsenko and Wanner, 2000).

Briefly, to remove the kanamycin cassette at the *fumB* locus, JW 4083-1 cells were transformed with the plasmid pCP20 that expresses the flippase enzyme (**Figure 6.1 a**). Thereafter, the cells were cured of the plasmid by incubation at 42 °C for 12 h. Subsequently, the cells were transformed with the plasmid pSC101 to introduce the high-efficiency lambda phage recombination machinery (**Figure 6.1 b**). In order to knockout the genes *fumA* and *fumC*, primers P1 and P2 were used to amplify a kanamycin cassette using plasmid pKD13 as the template, such that the PCR product will carry the homologous regions corresponding to the 5' flank of *fumA* and 3' flank of *fumC* (shown in red in Figure 6.1 a/b/c). After *DpnI* digestion, the ΔfumB strain was transformed with the PCR product by electroporation and selected on LB medium containing kanamycin. Kanamycin resistant colonies were screened by PCR using P3 and P6 primers to validate the insertion of the antibiotic cassette in the right locus as given in **Figure 6.1 c**. The cells were also checked for the absence of the wild-type genes, *fumA*, and *fumC* using primers P3/P4 and P5/P6 respectively (Table 6.1). The kanamycin cassette at the *fumA/C* gene locus was removed by expressing flippase in the strain resulting in the generation of marker free fumarate hydratase null strain (**Figure 6.1 d**).

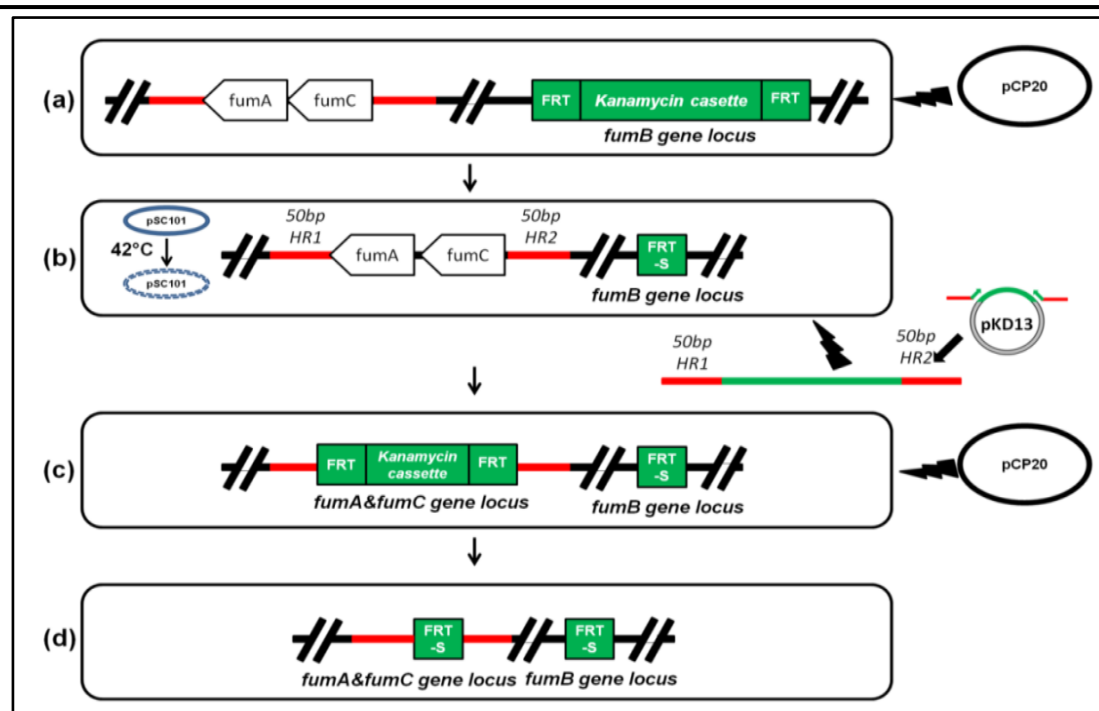


Figure 6.1. Schematic of the steps involved in generation of fumarate hydratase null strain (Δ fumACB) of *E. coli*

(a) Section of the genome of *E. coli* strain Δ fumB showing *fumA/C* loci. The *fumB* gene locus has been replaced by kanamycin resistance cassette flanked by flippase recombination target (FRT) sites. Transformation of the strain with plasmid pCP20, that expresses flippase, enables removal of the resistance cassette by recombination of the FRT sites. (b) The kanamycin sensitive Δ fumB strain was transformed with pSC101 (a plasmid that expresses lambda phage homologous recombination machinery) followed by electroporation of the cells with PCR product flanked by sequences for homologous recombination. The cells were selected on a kanamycin containing LB plate. Plasmid pSC101 is cured of the resulting strain, Δ fumACB, by growing the cells at 42 °C. (c) Transformation of Δ fumACB strain with pCP20 to generate marker free fumarate hydratase null strain as shown in (d).

6.2.6. Complementation assays in *E. coli*

pQE30 plasmids containing different truncation constructs of the *P. falciparum* enzyme were transformed into the *E. coli* Δ fumACB strain and selected on LB plate containing 100 μ g/ml ampicillin and 50 μ g/ml kanamycin. A single colony from the plate was inoculated into 10 ml LB broth and grown overnight. An aliquot of each of the cultures was washed three times with sterile M9 medium to remove traces of LB. The cells were resuspended in M9 medium and an aliquot of the suspension was spread on a minimal medium plate containing the appropriate carbon source and antibiotics. The selection plate contained, M9 salts, trace elements (EDTA, 13.4 mM; FeCl₃-6H₂O, 3.1 mM; ZnCl₂, 0.62 mM; CuCl₂-2H₂O, 76 μ M; CoCl₂-2H₂O, 42 μ M; H₃BO₃, 162 μ M; MnCl₂-4H₂O, 8.1 μ M), 10 μ g/ml thiamine, 10 μ g/ml biotin, 0.3 mM calcium chloride, 1 mM magnesium chloride, 1.5% agar, 0.4% of

one of the following carbon sources; L-malate, fumarate, L/D-tartrate, mesaconate, and itaconate.

6.2.7. Mercaptosuccinic acid mediated inhibition of FH

Multiple colonies of the Δ fumACB strain expressing PffH Δ 40 were picked from a LB agar plate and inoculated into 5 ml M9 minimal medium with 20 mM fumarate as the sole carbon source and appropriate antibiotics (kanamycin and ampicillin). The cells were grown overnight and an aliquot of the culture was washed twice with M9 minimal medium. The cell pellet was resuspended in M9 medium to the original culture volume and used as a pre-inoculum. 100-200 μ l of this suspension were added to tubes containing 5 ml of M9 minimal medium with fumarate as the sole carbon source and appropriate antibiotics (kanamycin and ampicillin). MSA was added to the medium to a final concentration ranging from 5 mM to 1 μ M and the growth of the cultures was monitored by measuring the absorbance at 600 nm. OD₆₀₀ was measured at the end of 10 h and the data were plotted for estimating the IC₅₀ value for the inhibitor.

6.3. Results and discussion

6.3.1. Multiple sequence alignment

Fumarate hydratase (FH) gene is present in all *Plasmodium* species for which complete genome sequence is available. In *P. falciparum* the gene is present on chromosome 9, in highly syntenic loci (amongst *Plasmodium* species) (PlasmoDB). The *Plasmodium* FH protein sequences are longer than class-I fumarate hydratases present in most other eukaryotic/prokaryotic organisms.

P_vivax	1MRNFARIPLCRPPPGKRLSRGAHLG.....GKHPFRLNKANINTLSN
P_inui	1MRNFVRIPLCRPPSGKYLSKSAHLG.....GKQPFRRNANINTVRN
P_knowlesi	1MRNFTRILLCRSPSGKLSKSAHLG.....GNHFRFKKAHIKTLHN
P_fragile	1MRNFARIPLCRP.....LG.....GKHPFRRNKAQIKTLHN
P_yoelii	1	MVGYQQARKFKRIHKLFPPYITICTNNLVEISGKNNINN.....INNINNINKLNINTINN
P_berghei	1	MVGYQKIRKFKKVPKLFPPYITICTSNFIGVHGKHHIRNISNINNIRNINNINKLNINTLNN
P_vinckei	1MGIHGKKNQISN.....INKINKLNINTLNN
P_chabaudi	1	MVAYQKVRRFKVPKLSFSYITICTNKFMGIHGKKNHISN.....INKINKLNINTLNN
P_gallinaceum	1MLNFKNIPLLFSKKIY.....GIKTVNINSI.YKINKLNINTLNN
P_gaboni	1MIKFKGGSILLSH.NAYF.....K.YNLYLKKKIRCYVNNIYRRDVNTLNN
P_falciparum	1MIKFKEASILLSHKNAYL.....Q.YNLYFKKIRCVCYHKIYRRHMNSLNS
P_reichenowi	1MIKFKEASILLSHKNAYI.....K.YNLYFKKIRCVCYNKIYRRHMNTLNS
Geobacter	1MSTKP
Klebsiella	
E_coli_FUMA	1MSNKP
E_coli_FUMB	1MSNKP
Hipaea	
Bordetella	
Mesorhizobium	
Zymomonas	
Vibrio	
Neisseria	
P_vivax	43	FLDVLEFEEGKEDETEYRRIDDLISKYIEVIKLRDNP.I.NQSKYYGYNFENEENFFHPNGELK.
P_inui	43	FLDVLEFEDAKEDETEYRRIDDLISKYVEVIKIKESPI.NQSKYYGYNFENEDNFFHPNGELK.
P_knowlesi	43	FLDVLEFEEGKEDDTEYRRIDDLISKYIEVVKIKDSP.I.NESKYYGYNFENEDNFFHPNGELK.
P_fragile	32	FLDVLEFEEGKEDDTEYRRIDDLISKYIEVIKIKDSP.I.NESKYYGYNFENEENFFDPNGELKK
P_yoelii	55	FLDTFEFEGKNDGIEYRRDLDELISKYIEVIKFN.N.KINDDNKYDINYEDENEFFDDNGNLKI
P_berghei	64	FLDIFEFEEKGNDNIEYRRDLDELISKYIEVIKFDN.KINENSKYYDINYEDENEFFDDNGNLKI
P_vinckei	26	FLDTFEFEEKGNDGIEYKRLDELISKYIEVIKLDNNKINKDSKYDINYEDENEFFDDNGNLKI
P_chabaudi	52	FLDIFEFEEKGNDGIEYRRDLDELISKYIEVIKLDNNKINKDSKYDINYEDENEFFDDNGNLKI
P_gallinaceum	40	FLDVLDFEE..EEDIEYTRIDELISKYIETVKINEDIF.NKTKYVGYDFTDNNFFDKNGNLIK
P_gaboni	44	FIDILSFRNDEDDIEYKVEDLSKYIEVIKMNKSSM.NETKYGYNFKDENNFLDEHGNIKE
P_falciparum	45	FIDILSFRNE..DDIEYKVEDLSKYIEVIKINKSPM.NETKYGYNFKEEYNFLDEHGNIKE
P_reichenowi	45	FIDILSFRNEE.DDIEYKVEDLSKYIEVIKINKSPM.NETKYGYNFKEENNFLDEHGNIKE
Geobacter	6	FVYQEPFP.LEKDETSYYKIPDSEKYVSVATF.....
Klebsiella	
E_coli_FUMA	6	FHYQAPFP.LKKDDTEYLLT..SEHVSVEF.....
E_coli_FUMB	6	FIYQAPFP.MGKDNTTEYLLT..SDYVSVADF.....
Hipaea	
Bordetella	
Mesorhizobium	
Zymomonas	
Vibrio	
Neisseria	
P_vivax	104	NLPEQ.VRQNEGERVKEYLHVPFV.LAKLCEYAFKEIL.FFLNKKHLKQLSN.ILNDG.ESSKNDK
P_inui	104	KLPEQ.VMQSEGERIKEYIHPFV.LAKLCECAFREIL.FFLNKKHLKQLSN.ILNDE.ESSKNDK
P_knowlesi	104	NLPEQ.VRQNEVERIKEYIHPFV.LTKLCEYAFREIL.FFLNKKHLKQLSN.ILKDG.ESSKNDK
P_fragile	94	NLPEQ.VIQNEGERIKEYIHPFV.LTKLCEYAFKEIL.FFLNKKHLKQLSN.ILNDG.ESSKNDK
P_yoelii	117	KNN..YEKESKNVIKEYIHPFV.LTKLCEYALKEIL.FFLNKKHLKQLSN.ILIDK.ESSKNDK
P_berghei	126	KNN..YEKESKNIMKEYIHPFV.LTKLCEYALKEIL.FFLNKKHLKQLSN.ILMDK.ESSKNDK
P_vinckei	89	KND..CEKKSNNVMKEYLHVPFV.LTKLCEYALKEIL.FFLSKKHLKQLSN.ILMDK.ESSKNDK
P_chabaudi	115	KND..CEKNNKNVMKEYIHPFV.LTKLCEYALKEIL.FFLNKKHLKQLSN.ILIDK.ESSKNDK
P_gallinaceum	100	YSKQDT...NKKDAKEYIHPFV.LTKLCEYAFKEIL.FFLNKKHLNQLSN.ILYDK.ESSKNDK
P_gaboni	106	YINNENKKLLDKNYEKEYIHPFV.LTKLCEYAFKEIL.FFLNKKHLKQLSN.ILQDK.ESSKNDK
P_falciparum	105	YIYNENKKLLYKNYEKEYIHPFV.LTKLCEYAFKEIL.FFLNKKHLKQLSN.ILQDK.ESSKNDK
P_reichenowi	106	YIYNENKKLLHKNYEKEYIHPFV.LTKLCEYAFKEIL.FFLNKKHLKQLSN.ILQDK.ESSKNDK
Geobacter	37EGKEVLKVDPEALTVLANTAMRDV.SFLLRPEHNE.SVAK.ILRDP.EASQNDK
Klebsiella	1EASDNDK
E_coli_FUMA	35EGQEILKVAP.EALTL.LARQ.AFH.DAS.FMLRPAHQ.QVAD.ILRDP.EASENDK
E_coli_FUMB	35DGETILKVEPEALTL.LAQQ.AFH.DAS.FMLRPAHQ.QVAA.ILHDP.EASENDK
Hipaea	1MAEVRVSVKDI.EEA.VYK.LALEA.YH.IPEDVLEAEKK.AYEKE.KSPVAKQ
Bordetella	1MRF.IEAAH.IVD.SIAN.ALQ.FV.SHHHP.PDFVQ.IAL.KR.AYQAET.QAP.AAN
Mesorhizobium	1MGSRTRT.IAGND.IIRSVAD.ALQYI.SYHP.PDY.IRSL.SQ.AYARE.QSPA.KN
Zymomonas	1MTV.IHQND.LIDSITD.ALQ.FI.AC.YHP.KDF.ID.SLYQ.AYQKE.ENPV.ARD
Vibrio	1MTV.IRRQD.VISSVAD.ALQYI.SYHP.LDFVKA.LEK.AYQRE.ESSQA.AKD
Neisseria	1MTV.IKQED.FIQSICD.AFQ.FI.SYHP.PKDY.IDA.LYK.AWQKE.ENPA.AKD

Figure 6.2. N-terminal region of the multiple sequence alignment of *Plasmodium* and bacterial class-I fumarate hydratase sequences.

The underlined region, corresponding to 120 amino acids at the N-terminus, shows the part of the *Plasmodium* sequence that is not present in bacterial sequences. The sequences were downloaded from NCBI database and alignment was done using Clustal omega (Sievers et al., 2011) with default parameters. The colour coding is according to the residue conservation based on BLOSUM62 matrix and was generated using ESPRINT 3.0 (Robert and Gouet, 2014).

Chapter 6. Preliminary biochemical characterization of PffH

P. vivax	1MRNFARIPLCRPPPGKRLSRGAHLG.....GKHFFRLNKANINTLSN
P. inui	1MRNFVRIPLCRPPSGKYLKSAHLG.....GKQPFRLNKANINTVRN
P. knowlesi_strainH	1MRNFTRILLCRSPSGKCLSKSAHLG.....GNHFFRFKKAHIKTLHN
P. fragile	1MRNFARIPLCRPP.....LG.....GKHFFRFNKAQIKTLHN
P. yoelii	1	MVGYQQARKFKRIHKLFPYITCTNNLVEISGKNNINN.....INNINNNIKLININTLNN
P. berghei	1	MVGYQKIRKFKKVPKLFYITCTSNFIVGHGKKHIRINISNINNIRNINNNIKLININTLNN
P. vinckei	1MGIHGKNQISN.....INKNINIKLININTLNN
P. chabaudi	1	MVAYQKVRKFKKVPKLFYITCTNFKFMGIHGKNHISN.....INKNINIKLININTLNN
P. gallinaceum	1MLNFKNIPLLFSKTIY.....GIKTVINSI.YKINIKLININTLNN
P. gaboni	1MIKFKGSSILLSH.NAYF.....K..YNLYLKKIRCYNNIYRRDVTNLNN
P. falciparum_3D7	1MIKFKKASILLSHKNAYL.....Q..YNLYFKKIRCVCYHKIYRRHMNSLNS
P. reichenowi	1MIKFKKASILLSHKNAYI.....K..YNLYFKKIRCVCYHKIYRRHMNTLNS
Variation 1		
P. vivax	43	FDDVLEFPEGKEDETEYRRIDDDLSKYIEVIKLRDNPIT.NQSKYVGYNFENEENFFHFNGEELK.
P. inui	43	FDDVLEFPEGKEDDETEYRRIDDDLSKYIEVIKLRDNPIT.NQSKYVGYNFENEENFFHFNGEELK.
P. knowlesi_strainH	43	FDDVLEFPEGKEDDETEYRRIDDDLSKYIEVIKLRDNPIT.NQSKYVGYNFENEENFFHFNGEELK.
P. fragile	32	FDDVLEFPEGKEDDETEYRRIDDDLSKYIEVIKLRDNPIT.NQSKYVGYNFENEENFFHFNGEELK.
P. yoelii	55	FDDVLEFPEGKEDDETEYRRIDDDLSKYIEVIKLRDNPIT.NQSKYVGYNFENEENFFHFNGEELK.
P. berghei	64	FDDVLEFPEGKEDDETEYRRIDDDLSKYIEVIKLRDNPIT.NQSKYVGYNFENEENFFHFNGEELK.
P. vinckei	26	FDDVLEFPEGKEDDETEYRRIDDDLSKYIEVIKLRDNPIT.NQSKYVGYNFENEENFFHFNGEELK.
P. chabaudi	52	FDDVLEFPEGKEDDETEYRRIDDDLSKYIEVIKLRDNPIT.NQSKYVGYNFENEENFFHFNGEELK.
P. gallinaceum	40	FDDVLEFPEGKEDDETEYRRIDDDLSKYIEVIKLRDNPIT.NQSKYVGYNFENEENFFHFNGEELK.
P. gaboni	44	FDDVLEFPEGKEDDETEYRRIDDDLSKYIEVIKLRDNPIT.NQSKYVGYNFENEENFFHFNGEELK.
P. falciparum_3D7	45	FDDVLEFPEGKEDDETEYRRIDDDLSKYIEVIKLRDNPIT.NQSKYVGYNFENEENFFHFNGEELK.
P. reichenowi	45	FDDVLEFPEGKEDDETEYRRIDDDLSKYIEVIKLRDNPIT.NQSKYVGYNFENEENFFHFNGEELK.
▼		
P. vivax	104	NLPEQ.VRQNEGERVKEYEHPVPPFVLTCLCEYAFKEILFFLNKHLKQLNSILNDGESSKNDK
P. inui	104	NLPEQ.VMQSEGERIKKEYEHPVPPFVLTCLCEYAFKEILFFLNKHLKQLNSILNDGESSKNDK
P. knowlesi_strainH	104	NLPEQ.VRQNEVERIKKEYEHPVPPFVLTCLCEYAFKEILFFLNKHLKQLNSILNDGESSKNDK
P. fragile	94	NLPEQ.VIQNEGERIKKEYEHPVPPFVLTCLCEYAFKEILFFLNKHLKQLNSILNDGESSKNDK
P. yoelii	117	KNN..YKESKKNVTKKEYEHPVPPFVLTCLCEYAFKEILFFLNKHLKQLNSILNDGESSKNDK
P. berghei	126	KNN..YKESKKNVTKKEYEHPVPPFVLTCLCEYAFKEILFFLNKHLKQLNSILNDGESSKNDK
P. vinckei	89	KND..CEKSKSNVTKKEYEHPVPPFVLTCLCEYAFKEILFFLNKHLKQLNSILNDGESSKNDK
P. chabaudi	115	KND..CEKSKSNVTKKEYEHPVPPFVLTCLCEYAFKEILFFLNKHLKQLNSILNDGESSKNDK
P. gallinaceum	100	YSKQDT...NKKDAKEYEHPVPPFVLTCLCEYAFKEILFFLNKHLKQLNSILNDGESSKNDK
P. gaboni	106	YINNENKLLDKNYEKEYEHPVPPFVLTCLCEYAFKEILFFLNKHLKQLNSILNDGESSKNDK
P. falciparum_3D7	105	YIYNENKLLDKNYEKEYEHPVPPFVLTCLCEYAFKEILFFLNKHLKQLNSILNDGESSKNDK
P. reichenowi	106	YIYNENKLLDKNYEKEYEHPVPPFVLTCLCEYAFKEILFFLNKHLKQLNSILNDGESSKNDK
▼		
P. vivax	166	YVAMTLIKNAVISAEQNLPGCQDGTGAILGKKDEELTTYEHKYLNLGVYNAYRNNFRYSQ
P. inui	166	YVAMTLIKNAVISAEQNLPGCQDGTGAILGKKDEELTTYEHKYLNLGVYNAYRNNFRYSQ
P. knowlesi_strainH	166	YVAMTLIKNAVISAEQNLPGCQDGTGAILGKKDEELTTYEHKYLNLGVYNAYRNNFRYSQ
P. fragile	156	YVAMTLIKNAVISAEQNLPGCQDGTGAILGKKDEELTTYEHKYLNLGVYNAYRNNFRYSQ
P. yoelii	178	YVAMTLIKNAVISAEQNLPGCQDGTGAILGKKDEELTTYEHKYLNLGVYNAYRNNFRYSQ
P. berghei	187	YVAMTLIKNAVISAEQNLPGCQDGTGAILGKKDEELTTYEHKYLNLGVYNAYRNNFRYSQ
P. vinckei	150	YVAMTLIKNAVISAEQNLPGCQDGTGAILGKKDEELTTYEHKYLNLGVYNAYRNNFRYSQ
P. chabaudi	176	YVAMTLIKNAVISAEQNLPGCQDGTGAILGKKDEELTTYEHKYLNLGVYNAYRNNFRYSQ
P. gallinaceum	159	YVAMTLIKNAVISAEQNLPGCQDGTGAILGKKDEELTTYEHKYLNLGVYNAYRNNFRYSQ
P. gaboni	169	YVAMTLIKNAVISAEQNLPGCQDGTGAILGKKDEELTTYEHKYLNLGVYNAYRNNFRYSQ
P. falciparum_3D7	168	YVAMTLIKNAVISAEQNLPGCQDGTGAILGKKDEELTTYEHKYLNLGVYNAYRNNFRYSQ
P. reichenowi	169	YVAMTLIKNAVISAEQNLPGCQDGTGAILGKKDEELTTYEHKYLNLGVYNAYRNNFRYSQ
▼		
P. vivax	229	LSPLSMPSEANTKNNLPCQIEIYSSVRRGGKALGGATYITSSAPITSTYITSSA.....
P. inui	229	LSPLSMPSEANTKNNLPCQIEIYSSVRRGGNAPSTASASVASASVASASV.....
P. knowlesi_strainH	229	LSPLSMPSEANTKNNLPCQIEIYSSVRRGAKAHGVKTPPGVQL.....SA.....
P. fragile	219	LSPLSMPSEANTKNNLPCQIEIYSSVRRGGKALGGVITPGVRA.....SP.....
P. yoelii	241	LSPINMFEINTKNNLPCQIEIYSSVRRKKNL.....
P. berghei	250	LSPINMFEINTKNNLPCQIEIYSSVRRKKNL.....
P. vinckei	213	LSPINMFEINTKNNLPCQIEIYSSVRRKKNL.....
P. chabaudi	239	LSPINMFEINTKNNLPCQIEIYSSVRRKKNL.....
P. gallinaceum	222	LSPINMFEINTKNNLPCQIEIYSSVRRKKNL.....
P. gaboni	232	LSPINMFEINTKNNLPCQIEIYSSVRRKKNL.....
P. falciparum_3D7	231	LSPINMFEINTKNNLPCQIEIYSSVRRKKNL.....
P. reichenowi	232	LSPINMFEINTKNNLPCQIEIYSSVRRKKNL.....
Variation 2		
P. vivax	283	...PTTSTTYTT...SNAYTASNETTCTASGGPAPKYELIFIAKGGGSANKTFLFQOTKSIIL
P. inui	278ASASVASAPPTASSPKYELIFIAKGGGSANKTFLFQOTKSIIL
P. knowlesi_strainH	273SSTAP.....IDSSPKYELIFIAKGGGSANKTFLFQOTKSIIL
P. fragile	263PSSPPTCAASTASIAKYELIFIAKGGGSANKTFLFQOTKSIIL
P. yoelii	273NDKIKKDPKYELIFIAKGGGSANKTFLFQOTKSIIL
P. berghei	282NDKIKKDPKYELIFIAKGGGSANKTFLFQOTKSIIL
P. vinckei	245NEQIKKDPKYELIFIAKGGGSANKTFLFQOTKSIIL
P. chabaudi	271NYPKIKKDPKYELIFIAKGGGSANKTFLFQOTKSIIL
P. gallinaceum	260NEKLNKDRHNYLYDGPKYELIFIAKGGGSANKTFLFQOTKSIIL
P. gaboni	295	NQHLNLVEDIQNNKVKHINHISIKRPNNEHLYHGPKYELIFIAKGGGSANKTFLFQOTKSIIL
P. falciparum_3D7	281	..NVKHNKIDITTRQIDSKENQKSTIKKQNVDFLYDGPKYELIFIAKGGGSANKTFLFQOTKSIIL
P. reichenowi	282	..NVKHNKIDITTSQMDSKENQKSTIKKQNVDFLYDGPKYELIFIAKGGGSANKTFLFQOTKSIIL

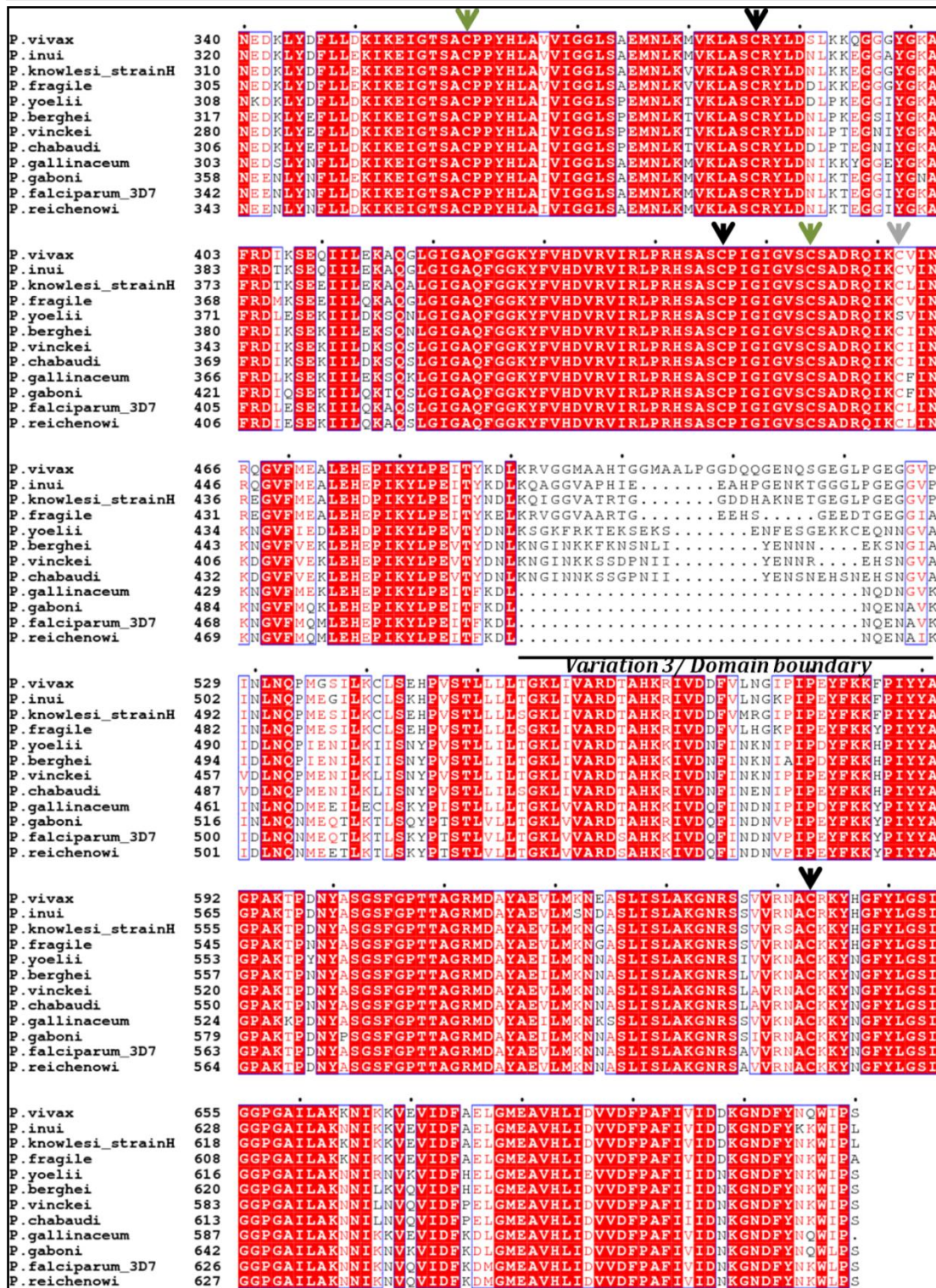


Figure 6.3. Multiple sequence alignment of Class I fumarate hydratase from different *Plasmodium* species.

The alignment shows a high degree of conservation amongst class-I fumarate hydratase protein sequences from different *Plasmodium* species. However, there are three regions, highlighted using the black bar, where there are variations; the N-terminal region of around 40 residues (variation 1), residues from 250-310 (variation 2), and residues from 490 to 530 corresponding to the domain boundary (variation 3) (*P. vivax* numbering). Cysteines that might be involved in iron-sulfur cluster ligation are shown by green arrows; those that are conserved in *Plasmodium* sequences in black arrows and the ones that are not conserved are

highlighted by grey arrows. The sequences were downloaded from NCBI database and alignment was done using Clustal omega (Sievers et al., 2011) with default parameters. The colour coding is according to the residue conservation based on BLOSUM62 matrix and was generated using ESPRIPT 3.0 (Robert and Gouet, 2014).

Examination of the multiple sequence alignment of protein sequence of *Plasmodium* FH with that of bacterial FH, shows a 120 amino acid insertion at the N-terminus that is present in *Plasmodium* FHs (Figure 6.2). The cysteines involved in ligation of the cluster though not unambiguously evident in the alignment with bacterial sequences, are evident from the alignment of PffH with two-subunit type class I FH sequences (Appendix Figure A6.1) and are highlighted in Figure 6.3.

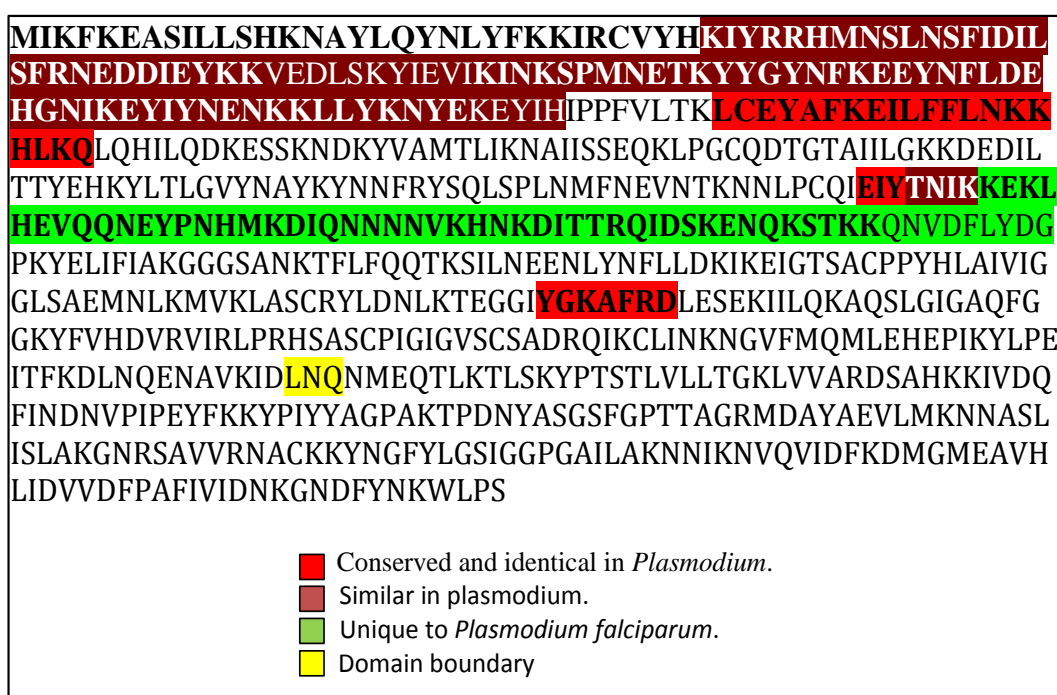


Figure 6.4. Sequence features of *P. falciparum* fumarate hydratase.

Conserved and unique features in the PffH sequence are highlighted in different colours.

Plasmodium FH proteins share high sequence identity amongst themselves as can be seen from the multiple sequence alignment in Figure 6.3. Multiple sequence alignment of *Plasmodium* FH sequences with FH sequences from other organisms shows an insertion of around 56 amino acids specific to genus *Plasmodium* shown in green in Figure 6.4 and sequence highlighted in Figure 6.3 as ‘variation 2’. The sequence of the insertion is not conserved amongst *Plasmodium* genus. The role of this insertion is not known. Though there is a 120 amino acid insertion at the N-terminus of the *Plasmodium* proteins (compared to bacterial FH sequences), except for 40 residues at the N-terminus, rest of them are conserved amongst *Plasmodium* sequences and hence might be important for

function. This forms the basis of generating expression constructs for the proteins PffH Δ 40, in which 40 residues from the N-terminus is removed and PffH Δ 120, wherein 120 residues from the N-terminus is removed. The results of the multiple sequence alignment are projected onto the *P. falciparum* FH sequence—as conserved and unique features— and shown in **Figure 6.4**.

6.3.2. Prediction of mitochondrial targeting sequence

Biochemical evidence suggests that the PffH is mitochondrially localized (Bulusu et al., 2011). Mitochondrial targeting signals are rich in amphipathic α -helices that help in translocation of proteins across the mitochondrial membrane (Roise et al., 1986). In order to express the recombinant protein in *E. coli*, it is preferable to use the DNA sequence corresponding to only the mature protein with the signal peptide deleted. In order to predict the mitochondrial targeting signal in different FH sequences of *Plasmodium* species, various tools such as MitoprotII, TargetP, MitoFates, and PlasMIT were used. **Table 6.3** summarizes the results of the analysis from different prediction softwares for *Plasmodium* FH protein sequences. As a positive control for the analysis, *P. falciparum* dihydroorotate dehydrogenase (PfdHODH), a well characterized protein with canonical mitochondrial targeting sequence was used.

As evident from the Table 6.3, except for FH sequence of *Plasmodium knowlesi*, the targeting sequence is not predicted by the tools used in the analysis. Especially, for *P. falciparum* FH sequence, none of the tools were able to predict the localization or the signal sequence. One of the tools used in the analysis, PlasMIT, is an artificial neural network based prediction tool developed specifically for predicting mitochondrial transit peptides specific to *P. falciparum*. Unfortunately, the authors report that of all the mitochondrial proteins predicted by the tool, fumarate hydratase is the only 'false negative' (Bender et al., 2003a). This raises doubts on whether FH in *Plasmodium* species is targeted to the mitochondrion using N-terminal signal sequence. There is a possibility that PffH might get localized to the mitochondrion using an internal signal sequence or an unconventional mitochondrial localization signal. Since none of the tools were able to predict an unambiguous signal sequence in *P. falciparum* FH sequence, for generating expression constructs corresponding to mature protein, read out from only multiple sequence alignment was considered.

Table 6.3. Mitochondrial targeting sequence prediction

S.No	Protein	MitoprotII (Claros and Vincens, 1996)	TargetP (Emanuelsson et al., 2000)	MitoFates (Fukasawa et al., 2015)	PlasMIT (Bender et al., 2003b)
1	<i>P. falciparum</i>	CS: NP P:0.88	CS:NP P:0.344	CS:38 P:0.302	Non-mito (99%)
2	<i>P. reichenowi</i>	CS:NP P: 0.97	CS: NP P:.264	CS:38 P:0.294	Non-mito (99%)
3	<i>P. gaboni</i>	CS:37 P: 0.92	CS:NP P:0.399	CS:28 P:0.240	Non-mito (99%)
4	<i>P. gallinaceum</i>	CS:NP P: 0.85	CS:NP P:0.176	CS:57 P:0.013	Mito (91%)
5	<i>P. knowlesi</i>	CS: 13 P:0.9928	CS:11 P:0.877	CS:32 P:0.691	Mito (91%)
6	<i>P. fragile</i>	CS:21 P:0.83	CS:13 P:0.828	CS:12 P:0.250	Non-mito (99%)
7	<i>P. vinckei</i>	CS:NP P:0.1488	CS:NP P:0.088	CS:45 P:0.005	Mito (91%)
8	<i>P. chabaudi</i>	CS:NP P:0.89	CS:9 P:0.661	CS:10 P:0.174	Mito (91%)
9	<i>P. inui</i>	CS:13 P:0.97	CS:50 P:0.858	CS:42 P:0.318	Mito (91%)
10	<i>P. vivax</i>	CS:13 P:0.96	CS:29 P:0.816	CS:21 P:0.630	Non-mito (99%)
11	<i>P. berghei</i>	CS:46 P:0.85	CS:NP P:0.262	CS:37 P:0.251	Mito (91%)
12	<i>P. yoelii</i>	CS:NP P:0.435	CS:NP P:0.273	CS:9 P:0.078	Mito (91%)
13	Pf DHODH	CS:24 P:0.50	CS:NP P:0.349	CS:23 P:0.996	Mito (91%)

A probability value of more than 0.5 is considered significant. Boxes shaded in green correspond to sequences for which the cleavage sequence was predicted with a probability value of more than 0.5. CS-cleavage sequence; P-probability; Pf-Plasmodium falciparum; mito-mitochondrially localized; non-mito- not localized to mitochondria; NP- not predictable.

6.3.3. Cloning, expression and purification

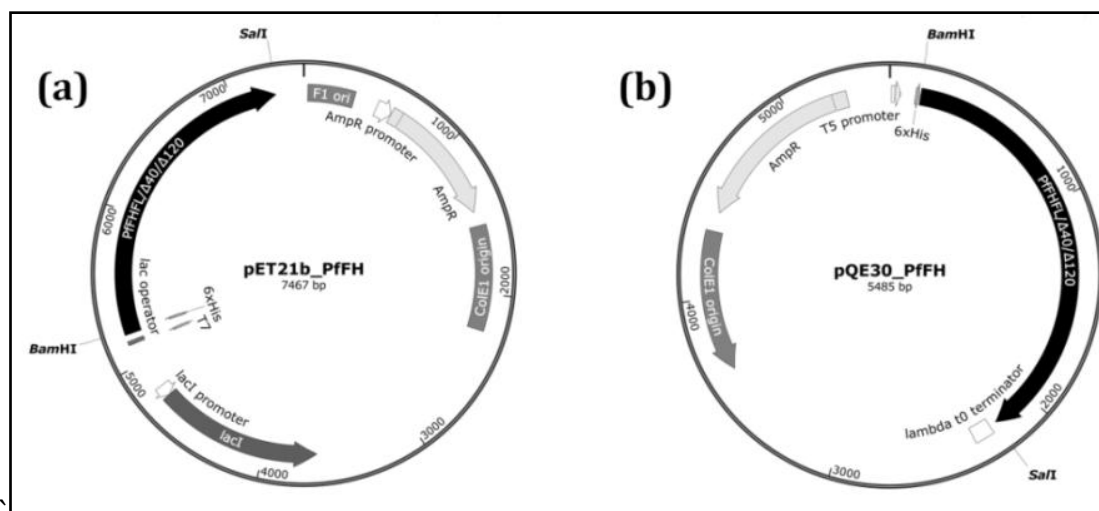


Figure 6.5. Vector maps of expression constructs of PffFH gene.

The clones generated were used for expression of different N-terminal truncated proteins and the full length of *P. falciparum* FH. **(a)** pET21b constructs for recombinant protein expression of PffFHFL, PffFHΔ40 and PffFHΔ120. **(b)** pQE30 constructs of PffFHFL, PffFHΔ40 and PffFHΔ120 genes for functional complementation in *E. coli*. AmpR, β -lactamase gene; 6XHIS, 6X histidine tag; T7, T7 phage promoter; CTD, C-terminal domain.

Constructs containing the full-length *Plasmodium* FH were generated using both pET21b and pQE30 as the backbone (**Figure 6.5**). N-terminal truncation constructs, based on the alignment with bacterial and two-subunit archaeal sequences, were also generated. The clones were confirmed by both insert release (**Figure 6.6**) and sequencing. Constructs in pET21b were used for recombinant protein expression in the *E. coli* strain BL21(DE3)-RIL. The full-length and N-terminal truncation constructs have N-terminal (His)₆ tag. All three proteins expressed well upon IPTG induction (**Figure 6.7a and 6.8**).

Purification of all the three constructs was attempted using Ni-NTA affinity chromatography. Examination of different fractions from the purification process on SDS-PAGE showed that more than 90% of the protein was found in the insoluble fraction (**Figure 6.7 a**). Moreover, the eluates contained multiple impurities; both of higher and lower molecular weight, along with the protein of interest (**Figure 6.7 b**).

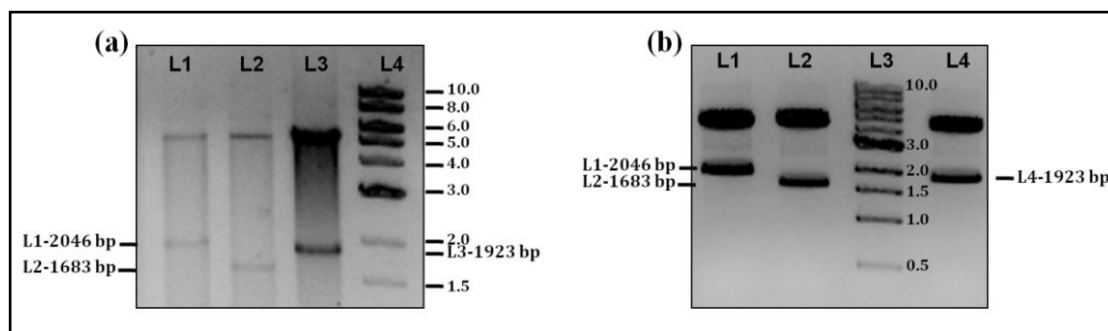


Figure 6.6. Validation of plasmid constructs.

(a) Clones generated for recombinant expression of PffHFL (L1), PffH Δ 120 (L2) and Pff Δ 40 (L3) in pET21b were validated using release of the cloned segment using the restriction enzymes, BamHI and Sall. L4, 1kb DNA ladder. **(b)** Cloning of PffHFL (L1), PffH Δ 120 (L2) and PffH Δ 40 (L4) in pQE30 was validated using BamHI and Sall. L3, 1kb DNA ladder.

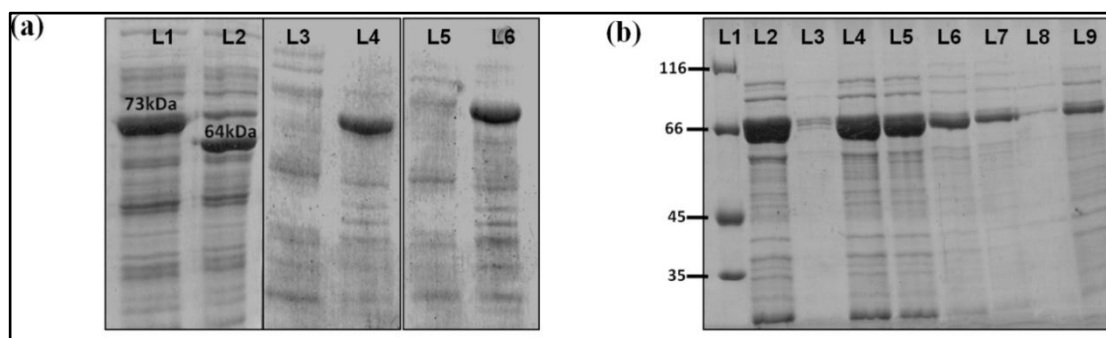


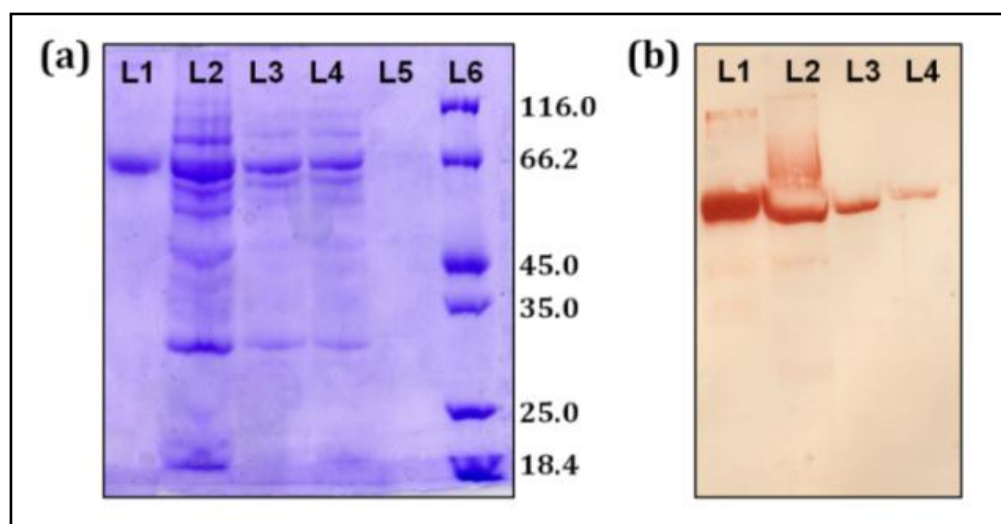
Figure 6.7. Expression of PffH Δ 40 and PffH Δ 120 in BL21(DE3)-RIL and purification of PffH Δ 40.

(a) BL21 (DE3)-RIL strain expressing PffH Δ 40 and PffH Δ 120 was lysed and soluble and insoluble fractions were analysed by SDS-PAGE. All fractions correspond to 250 μ l culture equivalent. L1 and L2, whole cell lysate of cells expressing PffH Δ 40 and PffH Δ 120, respectively. L3 and L5, the soluble fraction obtained after lysis of cells expressing PffH Δ 40 and PffH Δ 120, respectively. L4 and L6, pellet fraction after lysis of cells expressing PffH Δ 40 and PffH Δ 120, respectively. **(b)** The protein, PffH Δ 40 was recombinantly expressed in BL21 (DE3)-RIL strain and purified using Ni-NTA chromatography. The bead-bound protein was eluted with different concentrations of imidazole and the eluates analysed using SDS-PAGE followed by staining with Coomassie Brilliant Blue (CBB). L1, protein molecular weight marker; L2 and L3, 150 mM imidazole eluate; L4 and L5, 300 mM imidazole eluate; L6 and L7, 750 mM imidazole eluate, L8 and L9, 1 M imidazole eluate. Molecular weight of marker proteins is indicated in kDa.

The amount of soluble protein obtained was relatively higher (2 mg/L) for the truncated protein, PffH Δ 40 compared to the full length and PffH Δ 120. Extensive efforts, summarized in **Table 6.4**, taken to improve the yield of soluble protein (PffH Δ 40) were unsuccessful. Western blot of the eluates probed with α -(His)₆ antibody showed single bands corresponding to the protein PffH Δ 40 as shown in **Figure 6.9 b**.

Table 6.4. Efforts to improve the solubility of the PffH Δ 40

S.No	Variable	Results
1	Bacterial Strains C41 (DE3), C42 (DE3), Lemo21(DE3), BL21(DE3) Δ iscR.	No improvement in yield
2	Temperature Pre-induction temperature (in °c) : 37, 27 Post-induction temperature (in °c): 20, 16, 4	No improvement in yield
3	Co-expression plasmids Chaperone plasmids (Takara clonotech kit) pDB1818 (<i>Isc</i> operon)	No improvement in yield
4	Medium additives Benzyl alcohol Iron and sulfur supplement	No improvement in yield

**Figure 6.9. Western blotting of purified PffH Δ 40 with α -His antibody.**

(a) Ni-NTA purified fractions of PffH Δ 40. L1, electro eluted protein; L2, 250 mM imidazole eluate from Ni-NTA purification; L3, 500 mM imidazole eluate; 1M imidazole eluate; L6, protein molecular weight marker. **(b)** Western blot probed with α -(His)₆ antibody. The 1^o antibody was used at a titer of 1:4000. HRP-tagged secondary antibody was used and the blot was developed using 3-amino-9-ethylcarbazole. L1, electroeluted protein; L2, 250 mM imidazole eluate ; L3, 500 mM imidazole eluate; L4, 1M imidazole eluate.

6.3.4. Generation and testing of α -PffH Δ 40 antibody

PffH Δ 40 protein was used to raise antibodies in rabbit using standard protocols mentioned in section 2.3.4. PffH Δ 40 could not be purified to homogeneity from the soluble fraction. In order to obtain pure protein, purification of the same was performed from inclusion body. After 2M urea wash, the inclusion body was solubilized in 6M guanidinium hydrochloride (GndHCl). The solubilized protein was subjected to Ni-NTA chromatography under denaturing condition. The eluates were loaded on SDS-PAGE and the band corresponding to PffH Δ 40 was subjected to electroelution to obtain pure

protein (**Figure 6.10 a**). Probing of the eluted protein with α -(His)₆ antibody gave a single band (**Figure 6.10 b**) showing the presence of (His)₆-tag in the protein. The antibody generated was used to probe the Ni-NTA eluate containing PffH Δ 40 obtained from soluble fraction. Unlike a single specific band obtained with α -(His)₆ antibody (**Figure 6.9 b**), in this blot multiple lower bands were seen along with a band corresponding to protein of interest (**Figure 6.10 c**). These bands probably correspond to degradation of recombinant protein. It should be noted that the degradation is evident even in the presence of protease cocktail inhibitor in the lysis and elution buffer. This may be due to thermolabile nature of mesophilic class-I FH (Woods et al., 1988).

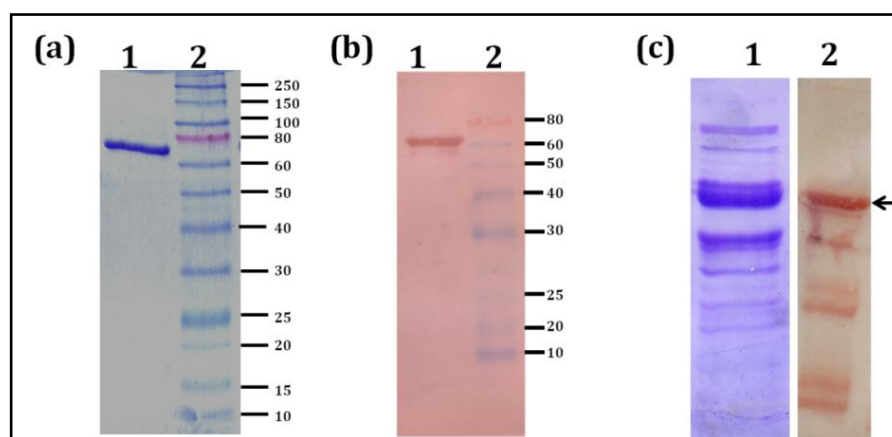


Figure 6.10. Generation and testing of PffH Δ 40 specific antibody.

(a) Purification of PffH Δ 40 from inclusion body by excision of the band of interest from a CBB stained gel followed by electroelution. L1, electroeluted protein; L2, protein molecular weight marker (in kDa). **(b)** Validation of the electroeluted protein with α -HIS antibody. L1, electroeluted protein probed with the α -HIS antibody; L2, prestained protein molecular weight marker. **(c)** Western blot probed with α -PffH Δ 40 antibody against Ni-NTA purified soluble PffH Δ 40; L1, 250 mM imidazole eluates and L2, blot probed with PffH Δ 40 specific antibody. The arrow shows the position of PffH Δ 40. Degradation of protein bands are clearly seen when probed with protein specific antibody but not with α -(His)₆ antibody.

6.3.5. Fumarate hydratase activity

Ni-NTA eluates were directly used for checking the catalytic activity. The fumarate to malate conversion was monitored at 240 nm ($\Delta\epsilon = 2440 \text{ M}^{-1} \text{ cm}^{-1}$). The protein was found to be active as seen by the time-dependent change in absorbance (**Figure 6.11 b**). The specific activity of the protein for fumarate was $1 \mu\text{mol min}^{-1} \text{ mg}^{-1}$ and for malate was $10 \text{ nmol min}^{-1} \text{ mg}^{-1}$. The fact that the protein was active without any *in vitro* reconstitution suggests that at least a part of the protein molecules are cluster bound. This is also evident from the absorbance at 420 nm of the purified protein immediately after purification (**Figure 6.11 a**). The activity of the protein was further confirmed by

incubating the partially purified protein with [2, 3]¹³C-fumarate. NMR spectrum of the reaction mixture after removing the protein by heat precipitation showed peaks corresponding to [2, 3]¹³C-malate, confirming the chemical identity of the product. The spectrum is shown in the **Figure 6.11 c**.

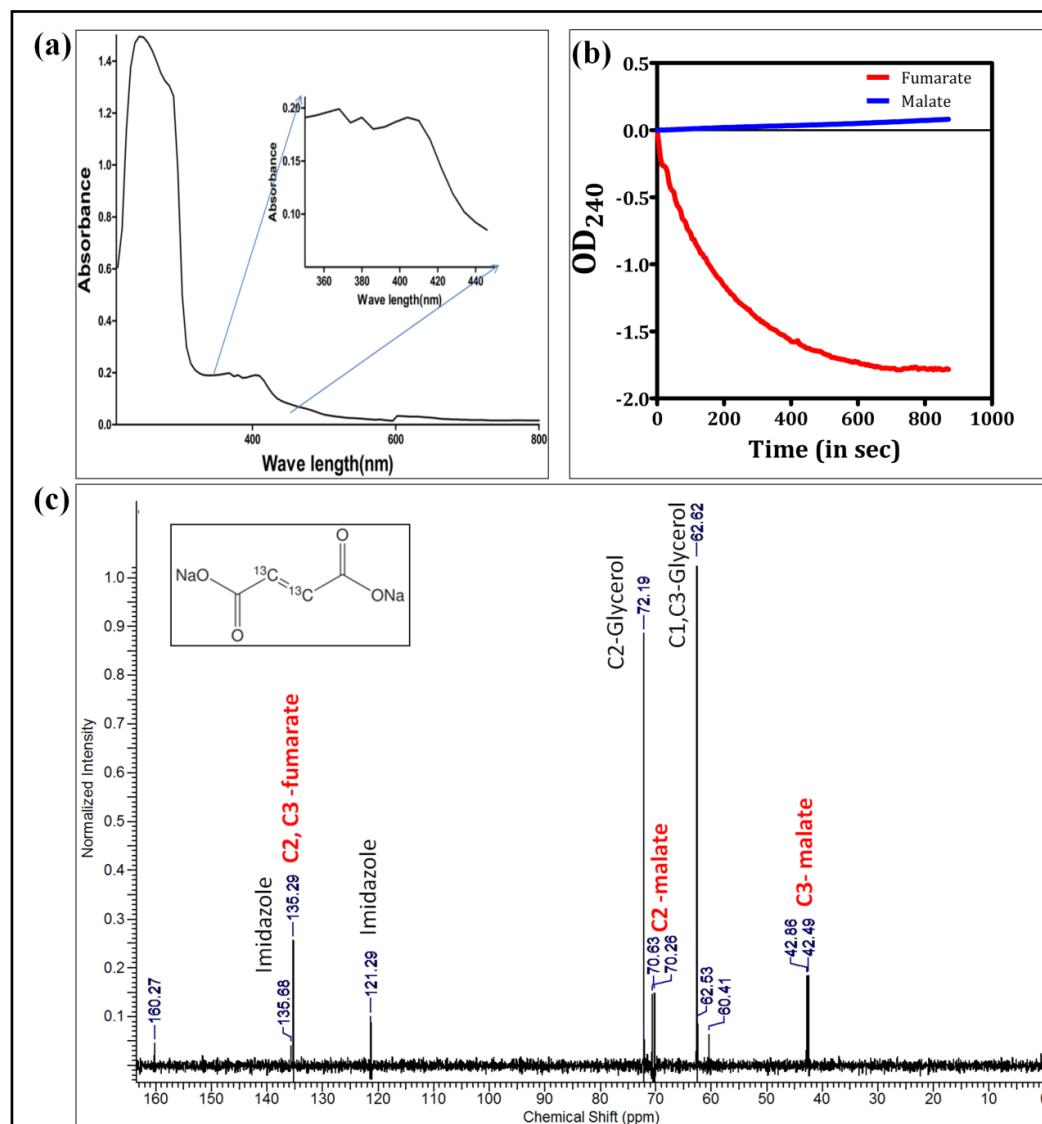


Figure 6.11. Activity of PffHΔ40 and characterization of Fe-S cluster

(a) A wavelength scan of Ni-NTA eluates shows the characteristic peak at 420 nm that corresponds to a 4Fe-4S type Fe-S cluster. **(b)** The time scan at 240 nm shows the conversion of fumarate to malate (red) and malate to fumarate (blue) using 75 μg of partially purified PffHΔ40. The reaction was initiated by the addition of the enzyme to a reaction mixture containing either 1mM fumarate/malate in 50 mM Tris-HCl, pH7.4 at 37 °C. **(c)** Validation of activity by ¹³C-NMR. The NMR spectra of assay mixture consisting of 50 μM 2,3-[¹³C]-fumarate in 100 mM potassium phosphate, pH 7.4, incubated with 100 μg of purified PffHΔ40 enzyme, shows the presence of peaks corresponding to both ¹³C-malate and unreacted ¹³C-fumarate. This validates the fumarate hydratase activity of PffHΔ40. The inset shows the chemical structure of ¹³C-fumarate used in this assay. The spectra represent the average of 3000 scans acquired using Bruker 400MHz NMR spectrophotometer.

6.3.6. Functional complementation of PffH in fumarate hydratase null *E. coli* strain

E. coli has three genes that encode for fumarate hydratase; *fumA* and *fumB* of the class-I type and *fumC* of the class-II type. *FumA* and *fumC* genes are in tandem and are driven by a common promoter. Recently, another gene, *fumD* was identified to have fumarate hydratase activity, though the primary substrate for this enzyme is mesaconate (Kronen and Berg, 2015). *E. coli fumD* has weak activity on fumarate with an apparent K_m value close to 1mM and hence, might not have a significant contribution *in vivo* to the overall fumarate hydratase activity. A triple knockout strain of *E. coli* Δ *fumACB*, in which the three major FH genes are deleted, was generated.

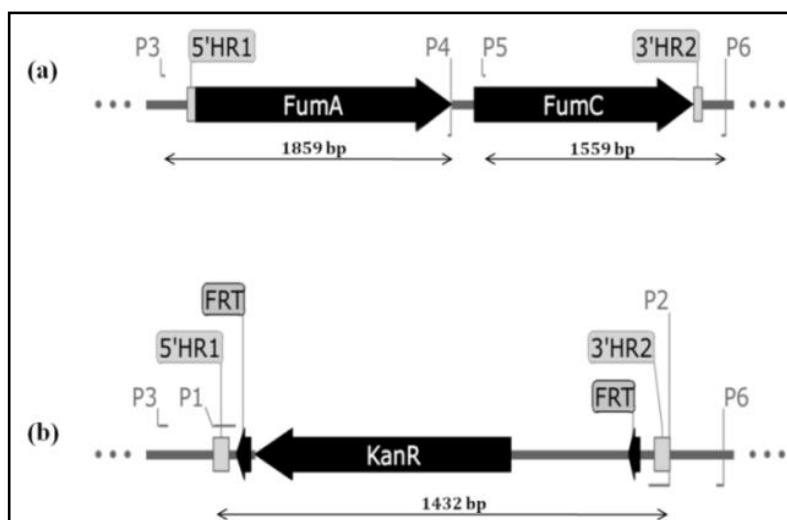


Figure 6.12. Genotype of *E. coli* Δ *fumACB* strain.

(a) The relative orientation of *fumA* and *fumC* genes in the Δ *fumB* strain and the location of primers (P3-P6) used for validation of the knockout. 5'HR1 and 3'HR2 represent the 30bp homologous regions used for gene replacement with kanamycin resistant marker. **(b)** *fumA/C* gene loci after homologous recombination and replacement with kanamycin resistance marker flanked by FRT sites. The orientation of the primers (P1 and P2) used for amplification by PCR of the kanamycin cassette is shown.

Deletion of the gene was validated by PCR using genomic DNA of the mutant strain as template and appropriate primers as shown in **Figure 6.12**. **Figure 6.13** shows the results of genotyping. The absence of the genes *fumA* and *fumC*, is evident from the PCR results. As expected, while the strain was able to grow normally in malate containing minimal medium, it was not able to grow on M9 minimal medium containing fumarate as the sole carbon source (**Figure 6.13 c**).

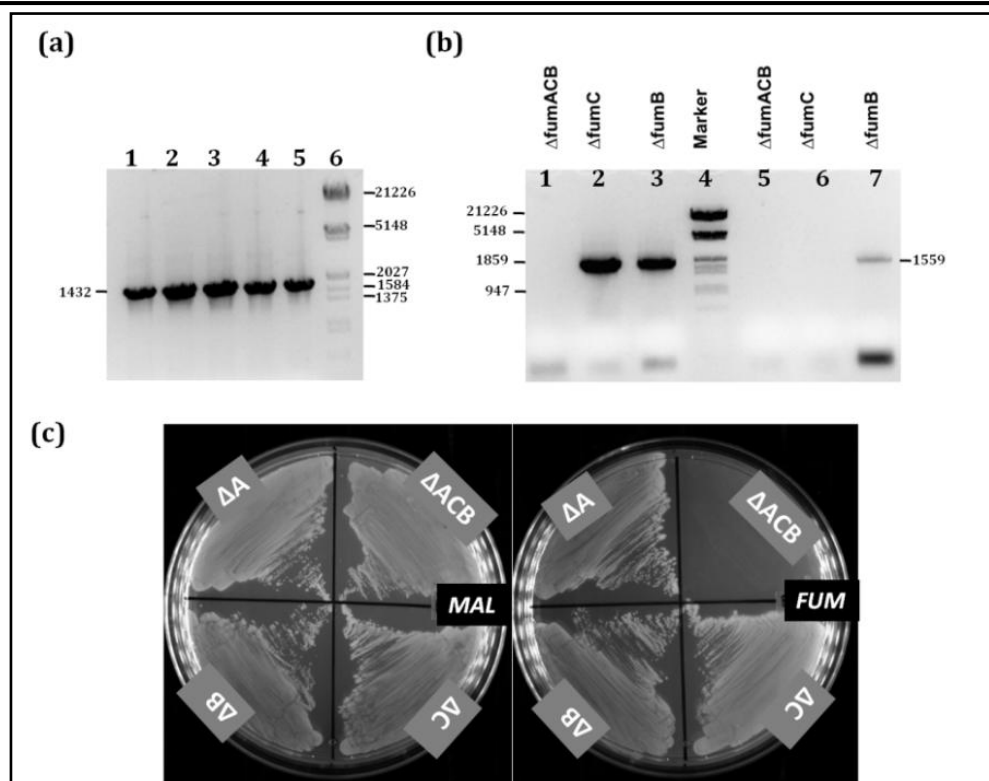


Figure 6.13. Genotyping and phenotyping of the Δ fumACB strain.

(a) PCR amplified products using primers P1 and P2 and genomic DNA of 5 different colonies selected on kanamycin plate as template, showing the presence the kanamycin selection cassette integrated into the right loci. **(b)** Lane 1-3 represents the amplicons obtained on performing a PCR to check the presence/absence of *fumA* gene using primers P3 and P4 and genomic DNA from different *E. coli* strains (mentioned in the figure) as template. Lane 5-7 represents the amplicons obtained on performing a PCR to check the presence/absence of *fumC* gene using primers P5 and P6 and genomic DNA from different FH knockout strains (mentioned in the figure) as template. **(c)** Growth phenotype of various strains with at least one copy of fumarate hydratase gene deleted. As it is evident from the phenotype, Δ fumACB strain is not able to grow on fumarate containing minimal medium.

6.3.7. Functional complementation with PffH

In order to check if PffH protein could functionally complement fumarate hydratase deficiency in Δ fumACB strain of *E. coli*, the bacterial cells were transformed with plasmids, pQE-PffHFL, pQE-PffH Δ 40, and pQE-PffH Δ 120, expressing full-length and N-terminal truncated versions of the *P. falciparum* enzyme. *E. coli* Δ fumACB strain transformed with pQE30 vector served as a negative control. At the end of 48 hours, the growth phenotype was scored and it was observed that all the strains grew equally well on malate/glucose containing-M9 medium plates (**Figure 6.14 a and b**). In the fumarate containing M9 plate, the cells with PffH Δ 40 and PffHFL grew faster, whereas, the growth rate of cells with and PffH Δ 120 was slower and no growth was seen in cells carrying just the empty plasmid (pQE30) (**Figure 6.14 c**). This shows that the *P. falciparum* FH can functionally

complement the enzymatic role of fumarate hydratase in Δ fumACB strain. This validates that *Plasmodium* enzyme is indeed fumarate hydratase. The observation that PffH Δ 120 supplemented strain grew slower than PffH Δ 40 shows that residue 40-120 play a role in the structure and/or function of the enzyme despite the fact that these residues are conserved only in *Plasmodium* fumarate hydratase sequences and not in others.

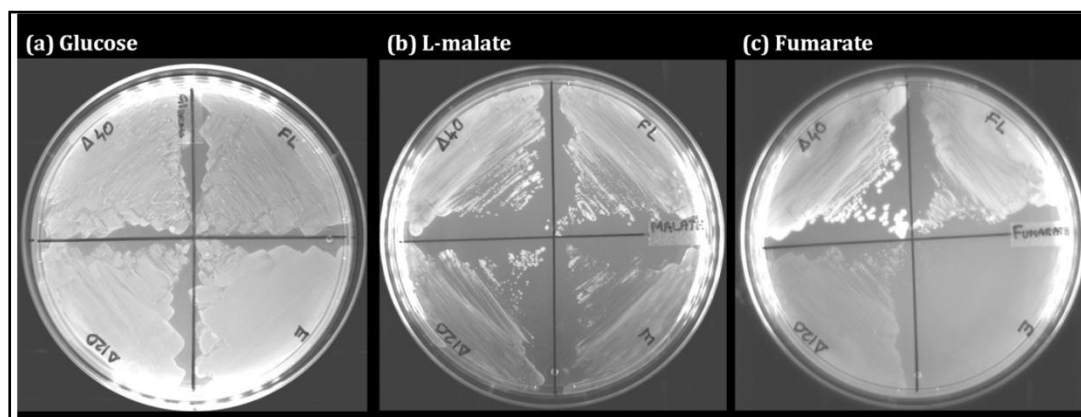


Figure 6.14. Complementation of the Δ fumACB strain with PffH gene

Δ fumACB strains expressing different truncation constructs of PffH (FL-PffHFL, Δ 40-PffH Δ 40 and Δ 120-PffH Δ 120) were generated to see functional complementation in M9 medium with different carbon sources. As a control, the growth phenotype of the strain with just the pQE30 plasmid (E) was used for comparison. Expression of PffH restored the growth on M9-fumarate medium (panel c) and maximal rescue was observed with PffH Δ 40. The growth of all the four strains was similar when either glucose (panel a) or malate (panel b) was used as the sole carbon source. This suggests that FH is not needed for growth on these substrates. The experiment was repeated twice and the images correspond to one of the replicates.

6.3.8. Substrate promiscuity of PffH

Substrate promiscuity in class-I FHs has been reported earlier (van Vugt-Lussenburg et al., 2013; Kronen and Berg, 2015). In order to check if PffH can catalyze hydration/dehydration of other dicarboxylic acids reported to be substrates for FH from other organisms, the Δ fumACB strain carrying different constructs of PffH was grown on M9 medium with meso-tartrate, mesaconate or D-tartrate as the sole carbon source. Growth phenotype under the different conditions was scored after incubating the plates at 37 °C for 48 h. The results are summarized in **Figure 6.15**. The growth on meso-tartrate is clearly independent of the presence of PffH as the cells having just the vector backbone grow well on this (**Figure 6.15 a**).

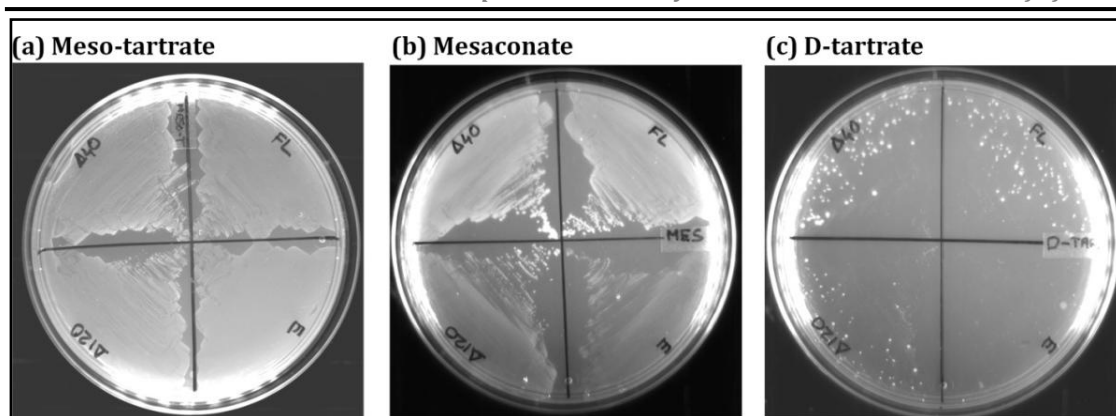


Figure 6.15. Growth phenotype of PffH expressing Δ fumACB strain on promiscuous substrates

Cells expressing PffHFL, PffH Δ 40 and PffH Δ 120 grew well when D-tartrate or mesaconate (panel b and c respectively) was used as a sole carbon source, compared to the strain expressing just the vector (E). The picture represents growth at the end of 48 h. The experiment was repeated twice and the images correspond to one of the replicates.

Cells expressing PffH Δ 40 and PffHFL in the presence of mesaconate as the carbon source show significantly better growth than PffH Δ 120 (**Figure 6.15 b**). The growth of cells carrying just the vector backbone was the poorest suggesting that the Δ fumACB strain has weak ability to utilize mesaconate as carbon source. This growth could be attributed to the presence of fumD, which has been reported to have activity on mesaconate (Kronen and Berg, 2015). The dramatic increase in growth seen upon expression of PffH (PffH Δ 40 and PffHFL) clearly indicates that the parasite enzyme metabolizes mesaconate.

Cells expressing all the three constructs of PffH showed weak growth on D-tartrate containing medium (**Figure 6.15 c**), while cells containing the plasmid vector alone failed to grow. This observed growth with only few isolated colonies is significantly weaker when compared to that on fumarate and mesaconate that yielded a lawn. This either suggests that the activity of PffH on D-tartrate is very poor or D-tartrate is not sufficiently transported in to the cell.

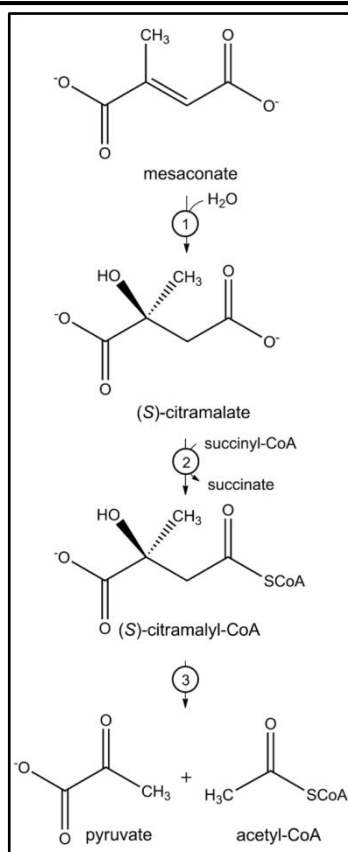


Figure 6.16. Mesaconate utilization pathway in *E. coli*

Mesaconate is converted to citramalate by the action of the enzyme mesaconase/fumarase. The citramalate is activated by the addition of Co-A molecule by the enzyme succinyl-CoA:(S)-citramalate CoA-transferase. The citramalyl-CoA is subsequently cleaved into pyruvate and acetyl-CoA. 1, mesaconase; 2, succinyl-CoA:(S)-citramalate CoA-transferase; 3, (S)-citramalyl-CoA lyase. Figure reproduced from Kronen and Berg, 2015.

Activity of fumarate hydratase on mesaconate and D-tartrate will result in the formation of citramalate and oxaloacetate, respectively. While citramalate is metabolized in the cell to produce pyruvate and acetyl-CoA by the action of enzymes succinyl-CoA:(S)-citramalate CoA-transferase and citramalyl-CoA lyase as shown in the **Figure 6.16** (Kronen and Berg, 2015), oxaloacetate is converted to malate by the action of the enzyme malate dehydrogenase. These products can enter the metabolic pathways and fuel the growth of cells expressing active FH.

Taken together, these results show that the substrate promiscuity profile of the PffH is similar to that obtained from the *in vitro* studies on class-I enzymes from other organisms (Woods et al., 1988; Flint, 1994; van Vugt-Lussenburg et al., 2013; Kronen and Berg, 2015). From the growth profiles we conclude that the order of substrate utilization efficiency of PffH is fumarate followed by mesaconate with D-tartrate being the least preferred.

6.3.8. Growth phenotype of cells expressing PffH on L-tartrate and itaconate

Class I fumarate hydratases reported till date are highly stereospecific and do not catalyse the dehydration of the enantiomer of their substrates *viz.*, D-malate and L-tartrate. To test if the Pf enzyme also behaves in a similar manner, growth phenotype of Δ fumACB cells expressing PffH was tested on minimal medium containing L-tartrate as the sole carbon source (Figure 6.16). Only cells expressing PffH (PffHFL/PffH Δ 40/PffH Δ 120) were able to grow on this medium. The growth rescue on L-tartrate was indeed surprising as there are no earlier reports suggesting it to be a substrate for either class-I/II fumarate hydratases. A possible explanation for the growth phenotype could be that the expressed PffH is playing a secondary but critical role required for the growth of Δ fumACB. Future *in vitro* studies on purified parasite FH should answer on the promiscuous activity of this enzyme on L-tartrate.

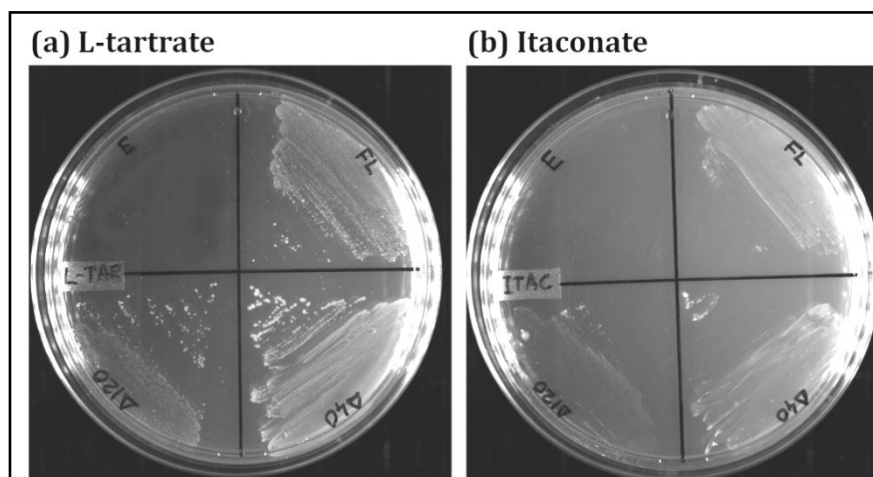


Figure 6.16. Growth phenotype of PffH expressing Δ fumACB strain on L-tartrate and itaconate

Δ fumACB cells expressing PffHFL, PffH Δ 40 and PffH Δ 120 grew when L-tartrate or itaconate (panel a and b respectively) were used as a sole carbon source. There was no growth seen of Δ fumACB cells containing just the vector (E) in the same medium. L-tartrate and itaconate are not reported to be substrates of class I FHs. The molecular mechanism behind the observed growth phenotype is unclear. The picture represents growth at the end of 48 h. The experiment was repeated twice and the images correspond to one of the replicates.

Our studies thus far have shown that PffH can catalyze the hydration of fumarate and its analogue mesaconate (methylfumarate). We extended our studies to examine the ability of the enzyme to accept itaconate as the substrate. The structure of three dicarboxylic acids (fumarate, mesaconate and itaconate) and their products obtained upon hydration are shown in **Figure 6.17 a**.

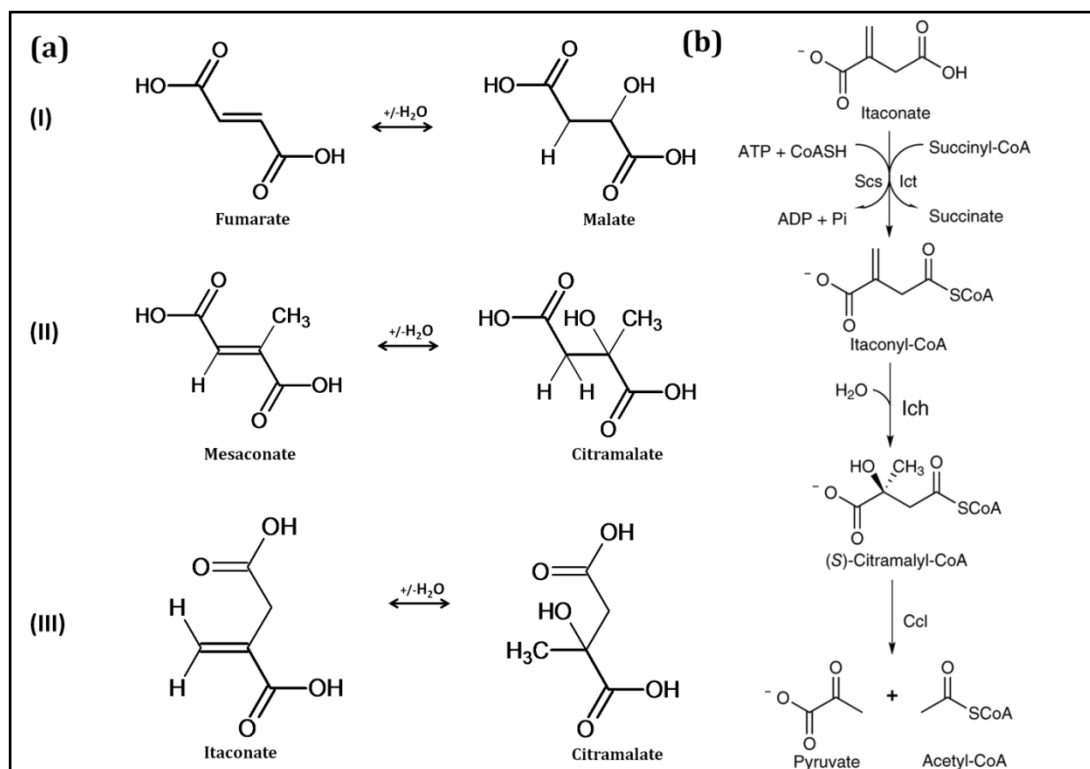


Figure 6.17. Metabolism of itaconate and L-tartrate.

(a) Chemical structures of substrates and products acted upon by fumarate hydratase. (I) fumarate to malate conversion (II) mesaconate to citramalate conversion (III) itaconate to citramalate conversion. *In vitro* studies have shown that the enzyme can use fumarate and mesaconate as substrates. Currently, there are no direct evidence available showing itaconate as a substrate for the enzyme. However, the complementation studies using PffH implies a direct or an indirect role of the enzyme in itaconate utilization. **(b)** Pathway showing enzymes involved in itaconate metabolism. Scs, succinyl coA synthetase; Ict, itaconylcoA transferase; Ich, itaconylcoA hydratase; Ccl, citramalyl-CoA lyase. Panel (b) reproduced from Sasikaran et al., 2014.

Addition of water to the olefinic bond in itaconate would result in the production of citramalate. If the PffH has promiscuous activity on itaconate, the cells expressing this enzyme would generate citramalate which can get metabolized as shown in **Figure 6.17 b**, thereby enabling growth. *ΔfumACB* strain expressing the PffH constructs and cells carrying only the plasmid vector were examined for their growth phenotype on minimal medium plates containing itaconate as the sole carbon source (**Figure 6.16 b**). The cell carrying just the empty vector failed to grow under these conditions and albeit weak, cells carrying the full length and deletion constructs of PffH showed growth.

Although the complementation results appear to suggest that PffH has promiscuous activity on itaconate, *in vitro* validation on the enzyme is necessary. Pathway of itaconate degradation has been reported to be operative in mammalian mitochondria, *Salmonella* spp., *Pseudomonas* species, and *Micrococcus* species (Wang et al., 1961; Martin

et al., 1961; Cooper et al., 1965). The enzymes involved in this pathway have been recently identified in *Yersinia pestis* and *Pseudomonas* (Sasikaran et al., 2014a). The pathway showing enzymes and the intermediates involved in the conversion of itaconate to acetyl-coA and pyruvate in *Yersinia pestis* (Yp) is shown in **Figure 6.17 a**. A BlastP search was performed against *E. coli* proteins using protein sequences of YpIct, YpIch, and YpCcl as query. Citrate lyase of *E. coli* was obtained as a hit with significant similarity (e-value of $8e-33$ and sequence identity of 32 %) to YpCcl. However, there were no significant hits available for either YpIct or YpIch.

6.3.9. Mercaptosuccinic acid mediated inhibition

The growth of *E. coli* Δ fumACB strain on fumarate minimal medium is conditional to supplementation with PffH Δ 40 expression construct. This was exploited to test the inhibitory potential of malate analog, mercaptosuccinic acid (**Figure 6.18 a**) on PffH Δ 40. Mercaptosuccinate inhibited the growth with an IC₅₀ of 482 ± 0.02 μ M (**Figure 6.18 b**). Mercaptosuccinate used is a mixture of D and L-mercaptosuccinate. Based on the stereochemistry of the reaction one would expect only L-mercaptosuccinate to inhibit the enzyme and not the D-isofom. Hence, the effective IC₅₀ value for L-mercaptosuccinate could be lower. MSA inhibited the growth of the strain, Δ fumACB when grown in fumarate containing minimal media but not in malate containing minimal media. This shows that the inhibition is specific to fumarate to malate interconversion catalyzed by PffH Δ 40 (**Figure 6.18 c**). This data forms the proof-of-concept showing that this strain can be used to screen molecules against PffH.

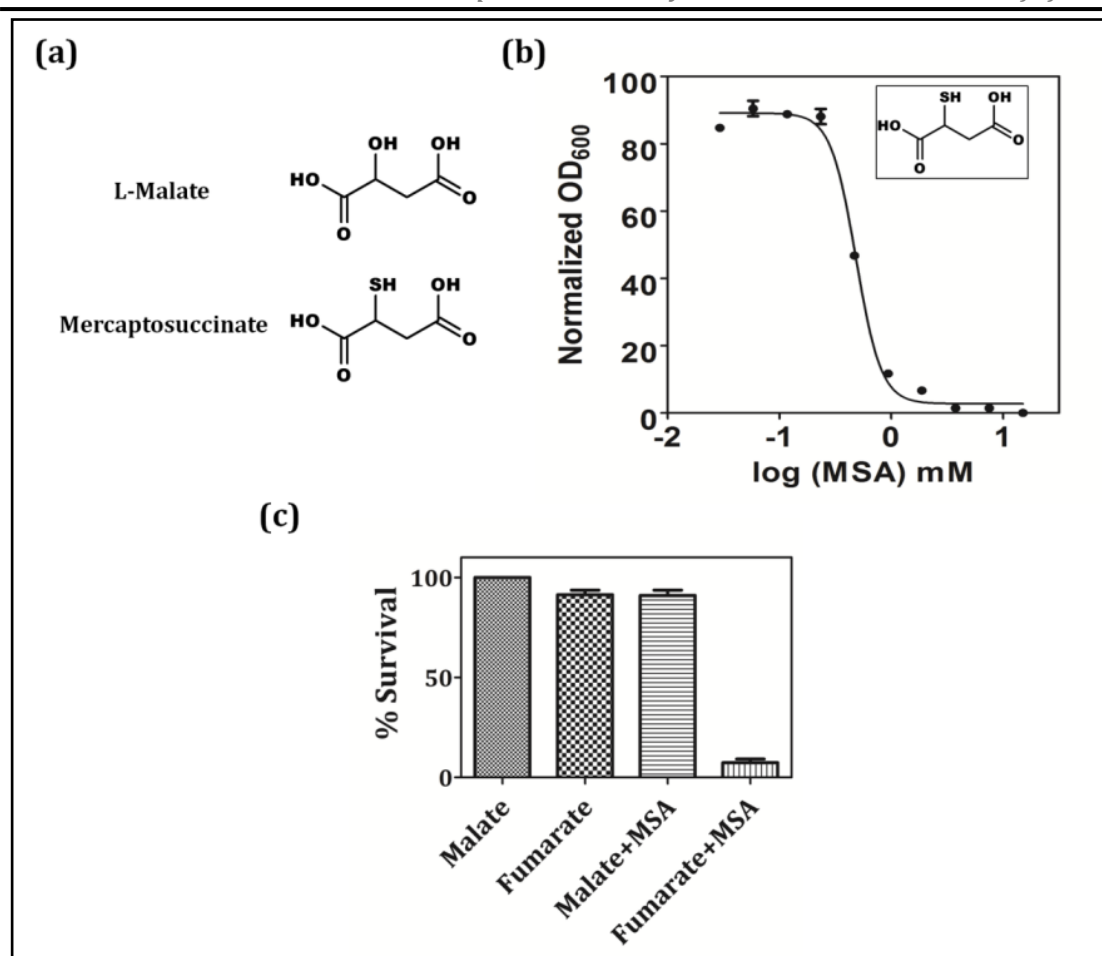


Figure 6.18. Mercaptosuccinate mediated inhibition of *E. coli* Δ fumACB strain expressing Pff Δ 40.

(a) Chemical structure of malate and of inhibitors used for screening. **(b)** Plot showing inhibition of PffH Δ 40 supplemented Δ fumACB strain on fumarate minimal medium by mercaptosuccinate. IC₅₀ obtained was $482 \pm 0.02 \mu\text{M}$. The experiment was done in duplicates and repeated twice. The error bars represent the standard error of mean obtained from two independent experiments. **(c)** Growth of *E. coli* strain Δ fumACB expressing PffH Δ 40 in different media conditions. The growth was normalized against OD₆₀₀ value obtained in 20 mM malate containing M9 minimal medium. While the growth on fumarate and malate containing minimal medium was comparable, the growth was severely inhibited in the presence of 3 mM MSA. However, there was no growth inhibition seen in medium containing malate and MSA. This shows that MSA acts specifically inhibits the enzymatic step PffH Δ 40 and has minimal off-target effects at the concentration used. The experiment was done in duplicates and repeated thrice. The error bars represent the standard error of mean obtained from three independent experiments.

6.3.10. Mercaptosuccinic acid mediated inhibition of *P. falciparum* in vitro cultures

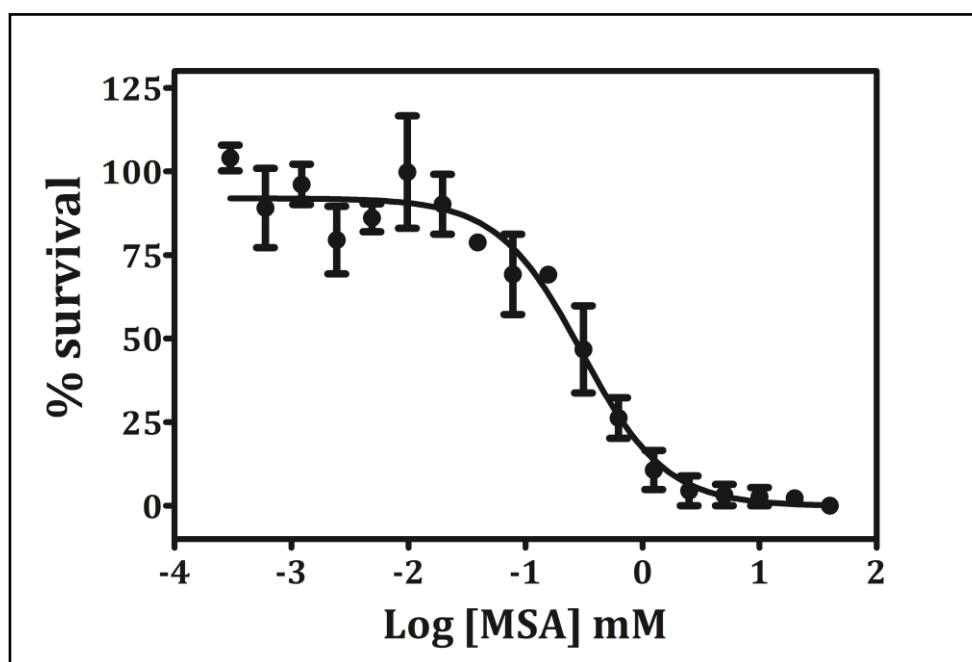


Figure 6.19. Mercaptosuccinate (MSA) inhibits *P. falciparum* growth.

The plot shows the IC_{50} of mercaptosuccinate mediated inhibition of in vitro culture of *P. falciparum*

MSA inhibition of the growth of Δ fumACB strain of *E. coli* expressing PffH Δ 40, on fumarate containing minimal media suggests that MSA is directly inhibiting the *Plasmodium* enzyme. In order to check if this could have an effect on the growth of *P. falciparum* in in vitro culture, a drug susceptibility test was performed. For this, the culture was incubated with different concentration of MSA and parasitemia was estimated at the end of 48 h. The parasitemia of the untreated culture was used for normalization. **Figure 6.19** shows the plot of normalized parasitemia versus log of MSA concentration. An IC_{50} value of $302 \pm 0.8 \mu\text{M}$ was obtained from the fit.

6.4. Summary and future perspectives.

Recombinant PffH was partially purified and was found to be active. Extensive efforts to optimize the growth conditions, strains and co-expression of chaperones, did not help to increase the yield of the protein in the soluble fraction. Deletion of the *Plasmodium*-specific 56 amino acid insertion (from 257-312) might help in improving solubility. The fact that C-terminal domain is soluble shows that the insolubility of the full-length protein

and truncation constructs is primarily because of the N-terminal domain. A fumarate hydratase null strain was developed that can be used to functionally complement fumarate hydratases from other organisms. Additionally, cells expressing PffH were able to grow on mesaconate, D-tartrate, L-tartrate or itaconate as the sole carbon source. The strain can also be used to screen for inhibitors against fumarate hydratases. As a proof of concept, mercaptosuccinate has been shown to inhibit the growth of PffH Δ 40 in fumarate containing M9 minimal media. MSA was found to inhibit the *P. falciparum* growth with an IC₅₀ of $302 \pm 0.8 \mu\text{M}$. The mechanism of growth inhibition by MSA can be investigated by NMR based metabolomic study using ¹³C-labeled fumarate as a tracer.

Chapter 7

***Biochemical and structural
characterization of two subunit class***

***I fumarate hydratase from
thermophilic archaeon,***

Methanocaldococcus jannaschii

Chapter 7

Biochemical and structural characterization of two subunit class I fumarate hydratase from thermophilic archaeon, *Methanocaldococcus jannaschii*

ABSTRACT

The two subunit class I fumarate hydratases are present in both archaea and bacteria but not in eukaryotes. Class I single subunit fumarate hydratases (C I-FH_{ss}) are present in many eukaryotic pathogens and biochemical and structural characterization is difficult owing to the thermolability of the protein and highly oxygen-sensitive nature of the iron-sulfur cluster. Studying the thermostable homolog of the enzyme that has better structural stability would enable the understanding of the characteristics of class I fumarate hydratases in general. As the Plasmodium FH was difficult to purify in significant quantities for thorough biochemical and structural characterization, Methanocaldococcus jannaschii fumarate hydratase was chosen as a model to understand the Fe-S cluster containing fumarate hydratase. Moreover, studying the class I two-subunit FH (C I-FH_{ts}) enzyme would also throw light on unique biochemical/biophysical features of this subset of proteins as well. Towards this, we have recombinantly expressed in E. coli and purified individual subunits and the complex of the two subunits of the Methanocaldococcus jannaschii (Mj) fumarate hydratase (FH). Basic characterization including oligomeric status, subunit-interaction, and thermostability of the individual subunits and of the complex were performed. The nature and stoichiometry of the cluster were probed using tools such as UV-Visible spectrophotometry, electron paramagnetic resonance, and native mass spectrometry. The iron-sulfur cluster could be reconstituted on to the α -subunit alone. The α -subunit alone was found to be active and the activity was enhanced 50 fold upon addition of stoichiometric amounts of β -subunit. The structure of the β -subunit has been solved by X-ray crystallography using molecular replacement. Comparison of this structure with the recently published structure of C I-FH_{ss} from Leishmania major shows many conserved features between the two.

7.1. INTRODUCTION

Class I fumarate hydratases are divided into single and two-subunit type enzymes depending on the number of genes that encode the functional protein. Two subunit proteins are found only in prokaryotes and archaea but not in eukaryotes. The domain

architecture of both types of proteins is shown in **Figure 7.1**. It is not known which of the two (single subunit vs. two subunit) is the more ancestral protein and hence we cannot comment on whether the two subunit type of FH was formed by a domain fission event of the single subunit FH's. A phylogenetic analysis of FH sequences from different organisms should inform us on the domain organization of the ancestral protein. Multiple sequence alignment of two subunit FH has shown that there is high degree of sequence conservation between single subunit class I fumarate hydratase (C I-FH_{ss}) and two subunit class I fumarate hydratase (C I-FH_{ts}) sequences.

C I-FH_{ts} has been studied from *Pelotomaculum thermopropionicum* (Shimoyama et al., 2007a), a thermophilic bacteria and *Pyrococcus furiosus*, a thermophilic archaea (van Vugt-Lussenburg et al., 2009a). From both these studies, the following conclusions can be arrived at; both the subunits associate to form functional protein which is a dimer of a heterodimer, the protein complex is thermostable with optimal activity at high temperature, and EPR studies show the presence of a [4Fe-4S] type iron-sulfur cluster. The structure of the β -subunit of *Archaeoglobus fulgidus* FH (PDB ID: 2ISB) has been solved by a structural genomics consortium and has been deposited in PDB and this is the only structural information about two-subunit type FH. A study on the structure of CI-FH_{ss} from *Leishmania*, that was recently reported is a valuable starting point to study the structure-function correlation in this class of enzymes (Feliciano et al., 2016).

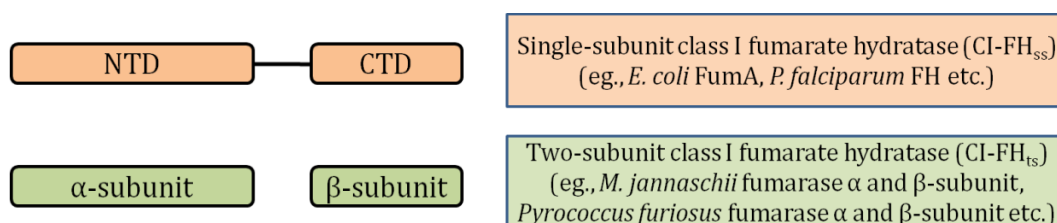


Figure 7.1. Domain organization in single-subunit (top) and two-subunit fumarate hydratase.

In single subunit fumarate hydratases (FH), the N-terminal and the C-terminal domains (NTD and CTD) are connected by a linker segment. In two subunit type FH, the two domains, annotated as α - and β -subunits, are encoded by two different genes. These subunits assemble to form a functional protein complex.

CI-FHs are known to exhibit promiscuity with respect to substrates catalyzed. This aspect has not been investigated for CI-FH_{ts}. It is known that in [4Fe-4S] cluster containing enzymes, there are three cysteines from the protein that coordinate the 3 iron atoms in the cluster and the 4th iron atom is held loosely by a hydroxyl ion. In CI-FH, though certain cysteine residues are proposed to be involved in cluster ligation based on multiple sequence alignment and conservation of residues, a biochemical validation for the same is

not available for CI-FH_{ts}. The role of individual subunits with respect to iron-sulfur cluster coordination and catalysis is still not clear. L-tartrate dehydratases (L-ttd) are similar to CI-FH_{ts} with respect to sequence conservation and the use of [4Fe-4S] cluster in catalysis. The high degree of sequence conservation makes it difficult to discern and annotate a protein sequence as either L-ttd or CI-FH_{ts}. Moreover, the biochemical information on this protein is based on only limited studies done on *Pseudomonas putida* L-ttd (Kelly and Scopes, 1986), *E. coli* L-ttd (Reaney et al., 1993) and the enzyme from L-tartrate fermenting anaerobic bacteria (Schink, 1984). L-tartrate metabolism has been well studied in *E. coli* (Reaney et al., 1993; Kim et al., 2007; Kim and Unden, 2007). L-ttd from *E. coli* displays no activity against fumarate, D-malate, and D-tartrate. The structure of L-ttd has been recently predicted from just the primary sequence using constraints derived from sequence co-evolution and modeling (Ovchinnikov et al., 2015).

7.2. Materials and methods

7.2.1. Cloning, expression and purification of MjFH

The two subunit genes, *MjFHα*, and *MjFHβ* were PCR amplified from Mj genomic DNA (procured from ATCC) using the primers # 1-4 in **Table 7.1** and cloned into two tandem multiple cloning site (MCS) of pET-Duet vector, using the enzymes *BamHI* and *Sall* for *MjFHα* subunit; *NdeI* and *XhoI* for *MjFHβ* subunit such that they can be co-expressed from the same plasmid. For expressing the individual subunits separately, the same primers and restriction sites were used. The cloning was confirmed by insert release and sequencing.

Table 7.1. Sequence of primers used to clone *MjFHα* and *MjFHβ* in pET-DUET vector

#	Primer name	Primer sequence (5' to 3')
1	MjFHα_ <i>BamHI</i> _up	CGCGGATCCGAAAATCTCCGATGTTGTTGTTGAATTATTTAG
2	MjFH α_ <i>Sall</i> _down	ACGCGT CGACT TATAATTTAGCATCCAATTTTATTCTTTTAATTGCC
3	MjFH β_ <i>NdeI</i> _up	CTAATTC CATATG GGAATATACATTTAACAAATTAACAAAAAGATG
4	MjFH β_ <i>XhoI</i> _down	CCGCT CGAGT TATAATCCTATCAATTCATTAAGCTTTTCATAAAC

Sequences corresponding to the restriction sites are in bold.

BL21 (DE3)-RIL strain was used for expression of (His)₆-tagged *MjFHα* and untagged *MjFHβ*. For protein expression, cultures were grown to mid-log phase (OD₆₀₀ of 0.4-0.6) at 37 °C and then pre-chilled at 16 °C for 20 min. IPTG was added for induction to a final concentration of 0.3 mM and grown for 16 h at 16 °C. The cells were harvested by centrifugation and stored at -80 °C until further use. The cell pellets (corresponding to 800 ml culture) once removed from -20°C/-80 °C, were kept on ice for 10 min along with the 30 ml of lysis buffer (20 mM Tris-HCl, pH 8; 5% glycerol; 1 mM DTT and 1 mM PMSF).

The cells were resuspended in the lysis buffer and lysed using 4 cycles of French® pressure cell press (Thermo IEC Inc., USA) at 1000 psi. The cell lysate was cleared of the debris by centrifuging at 30,000 x g for 30 min at 4 °C. The supernatant was carefully decanted without disturbing the pellet and was then incubated at 70 °C in a water bath for 30 min to allow the precipitation of *E. coli* proteins and then centrifuged at 30,000 x g for 30 min and the resulting supernatant recovered. The solution was subjected to polyethylenimine precipitation (0.001% v/v) to remove DNA. The precipitated DNA was removed by centrifugation and the supernatant was subjected to anion-exchange chromatography using a Q-sepharose column. Briefly, the column was equilibrated with the buffer containing 20 mM Tris-HCl, pH 8.0 and 5% glycerol, and the protein solution was injected into the column. 1 column volume of the same buffer was passed to remove any unbound protein. The desired protein was then eluted from the column using gradient of increasing sodium chloride concentration. The eluted protein was checked for purity on SDS-PAGE. Appropriate fractions were pooled and dialysed against buffer containing 20 mM Tris-HCl, pH 7.4 and 5 % glycerol. After dialysis, the protein was aliquoted, flash frozen in liquid nitrogen and stored at – 80 °C for future use or directly used for reconstitution.

7.2.2. Mass spectrometry

For the accurate estimation of the molecular weight of both the subunits of MjFH, the protein sample was analysed using LC-ESI-MS. An aliquot of protein solution of concentration of 1 mg/ml was dialysed against 10 mM ammonium acetate (a volatile buffer) containing 1 mM DTT and used for the analysis. The spectra were acquired in an ESI-QTOF maXis mass spectrometer (Bruker Daltonics, Bremen, Germany), with an online Agilent 1100 series HPLC. The spectrometer was calibrated using an external standard, caesium iodide in the m/z range of 500-6000. The spectra were acquired in the positive ion mode with a capillary voltage of 4500 V. Data processing was done using Data analysis 4.1 software (Bruker Daltonics, Bremen, Germany). The raw spectra were smoothed using 5 cycles of Savitzky-Golay algorithm subsequent to which multiple charge states of the protein were identified through “charge deconvolution” option available in the tool.

7.2.3. Interaction of MjFH α and MjFH β

7.2.3.1. Pull-down

The MjFH α -subunit is tagged at the N-terminus with (His)₆-tag. For checking the interaction of α - with the β -subunit, α -subunit bound Ni-NTA beads were incubated with

an excess of β -subunit and incubated at room temperature for 30 min in buffer containing 20 mM Tris-HCl, pH 7.4. The beads were washed with the same buffer and elution of α -subunit was done using a buffered solution containing 500 mM imidazole. An aliquot of the eluate was loaded onto SDS-PAGE for separation and stained with Coomassie Brilliant Blue (CBB) for visualization.

7.2.3.2. Analytical gel filtration

The oligomeric state of both the subunits and the co-purified protein was probed by size-exclusion chromatography on an analytical Superdex 200 10/300 GL column (10 mm X 300 mm) (GE Health Care Life Sciences) attached to an AKTA Basic HPLC system equipped with UV900 detector. The column was equilibrated with Buffer A (50 mM Tris-HCl, pH 7.4 and 100mM KCl) and calibrated using molecular weight standards; blue dextran (2000 kDa), β -amylase (200 kDa), alcohol dehydrogenase (150 kDa), bovine serum albumin (66 kDa), carbonic anhydrase (29 kDa) and cytochrome c (12.4 kDa). Elution volume of the blue dextran corresponds to the void volume of the column. A standard curve was plotted using ratio of the elution volume to void volume of these standards against their log molecular weight. The flow rate was maintained at 0.5 ml min⁻¹. 100 μ l of purified protein (10 μ M) (MjFH α , MjFH β , and the co-expressed protein) was loaded onto the column and the elution was monitored simultaneously at both 280 nm and 220 nm. The molecular weight of the MjFH subunits and that of the complex was calculated by interpolation of the elution volume on the standard curve. To examine the nature of the inter and intra-subunit interaction, individual and co-expressed subunits were loaded into the column after equilibration with Buffer A containing 1 M NaCl and 2 mM β -mercaptoethanol in two separate chromatographic experiments.

7.2.3.3. Isothermal calorimetry

To examine the thermodynamics of the interaction of α - and β - subunits and to estimate the dissociation constant (K_d) MicroCal VP-ITC machine was used. 681 μ M MjFH β was taken in the syringe and 75 μ M of MjFH α was kept in the cell. 30 injections of 10 μ l each were done and the cell contents were stirred at 300 rpm throughout the titration. The titration was performed at a constant temperature of 25 °C Data were processed using Origin software. The best fit model was used for the K_d estimation.

7.2.4. Characterization of iron-sulfur cluster

7.2.4.1. Reconstitution of the cluster

Reconstitution was performed starting with frozen aliquots of protein stored at -80 °C. The protein solution was incubated in anaerobic chamber (Coy, USA) for 1 h to remove all traces of oxygen. All the subsequent steps were performed under anaerobic condition in the chamber. Standard protocols were followed for reconstitution (Beinert et al., 1996; Yano et al., 1996). Briefly, around 30-60 μ M protein was used for reconstitution. The reconstitution procedure was initiated by the addition of 50 fold excess of DTT to the protein solution followed by stirring for 30 min. Subsequently, 10 fold excess of ferrous ammonium sulfate was added and stirred for 1 h. Following this, 10 fold excess of lithium sulphide/ sodium sulfide was added and stirred for another 3 h. Excess iron and sulfur was removed by dialysing the protein solution against the buffer containing 50 mM Tris-HCl, pH 7.4 and 5% glycerol. The dialysed protein was used for activity measurements.

7.2.4.2. Spectroscopic methods

For detection of metal-thiolate charge transfer band in the visible region, a 30 μ M solution of the protein was taken in an anaerobically sealed 1 cm path length cuvette and a wavelength scan was performed from 600 to 220 nm. For visible CD measurements, 30 μ M protein was taken in a 1 cm path length cuvette that was anaerobically sealed and ellipticity values were recorded from 800 to 280 nm using a Jasco J-810 spectropolarimeter.

7.2.4.3. Colorimetric estimation of iron and acid-labile sulfide in the protein

To estimate the stoichiometry of iron and sulfur the protein solution soon after reconstitution was passed through a Zeba™ Spin Desalting Columns, 7K MWCO, 10 ml, to remove unbound iron and sulphur. Lithium sulphide was used as a sulphide source in reconstitution of protein for use in this experiment. Standard protocol for iron and acid-labile sulphide estimation were followed. Briefly, for iron estimation, 100 μ l protein solution was treated with equal volume of 21.7 % nitric acid and incubated at 95 °C for 30 min. The precipitated protein was removed by centrifugation. The supernatant was reacted with ferene in the presence of ascorbic acid. The blue coloured complex that is formed by the reaction of ferene with ferrous ion is measured at 593 nm. Known concentrations of ferrous ammonium sulphate solution were used to plot the standard curve (Hennessy et al., 1984; Pierik, web document).

For sulphide estimation standard protocol was followed (Beinert, 1983). Briefly, the 200 μ l of protein solution was reacted with 600 μ l of 1% zinc acetate solution and 50

μl of 7% sodium hydroxide to form zinc sulphide. The cloudy solution formed was centrifuged to collect a thick pellet of zinc sulphide. To the pellet 150 μl of an acidic solution of N, N-dimethyl-p-phenylenediamine (DMPD) (0.1 % w/v in 5 N HCl) was added to dissolve the pellet. Immediately, 150 μl of 10 mM ferric chloride solution was added to form methylene blue, the absorbance of which was measured at 670 nm. The presence of protein causes a decreased estimate of methylene blue and hence the readings were corrected by performing the assay on a solution that has equivalent amount of apoprotein. Different dilutions made from a stock solution of 2 mM lithium sulphide dissolved in water were used to plot the standard curve.

7.2.4.4. Native mass spectrometry

Non-covalent mass spectrometry measurements were performed on an ESI-QTOF mass spectrometer (maXis impact, Bruker Daltonics, Bremen, Germany) with an online ESI-nanospray source was used. A 10 μM of MjFH $\alpha\beta$ protein was dialysed against 10 mM ammonium acetate was injected through a nano-flow probe silica tip with inner diameter of 10 μM (New Objectives, Woburn, MA, USA). A syringe pump (operated using a stepper motor) connected to a needle was used for injection of the protein. The protein was passed through a 5 μl loop and subsequently into the spray chamber at the rate of 0.8 $\mu\text{l min}^{-1}$. The source temperature was set at 45 °C with a capillary voltage of 1200 V. The dry gas flow rate was maintained at 5.0 l min^{-1} . Data were recorded in positive ion mode.

7.2.4.5. Electron paramagnetic resonance

For EPR studies the reconstituted protein was concentrated to around 100 μM . In addition to normal buffer components (50 mM Tris-HCl, pH 7.4, 5% glycerol, ferrous ammonium sulphate, and sodium sulfide), 50 % glycerol was also added to the protein. The protein solution was anaerobically transferred to a quartz tube meant for EPR studies. The tube containing the protein was slowly and gently immersed into liquid nitrogen solution. Presence of glycerol ensured that the solution did not freeze. This was essential as freezing could cause expansion of the solution and rupture of the tube. The EPR spectra was recorded on an X-band Bruker ER 200 CW EPR spectrometer equipped with liquid helium cooled cryostat. The spectra were recorded at 4 K and at 60 K. All the spectra were acquired using 9.3 GHz of microwave power. The g-value for the electron was calculated from each of the spectra using the following equation,

$$g = 0.7145 * \nu \text{ (in MHz)} / B_0 \text{ (in Gauss)},$$

where, g is the dimensionless quantity that characterizes the gyromagnetic ratio and the magnetic moment of a particle; ν is the frequency of the microwave used and B_0 is the magnetic field strength in Gauss.

7.2.5. Thermostability of the individual subunits and the complex

Thermostability of the individual subunits and that of the complex was measured using circular dichroism by monitoring the change in ellipticity at 222 nm upon gradual increase in temperature. The proteins were dialysed against buffer containing 20 mM sodium phosphate, pH 6.4. Temperature was increased at the rate of 1 °C min⁻¹. The ellipticity value was recorded at 222 nm at each temperature.

7.2.6. Enzyme activity

7.2.6.1. Spectrophotometric assay

The conversion of fumarate to malate was monitored by a drop in absorbance at 240nm caused by fumarate depletion ($\Delta\epsilon_{240}=22,400 \text{ M}^{-1} \text{ cm}^{-1}$). For activity measurements, the reconstituted protein was dialyzed against 50 mM Tris, pH 7.4 for 3 h in the anaerobic chamber. Dialysis was performed to remove unbound iron and sulfur.

7.2.6.2. Complementation assay

pET-DUET based plasmid constructs expressing individual subunits and the construct co-expressing both the subunits were separately transformed into the *E. coli* ΔfumACB strain (details of the strain mentioned in section 6.2.5) containing the plasmid pACT7. The plasmid encodes for T7 RNA polymerase under a constitutive promoter thereby enabling the use of T7 based expression systems in the strain. The transformants were selected on LB plate containing ampicillin, chloramphenicol and kanamycin. A single colony from the plate was inoculated into 10 ml LB medium and grown overnight. An aliquot of each of the culture was washed three times with autoclaved M9 medium to remove traces of LB medium. The washed cells were resuspended in M9 medium and an aliquot of the suspension was streaked on a minimal medium plate containing the appropriate carbon source (20 mM of either fumarate or malate), 100 μM IPTG and appropriate antibiotics. The plates were incubated at 37 °C for 110 h and growth phenotype was scored.

7.2.7. Structure solution of MjFH beta subunit using X-ray crystallography

Microbatch method (Chayen et al., 1992) was used for screening all the conditions available in Hampton research crystal screen. A 72 well multi-well plate from Grenier-Bio was used. All the screens *viz.*, crystal screen, Index screen, salt screen (96 different

conditions) and PEG-Ion screen containing 48 different conditions were used. 3 μ l of protein and 3 μ l of buffer from different conditions were placed under silicone oil and left undisturbed at room temperature for 3 days, for the crystals to form. Different concentrations of the protein of each subunit were also used and crystal trays were set both in aerobic and anaerobic conditions. After 3 days, the plates were examined under light microscope for the presence of crystals. The crystals obtained were diffracted using a Rigaku RU200 X-ray diffractometer equipped with a rotating anode type light source with an osmic mirror that gives the monochromatic light source of wavelength 1.54179 Å. For detection an image plate of type MAR scanner, 345 mm was used.

For structure solution, various packages available in CCP4 suite (Winn et al., 2011) and Phenix modules (Adams et al., 2010) were used. Briefly, MOSFLM was used for data collection (Battye et al., 2011), REFMAC 5.0 (Murshudov et al., 2011) and Phenix_refine 1.9_1692 (Afonine et al., 2012) for refinements, SCALA for data reduction and scaling (Evans, 2006), and PHASER for phasing (McCoy et al., 2007). The structure solution was obtained using molecular replacement (MR). The template used for MR was *Archaeoglobus fulgidus* FH β -subunit (PDB ID: 2ISB). The structure solution was validated using wwwPDB validation tool (Berman et al., 2003) and deposited in RCSB-PDB (www.rcsb.org) (Berman et al., 2000).

7.3. Results and discussion

7.3.1. Taxonomic distribution and phylogenetic analysis

A survey of Pfam database (Finn et al., 2014) reveals that out of 1140 unique sequences, there are 516 sequences deposited for α -subunit and 503 sequences for β -subunit. The Pfam ID for α -subunit - and β -subunit are PF05681 and PF05683 respectively. Two-subunit architecture of class I fumarate hydratase is seen mostly in archaea and to a lesser extent in prokaryotes. None of the eukaryotic sequences deposited, have two-subunit type class I fumarate hydratase. The multiple sequence alignment of biochemically characterized FHs of both single two subunit type fumarases reveals good sequence conservation (**Figure 7.2**). The alignment also reveals the domain boundary in single subunit type FHs.

It has been noted earlier that the two-subunit L-tartrate dehydratase (L-Ttd) that catalyses the dehydration of L-tartrate to oxaloacetate, has iron-sulfur cluster and share high level of sequence similarity to single-subunit class I fumarases (CI-FH_{ss}) (Reaney et al., 1993). It should be noted that, two subunit class I fumarases (CI-FH_{ts}) were identified later (Shimoyama et al., 2007a). Similarly, the enzyme mesaconate hydratase/mesaconase that catalyzes the conversion of mesaconate to citramalate also shares high degree of

sequence similarity with class I fumarases (Kronen et al., 2015; Kronen and Berg, 2015). Recently, a gene *fumD* has been identified in *E. coli* that has preferential activity on mesaconate over fumarate (Kronen and Berg, 2015). The multiple sequence alignment of protein sequences of L-tartrate dehydratase (L-Ttd), single- and two-subunit type class I FH sequences from different bacteria and archaea, and mesaconate hydratase, shows good degree of sequence conservation that includes the conserved cysteines that are involved in cluster ligation (**Figure 7.3**).

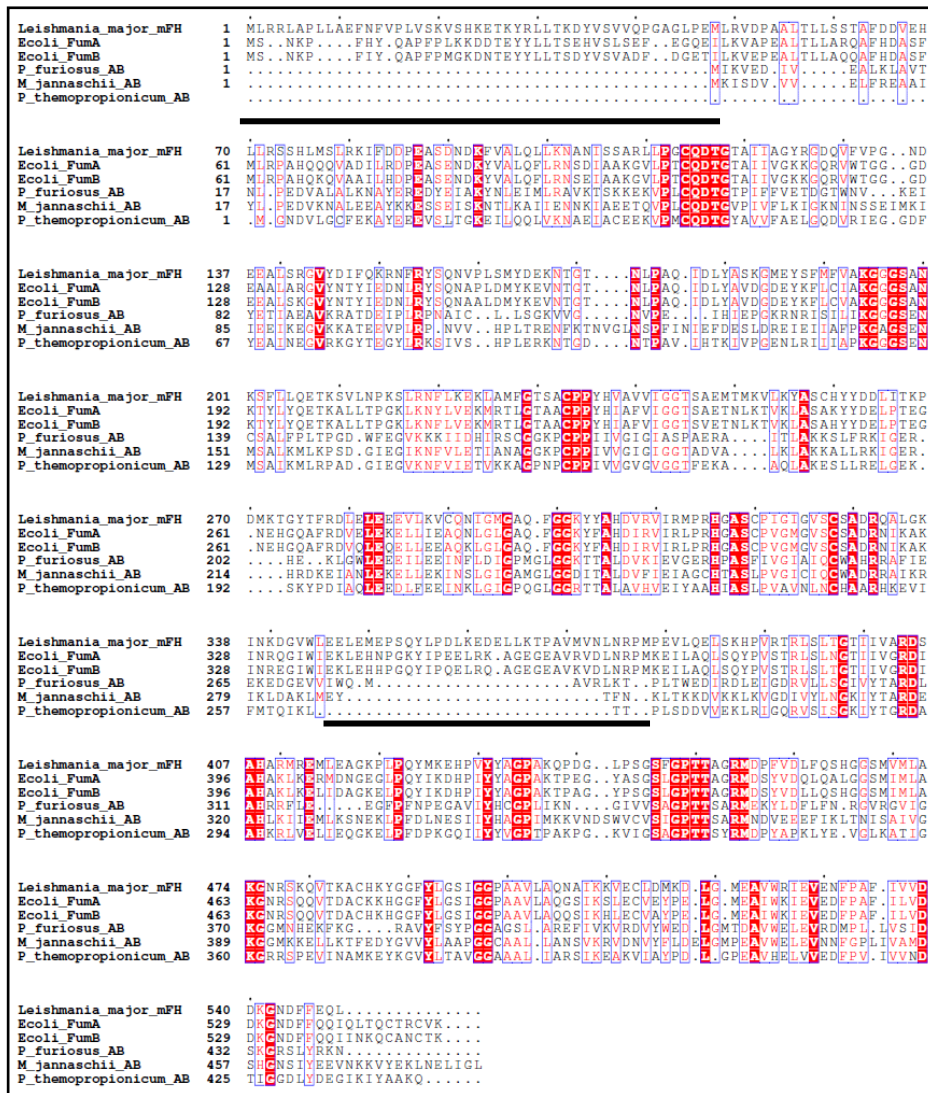


Figure 7.2. Multiple sequence alignment of biochemically characterized FH sequences

The alignment shows good degree of similarity between single-subunit class I fumarate hydratase (CI-FH_{SS}) and two-subunit class I fumarate hydratase (CI-FH_{TS}). It should be noted that CI-FH_{SS} sequences are longer than CI-FH_{TS}. The difference is due to extra residues at the N-terminus and the linker region connecting the two domains. Both these regions are not conserved. The linker region and the N-terminus are highlighted in the figure.

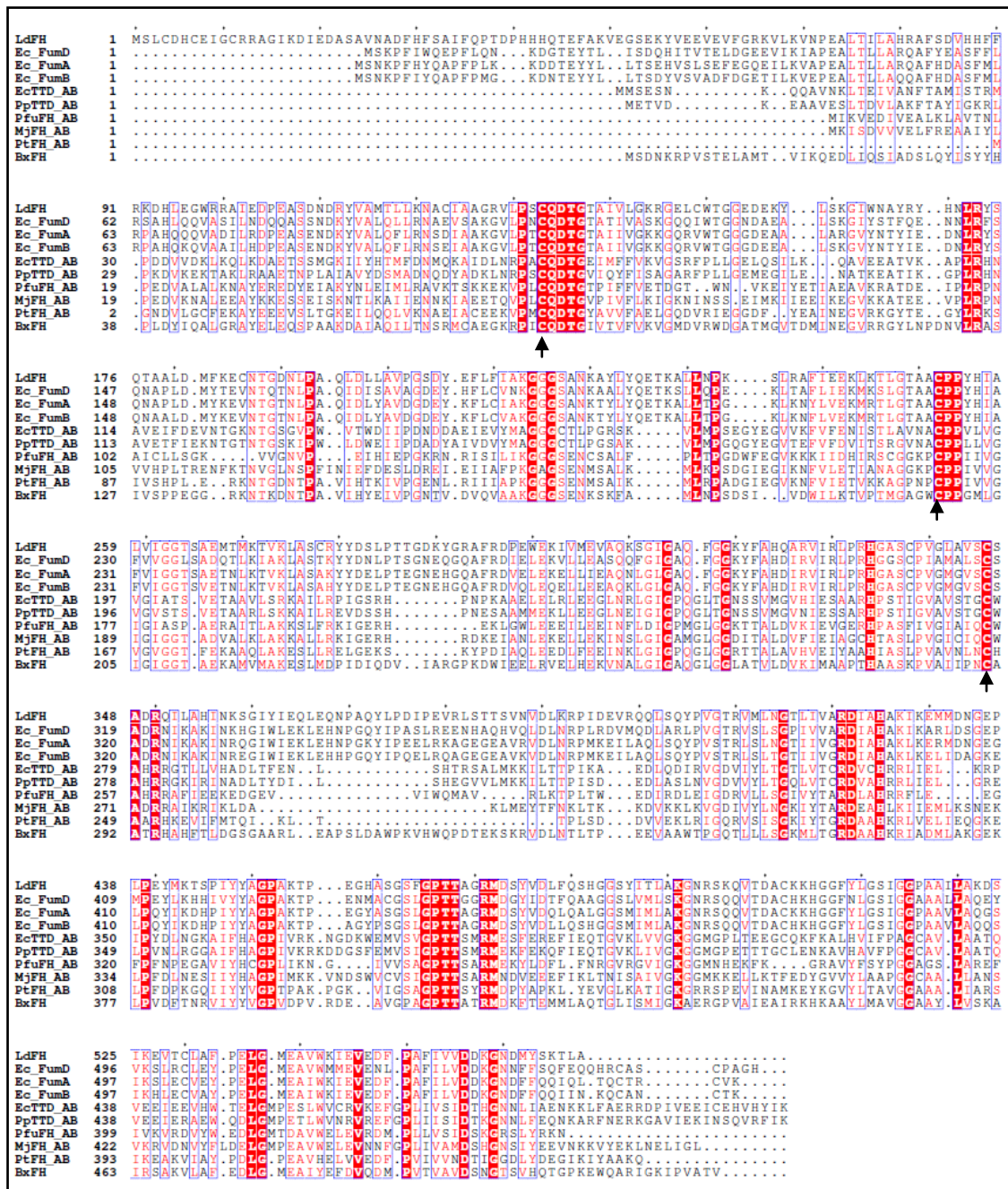


Figure.7.3. Multiple sequence alignment of single-subunit fumarate hydratase (LdFH, Ec_FumA, Ec_FumB, BxjFH), two-subunit fumarate hydratases (MjFH_AB, Pffh_AB, Ptfh_AB), mesaconase (Ec_FumD), and two subunit L-tartrate dehydratase (EcTTD_AB and PpTTD_AB).

The earlier observed high degree of similarity between L-Ttd sequences and class I fumarate hydratase is also seen with two-subunit I fumarate hydratases. Moreover, as is evident from the alignment sequence conservation is also observed between L-tartrate dehydratase, class I FH and mesaconase. Cysteine residues that might be involved in Fe-S cluster ligation are highlighted with an arrow. Ec, *E. coli*; Ld, *Leishmania donovani*; Pp, *Pseudomonas putida*; Bx, *Burkholderia xerovorans*; TTD, L-tartrate dehydratase; Mj, *Methanocaldococcus jannaschii*; Pt, *Pelotomaculum thermopropionicum*; Pfu, *Pyrococcus furiosus*; AB, concatenated sequences of α and β -subunits.

LdFH	100%										
Ec_Fum D	55.8%	100%									
Ec_Fum A	62.9%	67.3%	100%								
Ec_Fum B	62.5%	66.4%	89.5%	100%							
EcTTD_ AB	22.4%	20.4%	21.4%	22.0%	100%						
PpTTD_ AB	23.2%	23.0%	23.2%	23.8%	64.4%	100%					
PfuFH_ AB	24.4%	25.1%	26.7%	26.5%	33.7%	34.4%	100%				
MjFH_A B	28.1%	27.5%	28.7%	28.1	35%	33.9%	45.5%	100%			
PtFH_A B	32.1%	29.8%	32.1%	34.1%	32.3%	31.9%	37.1%	43.4%	100%		
BxFH	27.1%	26.5%	29.0%	28.0%	25.3%	23.8%	33.7%	32.9%	43.4%	100%	
	LdFH	Ec_Fu mD	Ec_Fu mA	Ec_Fu mB	EcTTD_ AB	PpTTD_ AB	PfuFH_ AB	MjFH_ AB	PtFH_ AB	BxF H	

Table 7.1. Protein sequence identity between primary sequences of single and two-subunit fumarate hydratase, two subunit L-tartrate dehydratase, and mesaconase.

It has also been speculated that all fumarases will have mesaconate activity and all mesaconases may have fumarase activity, although with varying level of efficiencies (Kronen et al., 2015). **Table 7.1** provides the identity in percentage between CI-FH_{ss}, CI-FH_{ts}, mesaconase and L-Ttd protein sequences. Sequence features that determine the efficiency of catalysis towards different substrates is still not identified. It should be noted that D-tartrate, mesaconate, and fumarate are also substrates for C II-FH that does not contain Fe-S cluster. **Table 7.2** shows the molecules that were tested for activity/binding on class II FHs (Teipel et al., 1968).

Table 7.2. Specificity of class II fumarate hydratase. The table is reproduced from (Dixon and Webb, 2014)

SPECIFICITY OF FUMARATE HYDRATASE		
<i>Substrates</i>	<i>Competitive inhibitors</i>	<i>Inactive substances</i>
L-malate	D-malate	L-aspartate
fumarate	citrate	D-aspartate
	D-tartrate	fumarate monomethyl ester
	L-2-hydroxy-3-sulphopropionate	fumaric dimethyl ester
	maleate	crotonate
	mesaconate	acetoacetate
	<i>trans</i> aconitate	acetate
	succinate	butyrate
	malonate	acetylenedicarboxylate
	adipate	L-cysteate
	glutarate	
	glycine	

BLASTP results using FumC/FumA sequence from *E. coli* against Cyanobacteria, the most ancient group of bacteria, showed that they have only the class II iron independent enzyme and not the class I FH. This unambiguously shows that class II FHs are more ancestral than class I type FH. To answer the question as to which is a more ancestral protein amongst CI FHs, we checked for the presence of both single and two subunit type fumarases in phylogenetically early branching group of organisms like Firmicutes and Candidate phyla radiation (CPR) group of bacteria (Hug et al., 2016) using the BLASTP tool. We found that with a few exceptions, almost all these organisms have two subunit type class I fumarate hydratase. Hence, we propose that the single subunit fumarate hydratase is a more recent version of FH that resulted after a domain fusion event between the α and β subunits of CI-FH_{ts}.

A phylogenetic analysis reveals that the two subunit type FH forms a separate clade that clusters separately (**Figure 7.4**). In addition, the two subunit type enzymes are further divided into two subtypes. The significance of this divergence is not clear. L-tartrate dehydratases, that catalyse the conversion of tartrate to oxaloacetate share close similarity with two subunit class-I fumarases. L-ttd are absent in eukaryotes and are present only in archaea and prokaryotes. The β -subunit of class I fumarate hydratases in few instances are fused to domains other than alpha subunit; to protein kinase domain in *Strongylocentrotus purpuratus* (W4Y8Y1_STRPU), fumarate reductase flavoprotein in *Amphimedon queenslandica* (Sponge)(I1EJK5_AMPQE), and to serine acetyltransferase domain in *Entamoeba dispar* (B0EPH7_ENTDS). Similarly, in one sequence (*Yersinia enterocolitica*, W8TUY3_YEREN) the alpha subunit is fused to a haloacid dehalogenase like hydrolase domain.

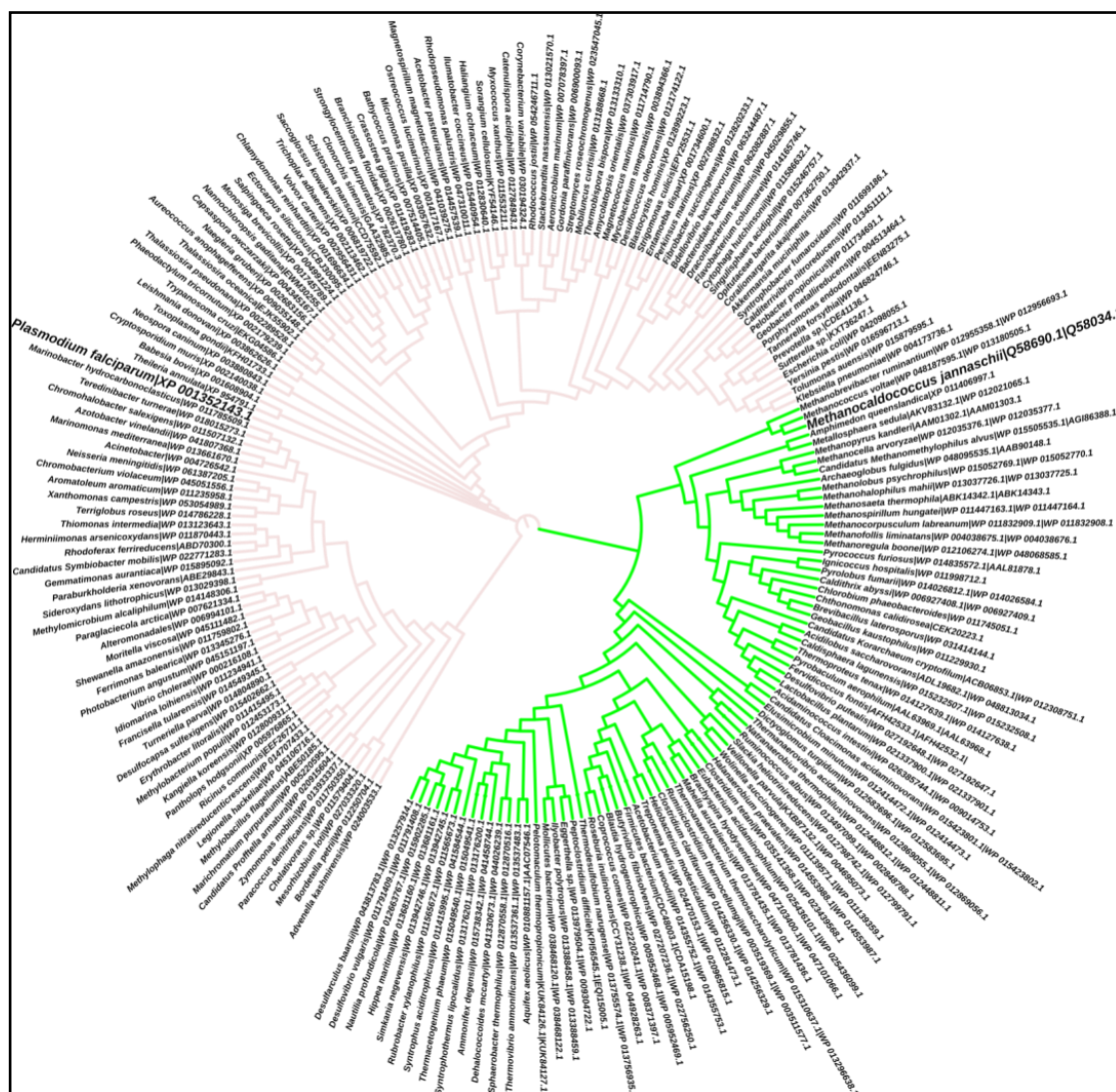


Figure 7.4. Phylogenetic tree of class I fumarate hydratases.

Single-subunit class I FH and concatenated sequences of two-subunit class I FH, representing all the taxa in which these proteins are present were used for the analysis. The alignment, evolutionary model selection and the tree construction were done using MEGA 7.0. The tree is not bootstrapped and is presented here just to show that the two subunit FH sequences (shown in green lines) segregate into a separate branch. MjFH and PffFH representing two and single subunit FH respectively, are highlighted using bigger font. The name of the organism and the accession number of the protein sequence used are presented.

7.3.2. Cloning, expression and purification

Based on previous reports available, it was clear that the two subunits of FH when expressed heterologously, associate strongly to form a complex. However, information on the role of each subunit with respect to their structure and function was unknown. In order to have a holistic understanding of the CI-FH_{ts}, we made clones to express the individual subunits, which will be denoted as MjFH α and MjFH β subunits, as well as to co-express the subunits.

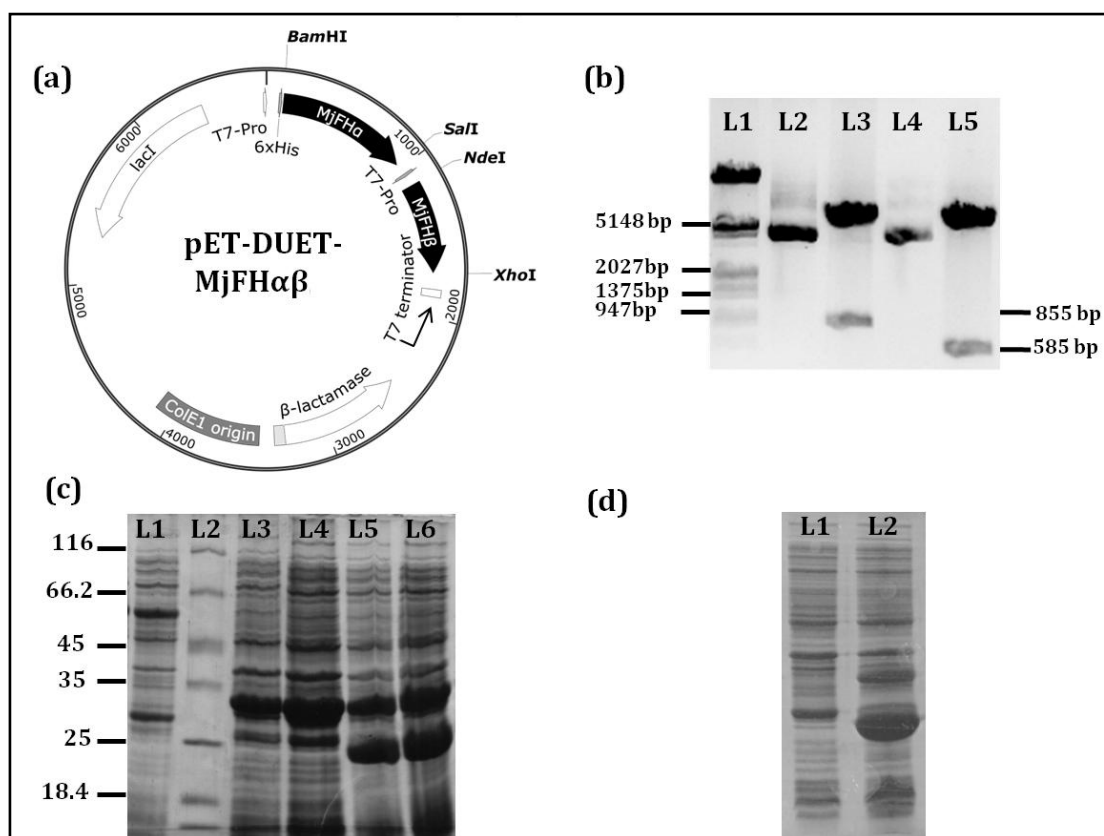


Figure 7.5. Cloning and expression of MjFH subunits.

(a) Vector map showing the restriction enzymes sites used for cloning the two subunits of MjFH. MjFH α subunit was cloned into BamHI and SalI sites, whereas the β -subunit gene was cloned into NdeI and XhoI sites. MjFH α subunit is expressed with a N-terminal (His)₆-tag and the MjFH β subunit is expressed as an untagged protein. **(b)** Cloning of both subunits was validated by releasing the insert using appropriate restriction enzymes. L1, DNA ladder; L2 and L4, undigested supercoiled plasmid DNA (pETDUET) containing MjFH α and MjFH β genes respectively; L3, plasmid DNA, pETDUET-MjFH α digested with BamHI and SalI, releasing the insert corresponding to MjFH α gene of size 855 bp; L5, plasmid DNA digested with NdeI and XhoI, releasing the insert corresponding to MjFH β gene of size 585 bp. **(c)** SDS-PAGE showing the expression of MjFH α and MjFH $\alpha\beta_{CE}$. L1, lysate from uninduced BL21 (DE3)-RIL cells; L2, protein molecular weight maker (molecular weight of the maker proteins are given in kDa); L3 and L4, cell lysate corresponding to 150 μ l and 250 μ l of induced culture expressing MjFH α , respectively; L5 and L6, cell lysate corresponding to 150 μ l and 250 μ l of induced culture expressing MjFH $\alpha\beta_{CE}$, respectively. **(d)** SDS-PAGE showing the expression of MjFH β in BL21(DE3)-RIL strain. L1, cell lysate corresponding to 150 μ l uninduced culture expressing MjFH β and L2, cell lysate corresponding to 250 μ l of induced culture expressing MjFH β . 300 μ M IPTG was used for all inductions.

The clones were made in pET-DUET vector that permits co-expression of genes from independent promoter (**Figure 7.5 a**). The complex containing the both the subunits obtained by co-expression will be referred to as MjFH $\alpha\beta$. All the clones were made and validated by insert release (**Figure 7.5 b**) and sequencing. The clones generated were

used for protein expression in BL21 (DE3)-RIL strain. Upon induction with 300 μ M IPTG, there was a significant overexpression of desired protein/s. (**Figure 7.5 c and d**).

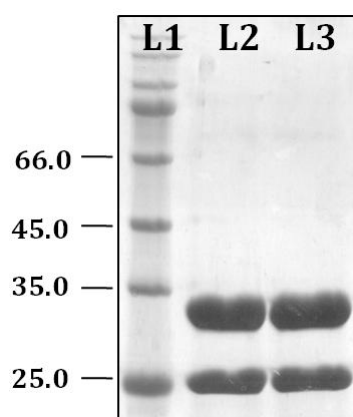


Figure 7.6. Ni-NTA chromatography on lysate from cells co-expressing both subunits.

SDS-PAGE of eluates from Ni-NTA chromatography showing the presence of both subunits. This suggests strong interaction between the subunits. L1, protein molecular weight marker (molecular weight in kDa indicated to the left of the panel); L2, 250 mM imidazole eluate 1; L3, 250 mM imidazole eluate 2.

Ni-NTA chromatography was performed on the lysate from cells co-expressing both the subunits. The imidazole eluates were analysed using SDS-PAGE. As shown in **Figure 7.6**, the eluates contained both (His)₆-tagged MjFH α subunit along with the untagged MjFH β subunit. This indicates that the two subunits interact and form a tight complex. Thus the FH subunits from *M. jannaschii* interact with each other as observed for two-subunit class I FH from other organisms (Shimoyama et al., 2007a; van Vugt-Lussenburg et al., 2009b). For all further studies we used the protein purified by thermal precipitation followed by anion-exchange chromatography, as the yield of the protein was much higher compared to that of Ni-NTA chromatography.

Purification profile of the MjFH α and MjFH β that involved thermal precipitation of *E. coli* proteins followed by anion exchange chromatography is presented in **Figure 7.7 a and b**. Upon purification of the co-expressed subunits using the same protocol, it was found that the fractions obtained after anion exchange had both MjFH α and MjFH β (**Figure 7.7 c**). This is in agreement with the behavior of the subunits in Ni-NTA chromatography. The purity of the subunits and that of the complex were examined by SDS-PAGE (**Figure 7.7 d**).

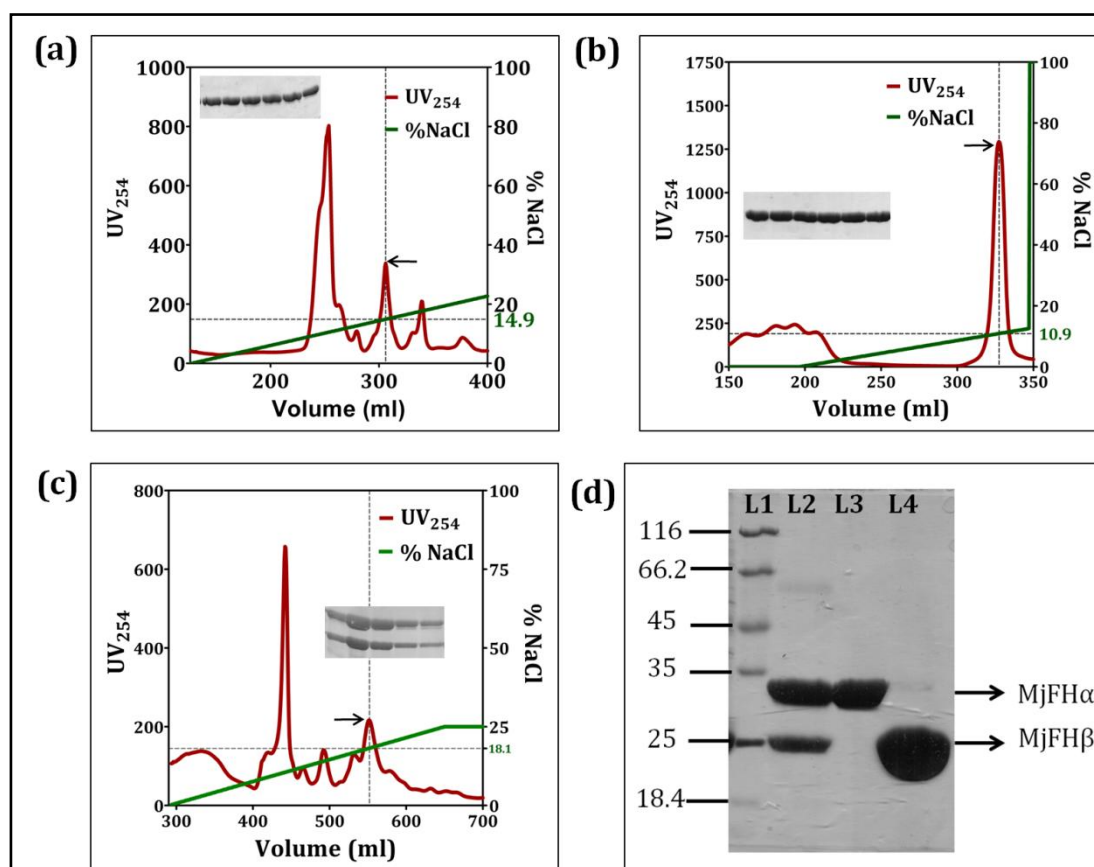


Figure 7.7. Purification of MjFH α , MjFH β and MjFH $\alpha\beta$.

(a) Elution profile from anion-exchange chromatography showing the purification profile of MjFH α . The protein was eluted with NaCl gradient and fraction containing pure protein was obtained at around 15 % NaCl (indicated by an arrow). Inset shows the SDS-PAGE of the protein fractions. **(b)** Elution profile from anion-exchange chromatography showing the purification profile of MjFH β . The protein was eluted with NaCl gradient and fraction containing pure protein was obtained at around 11 % NaCl (indicated by an arrow). Inset shows the SDS-PAGE of the protein fractions under the corresponding peak indicated by the dotted vertical line. **(c)** Elution profile from anion-exchange chromatography showing the purification of MjFH $\alpha\beta$. The protein was eluted with NaCl gradient and fractions containing pure protein were obtained at around 18 % NaCl (indicated by an arrow). Inset shows the SDS-PAGE of the protein fractions. MjFH α and MjFH β when co-expressed purify together as a complex. **(d)** SDS-PAGE of purified MjFH subunits. L1, protein molecular weight marker (molecular weight of the marker proteins are shown in kDa); L2, purified MjFH $\alpha\beta$; L3, purified MjFH α ; L4, purified MjFH β .

7.3.3. Oligomeric state and subunit interaction

To determine the oligomeric state of the subunits and that of the complex, analytical size exclusion chromatography was used. The column was calibrated with proteins of known molecular weight (mentioned in **Figure 7.8 a**) and a standard curve was obtained by linear regression. The equation of the line obtained from the fit was,

$$Y = [(-1.53) * V_e/V_o + 4.61],$$

where Y is log molecular weight of the protein, V_e , the elution volume of protein and V_o , the void volume. The void volume is the elution volume of blue dextran which was 8.545 ml. 100 μ l of protein solution containing 10 μ M of each of the protein (individual subunit/complex) was injected to estimate the elution volume. The molecular weight was calculated from the elution volume by interpolation in the standard curve. The elution profile of the individual subunits and that of the complex is shown in **Figure 7.8 b**. The elution volume of different proteins is given in **Table 7.3**. From the table it is clear that MjFH α is a constitutive dimer and MjFH β is a monomer.

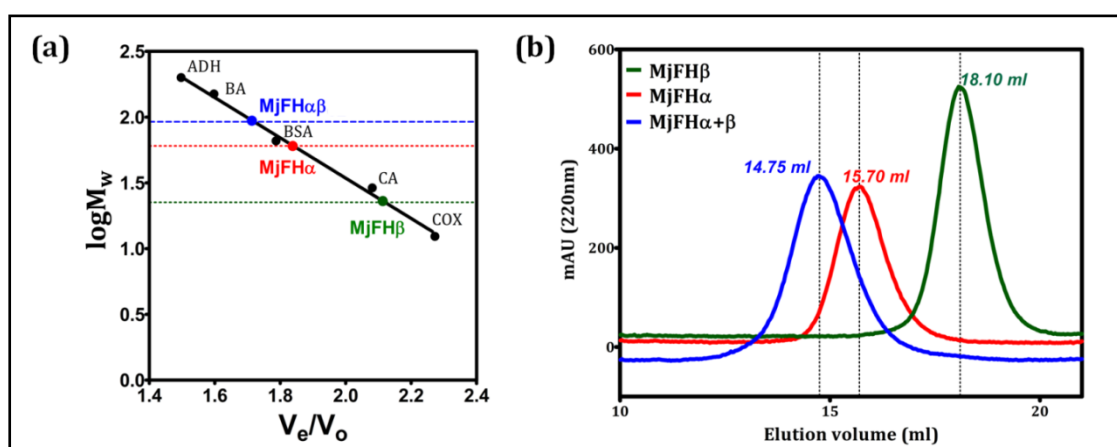


Figure 7.8. Analytical gel filtration to infer oligomeric status of MjFH.

100 μ l of 10 μ M protein solution was injected into an analytical gel filtration column that was equilibrated with 50 mM potassium phosphate buffer containing 100 mM potassium chloride. The flow rate was maintained at 0.5 ml/min and the eluate from the column was continuously monitored at 220 nm. The column was calibrated with proteins of standard molecular weight (shown in the inset). **(a)** Standard curve fit using elution volume (black dots) of standard proteins indicated. ADH, alcohol dehydrogenase; BA, β -amylase; BSA, bovine serum albumin; CA, carbonic anhydrase; COX, cytochrome *c*-oxidase. **(b)** Overlay of chromatograms corresponding to MjFH α , MjFH β , and MjFH $\alpha\beta$. The elution volume of these proteins shows that MjFH α is a constitutive dimer; MjFH β is a monomer and MjFH $\alpha\beta$ is dimer of a heterodimer ($2\alpha+2\beta$).

The elution volume of the complex is close to the expected molecular weight of the complex containing dimer of a heterodimer. Hence, the complex contains two subunits of MjFH α and two subunits of MjFH β . The α -subunit remained associated as a dimer even in the presence of 2 mM β -mercaptoethanol and also in 1M KCl. Similarly, the elution volume of the complex remained unchanged under these conditions. This suggests that the MjFH α dimer and complex assemble tightly and are not broken by salt and the possibility of disulfide bonds in these interactions can also be ruled out. However, it should be noted that not all disulfide bonds can be readily reduced by β -ME.

Table 7.3. Oligomeric state of MjFH

Protein	Condition	Elution volume	M. wt (calc.)	M. wt of monomer (thoret.)	Oligomeric state
MjFH α	AGF Buffer	15.70	60.39	32.56 (α)	Dimer
MjFH α	AGF buffer+ 1M KCl	15.71	59.87	32.56 (α)	Dimer
MjFH α	AGF buffer+ 2 mM β -ME	15.70	60.39	32.56 (α)	Dimer
MjFH β	AGF buffer	18.10	22.69	21.86 (β)	Monomer
MjFH $\alpha\beta$	AGF buffer	14.75	92.20	54.43 ($\alpha+\beta$)	2 α +2 β
MjFH $\alpha\beta$	AGF buffer+ 1M KCl	14.65	94.28	54.43 ($\alpha+\beta$)	2 α +2 β
MjFH $\alpha\beta$	AGF buffer+ 2 mM β -ME	14.68	93.12	54.43 ($\alpha+\beta$)	2 α +2 β

AGF, analytical gel filtration buffer: 50 mM Tris-HCl, pH 7.4.

To probe further into the stoichiometry of the complex and to understand the nature of the interaction, we resorted to isothermal calorimetry. Binding of the two subunits would result in a heat change which can be monitored using a calorimeter. For this, 70 μ M of MjFH α and 681 μ M of MjFH β , in 50 mM potassium phosphate buffer containing 2 mM TCEP, were taken in cell and syringe of the calorimeter, respectively. Titration of α -subunit with β -subunit showed an endothermic heat change with ΔH value of 4.156 kCal/mol and positive entropic contribution with ΔS value of 42.1 cal/mol/deg. An endothermic heat change in an interaction happens when more number of bonds are broken than formed. This usually happens when the association is dominated by hydrophobic interactions thereby causing release of water molecules from the subunit surfaces that would eventually become the interface (Abraham et al., 2005; Luke et al., 2005; Tanford, 1978). Hence, it can be concluded that the interaction of the subunits is entropically favored and enthalpically disfavored. The thermogram obtained from the subunit titration was subtracted from that obtained using just the titration of MjFH β with buffer. The resultant thermogram is shown in **Figure 7.9**. It fits best to one-site binding model. The equation of the model used is as given below and is reproduced from 'ITC data analysis in Origin' manual, MicroCal, LLC, USA pg. 106-107;

$$Q = \frac{nM_t \Delta H V_o}{2} \left[1 + \frac{X_t}{nM_t} + \frac{1}{nKM_t} - \sqrt{\left(1 + \frac{X_t}{nM_t} + \frac{1}{nKM_t} \right)^2 - \frac{4X_t}{nM_t}} \right]$$

where K = Binding constant; n = # of sites; V_o = active cell volume; M_t and $[M]$ are bulk and free concentration of macromolecule (MjFH α) in V_o ; X_t and $[X]$ are bulk and free concentration of ligand (in this case MjFH β), and θ = fraction of sites occupied by ligand X ; $Q = n M_t \Delta H V_o$.

This is in agreement with the stoichiometry of the complex as inferred through analytical gel filtration. The K_d value of the interaction was found to be 694 nM. Thus, it can be concluded that the complex has two copies of MjFH α and two copies of MjFH β .

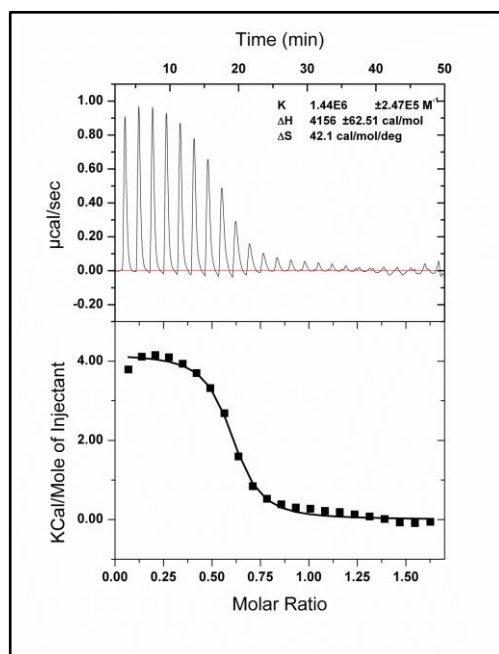


Figure 7.9. Thermogram obtained by titration of MjFH α with MjFH β in an isothermal calorimeter.

Titration of MjFH β (in syringe) with MjFH α (in cell) shows that the K_d value of the interaction is 694 nM. The thermogram fit well to a one-site binding equation, in Origin data processing suite for ITC, further confirming that there is 1:1 stoichiometry in the MjFH $\alpha\beta$ complex.

7.3.4. Biophysical characterization and thermostability

Aromatic amino acids in proteins exhibit fluorescence properties when excited in the UV region of electromagnetic spectrum. Unique among these residues is the tryptophan fluorescence that is highly sensitive to the environment because of the large excited state dipole moment (Pierce and Boxer, 1995). Hence, intrinsic tryptophan fluorescence, in particular the λ_{\max} (emission) and the intensity of emission, in proteins provide a qualitative understanding of the tryptophan environment. A well buried tryptophan exhibits a blue shifted emission maximum that ranges from 309 nm as seen in azurin protein to 335 nm in a partially buried configuration, whereas a completely solvent exposed tryptophan has an emission maximum of around 350 nm. In general, tryptophan being a hydrophobic residue is expected to be found in the hydrophobic core of the protein, in the oligomeric interfaces or in the interface of two interacting proteins. Hence,

the λ_{\max} of emission of intrinsic tryptophan fluorescence of proteins is used as an indicator of how well the protein is folded. (Teale and Weber, 1957; Szabo et al., 1983; Royer, 2006).

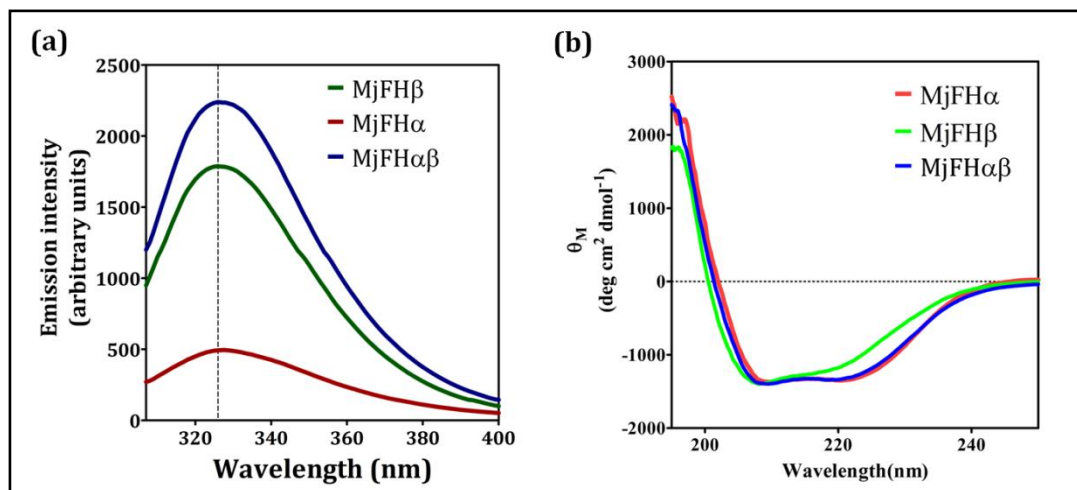


Figure 7.10. Intrinsic tryptophan fluorescence and far-UV circular dichroism spectra of MjFH.

(a) Intrinsic tryptophan fluorescence of individual subunits of MjFH and that of the complex. The emission maxima is indicated by a dotted vertical line and corresponds to 326 nm. This corresponds to a buried tryptophan and hence, a well folded protein. **(b)** Far-UV CD measurement of the $\alpha\beta$ complex and the individual subunits of MjFH using. The CD profile shows that all the three protein samples have well ordered secondary structure.

MjFH α and MjFH β have one and two tryptophans, respectively in their primary sequence. Intrinsic tryptophan fluorescence from the individual subunits and from the complex, when excited at 295 nm showed a λ_{\max} of emission of 326 nm (dotted line in Figure 7.10 a), suggesting that all the proteins are well folded (**Figure 7.10**). Since multiple factors influence intensity of fluorescence emission and not much information can be inferred from steady state fluorescence studies, interpretation on the intensity value of the individual subunits and of the complex would need further experimental validation. Examination of far-UV circular dichroism spectra of MjFH α , MjFH β , and MjFH $\alpha\beta$ (**Figure 7.10 b**) confirms well ordered secondary structure in these proteins. For both fluorescence and CD experiments the proteins were dialyzed against 20 mM potassium phosphate buffer, pH 6.4 and the spectra shown are blank (buffer alone) subtracted. Melting experiments using far-UV circular dichroism spectropolarimeter showed that both the individual subunits and the complex were indeed thermostable with T_m of around 90 °C (**Figure 7.11**). There was a slight increase in the thermostability of MjFH α upon complex formation.

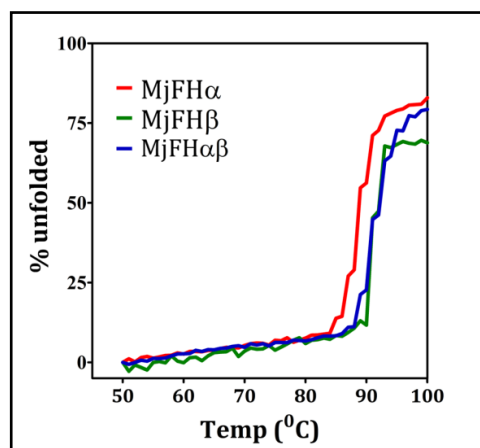


Figure 7.11. Thermostability of the MjFH α , MjFH β and MjFH $\alpha\beta$.

(a) Thermostability of the individual subunits and that of the complex of MjFH. The ellipticity at 222 nm was measured as a function of temperature as the measure of the protein stability. It can be seen from the profile that MjFH β is slightly more stable than that of MjFH α and the complex is as stable as that of MjFH β . This suggests that complex formation leads to slight increase in the stability of MjFH α .

7.3.5. Mass spectrometry of MjFH subunits

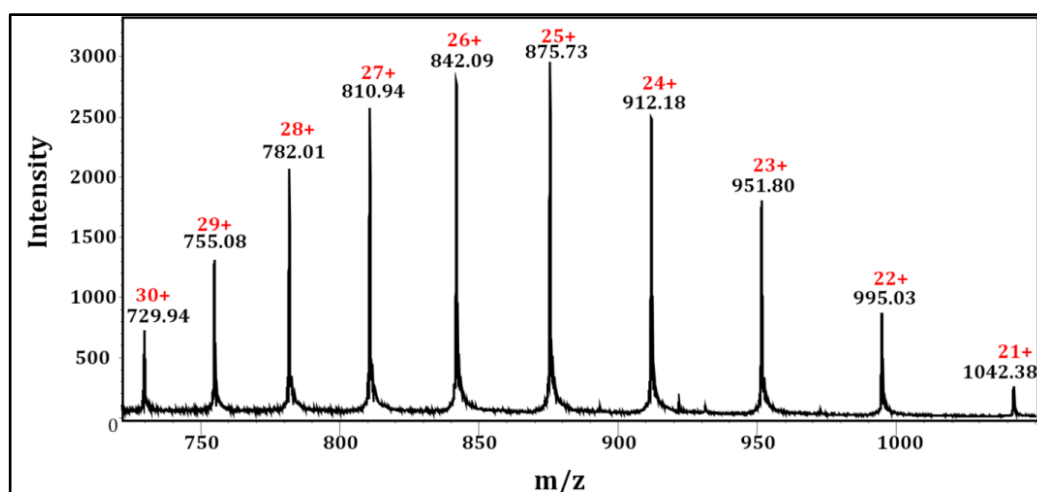


Figure 7.12. ESI-MS of purified MjFH β protein.

The mass of purified MjFH β was measured by LC-ESI-MS. The charge state of the peak was automatically assigned using 'Charge deconvolution' option in the Bruker data analysis tool. The observed mass of the protein is 21868 Da which is in agreement with the theoretical mass of the protein, 21868 Da.

Mass spectrometry of the individual subunits showed that MjFH β -subunit exists as single species with mass (21868 Da) close to that theoretically calculated mass of 21868 Da for the full length protein (**Figure 7.12**).

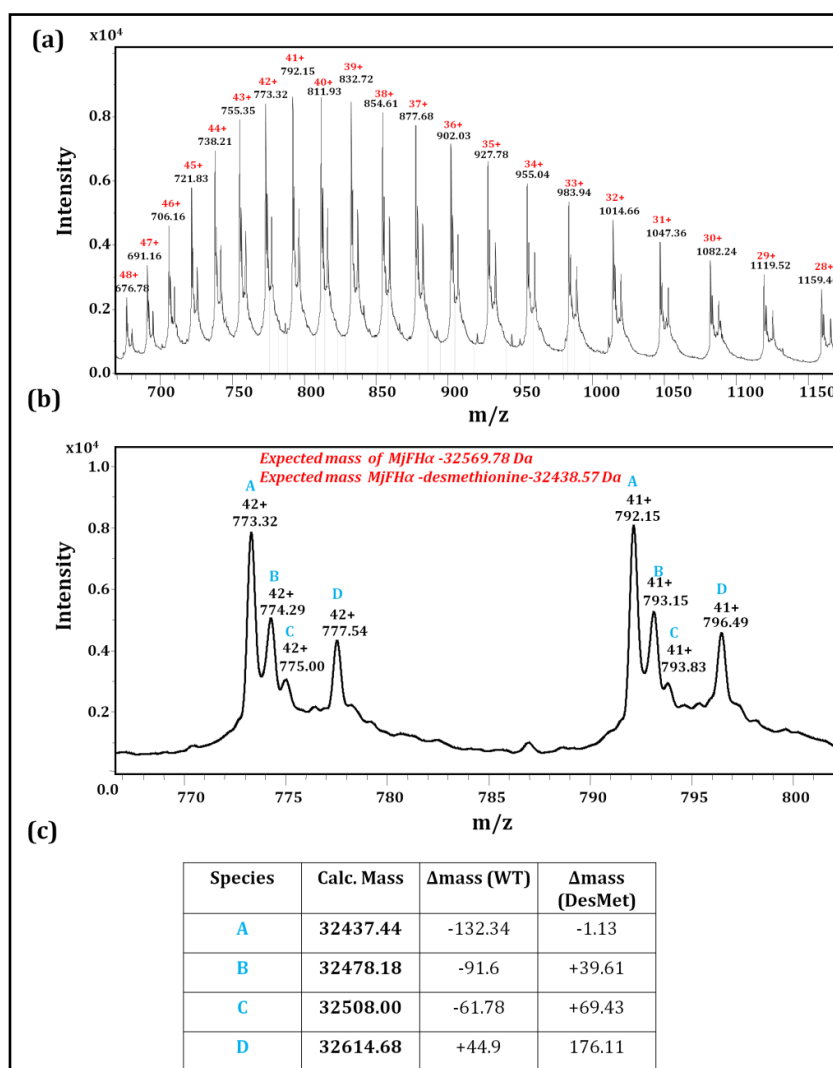


Figure 7.13. ESI-MS of purified MjFH α .

(a) ESI-MS showing the charge state distribution of MjFH α . **(b)** Two of the charge states 42+ and 41+ have been zoomed-in for better clarity. As can be seen, there are four different species (A, B, C, and D) present in each of the charge states. **(c)** Table showing the calculated mass of the four different species along with difference in mass from the wild-type and desmethionine forms of the protein. Major form of the protein is the desmethionine form.

The alpha subunit on the other hand showed four different populations (**Figure 7.13 b**), with the major population being the desmethionine form of the protein (**Figure 7.13 c**). Species B and D might correspond to acetylated form of the desmethionine and the wild-type protein respectively. It is known that removal of the initiator methionine from the N-terminus is often key for the stability of the protein. The initiator methionine is removed by methionine aminopeptidases that are present in all kingdoms of life. The extent of removal of the initiator methionine is dependent on the neighboring residues (Liao et al., 2004).

7.3.6. Type of the cluster and stoichiometry

For all the experiments described in this section reconstituted protein was used. For proteins containing 3Fe-4S clusters, addition of just excess iron in the presence of reducing agent is shown to be enough to obtain a 4Fe-4S cluster and hence an active enzyme (Flint et al., 2002; Kennedy and Beinert, 1988; Hofmeister et al., 1994; van Vugt-Lussenburg et al., 2013). However, upon purification of the MjFH proteins, we found that there was not enough iron and sulphide content corresponding to 3Fe-4S cluster and hence, in addition to excess iron, a sulphide source was also used. This protocol is generally followed for reconstituting the cluster in aerobically purified apoproteins (Yano et al., 1996; Liu et al., 2016).

7.3.6.1. Spectroscopic characterisation

Metalloenzymes in which the metal ion is coordinated to a electronegative ligand exhibit ligand to metal charge transition (LMCT). Depending on the electronegativity of the ligand the absorption is either in the visible region or in the UV region. For soft ligands (weak electronegativity) like sulfur, LMCT absorption is observed as intense band in the low energy visible region (Solomon et al., 2006; Bertini et al., 2006). This property is responsible for the brown coloration of Fe-S cluster containing proteins.

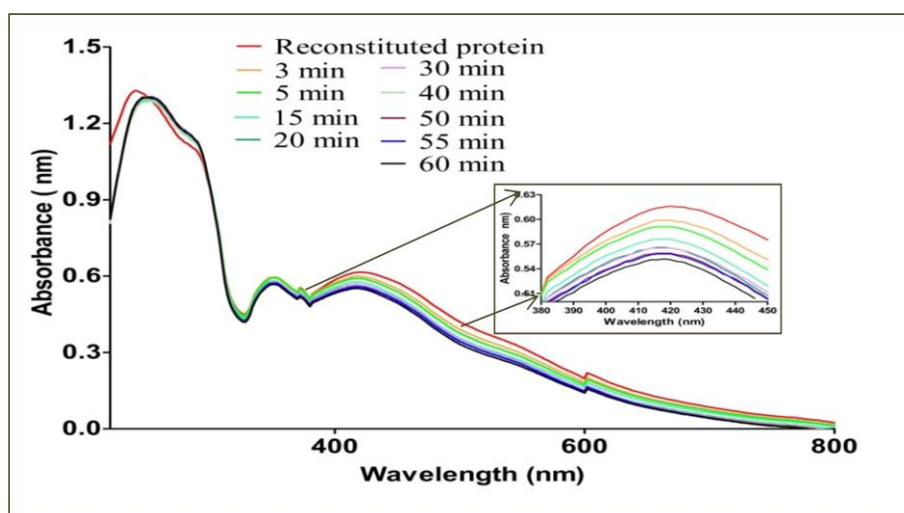


Figure 7.14. Presence of Fe-S cluster in MjFH $\alpha\beta$.

Upon spectrophotometric examination of the reconstituted protein it was evident that there was an absorbance peak around 420 nm which usually corresponds to the presence of 4Fe-4S cluster. Further, upon exposure to air, there was a time-dependant drop in the intensity of the 420 nm peak alone but not that corresponding to 280 nm. This shows that the cluster, as expected, is oxygen sensitive and hence degrades with time, thereby, causing a drop in absorbance at 420 nm.

Wavelength scan of the reconstituted α/β -complex showed two absorbance maxima in the visible region, one at 415nm and the other at 360 nm (**Figure 7.14**). This is characteristic of a 4Fe-4S cluster (Evert C. Duin et al., 1997). Moreover, upon exposure to air there was a time dependent drop in the absorbance in these regions suggesting oxidation of the cluster (shown in the inset of the figure). Broadness of the peak seen in absorption spectra is due to multiple unresolved transitions. In such cases use of circular dichroism comes handy, provided the molecule is chiral or has groups in chiral environment. The S to Fe (II)/ (III) charge transition band displays Cotton effect. Iron-sulfur proteins have been studied extensively using visible CD (Stephens et al., 1978). The phenomenon wherein there is a change in the ellipticity/optical rotation with change in wavelength around the absorption region of the chromophore is called Cotton effect. Because Fe-S cluster containing proteins absorb in the visible region and since they reside in the chiral environment of the protein, Cotton effect is displayed. One can infer the absorption maxima of the chromophore from the point of inflection (where the curve reaches zero) of the bisignate CD spectrum. In many cases, visible CD is considered to be more sensitive to changes in cluster environment compared to that of absorption spectra (Stephens et al., 1978).

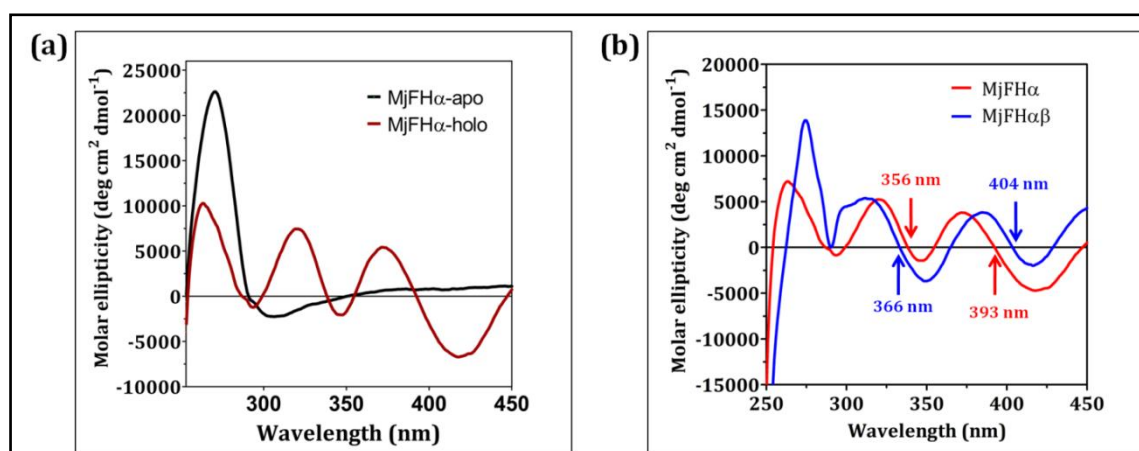


Figure 7.15. Visible circular dichroism for Fe-S reconstituted MjFH α and MjFH $\alpha\beta$.

(a) Comparison of the CD spectrum of MjFH α apo and the holo protein. Unlike for the apoprotein, the holoprotein exhibits a dichroic pattern in the visible region. **(b)** Comparison of the visible CD profile of MjFH α and MjFH $\alpha\beta$. Though the overall pattern in the visible region remains the same, it should be noted that the inflection point for MjFH $\alpha\beta$ is 404 nm that is 11nm different from that of the MjFH α holo protein. There is also a 10 nm shift in the absorption band around 360 nm. This clearly shows that addition of MjFH β does have an effect on the iron-sulfur cluster. It should also be noted that the cluster in both these proteins displays negative Cotton effect which is pronounced for MjFH α at the 404nm region and MjFH $\alpha\beta$ at the 366 nm region.

CD spectra of the holo MjFH α (**Figure 7.16**) shows characteristic pattern seen for Fe-S cluster containing proteins. The unreconstituted protein doesn't show any CD effect in the visible region. Moreover, the CD spectrum of the MjFH $\alpha\beta$ was slightly different from that of MjFH α (**Figure 7.16 b**) which might be due to changes in the cluster environment brought about by the binding of MjFH β . This suggests that MjFH β might be in close proximity of the cluster. As the iron-sulfur cluster is essential for its activity (see section 7.3.7), we used visible CD to probe the environment of the cluster as a function of temperature.

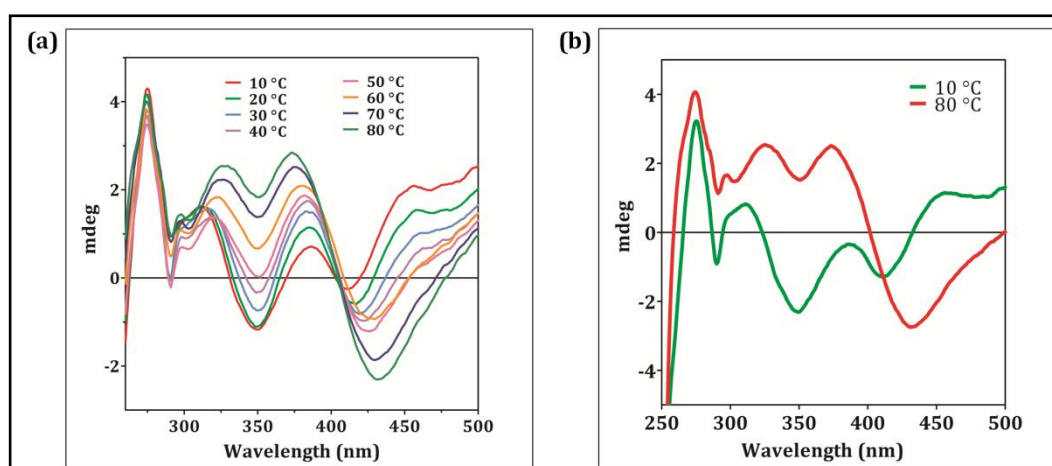


Figure 7.16. Effect of temperature on cluster environment.

(a) Visible CD spectra were acquired for MjFH $\alpha\beta$ at different temperatures under anaerobic conditions. An obvious observation is the increase in the magnitude of negative Cotton effect in the 400 nm region and decrease in the 360 nm region. (b) For better clarity the visible CD spectra obtained at 10 °C and at 80 °C alone are shown. It can be seen that there are significant changes in the cluster environment upon increase in temperature. Its relevance to structure and function of the protein needs further investigation.

An overlay of the spectrum at different temperatures (**Figure 7.16**) showed that there are significant changes in the cluster environment with respect to temperature. The exact mechanism causing the change needs to be understood by further experimentation.

7.3.6.2. Electron paramagnetic resonance (EPR)

To further validate the nature of the cluster, EPR analysis was done on reconstituted MjFH α and MjFH $\alpha\beta$. The characteristic pattern with a g-value of 2.01 observed in the spectrum of both the proteins is typical of an oxidized form of 3Fe-4S cluster (**Figure 7.17**). Spin lattice relaxation rate varies with the nature of the cluster with the least value for [2Fe-2S] cluster followed by [3Fe-4S] and [4Fe-4S]²⁺. Since the relaxation rate for

[2Fe-2S] is the least, its EPR signal should be observed at temperatures in the range of 60-100 K (Bennett, 2010a). The fact that the EPR signal completely disappeared at 60K for both MjFH α and MjFH $\alpha\beta$ supports the [3Fe-4S] nature of the cluster. Sensitivity of the peak intensity to changes in temperature in the range of 10-60 K for both protein preparations further confirmed the nature of the cluster. This is in concordance with earlier reports on class I FH from other organisms (Shimoyama et al., 2007b; Flint et al., 2002; van Vugt-Lussenburg et al., 2013).

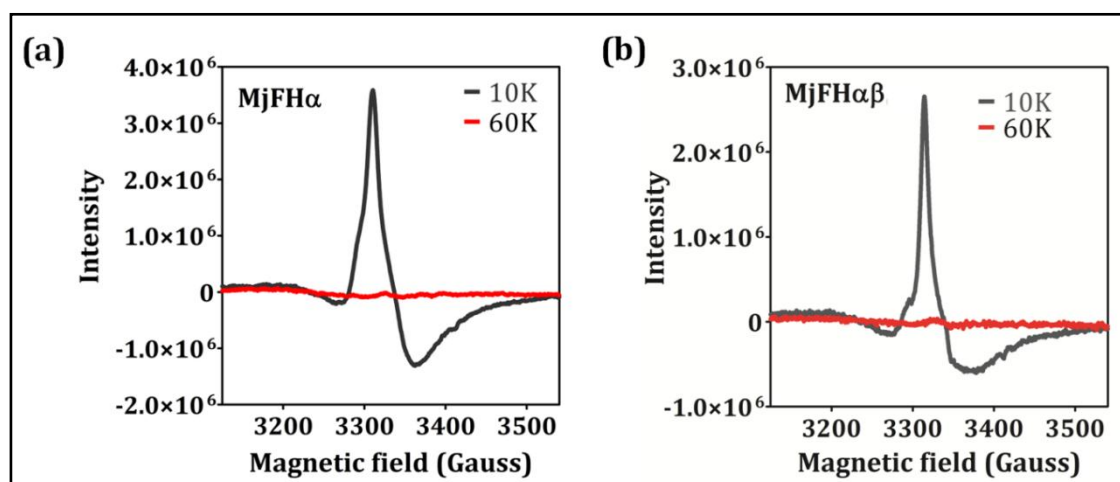


Figure 7.17. EPR spectroscopic analysis of reconstituted MjFH α and MjFH $\alpha\beta$.

(a) 100 μ M reconstituted MjFH α was used for the analysis. The B_0 value at maximum intensity of the signal was 3309.08 gauss. This corresponds to a g -value of 2.01. The EPR pattern clearly corresponds to an oxidized form of the [4Fe-4S] cluster, [3Fe-4S] that is EPR active. This is further confirmed by the fact that the pattern is temperature sensitive. Upon increasing the temperature, the pattern completely disappears. It should be noted that 2Fe-2S cluster shows paramagnetic property even up to 100 K (Bennett, 2010). **(b)** The pattern observed for MjFH $\alpha\beta$ (100 μ M) is similar to that seen for MjFH α showing that the nature of the cluster is the same. The B_0 value at maximum intensity of the signal was 3313.8 gauss. This corresponds to a g -value of 2.01. In conclusion, it is clear that for the assembly of the cluster, residues in the MjFH α subunit alone are sufficient.

7.3.6.3. Stoichiometry of iron and sulfur

Colorimetric analysis for the protein bound iron and the acid-labile sulfide showed that there is 4.1 ± 0.8 mole of Fe and 4.8 ± 0.4 mole of inorganic sulfide per mole of α -subunit. (Figure 7.18). This is close to the expected [4Fe-4S] type of cluster present in the protein. To further validate the stoichiometry, native mass spectrometry was done on the reconstituted α/β -complex. The source conditions ensure that even non-covalent interactions are preserved during ionization.

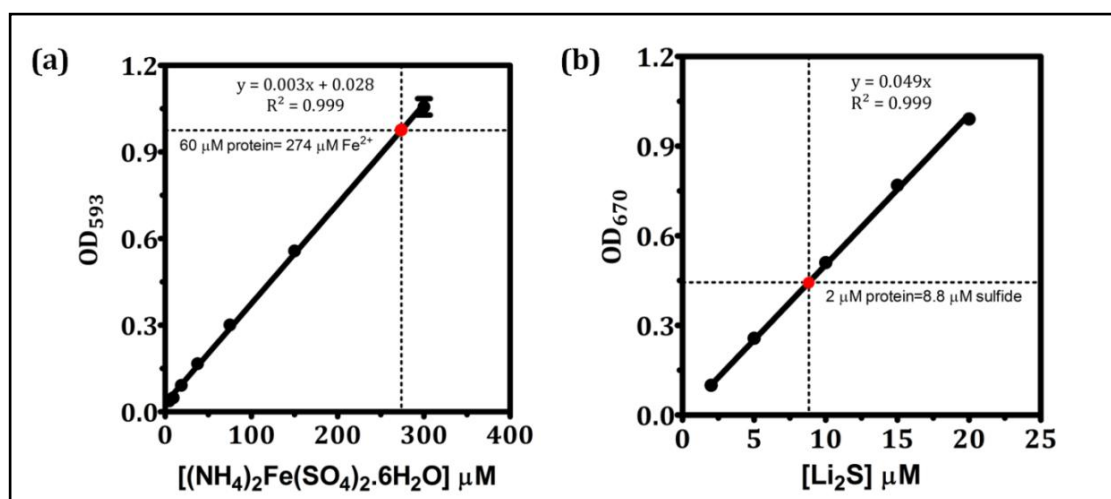


Figure 7.18. Colorimetric estimation of iron and sulfide content in MjFH $\alpha\beta$

(a) Standard curve for iron estimation with the red dot corresponding to the level of iron in the protein. (b) Standard curve used for sulfide estimation. The red dot corresponds to the amount of sulfide in the protein sample. The experiment was performed once in duplicates and the error bars indicates the standard deviation the values obtained.

There was a mixture of many species observed in the spectra as shown in the **Figure 7.19**. Three peaks in the lower m/z range of 2187.92, 2430.69 and 2734.41 were unambiguously assigned a charge state as calculated from its isotope distribution pattern as described in the methods section. The overall spectra along with zoomed in images of each of the three peaks are presented in the **appendix I Figure A7.1, A7.2, and A7.3**. In high m/z range, the isotopic peaks were not well resolved and hence this information could not be used to calculate the charge state of the peaks. Therefore, the m/z value of these peaks (shown in **Figure 7.19**) were compared to all theoretically possible m/z values corresponding to a charge state ranging from 1 to 40 of protein complexes containing different stoichiometry of MjFH α , MjFH β subunits and the Fe-S cluster. From this analysis, each peak was assigned to the species that has the closest m/z value to that theoretically estimated and thus, the charge state was inferred indirectly. A particular species of protein complex was assigned to peaks for which a close match was found and the final analysis is schematically presented in **Figure 7.20**. The difference between theoretical and experimental mass is given in a tabulated form in **appendix I Table A7.1**. As is evident from the figure, most of the peaks belong to the dimer of MjFH α -subunit containing different stoichiometry of iron and sulfur. Most abundant species was MjFH α dimer in which each monomer contains a 4Fe-4S cluster. The condition used at the source was gentle enough to retain the dimeric complex of MjFH α subunit in the gas phase. Under the same conditions, however, very low abundance of heteromer (MjFH α +MjFH β)

population was observed. It can be concluded that under the conditions used, the complex of MjFH α dimer is more tightly held compared to MjFH α -MjFH β complex. Put together EPR, colorimetric based assay and native mass spectrometry suggest that the protein has a 4Fe-4S type iron-sulfur cluster.

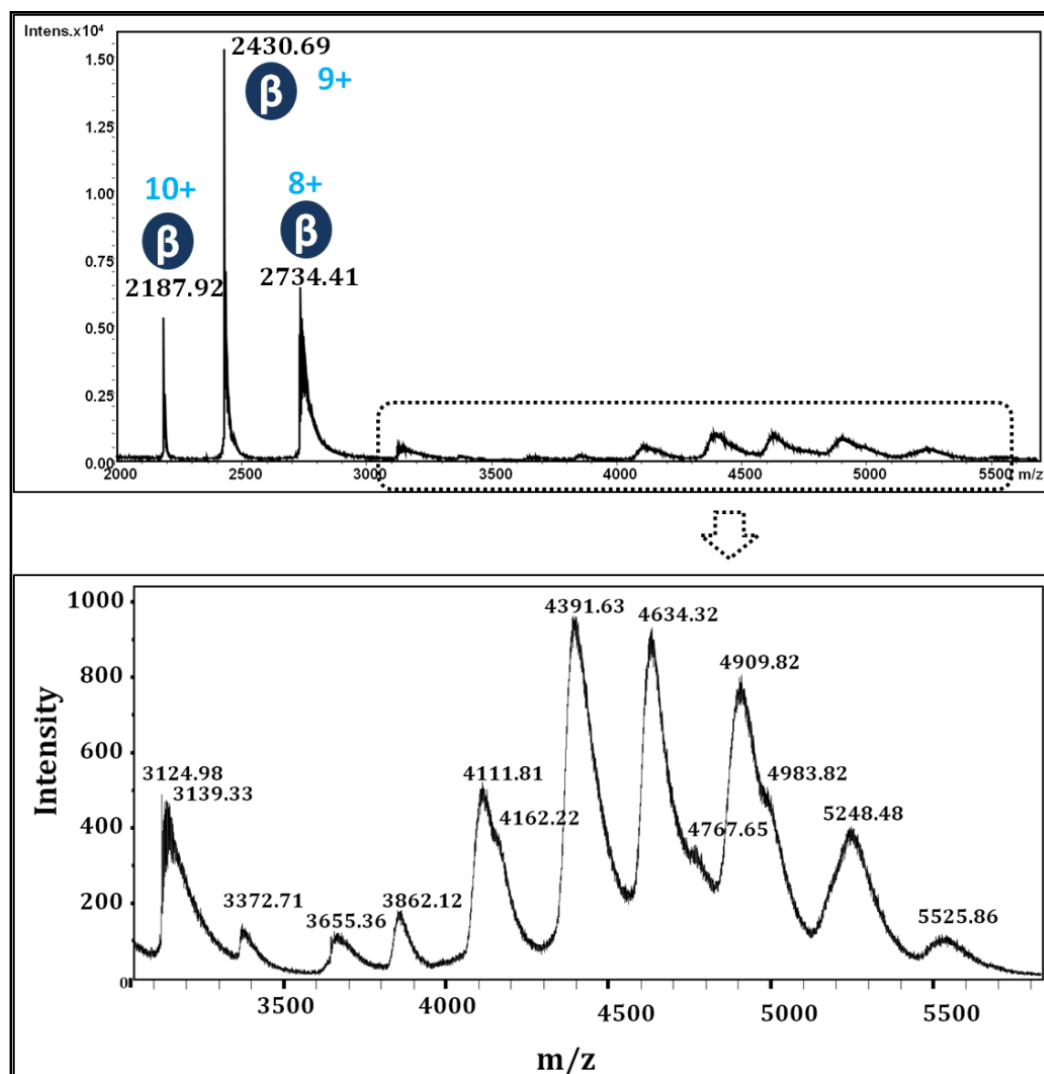


Figure 7.19. Native mass spectrometry of reconstituted MjFH $\alpha\beta$.

The reconstituted MjFH $\alpha\beta$ was dialyzed against 10 mM ammonium acetate and used for native mass spectrometry. The upper panel shows the complete spectrum that was obtained. Three prominent peaks in the low m/z range correspond to 10+, 9+, 8+ charge states of MjFH β subunit (enclosed in blue circle). The charge state of these peaks was calculated from their isotope distribution. The peaks in the high m/z region are highlighted by a rectangle. The lower panel shows a zoom-in of the spectrum containing peaks in the high m/z region. The masses were calculated by the peak finding tool in Data analysis 4.1 suite provided with maXis impact, Bruker Daltonics. The isotope distribution of the peaks in the higher m/z region was not resolved well-enough for unambiguous charge state assignment.

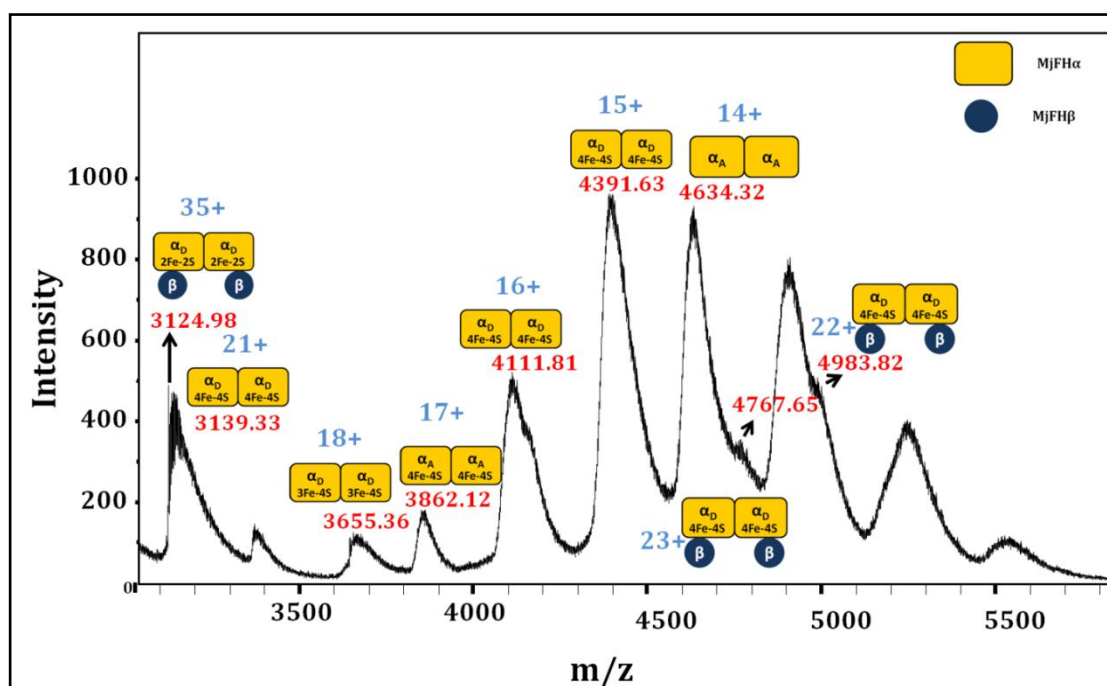


Figure 7.20. Assignment of different species of protein complex to the various peaks.

Numbers in red are m/z value of a peak for which a particular species was assigned. Numbers in blue are the charge states of peaks.

7.3.7. Functional complementation in *E. coli*

Fumarase null strain of *E. coli* has all three copies of fumarate hydratase deleted and hence cannot grow in minimal medium with fumarate as the sole carbon source (see section 6.3.6 for further details). Expression of fumarate hydratase that converts fumarate to malate would rescue its growth phenotype on fumarate minimal medium. Strain transformed with the plasmid co-expressing MjFHα and MjFHβ-subunit was able to grow, albeit at a slower rate compared to *P. falciparum* fumarate hydratase supplemented strain, in fumarate minimal medium (for PjFH results see section 6.3.7). Strain transformed with plasmid expressing either alpha or beta subunit failed to rescue the growth (**Figure 7.21 b**). All these strains could grow in malate minimal medium which was used as a positive control (**Figure 7.21 a**).

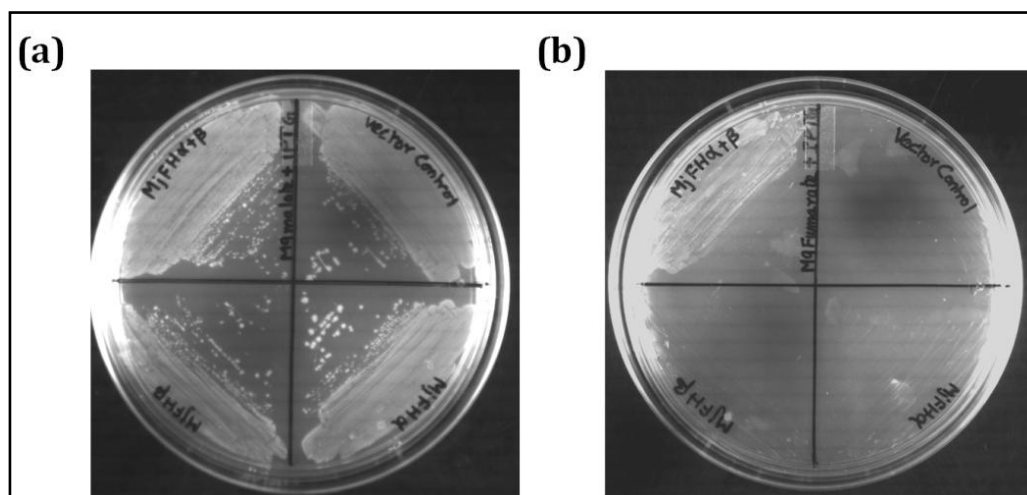


Figure 7.21. Functional complementation of fumarase activity in a fumarase null *E. coli* strain, Δ fumACB.

Fumarase null *E. coli* strain Δ fumACB was transformed with T7 RNA polymerase expressing plasmid, pACT7. This renders the strain compatible with pET based expression systems. The strain was then transformed with pETDUET plasmid expressing MjFH α , MjFH β , and MjFH $\alpha\beta$. As a negative control, the strain was also transformed with just the pETDUET plasmid. The cultures were grown overnight in LB and equal number of cells were plated in minimal medium plates containing IPTG and either fumarate/malate as the sole carbon source. The growth phenotype was scored after 4 days of incubation. Prolonged incubation was needed as the protein has weak activity at 37 °C. **(a)** All the cultures grew well in the malate containing minimal medium plate suggesting that none of these had any growth defect under permissive growth condition. **(b)** Only the cells expressing MjFH $\alpha\beta$ were able to grow in fumarate minimal medium plate validating the fumarate hydratase activity of the Mj protein.

7.3.8. Enzyme activity

The reconstituted MjFH α and MjFH $\alpha\beta$ were tested for fumarase activity using spectrophotometry based assay. Fumarate to malate conversion by the enzyme would result in a drop in absorbance at 240 nm. Both the reconstituted MjFH α and MjFH $\alpha\beta$ were found to be active. It was seen that upon addition of MjFH β to reconstituted MjFH α , the activity increased dramatically, further substantiating the role of MjFH β on the catalytic activity of MjFH $\alpha\beta$ (**Figure 7.22 a**). The pH optimum for fumarate to malate conversion for MjFH $\alpha\beta$ was found to be 7.25 (**Figure 7.22 b**). The kinetic parameters for the activity on fumarate were obtained from the v versus [fumarate] plot for both the proteins. The data for MjFH α fit well to Michaelis-Menten equation. A V_{\max} value of $0.32 \pm 0.01 \mu\text{mol min}^{-1} \text{mg}^{-1}$ and a K_m value of $109.4 \pm 8.32 \mu\text{M}$ was obtained from the fit (**Figure 7.22 c**). The v versus [fumarate] data for MjFH $\alpha\beta$ displayed non-Michaelis-Menten (MM) behavior. A comparative fit analysis between Michaelis-Menten and positive cooperativity revealed a better fit of the data to positive cooperativity. A V_{\max} value of $16.97 \pm 1.25 \mu\text{mol min}^{-1}$

mg^{-1} , Hill's coefficient of 2.08 and K_m of $111.8 \pm 11.8 \mu\text{M}$ was obtained from the fit (Figure 7.22 d).

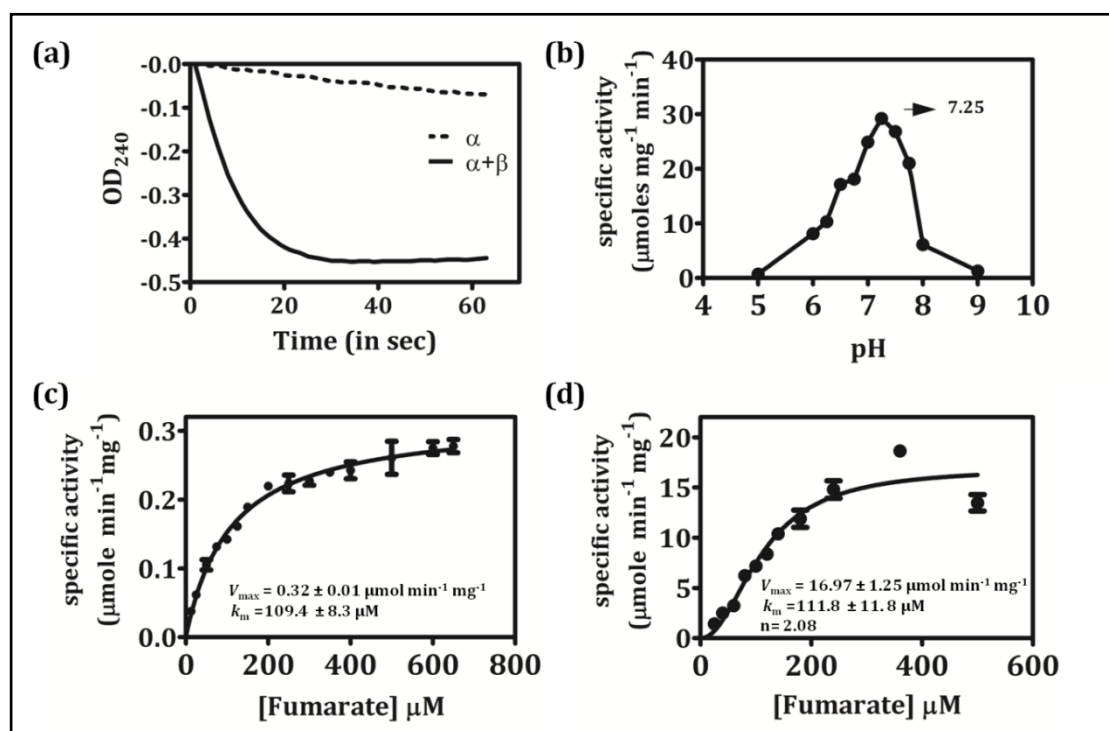


Figure 7.22. Kinetic characterization of MjFH.

(a) The plot shows the activation of MjFH α activity upon addition of MjFH β . For this experiment, 6 μg of reconstituted MjFH α and 3 μg of MjFH β were used. **(b)** The pH optima of fumarase activity was found to be 7.25. For this 0.15 μM of reconstituted MjFH $\alpha\beta$ and 350 μM fumarate was used to check activity in solution buffered at different pH values. A mixture containing 50 mM each of MES, glycine and HEPES was used to prepare solutions of different pH. The assay was performed at 50 °C. **(c)** v vs. [fumarate] plot for reconstituted MjFH α . Kinetic parameters obtained from the fit are shown. **(d)** v vs. [fumarate] plot for reconstituted MjFH $\alpha\beta$ using fumarate as substrate. The data was subjected to a comparative fit analysis across MM and Hill equation for positive cooperativity and was found to best fit the positive cooperativity model. The parameters obtained from the fit are shown. n , Hill's coefficient.

7.3.9. Structure of MjFH β subunit

7.3.9.1. Crystallization, data collection and structure solution

The two biochemically distinct fumarases, class I and class II, share no homology in their primary sequences. Hence, it is unlikely that the structure of these would be similar. With all the apicomplexan organisms using class I FH and the added finding that it plays an essential role in some of these organism (Coustou et al., 2006; Ke et al., 2015) provides a rationale for a detailed structural characterization of this class of enzyme. The RCSB Protein Data Bank (RCSB-PDB) currently has one model of single subunit class I FH from *Leishmania* (PDB ID-5L2R) and two model for the β -subunit of two-subunit type class I

FH; one from *Archaeoglobus fulgidus* (PDB ID:2ISB deposited by structural genomics consortium) and the model deposited from our study, 5DNI from *M. jannaschii*. In multiple instances the initial biochemical understanding of difficult to study mesophilic enzymes have come from their thermophilic counterpart. This extrapolation is justified because of the highly similar nature of functioning of both thermophilic and mesophilic enzymes at the mechanistic level albeit with different temperature optima. With an aim to understand both common (with respect to single subunit CI FH) and unique features of two-subunit type class I FH, we attempted crystallization of individual subunits of MjFH and that of the complex. Crystallization of reconstituted protein of MjFH α and MjFH $\alpha\beta$ was also attempted in completely anaerobic conditions. Microbatch method under oil was used for screening different conditions of crystallization. Many screening conditions provided by Hampton research were tested against these proteins. In all the conditions attempted only MjFH β crystallized. The condition that yielded crystal was 0.1M Bis-Tris, pH 5.5, and 25 % polyethylene glycol-3350 (PEG-3350) incubated with equal volume of protein at room temperature. The morphology of the crystal is shown in **Figure 7.23**.

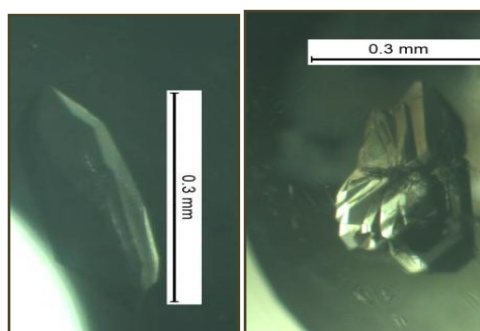


Figure 7.23. Morphology of MjFH β crystals

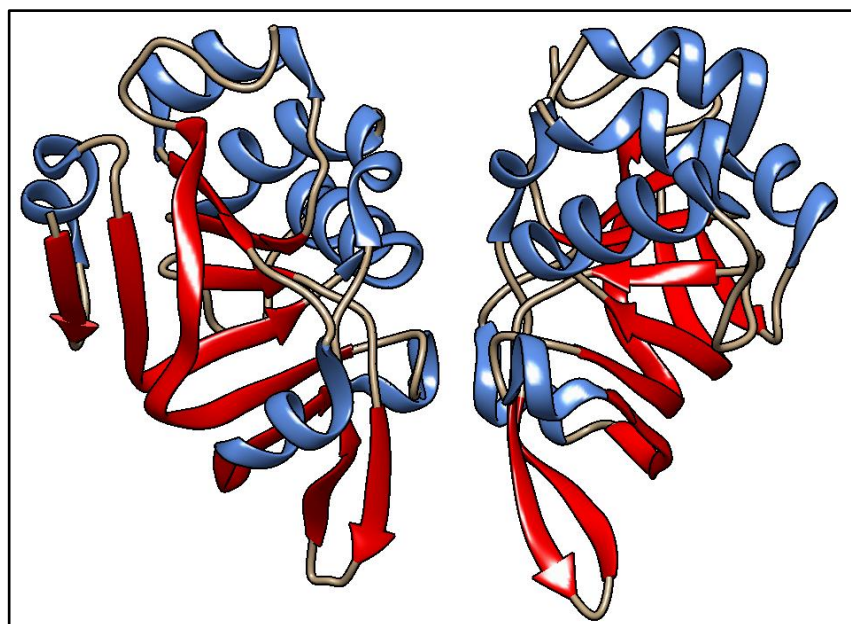
The crystals were obtained in the condition containing 0.1M Bis-Tris, pH 5.5, and 25 % polyethylene glycol-3350. The crystal shown in the right panel was used for data collection

The crystal diffracted well to a maximum resolution of 2.23 Å. Data statistics was good up to a resolution of 2.3 Å and the data up to this resolution was used for scaling. Phase information of the model was obtained using molecular replacement. 2ISB was used as a template for the molecular replacement. The data and refinement statistics are shown in **Table 7.3**. As is evident from the table the asymmetric unit has two subunits of MjFH β subunit and the structure was solved with a space group P6₁. The two subunits form a crystallographic dimer and do not have any physiological relevance as we have shown through analytical gel filtration that MjFH β is a monomer in solution.

Table 7.3. Data collection and refinement statistics

Statistic	Value
PDB ID	5DNI
Space group	P6 ₁
Cell parameters	
Length (Å)	a=85.61, b=85.61, c=121.83
Angle	$\alpha=90^\circ$, $\beta=90^\circ$, $\gamma=120^\circ$
Resolution (Å)	2.3
Mean B-factor (Å ²)	49.0
R _{merge} (%)	12.7
Completion (%)	100
$\langle I \rangle / \langle sI \rangle$	4.58
No. of observed reflections	22550
No. of unique reflections	22550
R _{work} (%)	20.3
R _{free} (%)	23.9
RMSD from ideal value	
Bond length (Å)	0.008
Bond angle (°)	1.176
No. of subunits/ ASU	2

ASU, asymmetric unit; $\langle I \rangle / \langle sI \rangle$, intensity/standard deviation of intensity; RMSD, root mean square deviation

**Figure 7.24. Structure of MjFH β (PDB ID: 5DNI)**

The asymmetric unit contains two chains. The chains are coloured based on secondary structure, with helices coloured blue and the sheets coloured red. Figure was generated using UCSF-Chimera (Pettersen et al., 2004).

Figure 7.24 shows the structure of MjFH β coloured based on the secondary structure information. The density corresponding to last 12 amino acids was not obtained and hence not modeled into the final structure. The lack of density might be due to highly

disordered nature of these residues. Additional electron density apart from the protein backbone was fit to ligands like polyethylene glycol, glycerol and ethylene glycol. Chain A has one molecule of each of them, whereas chain B has one molecule of glycerol and ethylene glycol. Extra electron density, with an $2F_0-F_C$ value of 6, was found in the interface of two subunits and was fit to a chloride ion. The residue Ile77 in chain A and chain B is a Ramachandran outlier with $\phi = -160^\circ$ and $\Psi = 66.8^\circ$ in chain A and with $\phi = -152.5^\circ$ and $\Psi = 69.1^\circ$ in chain B. The side chain of Arg-84 from chain A was found to have a non-rotameric side chain. TYR-18 in chain A was the only RSRZ outlier (a quantitative estimate of the fit of residues to electron density) with a value of 2.6. The occupancy value for all residues of chain A and B, the ligands, water molecules in both chains and the chloride ion was 1. There were 17 close contacts in the asymmetric unit mostly localized to the interface of the two chains.

7.3.9.2. Structural features of MjFH β

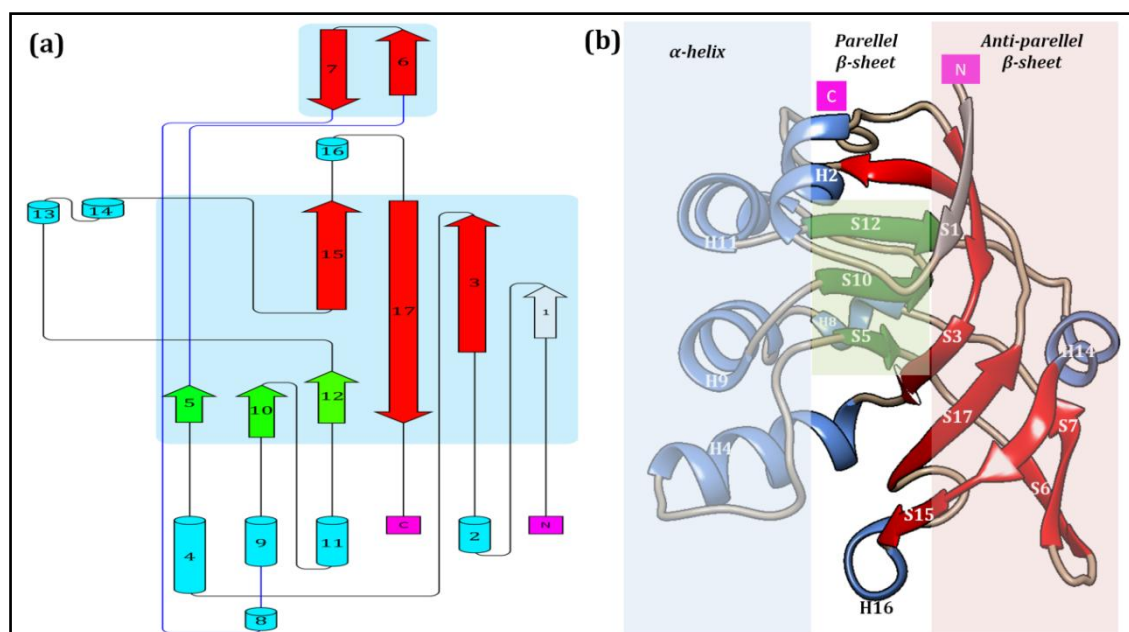


Figure 7.25. Topology and annotation of secondary structural features of MjFH β

(a) Topology diagram representing the secondary structural features in MjFH β . The figure was generated using Pro-Origami (Stivala et al., 2011) and edited using Inkscape (<https://inkscape.org/en/>). (b) The structure of MjFH β with helices and sheets labeled based on the topology diagram. The helices are labeled with a prefix H and the sheets are labeled with a prefix S. The numbering is based on the hierarchical occurrence of the secondary structural feature starting from the N-termini in the primary sequence of the protein. Highlighted in the figure using coloured rectangles are secondary structural features in the order of occurrence in the protein (from right to left): antiparallel β -sheets (in red) followed by parallel β -sheet (in green) and then the α -helices (in blue). This is the characteristic feature of swiveling $\beta/\beta/\alpha$ fold containing proteins (SCOPE database (Fox et al., 2014)).

The structure of MjFH β consists of 9 β -sheets and 8 α -helices connected with loops as evident from the topology diagram in **Figure 7.25 a**. The SCOPe database classifies the fold of MjFH β as “swiveling $\beta/\beta/\alpha$ ”. This fold is considered to be a highly mobile segment in multi-domain proteins containing this domain. The fold is characterized by the presence of a layer of anti-parallel β -sheet, parallel β -sheet and a layer of α -helices as depicted in **Figure 7.25 b**. The **Figure 7.26** shows the primary sequence of MjFH β along with structural features derived from 5DNI (MjFH β), residue conservation and solvent accessibility. It should be noted that with a few exceptions highly conserved residues are located in coils or in the boundary of a helix/sheet with a coil.

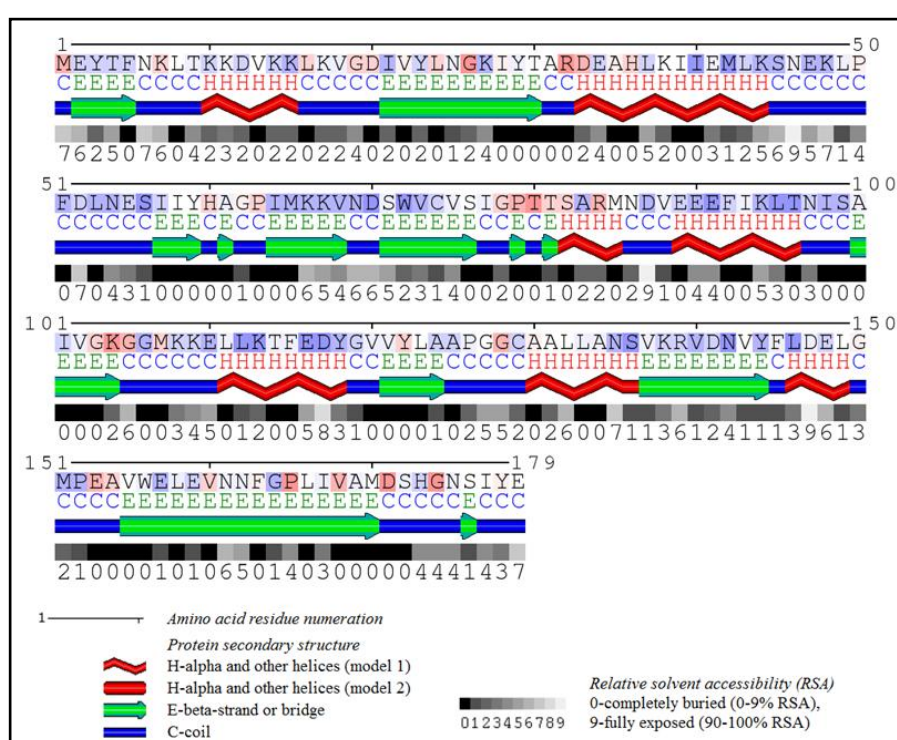


Figure 7.26. Primary sequence of MjFH α with secondary structural features, sequence conservation and solvent accessibility.

The legend for different features highlighted is given below in the figure. The figure was generated using Polyview-2D (Porollo et al., 2004)

The two monomers (chain A and B) present in the asymmetric unit were aligned using UCSF-chimera to check any structural differences between them. The structures aligned with an RMSD value of 0.43 Å², indicating very high structural overlap between the two. The aligned structure is shown in **Figure 7.27a**. A notable difference between the two chains is the position of β -sheets S6 and S7. This is also expected as the region has high average B-factor as shown in **Figure 7.27 b**.

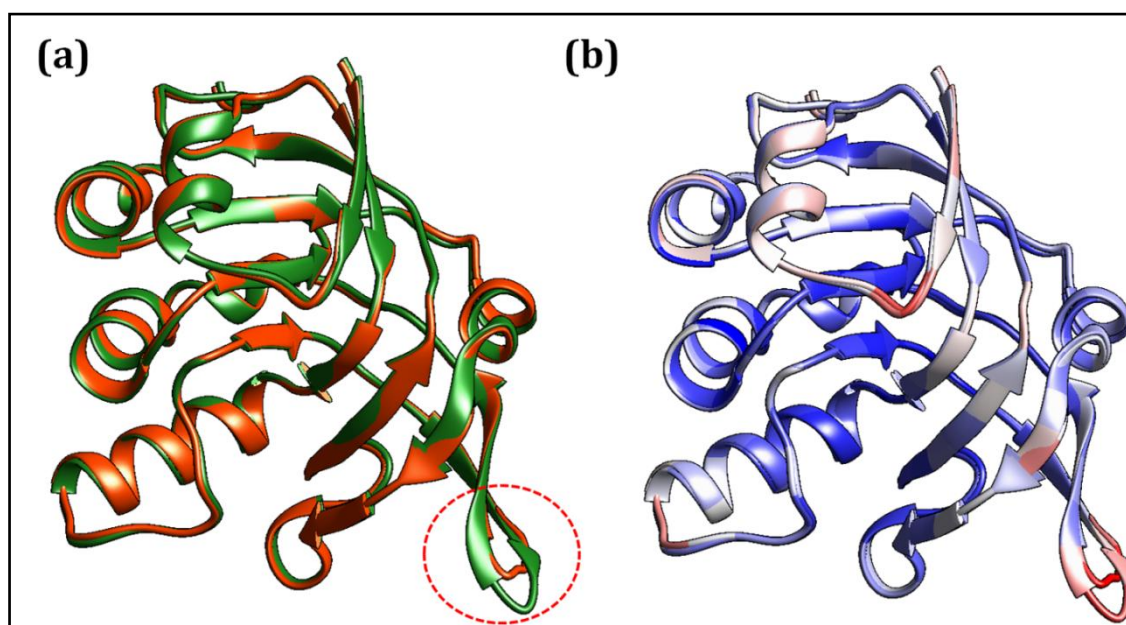


Figure 7.27. Structural alignment and B-factor distribution of Chain A and B of MjFH β

(a) Structural alignment of chain A and chain B of 5DNI. The structure superposed with an RMSD value of 0.42 Å². A notable difference is the position of β -sheets S6, β -sheet S7 and the loop connecting them (highlighted with a red circle). **(b)** The aligned chain A and chain B are coloured based on average b-factor values. A blue to red colouring pattern was chosen in UCSF-Chimera structure analysis tool with blue representing the lowest B-factor value and red representing higher values. It should be noted that β -sheets S6 and S7 and the loop connecting them has high B-factor value explaining the difference in their position in both chains.

7.3.9.3. Comparison of MjFH β structure with other available class I FH structures

Apart from the structure of MjFH β , currently, there are only three other structures available that belong to enzymes from class I fumarate hydratase family. The β -subunit of two-subunit type fumarate hydratase from *Archaeoglobus fulgidus* (PDB ID: 2ISB); complete structure of the single subunit type fumarate hydratase from *Leishmania major* (PDB ID: 5L2R); and finally a predicted model for the two-subunit L-tartrate dehydratase (which shares significant sequence similarity with C I-FH family of enzymes) from *E. coli*. It should be noted that while the first two structures are obtained through X-ray crystallography, the structure of L-tartrate dehydratase from *E. coli* was ‘predicted’ using a co-evolutionary algorithm combined with the modeling tool Rosetta (Ovchinnikov et al., 2015). Our attempts to crystallize the holo- structure of MjFH $\alpha\beta$ failed even after repeated attempts. Hence, a comparison of the available class I FH structures with MjFH β structure was performed to identify functionally key residues involved in subunit

interaction and catalysis. **Figure 7.28** shows the structural superposition of chain A of 5DNI with other structures.

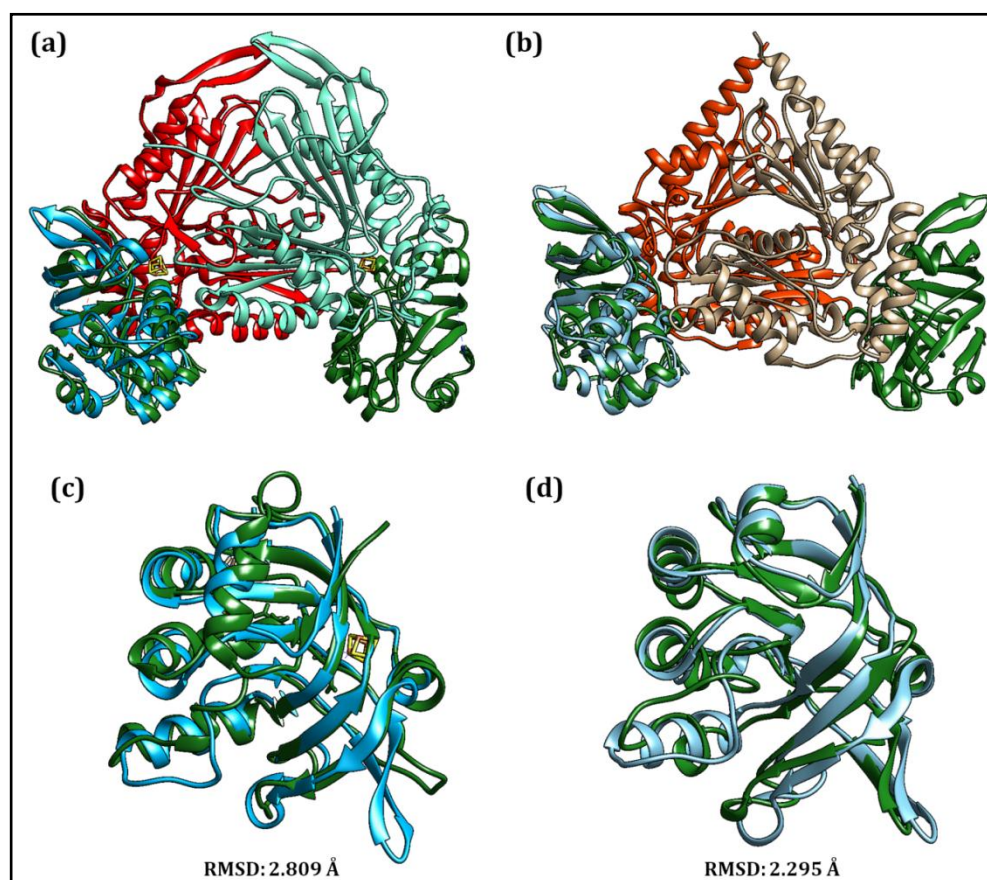


Figure 7.28. Structural superposition of chain A of 5DNI with FH from *Leishmania* (5L2R) and *L*-tartrate dehydratase.

(a) Structural alignment of 5L2R with chain A of 5DNI. N-terminal domain (NTD) of the *Leishmania* protein is shown in red and aquamarine colour. The CTD of both the chains are shown in green. Chain A of 5DNI is shown in sky blue colour. **(b)** Structural alignment of *L*-tartrate dehydratase (*L*-ttd) with chain A of 5DNI. The α -subunit of the two chains of *E. coli* protein is coloured red and sand brown. Both the β -subunits are coloured green. Chain A of 5DNI is shown in sky blue colour. **(c)** A close-up view on the structural alignment of CTD of 5L2R and chain A of 5DNI. The averaged RMSD value for all the pairs of amino acids aligned was 2.809. **(d)** Structural alignment of β -subunit of *L*-ttd. The averaged RMSD value for all the pairs of amino acids aligned was 2.295.

The RMSD value for the alignment of chain A with LmFH-2 structure (5L2R) and the *L*-ttd structure is 2.809 Å and 2.295 Å. A notable difference in the alignment of 5DNI with 5L2R is the difference in position of residues in 5L2R that corresponds to S6 and S7 in 5DNI. Whereas the residue in the segment forms β -sheet in 5DNI, the corresponding residues in 5L2R form coiled region.

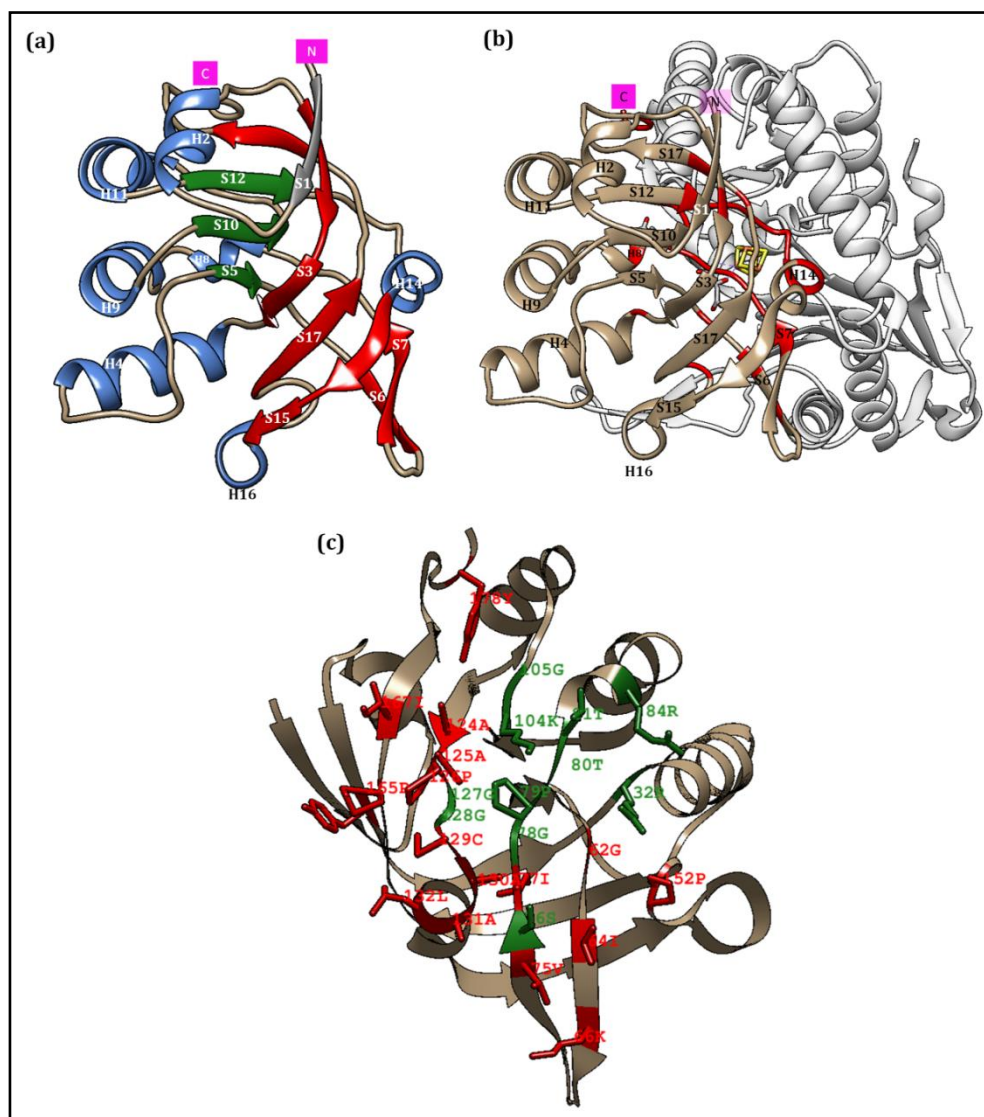


Figure 7.29. Mapping of potential interface forming residues in MjFH β from structural alignment.

(a) The structure of MjFH β with secondary structures numbered is provided for reference. (b) Structural alignment of chain A of 5DNI with 5L2R. Only the NTD from the corresponding chain to which 5DNI was aligned is shown in cartoon representation and the rest of the structure was removed for clarity. The residues that might form the interface are highlighted in red colour. (c) The residues that might be forming the interface is highlighted to display the residue number along with side chain. Residues in the interface that are conserved based on multiple sequence alignment is coloured green and the non-conserved residues are coloured red.

In order to map the residues in MjFH β that are involved in interacting with MjFH α , we sought to use the structural superposition between MjFH β and the CTD of 5L2R. Once the alignment was obtained, the residues in MjFH β within 4 Å distance cutoff from residues of NTD were selected. The highlighted residues in the interface along with their positioning on the overall structure are presented in **Figure 7.29**.

7.3.9.4. Malate binding sites in MjFH β subunit

From the structure of malate bound LmFH2, it is clear that majority of the residues involved in malate binding are from the C-terminal domain of the protein which is homologous to MjFH β subunit. In LmFH-2 the binding of malate is mediated by contacts between the two carboxyl- and the hydroxyl functional groups of malate with the side chain of R173 and D135 from NTD and R421, R471, T467, T468, and K491 from CTD. Identical residues are present in MjFH β subunit at the corresponding positions. In order to compare the orientation of side chain of these residues from MjFH β subunit with that LmFH-2 CTD, a structural superposition of the two was performed and the result is shown in **Figure 7.30**. For this both chain A and chain B of MjFH β were used.

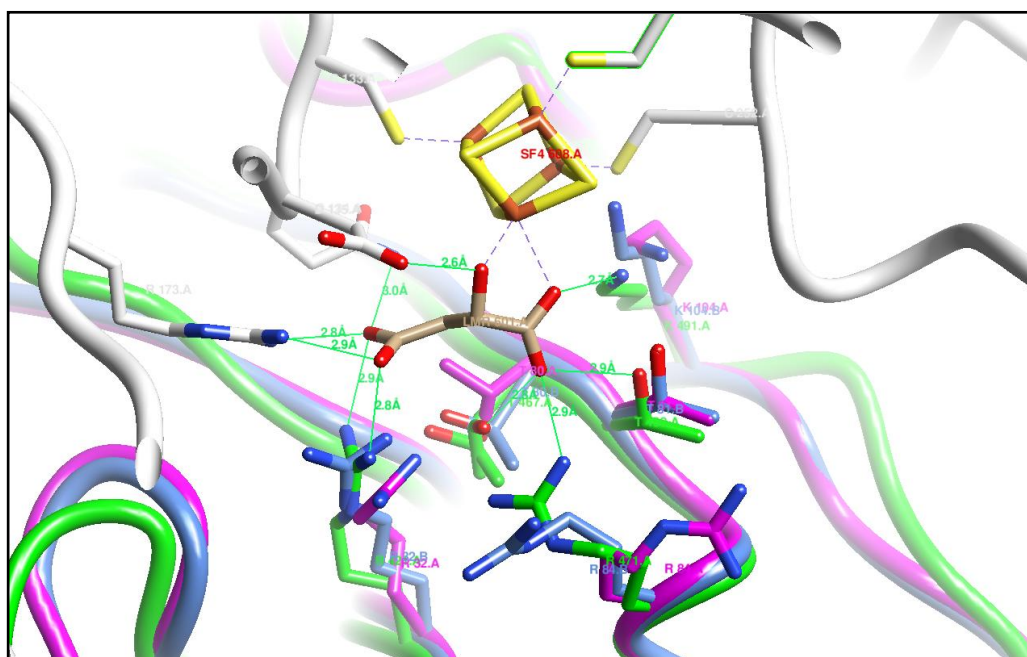


Figure 7.30. Residues involved in malate binding in MjFH β and LmFH2 C-terminal domain.

The backbone of LmFH2-CTD, LMFH2-NTD, MjFH β chain A, MjFH β chain B are shown in green, white, pink and blue, respectively. The iron sulfur cluster is shown with sulfurs coloured yellow and iron coloured brown. The cysteinyl- side chain involved in cluster ligation is also shown. Contacts between the residues of LmFH2 with malate are coloured green. L-malate is shown in sand brown colour.

As evident from the figure, the side chains of the residues from MjFH β viz., R32, T80, T81, R84, and K104 are poised to bind malate and could do so with only a minor conformational rearrangement. Only exception to this is the side chain of R84 from chain A of MjFH β subunit. R84 is the only residue with a non-rotameric side chain conformation in MjFH β . The role of MjFH β in malate binding could explain the increase in activity seen for the MjFH $\alpha\beta$ complex.

7.4. Summary and future perspective

Fumarases belong to the category of enzymes where the same chemistry is catalysed by two non-homologous enzymes. Iron dependent fumarases are one of the ancient enzymes present in early branching organisms in the tree of life but the reason as to why it has been retained in aerobic organisms is still not known. Many organisms as exemplified by *E. coli* have both classes of enzymes. Moreover, the *E. coli* genome codes for two different class I fumarate hydratases viz., *fumA* and *fumB*; the former expressed under aerobic conditions and the latter in anaerobic conditions. The only other example where similar scenario prevails is the case of serine dehydratase wherein, the Fe-S cluster containing enzyme has more affinity for the substrate compared to the non-homologous iron independent serine dehydratases (Grabowski et al., 1993; Hofmeister et al., 1994). Such an explanation does not answer the puzzle of why Fe-S cluster containing fumarate hydratases are still used by many organisms, because both the classes of enzymes have comparable catalytic efficiency (Flint and Allen, 1996). However, a detailed kinetic and structural characterization of class I enzyme might offer additional insight into the differences between these two classes of fumarases.

In this study, we have performed biochemical and structural investigation of *M. jannaschii* FH which belongs to a two subunit type class I FH. The individual subunits and the complex were purified to homogeneity. The purified proteins were found to be structured and thermostable by using intrinsic tryptophan fluorescence and circular dichroism based experiments, respectively. The subunits were found to interact strongly and the thermodynamics of interaction was studied using isothermal calorimetry. The mass of the individual subunits were analysed by ESI-MS. Whereas the MjFH β subunit had a mass similar to the theoretically predicted one, MjFH α subunit was present as four different species. Upon examination of the masses it was found that the desmethionine form is the major species of the protein. A conventional *in vitro* reconstitution procedure was followed to incorporate the cluster in the proteins. Spectrophotometric, EPR, and visible CD based experiments suggested that MjFH α has all the components necessary to bind the cluster and the cluster is of 4Fe-4S type. Native mass spectrometry of the reconstituted MjFH $\alpha\beta$ further confirmed the type of the cluster.

MjFH $\alpha\beta$ complex was able to successfully rescue the growth of fumarase null *E. coli* strain in fumarate containing M9 minimal media. This shows that the presence of both the subunits is essential for optimal functioning of the enzyme *in vivo*. This result was further substantiated by kinetic studies performed with the recombinantly purified

proteins. Reconstituted MjFH α and MjFH $\alpha\beta$ were both found to be active. However, MjFH $\alpha\beta$ was found to have at least 50 fold higher activity compared to reconstituted MjFH α . The kinetic parameters for the fumarate to malate conversion for both the proteins were derived from the substrate titration plots. The plot obtained for MjFH α fit well to MM equation whereas, MjFH $\alpha\beta$ showed non-MM behavior. The data fit well to the positive cooperativity model. The addition of MjFH β seems to bring about an increase in V_{\max} of the functional complex MjFH $\alpha\beta$ while the K_m remained largely the same.

The structure of MjFH β subunit was solved using X-ray crystallography. The phase information for the data was obtained by molecular replacement using the β -subunit structure of *Archaeoglobus fulgidus* FH β subunit already available in the RCSB protein data bank (PDB ID: 2ISB). Analysis of the structure showed that it has a swiveling $\beta/\beta/\alpha$ domain (Fold C.8). According to SCOPe database, the domain is considered to be highly mobile in most of the multi-domain proteins where it is present. Structural alignment with other available CI-FH structures was performed to map the interface residues. Many conserved features present in CTD of single subunit CI FH are also present in MjFH β protein.

Structure solution of the MjFH $\alpha\beta$ complex along with the cluster in substrate/inhibitor bound form would reveal additional insights into the mechanism of action of two subunit class I FH. Further, this enzyme is good model system to delineate factors that play critical role in substrate promiscuity that is generally seen in this class of enzymes.

Chapter 8
**CONCLUSIONS AND FUTURE
DIRECTIONS**

Chapter 8

CONCLUSIONS AND FUTURE DIRECTIONS

*Energy requirement of the intraerythrocytic stages of *P. falciparum* is largely met by glycolysis and the reactions of the TCA cycle along with oxidative phosphorylation are known to play only a minor role in terms of ATP generation. High glycolytic flux combined with the lack of regulatory roles of key enzymes in Plasmodium glycolytic pathway further suggest the importance of excessive reliance on glycolysis. However, metabolic labelling studies have shown the presence of a fully functional TCA cycle fuelled by glutamine-derived α -ketoglutarate and PEP derived oxaloacetate. Earlier studies from our laboratory have shown that fumarate generated from purine nucleotide cycle also, can anaplerotically drive the TCA flux mediated by the enzymes fumarate hydratase and malate-quinone oxidoreductase. Two major objectives of the current study were to investigate the physiological significance of the PNC mediated fumarate anaplerosis and to biochemically characterise class I fumarate hydratase which is biochemically and structurally very distinct from the human fumarate hydratase. These objectives have been approached using different strategies and are presented as two different sections in this thesis. This chapter provides an overall summary of the work done and future directions.*

8.1. Metabolic significance of fumarate generated from purine salvage pathway in *P. falciparum*

Fumarate is generated as a by-product in the AMP synthesis pathway of the parasite. An earlier study from our laboratory has shown that fumarate can be metabolised by the parasite to pyruvate, lactate, malate and aspartate. The key enzymes involved in fumarate metabolism are fumarate hydratase and malate-quinone oxidoreductase. The possible significance of fumarate metabolism has been reviewed (Jayaraman et al., 2012). In the current study, it is shown that fumarate hydratase is expressed during the intraerythrocytic stages of the parasite by RT-PCR on parasite RNA and Western blotting of parasite lysate using PfFH-C-terminal domain specific antibodies. In order experimentally test the metabolic significance of fumarate generated during AMP synthesis, two strategies were attempted: an indirect strategy involving the use of YAPRT expressing *P. falciparum* strain and a direct strategy involving knockout/knockdown of the fumarate hydratase at the gene/protein level.

ADSS and ASL mediated conversion of IMP to AMP, in which fumarate is generated as a by-product, is the sole pathway for AMP generation in the *P. falciparum*. Inhibition of ADSS by hadacidin is therefore, lethal for the parasites (Webster et al., 1984). There are no means direct means available by which one can selectively deplete fumarate generated in this pathway, thereby study the importance of the metabolite, without interfering with AMP production. *yAPRT* that catalyses the phosphoribosylation of adenine to AMP (without generating fumarate) can serve as an alternate pathway for generating AMP in the parasite, provided adenine is supplemented in the culture medium (apart from hypoxanthine). In *yAPRT* expressing parasite, addition of hadacidin would lead to selective depletion of fumarate without perturbing the levels of AMP. The sensitivity of *yAPRT*⁺ parasites to hadacidin treatment can be used as an indicator to probe the essentiality of fumarate. For this, *yAPRT* was expressed episomally from a centromere plasmid in 3D7 strain of *P. falciparum*. The enzyme was found to be functional in the parasite compartment as evident from adenine phosphoribosylation activity of *yAPRT*⁺ parasite lysate and by the increased sensitivity of the *yAPRT*⁺ parasites (IC₅₀ = 1.2 μM) to 2-fluoroadenine as compared to wild-type parasites (IC₅₀ = 9μM). Growth of the Wt and *yAPRT*⁺ parasites were tested on medium supplemented with adenine alone, hypoxanthine alone and a combination of adenine and hypoxanthine. For reasons that are not clear as yet, the combined presence of adenine and hypoxanthine was toxic to *yAPRT*⁺ parasites but not for wild-type parasites. Adenine and hypoxanthine when individually present were not toxic to either of the parasites. Hadacidin sensitivity on *yAPRT*⁺ parasites was tested in medium supplemented with adenine or hypoxanthine as purine source. In both the conditions tested, hadacidin was lethal to *yAPRT*⁺ parasite. This suggests that either fumarate is essential or sufficient AMP is not generated in *yAPRT*⁺ parasites under the conditions used. However, supplementation of excess fumarate in the medium was able to only partially rescue the hadacidin mediated inhibition. Optimizing media conditions by addition of supplements like guanosine, orotate etc., to ensure sufficient levels of AMP and GMP is present in the parasite compartment followed by testing hadacidin sensitivity on *yAPRT*⁺ parasites would provide more clarity on the essentiality of fumarate generated as a by-product of AMP synthesis in the parasite.

In the direct strategy, we generated *P. falciparum* strain in which fumarate hydratase protein levels could be controlled using a degron based strategy (Muralidharan et al., 2011). For this, a regulatable fluorescent affinity (RFA) tag coding for GFP, DHFR degradation domain, and a 3XHA tag in tandem was integrated 3' to the FH coding region by single crossover recombination. After three rounds of drug cycling, the strain was validated by PCR-based genotyping. The results indicated the integration of the plasmid

at the expected locus and also the presence of an episomal copy of the plasmid. The gene in the plasmid does not have a promoter of its own and hence, the presence of the episomal copy of the plasmid does not hinder either in studying the essentiality of the protein (by removal of trimethoprim) or for examining its localization. Colocalization of GFP signal with the MitoTracker staining pattern shows the mitochondrial localization of the protein. Removal of trimethoprim from the culture medium did not cause any lethality to the parasites. This could be due to the fact that the RFA-tagged FH is localized to the mitochondria and hence, inaccessible to the proteasomal machinery which is predominantly present in the cytosol. Alternate conditional knockout strategies (Ganesan et al., 2016) needs to be tested to study the essentiality of the gene.

During the course of our study, a report on the genetic investigation on the tricarboxylic acid cycle of the parasite was published (Ke et al., 2015). According to the study, fumarate hydratase and malate quinone oxidoreductase were the only enzymes of the TCA cycle of *P. falciparum* that were essential and could not be genetically disrupted. *P. berghei* is an alternate model system to understand *Plasmodium* biology and is more amenable to genetic manipulation. As the FH gene proved to be essential in *P. falciparum* the susceptibility of *P. berghei* FH gene locus to genetic recombination was tested using 3' HA tagging strategy. The parasites carrying HA-tagged FH were successfully generated and the genotype was validated by PCR and Southern blotting. Subsequent to this, knockout of the gene using double-crossover recombination was performed and recombinant parasites selected for growth on pyrimethamine were obtained. Southern blotting and PCR was performed to validate gene disruption. The FHKO parasites were viable even after multiple passages and cause lethality to mice. This shows that the gene is not essential for the parasite during intraerythrocytic growth of *P. berghei*. Limiting dilution cloning of FHKO parasites was attempted twice and was not successful. The procedure needs to be repeated and upon obtaining a clonal population, the phenotype of the parasite in sexual stages can be examined.

8.2. NMR-based strategy to study the cellular fate of ammonia

The net reaction in purine nucleotide cycle, that involves the operation of the enzymes ADSS, ASL, and AMPD, is conversion of a molecule of aspartate to one molecule each of fumarate and ammonia. The fate of this ammonia in the parasite is not known. To study this, we intended to develop an NMR-based strategy to trace the fate of nitrogen by following its incorporation into primary aliphatic amines (that includes amino acids as well as ammonia). The strategy was standardized using *E. coli* as a model system, as the nitrogen metabolism in the organism is well studied. A key step in the strategy was to

acetylate the extracted metabolites to convert all aliphatic primary amino groups to amides group. This is to minimize the chemical exchange of proton attached to nitrogen and facilitate the use of NMR to identify metabolites.

The protocol involved the use of acetic anhydride to acetylate primary aliphatic amines in the presence of triethylamine as a base. The protocol was first tested on standard metabolites like glutamate, asparagine, GABA and ammonia. Acquisition of 1D ^1H -NMR and 2D ^1H - ^{15}N -HSQC spectrum of acetylation reaction mixture confirmed the acetylation of these metabolites. OPA based fluorescent assay was used to estimate unacetylated amino acids after the reaction and hence the extent of acetylation. Metabolites were extracted from *E. coli* culture grown in minimal medium containing ^{15}N -labelled ammonium chloride as the sole nitrogen source. The metabolites were acetylated using the protocol described earlier and analysed by ^1H - ^{15}N -HSQC that showed cross peaks corresponding to 47 different metabolites. To establish the identity of the metabolites a ^{15}N -edited TOCSY-HSQC experiment was performed on the derivatized *E. coli* metabolites. This led to the identification of metabolites such as glycine, proline, alanine, glutamate, threonine, leucine, arginine, cysteine, histidine and serine. The intensity of the correlated aliphatic cross-peak is dependent on the efficient transfer of magnetization. In multidimensional NMR experiments, the intensity of the cross-peaks gets weaker across successive bonds which can be overcome by increasing the acquisition time or using higher concentration of metabolites. Repeating the experiment with metabolites extracted from a higher culture volume would aid in the identification of many more metabolites. Acquisition of multidimensional NMR spectra on acetylated standard metabolites can also be used to generate a reference table containing chemical shift values that would aid in establishing the identity of metabolites.

8.3. Biochemical and structural characterisation of class I fumarate hydratase

All parasites belonging to the apicomplexan and kinetoplastids depend solely on Class I fumarate hydratase for the conversion of fumarate to malate. *P. falciparum* fumarate hydratase was predicted to be mitochondrially localised. In order to biochemically characterise PffH, the protein was heterologously expressed in *E. coli* as a C-terminal (His)₆-tagged protein. The majority of the protein was found to be in inclusion bodies. A small amount of protein present in the soluble fraction was partially purified using Ni-NTA chromatography. Western blot of the protein with anti-protein antibody showed that majority of the impurities present were the degradation products of PffH. The partially purified protein was shown to be active using NMR and spectrophotometric based assay. A fumarate hydratase null strain of *E. coli*, ΔfumACB was generated and the genotype

validated by PCR. The strain failed to grow in minimal medium containing fumarate as the sole carbon source. Expression of PffH in Δ fumACB strain was shown to complement the growth deficiency in minimal medium containing fumarate as the sole carbon source further confirming the activity of the enzyme. The PffH expressing, fumarate hydratase-null strain was also able to grow on mesaconate and D-tartrate suggesting that PffH has promiscuous activity on these substrates. Mercaptosuccinic acid, a malate analogue was found to inhibit the growth of Δ fumACB strain expressing PffH with an IC₅₀ of 400 μ M. The growth was rescued by malate suggesting specific action of the molecule on the enzyme. The molecule was also found to inhibit the asexual stage growth of *P. falciparum* with an IC₅₀ value of 300 μ M.

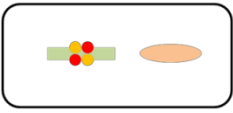

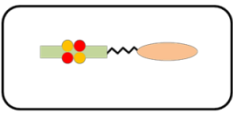
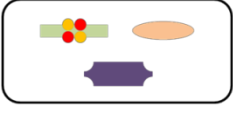
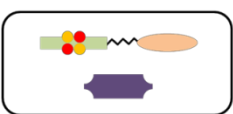
M. jannaschii fumarate hydratase belongs to two-subunit type fumarate hydratase. The two subunits were co-expressed in *E. coli* and purified to homogeneity. The MjFH α subunit was found to be a dimer and the β -subunit, a monomer. As inferred from the elution volume in analytical size-exclusion chromatography, the complex was found to be an assembly of 2 molecules of MjFH α and two molecules of MjFH β . The subunits were found to interact with a K_d value of 694 nM as estimated using isothermal calorimetry. The protein was found to have an iron-sulfur cluster of the type 4Fe-4S as evident from EPR, native mass spectrometry and colorimetry experiments. The structure of MjFH β subunit was solved using X-ray crystallography to a resolution of 2.34 Å. The protein was found to have a swivelling $\beta/\beta/\alpha$ fold.

Further experiments to obtain a crystal structure of the holo protein complex of MjFH $\alpha\beta$ followed by site-directed mutagenesis of key residues as inferred from the structure would aid in mechanistic understanding of the functioning of the enzyme.

8.4. Taxonomic distribution of two classes of fumarate hydratase

Class I Fe-S cluster containing fumarate hydratase are present in archaea, prokaryotes and lower eukaryotes. Amongst these, archaea have only the two-subunit type enzyme and lower eukaryotes have single-subunit enzyme. Prokaryotes have both types. Class II FH is present widely in all domains of life. Many organisms have both classes of enzymes. The taxonomic distribution of class I FH along with the co-occurrence of class II enzyme is not catalogued till now. We have observed five different types of FH distribution and this is schematically shown in **Figure 8.1**. Availability of an inventory of the distribution of FH across organisms belonging to different taxa could serve to draw connection between life-style of the organism and metabolic adaptation. Such cataloguing could also be starting

material to address questions related to physiological significance of the type of fumarate hydratase present in an organism.

Type of FH	Archaea	Bacteria	Eukaryotes
	<i>Methanocaldococcus jannaschii</i> <i>Pyrococcus furiosus</i> <i>Archaeoglobus fulgidus</i> <i>Korarchaeum cryptofilum</i>	<i>Pelotomaculum thermopropionicum</i>	None
	<i>Halogramum rubrum</i>	?	<i>Saccharomyces cerevisiae</i> <i>Homo Sapiens</i> <i>Arabidopsis thaliana</i>
	<i>Ignicoccus hospitalis</i> #	<i>Zymomonas mobilis</i>	<i>Plasmodium falciparum</i> <i>Toxoplasma gondii</i> <i>Leishmania donovani</i>
	<i>Thermoproteus tenax</i>	<i>Clostridium botulinum</i>	None
	<i>Halolamina sediminis</i> #	<i>Escherichia coli</i> <i>Bordetella petrii</i> <i>Vibrio cholerae</i>	<i>Micromonas commoda</i> <i>Naegleria gruberi</i>

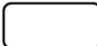



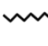



 Cell boundary
  α -subunit
  β -subunit
 Fe-S cluster
  Linker
  Class II FH
 Class I two-subunit FH
 Class I single-subunit FH

Figure 8.1. Distribution of class I and class II FH

Based on the presence of the type of fumarate hydratase, there are five different distribution types seen. A few representative organisms from each type are also listed.# No other organism is present in the taxa having this type of FH distribution.

It is enigmatic as to why some organisms have both classes of enzymes. The major difference between enzymes of the two classes is the oxygen sensitivity. However, in *E. coli* grown in aerobic conditions, class I FH accounts for the majority of the fumarate hydratase activity with only a minor contribution from the class II enzyme (Woods et al., 1988). Hence, oxygen sensitivity alone does not explain the presence or the use of one class of FH over the other. Other difference between class I and class II FH is with respect

to substrate promiscuity and capability to perform isomerization reactions. It has been reported that class I FH is less promiscuous than class II FH (Flint, 1994). Moreover, only class I enzyme can catalyse isomerization of enol to keto oxaloacetate. It has been suggested that this property of class I FH might be critical to prevent suicide inactivation of succinate dehydrogenase by enol oxaloacetate which is formed by the action of SDH on malate (Flint, 1994).

Appendix-I

Appendix -I

Table A1. Phenotype of genetic knockouts of genes involved in energy metabolism in *Plasmodium* spp.

S.No	Gene	Org.	Phenotype (IE stages)	Phenotype (sexual stages)	Reference
1	Phosphoenolpyruvate carboxylase (PEPC)	<i>Pf</i>	Severely reduced growth rate. Partial rescue of growth by the addition of 5mM malate/fumarate.	N.A	(Storm et al., 2014)
		<i>Pb</i>	Reduced growth rate in erythrocytes (life cycle extended by 4hrs). However, the strain was virulent. Parasites primarily reside in reticulocytes. Overgrown by wild-type parasites in competition experiments	Defects in gametocyte production, male gamete formation, female gamete viability resulting in very low levels of oocyst formation and failure to enter sporogony.	(Srivastava et al., 2015)
2	Glutamate dehydrogenase a (GDHa)	<i>Pf</i>	Dipensable for IE stage growth.	N.A	(Storm et al., 2011)
		<i>Pb</i>	Dipensable for IE stage growth.	Dipensable for mosquito stage development	(Srivastava et al., 2016)
3	Glutamate dehydrogenase 2/b (GDHb)	<i>Pb</i>	Inability to clone by limiting dilution. This could be due to essentiality of the gene for IE stage growth.	N.A	(Srivastava et al., 2016)
4	Glutamate dehydrogenase 3/c (GDHc)	<i>Pb</i>	Dipensable for IE stage growth.	Dipensable for mosquito stage development	(Srivastava et al., 2016)
5	Glycerol kinase (GK)	<i>Pf</i>	50% reduction in growth rate attributed to reduced phospholipid incorporation in the parasite membrane.	N.A	(Naidoo and Coetzer, 2013)
6	Pyruvate dehydrogenase (PDH) Pf (E1α) Pb(E1α and E3 subunits)	<i>Pf</i>	Dipensable for IE stage growth.	N.A	(Cobbold et al., 2013)
		<i>Py</i>	Dipensable for IE stage growth.	No defect in gametocyte formation, mosquito and early	(Pei et al., 2010)

				liver stage development. The parasites could not form exo-erythrocytic merozoites during late liver stage development.	
7	Branched chain keto acid dehydrogenase (BCKDH)	<i>Pb</i>	No growth in erythrocytes. Growth restricted to only reticulocytes	Reduced number of gametocytes and impaired gametocyte development. Significantly reduced number of oocyst formation and failure to establish sporogony	(Oppenheim et al., 2014)
8	Citrate synthase (CS)	<i>Pf</i>	Dipensable for IE stage growth.	N.A	(Ke et al., 2015)
9	Aconitase (Aco)	<i>Pf</i>	Dipensable for IE stage growth.	Reduced gametocytogenesis and lack of ability to undergo exflagellation and form oocysts	(Ke et al., 2015)
		<i>Pb</i>	Dipensable for IE stage growth.	Failed to form ookinetes	(Srivastava et al., 2016)
10	Isocitrate dehydrogenase (IDH)	<i>Pf</i>	Dipensable for IE stage growth.	N.A	(Ke et al., 2015)
11	Succinyl-CoA synthetase (α-subunit)	<i>Pf</i>	Dipensable for IE stage growth.	N.A	(Ke et al., 2015)
12	Succinate dehydrogenase (SDH)[#] F_p-subunit	<i>Pf</i>	1) Dipensable for IE stage growth. 2) Growth rate reduced by 50%. Succinate supplementation rescued the growth phenotype	1) N.A 2) N.A	1. (Ke et al., 2015) 2. (Tanaka et al., 2012)
		<i>Pb</i>	Dipensable for IE stage growth.	Impaired ookinete formation and failure to form oocyst	(Hino et al., 2012)
13	Fumarate hydratase (FH)	<i>Pf</i>	Essential gene. Refractory to knockout	N.A	(Ke et al., 2015)
14	Malate-quinone oxidoreductase (MQO)	<i>Pb</i>	Essential gene. Refractory to knockout	N.A	(Ke et al., 2015)
15	Alternate NADH dehydrogenase (Ndh-2)	<i>Pb</i>	Dipensable for IE stage growth.	Arrested oocyst maturation	(Boysen and Matuschewski, 2011)
16	ATP synthase beta subunit	<i>Pf</i>	Essential gene. Refractory to	N.A	(Balabaskaran Nina et al.,

			knockout		2011)
		<i>Pb</i>	Dipensable for IE stage growth.	Arrested at ookinete stages. Does not progress into oocyst stage. The ookinets were motile but not viable in the mosquito mid-gut.	(Sturm et al., 2015)
17	Aspartate aminotransferase	<i>Pb</i>	Essential gene. Refractory to knockout	N.A	(Srivastava et al., 2015)
18	Malate dehydrogenase	<i>Pb</i>	Parasites were virulent. Growth rate comparable to wild-type parasites in competition experiments. Parasite primarily resides in reticulocyte.	~50% reduction in the number of gametocyte and ookinetes formed. However, parasites were able to complete transmission through mosquito stages and establish successful infection in mice.	(Srivastava et al., 2015)
19	α-keto glutarate dehydrogenase (E1 subunit)	<i>Pf</i>	Dipensable for IE stage growth.	Normal gametocyte maturation but reduced oocyst formation	(Ke et al., 2015)
20	Ornithine amino transferase	<i>Pb</i>	Dipensable for IE stage growth.	Normal mosquito stage development	(Srivastava et al., 2016)
21	TRP, putative GABA transporter	<i>Pb</i>	Inability to clone by limiting dilution. This could be due to essentiality of the gene for IE stage growth.	N.A	(Srivastava et al., 2016)
22	Lysine decarboxylase	<i>Pb</i>	Dipensable for IE stage growth.	Normal mosquito stage development	(Srivastava et al., 2016)
23	Phosphoenolpyruvate carboxykinase	<i>Pb</i>	Dipensable for IE stage growth.	Failure to form oocyst	(Srivastava et al., 2016)
24	Glutamate synthase	<i>Pb</i>	Dipensable for IE stage growth.	Failure to form oocyst	(Srivastava et al., 2016)

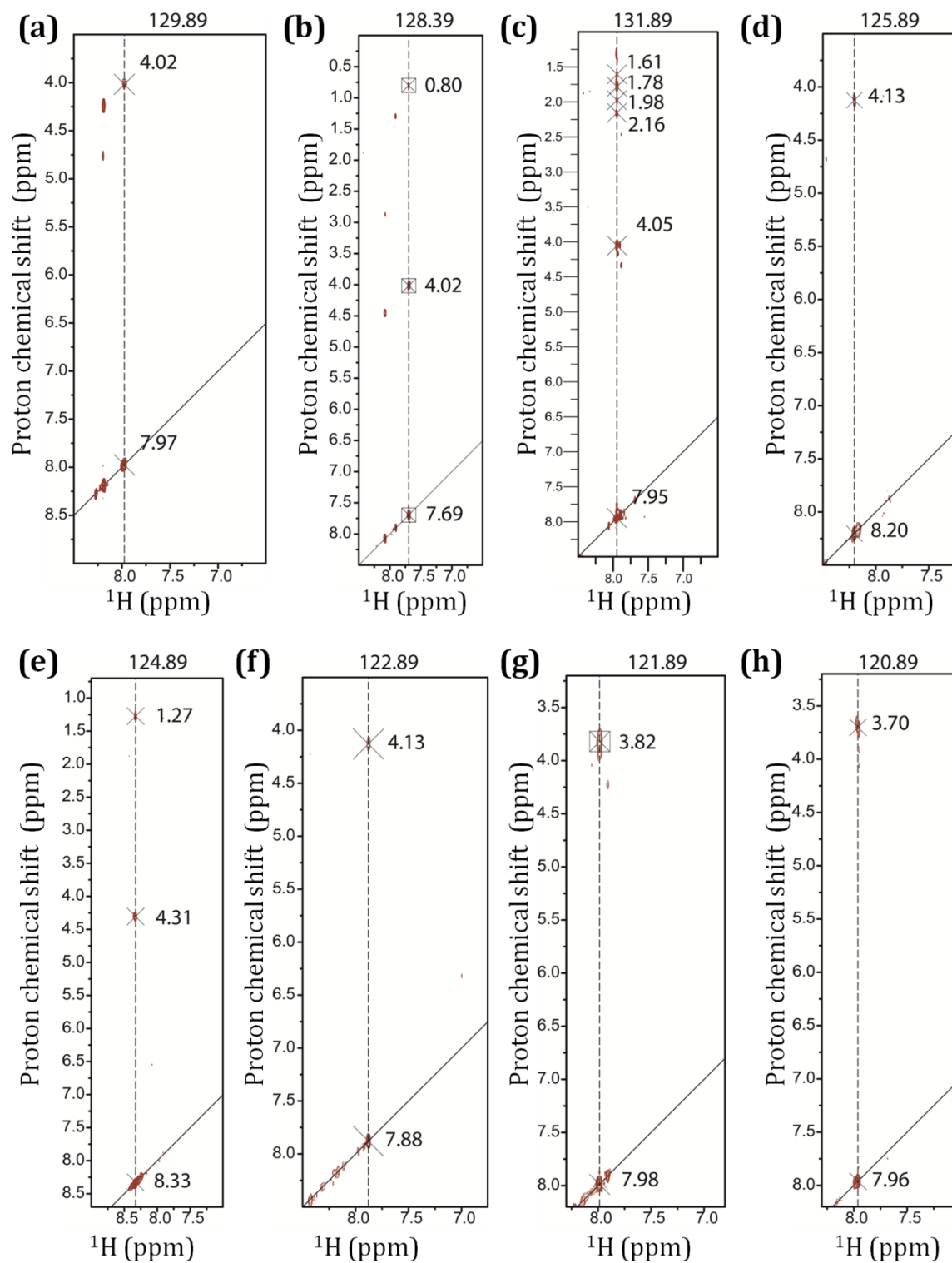
N.A., Not applicable as the study has not been carried out; IE, Intraerythrocytic

Table A4.1. List of chemical shift values in the ^{15}N and proton dimension for different cross peaks in 2D-HSQC spectrum acquired on acetylated total *E. coli* metabolites.

S.No	^{15}N (ppm)	H (ppm)
1	114.54	8.259
2	114.599	8.198
3	114.186	8.105
4	114.245	7.781
5	114.186	7.498
6	114.186	7.402
7	114.245	8.776
8	116.133	8.086
9	115.071	7.758
10	115.897	7.826
11	116.959	8.012
12	116.969	8.083
13	121.089	8.314
14	120.263	7.97
15	120.440	7.851
16	121.089	7.826
17	121.856	7.855
18	122.269	7.771
19	122.8	7.739
20	123.744	8.346
21	123.626	8.243
22	123.862	8.009
23	125.161	8.159
24	126.636	8.112
25	126.223	8.076
26	126.695	8.112
27	127.167	7.797
28	128.642	7.951
29	130.176	8.067
30	129.114	7.768
31	130.176	7.839
32	130.766	7.806
33	130.707	7.758
34	130.235	8.063
35	128.878	7.565
36	130.176	7.839
37	129.94	7.806
38	131.710	7.816
39	131.887	7.758
40	132.418	7.729
41	133.834	7.594
42	135.545	7.781
43	135.958	7.668
44	135.899	7.839
45	135.958	7.839
46	136.725	7.787
47	136.017	8.3585

Table A 4.2. Chemical shifts values obtained from ^{15}N -edited 3D-TOCSY-HSQC spectrum of acetylated total *E. coli* metabolites

#	15N (ppm)	H-N-C=O (ppm)	H α	Aliphatic-H	Strip
1	132.39	7.87	4.07	1.63	N-acetylleucine (4.12 f)
2	131.89	7.94	4.05	2.05,1.84,1.48,1.29	A4.1 c
3	131.89	7.89			
4	130.89	7.93	4.10	2.33,1.83	N-acetylglutamate (4.12 e)
4	129.89	8.18	4.76	4.23,1.28	N-acetylthreonine (4.12 d)
5	129.89	7.97	4.01		A4.1a
6	128.89	7.90	4.07	1.29	N-acetylalanine (4.12 c)
7	128.89	7.69	4.02	0.8	A4.1b
8	127.39	7.92	4.76	3.09,1.46,1.28	N-acetylarginine (4.12 g)
9	125.89	8.2	4.13		A4.1 d
10	124.89	8.32	4.30	1.27	A4.1 e
11	123.89	8.47	4.70	3.24,2.91,1.83	N-acetyl proline (4.12 b)
12	123.89	8.38			
13	122.89	7.88	4.13		A4.1 f
14	121.89	7.98	3.82		A4.1 g
15	121.89	8.44	4.079	3.91,3.70	N-acetylcysteine (4.12 h)
16	120.39	7.96	4.10	3.7	N-acetylserine (4.12 j)
17	120.39	8.10	3.92	3.38	N-acetylhistidine (4.12 i)
18	120.89	7.98	3.38	2.39	A4.1 i
19	120.89	7.96	3.70		A4.1 h
20	117.39	8.20	3.74		N-acetylglycine (4.12 a)
21	115.89	8.04	3.73		A4.1 j
22	116.39	7.96	4.24		A4.1 k
23	114.89	7.90	4.26		A4.1 l
24	115.39	8.32	4.50		A4.1 o
25	114.39	8.38	4.46		A4.1 n
26	113.89	7.5	6.77		A4.1 p
27	112.39	7.52			
28	112.39	6.82			
29	104.39	7.91	1.289		A4.1 q
30	103.89	7.91	4.06	1.29	A4.1 m



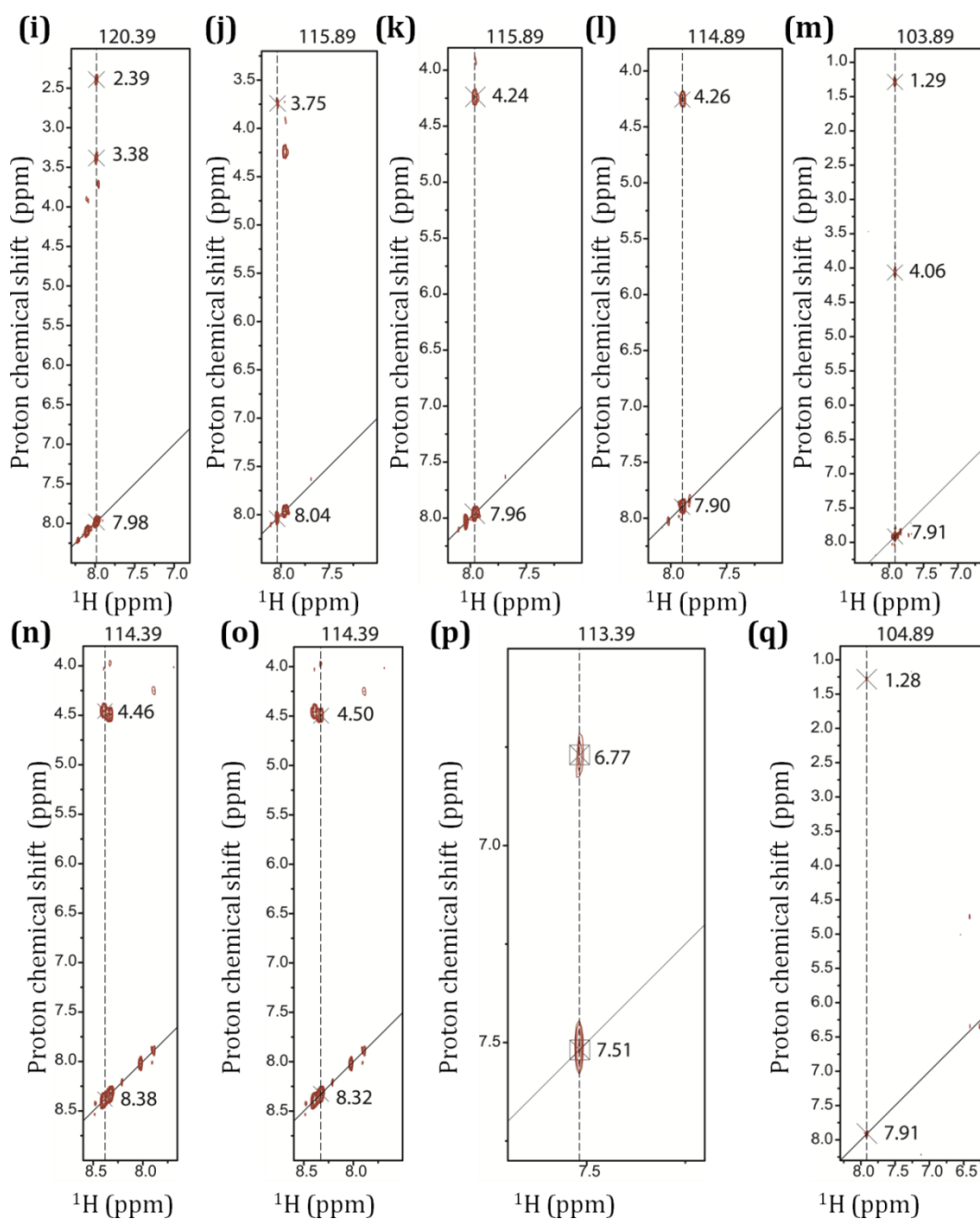


Figure A4.1. Strip plots from 3D ^{15}N -edited TOCSY-HSQC spectrum corresponding to metabolites for which the identity could not be established

P. knowlesi	1MRFNTRILLCRSPSGKCLSKSAHLGCGH.....PFRPKAHIKTLHNFVLEFEFGKEDDTEYRRIDELSKYIEVVKIKDS
P. fragile	1MRFNARIPLCRP.....LGGKH.....PF.....RFNKAQIKTLHNFVLEFEFGKEDDTEYRRIDELSKYIEVVKIKDS
P. yoellii	1	MVGYQQAARFKRRIHKLFPYITICTNNLVRISGKNN.....INNINNINNINKLNINTINNFDLTFEFGKGNDDIEYRRLDLDSKYIEVVKFNK
P. berghei	1	MVGYQKIRKFKPKVPLFPYITICTNSFIVGCHKHRIARNISNINNINNKLNINTINNFDLTFEFGKGNDDIEYRRLDLDSKYIEVVKFNK
P. vinckei	1MGIHGKNO.....IS.....NINKLNINTLNFDLTFEFGKGNDDIEYRRLDLDSKYIEVVKLNDD
P. chabaudi	1	MVAYQKVRFRKVPVSLFSYITICTNFKMGIHGKNN.....IS.....NINKLNINTLNFDLTFEFGKGNDDIEYRRLDLDSKYIEVVKLNDD
P. gallinaeum	1MLNFKNIPLLFSKK.....IYGIKTVNIN.....SI.....YKINKLNINTLNFDLTFEFGKGNDDIEYRRLDLDSKYIEVVKLNDD
P. falciptarum	1MIKPKKASILLSHKNAYLQYNLYPKKIR.....CV.....YKIKYRRHMNSLNSFDLILSPRN.....EDDIEYKVVEDLSKYIEVVKINKS
P. reichenowi	1MIKPKKASILLSHKNAYLQYNLYPKKIR.....CV.....YKIKYRRHMNSLNSFDLILSPRN.....EDDIEYKVVEDLSKYIEVVKINKS
E. coli_PuM8	1MSNKPFYIO.....APFPM.....GKDNTEYLL.....TSDYVADFD.....
G. metallireducens	1MSTKPFYIO.....EPFPL.....EKDETSYKIPDSEKVVSVAFPE.....
B. petrii		
V. cholerae		
N. meningitidis		
A. vinelandii		
Acinetobacter		
Metallosphaera		
Feridococcus		
Pyrolobus		
Thermoproteus		
Acidilobus		
Caldisphaera		
P. knowlesi	78	PIN.ESKYYGYNFENEDNFFHPNGELKNL..PEQVQRNEVERIKKEYIHPPFVLTKECYAPREILFFLNKKHKKQSNIKKQSSKNDHYVAMT
P. fragile	67	PIN.ESKYYGYNFENEENFFDPPNGELKKNL..PROVIONGERIKKEYIHPPFVLTKECYAPKEILFFLNKKHKKQSNIKKQSSKNDHYVAMT
P. yoellii	90	IND.DNKYYDINYEDENEFFDDNGNLKIK..NNEKESKKNIMKEYIHPPFVLTKECYALKEILFFLNKKHKKQSNIKKQSSKNDHYVAMT
P. berghei	99	INE.NSKYYDINYEDENEFFDDNGNLKIK..NNEKESKKNIMKEYIHPPFVLTKECYALKEILFFLNKKHKKQSNIKKQSSKNDHYVAMT
P. vinckei	61	KINKSKYYDINYEDENEFFDDNGNLKIK..NDEKESKKNVMKEYIHPPFVLTKECYALKEILFFLNKKHKKQSNIKKQSSKNDHYVAMT
P. chabaudi	87	KINKSKYYDINYEDENEFFDDNGNLKIK..NDEKESKKNVMKEYIHPPFVLTKECYALKEILFFLNKKHKKQSNIKKQSSKNDHYVAMT
P. gallinaeum	73	IPN.KTKYVGYDPTDNTNFFDKNGIKIKY..SKQDINKKDAKEYIHPPFVLTKECYAPKEILFFLNKKHKKQSNIKKQSSKNDHYVAMT
P. falciptarum	78	PMN.ETKYYGYNPKEEYNFLDEHGNIKEYIYENKLLKKNYEKEYIHPPFVLTKECYAPKEILFFLNKKHKKQSNIKKQSSKNDHYVAMT
P. reichenowi	79	PMN.ETKYYGYNPKEEYNFLDEHGNIKEYIYENKLLKKNYEKEYIHPPFVLTKECYAPKEILFFLNKKHKKQSNIKKQSSKNDHYVAMT
E. coli_PuM8	36GETILKVEPALTLIAQQPHDASFMLRPAHQKQVAALHDPPEASQNDHYVALQ
G. metallireducens	38GKEVLKVDPEALTLIAQAMRDASFMLRPAHQKQVAALHDPPEASQNDHYVALQ
B. petrii	1MRFEAARVDSANALQFVSHHPPDFVQALRRAYQAEIAPANAALLO
V. cholerae	1MTVIRKQDVISVADALQYISYTHPDLFVKALEXAPYREESQAANDSTAQ
N. meningitidis	1MTVIRKQDVISVADALQYISYTHPDLFVKALEXAPYREESQAANDSTAQ
A. vinelandii	1MTVIRKQDVISVADALQYISYTHPDLFVKALEXAPYREESQAANDSTAQ
Acinetobacter	1MTVIRKQDVISVADALQYISYTHPDLFVKALEXAPYREESQAANDSTAQ
Metallosphaera	1MSTQTFYSVRRVSELYKALTVIPKDVVERLCKAYRMEQSELGHRVLDT
Feridococcus	1MELNESFNKLVKLSGFINVVAIKSDDVNEKLELIRRESDVGLVYRA
Pyrolobus	1MORKLVDAIVEAIRIATRPLDVEAIRS..LAARSEGAACKQLOA
Thermoproteus	1MNLSEVYMRARAKAITRASIAPADVVSALRRARVSESEAAQVQGA
Acidilobus	1MGTTEQDLVGFYEMIRTAAISIPEDVYRALKECYRETNPLAKKQLEA
Caldisphaera	1MGTTESELTGFYELIKTASTSPADVYELKTYRETNPLAKKQLEA
P. knowlesi	171	LTKNAVISAQNLPSCODTGAAILGKXKDE.EI.....LITYEHKYLNLGVNAY..RNNFRYSOLSPLSMFESENKNNLPCOIRIYSSVRGAK
P. fragile	161	LTKNAVISAQNLPSCODTGAAILGKXKDE.EI.....LITYEHKYLNLGVNAY..RNNFRYSOLSPLSMFESENKNNLPCOIRIYSSVRGAK
P. yoellii	183	LTKNAVISAQNLPSCODTGAAILGKXKDE.EI.....LITYEHKYLNLGVNAY..KKNFRYSOLSPINMFEINNNLPCOIRIYSSNKKKE
P. berghei	192	LTKNAVISAQNLPSCODTGAAILGKXKDE.EI.....LITYEHKYLNLGVNAY..KKNFRYSOLSPINMFEINNNLPCOIRIYSSNKKKE
P. vinckei	155	LTKNAVISAQNLPSCODTGAAILGKXKDE.EI.....LITYEHKYLNLGVNAY..KKNFRYSOLSPINMFEINNNLPCOIRIYSSNKKKE
P. chabaudi	181	LTKNAVISAQNLPSCODTGAAILGKXKDE.EI.....LITYEHKYLNLGVNAY..KKNFRYSOLSPINMFEINNNLPCOIRIYSSNKKKE
P. gallinaeum	164	LTKNAVISAQNLPSCODTGAAILGKXKDE.EI.....LITYEHKYLNLGVNAY..KKNFRYSOLSPINMFEINNNLPCOIRIYSSNKKKE
P. falciptarum	173	LTKNAVISAQNLPSCODTGAAILGKXKDE.EI.....LITYEHKYLNLGVNAY..KKNFRYSOLSPINMFEINNNLPCOIRIYSSNKKKE
P. reichenowi	174	LTKNAVISAQNLPSCODTGAAILGKXKDE.EI.....LITYEHKYLNLGVNAY..KKNFRYSOLSPINMFEINNNLPCOIRIYSSNKKKE
E. coli_PuM8	90	PLRNEIAAANFELPSCODTGAIVGKXKDE.QV.W.....TGGDEEAISKVYNTI..IENLRYSONAALDMYKVVGGSLPAQIDLY.....
G. metallireducens	92	PLRNEIAAANFELPSCODTGAIVGKXKDE.QV.W.....TGGDEEAISKVYNTI..IENLRYSONAALDMYKVVGGSLPAQIDLY.....
B. petrii	51	ILINSRMCAEGRHPLCODTGAIVVFKVGM.DVWRWDG..ATMSVDDMNEGVRRAYNPNPNVLRASLADPAGSRKMKDPTAVIHHMS.....
V. cholerae	51	ILINSRMCAEGRHPLCODTGAIVVFKVGM.DVWRWDG..ATMSVDDMNEGVRRAYNPNPNVLRASLADPAGSRKMKDPTAVIHHMS.....
N. meningitidis	52	ILINSRMCAEGRHPLCODTGAIVVFKVGM.DVWRWDG..ATMSVDDMNEGVRRAYNPNPNVLRASLADPAGSRKMKDPTAVIHHMS.....
A. vinelandii	51	ILINSRMCAEGRHPLCODTGAIVVFKVGM.DVWRWDG..ATMSVDDMNEGVRRAYNPNPNVLRASLADPAGSRKMKDPTAVIHHMS.....
Acinetobacter	52	ILINSRMCAEGRHPLCODTGAIVVFKVGM.DVWRWDG..ATMSVDDMNEGVRRAYNPNPNVLRASLADPAGSRKMKDPTAVIHHMS.....
Metallosphaera	52	IMKNIIEVATKRNLLCODTGAIVVFKVGM.DVWRWDG..ATMSVDDMNEGVRRAYNPNPNVLRASLADPAGSRKMKDPTAVIHHMS.....
Feridococcus	52	WKKNISIALERKAPLCODTGAIVVFKVGM.DVWRWDG..ATMSVDDMNEGVRRAYNPNPNVLRASLADPAGSRKMKDPTAVIHHMS.....
Pyrolobus	47	VLRRNIEVAAREGRPLCODTGAIVVFKVGM.DVWRWDG..ATMSVDDMNEGVRRAYNPNPNVLRASLADPAGSRKMKDPTAVIHHMS.....
Thermoproteus	49	ILKNDIDACTRKKVPLCODTGAIVVFKVGM.DVWRWDG..ATMSVDDMNEGVRRAYNPNPNVLRASLADPAGSRKMKDPTAVIHHMS.....
Acidilobus	50	ILKNDIDACTRKKVPLCODTGAIVVFKVGM.DVWRWDG..ATMSVDDMNEGVRRAYNPNPNVLRASLADPAGSRKMKDPTAVIHHMS.....
Caldisphaera	50	ILKNDIDACTRKKVPLCODTGAIVVFKVGM.DVWRWDG..ATMSVDDMNEGVRRAYNPNPNVLRASLADPAGSRKMKDPTAVIHHMS.....
P. knowlesi	259	AHGVK.....TPPGVQLSASSTAP.....DSSPRYEIIFIAAGCGSANKTFI..FOOTKSLNE.....GKLYDFLLRKT
P. fragile	249	AHGCV.....TPPGVRASSPSSPTCAAS.....ASIAKYEIIFIAAGCGSANKTFI..FOOTKSLNE.....GKLYDFLLRKT
P. yoellii	271	WLNDK.....TPPGVRASSPSSPTCAAS.....KKDPRYEIIFIAAGCGSANKTFI..FOOTKSLNE.....GKLYDFLLRKT
P. berghei	280	WLNDK.....TPPGVRASSPSSPTCAAS.....KKDPRYEIIFIAAGCGSANKTFI..FOOTKSLNE.....GKLYDFLLRKT
P. vinckei	243	WLNEQ.....TPPGVRASSPSSPTCAAS.....KKMPPYEIIFIAAGCGSANKTFI..FOOTKSLNE.....GKLYDFLLRKT
P. chabaudi	269	HLNYP.....TPPGVRASSPSSPTCAAS.....KKMPPYEIIFIAAGCGSANKTFI..FOOTKSLNE.....GKLYDFLLRKT
P. gallinaeum	252	KENS.....TPPGVRASSPSSPTCAAS.....YDCPPYEIIFIAAGCGSANKTFI..FOOTKSLNE.....GKLYDFLLRKT
P. falciptarum	261	LHEVQNEYPNHHKDIQNNNVKHNKDIITRQDSKEMQSTKQNDIF..YDCPPYEIIFIAAGCGSANKTFI..FOOTKSLNE.....GKLYDFLLRKT
P. reichenowi	262	LHEVQNEYPNHHKDIQNNNVKHNKDIITRQDSKEMQSTKQNDIF..YDCPPYEIIFIAAGCGSANKTFI..FOOTKSLNE.....GKLYDFLLRKT
E. coli_PuM8	172AVDGDYKPLVAVAGCGSANKTYLYQETKALLTP..GKLYDFLLRKT
G. metallireducens	174AVDGDYKPLVAVAGCGSANKTYLYQETKALLTP..GKLYDFLLRKT
B. petrii	147VGGDIDITVAAGCGSADAKAGY.....AMLNPS.....GSIADWVVAQL
V. cholerae	137VPGDKVDTQIAAGCGSENKTKM.....VMLNPS.....DIAEWEVETV
N. meningitidis	137VPGDKVDTQIAAGCGSENKTKM.....VMLNPS.....DIAEWEVETV
A. vinelandii	137VPGDKVDTQIAAGCGSENKTKM.....VMLNPS.....DIAEWEVETV
Acinetobacter	137VPGDKVDTQIAAGCGSENKTKM.....VMLNPS.....DIAEWEVETV
Metallosphaera	138KDKIRITALPKCGSENMSL.....KMLRPADGILGAKKFLVETI
Feridococcus	135RENSYADVQVLYAGCGSARPSA.....RTLDPAGWGSIAKXVIVV
Pyrolobus	130PAKSEILIVVVPKCGSEYPAAL.....YVVPKAGLEAALKEVIAV
Thermoproteus	131FDGDLQPTVVPKCGSELPAKA.....MVLPPGATLRDIPKIVIAV
Acidilobus	132VEGDKLVVMTKCGSEFPATL.....MSEPIIGPKKSGVITD
Caldisphaera	132VEGDKLVVMTKCGSEFPATL.....MSEPIIGPKKSGVITD

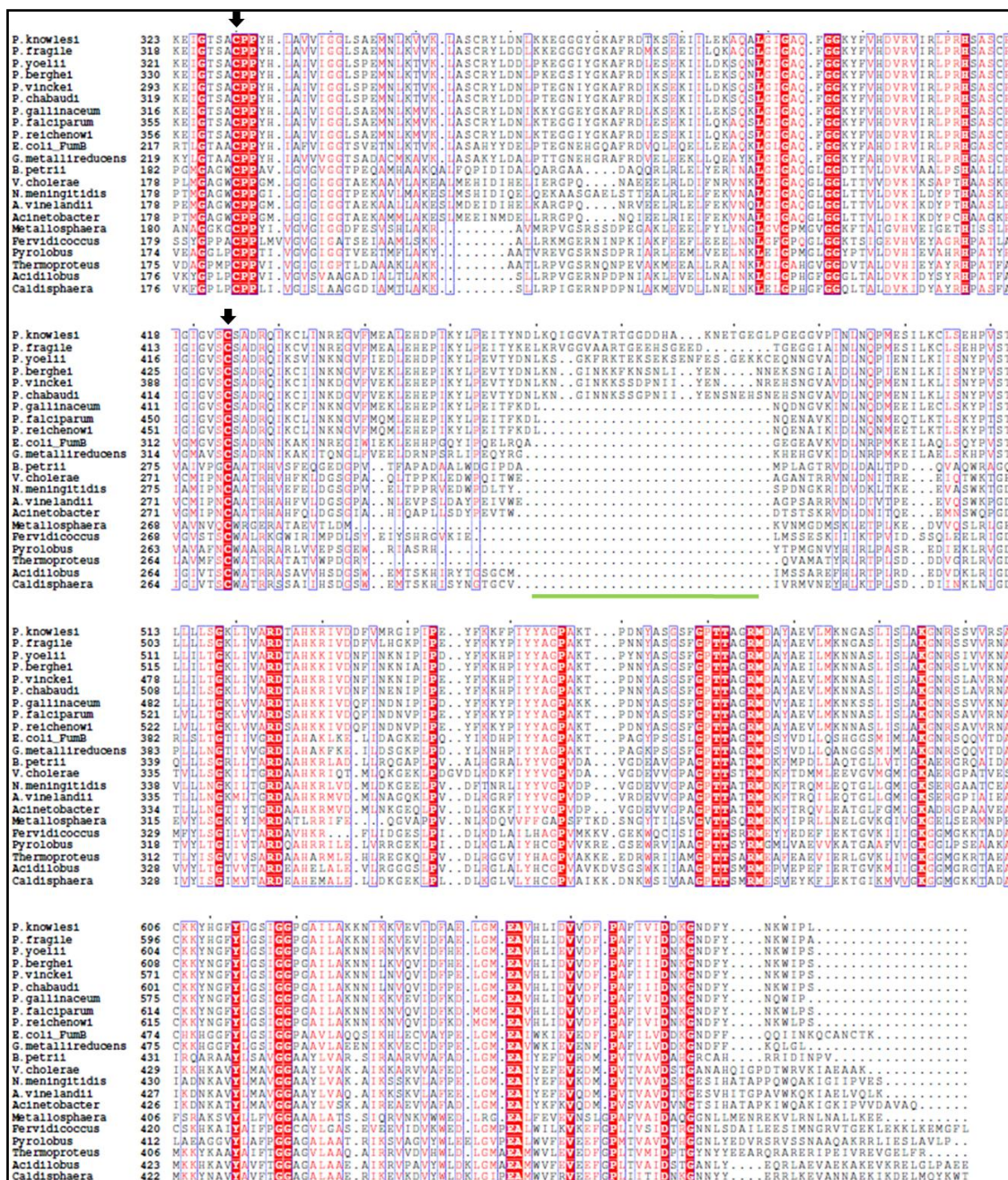


Figure A6.1. Multiple sequence alignment of single-subunit FH sequence from different *Plasmodium* spp. and two-subunit class I FH sequences from archaea and bacteria.

The black solid line shows 120 amino acid insertion at the N-terminal in *Plasmodium* FH sequences. The black arrow shows invariant cysteine residues that might be involved in Fe-S cluster ligation. The green bar indicates the boundary between the N- and C-terminal domains.

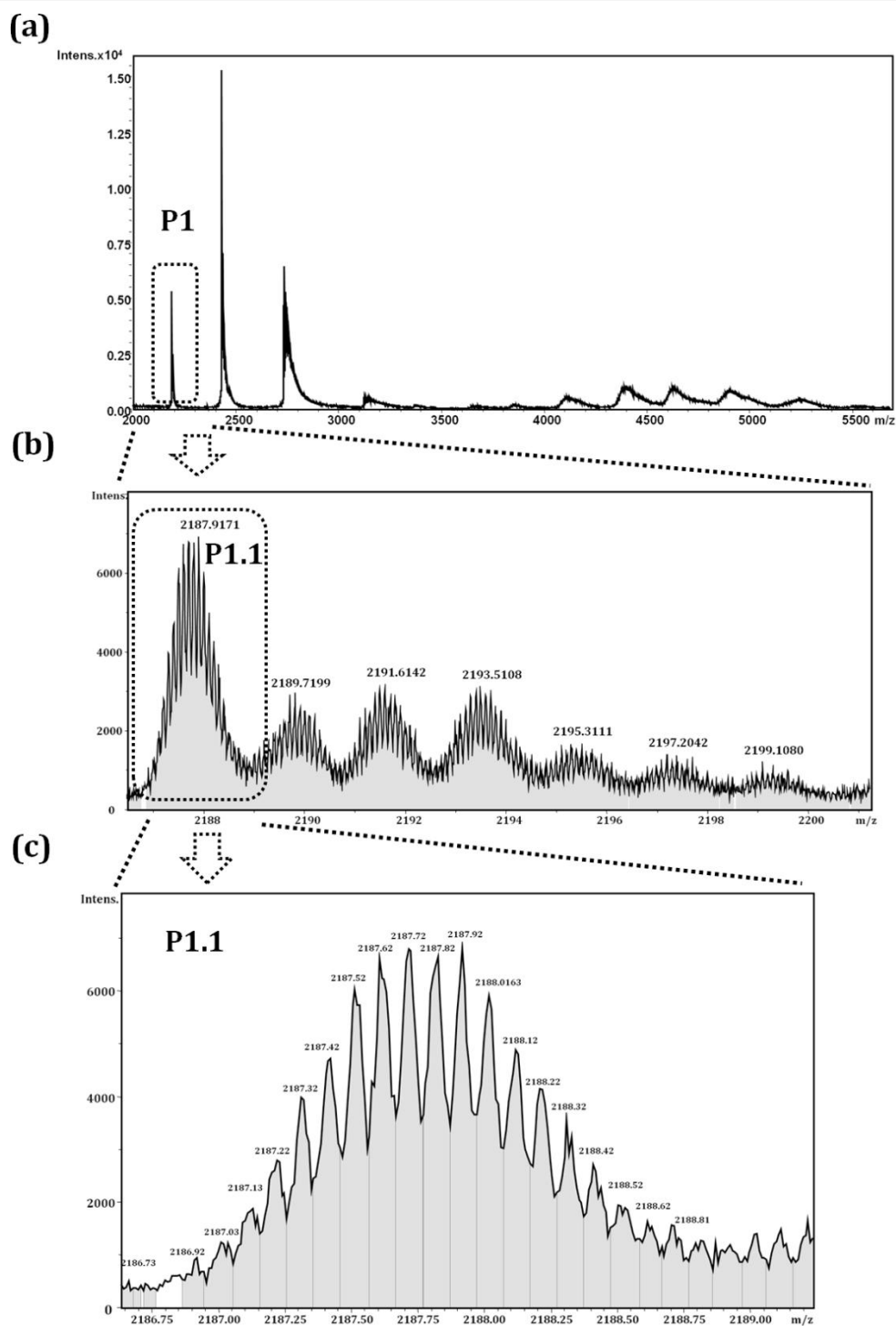


Figure A.7.1. Native mass spectrometry of MjFHαβ

(a) Complete mass spectrum (m/z from 2000 to 5500) of reconstituted MjFHαβ with the first peak with the lowest m/z value highlighted by a rectangular boundary. **(b)** Zoom-in of peak 1 shows the presence of adducts with mass increment of 19 Da. The first peak is highlighted by a rectangular boundary. **(c)** Peak 1.1 is further zoomed-in to highlight the isotope distribution. Peak 1.1 corresponds to 10+ charge state of β -subunit alone as calculated by using the difference in mass (0.10) between adjacent isotope peaks.

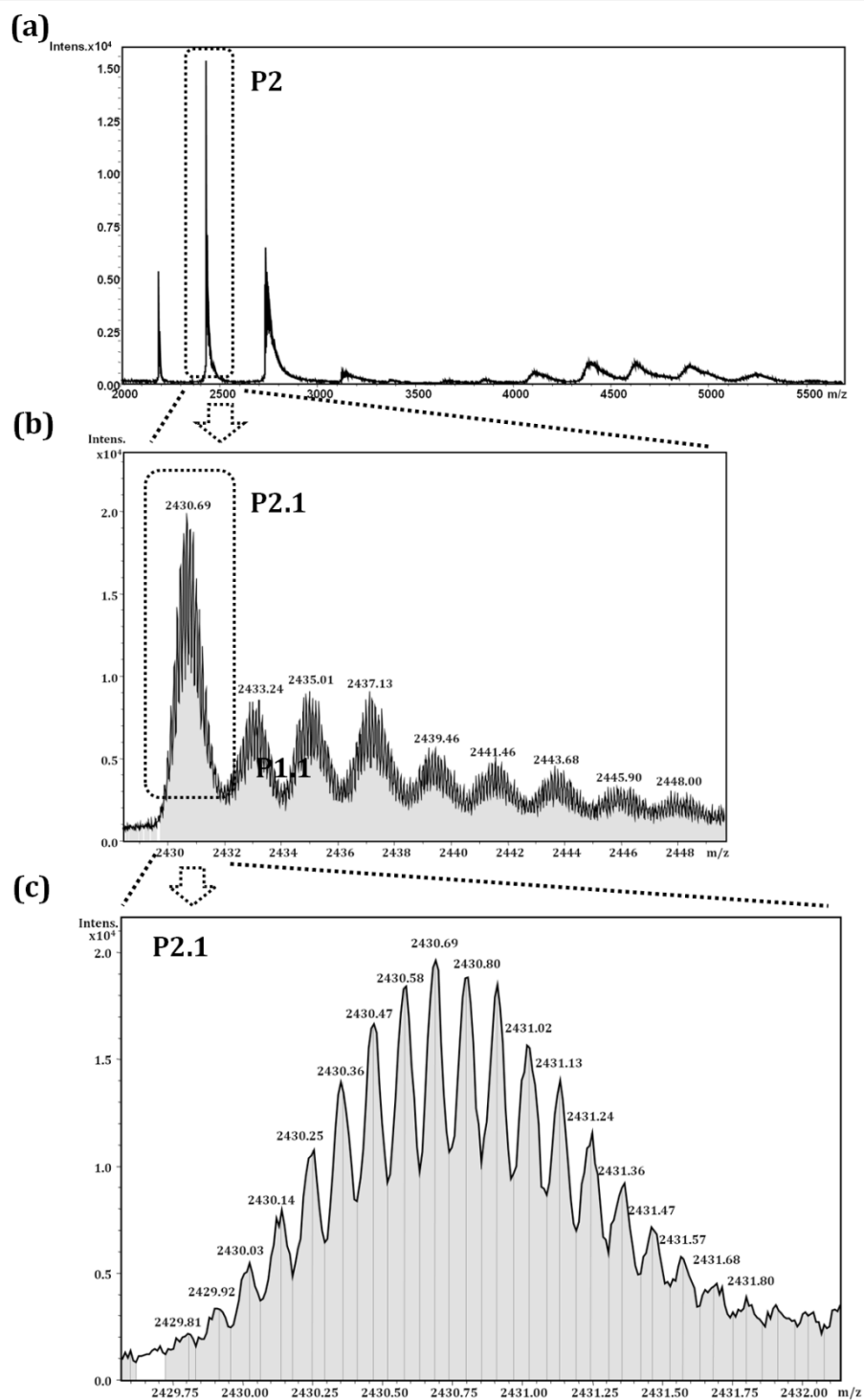


Figure A.7.2. Native mass spectrometry of MjFHαβ

(a) Complete mass spectrum (m/z from 2000 to 5500) of reconstituted MjFHαβ with the second peak highlighted by a rectangular boundary. **(b)** Zoom-in of peak 2 shows the presence of adducts with mass increment of 23 Da. The first peak is highlighted by a rectangular boundary. **(c)** Peak 2.1 is further zoomed-in to highlight the isotope distribution. Peak 2.1 corresponds to 9+ charge state of β-subunit alone as calculated by using the difference in mass (0.11) between adjacent isotope peaks.

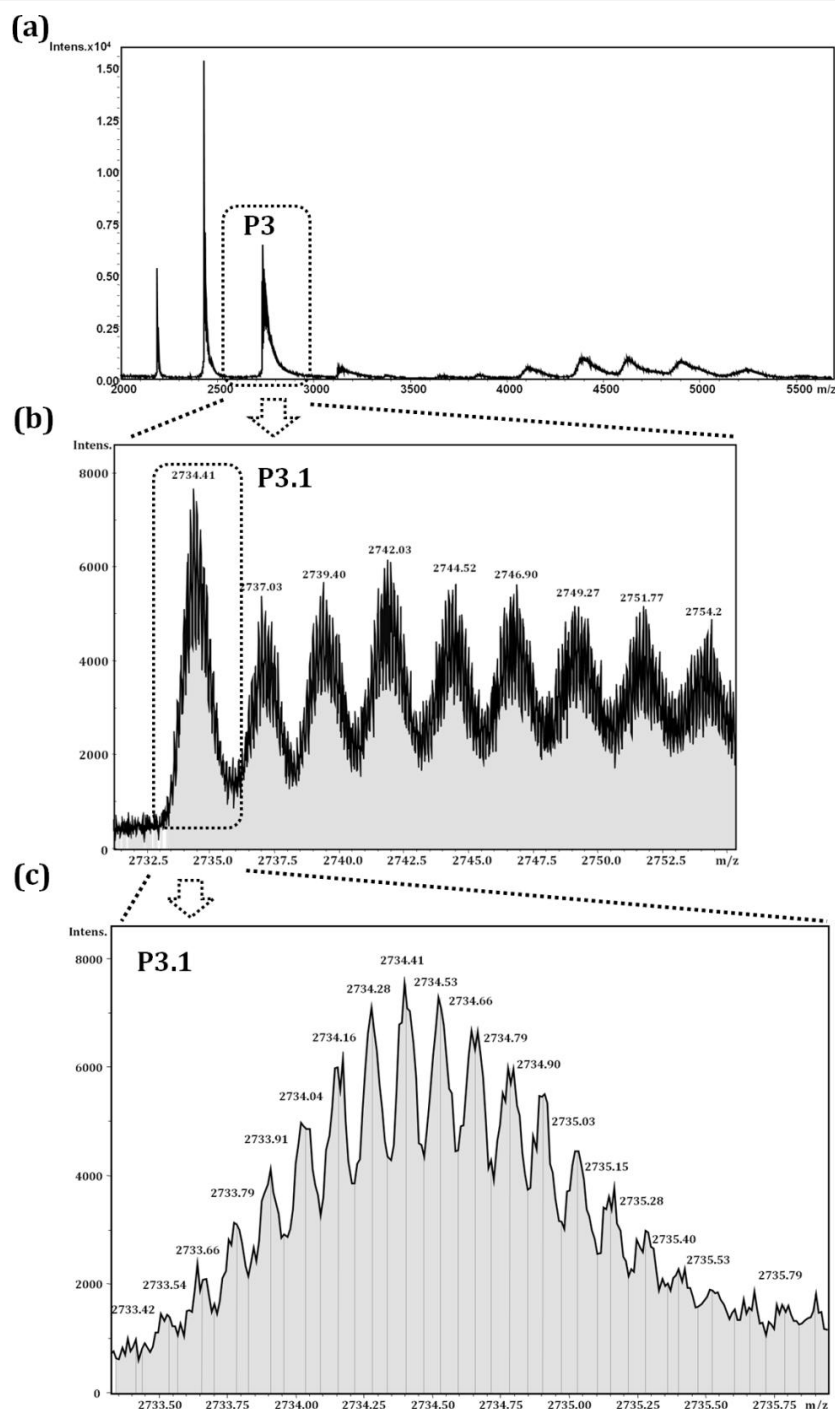


Figure A.7.3. Native mass spectrometry of MjFHαβ

(a) Complete mass spectrum (m/z from 2000 to 5500) of reconstituted MjFHαβ with the third peak highlighted by a rectangular boundary. **(b)** Zoom-in of peak 3 shows the presence of adducts with mass increment of 21Da . The first peak (P3.1) is highlighted by a rectangular boundary. **(c)** Peak 3.1 is further zoomed-in to highlight the isotope distribution. Peak 3.1 corresponds to 9+ charge state of β-subunit alone as calculated by using the difference in mass (0.12) between adjacent isotope peaks.

Table A7.1. Observed m/z values obtained from the native reconstituted MjFH $\alpha\beta$. Peaks have been assigned to various possible stoichiometries of MjFH α , MjFH β and Fe-S cluster, and compared with theoretical m/z values.

S.N O	Stoichiometry of complex	Charge state	Theoretical m/z	Experimental m/z
1	(MjFH α) ₂ +(MjFH β) ₂ + [2Fe-2S] ₂	35+	3124.24	3124.98
2	(MjFH α_D) ₂ + [4Fe-4S] ₂	21+	3140.26	3139.33
3	(MjFH α_D) ₂ + [3Fe-4S] ₂	18+	3657.38	3655.36
4	(MjFH α) ₂ + [4Fe-4S] ₂	17+	3858.06	3862.12
5	(MjFH α_D) ₂ + [4Fe-4S] ₂	16+	4114.43	4111.81
6	(MjFH α_D) ₂ + [4Fe-4S] ₂	15+	4388.66	4391.63
7	(MjFH α) ₂	14+	4634.92	4634.32
8	(MjFH α_D) ₂ +(MjFH β) ₂ + [2Fe-2S] ₂	23+	4768.88	4767.65
9	(MjFH α_D) ₂ +(MjFH β) ₂ + [2Fe-2S] ₂	22+	4985.605	4983.82

α_D , desmethionine form of MjFH α subunit

Appendix-II

NATURE PUBLISHING GROUP LICENSE TERMS AND CONDITIONS

Dec 31, 2016

This Agreement between Vijay Jayaraman ("You") and Nature Publishing Group ("Nature Publishing Group") consists of your license details and the terms and conditions provided by Nature Publishing Group and Copyright Clearance Center.

License Number	4019140446970
License date	Dec 31, 2016
Licensed Content Publisher	Nature Publishing Group
Licensed Content Publication	Nature Reviews Microbiology
Licensed Content Title	Looking under the skin: the first steps in malarial infection and immunity
Licensed Content Author	Robert Ménard, Joana Tavares, Ian Cockburn, Miles Markus, Fidel Zavala et al.
Licensed Content Date	Sep 16, 2013
Licensed Content Volume Number	11
Licensed Content Issue Number	10
Type of Use	reuse in a dissertation / thesis
Requestor type	academic/educational
Format	print
Portion	figures/tables/illustrations
Number of figures/tables /illustrations	1
High-res required	no
Figures	Figure 1
Author of this NPG article	no
Your reference number	
Title of your thesis / dissertation	Crosstalk between purine salvage and energy metabolism in Plasmodium
Expected completion date	Nov 2016
Estimated size (number of pages)	280
Requestor Location	Vijay Jayaraman JNCASR, Jakkur Bangalore Bangaluru, 560064 India Attn: Vijay Jayaraman
Billing Type	Invoice
Billing Address	Vijay Jayaraman JNCASR, Jakkur Bangalore Bangaluru, India 560064 Attn: Vijay Jayaraman
Total	0.00 USD

ELSEVIER LICENSE TERMS AND CONDITIONS

Dec 31, 2016

This Agreement between Vijay Jayaraman ("You") and Elsevier ("Elsevier") consists of your license details and the terms and conditions provided by Elsevier and Copyright Clearance Center.

License Number	3967450538601
License date	Oct 14, 2016
Licensed Content Publisher	Elsevier
Licensed Content Publication	Trends in Parasitology
Licensed Content Title	Apicomplexan Energy Metabolism: Carbon Source Promiscuity and the Quiescence Hyperbole
Licensed Content Author	Damien Jacot,Ross F. Waller,Dominique Soldati-Favre,Dougal A. MacPherson,James I. MacRae
Licensed Content Date	January 2016
Licensed Content Volume Number	32
Licensed Content Issue Number	1
Licensed Content Pages	15
Start Page	56
End Page	70
Type of Use	reuse in a thesis/dissertation
Intended publisher of new work	other
Portion	figures/tables/illustrations
Number of figures/tables /illustrations	1
Format	both print and electronic
Are you the author of this Elsevier article?	No
Will you be translating?	No
Order reference number	
Original figure numbers	Figure I
Title of your thesis/dissertation	Crosstalk between purine salvage and energy metabolism in Plasmodium
Expected completion date	Nov 2016
Estimated size (number of pages)	280
Elsevier VAT number	GB 494 6272 12
Requestor Location	Vijay Jayaraman JNCASR, Jakkur Banaglore Bangaluru, 560064 India Attn: Vijay Jayaraman
Total	0.00 USD
Terms and Conditions	



Confirmation Number: 11598774
Order Date: 10/14/2016

Customer Information

Customer: Vijay Jayaraman
Account Number: 3001072492
Organization: Vijay Jayaraman
Email: vijayj@jncasr.ac.in
Phone: +91 8022082813
Payment Method: Invoice

This is not an invoice

Order Details

Future medicinal chemistry

Billing Status:
N/A

Order detail ID: 70135289
ISSN: 1756-8919
Publication Type: Journal
Volume:
Issue:
Start page:
Publisher: Future Science

Permission Status: **Granted**
Permission type: Republish or display content
Type of use: Thesis/Dissertation
Order License Id: 3967460194072

Requestor type	Author of requested content
Format	Print, Electronic
Portion	image/photo
Number of images/photos requested	1
Title or numeric reference of the portion(s)	Figure1
Title of the article or chapter the portion is from	Targeting the mitochondrial electron transport chain of Plasmodium falciparum: new strategies towards the development of improved antimalarials for the elimination era
Editor of portion(s)	NA
Author of portion(s)	NA
Volume of serial or monograph	NA
Issue, if republishing an article from a serial	NA
Page range of portion	1
Publication date of portion	Nov, 2016
Rights for	Main product
Duration of use	Life of current edition

**ELSEVIER LICENSE
TERMS AND CONDITIONS**

Dec 31, 2016

This Agreement between Vijay Jayaraman ("You") and Elsevier ("Elsevier") consists of your license details and the terms and conditions provided by Elsevier and Copyright Clearance Center.

License Number	4019160006456
License date	Dec 31, 2016
Licensed Content Publisher	Elsevier
Licensed Content Publication	Trends in Endocrinology & Metabolism
Licensed Content Title	AMPK functions as an adenylyate charge-regulated protein kinase
Licensed Content Author	Jonathan S. Oakhill, John W. Scott, Bruce. E. Kemp
Licensed Content Date	March 2012
Licensed Content Volume Number	23
Licensed Content Issue Number	3
Licensed Content Pages	8
Start Page	125
End Page	132
Type of Use	reuse in a thesis/dissertation
Intended publisher of new work	other
Portion	figures/tables/illustrations
Number of figures/tables /illustrations	1
Format	both print and electronic
Are you the author of this Elsevier article?	No
Will you be translating?	No
Order reference number	
Original figure numbers	Figure I
Title of your thesis/dissertation	Crosstalk between purine salvage and energy metabolism in Plasmodium
Expected completion date	Nov 2016
Estimated size (number of pages)	280
Elsevier VAT number	GB 494 6272 12
Requestor Location	Vijay Jayaraman JNCASR, Jakkur Banaglore Bangaluru, 560064

**ELSEVIER LICENSE
TERMS AND CONDITIONS**

Dec 31, 2016

This Agreement between Vijay Jayaraman ("You") and Elsevier ("Elsevier") consists of your license details and the terms and conditions provided by Elsevier and Copyright Clearance Center.

License Number	4019270714574
License date	Dec 31, 2016
Licensed Content Publisher	Elsevier
Licensed Content Publication	Phytochemistry
Licensed Content Title	Fumarate: Multiple functions of a simple metabolite
Licensed Content Author	Wagner L. Araújo, Adriano Nunes-Nesi, Alisdair R. Fernie
Licensed Content Date	June 2011
Licensed Content Volume Number	72
Licensed Content Issue Number	9
Licensed Content Pages	6
Start Page	838
End Page	843
Type of Use	reuse in a thesis/dissertation
Intended publisher of new work	other
Portion	figures/tables/illustrations
Number of figures/tables /illustrations	1
Format	both print and electronic
Are you the author of this Elsevier article?	No
Will you be translating?	No
Order reference number	
Original figure numbers	Figure 1
Title of your thesis/dissertation	Crosstalk between purine salvage and energy metabolism in Plasmodium
Expected completion date	Nov 2016
Estimated size (number of pages)	280
Elsevier VAT number	GB 494 6272 12
Requestor Location	Vijay Jayaraman JNCASR, Jakkur Bangalore Bangaluru, 560064

**ELSEVIER LICENSE
TERMS AND CONDITIONS**

Dec 31, 2016

This Agreement between Vijay Jayaraman ("You") and Elsevier ("Elsevier") consists of your license details and the terms and conditions provided by Elsevier and Copyright Clearance Center.

License Number	4019310135985
License date	Dec 31, 2016
Licensed Content Publisher	Elsevier
Licensed Content Publication	Bioorganic & Medicinal Chemistry
Licensed Content Title	Reactivity of dimethyl fumarate and methylhydrogen fumarate towards glutathione and N-acetyl-L-cysteine—Preparation of S-substituted thiosuccinic acid esters
Licensed Content Author	Thomas J. Schmidt, Muharrem Ak, Ulrich Mrowietz
Licensed Content Date	1 January 2007
Licensed Content Volume Number	15
Licensed Content Issue Number	1
Licensed Content Pages	10
Start Page	333
End Page	342
Type of Use	reuse in a thesis/dissertation
Intended publisher of new work	other
Portion	figures/tables/illustrations
Number of figures/tables /illustrations	1
Format	both print and electronic
Are you the author of this Elsevier article?	No
Will you be translating?	No
Order reference number	
Original figure numbers	Figure 1
Title of your thesis/dissertation	Crosstalk between purine salvage and energy metabolism in Plasmodium
Expected completion date	Nov 2016
Estimated size (number of pages)	280
Elsevier VAT number	GB 494 6272 12
Requestor Location	Vijay Jayaraman JNCASR, Jakkur Banaglore

**NATURE PUBLISHING GROUP LICENSE
TERMS AND CONDITIONS**

Dec 31, 2016

This Agreement between Vijay Jayaraman ("You") and Nature Publishing Group ("Nature Publishing Group") consists of your license details and the terms and conditions provided by Nature Publishing Group and Copyright Clearance Center.

License Number	4019380147964
License date	Dec 31, 2016
Licensed Content Publisher	Nature Publishing Group
Licensed Content Publication	Nature Reviews Molecular Cell Biology
Licensed Content Title	Iron-sulphur cluster biogenesis and mitochondrial iron homeostasis
Licensed Content Author	Tracey A. Rouault and Wing-Hang Tong
Licensed Content Date	Apr 1, 2005
Licensed Content Volume Number	6
Licensed Content Issue Number	4
Type of Use	reuse in a dissertation / thesis
Requestor type	academic/educational
Format	print and electronic
Portion	figures/tables/illustrations
Number of figures/tables /illustrations	1
High-res required	no
Figures	Figure 1
Author of this NPG article	no
Your reference number	
Title of your thesis / dissertation	Crosstalk between purine salvage and energy metabolism in Plasmodium
Expected completion date	Nov 2016
Estimated size (number of pages)	280
Requestor Location	Vijay Jayaraman JNCASR, Jakkur Banaglore Bangaluru, 560064 India Attn: Vijay Jayaraman
Billing Type	Invoice
Billing Address	Vijay Jayaraman JNCASR, Jakkur Banaglore

References

REFERENCES

- A Pradet, and P Raymond (1983) Adenine Nucleotide Ratios and Adenylate Energy Charge in Energy Metabolism. *Annu. Rev. Plant Physiol.* 34, 199–224
- Abraham, T., Lewis, R. N. A. H., Hodges, R. S., and McElhaney, R. N. (2005) Isothermal titration calorimetry studies of the binding of a rationally designed analogue of the antimicrobial peptide gramicidin S to phospholipid bilayer membranes. *Biochemistry.* 44, 2103–12
- Adam, J., Yang, M., Bauerschmidt, C., Kitagawa, M., O'Flaherty, L., Maheswaran, P., Özkan, G., Sahgal, N., Baban, D., Kato, K., Saito, K., Iino, K., Igarashi, K., Stratford, M., Pugh, C., Tennant, D. A., Ludwig, C., Davies, B., Ratcliffe, P. J., El-Bahrawy, M., Ashrafian, H., Soga, T., and Pollard, P. J. (2013) A role for cytosolic fumarate hydratase in urea cycle metabolism and renal neoplasia. *Cell Rep.* 3, 1440–8
- Adams, K. L., and Palmer, J. D. (2003) Evolution of mitochondrial gene content: gene loss and transfer to the nucleus. *Mol. Phylogenet. Evol.* 29, 380–95
- Adams, P. D., Afonine, P. V., Bunkóczi, G., Chen, V. B., Davis, I. W., Echols, N., Headd, J. J., Hung, L.-W., Kapral, G. J., Grosse-Kunstleve, R. W., McCoy, A. J., Moriarty, N. W., Oeffner, R., Read, R. J., Richardson, D. C., Richardson, J. S., Terwilliger, T. C., Zwart, P. H. (2010) PHENIX: a comprehensive Python-based system for macromolecular structure solution. *Acta Crystallogr. Sect. D Biol. Crystallogr.* 66, 213–221
- Admyre, T., Amrot-Fors, L., Andersson, M., Bauer, M., Bjursell, M., Drmota, T., Hallén, S., Hartleib-Geschwindner, J., Lindmark, B., Liu, J., Löfgren, L., Rohman, M., Selmi, N., and Wallenius, K. (2014) Inhibition of {AMP} Deaminase Activity Does Not Improve Glucose Control in Rodent Models of Insulin Resistance or Diabetes. *Chem. Biol.* 21, 1486–1496
- Afonine, P. V., Grosse-Kunstleve, R. W., Echols, N., Headd, J. J., Moriarty, N. W., Mustyakimov, M., Terwilliger, T. C., Urzhumtsev, A., Zwart, P. H., Adams, P. D. (2012) Towards automated crystallographic structure refinement with phenix.refine. *Acta Crystallogr. Sect. D Biol. Crystallogr.* 68, 352–367
- Agar, J. N., Krebs, C., Frazzon, J., Huynh, B. H., Dean, D. R., and Johnson, M. K. (2000) IscU as a scaffold for iron-sulfur cluster biosynthesis: sequential assembly of [2Fe-2S] and [4Fe-4S] clusters in IscU. *Biochemistry.* 39, 7856–62
- Alfonzo, J. D., Sahota, A., and Taylor, M. W. (1997) Purification and characterization of adenine phosphoribosyltransferase from *Saccharomyces cerevisiae*. *Biochim. Biophys. Acta - Protein Struct. Mol. Enzymol.* 1341, 173–182
- Aly, A. S. I., Downie, M. J., Mamoun, C. Ben, and Kappe, S. H. I. (2010) Subpatent infection with nucleoside transporter 1-deficient *Plasmodium* blood stage parasites confers sterile protection against lethal malaria in mice. *Cell. Microbiol.* 12, 930–8

-
- Androes, G. M., and Calvin, M. (1962) Electron paramagnetic resonance in biology. *Biophys. J.* 2, 217–58
- Araújo, W. L., Nunes-Nesi, A., and Fernie, A. R. (2011) Fumarate: Multiple functions of a simple metabolite. *Phytochemistry.* 72, 838–843
- Arinze, I. J. (2005) Facilitating understanding of the purine nucleotide cycle and the one-carbon pool: Part I: The purine nucleotide cycle. *Biochem. Mol. Biol. Educ.* 33, 165–168
- Arisue, N., and Hashimoto, T. (2015) Phylogeny and evolution of apicomlasts and apicomplexan parasites. *Parasitol. Int.* 64, 254–259
- Arnot, D. E., and Gull, K. (1998) The Plasmodium cell-cycle: facts and questions. *Ann. Trop. Med. Parasitol.* 92, 361–5
- Ashrafiyan, H., Czibik, G., Bellahcene, M., Aksentijević, D., Smith, A. C., Mitchell, S. J., Dodd, M. S., Kirwan, J., Byrne, J. J., Ludwig, C., Isackson, H., Yavari, A., Støttrup, N. B., Contractor, H., Cahill, T. J., Sahgal, N., Ball, D. R., Birkler, R. I. D., Hargreaves, I., Tennant, D. A., Land, J., Lygate, C. A., Johannsen, M., Kharbanda, R. K., Neubauer, S., Redwood, C., de Cabo, R., Ahmet, I., Talan, M., Günther, U. L., Robinson, A. J., Viant, M. R., Pollard, P. J., Tyler, D. J., and Watkins, H. (2012) Fumarate is cardioprotective via activation of the Nrf2 antioxidant pathway. *Cell Metab.* 15, 361–71
- Atkinson, D. E., and Walton, G. M. (1967) Adenosine triphosphate conservation in metabolic regulation. Rat liver citrate cleavage enzyme. *J. Biol. Chem.* 242, 3239–41
- Baba, T., Ara, T., Hasegawa, M., Takai, Y., Okumura, Y., Baba, M., Datsenko, K. A., Tomita, M., Wanner, B. L., and Mori, H. (2006) Construction of Escherichia coli K-12 in-frame, single-gene knockout mutants: the Keio collection. *Mol. Syst. Biol.* 2, 2006.0008
- Balabaskaran Nina, P., Morrissey, J. M., Ganesan, S. M., Ke, H., Pershing, A. M., Mather, M. W., and Vaidya, A. B. (2011) ATP synthase complex of Plasmodium falciparum: dimeric assembly in mitochondrial membranes and resistance to genetic disruption. *J. Biol. Chem.* 286, 41312–22
- Bannister, L. H., Hopkins, J. M., Fowler, R. E., Krishna, S., and Mitchell, G. H. (2000) A brief illustrated guide to the ultrastructure of Plasmodium falciparum asexual blood stages. *Parasitol. Today.* 16, 427–33
- Barak, R., Giebel, I., and Eisenbach, M. (1996) The specificity of fumarate as a switching factor of the bacterial flagellar motor. *Mol. Microbiol.* 19, 139–44
- Bardella, C., El-Bahrawy, M., Frizzell, N., Adam, J., Ternette, N., Hatipoglu, E., Howarth, K., O’Flaherty, L., Roberts, I., Turner, G., Taylor, J., Giaslakitotis, K., Macaulay, V. M., Harris, A. L., Chandra, A., Lehtonen, H. J., Launonen, V., Aaltonen, L. A., Pugh, C. W., Mihai, R., Trudgian, D., Kessler, B., Baynes, J. W., Ratcliffe, P. J., Tomlinson, I. P., and Pollard, P. J. (2011) Aberrant succination of proteins in fumarate hydratase-deficient mice and HLRCC patients is a robust biomarker of mutation status. *J. Pathol.* 225, 4–11
-

- Battye, T. G. G., Kontogiannis, L., Johnson, O., Powell, H. R., and Leslie, A. G. W. (2011) iMOSFLM: a new graphical interface for diffraction-image processing with MOSFLM. *Acta Crystallogr. D. Biol. Crystallogr.* 67, 271–81
- Bearne, S. L., and Wolfenden, R. (1995) Enzymic hydration of an olefin: the burden borne by fumarase. *J. Am. Chem. Soc.* 117, 9588–9589
- Beinert, H. (1983) Semi-micro methods for analysis of labile sulfide and of labile sulfide plus sulfane sulfur in unusually stable iron-sulfur proteins. *Anal. Biochem.* 131, 373–378
- Beinert, H. (2000) A tribute to sulfur. *Eur. J. Biochem.* 267, 5657–5664
- Beinert, H., Emptage, M. H., Dreyer, J. L., Scott, R. A., Hahn, J. E., Hodgson, K. O., and Thomson, A. J. (1983) Iron-sulfur stoichiometry and structure of iron-sulfur clusters in three-iron proteins: evidence for [3Fe-4S] clusters. *Proc. Natl. Acad. Sci. U. S. A.* 80, 393–6
- Beinert, H., Kennedy, M. C., and Stout, C. D. (1996) Aconitase as Iron-Sulfur Protein, Enzyme, and Iron-Regulatory Protein. *Chem. Rev.* 96, 2335–2374
- Bender, A., van Dooren, G. G., Ralph, S. A., McFadden, G. I., and Schneider, G. (2003) Properties and prediction of mitochondrial transit peptides from *Plasmodium falciparum*. *Mol. Biochem. Parasitol.* 132, 59–66
- Bennett, B. (2010) *Metals in Biology*, 10.1007/978-1-4419-1139-1
- Berg, J. M., Tymoczko, J. L., and Stryer, L. (2002) Purine Bases Can Be Synthesized de Novo or Recycled by Salvage Pathways
- Berman, H. M., Westbrook, J., Feng, Z., Gilliland, G., Bhat, T. N., Weissig, H., Shindyalov, I. N., and Bourne, P. E. (2000) The Protein Data Bank. *Nucleic Acids Res.* 28, 235–42
- Berman, H., Henrick, K., and Nakamura, H. (2003) Announcing the worldwide Protein Data Bank. *Nat. Struct. Biol.* 10, 980–980
- Bertini, I., Gray, H. B., Stiefel, E. I., and Valentine, J. S. (2006) *Biological inorganic chemistry : structure and reactivity*
- Bertrand, P., More, C., Guigliarelli, B., Fournel, A., Bennett, B., and Howes, B. (1994) Biological polynuclear clusters coupled by magnetic interactions: From the point dipole approximation to a local spin model. *J. Am. Chem. Soc.* 116, 3078–3086
- Biagini, G. A., Fisher, N., Berry, N., Stocks, P. A., Meunier, B., Williams, D. P., Bonar-Law, R., Bray, P. G., Owen, A., O'Neill, P. M., and Ward, S. A. (2008) Acridinediones: selective and potent inhibitors of the malaria parasite mitochondrial bc1 complex. *Mol. Pharmacol.* 73, 1347–55
- Biagini, G. A., Viriyavejakul, P., O'Neill, P. M., Bray, P. G., and Ward, S. A. (2006) Functional characterization and target validation of alternative complex I of *Plasmodium falciparum* mitochondria. *Antimicrob. Agents Chemother.* 50, 1841–51

-
- Birrell, J. A., Laurich, C., Reijerse, E. J., Ogata, H., and Lubitz, W. (2016) Importance of Hydrogen Bonding in Fine Tuning the [2Fe-2S] Cluster Redox Potential of HydC from *Thermotoga maritima*. *Biochemistry*. 10.1021/acs.biochem.6b00341
- Blanchard, J. S., and Cleland, W. W. (1980) Use of isotope effects to deduce the chemical mechanism of fumarase. *Biochemistry*. 19, 4506–4513
- Blatnik, M., Thorpe, S. R., and Baynes, J. W. (2008) Succination of proteins by fumarate: mechanism of inactivation of glyceraldehyde-3-phosphate dehydrogenase in diabetes. *Ann. N. Y. Acad. Sci.* 1126, 272–5
- Blume, M., Nitzsche, R., Sternberg, U., Gerlic, M., Masters, S. L., Gupta, N., and McConville, M. J. (2015) A *Toxoplasma gondii* Gluconeogenic Enzyme Contributes to Robust Central Carbon Metabolism and Is Essential for Replication and Virulence. *Cell Host Microbe*. 18, 210–20
- Boettcher, M., Lawson, A., Ladenburger, V., Fredebohm, J., Wolf, J., Hoheisel, J. D., Frezza, C., and Shlomi, T. (2014) High throughput synthetic lethality screen reveals a tumorigenic role of adenylate cyclase in fumarate hydratase-deficient cancer cells. *BMC Genomics*. 15, 158
- Boitz, J. M., Strasser, R., Yates, P. A., Jardim, A., and Ullman, B. (2013) Adenylosuccinate synthetase and adenylosuccinate lyase deficiencies trigger growth and infectivity deficits in *Leishmania donovani*. *J. Biol. Chem.* 288, 8977–90
- Bomsel, J.-L., and Pradet, A. (1968) Study of adenosine 5'-mono-, di- and triphosphates in plant tissues. IV. Regulation of the level of nucleotides, in vivo, by adenylate kinase: Theoretical and experimental study. *Biochim. Biophys. Acta - Bioenerg.* 162, 230–242
- Bonomi, F., Iametti, S., Morleo, A., Ta, D., and Vickery, L. E. (2008) Studies on the mechanism of catalysis of iron-sulfur cluster transfer from IscU[2Fe2S] by HscA/HscB chaperones. *Biochemistry*. 47, 12795–801
- Boysen, K. E., and Matuschewski, K. (2011) Arrested oocyst maturation in *Plasmodium* parasites lacking type II NADH:ubiquinone dehydrogenase. *J. Biol. Chem.* 286, 32661–71
- Bradford, M. M. (1976) A rapid and sensitive method for the quantitation of microgram quantities of protein utilizing the principle of protein-dye binding. *Anal. Biochem.* 72, 248–254
- Brown, W. M., Yowell, C. A., Hoard, A., Vander Jagt, T. A., Hunsaker, L. A., Deck, L. M., Royer, R. E., Piper, R. C., Dame, J. B., Makler, M. T., and Vander Jagt, D. L. (2004) Comparative structural analysis and kinetic properties of lactate dehydrogenases from the four species of human malarial parasites. *Biochemistry*. 43, 6219–29
- Buchanan, J. M. (1973) The amidotransferases. *Adv. Enzymol. Relat. Areas Mol. Biol.* 39, 91–183
-

- Bulusu, V., Jayaraman, V., and Balaram, H. (2011) Metabolic fate of fumarate, a side product of the purine salvage pathway in the intraerythrocytic stages of *Plasmodium falciparum*. *J. Biol. Chem.* 286, 9236–9245
- Cammack, S. (1999) *Advances in inorganic chemistry*, First (Cammack, S. ed), Academic Press, 10.1017/CBO9781107415324.004
- Canfield, C. J., Pudney, M., and Gutteridge, W. E. (1995) Interactions of atovaquone with other antimalarial drugs against *Plasmodium falciparum* in vitro. *Exp. Parasitol.* 80, 373–81
- Cassera, M. B., Hazleton, K. Z., Riegelhaupt, P. M., Merino, E. F., Luo, M., Akabas, M. H., and Schramm, V. L. (2008) Erythrocytic adenosine monophosphate as an alternative purine source in *Plasmodium falciparum*. *J. Biol. Chem.* 283, 32889–99
- Cavanagh, J., Fairbrother, W., Palmer III, A., Rance, M., and Skelton, N. (2007) Protein NMR spectroscopy. *Principles and Practice.*, 10.1093/cid/cis040
- Cerdan, S., and Seelig, J. (1990) NMR Studies of Metabolism. *Annu. Rev. Biophys. Biophys. Chem.* 19, 43–67
- Chaikuad, A., Fairweather, V., Conners, R., Joseph-Horne, T., Turgut-Balik, D., and Brady, R. L. (2005) Structure of lactate dehydrogenase from *Plasmodium vivax*: complexes with NADH and APADH. *Biochemistry.* 44, 16221–8
- Chaleckis, R., Murakami, I., Takada, J., Kondoh, H., and Yanagida, M. (2016) Individual variability in human blood metabolites identifies age-related differences. *Proc. Natl. Acad. Sci. U. S. A.* 113, 4252–9
- Chan, M., and Sim, T.-S. (2005) Functional analysis, overexpression, and kinetic characterization of pyruvate kinase from *Plasmodium falciparum*. *Biochem. Biophys. Res. Commun.* 326, 188–96
- Chaudhary, K., Darling, J. A., Fohl, L. M., Sullivan, W. J., Donald, R. G. K., Pfefferkorn, E. R., Ullman, B., and Roos, D. S. (2004) Purine salvage pathways in the apicomplexan parasite *Toxoplasma gondii*. *J. Biol. Chem.* 279, 31221–7
- Chayen, N. E., Shaw Stewart, P. D., and Blow, D. M. (1992) Microbatch crystallization under oil — a new technique allowing many small-volume crystallization trials. *J. Cryst. Growth.* 122, 176–180
- Cheng, Q. (2008) Perspectives in Biological Nitrogen Fixation Research. *J. Integr. Plant Biol.* 50, 786–798
- Chiodini, P. L., Conlon, C. P., Hutchinson, D. B. A., Farquhar, J. A., Hall, A. P., Peto, T. E. A., Birley, H., and Warrell, D. A. (1995) Evaluation of atovaquone in the treatment of patients with uncomplicated *Plasmodium falciparum* malaria. *J. Antimicrob. Chemother.* 36, 1073–1078

-
- Christophers, S., and Fulton, J. (1939) Experiments with Isolated Malaria Parasites (*Plasmodium knowlesi*) Free from Red Cells. *Ann. Trop. Med. Parasit.* [online] <http://www.cabdirect.org/abstracts/19402900333.html> (Accessed June 4, 2016)
- Claros, M. G., and Vincens, P. (1996) Computational method to predict mitochondrially imported proteins and their targeting sequences. *Eur. J. Biochem.* 241, 779–86
- Clinch, K., Crump, D. R., Evans, G. B., Hazleton, K. Z., Mason, J. M., Schramm, V. L., and Tyler, P. C. (2013) Acyclic phosph(on)ate inhibitors of *Plasmodium falciparum* hypoxanthine-guanine-xanthine phosphoribosyltransferase. *Bioorg. Med. Chem.* 21, 5629–46
- Cobbold, S. A., Vaughan, A. M., Lewis, I. A., Painter, H. J., Camargo, N., Perlman, D. H., Fishbaugher, M., Healer, J., Cowman, A. F., Kappe, S. H. I., and Llinás, M. (2013) Kinetic flux profiling elucidates two independent acetyl-CoA biosynthetic pathways in *Plasmodium falciparum*. *J. Biol. Chem.* 288, 36338–50
- Cohen-Ben-Lulu, G. N., Francis, N. R., Shimoni, E., Noy, D., Davidov, Y., Prasad, K., Sagi, Y., Cecchini, G., Johnstone, R. M., and Eisenbach, M. (2008) The bacterial flagellar switch complex is getting more complex. *EMBO J.* 27, 1134–1144
- Collins, D. J., Zhou, H.-C., Collins, D. J., and Zhou, H. (2011) Iron-Sulfur Models of Protein Active Sites. in *Encyclopedia of Inorganic and Bioinorganic Chemistry*, John Wiley & Sons, Ltd, Chichester, UK, 10.1002/9781119951438.eibc0108
- Cooper, R. A., Itiaba, K., and Kornberg, H. L. (1965) The utilization of aconate and itaconate by *Micrococcus* sp.. *Biochem. J.* 94, 25–31
- Coustou, V., Biran, M., Besteiro, S., Rivière, L., Baltz, T., Franconi, J.-M., and Bringaud, F. (2006) Fumarate Is an Essential Intermediary Metabolite Produced by the Procyclic *Trypanosoma brucei*. *J. Biol. Chem.* 281, 26832–26846
- Coustou, V., Biran, M., Besteiro, S., Rivière, L., Baltz, T., Franconi, J.-M., and Bringaud, F. (2006) Fumarate Is an Essential Intermediary Metabolite Produced by the Procyclic *Trypanosoma brucei*. *J. Biol. Chem.* 281, 26832–26846
- Cutsail, G. E., Telsner, J., and Hoffman, B. M. (2015) Advanced paramagnetic resonance spectroscopies of iron-sulfur proteins: Electron nuclear double resonance (ENDOR) and electron spin echo envelope modulation (ESEEM). *Biochim. Biophys. Acta - Mol. Cell Res.* 1853, 1370–1394
- Dailey, H. A., Finnegan, M. G., and Johnson, M. K. (1994) Human ferrochelatase is an iron-sulfur protein. *Biochemistry.* 33, 403–7
- Danne, J. C., Gornik, S. G., Macrae, J. I., McConville, M. J., and Waller, R. F. (2013) Alveolate mitochondrial metabolic evolution: dinoflagellates force reassessment of the role of parasitism as a driver of change in apicomplexans. *Mol. Biol. Evol.* 30, 123–39
- Datsenko, K. A., and Wanner, B. L. (2000) One-step inactivation of chromosomal genes in *Escherichia coli* K-12 using PCR products. *Proc. Natl. Acad. Sci. U. S. A.* 97, 6640–5
-

- de Koning, H. P., Bridges, D. J., and Burchmore, R. J. S. (2005) Purine and pyrimidine transport in pathogenic protozoa: from biology to therapy. *FEMS Microbiol. Rev.* 29, 987–1020
- De la Fuente, I. M., Cortés, J. M., Valero, E., Desroches, M., Rodrigues, S., Malaina, I., and Martínez, L. (2014) On the dynamics of the adenylate energy system: homeorhesis vs homeostasis. *PLoS One.* 9, e108676
- Dean, P., Major, P., Nakjang, S., Hirt, R. P., and Embley, T. M. (2014) Transport proteins of parasitic protists and their role in nutrient salvage. *Front. Plant Sci.* 5, 153
- Delaglio, F., Grzesiek, S., Vuister, G., Zhu, G., Pfeifer, J., and Bax, A. (1995) NMRPipe: A multidimensional spectral processing system based on UNIX pipes. *J. Biomol. NMR.* 6, 277–293
- Denton, H., Thong, K. W., and Coombs, G. H. (1994) *Eimeria tenella* contains a pyrophosphate-dependent phosphofructokinase and a pyruvate kinase with unusual allosteric regulators. *FEMS Microbiol. Lett.* 115, 87–91
- Derr, R. F., and Zieve, L. (1972) Adenylate energy charge: Relation to guanylate energy charge and the adenylate kinase equilibrium constant. *Biochem. Biophys. Res. Commun.* 49, 1385–1390
- Desai, S. A., Krogstad, D. J., and McCleskey, E. W. (1993) A nutrient-permeable channel on the intraerythrocytic malaria parasite. *Nature.* 362, 643–6
- Desjardins, R. E., Canfield, C. J., Haynes, J. D., and Chulay, J. D. (1979) Quantitative assessment of antimalarial activity in vitro by a semiautomated microdilution technique. *Antimicrob. Agents Chemother.* 16, 710–8
- Dieterle, F., Riefke, B., Schlotterbeck, G., Ross, A., Senn, H., and Amberg, A. (2011) NMR and MS Methods for Metabonomics. in *Methods in molecular biology* (Clifton, N.J.), pp. 385–415, 691, 385–415
- Dik, E., Naamati, A., Asraf, H., Lehming, N., and Pines, O. (2016) Human Fumarate Hydratase Is Dual Localized by an Alternative Transcription Initiation Mechanism. *Traffic.* 17, 720–732
- Dixon, M., and Webb, E. C. (2014) *Enzymes*, Elsevier Science
- Dobson, A., Lafferty, K. D., Kuris, A. M., Hechinger, R. F., and Jetz, W. (2008) Colloquium paper: homage to Linnaeus: how many parasites? How many hosts? *Proc. Natl. Acad. Sci. U. S. A.* 105, 11482–11489
- Domin, B. A., Mahony, W. B., and Zimmerman, T. P. (1988) Purine nucleobase transport in human erythrocytes. Reinvestigation with a novel ‘inhibitor-stop’ assay. *J. Biol. Chem.* 263, 9276–84
- Donaldson, T. M., Ting, L.-M., Zhan, C., Shi, W., Zheng, R., Almo, S. C., and Kim, K. (2014) Structural determinants of the 5'-methylthioinosine specificity of *Plasmodium* purine nucleoside phosphorylase. *PLoS One.* 9, e84384

-
- Downie, M. J., Kirk, K., and Mamoun, C. Ben (2008) Purine salvage pathways in the intraerythrocytic malaria parasite *Plasmodium falciparum*. *Eukaryot. Cell.* 7, 1231–7
- Drevland, R. M., Jia, Y., Palmer, D. R. J., and Graham, D. E. (2008) Methanogen homoaconitase catalyzes both hydrolyase reactions in coenzyme B biosynthesis. *J. Biol. Chem.* 283, 28888–96
- Ducati, R. G., Namanja-Magliano, H. A., and Schramm, V. L. (2013) Transition-state inhibitors of purine salvage and other prospective enzyme targets in malaria. *Future Med. Chem.* 5, 1341–60
- Eaazhisai, K., Jayalakshmi, R., Gayathri, P., Anand, R. P., Sumathy, K., Balaram, H., and Murthy, M. R. N. (2004) Crystal structure of fully ligated adenylosuccinate synthetase from *Plasmodium falciparum*. *J. Mol. Biol.* 335, 1251–64
- El Bissati, K., Downie, M. J., Kim, S.-K., Horowitz, M., Carter, N., Ullman, B., and Ben Mamoun, C. (2008) Genetic Evidence for the Essential Role of PfNT1 in the Transport and Utilization of Xanthine, Guanine, Guanosine and Adenine by *Plasmodium falciparum*. *Mol. Biochem. Parasitol.* 161, 130–139
- Emanuelsson, O., Nielsen, H., Brunak, S., and von Heijne, G. (2000) Predicting subcellular localization of proteins based on their N-terminal amino acid sequence. *J. Mol. Biol.* 300, 1005–16
- Emwas, A.-H. M. (2015) The Strengths and Weaknesses of NMR Spectroscopy and Mass Spectrometry with Particular Focus on Metabolomics Research. in *Methods in molecular biology* (Clifton, N.J.), pp. 161–193, 1277, 161–193
- Eprintsev, A. T., Fedorin, D. N., Starinina, E. V., and Igamberdiev, A. U. (2014) Expression and properties of the mitochondrial and cytosolic forms of fumarase in germinating maize seeds. *Physiol. Plant.* 152, 231–40
- Esch, G., and Fernandez, J. (1993) A Functional Biology of Parasitism. 10.1007/978-94-009-1497-1
- Evans, P. (2006) Scaling and assessment of data quality. *Acta Crystallogr. Sect. D Biol. Crystallogr.* 62, 72–82
- Evert C. Duin, , Meghan E. Lafferty, , Brian R. Crouse, , Ronda M. Allen, Indrajit Sanyal, Dennis H. Flint, and Michael K. Johnson .(1997) [2Fe-2S] to [4Fe-4S] Cluster Conversion in *Escherichia coli* Biotin Synthase†. 10.1021/BI9706430
- Feliciano, P. R., Drennan, C. L., and Nonato, M. C. (2016) Crystal structure of an Fe-S cluster-containing fumarate hydratase enzyme from *Leishmania major* reveals a unique protein fold. *Proc. Natl. Acad. Sci.* 113, 9804–9809
- Feliciano, P. R., Gupta, S., Dyszy, F., Dias-Baruffi, M., Costa-Filho, A. J., Michels, P. A. M., and Nonato, M. C. (2012) Fumarate hydratase isoforms of *Leishmania major*: Subcellular localization, structural and kinetic properties. *Int. J. Biol. Macromol.* 51, 25–31
-

- Fibriansah, G., Veetil, V. P., Poelarends, G. J., and Thunnissen, A.-M. W. H. (2011) Structural Basis for the Catalytic Mechanism of Aspartate Ammonia Lyase. *Biochemistry*. 50, 6053–6062
- Finn, R. D., Bateman, A., Clements, J., Coggill, P., Eberhardt, R. Y., Eddy, S. R., Heger, A., Hetherington, K., Holm, L., Mistry, J., Sonnhammer, E. L. L., Tate, J., and Punta, M. (2014) Pfam: the protein families database. *Nucleic Acids Res.* 42, D222-30
- Fishbein, W., Armbrustmacher, V., and Griffin, J. (1978) Myoadenylate deaminase deficiency: a new disease of muscle. *Science* (80-).
- Flamholz, A., Noor, E., Bar-Even, A., and Milo, R. (2012) eQuilibrator--the biochemical thermodynamics calculator. *Nucleic Acids Res.* 40, D770-5
- Flint, D. H. (1993) Escherichia coli fumarase A catalyzes the isomerization of enol and keto oxalacetic acid. *Biochemistry*. 32, 799–805
- Flint, D. H. (1994) Initial Kinetic and Mechanistic Characterization of Escherichia coli Fumarase A. *Arch. Biochem. Biophys.* 311, 509–516
- Flint, D. H., and Allen, R. M. (1996) Iron-Sulfur Proteins with Nonredox Functions. *Chem. Rev.* 96, 2315–2334
- Flint, D. H., Emptage, M. H., and Guest, J. R. (1992) Fumarase a from Escherichia coli: purification and characterization as an iron-sulfur cluster containing enzyme. *Biochemistry*. 31, 10331–7
- Flint, D. H., Emptage, M. H., Finnegan, M. G., Fu, W., and Johnson, M. K. (1993) The role and properties of the iron-sulfur cluster in Escherichia coli dihydroxy-acid dehydratase. *J. Biol. Chem.* 268, 14732–42
- Fontecave, M. (2006) Iron-sulfur clusters: ever-expanding roles. *Nat. Chem. Biol.* 2, 171–174
- Fox, N. K., Brenner, S. E., and Chandonia, J.-M. (2014) SCOPe: Structural Classification of Proteins--extended, integrating SCOP and ASTRAL data and classification of new structures. *Nucleic Acids Res.* 42, D304-9
- Frame, I. J., Deniskin, R., Arora, A., and Akabas, M. H. (2015) Purine import into malaria parasites as a target for antimalarial drug development. *Ann. N. Y. Acad. Sci.* 1342, 19–28
- Frame, I. J., Deniskin, R., Rinderspacher, A., Katz, F., Deng, S.-X., Moir, R. D., Adjalley, S. H., Coburn-Flynn, O., Fidock, D. A., Willis, I. M., Landry, D. W., and Akabas, M. H. (2015) Yeast-based high-throughput screen identifies Plasmodium falciparum equilibrative nucleoside transporter 1 inhibitors that kill malaria parasites. *ACS Chem. Biol.* 10, 775–83
- Francia, M. E., and Striepen, B. (2014) Cell division in apicomplexan parasites. *Nat. Rev. Microbiol.* 12, 125–36
- Francia, M. E., Jordan, C. N., Patel, J. D., Sheiner, L., Demerly, J. L., Fellows, J. D., de Leon, J. C., Morrissette, N. S., Dubremetz, J. F., and Striepen, B. (2012) Cell Division in Apicomplexan

Parasites Is Organized by a Homolog of the Striated Rootlet Fiber of Algal Flagella. *PLoS Biol.* 10.1371/journal.pbio.1001444

Frizzell, N., Rajesh, M., Jepson, M. J., Nagai, R., Carson, J. A., Thorpe, S. R., and Baynes, J. W. (2009) Succination of Thiol Groups in Adipose Tissue Proteins in Diabetes: Succination inhibits polymerization and secretion of adiponectin. *J. Biol. Chem.* 284, 25772–25781

Frizzell, N., Thomas, S. A., Carson, J. A., and Baynes, J. W. (2012) Mitochondrial stress causes increased succination of proteins in adipocytes in response to glucotoxicity. *Biochem. J.* 445, 247–54

Fry, M., and Beesley, J. E. (1991) Mitochondria of mammalian *Plasmodium* spp. *Parasitology.* 102 Pt 1, 17–26

Fry, M., and Pudney, M. (1992) Site of action of the antimalarial hydroxynaphthoquinone, 2-[trans-4-(4'-chlorophenyl) cyclohexyl]-3-hydroxy-1,4-naphthoquinone (566C80). *Biochem. Pharmacol.* 43, 1545–1553

Fu, R., Sutcliffe, D., Zhao, H., Huang, X., Schretlen, D. J., Benkovic, S., and Jinnah, H. A. (2015) Clinical severity in Lesch-Nyhan disease: the role of residual enzyme and compensatory pathways. *Mol. Genet. Metab.* 114, 55–61

Fukasawa, Y., Tsuji, J., Fu, S.-C., Tomii, K., Horton, P., and Imai, K. (2015) MitoFates: Improved Prediction of Mitochondrial Targeting Sequences and Their Cleavage Sites. *Mol. Cell. Proteomics.* 14, 1113–1126

Ganesan, S. M., Falla, A., Goldfless, S. J., Nasamu, A. S., and Niles, J. C. (2016) Synthetic RNA-protein modules integrated with native translation mechanisms to control gene expression in malaria parasites. *Nat. Commun.* 7, 10727

Gao, H., Leary, J., Carroll, K. S., Bertozzi, C. R., and Chen, H. (2007) Noncovalent complexes of APS reductase from *M. tuberculosis*: delineating a mechanistic model using ESI-FTICR MS. *J. Am. Soc. Mass Spectrom.* 18, 167–78

Gardner, M. J., Hall, N., Fung, E., White, O., Berriman, M., Hyman, R. W., Carlton, J. M., Pain, A., Nelson, K. E., Bowman, S., Paulsen, I. T., James, K., Eisen, J. A., Rutherford, K., Salzberg, S. L., Craig, A., Kyes, S., Chan, M.-S., Nene, V., Shallom, S. J., Suh, B., Peterson, J., Angiuoli, S., Pertea, M., Allen, J., Selengut, J., Haft, D., Mather, M. W., Vaidya, A. B., Martin, D. M. A., Fairlamb, A. H., Fraunholz, M. J., Roos, D. S., Ralph, S. A., McFadden, G. I., Cummings, L. M., Subramanian, G. M., Mungall, C., Venter, J. C., Carucci, D. J., Hoffman, S. L., Newbold, C., Davis, R. W., Fraser, C. M., and Barrell, B. (2002) Genome sequence of the human malaria parasite *Plasmodium falciparum*. *Nature.* 419, 498–511

Gaudin, Z., Cerveau, D., Marnet, N., Bouchereau, A., Delavault, P., Simier, P., and Pouvreau, J.-B. (2014) Robust Method for Investigating Nitrogen Metabolism of ¹⁵N Labeled Amino Acids Using AccQ•Tag Ultra Performance Liquid Chromatography-Photodiode Array-Electrospray Ionization-Mass Spectrometry: Application to a Parasitic Plant-Plant Interaction. *Anal. Chem.* 86, 1138–1145

-
- Gibala, M. J., Young, M. E., and Taegtmeyer, H. (2000) Anaplerosis of the citric acid cycle: role in energy metabolism of heart and skeletal muscle. *Acta Physiol. Scand.* 168, 657–65
- Ginsburg, H., Divo, A. A., Geary, T. G., Boland, M. T., and Jensen, J. B. (1986) Effects of mitochondrial inhibitors on intraerythrocytic *Plasmodium falciparum* in in vitro cultures. *J. Protozool.* 33, 121–5
- Ginsburg, H., Krugliak, M., Eidelman, O., and Cabantchik, Z. I. (1983) New permeability pathways induced in membranes of *Plasmodium falciparum* infected erythrocytes. *Mol. Biochem. Parasitol.* 8, 177–90
- Goldfless, S. J., Wagner, J. C., and Niles, J. C. (2014) Versatile control of *Plasmodium falciparum* gene expression with an inducible protein–RNA interaction. *Nat. Commun.* 5, 5329
- Grabowski, R., Hofmeister, A. E. M., and Buckel, W. (1993) Bacterial l-serine dehydratases: a new family of enzymes containing iron-sulfur clusters. *Trends Biochem. Sci.* 18, 297–300
- Gueirard, P., Tavares, J., Thiberge, S., Bernex, F., Ishino, T., Milon, G., Franke-Fayard, B., Janse, C. J., Menard, R., and Amino, R. (2010) Development of the malaria parasite in the skin of the mammalian host. *Proc. Natl. Acad. Sci.* 107, 18640–18645
- Guler, J. L., White, J., Phillips, M. A., and Rathoda, P. K. (2015) Atovaquone tolerance in *Plasmodium falciparum* parasites selected for high-level resistance to a dihydroorotate dehydrogenase inhibitor. *Antimicrob. Agents Chemother.* 59, 686–689
- Günther, H. (2013) *NMR Spectroscopy: Basic Principles, Concepts and Applications in Chemistry*, Wiley
- Gutteridge, W. E., Dave, D., and Richards, W. H. (1979) Conversion of dihydroorotate to orotate in parasitic protozoa. *Biochim. Biophys. Acta.* 582, 390–401
- Hancock, C. R., Brault, J. J., and Terjung, R. L. (2006) Protecting the cellular energy state during contractions: role of AMP deaminase. *J. Physiol. Pharmacol.* 57 Suppl 1, 17–29
- Hanssen, E., Goldie, K. N., and Tilley, L. (2010) Ultrastructure of the asexual blood stages of *Plasmodium falciparum*. *Methods Cell Biol.* 96, 93–116
- Haran, N., Kahana, Z. E., and Lapidot, A. (1983) In vivo ¹⁵N NMR studies of regulation of nitrogen assimilation and amino acid production by *Brevibacterium lactofermentum*. *J. Biol. Chem.* 258, 12929–33
- Hassan, H. F., and Coombs, G. H. (1988) Purine and pyrimidine metabolism in parasitic protozoa. *FEMS Microbiol. Rev.* 4, 47–83
- Hazleton, K. Z., Ho, M.-C., Cassera, M. B., Clinch, K., Crump, D. R., Rosario, I., Merino, E. F., Almo, S. C., Tyler, P. C., and Schramm, V. L. (2012) Acyclic immucillin phosphonates: second-generation inhibitors of *Plasmodium falciparum* hypoxanthine-guanine-xanthine phosphoribosyltransferase. *Chem. Biol.* 19, 721–30
-

-
- Hennessy, D. J., Reid, G. R., Smith, F. E., and Thompson, S. L. (1984) Ferene — a new spectrophotometric reagent for iron. *Can. J. Chem.* 62, 721–724
- Hernández, H., Hewitson, K. S., Roach, P., Shaw, N. M., Baldwin, J. E., and Robinson, C. V. (2001) Observation of the Iron-Sulfur Cluster in *Escherichia coli* Biotin Synthase by Nanoflow Electrospray Mass Spectrometry. *Anal. Chem.* 73, 4154–4161
- Hill, C., and London, W. (1978) The Pool Sizes of Adenine Nucleotides in Exponentially Growing , Stationary Phase and 2'-Deoxyadenosine- synchronized Cultures of *Schizosaccharomyces pombe* 972 h
- Hino, A., Hirai, M., Tanaka, T. Q., Watanabe, Y., Matsuoka, H., and Kita, K. (2012) Critical roles of the mitochondrial complex II in oocyst formation of rodent malaria parasite *Plasmodium berghei*. *J. Biochem.* 152, 259–68
- Hirano, Y., Takeda, K., and Miki, K. (2016) Charge-density analysis of an iron–sulfur protein at an ultra-high resolution of 0.48 Å. *Nature.* 534, 281
- Hofmeister, A. E. M., Albracht, S. P. J., and Buckel, W. (1994) Iron-sulfur cluster-containing l -serine dehydratase from *Peptostreptococcus asaccharolyticus*: Correlation of the cluster type with enzymatic activity. *FEBS Lett.* 351, 416–418
- Huang, S., Colmer, T. D., and Millar, A. H. (2008) Does anoxia tolerance involve altering the energy currency towards PPI? *Trends Plant Sci.* 13, 221–7
- Huberts, D. H. E. W., and van der Klei, I. J. (2010) Moonlighting proteins: an intriguing mode of multitasking. *Biochim. Biophys. Acta.* 1803, 520–5
- Huff, C. G. (1947) Life Cycle of Malarial Parasites. *Annu. Rev. Microbiol.* 1, 43–60
- Hug, L. A., Baker, B. J., Anantharaman, K., Brown, C. T., Probst, A. J., Castelle, C. J., Butterfield, C. N., Hermsdorf, A. W., Amano, Y., Ise, K., Suzuki, Y., Dudek, N., Relman, D. A., Finstad, K. M., Amundson, R., Thomas, B. C., Banfield, J. F. (2016) A new view of the tree of life. *Nat. Microbiol.* 1, 16048
- Huthmacher, C., Hoppe, A., Bulik, S., and Holzhütter, H.-G. (2010) Antimalarial drug targets in *Plasmodium falciparum* predicted by stage-specific metabolic network analysis. *BMC Syst. Biol.* 4, 120
- Hwang, T. L., and Shaka, A. J. (1995) Water Suppression That Works. Excitation Sculpting Using Arbitrary Wave-Forms and Pulsed-Field Gradients, Academic Press, 10.1006/jmra.1995.1047
- Jacot, D., Waller, R. F., Soldati-Favre, D., MacPherson, D. A., and MacRae, J. I. (2016) Apicomplexan Energy Metabolism: Carbon Source Promiscuity and the Quiescence Hyperbole. *Trends Parasitol.* 32, 56–70
- Janse, C. J., Ramesar, J., and Waters, A. P. (2006) High-efficiency transfection and drug selection of genetically transformed blood stages of the rodent malaria parasite *Plasmodium berghei*. *Nat. Protoc.* 1, 346–356
-

-
- Jayalakshmi, R., Sumathy, K., and Balaram, H. (2002) Purification and characterization of recombinant *Plasmodium falciparum* adenylosuccinate synthetase expressed in *Escherichia coli*. *Protein Expr. Purif.* 25, 65–72
- Jayaraman, V., Bulusu, V., and Balaram, H. (2012) Crosstalk between purine nucleotide metabolism and mitochondrial pathways in *Plasmodium falciparum*. *Curr. Sci.* 102, 757–766
- Jensen, K. P. (2006) Iron-sulfur clusters: Why iron? *J. Inorg. Biochem.* 100, 1436–1439
- Jensen, M. D., Conley, M., and Helstowski, L. D. (1983) Culture of *Plasmodium falciparum*: the role of pH, glucose, and lactate. *J. Parasitol.* 69, 1060–7
- Jiang, Y., Qian, X., Shen, J., Wang, Y., Li, X., Liu, R., Xia, Y., Chen, Q., Peng, G., Lin, S.-Y., and Lu, Z. (2015) Local generation of fumarate promotes DNA repair through inhibition of histone H3 demethylation. *Nat. Cell Biol.* 17, 1158–1168
- Jiang, Y., Qian, X., Shen, J., Wang, Y., Li, X., Liu, R., Xia, Y., Chen, Q., Peng, G., Lin, S.-Y., and Lu, Z. (2015) Local generation of fumarate promotes DNA repair through inhibition of histone H3 demethylation. *Nat. Cell Biol.* 17, 1158–1168
- Jinnah, H. A., Sabina, R. L., and Van Den Berghe, G. (2013) Metabolic disorders of purine metabolism affecting the nervous system. *Handb. Clin. Neurol.* 113, 1827–36
- Kanamori, K., Weiss, R. L., and Roberts, J. D. (1989) Ammonia assimilation pathways in nitrogen-fixing *Clostridium kluyverii* and *Clostridium butyricum*. *J. Bacteriol.* 171, 2148–54
- Karl, D. M. (1980) Cellular nucleotide measurements and applications in microbial ecology. *Microbiol. Rev.* 44, 739–796
- Karnkowska, A., Vacek, V., Zubáčová, Z., Treitli, S. C., Petrželková, R., Eme, L., Novák, L., Žárský, V., Barlow, L. D., Herman, E. K., Soukal, P., Hroudová, M., Doležal, P., Stairs, C. W., Roger, A. J., Eliáš, M., Dacks, J. B., Vlček, Č., and Hampl, V. (2016) A Eukaryote without a Mitochondrial Organelle. *Curr. Biol.* 26, 1274–1284
- Kawahara, K., Mogi, T., Tanaka, T. Q., Hata, M., Miyoshi, H., and Kita, K. (2009) Mitochondrial dehydrogenases in the aerobic respiratory chain of the rodent malaria parasite *Plasmodium yoelii yoelii*. *J. Biochem.* 145, 229–37
- Kay, L., Keifer, P., and Saarinen, T. (1992) Pure absorption gradient enhanced heteronuclear single quantum correlation spectroscopy with improved sensitivity. *J. Am. Chem. Soc.* 114, 10663–10665
- Ke, H., Lewis, I. A., Morrissey, J. M., McLean, K. J., Ganesan, S. M., Painter, H. J., Mather, M. W., Jacobs-Lorena, M., Llinás, M., Vaidya, A. B., Llinas, M., and Vaidya, A. B. (2015) Genetic investigation of tricarboxylic acid metabolism during the *Plasmodium falciparum* life cycle. *Cell Rep.* 11, 164–174
-

-
- Ke, H., Morrissey, J. M., Ganesan, S. M., Painter, H. J., Mather, M. W., and Vaidya, A. B. (2011) Variation among *Plasmodium falciparum* strains in their reliance on mitochondrial electron transport chain function. *Eukaryot. Cell.* 10, 1053–61
- Kelly, J. M., and Scopes, R. K. (1986) L-(+)-Tartrate dehydratase from *Pseudomonas putida* is an iron-sulphur enzyme. *FEBS Lett.* 202, 274–276
- Kennedy, M. C., and Beinert, H. (1988) The state of cluster SH and S²⁻ of aconitase during cluster interconversions and removal. A convenient preparation of apoenzyme. *J. Biol. Chem.* 263, 8194–8
- Kerscher, S., Dröse, S., Zickermann, V., and Brandt, U. (2008) The three families of respiratory NADH dehydrogenases. *Results Probl. Cell Differ.* 45, 185–222
- Kicska, G. A., Tyler, P. C., Evans, G. B., Furneaux, R. H., Kim, K., and Schramm, V. L. (2002) Transition state analogue inhibitors of purine nucleoside phosphorylase from *Plasmodium falciparum*. *J. Biol. Chem.* 277, 3219–25
- Kicska, G. A., Tyler, P. C., Evans, G. B., Furneaux, R. H., Schramm, V. L., and Kim, K. (2002) Purine-less death in *Plasmodium falciparum* induced by immucillin-H, a transition state analogue of purine nucleoside phosphorylase. *J. Biol. Chem.* 277, 3226–31
- Kim, O. Bin, and Uden, G. (2007) The L-tartrate/succinate antiporter TtdT (YgjE) of L-tartrate fermentation in *Escherichia coli*. *J. Bacteriol.* 189, 1597–603
- Kim, O. Bin, Lux, S., and Uden, G. (2007) Anaerobic growth of *Escherichia coli* on d-tartrate depends on the fumarate carrier DcuB and fumarase, rather than the l-tartrate carrier TtdT and l-tartrate dehydratase. *Arch. Microbiol.* 188, 583–589
- Kinch, L., Grishin, N. V., and Brugarolas, J. (2011) Succination of Keap1 and activation of Nrf2-dependent antioxidant pathways in FH-deficient papillary renal cell carcinoma type 2. *Cancer Cell.* 20, 418–20
- King, A., Selak, M. A., and Gottlieb, E. (2006) Succinate dehydrogenase and fumarate hydratase: linking mitochondrial dysfunction and cancer. *Oncogene.* 25, 4675–4682
- King, M. E., Honeysett, J. M., and Howell, S. B. (1983) Regulation of de novo purine synthesis in human bone marrow mononuclear cells by hypoxanthine. *J. Clin. Invest.* 72, 965–70
- Kinoshita, H., Nagasaki, J., Yoshikawa, N., Yamamoto, A., Takito, S., Kawasaki, M., Sugiyama, T., Miyake, H., Weber, A. P. M., and Taniguchi, M. (2011) The chloroplastic 2-oxoglutarate/malate transporter has dual function as the malate valve and in carbon/nitrogen metabolism. *Plant J.* 65, 15–26
- Kleine, T., Maier, U. G., and Leister, D. (2009) DNA transfer from organelles to the nucleus: the idiosyncratic genetics of endosymbiosis. *Annu. Rev. Plant Biol.* 60, 115–38
- Knox, C., Sass, E., Neupert, W., and Pines, O. (1998) Import into mitochondria, folding and retrograde movement of fumarase in yeast. *J. Biol. Chem.* 273, 25587–93
-

- Kobayashi, T., Sato, S., Takamiya, S., Komaki-Yasuda, K., Yano, K., Hirata, A., Onitsuka, I., Hata, M., Mi-ichi, F., Tanaka, T., Hase, T., Miyajima, A., Kawazu, S., Watanabe, Y., and Kita, K. Mitochondria and apicoplast of *Plasmodium falciparum*: behaviour on subcellular fractionation and the implication. *Mitochondrion*. 7, 125–32
- Kolling, D. J., Brunzelle, J. S., Lhee, S., Crofts, A. R., and Nair, S. K. (2007) Atomic resolution structures of rieske iron-sulfur protein: role of hydrogen bonds in tuning the redox potential of iron-sulfur clusters. *Structure*. 15, 29–38
- Kolling, D. R. J., Samoilova, R. I., Shubin, A. A., Crofts, A. R., and Dikanov, S. A. (2009) Proton environment of reduced Rieske iron-sulfur cluster probed by two-dimensional ESEEM spectroscopy. *J. Phys. Chem. A*. 113, 653–67
- Kollmann-Koch, A., and Eggerer, H. (1984) Nicotinic Acid Metabolism. Dimethylmaleate Hydratase. *Hoppe-Seyler's Zeitschrift für Physiol. Chemie*. 365, 847–858
- Kornberg, H. L. (1966) Anaplerotic sequences and their role in metabolism. *Essays Biochem*. 2, 1–31
- Kosaka, T., Uchiyama, T., Ishii, S., Enoki, M., Imachi, H., Kamagata, Y., Ohashi, A., Harada, H., Ikenaga, H., and Watanabe, K. (2006) Reconstruction and regulation of the central catabolic pathway in the thermophilic propionate-oxidizing syntroph *Pelotomaculum thermopropionicum*. *J. Bacteriol*. 188, 202–10
- Kovachevich, R., and Wood, W. A. (1955) Carbohydrate metabolism by *Pseudomonas fluorescens*. III. Purification and properties of a 6-phosphogluconate dehydrase. *J. Biol. Chem*. 213, 745–56
- Krager, A., Geisler, V., Lemma, E., Theis, F., and Lenger, R. (1992) Bacterial fumarate respiration. *Arch. Microbiol*. 158, 311–314
- Kraupp, M., Paskutti, B., Schön, C., and Marz, R. (1994) Inhibition of purine nucleobase transport in human erythrocytes and cell lines by papaverine. Investigation of structure-activity relationship. *Biochem. Pharmacol*. 48, 41–7
- Krebs, H. A. (1937) The intermediate metabolism of carbohydrates. *Lancet*. 230, 736–738
- Krebs, H. A., Salvin, E., and Johnson, W. A. (1938) The formation of citric and alpha-ketoglutaric acids in the mammalian body. *Biochem. J*. 32, 113–7
- Kronen, M., and Berg, I. A. (2015) Mesaconase/Fumarase FumD in *Escherichia coli* O157:H7 and Promiscuity of *Escherichia coli* Class I Fumarases FumA and FumB. *PLoS One*. 10, e0145098
- Kronen, M., Sasikaran, J., and Berg, I. A. (2015) Mesaconase Activity of Class I Fumarase Contributes to Mesaconate Utilization by *Burkholderia xenovorans*. *Appl. Environ. Microbiol*. 81, 5632–5638
- Kruk, J., Doskocz, M., Jodłowska, E., Zacharzewska, A., Łakomiec, J., Czaja, K., and Kujawski, J. (2016) NMR Techniques in Metabolomic Studies: A Quick Overview on Examples of Utilization. *Appl. Magn. Reson*. 10.1007/s00723-016-0846-9

-
- Krungskrai, J., Krungskrai, S. R., and Bhumiratana, A. (1993) Plasmodium berghei: partial purification and characterization of the mitochondrial cytochrome c oxidase. *Exp. Parasitol.* 77, 136–46
- Krungskrai, J., Krungskrai, S. R., Suraveratum, N., and Prapunwattana, P. (1997) Mitochondrial ubiquinol-cytochrome c reductase and cytochrome c oxidase: chemotherapeutic targets in malarial parasites. *Biochem. Mol. Biol. Int.* 42, 1007–14
- Kubišta, V., and Foustka, M. (1962) Inorganic Phosphate and the Rate of Glycolysis in Insect Muscle. *Nature.* 195, 702–703
- Kuijk, B. L. M. Van, Loo, N.-D. Van, Arendsen, A. F., Hagen, W. R., and Stams, A. J. M. (1996) Purification and characterization of fumarase from the syntrophic propionate-oxidizing bacterium strain MPOB. *Arch. Microbiol.* 165, 126–131
- Kumar, S., and Banyal, H. S. (1997) Purification and characterisation of the hexokinase of Plasmodium berghei, a murine malaria parasite. *Acta Vet. Hung.* 45, 119–26
- Kuzmanic, A., Pannu, N. S., and Zagrovic, B. (2014) X-ray refinement significantly underestimates the level of microscopic heterogeneity in biomolecular crystals. *Nat. Commun.* 5, 218–222
- LaGier, M. J., Tachezy, J., Stejskal, F., Kutisova, K., and Keithly, J. S. (2003) Mitochondrial-type iron-sulfur cluster biosynthesis genes (IscS and IscU) in the apicomplexan *Cryptosporidium parvum*. *Microbiology.* 149, 3519–30
- Lambros, C., and Vanderberg, J. P. (1979) Synchronization of Plasmodium falciparum erythrocytic stages in culture. *J. Parasitol.* 65, 418–20
- Landfear, S. M. (2011) Nutrient transport and pathogenesis in selected parasitic protozoa. *Eukaryot. Cell.* 10, 483–93
- Lane, A. N., and Fan, T. W.-M. (2015) Regulation of mammalian nucleotide metabolism and biosynthesis. *Nucleic Acids Res.* 43, 2466–2485
- Lauble, H., Kennedy, M. C., Beinert, H., and Stout, C. D. (1992) Crystal structures of aconitase with isocitrate and nitroisocitrate bound. *Biochemistry.* 31, 2735–2748
- Lee, C. C., Ribbe, M. W., and Hu, Y. (2014) Cleaving the N,N Triple Bond: The Transformation of Dinitrogen to Ammonia by Nitrogenases. in *Metal ions in life sciences*, pp. 147–176, 14, 147–176
- Lee, I. H., and Finkel, T. (2013) Metabolic regulation of the cell cycle. *Curr. Opin. Cell Biol.* 25, 724–9
- Lee, I. Y., Strunk, R. C., and Coe, E. L. (1967) Coordination among rate-limiting steps of glycolysis and respiration in intact ascites tumor cells. *J. Biol. Chem.* 242, 2021–8
- Legerton, T. L., Kanamori, K., Weiss, R. L., and Roberts, J. D. (1981) ¹⁵N NMR studies of nitrogen metabolism in intact mycelia of *Neurospora crassa*. *Proc. Natl. Acad. Sci. U. S. A.* 78, 1495–8
-

- Levine, R. A., and Taylor, M. W. (1982) Mechanism of adenine toxicity in *Escherichia coli*. *J. Bacteriol.* 149, 923–30
- Lian, L.-Y., Al-Helal, M., Roslani, A. M., Fisher, N., Bray, P. G., Ward, S. A., and Biagini, G. A. (2009) Glycerol: an unexpected major metabolite of energy metabolism by the human malaria parasite. *Malar. J.* 8, 38
- Liao, Y.-D., Jeng, J.-C., Wang, C.-F., Wang, S.-C., and Chang, S.-T. (2004) Removal of N-terminal methionine from recombinant proteins by engineered *E. coli* methionine aminopeptidase. *Protein Sci.* 13, 1802–10
- Lin, J. T., and Stewart, V. (1998) Nitrate assimilation by bacteria. *Adv. Microb. Physiol.* 39, 1–30, 379
- Linker, R. A., Lee, D.-H., Ryan, S., van Dam, A. M., Conrad, R., Bista, P., Zeng, W., Hronowsky, X., Buko, A., Chollate, S., Ellrichmann, G., Brück, W., Dawson, K., Goelz, S., Wiese, S., Scannevin, R. H., Lukashev, M., and Gold, R. (2011) Fumaric acid esters exert neuroprotective effects in neuroinflammation via activation of the Nrf2 antioxidant pathway. *Brain.* 134, 678–92
- Liu, L., Fu, T., Xu, X., Fu, C., Fang, M., Liu, Y., Xu, P., and Zhao, Y. (2015) Tracing the nitrogen metabolites of glycine using ¹⁵N-glycine and mass spectrometry. *Rapid Commun. Mass Spectrom.* 29, 645–653
- Liu, Y., Vinyard, D. J., Reesbeck, M. E., Suzuki, T., Manakongtreecheep, K., Holland, P. L., Brudvig, G. W., and Söll, D. (2016) A [3Fe-4S] cluster is required for tRNA thiolation in archaea and eukaryotes. *Proc. Natl. Acad. Sci. U. S. A.* 10.1073/pnas.1615732113
- Llinas, M., Bozdech, Z., Wong, E. D., Adai, A. T., and DeRisi, J. L. (2006) Comparative whole genome transcriptome analysis of three *Plasmodium falciparum* strains. *Nucleic Acids Res.* 34, 1166–1173
- Lloyd, S. J., Lauble, H., Prasad, G. S., and Stout, C. D. (1999) The mechanism of aconitase: 1.8 Å resolution crystal structure of the S642a:citrate complex. *Protein Sci.* 8, 2655–62
- Looareesuwan, S., Viravan, C., and Webster, H. (1996) Clinical studies of atovaquone, alone or in combination with other antimalarial drugs, for treatment of acute uncomplicated malaria in Thailand. *Am. J.*
- Lowenstein, J. M., and Goodman, M. N. (1978) The purine nucleotide cycle in skeletal muscle. *Fed. Proc.* 37, 2308–12
- Ludin, P., Woodcroft, B., Ralph, S. A., and Mäser, P. (2012) In silico prediction of antimalarial drug target candidates. *Int. J. Parasitol. Drugs drug Resist.* 2, 191–9
- Luke, K., Apiyo, D., and Wittung-Stafshede, P. (2005) Dissecting homo-heptamer thermodynamics by isothermal titration calorimetry: entropy-driven assembly of co-chaperonin protein 10. *Biophys. J.* 89, 3332–6
- Lüscher, A., Lamprea-Burgunder, E., Graf, F. E., de Koning, H. P., and Mäser, P. (2014) Trypanosoma brucei adenine-phosphoribosyltransferases mediate adenine salvage and

-
- aminopurinol susceptibility but not adenine toxicity. *Int. J. Parasitol. Drugs drug Resist.* 4, 55–63
- MacRae, J. I., Dixon, M. W., Dearnley, M. K., Chua, H. H., Chambers, J. M., Kenny, S., Bottova, I., Tilley, L., and McConville, M. J. (2013) Mitochondrial metabolism of sexual and asexual blood stages of the malaria parasite *Plasmodium falciparum*. *BMC Biol.* 11, 67
- Madrid, D. C., Ting, L.-M., Waller, K. L., Schramm, V. L., and Kim, K. (2008) *Plasmodium falciparum* purine nucleoside phosphorylase is critical for viability of malaria parasites. *J. Biol. Chem.* 283, 35899–907
- Marion, D., Driscoll, P. C., Kay, L. E., Wingfield, P. T., Bax, A., Gronenborn, A. M., and Clore, G. M. (1989) Overcoming the overlap problem in the assignment of proton NMR spectra of larger proteins by use of three-dimensional heteronuclear proton-nitrogen-15 Hartmann-Hahn-multiple quantum coherence and nuclear Overhauser-multiple quantum coherence spectroscopy: *Biochemistry.* 28, 6150–6156
- Markley, J. L., Brüschweiler, R., Edison, A. S., Eghbalnia, H. R., Powers, R., Raftery, D., and Wishart, D. S. (2017) The future of NMR-based metabolomics. *Curr. Opin. Biotechnol.* 43, 34–40
- Marr, J. J., Marr, J. J. (James J., and Müller, M. (1995) *Biochemistry and molecular biology of parasites*, Academic Press
- Martin, W. R., Frigan, F., and Bergman, E. H. (1961) Noninductive metabolism of itaconic acid by *Pseudomonas* and *Salmonella* species. *J. Bacteriol.* 82, 905–8
- Martínez-Gómez, K., Flores, N., Castañeda, H. M., Martínez-Batallar, G., Hernández-Chávez, G., Ramírez, O. T., Gosset, G., Encarnación, S., and Bolivar, F. (2012) New insights into *Escherichia coli* metabolism: carbon scavenging, acetate metabolism and carbon recycling responses during growth on glycerol. *Microb. Cell Fact.* 11, 46
- Marwan, W., Schäfer, W., and Oesterhelt, D. (1990) Signal transduction in *Halobacterium* depends on fumarate. *EMBO J.* 9, 355–62
- McCoy, A. J., Grosse-Kunstleve, R. W., Adams, P. D., Winn, M. D., Storoni, L. C., Read, R. J. (2007) Phaser crystallographic software. *J. Appl. Crystallogr.* 40, 658–674
- McGinnis, S., and Madden, T. L. (2004) BLAST: at the core of a powerful and diverse set of sequence analysis tools. *Nucleic Acids Res.* 32, W20-5
- Mechaly, A. E., Haouz, A., Miras, I., Barilone, N., Weber, P., Shepard, W., Alzari, P. M., and Bellinzoni, M. (2012) Conformational changes upon ligand binding in the essential class II fumarase Rv1098c from *Mycobacterium tuberculosis*. *FEBS Lett.* 586, 1606–11
- Ménard, R. (2005) Medicine: Knockout malaria vaccine? *Nature.* 433, 113–114
- Ménard, R. (2013) *Malaria: Methods and Protocols* (Ménard, R. ed), *Methods in Molecular Biology*, Humana Press, Totowa, NJ, 10.1007/978-1-62703-026-7
-

-
- Mendonça, A. G., Alves, R. J., and Pereira-Leal, J. B. (2011) Loss of genetic redundancy in reductive genome evolution. *PLoS Comput. Biol.* 7, e1001082
- Menendez, M. T., Teygong, C., Wade, K., Florimond, C., and Blader, I. J. (2015) siRNA Screening Identifies the Host Hexokinase 2 (HK2) Gene as an Important Hypoxia-Inducible Transcription Factor 1 (HIF-1) Target Gene in *Toxoplasma gondii*-Infected Cells. *MBio.* 6, e00462
- Mertens, E. (1991) Pyrophosphate-dependent phosphofructokinase, an anaerobic glycolytic enzyme? *FEBS Lett.* 285, 1–5
- Metheni, M., Lombès, A., Bouillaud, F., Batteux, F., and Langsley, G. (2015) HIF-1 α induction, proliferation and glycolysis of *Theileria*-infected leukocytes. *Cell. Microbiol.* 17, 467–72
- Millar, A. H., Wiskich, J. T., Whelan, J., and Day, D. A. (1993) Organic acid activation of the alternative oxidase of plant mitochondria. *FEBS Lett.* 329, 259–62
- Mogi, T., and Kita, K. (2009) Identification of mitochondrial Complex II subunits SDH3 and SDH4 and ATP synthase subunits a and b in *Plasmodium* spp. *Mitochondrion.* 9, 443–53
- Mommsen, T. P., and Hochachka, P. W. (1988) The purine nucleotide cycle as two temporally separated metabolic units: a study on trout muscle. *Metabolism.* 37, 552–6
- Mony, B. M., Mehta, M., Jarori, G. K., and Sharma, S. (2009) Plant-like phosphofructokinase from *Plasmodium falciparum* belongs to a novel class of ATP-dependent enzymes. *Int. J. Parasitol.* 39, 1441–53
- Morrison, D. A. (2009) Evolution of the Apicomplexa: where are we now? *Trends Parasitol.* 25, 375–82
- Mouesca, J.-M., and Lamotte, B. (1998) Iron–sulfur clusters and their electronic and magnetic properties. *Coord. Chem. Rev.* 178, 1573–1614
- Mullen, A. R., and DeBerardinis, R. J. (2016) Genetically-defined metabolic reprogramming in cancer. *Trends Endocrinol. Metab.* 23, 552–559
- Munagala, N. R., and Wang, C. C. (2003) Adenosine is the primary precursor of all purine nucleotides in *Trichomonas vaginalis*. *Mol. Biochem. Parasitol.* 127, 143–149
- Murakami, K. (1979) AMP deaminase from baker's yeast. Kinetic and molecular properties. *J. Biochem.* 86, 1331–6
- Muralidharan, V., Oksman, A., Iwamoto, M., Wandless, T. J., and Goldberg, D. E. (2011) Asparagine repeat function in a *Plasmodium falciparum* protein assessed via a regulatable fluorescent affinity tag. *Proc. Natl. Acad. Sci. U. S. A.* 108, 4411–4416
- Murphy, A. D., and Lang-Unnasch, N. (1999) Alternative oxidase inhibitors potentiate the activity of atovaquone against *Plasmodium falciparum*. *Antimicrob. Agents Chemother.* 43, 651–4

-
- Murphy, A. D., Doeller, J. E., Hearn, B., and Lang-Unnasch, N. (1997) Plasmodium falciparum: cyanide-resistant oxygen consumption. *Exp. Parasitol.* 87, 112–20
- Murshudov, G. N., Skubák, P., Lebedev, A. A., Pannu, N. S., Steiner, R. A., Nicholls, R. A., Winn, M. D., Long, F., Vagin, A. A. (2011) REFMAC 5 for the refinement of macromolecular crystal structures. *Acta Crystallogr. Sect. D Biol. Crystallogr.* 67, 355–367
- Naidoo, K., and Coetzer, T. L. (2013) Reduced glycerol incorporation into phospholipids contributes to impaired intra-erythrocytic growth of glycerol kinase knockout Plasmodium falciparum parasites. *Biochim. Biophys. Acta - Gen. Subj.* 1830, 5326–5334
- Naik, S. (2004) Mild and eco-friendly chemoselective acylation of amines in aqueous medium. *Arkivoc.* 2004, 55–63
- Ngwa, C. J., Scheuermayer, M., Mair, G. R., Kern, S., Brügl, T., Wirth, C. C., Aminake, M. N., Wiesner, J., Fischer, R., Vilcinskis, A., and Pradel, G. (2013) Changes in the transcriptome of the malaria parasite Plasmodium falciparum during the initial phase of transmission from the human to the mosquito. *BMC Genomics.* 14, 256
- Nixon, G. L., Pidathala, C., Shone, A. E., Antoine, T., Fisher, N., O'Neill, P. M., Ward, S. A., and Biagini, G. A. (2013) Targeting the mitochondrial electron transport chain of Plasmodium falciparum: new strategies towards the development of improved antimalarials for the elimination era. *Future Med. Chem.* 5, 1573–91
- Noodleman, L., Peng, C. Y., Case, D. A., and Mouesca, J.-M. (1995) Orbital interactions, electron delocalization and spin coupling in iron-sulfur clusters. *Coord. Chem. Rev.* 144, 199–244
- Nozawa, A., Fujimoto, R., Matsuoka, H., Tsuboi, T., and Tozawa, Y. (2011) Cell-free synthesis, reconstitution, and characterization of a mitochondrial dicarboxylate-tricarboxylate carrier of Plasmodium falciparum. *Biochem. Biophys. Res. Commun.* 414, 612–7
- Nunes-Nesi, A., Carrari, F., Gibon, Y., Sulpice, R., Lytovchenko, A., Fisahn, J., Graham, J., Ratcliffe, R. G., Sweetlove, L. J., and Fernie, A. R. (2007) Deficiency of mitochondrial fumarase activity in tomato plants impairs photosynthesis via an effect on stomatal function. *Plant J.* 50, 1093–106
- Nunes-Nesi, A., Fernie, A. R., and Stitt, M. (2010) Metabolic and Signaling Aspects Underpinning the Regulation of Plant Carbon Nitrogen Interactions. *Mol. Plant.* 3, 973–996
- Nyhan, W. L. (2014) Nucleotide Synthesis via Salvage Pathway. in *eLS*, John Wiley & Sons, Ltd, Chichester, UK, 10.1002/9780470015902.a0001399.pub3
- Nyhan, W. L. Disorders of purine and pyrimidine metabolism. *Mol. Genet. Metab.* 86, 25–33
-

-
- Ollagnier-de Choudens, S., Loiseau, L., Sanakis, Y., Barras, F., and Fontecave, M. (2005) Quinolinate synthetase, an iron-sulfur enzyme in NAD biosynthesis. *FEBS Lett.* 579, 3737–3743
- Olszewski, K. L., and Llinás, M. (2011) Central carbon metabolism of *Plasmodium* parasites. *Mol. Biochem. Parasitol.* 175, 95–103
- Oppenheim, R. D., Creek, D. J., Macrae, J. I., Modrzynska, K. K., Pino, P., Limenitakis, J., Polonais, V., Seeber, F., Barrett, M. P., Billker, O., McConville, M. J., and Soldati-Favre, D. (2014) BCKDH: the missing link in apicomplexan mitochondrial metabolism is required for full virulence of *Toxoplasma gondii* and *Plasmodium berghei*. *PLoS Pathog.* 10, e1004263
- Ouyang, J., Parakhia, R. A., and Ochs, R. S. (2011) Metformin activates AMP kinase through inhibition of AMP deaminase. *J. Biol. Chem.* 286, 1–11
- Ovchinnikov, S., Kinch, L., Park, H., Liao, Y., Pei, J., Kim, D. E., Kamisetty, H., Grishin, N. V., and Baker, D. (2015) Large-scale determination of previously unsolved protein structures using evolutionary information. *Elife.* 4, e09248
- Owen, O. E., Kalhan, S. C., and Hanson, R. W. (2002) The key role of anaplerosis and cataplerosis for citric acid cycle function. *J. Biol. Chem.* 277, 30409–12
- Ozsahin, H., Arredondo-Vega, F. X., Santisteban, I., Fuhrer, H., Tuchschild, P., Jochum, W., Aguzzi, A., Lederman, H. M., Fleischman, A., Winkelstein, J. A., Seger, R. A., and Herschfeld, M. S. (1997) Adenosine deaminase deficiency in adults. *Blood.* 89, 2849–55
- Painter, H. J., Morrisey, J. M., Mather, M. W., and Vaidya, A. B. (2007) Specific role of mitochondrial electron transport in blood-stage *Plasmodium falciparum*. *Nature.* 446, 88–91
- Pandelia, M.-E., Lanz, N. D., Booker, S. J., and Krebs, C. (2015) Mössbauer spectroscopy of Fe/S proteins. *Biochim. Biophys. Acta - Mol. Cell Res.* 1853, 1395–1405
- Parkinson, F. E., Damaraju, V. L., Graham, K., Yao, S. Y. M., Baldwin, S. A., Cass, C. E., and Young, J. D. (2011) Molecular biology of nucleoside transporters and their distributions and functions in the brain. *Curr. Top. Med. Chem.* 11, 948–72
- Paul Juretschke, H. (1984) Double-quantum ^1H NMR studies of nitrogen metabolism in yeast, No longer published by Elsevier, 10.1016/0014-5793(84)81254-5
- Pei, Y., Tarun, A. S., Vaughan, A. M., Herman, R. W., Soliman, J. M. B., Erickson-Wayman, A., and Kappe, S. H. I. (2010) *Plasmodium* pyruvate dehydrogenase activity is only essential for the parasite's progression from liver infection to blood infection. *Mol. Microbiol.* 75, 957–71
- Penner-Hahn, J. E. (1988) X-ray Absorption Spectroscopy for Characterizing Metal Clusters in Proteins, pp. 28–48, 10.1021/bk-1988-0372.ch002
-

-
- Pettersen, E. F., Goddard, T. D., Huang, C. C., Couch, G. S., Greenblatt, D. M., Meng, E. C., and Ferrin, T. E. (2004) UCSF Chimera--a visualization system for exploratory research and analysis. *J. Comput. Chem.* 25, 1605–12
- Pfander, C., Anar, B., Schwach, F., Otto, T. D., Brochet, M., Volkmann, K., Quail, M. A., Pain, A., Rosen, B., Skarnes, W., Rayner, J. C., and Billker, O. (2011) A scalable pipeline for highly effective genetic modification of a malaria parasite. *Nat. Methods.* 8, 1078–1082
- Phukan, K., Ganguly, M., and Devi, N. (2009) Mild and Useful Method for N-Acylation of Amines. *Synth. Commun.* 39, 2694–2701
- Pierce, D. W., and Boxer, S. G. (1995) Stark effect spectroscopy of tryptophan. *Biophys. J.* 68, 1583–91
- Pierik, A. J. Analysis of Metals and Acid-Labile Sulfide in Proteins
- Pierik, A. J., Hagen, W. R., Redeker, J. S., Wolbert, R. B. G., Boersma, M., Verhagen, M. F. J. M., Grande, H. J., Veeger, C., Mutsaers, P. H. A., Sands, R. H., And Dunham, W. R. (1992) Redox properties of the iron-sulfur clusters in activated Fe-hydrogenase from *Desulfovibrio vulgaris* (Hildenborough). *Eur. J. Biochem.* 209, 63–72
- Plaideau, C., Lai, Y.-C., Kviklyte, S., Zanou, N., Löfgren, L., Andersén, H., Vertommen, D., Gailly, P., Hue, L., Bohlooly-Y, M., Hallén, S., and Rider, M. H. (2014) Effects of Pharmacological {AMP} Deaminase Inhibition and *Ampd1* Deletion on Nucleotide Levels and {AMPK} Activation in Contracting Skeletal Muscle. *Chem. Biol.* 21, 1497–1510
- Pollard, P. J., Brière, J. J., Alam, N. A., Barwell, J., Barclay, E., Wortham, N. C., Hunt, T., Mitchell, M., Olpin, S., Moat, S. J., Hargreaves, I. P., Heales, S. J., Chung, Y. L., Griffiths, J. R., Dalgleish, A., McGrath, J. A., Gleeson, M. J., Hodgson, S. V, Poulson, R., Rustin, P., and Tomlinson, I. P. M. (2005) Accumulation of Krebs cycle intermediates and over-expression of HIF1 α in tumours which result from germline FH and SDH mutations. *Hum. Mol. Genet.* 14, 2231–9
- Pomel, S., Luk, F. C. Y., and Beckers, C. J. M. (2008) Host cell egress and invasion induce marked relocations of glycolytic enzymes in *Toxoplasma gondii* tachyzoites. *PLoS Pathog.* 4, e1000188
- POORTER, H., and BERGKOTTE, M. (1992) Chemical composition of 24 wild species differing in relative growth rate. *Plant, Cell Environ.* 15, 221–229
- Porollo, A. A., Adamczak, R., and Meller, J. (2004) POLYVIEW: a flexible visualization tool for structural and functional annotations of proteins. *Bioinformatics.* 20, 2460–2
- Portman, N., and Slapeta, J. (2014) The flagellar contribution to the apical complex: a new tool for the eukaryotic Swiss Army knife? *Trends Parasitol.* 30, 58–64
- Poulin, R., and Morand, S. (2000) The diversity of parasites. *Q. Rev. Biol.* 75, 277–293
- Pracharoenwattana, I., Zhou, W., Keech, O., Francisco, P. B., Udomchalothorn, T., Tschoep, H., Stitt, M., Gibon, Y., and Smith, S. M. (2010) *Arabidopsis* has a cytosolic fumarase
-

required for the massive allocation of photosynthate into fumaric acid and for rapid plant growth on high nitrogen. *Plant J.* 62, 785–95

Pranker, T. A. J. (1955) The Metabolism of the Human Erythrocyte: A Review. *Br. J. Haematol.* 1, 131–145

Prasad Maharjan, R., and Ferenci, T. (2003) Global metabolite analysis: the influence of extraction methodology on metabolome profiles of *Escherichia coli*. *Anal. Biochem.* 313, 145–154

Prasad, K., Caplan, S. R., and Eisenbach, M. (1998) Fumarate modulates bacterial flagellar rotation by lowering the free energy difference between the clockwise and counterclockwise states of the motor. *J. Mol. Biol.* 280, 821–8

Punta, M., Coghill, P. C., Eberhardt, R. Y., Mistry, J., Tate, J., Boursnell, C., Pang, N., Forslund, K., Ceric, G., Clements, J., Heger, A., Holm, L., Sonnhammer, E. L. L., Eddy, S. R., Bateman, A., and Finn, R. D. (2012) The Pfam protein families database. *Nucleic Acids Res.* 40, D290–301

Puthan Veetil, V., Fibriansah, G., Raj, H., Thunnissen, A.-M. W. H., and Poelarends, G. J. (2012) Aspartase/Fumarase Superfamily: A Common Catalytic Strategy Involving General Base-Catalyzed Formation of a Highly Stabilized aci - Carboxylate Intermediate. *Biochemistry.* 51, 4237–4243

Putignani, L., Tait, A., Smith, H. V., Horner, D., Tovar, J., Tetley, L., and Wastling, J. M. (2004) Characterization of a mitochondrion-like organelle in *Cryptosporidium parvum*. *Parasitology.* 129, 1–18

Quashie, N. B., Ranford-Cartwright, L. C., and de Koning, H. P. (2010) Uptake of purines in *Plasmodium falciparum*-infected human erythrocytes is mostly mediated by the human equilibrative nucleoside transporter and the human facilitative nucleobase transporter. *Malar. J.* 9, 36

Rahman, S. A., Cuesta, S. M., Furnham, N., Holliday, G. L., and Thornton, J. M. (2014) EC-BLAST: a tool to automatically search and compare enzyme reactions. *Nat. Methods.* 11, 171–174

Raimundo, N., Ahtinen, J., Fumić, K., Barić, I., Remes, A. M., Renkonen, R., Lapatto, R., and Suomalainen, A. (2008) Differential metabolic consequences of fumarate hydratase and respiratory chain defects. *Biochim. Biophys. Acta - Mol. Basis Dis.* 1782, 287–294

Raman, J., Ashok, C. S., I.N. Subbayya, S., Anand, R. P., T. Selvi, S., and Balaram, H. (2005) *Plasmodium falciparum* hypoxanthine guanine phosphoribosyltransferase. *FEBS J.* 272, 1900–1911

Raman, J., Mehrotra, S., Anand, R. P., and Balaram, H. (2004) Unique kinetic mechanism of *Plasmodium falciparum* adenylosuccinate synthetase. *Mol. Biochem. Parasitol.* 138, 1–8

-
- Reaney, S. K., Begg, C., Bungard, S. J., and Guest, J. R. (1993) Identification of the L-tartrate dehydratase genes (ttdA and ttdB) of *Escherichia coli* and evolutionary relationship with the class I fumarase genes. *J. Gen. Microbiol.* 139, 1523–30
- Rhodes, G. (2006) *Crystallography made crystal clear: a guide for users of macromolecular models*, Elsevier/Academic Press
- Riegelhaupt, P. M., Cassera, M. B., Fröhlich, R. F. G., Hazleton, K. Z., Hefter, J. J., Schramm, V. L., and Akabas, M. H. (2010) Transport of purines and purine salvage pathway inhibitors by the *Plasmodium falciparum* equilibrative nucleoside transporter PfENT1. *Mol. Biochem. Parasitol.* 169, 40–9
- Rivadeneira, E. M., Wasserman, M., and Espinal, C. T. (1983) Separation and concentration of schizonts of *Plasmodium falciparum* by Percoll gradients. *J. Protozool.* 30, 367–70
- Robert, X., and Gouet, P. (2014) Deciphering key features in protein structures with the new ENDscript server. *Nucleic Acids Res.* 42, W320–W324
- Rodrigues, T., Lopes, F., and Moreira, R. (2010) Inhibitors of the mitochondrial electron transport chain and de novo pyrimidine biosynthesis as antimalarials: The present status. *Curr. Med. Chem.* 17, 929–56
- Roessler, M. M., King, M. S., Robinson, A. J., Armstrong, F. A., Harmer, J., and Hirst, J. (2010) Direct assignment of EPR spectra to structurally defined iron-sulfur clusters in complex I by double electron-electron resonance. *Proc. Natl. Acad. Sci.* 107, 1930–1935
- Rohde, K. (1993) *Ecology of marine parasites: an introduction to marine parasitology*, CAB International Publication, CAB International
- Roise, D., Horvath, S. J., Tomich, J. M., Richards, J. H., and Schatz, G. (1986) A chemically synthesized pre-sequence of an imported mitochondrial protein can form an amphiphilic helix and perturb natural and artificial phospholipid bilayers. *EMBO J.* 5, 1327–34
- Roth, E. F., Calvin, M. C., Max-Audit, I., Rosa, J., and Rosa, R. (1988) The enzymes of the glycolytic pathway in erythrocytes infected with *Plasmodium falciparum* malaria parasites. *Blood.* 72, 1922–5
- Roth, M. (1971) Fluorescence reaction for amino acids. *Anal. Chem.* 43, 880–2
- Rouault, T. A., and Tong, W.-H. (2005) Iron-sulphur cluster biogenesis and mitochondrial iron homeostasis. *Nat. Rev. Mol. Cell Biol.* 6, 345–351
- Roy, S., Karmakar, T., Prahlada Rao, V. S., Nagappa, L. K., Balasubramanian, S., and Balaram, H. (2015) Slow ligand-induced conformational switch increases the catalytic rate in *Plasmodium falciparum* hypoxanthine guanine xanthine phosphoribosyltransferase. *Mol. Biosyst.* 11, 1410–24
- Royer, C. A. (2006) Probing protein folding and conformational transitions with fluorescence. *Chem. Rev.* 106, 1769–84
-

-
- Rupp, B. (2010) *Biomolecular crystallography: principles, practice, and application to structural biology*, Garland Science, New York
- Sambrook, J., and Russell, D. W. (2001) *Molecular Cloning - Sambrook & Russel*, 10.1002/humu.1186.abs
- Sanders-Loehr, J. (1988) Resonance Raman Spectroscopy of Iron—Oxo and Iron—Sulfur Clusters in Proteins, pp. 49–67, 10.1021/bk-1988-0372.ch003
- Sarpel, G., Barr, A. N., Lubansky, H. J., and Omachi, A. (1982) Erythrocyte phosphate content in Huntington's disease. *Neurosci. Lett.* 31, 91–6
- Saruta, F., Hirawake, H., Takamiya, S., Ma, Y.-C., Aoki, T., Sekimizu, K., Kojima, S., and Kita, K. (1996) Cloning of a cDNA encoding the small subunit of cytochrome b558 (cybS) of mitochondrial fumarate reductase (complex II) from adult *Ascaris suum*, 10.1016/0005-2728(96)00070-9
- Sasaki, R., Ikura, K., Katsura, S., and Chiba, H. (1976) Regulation of Human Erythrocyte AMP Deaminase by ATP and 2,3-Bisphosphoglycerate. *Agric. Biol. Chem.* 40, 1797–1803
- Sasikaran, J., Ziemski, M., Zadora, P. K., Fleig, A., and Berg, I. A. (2014) Bacterial itaconate degradation promotes pathogenicity. *Nat. Chem. Biol.* 10, 371–377
- Sasikaran, J., Ziemski, M., Zadora, P. K., Fleig, A., and Berg, I. A. (2014) Bacterial itaconate degradation promotes pathogenicity. *Nat. Chem. Biol.* 10, 371–7
- Scheibel, L. W., and Pflaum, W. K. (1970) Cytochrome Oxidase Activity in Platelet-Free Preparations of *Plasmodium falciparum*. *J. Parasitol.* 56, 1054
- Schink, B. (1984) Fermentation of tartrate enantiomers by anaerobic bacteria, and description of two new species of strict anaerobes, *Ruminococcus pasteurii* and *Ilyobacter tartaricus*. *Arch. Microbiol.* 139, 409–414
- Schmidt, T. J., Ak, M., and Mrowietz, U. (2007) Reactivity of dimethyl fumarate and methylhydrogen fumarate towards glutathione and N-acetyl-l-cysteine—Preparation of S-substituted thiosuccinic acid esters. *Bioorg. Med. Chem.* 15, 333–342
- Schnarrenberger, C., and Martin, W. (2002) Evolution of the enzymes of the citric acid cycle and the glyoxylate cycle of higher plants. A case study of endosymbiotic gene transfer. *Eur. J. Biochem.* 269, 868–83
- Schoepp-Cothenet, B., van Lis, R., Atteia, A., Baymann, F., Capowicz, L., Ducluzeau, A.-L., Duval, S., ten Brink, F., Russell, M. J., and Nitschke, W. (2013) On the universal core of bioenergetics. *Biochim. Biophys. Acta.* 1827, 79–93
- Schreiner, M. E., Fiur, D., Holatko, J., Patek, M., and Eikmanns, B. J. (2005) E1 enzyme of the pyruvate dehydrogenase complex in *Corynebacterium glutamicum*: molecular analysis of the gene and phylogenetic aspects. *J. Bacteriol.* 187, 6005–6018
- Schulze, A., and Harris, A. L. (2012) How cancer metabolism is tuned for proliferation and vulnerable to disruption. *Nature.* 491, 364–373
-

-
- Schuster, F. L. (2002) Cultivation of plasmodium spp. *Clin. Microbiol. Rev.* 15, 355–64
- Schut, G. J., Zhou, J., and Adams, M. W. W. (2001) DNA Microarray Analysis of the Hyperthermophilic Archaeon *Pyrococcus furiosus*: Evidence for a New Type of Sulfur-Reducing Enzyme Complex. *J. Bacteriol.* 183, 7027–7036
- Sciacovelli, M., Gonçalves, E., Johnson, T. I., Zecchini, V. R., da Costa, A. S. H., Gaude, E., Drubbel, A. V., Theobald, S. J., Abbo, S. R., Tran, M. G. B., Rajeeve, V., Cardaci, S., Foster, S., Yun, H., Cutillas, P., Warren, A., Gnanapragasam, V., Gottlieb, E., Franze, K., Huntly, B., Maher, E. R., Maxwell, P. H., Saez-Rodriguez, J., and Frezza, C. (2016) Fumarate is an epigenetic modifier that elicits epithelial-to-mesenchymal transition. *Nature.* 537, 544–547
- Sculley, D., Dawson, P., Emmerson, B., and Gordon, R. (1992) A review of the molecular basis of hypoxanthine-guanine phosphoribosyltransferase (HPRT) deficiency. *Hum. Genet.* 90, 195–207
- Shibata, H., Gardiner, W. E., and Schwartzbach, S. D. (1985) Purification, characterization, and immunological properties of fumarase from *Euglena gracilis* var. *bacillaris*. *J. Bacteriol.* 164, 762–8
- Shimoyama, T., Rajashekhara, E., Ohmori, D., Kosaka, T., and Watanabe, K. (2007) MmcBC in *Pelotomaculum thermopropionicum* represents a novel group of prokaryotic fumarases. *FEMS Microbiol. Lett.* 270, 207–13
- Shoemark, D. K., Cliff, M. J., Sessions, R. B., and Clarke, A. R. (2007) Enzymatic properties of the lactate dehydrogenase enzyme from *Plasmodium falciparum*. *FEBS J.* 274, 2738–48
- Shryock, J. C., Rubio, R., and Berne, R. M. (1986) Extraction of adenine nucleotides from cultured endothelial cells. *Anal. Biochem.* 159, 73–81
- Siehl, D. L., Subramanian, M. V., Walters, E. W., Lee, S. F., Anderson, R. J., and Toschi, A. G. (1996) Adenylosuccinate synthetase: site of action of hydantocidin, a microbial phytotoxin. *Plant Physiol.* 110, 753–8
- Sievers, F., Wilm, A., Dineen, D., Gibson, T. J., Karplus, K., Li, W., Lopez, R., McWilliam, H., Remmert, M., Söding, J., Thompson, J. D., and Higgins, D. G. (2011) Fast, scalable generation of high-quality protein multiple sequence alignments using Clustal Omega. *Mol. Syst. Biol.* 10.1038/msb.2011.75
- Skala, J., Capieaux, E., Balzi, E., Chen, W. N., and Goffeau, A. (1991) Complete sequence of the *Saccharomyces cerevisiae* LEU1 gene encoding isopropylmalate isomerase. *Yeast.* 7, 281–5
- Slavic, K., Straschil, U., Reiningger, L., Doerig, C., Morin, C., Tewari, R., and Krishna, S. (2010) Life cycle studies of the hexose transporter of *Plasmodium* species and genetic validation of their essentiality. *Mol. Microbiol.* 75, 1402–13
- Slavov, N., Botstein, D., and Caudy, A. (2014) Extensive Regulation of Metabolism and Growth during the Cell Division Cycle. *bioRxiv.* 10.1101/005629
-

- Smilkstein, M. J., Forquer, I., Kanazawa, A., Kelly, J. X., Winter, R. W., Hinrichs, D. J., Kramer, D. M., and Riscoe, M. K. (2008) A drug-selected *Plasmodium falciparum* lacking the need for conventional electron transport. *Mol. Biochem. Parasitol.* 159, 64–68
- Smith, T. G., Walliker, D., and Ranford-Cartwright, L. C. (2002) Sexual differentiation and sex determination in the Apicomplexa. *Trends Parasitol.* 18, 315–323
- Solomon, E. I., Gorelsky, S. I., and Dey, A. (2006) Metal-thiolate bonds in bioinorganic chemistry. *J. Comput. Chem.* 27, 1415–28
- Spear, W., Chan, D., Coppens, I., Johnson, R. S., Giaccia, A., and Blader, I. J. (2006) The host cell transcription factor hypoxia-inducible factor 1 is required for *Toxoplasma gondii* growth and survival at physiological oxygen levels. *Cell. Microbiol.* 8, 339–52
- Srivastava, A., Creek, D. J., Evans, K. J., De Souza, D., Schofield, L., Müller, S., Barrett, M. P., McConville, M. J., and Waters, A. P. (2015) Host reticulocytes provide metabolic reservoirs that can be exploited by malaria parasites. *PLoS Pathog.* 11, e1004882
- Stephens, P. J., Thomson, A. J., Dunn, J. B., Keiderling, T. A., Rawlings, J., Rao, K. K., and Hall, D. O. (1978) Circular dichroism and magnetic circular dichroism of iron-sulfur proteins. *Biochemistry.* 17, 4770–8
- Stivala, A., Wybrow, M., Wirth, A., Whisstock, J. C., and Stuckey, P. J. (2011) Automatic generation of protein structure cartoons with Pro-origami. *Bioinformatics.* 27, 3315–6
- Storm, J., Perner, J., Aparicio, I., Patzewitz, E.-M., Olszewski, K., Llinas, M., Engel, P. C., and Müller, S. (2011) *Plasmodium falciparum* glutamate dehydrogenase a is dispensable and not a drug target during erythrocytic development. *Malar. J.* 10, 193
- Storm, J., Sethia, S., Blackburn, G. J., Chokkathukalam, A., Watson, D. G., Breitling, R., Coombs, G. H., and Müller, S. (2014) Phosphoenolpyruvate carboxylase identified as a key enzyme in erythrocytic *Plasmodium falciparum* carbon metabolism. *PLoS Pathog.* 10, e1003876
- Sturm, A., Mollard, V., Cozijnsen, A., Goodman, C. D., and McFadden, G. I. (2015) Mitochondrial ATP synthase is dispensable in blood-stage *Plasmodium berghei* rodent malaria but essential in the mosquito phase. *Proc. Natl. Acad. Sci.* 112, 10216–10223
- Sturm, A., Mollard, V., Cozijnsen, A., Goodman, C. D., and McFadden, G. I. (2015) Mitochondrial ATP synthase is dispensable in blood-stage *Plasmodium berghei* rodent malaria but essential in the mosquito phase. *Proc. Natl. Acad. Sci.* 112, 10216–10223
- Subramanian, S. S., and Rao, M. R. (1968) Purification and properties of citraconase. *J. Biol. Chem.* 243, 2367–72
- Suhara, K., Takemori, S., Katagiri, M., Wada, K., Kobayashi, H., and Matsubara, H. (1975) Estimation of labile sulfide in iron-sulfur proteins. *Anal. Biochem.* 68, 632–636
- Szabo, A. G., Stepanik, T. M., Wayner, D. M., and Young, N. M. (1983) Conformational heterogeneity of the copper binding site in azurin. A time-resolved fluorescence study. *Biophys. J.* 41, 233–44

- Takeo, S., Kokaze, A., Ng, C. S., Mizuchi, D., Watanabe, J., Tanabe, K., Kojima, S., and Kita, K. (2000) Succinate dehydrogenase in *Plasmodium falciparum* mitochondria: molecular characterization of the SDHA and SDHB genes for the catalytic subunits, the flavoprotein (Fp) and iron-sulfur (Ip) subunits. *Mol. Biochem. Parasitol.* 107, 191–205
- Talman, A. M., Domarle, O., McKenzie, F., Ariey, F., and Robert, V. (2004) Gametocytogenesis : the puberty of *Plasmodium falciparum*. *Malar. J.* 3, 24
- Tanaka, T. Q., Hirai, M., Watanabe, Y., and Kita, K. (2012) Toward understanding the role of mitochondrial complex II in the intraerythrocytic stages of *Plasmodium falciparum*: Gene targeting of the Fp subunit. *Parasitol. Int.* 61, 726–728
- Tanford, C. (1978) The hydrophobic effect and the organization of living matter. *Science.* 200, 1012–8
- Taylor Ringia, E. A., and Schramm, V. L. (2005) Transition states and inhibitors of the purine nucleoside phosphorylase family. *Curr. Top. Med. Chem.* 5, 1237–58
- Teale, F. W., and Weber, G. (1957) Ultraviolet fluorescence of the aromatic amino acids. *Biochem. J.* 65, 476–82
- Teipel, J. W., Hass, G. M., and Hill, R. L. (1968) The substrate specificity of fumarase. *J. Biol. Chem.* 243, 5684–94
- ter Schure, E. G., Sillje, H. H. W., Vermeulen, E. E., Kalthorn, J.-W., Verkleij, A. J., Boonstra, J., and Verrips, C. T. (1998) Repression of nitrogen catabolic genes by ammonia and glutamine in nitrogen-limited continuous cultures of *Saccharomyces cerevisiae*. *Microbiology.* 144, 1451–1462
- Thomas, K. C., and Dawson, P. S. S. (1977) Variations in the Adenylate Energy Charge During Phased Growth (Cell Cycle) of *Candida utilis* Under Energy Excess and Energy-Limiting Growth Conditions. *J. Bacteriol.* 132, 36–43
- Thomas, S. A., Storey, K. B., Baynes, J. W., and Frizzell, N. (2012) Tissue distribution of S-(2-succino)cysteine (2SC), a biomarker of mitochondrial stress in obesity and diabetes. *Obesity (Silver Spring).* 20, 263–9
- Thompson, J. D., Higgins, D. G., and Gibson, T. J. (1994) CLUSTAL W: improving the sensitivity of progressive multiple sequence alignment through sequence weighting, position-specific gap penalties and weight matrix choice. *Nucleic Acids Res.* 22, 4673–4680
- Tielens, A. G. M. M., and Van Hellemond, J. J. (1998) The electron transport chain in anaerobically functioning eukaryotes. *Biochim. Biophys. Acta - Bioenerg.* 1365, 71–78
- Ting, L.-M., Gissot, M., Coppi, A., Sinnis, P., and Kim, K. (2008) Attenuated *Plasmodium yoelii* lacking purine nucleoside phosphorylase confer protective immunity. *Nat. Med.* 14, 954–8
- Tomlinson, I. P. M., Alam, N. A., Rowan, A. J., Barclay, E., Jaeger, E. E. M., Kelsell, D., Leigh, I., Gorman, P., Lamlum, H., Rahman, S., Roylance, R. R., Olpin, S., Bevan, S., Barker, K., Hearle,

- N., Houlston, R. S., Kiuru, M., Lehtonen, R., Karhu, A., Vilkki, S., Laiho, P., Eklund, C., Vierimaa, O., Aittomäki, K., Hietala, M., Sistonen, P., Paetau, A., Salovaara, R., Herva, R., Launonen, V., Aaltonen, L. A., and Multiple Leiomyoma Consortium (2002) Germline mutations in FH predispose to dominantly inherited uterine fibroids, skin leiomyomata and papillary renal cell cancer. *Nat. Genet.* 30, 406–10
- Tomlinson, I. P. M., Alam, N. A., Rowan, A. J., Barclay, E., Jaeger, E. E. M., Kelsell, D., Leigh, I., Gorman, P., Lamlum, H., Rahman, S., Roylance, R. R., Olpin, S., Bevan, S., Barker, K., Hearle, N., Houlston, R. S., Kiuru, M., Lehtonen, R., Karhu, A., Vilkki, S., Laiho, P., Eklund, C., Vierimaa, O., Aittomäki, K., Hietala, M., Sistonen, P., Paetau, A., Salovaara, R., Herva, R., Launonen, V., Aaltonen, L. A., and Multiple Leiomyoma Consortium (2002) Germline mutations in FH predispose to dominantly inherited uterine fibroids, skin leiomyomata and papillary renal cell cancer. *Nat. Genet.* 30, 406–10
- Tong, W.-H., Sourbier, C., Kovtunovych, G., Jeong, S. Y., Vira, M., Ghosh, M., Romero, V. V., Sougrat, R., Vaulont, S., Viollet, B., Kim, Y.-S., Lee, S., Trepel, J., Srinivasan, R., Bratslavsky, G., Yang, Y., Linehan, W. M., and Rouault, T. A. (2011) The Glycolytic Shift in Fumarate-Hydratase-Deficient Kidney Cancer Lowers AMPK Levels, Increases Anabolic Propensities and Lowers Cellular Iron Levels. *Cancer Cell.* 20, 315–327
- Tonhosolo, R., Gabriel, H. B., Matsumura, M. Y., Cabral, F. J., Yamamoto, M. M., D’Alexandri, F. L., Sussmann, R. A. C., Belmonte, R., Peres, V. J., Crick, D. C., Wunderlich, G., Kimura, E. A., and Katzin, A. M. (2010) Intraerythrocytic stages of *Plasmodium falciparum* biosynthesize menaquinone. *FEBS Lett.* 584, 4761–8
- Tornheim, K., and Lowenstein, J. M. (1972) The purine nucleotide cycle. The production of ammonia from aspartate by extracts of rat skeletal muscle. *J. Biol. Chem.* 247, 162–9
- Torrentino-Madamet, M., Almeras, L., Travaille, Sinou, Pophillat, Belghazi, Fourquet, Jammes, and Parzy (2011) Proteomic analysis revealed alterations of the *Plasmodium falciparum* metabolism following salicylhydroxamic acid exposure. *Res. Rep. Trop. Med.* Volume 2, 109
- Torres, R. J., and Puig, J. G. (2007) Hypoxanthine-guanine phosphoribosyltransferase (HPRT) deficiency: Lesch-Nyhan syndrome. *Orphanet J. Rare Dis.* 2, 48
- Trager, W., and Jensen, J. B. (1976) Human malaria parasites in continuous culture. *Science.* 193, 673–5
- Tronrud, D. E. (2007) Introduction to Macromolecular Refinement. in *Macromolecular Crystallography Protocols*, Volume 2, pp. 231–254, Humana Press, New Jersey, 364, 231–254
- Taboi, S., Sato, M., Ono, H., Kobayashi, K., and Hiraga, K. (1986) Mechanism of synthesis and localization of mitochondrial and cytosolic fumarases in rat liver. *Adv. Enzyme Regul.* 25, 461–84
- Ueda, M., Asano, Y., and Yamada, H. (1993) Purification and Characterization of Maleate Hydratase from *Arthrobacter* sp. strain MCI2612. *Biosci. Biotechnol. Biochem.* 57, 1545–1548

- Uyemura, S. A. (2000) Oxidative Phosphorylation, Ca²⁺ Transport, and Fatty Acid-induced Uncoupling in Malaria Parasites Mitochondria. *J. Biol. Chem.* 275, 9709–9715
- Vaidya, A. B., and Mather, M. W. (2000) Atovaquone resistance in malaria parasites. *Drug Resist. Updat.* 3, 283–287
- Vaidya, A. B., and Mather, M. W. (2009) Mitochondrial evolution and functions in malaria parasites. *Annu. Rev. Microbiol.* 63, 249–67
- van Dooren, G. G., Stimmler, L. M., and McFadden, G. I. (2006) Metabolic maps and functions of the Plasmodium mitochondrion. *FEMS Microbiol. Rev.* 30, 596–630
- van Heeswijk, W. C., Westerhoff, H. V, and Boogerd, F. C. (2013) Nitrogen assimilation in *Escherichia coli*: putting molecular data into a systems perspective. *Microbiol. Mol. Biol. Rev.* 77, 628–95
- Van Kuijk, B. L., Van Loo, N. D., Arendsen, A. F., Hagen, W. R., and Stams, A. J. (1996) Purification and characterization of fumarase from the syntrophic propionate-oxidizing bacterium strain MPOB. *Arch. Microbiol.* 165, 126–31
- van Schalkwyk, D. A., Priebe, W., and Saliba, K. J. (2008) The inhibitory effect of 2-halo derivatives of D-glucose on glycolysis and on the proliferation of the human malaria parasite *Plasmodium falciparum*. *J. Pharmacol. Exp. Ther.* 327, 511–7
- Van Vugt-Lussenburg, B. M. A., van der Weel, L., Hagen, W. R., and Hagedoorn, P.-L. (2013) Biochemical similarities and differences between the catalytic [4Fe-4S] cluster containing fumarases FumA and FumB from *Escherichia coli*. *PLoS One.* 8, e55549
- van Vugt-Lussenburg, B. M. A., van der Weel, L., Hagen, W. R., and Hagedoorn, P.-L. (2009) Identification of two [4Fe-4S]-cluster-containing hydro-lyases from *Pyrococcus furiosus*. *Microbiology.* 155, 3015–20
- van Vugt-Lussenburg, B. M. A., van der Weel, L., Hagen, W. R., and Hagedoorn, P.-L. (2013) Biochemical similarities and differences between the catalytic [4Fe-4S] cluster containing fumarases FumA and FumB from *Escherichia coli*. *PLoS One.* 8, e55549
- van Waarde, A. (1988) Operation of the purine nucleotide cycle in animal tissues. *Biol. Rev. Camb. Philos. Soc.* 63, 259–98
- Vander Jagt, D. L., Hunsaker, L. A., and Heidrich, J. E. (1981) Partial purification and characterization of lactate dehydrogenase from *Plasmodium falciparum*. *Mol. Biochem. Parasitol.* 4, 255–64
- Vivas, L., Easton, A., Kendrick, H., Cameron, A., Lavandera, J.-L., Barros, D., de las Heras, F. G., Brady, R. L., and Croft, S. L. (2005) *Plasmodium falciparum*: stage specific effects of a selective inhibitor of lactate dehydrogenase. *Exp. Parasitol.* 111, 105–14
- Voet, D., and Voet, J. G. (2011) *Biochemistry*, John Wiley & Sons
- Vranken, W. F., Boucher, W., Stevens, T. J., Fogh, R. H., Pajon, A., Llinas, M., Ulrich, E. L., Markley, J. L., Ionides, J., and Laue, E. D. (2005) The CCPN data model for NMR

-
- spectroscopy: Development of a software pipeline. *Proteins Struct. Funct. Bioinforma.* 59, 687–696
- Wächtershäuser, G. (1990) Evolution of the first metabolic cycles. *Proc. Natl. Acad. Sci. U. S. A.* 87, 200–4
- Wächtershäuser, G. (1992) Groundworks for an evolutionary biochemistry: The iron-sulphur world. *Prog. Biophys. Mol. Biol.* 58, 85–201
- Wächtershäuser, G. (2008) Iron-Sulfur World. in *Wiley Encyclopedia of Chemical Biology*, John Wiley & Sons, Inc., Hoboken, NJ, USA, 10.1002/9780470048672.wecb264
- Wang, M., Shen, Q., Xu, G., and Guo, S. (2014) New insight into the strategy for nitrogen metabolism in plant cells. *Int. Rev. Cell Mol. Biol.* 310, 1–37
- Wang, S. F., Adler, J., and Lardy, H. A. (1961) The pathway of itaconate metabolism by liver mitochondria. *J. Biol. Chem.* 236, 26–30
- WARBURG, O. (1956) On the origin of cancer cells. *Science.* 123, 309–14
- Weaver, T. (2005) Structure of free fumarase C from *Escherichia coli*. *Acta Crystallogr. D. Biol. Crystallogr.* 61, 1395–401
- Weaver, T., and Banaszak, L. (1996) Crystallographic studies of the catalytic and a second site in fumarase C from *Escherichia coli*. *Biochemistry.* 35, 13955–65
- Weaver, T., Lees, M., Zaitsev, V., Zaitseva, I., Duke, E., Lindley, P., McSweeney, S., Svensson, A., Keruchenko, J., Keruchenko, I., Gladilin, K., and Banaszak, L. (1998) Crystal structures of native and recombinant yeast fumarase. *J. Mol. Biol.* 280, 431–42
- Weber, A. L. (1997) Energy from redox disproportionation of sugar carbon drives biotic and abiotic synthesis. *J. Mol. Evol.* 44, 354–60
- Webster, G. C. (1955) Nitrogen Metabolism. *Annu. Rev. Plant Physiol.* 6, 43–70
- Webster, H. K., Whaun, J. M., Walker, M. D., and Bean, T. L. (1984) Synthesis of adenosine nucleotides from hypoxanthine by human malaria parasites (*Plasmodium falciparum*) in continuous erythrocyte culture: inhibition by hadacidin but not alanosine. *Biochem. Pharmacol.* 33, 1555–1557
- Wellems, T. E., Hayton, K., and Fairhurst, R. M. (2009) The impact of malaria parasitism: From corpuscles to communities. *J. Clin. Invest.* 119, 2496–2505
- Wiback, S. J., and Palsson, B. O. (2002) Extreme Pathway Analysis of Human Red Blood Cell Metabolism. *Biophys. J.* 83, 808–818
- Wilkinson, D. J., Smeeton, N. J., and Watt, P. W. (2010) Ammonia metabolism, the brain and fatigue; revisiting the link. *Prog. Neurobiol.* 91, 200–19
- Williams, J., Gill, G. S., and Trager, W. (1998) Prolonged extracellular development of *Plasmodium falciparum* and the favoring effect of carnitine. *Parasitol. Int.* 47, 107–119

- Winn, M. D., Ballard, C. C., Cowtan, K. D., Dodson, E. J., Emsley, P., Evans, P. R., Keegan, R. M., Krissinel, E. B., Leslie, A. G. W., McCoy, A., McNicholas, S. J., Murshudov, G. N., Pannu, N. S., Potterton, E. A., Powell, H. R., Read, R. J., Vagin, A., and Wilson, K. S. (2011) Overview of the CCP 4 suite and current developments. *Acta Crystallogr. Sect. D Biol. Crystallogr.* 67, 235–242
- Winter, R. W., Kelly, J. X., Smilkstein, M. J., Dodean, R., Bagby, G. C., Rathbun, R. K., Levin, J. I., Hinrichs, D., and Riscoe, M. K. (2006) Evaluation and lead optimization of anti-malarial acridones. *Exp. Parasitol.* 114, 47–56
- Wolf, Y. I., and Koonin, E. V (2013) Genome reduction as the dominant mode of evolution. *BioEssays.* 35, 829–837
- Woo, Y. H., Ansari, H., Otto, T. D., Klinger, C. M., Kolisko, M., Michálek, J., Saxena, A., Shanmugam, D., Tayyrov, A., Veluchamy, A., Ali, S., Bernal, A., del Campo, J., Cihlář, J., Flegontov, P., Gornik, S. G., Hajdušková, E., Horák, A., Janouškovec, J., Katris, N. J., Mast, F. D., Miranda-Saavedra, D., Mourier, T., Naeem, R., Nair, M., Panigrahi, A. K., Rawlings, N. D., Padron-Regalado, E., Ramaprasad, A., Samad, N., Tomčala, A., Wilkes, J., Neafsey, D. E., Doerig, C., Bowler, C., Keeling, P. J., Roos, D. S., Dacks, J. B., Templeton, T. J., Waller, R. F., Lukeš, J., Oborník, M., and Pain, A. (2015) Chromerid genomes reveal the evolutionary path from photosynthetic algae to obligate intracellular parasites. *Elife.* 10.7554/eLife.06974
- Woodrow, C. J., Burchmore, R. J., and Krishna, S. (2000) Hexose permeation pathways in *Plasmodium falciparum*-infected erythrocytes. *Proc. Natl. Acad. Sci. U. S. A.* 97, 9931–6
- Woods, S. A., Schwartzbach, S. D., and Guest, J. R. (1988) Two biochemically distinct classes of fumarase in *Escherichia coli*. *Biochim. Biophys. Acta.* 954, 14–26
- Woods, S. A., Schwartzbach, S. D., and Guest, J. R. (1988) Two biochemically distinct classes of fumarase in *Escherichia coli*. *Biochim. Biophys. Acta.* 954, 14–26
- Wrenger, C., Müller, I. B., Schifferdecker, A. J., Jain, R., Jordanova, R., and Groves, M. R. (2011) Specific inhibition of the aspartate aminotransferase of *Plasmodium falciparum*. *J. Mol. Biol.* 405, 956–71
- Wu, R. (1965) Rate-limiting factors in glycolysis and inorganic orthophosphate transport in rat liver and kidney slices. *J. Biol. Chem.* 240, 2373–81
- Xi, H., Schneider, B. L., and Reitzer, L. (2000) Purine catabolism in *Escherichia coli* and function of xanthine dehydrogenase in purine salvage. *J. Bacteriol.* 182, 5332–41
- Yamada, K. A., and Sherman, I. W. (1980) *Plasmodium lophurae*: Malaria induced nucleotide changes in duckling (*Anas domestica*) erythrocytes. *Mol. Biochem. Parasitol.* 1, 187–198
- Yamaoka, T., Kondo, M., Honda, S., Iwahana, H., Moritani, M., Ii, S., Yoshimoto, K., and Itakura, M. (1997) Amidophosphoribosyltransferase limits the rate of cell growth-linked de novo purine biosynthesis in the presence of constant capacity of salvage purine biosynthesis. *J. Biol. Chem.* 272, 17719–25

-
- Yang, M., Soga, T., Pollard, P. J., and Adam, J. (2012) The emerging role of fumarate as an oncometabolite. *Front. Oncol.* 2, 85
- Yano, T., Sled' V. D., Ohnishi, T., and Yagi, T. (1996) Expression and Characterization of the Flavoprotein Subcomplex Composed of 50-kDa (NQO1) and 25-kDa (NQO2) Subunits of the Proton-translocating NADH-Quinone Oxidoreductase of *Paracoccus denitrificans*. *J. Biol. Chem.* 271, 5907–5913
- Yardeni, T., Eckhaus, M., Morris, H. D., Huizing, M., and Hoogstraten-Miller, S. (2011) Retro-orbital injections in mice. *Lab Anim. (NY)*. 40, 155–60
- Yeh, E., and DeRisi, J. L. (2011) Chemical rescue of malaria parasites lacking an apicoplast defines organelle function in blood-stage *Plasmodium falciparum*. *PLoS Biol.* 9, e1001138
- Yogev, O., Yogev, O., Singer, E., Shaulian, E., Goldberg, M., Fox, T. D., and Pines, O. (2010) Fumarase: a mitochondrial metabolic enzyme and a cytosolic/nuclear component of the DNA damage response. *PLoS Biol.* 8, e1000328
- Yoshida, N., and Camargo, E. P. (1978) Ureotelism and ammonotelism in trypanosomatids. *J. Bacteriol.* 136, 1184–6
- Yoshino, M., and Murakami, K. (1982) AMP deaminase reaction as a control system of glycolysis in yeast. Activation of phosphofructokinase and pyruvate kinase by the AMP deaminase-ammonia system. *J. Biol. Chem.* 257, 2822–8
- Yotoko, K. S. C., and Elisei, C. (2006) Malaria parasites (Apicomplexa, Haematozoa) and their relationships with their hosts: Is there an evolutionary cost for the specialization? *J. Zool. Syst. Evol. Res.* 44, 265–273
- Young, J. A., Fivelman, Q. L., Blair, P. L., de la Vega, P., Le Roch, K. G., Zhou, Y., Carucci, D. J., Baker, D. A., and Winzeler, E. A. (2005) The *Plasmodium falciparum* sexual development transcriptome: A microarray analysis using ontology-based pattern identification. *Mol. Biochem. Parasitol.* 143, 67–79
- Zalkin, H. (1985) Glutamine amidotransferases. *Methods Enzymol.* 113, 263–4
- Zell, M. B., Fahnenstich, H., Maier, A., Saigo, M., Voznesenskaya, E. V, Edwards, G. E., Andreo, C., Schleifenbaum, F., Zell, C., Drincovich, M. F., and Maurino, V. G. (2010) Analysis of *Arabidopsis* with highly reduced levels of malate and fumarate sheds light on the role of these organic acids as storage carbon molecules. *Plant Physiol.* 152, 1251–62
- Zeuthen, T., Wu, B., Pavlovic-Djuranovic, S., Holm, L. M., Uzcategui, N. L., Duszenko, M., Kun, J. F. J., Schultz, J. E., and Beitz, E. (2006) Ammonia permeability of the aquaglyceroporins from *Plasmodium falciparum*, *Toxoplasma gondii* and *Trypanosoma brucei*. *Mol. Microbiol.* 61, 1598–608
- Zhao, A., Tsechansky, M., Ellington, A. D., and Marcotte, E. M. (2014) Revisiting and revising the purinosome. *Mol. Biosyst.* 10, 369–74
-

Zhao, H., French, J. B., Fang, Y., and Benkovic, S. J. (2013) The purinosome, a multi-protein complex involved in the de novo biosynthesis of purines in humans. *Chem. Commun. (Camb)*. 49, 4444–52

Zheng, P., and Li, H. (2011) Highly Covalent Ferric–Thiolate Bonds Exhibit Surprisingly Low Mechanical Stability. *J. Am. Chem. Soc.* 133, 6791–6798

Zientz, E., Bongaerts, J., and Uden, G. (1998) Fumarate regulation of gene expression in *Escherichia coli* by the DcuSR (dcuSR genes) two-component regulatory system. *J. Bacteriol.* 180, 5421–5